DOT/FAA/AR-xx/xx

Air Traffic Organization
NextGen & Operations Planning
Office of Research and
Technology Development
Washington, DC 20591

The FAA's Center of Excellence for UAS Research
ASSURE
Alliance for System Safety of UAS through Research Excellence

# Volume VI – UAS Airborne Collision Severity Evaluation – 14 CFR Part 29 Rotorcraft

June 2022

Final Report

U.S. Department of Transportation

**Federal Aviation Administration**

## NOTICE

**Technical Report Documentation Page**

| 1. Report No. | 2. Government Accession No. | 3. Recipient's Catalog No. |
|---|---|---|
| DOT/FAA/AR-xx/xx | | |

| 4. Title and Subtitle | 5. Report Date |
|---|---|
| **Volume VI – UAS Airborne Collision Severity Evaluation – 14 CFR Part 29 Rotorcraft** | **June 2022** |
| | 6. Performing Organization Code |
| 7. Author(s) | 8. Performing Organization Report No. |
| **Gerardo Olivares, Luis Gomez, Rodrigo Marco, Hoa Ly, Javier Calderon del Rey, Chris Duling, Mark Zwiener, Zack Perrin** | |
| 9. Performing Organization Name and Address | 10. Work Unit No. (TRAIS) |
| National Institute for Aviation Research<br>Wichita State University<br>1845 Fairmount<br>Wichita, KS 67260-0093 | 11. Contract or Grant No. |
| 12. Sponsoring Agency Name and Address | 13. Type of Report and Period Covered |
| U.S. Department of Transportation<br>Federal Aviation Administration<br>Office of Aviation Research<br>Washington, DC 20591 | 14. Sponsoring Agency Code |

15. Supplementary Notes

16. Abstract

| 17. Key Words | 18. Distribution Statement |
|---|---|
| **Crashworthiness, Airborne Collision, UAS, National Institute for Aviation Research, NIAR** | This document is available to the U.S. public through the National Technical Information Service (NTIS), Springfield, Virginia, 22161. This document is also available from the Federal Aviation Administration William J. Hughes Technical Center at actlibrary.tc.faa.gov. |

| 19. Security Classif. (of this report) | 20. Security Classif. (of this page) | 21. No. of Pages | 22. Price |
|---|---|---|---|
| Unclassified | Unclassified | | |

**Form DOT F 1700.7** (8-72) Reproduction of completed page authorized

REVISION HISTORY

| Revision | Description of Modifications | Release Date |
| --- | --- | --- |
| - | Initial release | 06/22/2022 |
| | - | |

ACKNOWLEDGEMENTS

The authors would like to thank all the Federal Aviation Administration (FAA) personnel that have been involved in this research project. In particular, the authors would like to thank Sabrina Saunders-Hodge, Hector Rea, Nick Lento, Bill Oehlschlager, Melanie Flavin, and Gerald Pilj for all their contributions and valuable input throughout the research.

The authors would like to thank:

1. Colonel Stephen P. Luxion and Hannah Thach from the FAA’s Center of Excellence for Uncrewed Aircraft Systems (ASSURE) for supporting this research.
2. The collaboration of the Industry Partner provided the information required to create the rotorcraft structure, bird strike validation data, and the rotorcraft components for testing.

The authors also acknowledge the contributions of the graduate research assistants, research engineers, and lab technicians from the National Institute for Aviation Research Virtual Engineering Laboratory: Armando De Abreu Barriga, Akhil Bhasin, Aswini Kona Ravi, Luis Daniel Castillo, Ankit Gupta, Tharun R. Chillakuru, Claudia Rojo Cazorla and Samuel J. De Abreu Barriga.

TABLE OF CONTENTS

LIST OF FIGURES

LIST OF TABLES

# LIST OF ACRONYMS

| | |
|---|---|
| ABS | Acrylonitrile Butadiene Styrene |
| ARC | Aviation Rulemaking Committee |
| BBA | Building Block Approach |
| CAD | Computer-Aided Design |
| CFR | Code of Federal Regulations |
| CG | Center of Gravity |
| COVID-19 | Coronavirus Disease 2019 |
| DIC | Digital Image Correlation |
| DOF | Degree of Freedom |
| ELoS | Equivalent Level of Safety |
| FAA | Federal Aviation Administration |
| FE | Finite Element |
| FEA | Finite Element Analysis |
| FEM | Finite Element Model |
| LiPo | Lithium-ion Polymer (battery) |
| MTOW | Maximum Take-Off Weight |
| NAS | National Airspace System |
| NIAR | National Institute for Aviation Research |
| NTSB | National Transportation Safety Board |
| OEM | Original Equipment Manufacturer |
| PCB | Printed Circuit Board |
| SPC | Single Point Constraint |
| SPH | Smoothed-Particle Hydrodynamics |
| sUAS | Small Uncrewed Aircraft System |
| UAH | University of Alabama in Huntsville |
| UAS | Uncrewed Aircraft System |
| UAV | Uncrewed Aircraft Vehicle |

# EXECUTIVE SUMMARY

According to the latest industry forecast studies, the Uncrewed Aircraft System (UAS) market volume is expected to reach 2.33 million units by 2024 [1]. Nonetheless, safety, regulatory, social, and technical challenges must be addressed before the sight of an uncrewed aircraft in the sky becomes as common and accepted by the public as its crewed counterpart. The primary goal of regulating UAS operations in the National Airspace System (NAS) is to assure an appropriate level of safety. The effect of an airborne collision between a UAS and a crewed aircraft is a concern to the public and government officials at all levels. Research is needed to define airborne hazard severity thresholds for collisions between uncrewed and crewed aircraft or collisions with people on the ground.

This report analyzes airborne collision scenarios between a 1.2 kg (2.7 lb.) quadcopter UAS and a 1.8 kg (4.0 lb.) fixed-wing UAS with a 14 CFR Part 29 rotorcraft. Detailed Finite Element Models of the UAS and the rotorcraft validated through NIAR's Building Block approach have been used to reduce the time and costs associated with physical testing at the full-scale level. The following critical areas for the rotorcraft were identified for analysis: the front cowling, horizontal stabilizer, rear servo, windshield, and main rotor blade. The collaboration of an industry partner facilitated the access to proprietary data to develop and validate the FEM. The severity evaluation criterion follows the guidelines of the ASSURE Airborne Collision Phase I program [2] and a new Blade Damage criterion defining four levels for damage assessment, as shown in the table below.

Table 1. Damage severity evaluation criteria.

| Severity | Airframe Damage Description | Blade Damage Description |
|---|---|---|
| **Level 1** | The airframe is undamaged.<br>Small deformations. | Blade undamaged.<br>Scratches or small dents on a rotor blade.<br>No crack initiation. |
| **Level 2** | Extensive permanent deformation on external surfaces.<br>Some deformation in internal structure.<br>No Skin Failure. | Large dents on a rotor blade.<br>Visible cracking of a rotor blade.<br>Skin debonding. |
| **Level 3** | Skin fracture.<br>Penetration of at least one component into the airframe. | Significant material loss leading to an imbalance on a single blade.<br>No crack initiation at the blade root or hub. |
| **Level 4** | Penetration of UAS into airframe and failure of the primary structure. | Complete rotor blade failure. |

An airborne collision between the rotorcraft's targets and a 1.2 kg (2.7 lb.) quadcopter UAS at a relative velocity of 20.1 – 97.2 m/s (39 - 189 knots) may result in a damage severity level of low-medium (level 1-3) in the front cowling, low-high (level 1-4) in the horizontal stabilizer, low-medium (level 1-2) in the rear servo, low-medium (level 1-2) in the windshield, and medium (level 2) in the main rotor blade. Equally, an airborne collision between the rotorcraft's targets and a 1.8 kg (4.0 lb.) fixed-wing UAS may result in a damage severity level of medium (level 2-3) in the front cowling, medium-high (level 2-4) in the horizontal stabilizer, low-medium (level 1-3) in the rear servo, medium-high (level 2-4) in the windshield, and medium (level 2) in the main rotor blade.

The findings from this research may be used to conservatively define airborne hazard severity thresholds for collisions between uncrewed sUAS (2.7 lb. Quadcopter and 4.0 Fixed Wing) and rotorcraft airframes certified under part *14 CFR Part 29*.

## 1. INTRODUCTION

Uncrewed Aircraft Systems (UASs) is the fastest-growing sector of the aviation industry today; according to The Association for Uncrewed Vehicles International (AUVSI), the largest trade group around UASs, estimates that by 2025 more than 100,000 jobs will be created in the US with an economic impact of more than $82 billion [1]. In addition, the UAS market volume is expected to reach 2.33 million units by 2024 [3]. Nonetheless, safety, regulatory, social, and technical challenges must be addressed before the sight of an uncrewed aircraft in the sky becomes as common and accepted by the public as its crewed counterparts.

The effect of an airborne collision between a UAS and a crewed aircraft is a concern to the public and government officials at all levels. The primary goal of regulating UAS operations in the National Airspace System (NAS) is to assure an appropriate level of safety. While the effects of bird impacts on airplanes are well documented, little is known about the effects of more rigid and higher mass UASs on aircraft structures and propulsion systems. This research evaluates the severity of small UAS (sUAS) (under 55 lb., as defined in the Small Uncrewed Aircraft Rule (*Part 107*)) collisions on rotorcraft airframes.

This research can help define airborne hazard severity thresholds for collisions between uncrewed and crewed aircraft. The results presented in this report focus on small quadcopter and fixed-wing UAS configurations impacting a 14 CFR Part 29 rotorcraft. A second report analyzes the severity level of UAS airborne collisions with general aviation aircraft [4]. Additional work on sUAS collisions against commercial transport and business jet was carried out within the A3 program [2] [5] [6].

### 1.1 BACKGROUND

#### 1.1.1 Uncrewed Aircraft Systems Categories

A UAS is an Uncrewed Aircraft Vehicle (UAV) and the equipment necessary for that aircraft's safe and efficient operation. A UAV is a component of a UAS. It is defined by statute as an aircraft that is operated without the possibility of direct human intervention from within or on the aircraft [7]. It either can fly autonomously or be piloted remotely.

Currently, there is no standard for the classification of UASs. Defense agencies have their standard, and civilian agencies worldwide have their ever-evolving categories and definitions for UASs. Currently, the Federal Aviation Administration (FAA) classifies UASs into the following categories:

- **Small Uncrewed Aircraft Rule (*Part 107*) [8]:** The rule does not cover the full spectrum of UAS types or weights. The FAA acknowledges that rulemaking is an incremental stage of adding UASs into the NAS. The small non-hobby or non-recreational UASs must be operated under the following limitations:
  - Uncrewed aircraft must weigh less than 55 lb. (25 kg).
  - It cannot be flown faster than a ground speed of 87 knots (100 mph).
  - It cannot be flown higher than 400 ft. (≈122 m) above ground level (AGL) unless flown within a 400 ft. radius of a structure and does not fly higher than 400 ft. above the structure's immediate uppermost limit.

        - Minimum visibility, as observed from the location of the control station, may not be less than three statute miles (sm).
        - The minimum distance from clouds is 500 ft (≈152 m) below a cloud and no less than 2,000 ft. (≈610 m) horizontally from the cloud.
    - **Micro-UAS:** The Aviation Rulemaking Committee (ARC) was focused on the flight over people and, in furtherance of that goal, identified four sUAS categories, defined primarily by the level of risk of injury posed, for operations over people. For each category, the ARC recommends a risk threshold that correlates to either a weight or an impact energy equivalent and, to the extent necessary to minimize the risks associated with that category, additional performance standards, and operational restrictions. The following is a summary of the category recommendations [9]:
        - For Category 1, an sUAS may operate over people if the mass (including accessories/payload, *e.g.*, cameras) is 250 g or less.
        - Under Categories 2, 3, and 4, an sUAS may operate over people if it does not exceed the impact energy threshold specified for each category, as certified by the manufacturer using industry consensus test methods, and if its operator complies with operational restrictions specified for each category.

#### 1.1.2 Uncrewed Aircraft Systems Market Size

The UAS market is divided into two groups: Hobbyist and Commercial. Table 2 presents the registration forecast for sUAS until 2024 [3].

Table 2. Registration forecast summary (million sUAS units) [3].

| | 2020 | 2021 | 2022 | 2023 | 2024 |
|---|---|---|---|---|---|
| Hobbyist (model aircraft) | 1.44 | 1.50 | 1.53 | 1.54 | 1.55 |
| Commercial (non-model aircraft) | 0.49 | 0.59 | 0.67 | 0.73 | 0.78 |
| TOTAL UASs | 1.93 | 2.09 | 2.20 | 2.27 | 2.33 |

##### 1.1.2.1 Hobbyist UAS Forecast

To operate in the NAS, the FAA must ensure that aircraft operators are aware of the system they are operating and that the agency also has the means to identify owners. One means to accomplish this is through aircraft registration and marking. On December 14, 2015, the FAA issued a rule requiring all UASs weighing more than 0.55 lb. (250 g) and less than 55 lb. (24.9 kg) to be registered using a new online system (UASs weighing more than 55 lb. must be registered using the existing Aircraft Registration Process). This registration rule aids in investigations and allows the FAA to gather data about UAS use.

The FAA forecasts the market each year according to the sales and registration records. This yearly update identifies the UAS market growth, predicts the following years, and determines an accurate count of the actual active vehicles. Figure 1 presents the most recent record on recreational UAS registration [3] since the rule was instated in 2015. Registrations reached 1.44 million UAS by the end of 2020, which is lower than what the FAA expected in its previous annual prediction. One of the factors affecting the slower registration rate has been the COVID-19 pandemic, which has changed the market's inertia.

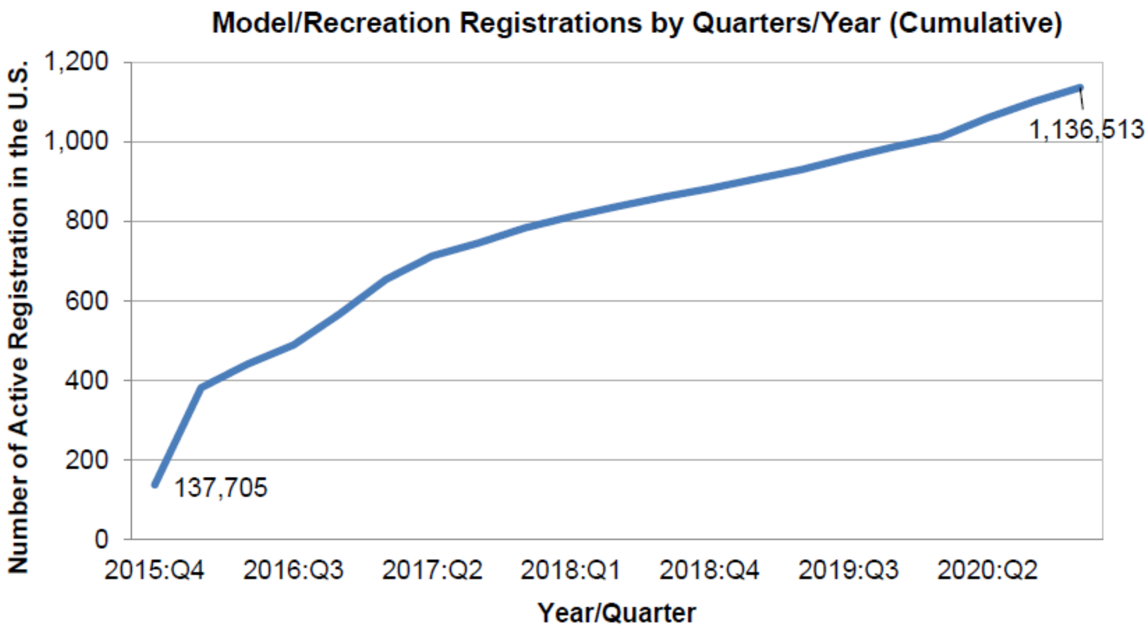


Figure 1. Recreational UAS registrations - December 2020 update [3].

1.1.2.2 Commercial UAS Forecast

In 2015, in support of the sUAS registration rule, a sales forecast for commercial sUASs was developed to derive the potential demand for the new online registration system. That forecast predicted that the potential sales of commercial sUAS requiring registration would grow to 2.7 million by 2020 [1]. The actual market did not evolve at the speed those predictions indicated, but it is constantly growing, as indicated in Figure 2. In addition, the FAA noted in its latest annual revision [3] that the regulatory clarity provided by Part 107 [8] in the recent update on Operation over People increases the opportunities for further integration of sUAS into the NAS.

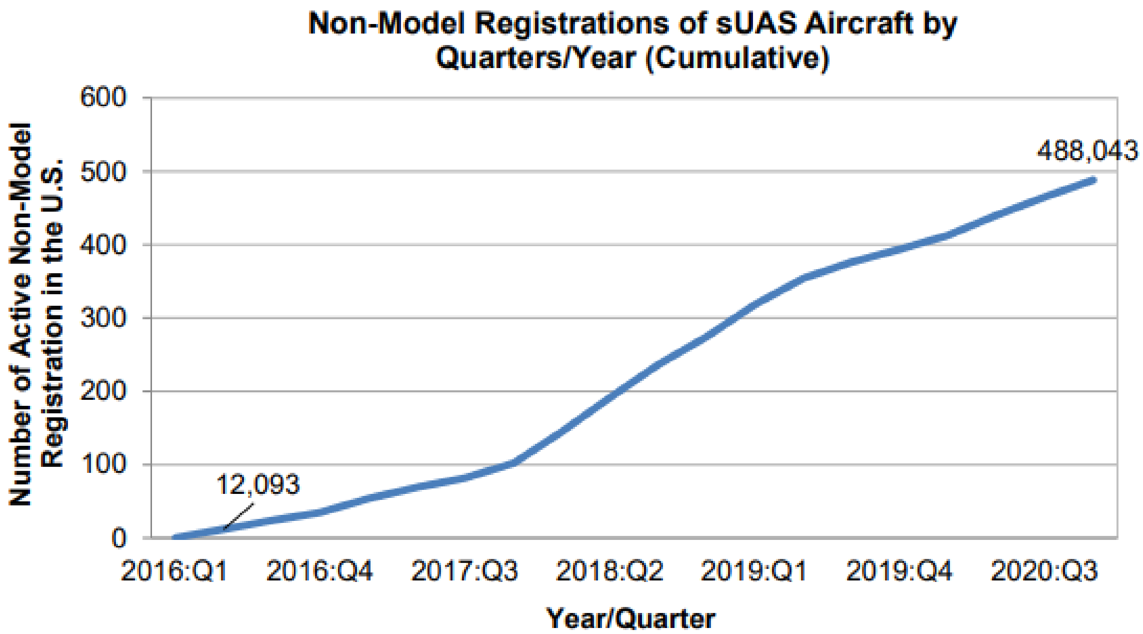


Figure 2. Commercial UAS registrations - December 2020 update [3].

The fast-growing UAS market demands waivers to operate beyond the existing Part 107 [8] regulations. Figure 3 shows the FAA's five most common waiver requests until December 2020. Waivers to operate commercial sUAS at night are the most repeated waiver request.

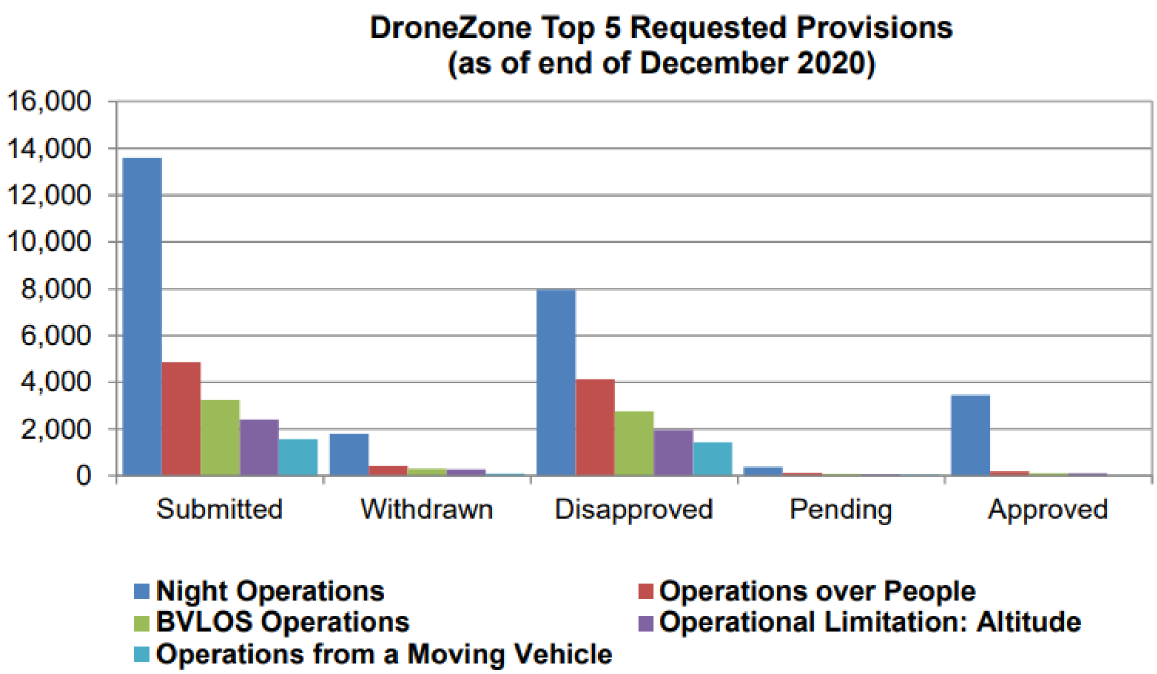


Figure 3 Five most common waiver requests to operate commercial UAS [3].

### 1.1.3 Uncrewed Aircraft Systems Impact Severity Classification

Conventional *Code of Federal Regulations Title 14 (14 CFR*) safety analyses [10] [11] [12] [13] include hazards to flight crew and occupants that may not be applicable to uncrewed aircraft. However, UAS operations may pose unique hazards to other aircraft and people on the ground. Therefore, it is necessary to determine hazard severity thresholds for UASs using safety characteristic factors that affect the potential severity of UASs in collisions with other aircraft on the ground or in airborne encounters and collisions with people on the ground. The factors that determine the outcome of an airborne collision are numerous and complex and highly dependent on the structural design and materials used to construct the UAS.

#### 1.1.3.1 Uncrewed Aircraft Systems Mid-Air Collisions Equivalent Level of Safety

The primary goal of regulating UAS operations in the NAS is to assure an appropriate level of safety. National aviation agencies quantify this goal as an "Equivalent Level of Safety" (ELoS) with crewed aviation. However, there are major key differences between crewed and uncrewed aviation that do not only lay in the separation of the pilot from the cockpit and the level of automation introduced but also in the variety of architectures and materials used for the construction of UASs. These differences could introduce new failure modes and, as a result, increase the perceived risk that needs to be evaluated [14].

To have an ELoS, according to the definition of the Range Commanders Council in its guidance on UAS operations, any UAS operation or test must show a level of risk to human life no greater than that for an operation or test of a piloted aircraft [15].

Although current crewed aviation regulations do not impose limits on fatality rates, a statistical analysis of historical data can provide valuable insight into crewed aviation's collision and fatality rates. It could be used to define the basis for the ELoS of UAS.

For an ELoS to be derived, accident statistics involving mid-air collisions are required. The National Transportation Safety Board (NTSB) has defined two categories of relevant collision accident scenarios; *(i)* in-flight collisions with obstacles such as birds, trees, power lines; and *(ii)* mid-air collisions with other aircraft. The latter could be used to define the UAS requirements. Data pertaining to this approach is presented in reference [14] to NTSB data compiled between 1983 and 2006. If this approach is used in the future as a reference metric to define the ELoS, it is recommended to conduct further studies that include updated NTSB data available.

Once the ELoS is defined based on historical data from crewed aviation, the next step is to develop a method to estimate the probability of mid-air collisions between UASs and crewed aircraft. Several authors have published methodologies on how to evaluate the risk of mid-air collisions between crewed aircraft and UASs [16] [15]; some of the midair collision models are based on a theory originally developed to predict the collision frequency of gas molecules [15]. This theory was similarly applied to air traffic [17] [18]. The collision frequency between a single UAS and transient air traffic is a product of the transient aircraft density, the combined frontal areas, and the relative closing velocity between the colliding crewed and uncrewed aircraft [16].

The aforementioned metrics provide statistical probabilities of UAS mid-air collisions according to specific parameters defined for the evaluation. It should be noted that not all collisions could lead to catastrophic accidents. The large variability of UAS sizes and the fact that not all aircraft systems are critical for remaining airborne means that the aircraft involved may survive certain collisions.

The risk assessment to develop an Airborne Collision UASs Impact Severity Classification can be divided into three elements:

- **Estimation of the probability of mid-air collision** between UASs and crewed aircraft. This will be a function of the operating airspace, aircraft operating within the airspace, and the UAS configurations operating within the shared airspace. Methods to estimate the probability of impact are presented in references [16] [15].
- **Evaluation of damage potential for typical UASs** classes based on weight, architecture, operational characteristics [altitude, velocity] mid-air collision scenarios per crewed aircraft class (commercial, general aviation, rotorcraft, etc.) to assess the damage severity to crewed aircraft. Several groups advocate using simplified ballistic penetration models [19], similarity principles to existing bird strike requirements, or kinetic energy thresholds [20] [21]. This project aims to evaluate the severity of a typical quadcopter and fixed-wing UAS airborne collision with detailed Finite Element (FE) models of the UASs and the target aircraft. These results will be compared with the proposed penetration mechanics and energy-based criteria.
- Once the probability of an airborne collision is determined, **the damage models obtained through the research presented in this study can be combined with the probabilistic collision models to define appropriate ELoS criteria.**

## 1.2 PROJECT SCOPE

Research is needed to establish airborne hazard severity thresholds for collisions between uncrewed and crewed aircraft. This research will help determine airworthiness requirements for uncrewed aircraft based on their potential hazard severity to other airspace users in the NAS. The resulting severity thresholds will be based on UAS characteristics (kinetic energy, structure, shape, materials, etc.) under credible encounter scenarios and will provide test criteria for evaluating applicable operational and airworthiness standards. The previous work performed by ASSURE in Phase I [5] [6] was focused on Narrow Body Commercial Aircraft and Business Jets operating under 14 CFR Part 25 requirements [10] encountering sUAS (2.7 lb. quadcopter and 4.0 lb. fixed-wing). This research will address mid-air collisions with rotorcraft airframes focusing on the front cowling, horizontal stabilizer, rear servo, windshield, and main rotor blade. Lessons learned, and the UAS Finite Element Models (FEMs) developed in Phase I of the ASSURE A3 project will be used for analysis.

The main research questions being answered through this report are [22]:

- What are the hazard severity criteria for a UAS collision (mass, kinetic energy, etc.)?
- What is the severity of a UAS collision with a rotorcraft in mid-air?
- Can the severity of a UAS mid-air collision with a rotorcraft be characterized into categories based on the UAS? What would those categories look like?
- Can a UAS impact be classified as similar to a bird strike?
- What are the characteristics of a UAS where it will not be a risk to a rotorcraft?

This research project will utilize a proven simulation technique, the Building Block Approach (BBA), to analyze the outcome and severity of typical impact scenarios. In addition, the numerical models will be validated with experimental data at the coupon and component levels to predict the full-scale UAS system-level response under impact.

Collision severity to the airframe will be evaluated following the damage severity level criterion developed in Task A3 [2], which ranks level 1 as the lowest (no damage) and level 4 as (primary structure compromised).

## 2. UAS PROJECTILE DEFINITION

In previous Task A3 research [5] [6], two sUAS FE models were developed to assess the damage of sUAS airborne collisions with commercial transport jet and business jet aircraft. The FE models were validated for impact velocities up to 128.6 m/s (250 knots) through several coupon, component, assembly, and full-scale testing efforts. In addition, to further validate the sUAS FEM for velocities that better represent those expected during mid-air collisions with rotorcraft, additional tests were conducted at higher (500 knots) and lower (50 knots) impact velocities than those investigated in Task A3.

The 2.7 lb. quadcopter FEM was created by reverse-engineering the DJI Phantom 3 Standard model [5]. Likewise, the 4.0 lb. fixed-wing FEM followed a similar reverse-engineering process to create a representative virtual Precision Hawk Lancaster Mark III [6] model. Figure 4 and Figure 5 show the quadcopter and fixed-wing models, respectively.

Figure 4. DJI Phantom 3.

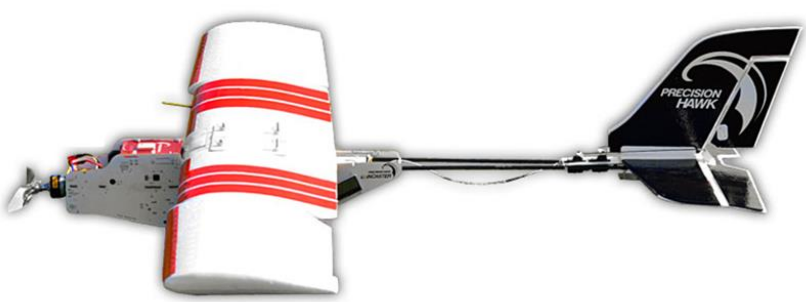


Figure 5. Precision Hawk Lancaster Hawkeye Mark III.

Figure 6 illustrates the process followed to reverse-engineer the UAS models during the Task A3 program [5] [6]. The process consisted of scanning the physical article to generate cloud point data of the geometry, creating the Computer-Aided Design (CAD) model, and discretizing the geometry.

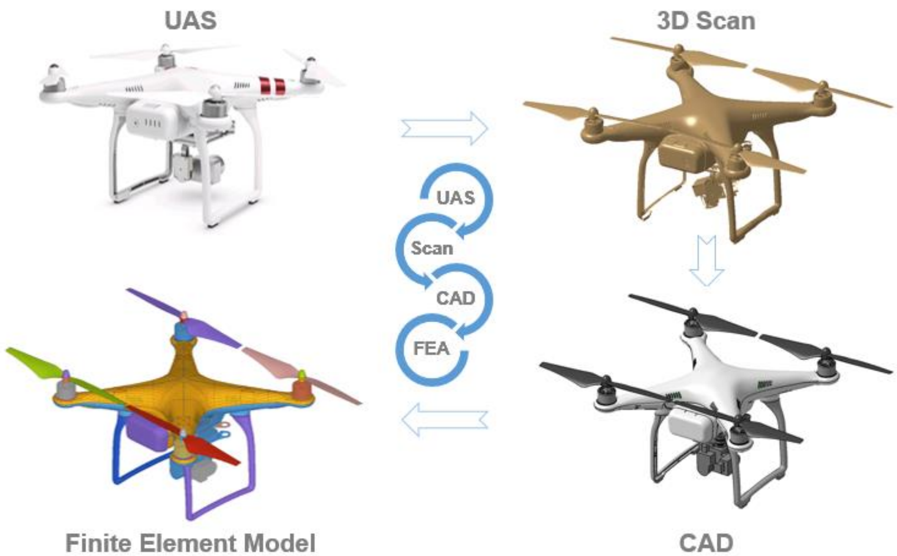


Figure 6. UAS FE modeling process.

The following subchapters summarize the work carried out during Task A3 [5] [6] to develop the FEM of the 2.7 quadcopter and the 4.0 lb. fixed-wing UAS. Furthermore, the validation results for the tests conducted in this research effort are also documented.

## 2.1 CAD DEFINITION

This chapter summarizes the process of developing the CAD models of the representative 2.7 lb. quadcopter and 4.0 fixed-wing UAS geometry. A more detailed description of the models can be found in A3 final report Volume II [5] and Volume III [6].

### 2.1.1 UAS 2.7 lb. Quadcopter

The DJI Phantom 3 was identified as the most common quadcopter in the sUAS market during Task A3 [5]. As a result, a physical Phantom 3 UAS was disassembled, scanned, and reverse-engineered to create the CAD geometry of the virtual model. Figure 7 illustrates the envelopes of the quadcopter at each of the three stages leading to the CAD creation: cloud point contour, polygonal mesh, and CAD geometry.

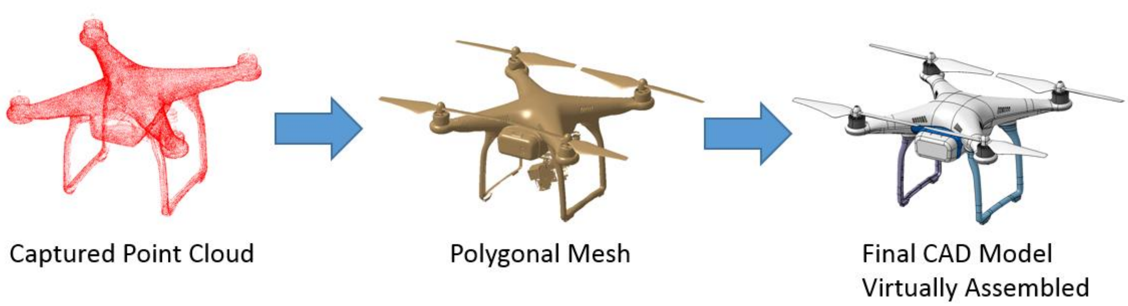


Figure 7. UAS 2.7 lb. quadcopter CAD model development steps.

Figure 8 shows an overall and an exploded view of the quadcopter that highlights the main sub-assemblies of the model.

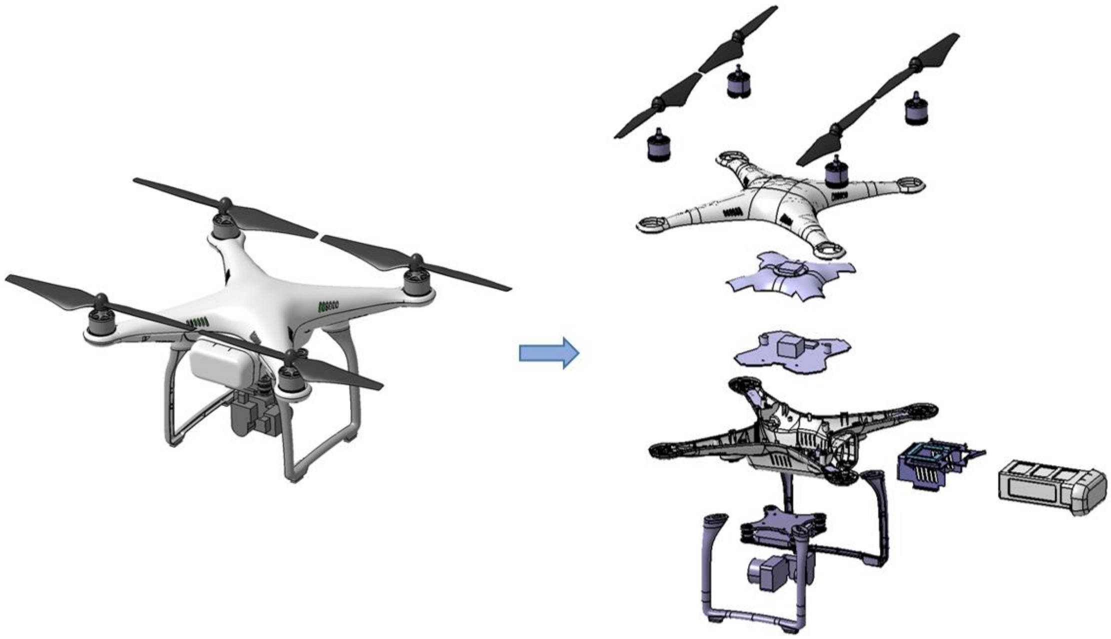

Figure 8. UAS 2.7 lb. quadcopter geometry model.

Table 3 gathers the most relevant specifications of the DJI Phantom 3 Standard [5]. This data was considered during the CAD creation and the FEM development processes.

Table 3. Relevant specifications of the DJI Phantom 3 Standard [5].

| | | |
|---|---|---|
| Mass | 1,216 g | 2.68 lb. |
| Diagonal | 350 mm | 13.8 in. |
| Max. Horizontal Speed | 16 m/s | 31 knots |
| Max. Service Ceiling | 6,000 m | 19,685 ft. |
| Electronic limit above ground | 120 m | 394 ft. |
| Max. Motor Speed | 1,240 rad/s | 11,840 rpm |
| Motors | 4x brushless DC motors; mass: 54 g | |
| Battery | 4x LiPo cells; capacity: 4480 mAh; mass: 363 g | |

2.1.2 UAS 4.0 lb. Fixed-Wing

The Precision Hawk Lancaster Mark-III was selected as a representative fixed-wing sUAS in the A3 program [6]. A physical article was disassembled and reverse-engineered to generate the CAD geometry. Figure 9 shows the CAD of the 4.0 lb. fixed-wing UAS.

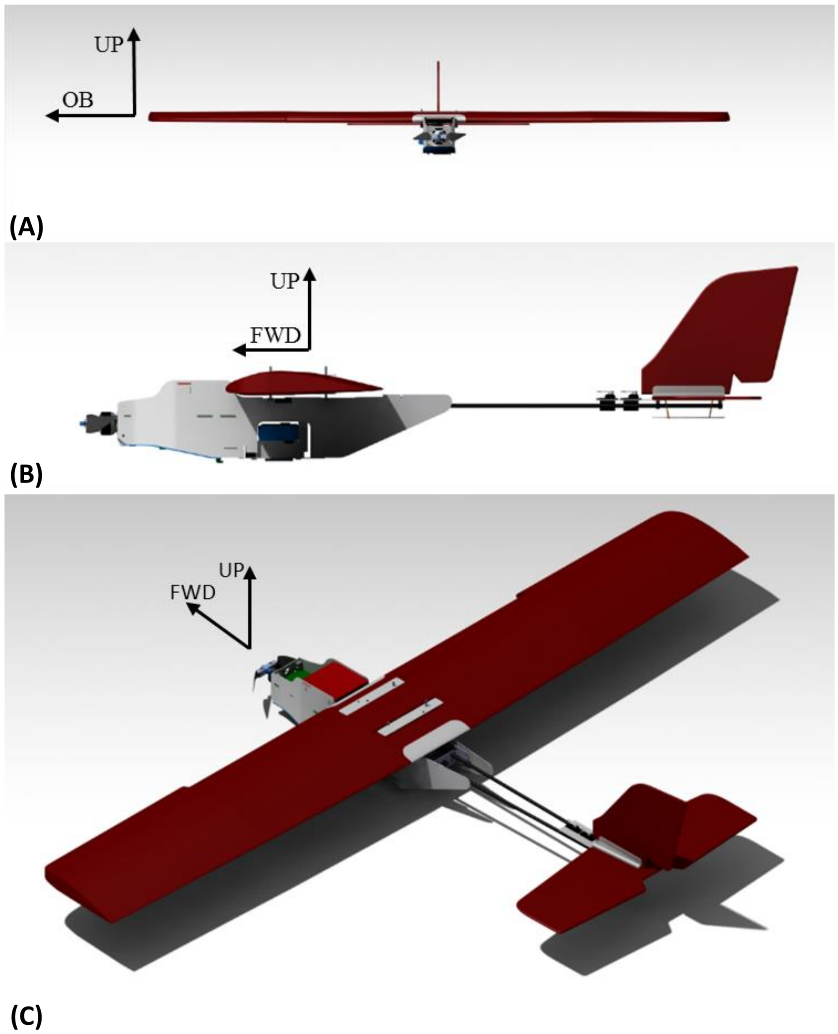


Figure 9. Fixed-wing CAD model: (A) front view, (B) side view, and (C) isometric view.

Figure 10 shows the CAD geometry of the fixed wing's sub-assemblies: motor and propeller, main body, tail, battery, wing, and camera. Table 4 gathers the most relevant specifications of the Precision Hawk Lancaster Mark III [6]. These specifications were considered for the CAD creation and FEM development processes. Note that the original fixed wing's MTOW (5.5 lb.) is higher than Task A3's UAS (4.0 lb.) [6]. This is due to the requirement in Task A3 [6] to develop a scaled-down version of the UAS to facilitate comparing a UAS airborne collision and a 4 lb. bird strike.

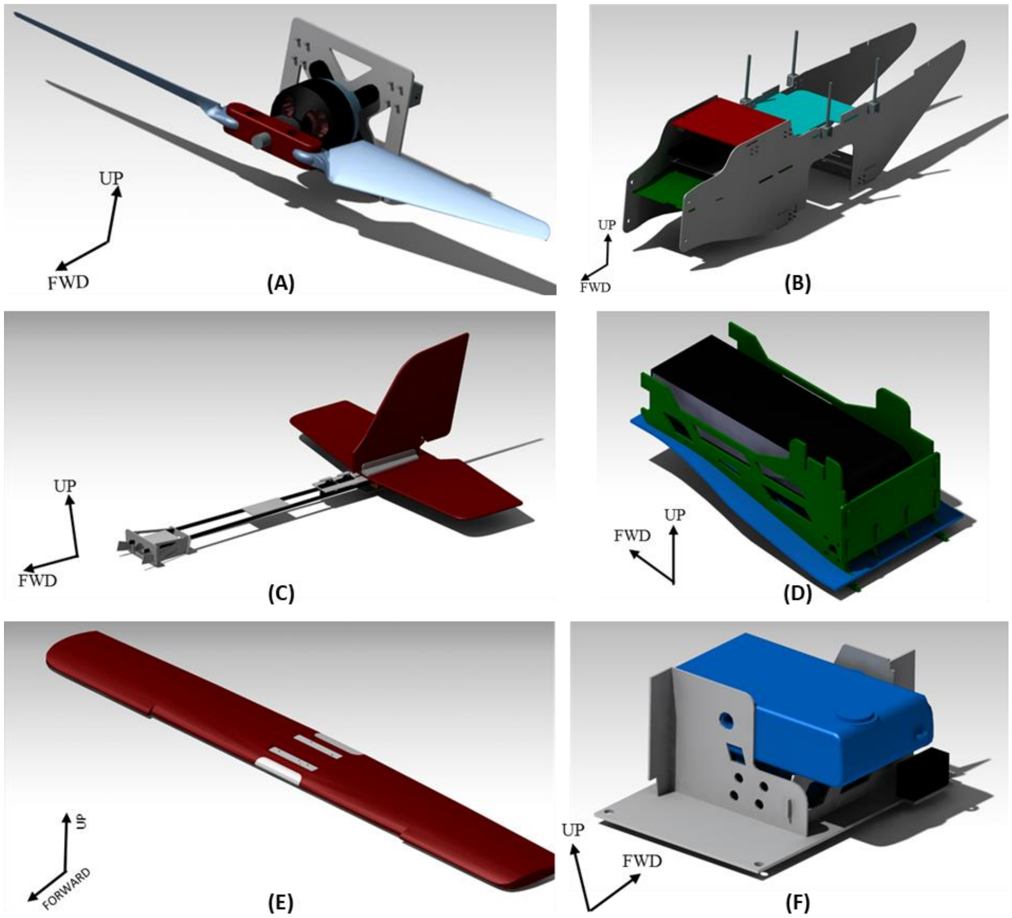


Figure 10. Fixed-wing UAS sub-assemblies: (A) motor & propeller, (B) main body, (C) tail, (D) battery, (E) wing, and (F) camera.

Table 4. Relevant specifications of the Precision Hawk Lancaster Hawkeye Mark III [6].

| | | |
|---|---|---|
| Mass (MTOW) | 2,495 g | 5.5 lb. |
| Wingspan | 1,500 mm | 4 ft. 11 in. |
| Length | 800 mm | 2 ft. 7.5 in. |
| Max. Horizontal Speed | 19.5 m/s | 38 knots |
| Max. Service Ceiling | 4,000 m | 13,120 ft. |

## 2.2 FINITE ELEMENT MODEL

This chapter summarizes the UAS FEM developed in Task A3 [5] [6]. This chapter also presents the validation results and updates applied to the UAS FEMs based on the additional component-level testing performed under this effort.

### 2.2.1 UAS 2.7 lb. Quadcopter

The 2.7 lb. quadcopter geometry was discretized following NIAR's mesh quality criteria, which allowed to capture most of the geometry features and keep a time step below 0.1 microseconds. Table 5 summarizes the mesh criteria followed for this FEM.

Table 5. Quadcopter mesh quality criteria.

| **Quality Parameter** | **Allowable Min.** | **Allowable Max.** |
|---|---|---|
| Element Size | 0.8 mm | 5 mm |
| Aspect Ratio | - | 5 |
| Quad Angle | 45° | 140° |
| Tria Angle | 30° | 120° |
| Warp Angle | - | 15° |
| Jacobian | 0.7 (2D Element)<br>0.5 (3D Element) | - |
| Time-step | 1E-7 s | - |

Figure 11 compares the quadcopter components' geometry and mesh, providing an example of the level of detail maintained during the discretization.

Material definition and calibration were carried out in Task A3 [5] through coupon level and other test experiments at the component level. The present quadcopter FEM preserves the same materials specifications. Figure 12 presents a color-coded exploded view of the 2.7 quadcopter FEM, specifying the materials applied to the virtual model.

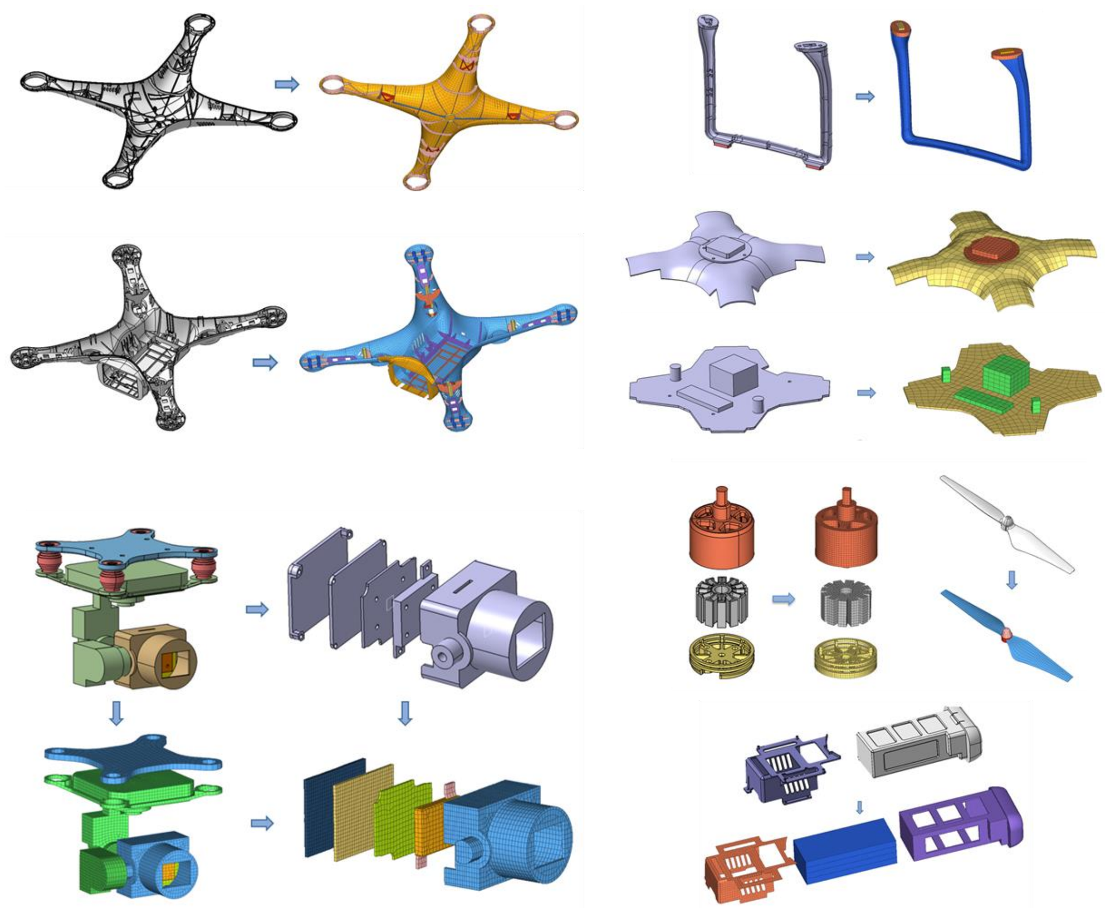

Figure 11. UAS 2.7 lb. quadcopter sub-assembly's CAD geometry and FE mesh.

| Code | Material |
|---|---|
| | Polycarbonate |
| | Nylon |
| | Cast Aluminum 520-F |
| | Steel 4030 |
| | G-10 Fiberglass (PCB) |
| | Li-Po Battery Cell |
| | Aluminum Film 1145-O |

Figure 12. UAS 2.7 lb. quadcopter materials.

Connections and contact definitions were determined and validated in the previous research [5]. Figure 13 illustrates the overall review of the 2.7 quadcopter FEM connections.

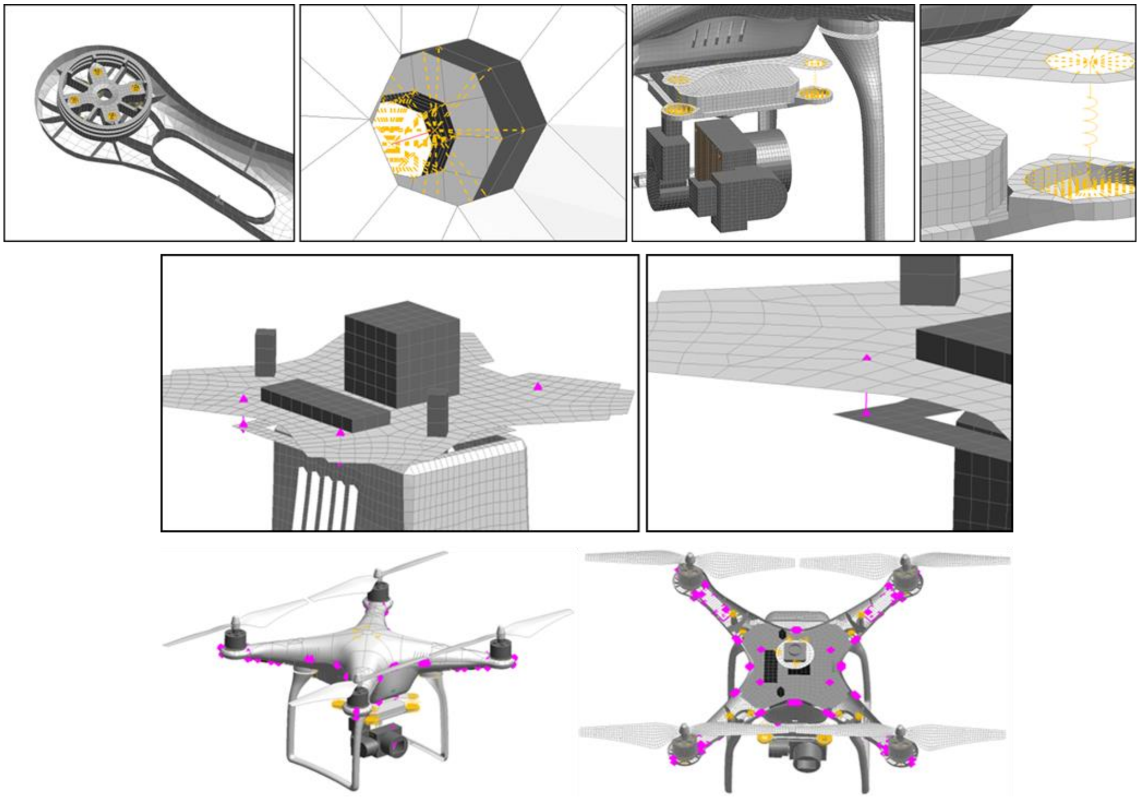

Figure 13. UAS 2.7 lb. quadcopter connections.

A final mass check was executed to confirm that the UAS mass distribution represents the 2.7 quadcopter physical model. Figure 14 shows the 2.7 lb. quadcopter FEM and the location of its center of gravity.

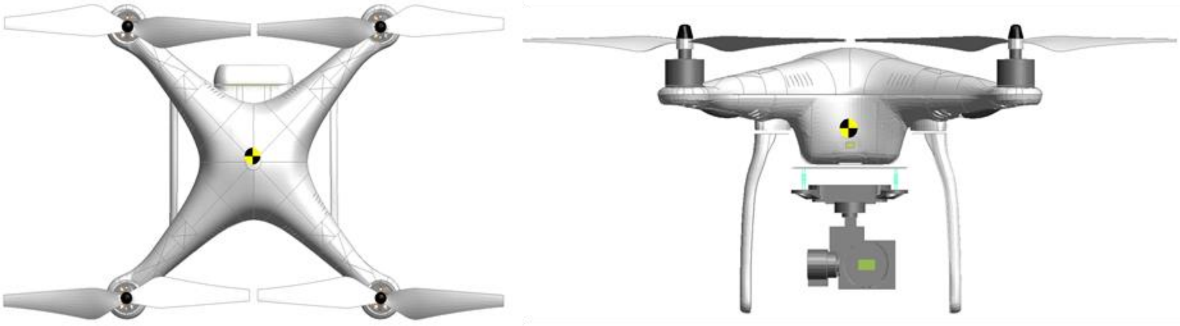

Figure 14. UAS 2.7 lb. quadcopter FEM center of gravity.

2.2.2 UAS 4.0 lb. Fixed-Wing

The CAD geometry was generated in a previous research program [6]. After the disassembling and scanning the fixed-wing UAS components, the geometry was discretized with 2D and 3D elements. Table 6 presents the quality criteria considered to mesh the 4.0 lb. fixed-wing model.

Table 6. Fixed-wing mesh quality criteria.

| **Quality Parameter** | **Allowable** | |
|---|---|---|
| | **Shell Elements** | **Solid Elements** |
| Min. Side Length | 1 mm | 1 mm |
| Max. Aspect Ratio | 5 | |
| Min. Quad Angle | 45° | - |
| Max. Quad Angle | 140° | - |
| Min. Tria Angle | 30° | - |
| Max. Tria Angle | 120° | - |
| Max. Warp Angle | 15° | |
| Min. Jacobian | 0.7 | 0.5 |

Figure 15 separates the model components based on the type of elements used for the discretization: 2D and 3D elements.

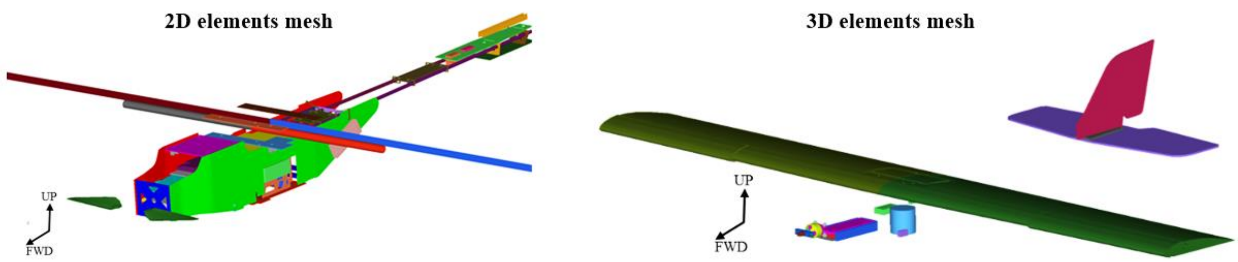


Figure 15. UAS 4.0 lb. fixed-wing parts modeled with 2D and 3D elements.

The definitions of materials, connections, and contacts are discussed in detail in Task A3's final report [6]. The same properties and specifications were kept for this research. In addition, all the component masses were documented during the reverse-engineering process to capture an accurate mass distribution in the virtual model. Figure 16 illustrates the 4.0 lb. fixed-wing FEM and the location of its center of gravity.

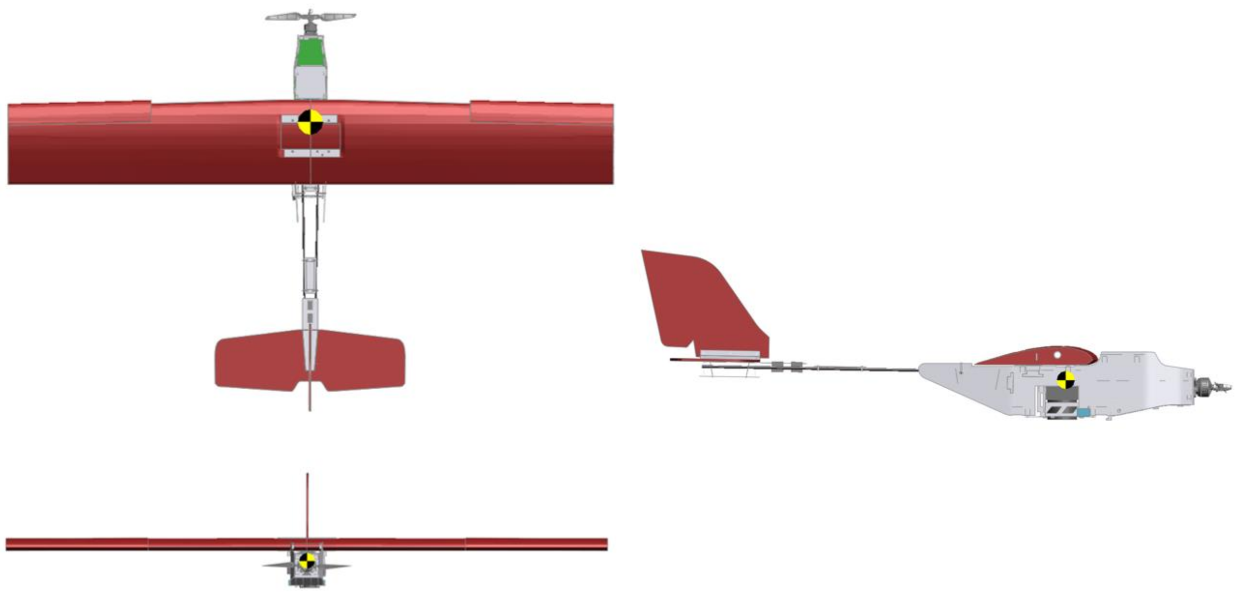

Figure 16. UAS 4.0 lb. fixed-wing FEM center of gravity.

## 2.3 COMPONENT LEVEL TESTS

This chapter presents the analysis work performed to replicate the component level tests and the validation results for the different UAS FEM components. Previous work in Task A3 [5] [6] validated the UAS components for up to 250 knots impact velocities. However, the impact speeds involved in a UAS collision with a rotorcraft could be much higher due to the blades' rotational velocity or smaller during a hovering situation. As a result, additional physical component level tests were conducted to validate further the UAS FEM components in between 50 and 500 knots. Tests were conducted at the University of Alabama in Huntsville (UAH).

This exercise considered two UAS models: DJI Phantom 3 and the Precision Hawk Lancaster Mark III. In continuation of previous Task A3 work [5] [6], the following components were evaluated during testing: battery, motor, and camera. The components were impacted against two different thickness aluminum panels: 1.6 mm (0.063 in.) and 6.35 mm (0.25 in.). These thicknesses are representative of the lower and upper thresholds for aluminum aerospace structures such as skins, spars, ribs, etc. In addition, with the aim of capturing and characterizing the slicing behavior of the battery when impacting against a thin body such as a helicopter blade, the battery was impacted against an aluminum sharp edge target that simulates the leading edge shape of a rotorcraft blade.

The following subchapters summarize the test preparation, instrumentation, output data, simulations, and validation results of the different UAS components.

2.3.1  Selection of Components for Ballistic Tests

Previous Task A3 [5] [6] identified that high mass and high stiffness components in the UAS cause the most damage during the impact. Consequently, those items were selected for ballistic testing to characterize, calibrate and validate their corresponding FEM. The components selected for ballistic testing were the battery and motor of the quadcopter and fixed-wing UAS, and the quadcopter's camera.

Figure 17 presents, from left to right, the battery, motor, and camera of quadcopter UAS. Figure 18 shows the fixed-wing UAS battery and motor.


Figure 17. Quadcopter UAS components for the ballistic test.


Figure 18. Fixed-Wing UAS components for the ballistic test.

2.3.2  Test Conditions

The tests were performed inside a closed cylindrical test chamber with instrumented targets to capture high-speed footage of the impact, load history data, strain outputs, and Digital Image Correlation (DIC) data. Three impact speeds were selected for testing: 50, 120, and 500 knots. This data complements the previous work in Task A3 [5] [6] that looked into an impact speed of 250 knots. The following subchapter presents the test setup and the instrumentation used for testing.

2.3.2.1 Test Setup

The test setup was divided into two assemblies: the fixed test frame and the test fixture. The fixed test frame was created to facilitate the assembling and disassembling the different test fixtures involved in the experiments.

The test fixture was used to hold the aluminum target plate by sandwiching it with two squared steel frames bolted together. The assembled test fixture, including the aluminum panel, was then attached to the fixed frame using four corner bolts through compression load cells.

The sharp blade was held by four steel L-brackets bolted to the steel c-channel that connects this assembly with the fixed test frame. All fixture components were sized to prevent permanent deformation.

Figure 19 presents the aluminum panel and the sharp edge test setups, including the corresponding fixed test frame and fixtures.

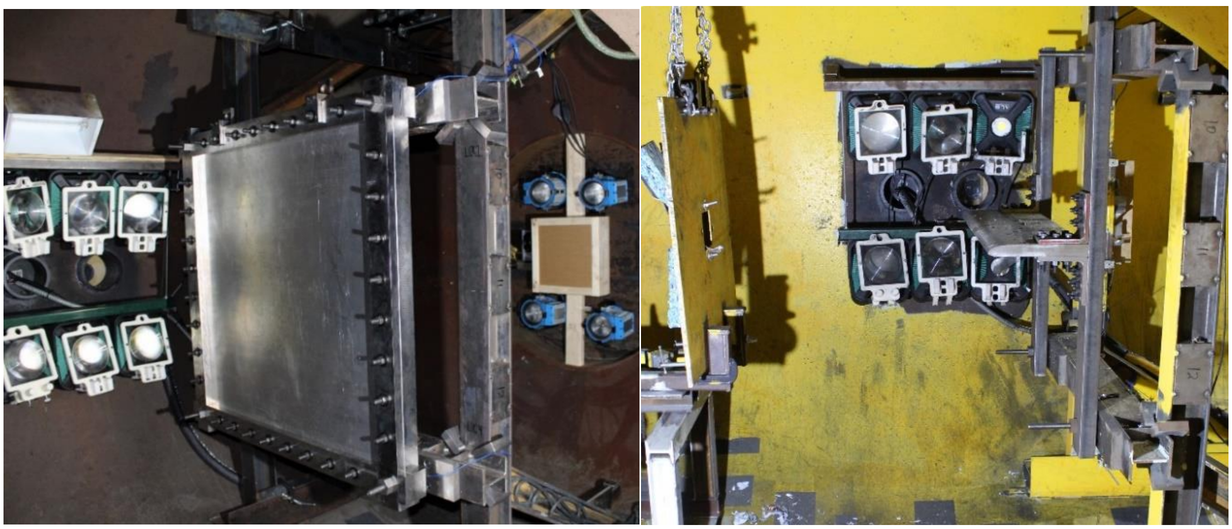

Figure 19. Aluminum panel test setup (left) and sharp edge test setup (right).

2.3.2.2 Test Equipment and Instrumentation

The following equipment and instrumentation were used on all the impact tests:

I. Compressed gas gun system:
   A large compressed gas gun system accelerated the projectile up to 257.2 m/s (500 knots) and impacted the desired location. The projectile's maximum diameter was 57.15 mm (2.25 in.) without the sabot. The acceptable deviation of the launch was determined at 5 % for the velocity and 5 degrees with respect to the nominal trajectory line. Figure 20 shows the compressed gas gun system used for component-level testing.

Figure 20. Compressed gas gun, reservoir, barrel, and test chambers.

II. Projectile sabot:
Two different sabot designs were created to accelerate the projectile along the launching barrel uniformly. A foam-based sabot was used for low-velocity tests, while an ABS 3D-printed sabot was used for the high-energy impacts. Figure 21 shows the foam and ABS sabots.

Figure 21. Foam sabot quadcopter motor (left), ABS sabot fixed-wing motor (right).

III. Load cells:

Four PCB Piezotronics Model 204C uniaxial force rings recorded the load-time history of the test. The load cells had a 40,000 lbf load capacity with a sampling rate of 1 MHz. Figure 22 shows a typical uniaxial load cell.

Figure 22. Typical uniaxial load cell.

The force transducers were located between the fixed test frame and the test fixture assembly. Figure 23 shows the location and numbering convention used for the four load cells once installed in the fixed test frame.

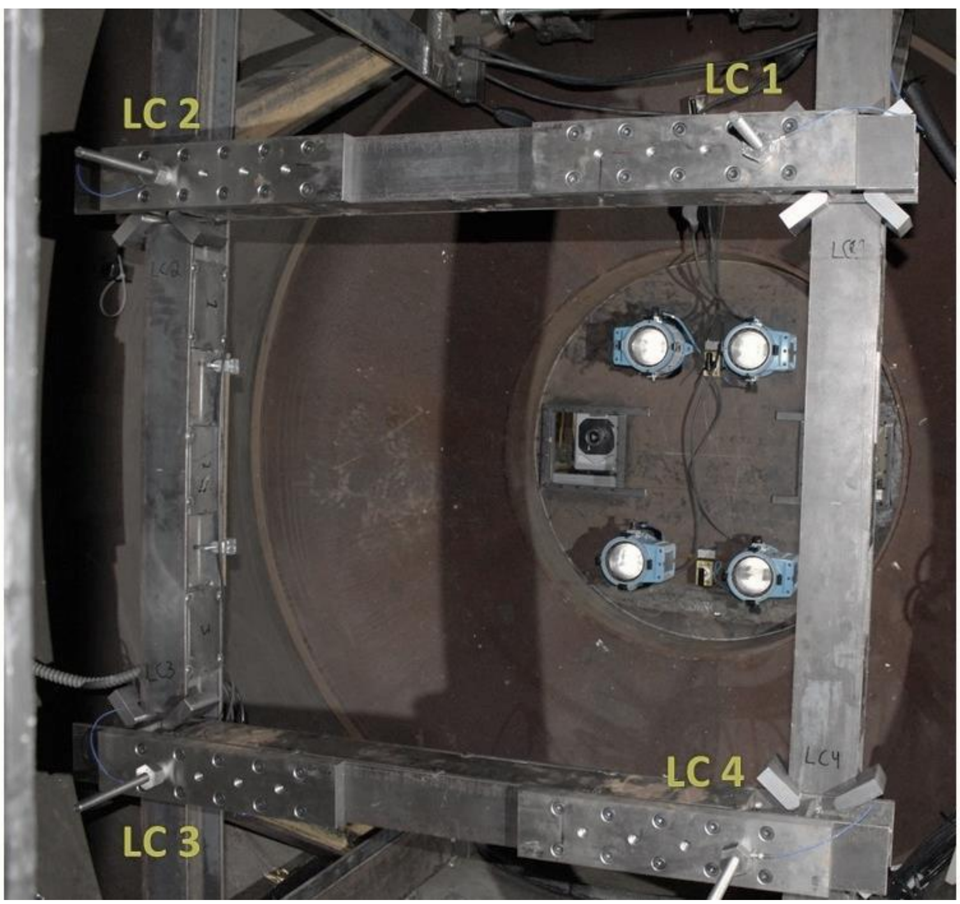


Figure 23. Load cell locations and numbering convention.

IV. Strain gages:

Thirteen ¼-inch, 350-ohm standard elongation strain gages were installed on each aluminum panel. Figure 24 illustrates the location and nomenclature of the strain gages on the aluminum panel rear surface. The data acquisition system sampled results at a rate of 1 MHz. Table 7 presents the general specifications of the strain gages.

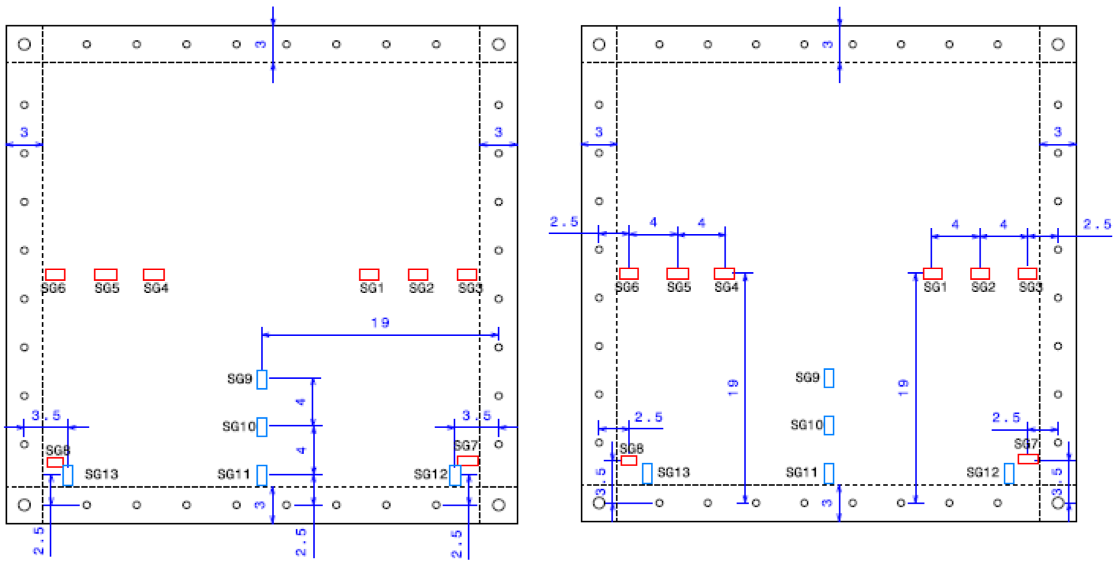


Figure 24. Strain gages location – Panel rear view.

Table 7. Strain gage specifications.

| | |
|---|---|
| Gage ID | K-216.31-2041 |
| Gage Resistance | 350 ± 0.3% Ω |
| Gage Factor | 2.155 ± 0.5% |
| Transverse Sensitivity | +0.3±0.2% |
| Adhesive | AE-10 |
| Post Curve | N/A |

V. High-speed video cameras

Four high-speed video cameras recorded the test at frame rates of 40,000 (camera 1 & 2) and 20,000 (camera 3 & 4) frames per second. Cameras 1 and 2 were positioned perpendicular to the shot line at the top and side of the test chamber, respectively. Camera 3 was located on the side of the test chamber and recorded the target through an angled mirror, providing an off-axis view of the impact. Camera 4 was positioned at the end of the barrel, providing a front view of the target.

VI. DIC system:
High-Speed DIC was used for the aluminum plate testing to capture the panel's maximum displacement and in-plain strains at different locations. To capture the displacement field, the rear surface of the aluminum panel was sprayed with white base paint and a black speckle pattern. These tests were recorded at 20,000 frames per second.

VII. Velocity measurement:
The impact velocity was determined using the high-speed cameras (1 & 2) footage, positioned perpendicular to the shot-line. The UAS traveled distance was estimated by the background scale pattern in the video images.

### 2.3.3 Component Level Tests Results and Validation

The following subchapters summarize the work done to replicate the twenty-three component tests through simulation and the validation results for each one of the UAS components evaluated. Due to the lengthy documentation of the simulation work, detailed information on the validation results is provided in APPENDIX A.

Using the test documentation and information provided by UAH, a numerical model of the test fixture was created for each one of the different configurations. After that, twenty-three simulations were set up to capture the projectile orientation and velocity observed during the physical test. Finally, results from these analyses were compared against the test data. When possible, this comparison included: high-speed kinematics, load time history, strain data (physical and DIC), and panel displacement.

### 2.3.3.1 Test Matrix

Table 8 and Table 9 summarize the component level matrix of the quadcopter and fixed-wing component level tests, respectively.

Table 8. Quadcopter component-level test matrix summary.

| Test Number | Iteration | Panel Type | Projectile Type | Projectile Weight [g] | Impact Velocity [knots] | Impact Velocity [m/s] | Deviation from nominal velocity | Impact Energy [J] | Panel Penetration (Y/N) | Peak Load [N] | Permanent Deformation (H x V) [mm x mm] | Max. Panel Displacement [mm] |
|---|---|---|---|---|---|---|---|---|---|---|---|---|
| 01 | 1 | Sharp Edge | Battery A | 350.80 | 510.7 | 262.73 | 2.14 % | 12,107.0 | NA | 17,778.3 | NA | NA |
| | 2 | | | 350.80 | 516.6 | 265.76 | 3.32 % | 12,388.4 | NA | 18,964.3 | NA | NA |
| 02 | 1 | 0.063" Al. Panel | | 344.20 | 503.6 | 259.07 | 0.72 % | 11,551.2 | Y | 2,564.7 | NA | 6.75 |
| | 2 | | | 343.40 | 500.6 | 257.53 | 0.12 % | 11,387.5 | Y | 2,297.1 | 211.5 x 76.29 | 5.58 |
| 03 | 1 | 0.25" Al. Panel | | 342.90 | NA | NA | NA | NA | N | NA | NA | NA |
| | 2 | | | 343.40 | 500.6 | 257.53 | 0.12 % | 11,387.5 | N | 45,803.9 | 154.19 x 137.72 | 41.29 |
| 04 | 1 | 0.063" Al. Panel | Motor A | 51.40 | 513 | 263.91 | 2.60 % | 1,790.0 | Y | 609.3 | 72.46 x 81.05 | N/A |
| | 2 | | | 51.10 | 507 | 260.82 | 1.40 % | 1,738.1 | Y | 809.2 | 62.24 x 85.06 | 3.35 |
| 05 | 1 | 0.25" Al. Panel | | 51.00 | 520 | 267.51 | 4.00 % | 1,824.8 | N | 10,871.5 | 60.98 x 44.89 | 13.70 |
| | 2 | | | 50.60 | NA | NA | N/A | NA | N | 9,724.9 | 57.59 x 68.75 | NA |
| 06 | 1 | 0.063" Al. Panel | Camera | 51.90 | 508 | 261.34 | 1.60 % | 1,772.3 | Y | 1,986.6 | 160.59 x128.03 | 7.00 |
| | 2 | | | 52.90 | 518 | 266.48 | 3.60 % | 1,878.3 | Y | 3,260.9 | 110.59 x 110.66 | 4.56 |
| 07 | 1 | 0.25" Al. Panel | | 52.40 | 522 | 268.54 | 4.40 % | 1,889.4 | N | 17,787.4 | 45.72 x 57.74 | 12.84 |
| | 2 | | | 53.10 | 521 | 268.03 | 4.20 % | 1,907.3 | N | 18,556.7 | 59.96 x 38.15 | 12.75 |
| 08 | 1 | 0.063" Al. Panel | Battery A | 343.20 | 52 | 26.75 | 4.00 % | 122.8 | N | 9,630.4 | 69.33 x 57.79 | 15.54 |
| | 2 | | | 343.70 | 51.5 | 26.49 | 3.00 % | 120.6 | N | 8,502.4 | 57.96 x 60.61 | 15.51 |
| 09 | 1 | 0.063" Al. Panel | | 342.60 | 120.87 | 62.18 | 0.73 % | 662.3 | N | 7,211.4 | 69.94 x 77.57 | 23.60 |
| | 2 | | | 343.10 | 118.5 | 60.96 | -1.25 % | 637.5 | N | 7,589.8 | 64.65 x 73.38 | 24.33 |
| 10 | 1 | 0.25" Al. Panel | | 343.80 | 116 | 59.68 | -3.33 % | 612.2 | N | 12,369.0 | 34.95 x 31.77 | 10.64 |
| | 2 | | | 334.50 | 122 | 62.76 | 1.67 % | 658.8 | N | 13,567.0 | 48.44 x 44.93 | 12.05 |
| 11 | 1 | 0.063" Al. Panel | Motor A | 50.80 | 124 | 63.79 | 3.33 % | 103.4 | N | 1,415.2 | 33.01 x 40.96 | 9.97 |
| | 2 | | | 51.80 | 120 | 61.73 | 0.00 % | 98.7 | N | 1,408.8 | 35.29 x 40.88 | 9.83 |
| 12 | 1 | 0.063" Al. Panel | | 51.30 | 57 | 29.32 | 14.00 % | 22.1 | N | 1,739.4 | 22.86 x 23.92 | 5.90 |
| | 2 | | | 50.80 | 57 | 29.32 | 14.00 % | 21.8 | N | 1,208.4 | 24.12 x 18.31 | 6.09 |
| 13 | 1 | 0.063" Al. Panel | Camera | 51.30 | 121 | 62.25 | 0.83 % | 99.4 | N | 1,122.8 | 40.63 x 37.05 | 8.92 |
| | 2 | | | 52.30 | 123 | 63.28 | 2.50 % | 104.7 | N | 1,839.0 | 38.11 x 38.28 | 9.67 |
| 14 | 1 | 0.063" Al. Panel | | 52.30 | 53 | 27.27 | 6.00 % | 19.4 | N | 1,692.0 | 20.36 x 19.87 | 5.67 |
| | 2 | | | 52.20 | 48.6 | 25.00 | -2.80 % | 16.3 | N | 1,525.7 | 26.65 x 20.91 | 5.59 |

Table 9. Fixed-wing component-level test matrix summary.

| Test Number | Iteration | Panel Type | Projectile Type | Projectile Weight [g] | Impact Velocity [knots] | Impact Velocity [m/s] | Deviation from nominal velocity | Impact Energy [J] | Panel Penetration (Y/N) | Peak Load [N] | Permanent Deformation (H x V) [mm x mm] | Max. Panel Displacement [mm] |
|---|---|---|---|---|---|---|---|---|---|---|---|---|
| 15 | 1 | Sharp Edge | Battery B | NA | 509.5 | 262.11 | 1.90 % | NA | NA | 23,069.6 | NA | NA |
| | 2 | | | 259.60 | 498.87 | 256.64 | -0.23 % | 8,549.2 | NA | 23,202.2 | NA | NA |
| 16 | 1 | 0.063" Al. Panel | | 264.80 | 509.5 | 262.11 | 1.90 % | 9,096.0 | Y | 1,828.9 | 160.32 x 138.17 | 4.35 |
| | 2 | | | 259.60 | 499.46 | 256.94 | -0.11 % | 8,569.4 | Y | 1,341.3 | 210.29 x 143.31 | 4.33 |
| 17 | 1 | 0.25" Al. Panel | | 263.90 | 499.46 | 256.94 | -0.11 % | 8,711.4 | N | 45,298.8 | 140.50 x 91.62 | 28.32 |
| | 2 | | | 264.00 | 501.2 | 257.84 | 0.24 % | 8,775.5 | N | 44,350.8 | 138.82 x 90.06 | 28.18 |
| 18 | 1 | 0.063" Al. Panel | Motor B | 75.90 | 527 | 271.11 | 5.40 % | 2,789.4 | Y | 718.2 | 68.35 x 116.81 | 2.61 |
| | 2 | | | 76.00 | 525 | 270.08 | 5.00 % | 2,771.9 | Y | 770.2 | 67.69 x 137.63 | 2.44 |
| 19 | 1 | 0.25" Al. Panel | | 76.10 | 527 | 271.11 | 5.40 % | 2,796.7 | N | NA | 74.90 x 65.86 | 18.14 |
| | 2 | | | 76.50 | 522.5 | 268.80 | 4.50 % | 2,763.6 | N | 17,969.4 | 73.14 x 60.25 | 18.15 |
| 20 | 1 | 0.063" Al. Panel | Battery B | 264.40 | 52 | 26.75 | 4.00 % | 94.6 | N | 4,469.5 | 26.23 x 19.20 | 12.54 |
| | 2 | | | 264.40 | 52 | 26.75 | 4.00 % | 94.6 | N | 3,133.0 | 30.50 x 33.08 | 12.24 |
| 21 | 1 | 0.063" Al. Panel | | 264.00 | 119.68 | 61.57 | -0.27 % | 500.4 | N | 11,839.6 | 48.27 x 45.28 | 19.32 |
| | 2 | | | 265.10 | 120.87 | 62.18 | 0.73 % | 512.5 | N | 11,652.7 | 52.35 x 45.28 | 19.35 |
| 22 | 1 | 0.063" Al. Panel | Motor B | 76.20 | 49 | 25.21 | -2.00 % | 24.2 | N | 1,844.3 | 17.83 x 25.02 | 7.20 |
| | 2 | | | 76.60 | 52 | 26.75 | 4.00 % | 27.4 | N | 2,087.3 | 19.01 x 24.83 | 7.05 |
| 23 | 1 | 0.063" Al. Panel | | 76.70 | 123 | 63.28 | 2.50 % | 153.6 | Y | 3,763.6 | 54.66 x 36.75 | 6.27 |
| | 2 | | | 76.80 | 123 | 63.28 | 2.50 % | 153.8 | Y | 3,409.9 | 58.45 x 35.51 | 6.62 |

#### 2.3.3.2 Test Fixture FEM

The test fixture is divided into two sub-assemblies: the fixed test frame and the individual test fixture (aluminum panel or sharp edge). The fixed test frame consists of structural steel I-beam members that create a robust structure to facilitate the installation of the individual target fixtures. The fixed test frame was rigidly anchored to the top and bottom of the cylindrical test chamber. Figure 25 illustrates the fixed test frame geometry and corresponding CAD geometry inside the test chamber. In addition, two test fixtures were developed for each test: the aluminum panel and the sharp edge. Each fixture was designed to be attached to the fixed test frame at the load cells region, channeling the load path through the connecting bolts that transfer the impact load through the load cells, producing the test load-time history. Figure 26 shows the aluminum panel and sharp edge test fixtures.

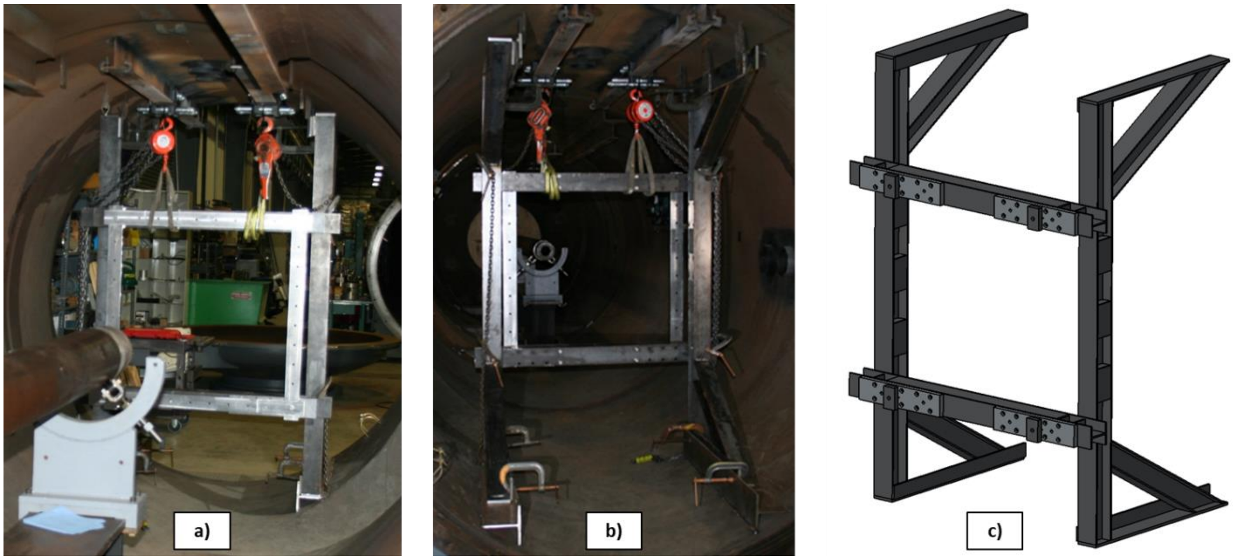


Figure 25. Fixed test frame: a) front view, b) rear view, and c) CAD.

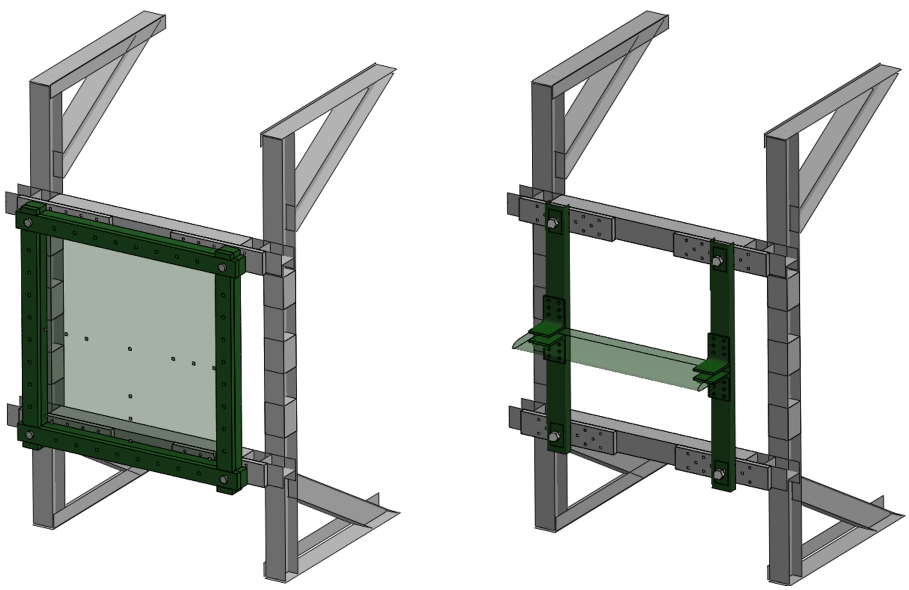

Figure 26. Aluminum panel fixture (left) and sharp edge fixture (right).

### 2.3.4 Component Level Test Summary

All twenty-three tests were simulated based on the initial conditions provided in the UAH test report (see APPENDIX B). Projectile orientation, test impact velocity, impact location on the target, and test boundary conditions were replicated. To support the validation effort, the following data was compared between testing and simulation results:

a. Test video kinematics
b. Load cells' time history
c. Strain gages time history
d. Digital Image Correlation (DIC) in-plane strain contour.
e. Panel maximum displacement
f. Target damage
g. Projectile damage

Due to the lengthy documentation of the simulation work, detailed information on the validation results for each component-level test is provided in APPENDIX A.

#### 2.3.4.1 Battery Risk of Fire Assessment

Battery risk is associated with the possibility of the Lithium-Ion Polymer cells of the battery overheating, sparking, or setting on fire due to the deformation sustained during the impact. This behavior was first observed during the component level testing on Task A3 [5], and it was observed again during the low-speed tests of this testing effort. Figure 27 shows images captured by the post-test cameras inside the test chamber. Table 10 summarizes the Fire Risk outcome from each battery test (APPENDIX B). Note that “Battery A” belongs to the 1.2 kg (2.7 lb.) quadcopter and “Battery B” to the 1.81 kg. (4.0 lb.) fixed-wing UAS.

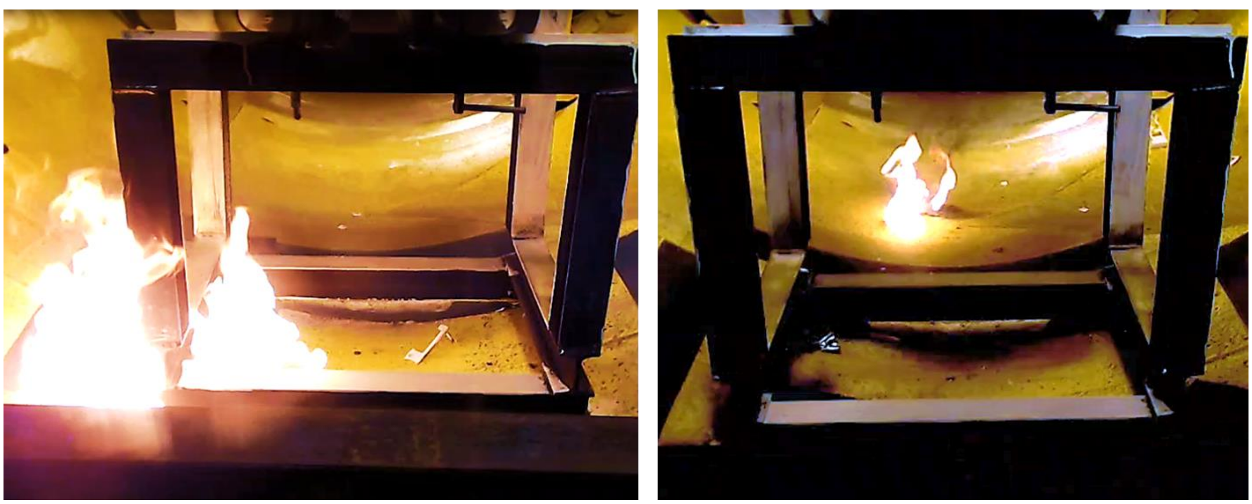

Figure 27. Battery fire risk.

Table 10. Battery tests – Fire risk.

| Test | Projectile | Target | Velocity [knots] | Fire Risk |
|---|---|---|---|---|
| 01 | Battery A | Sharp edge | 500 | No |
| 02 | Battery A | 0.063 in. AL panel | 500 | Yes |
| 03 | Battery A | 0.25 in. AL panel | 500 | No |
| 08 | Battery A | 0.063 in. AL panel | 50 | No |
| 09 | Battery A | 0.063 in. AL panel | 120 | Yes |
| 10 | Battery A | 0.25 in. AL panel | 120 | Yes |
| 15 | Battery B | Sharp edge | 500 | No |
| 16 | Battery B | 0.063 in. AL panel | 500 | No |
| 17 | Battery B | 0.25’ AL panel | 500 | No |
| 20 | Battery B | 0.063 in. AL panel | 50 | No |
| 21 | Battery B | 0.063 in. AL panel | 120 | Yes |

## 2.4 UAS FINITE ELEMENT MODEL VALIDATION

The sUAS models introduced in previous chapters were developed following the BBA. This exercise was initiated during the A3 program when the 1.2 kg (2.7 lb.) quadcopter [5] and the 1.81 kg (4.0 lb.) fixed-wing [6] UAS were reverse-engineered. These models are supported and validated by the following testing data:

- Coupon level data for material characterization from Task A3 [5].
- Sub-component tests were carried out to verify the UAS case polycarbonate material (drop tower test) from Task A3 [5].
- Ballistic component-level test of the battery, motor, and camera from Task A3 [5] [6]. The validation impact velocity range was 250 knots for this program.
- Full-scale test through a free drop test of the UAS from Task A3 [5].
- The full scale at low velocity from the Ground Collision Task A14 program [23].
- National Research Council (NRC) of Canada full-scale level test with DJI Phantom 3 [24] up to 250 knots.
- Task A16 ballistic component-level test (see APPENDIX A) for impact velocity up to 500 knots.
- Task A16 full-scale level test against rotorcraft targets (see Chapter 4).
- Task A17 Engine Ingestion component and full-scale level testing against representative engine fan blades for impact velocities up to 700 knots [25].

These models are intended to assess impact severity levels for mid-air collisions between sUAS and rotorcraft structures.

## 3. TARGET DEFINITION - ROTORCRAFT

This chapter covers the modeling of the rotorcraft airframes subjected to UAS impacts. The targets selected for this study are based on a collaboration between NIAR and the Industry Partner. As a result of this collaboration, the Industry Partner shared with NIAR the following technical data and test articles:

- Detail CAD geometry for the front cowling, horizontal stabilizer, rear servo, and windshield components.
- Detail bill of material (BOM) and layup information for the front cowling, horizontal stabilizer, rear servo, and windshield components.
- Bird strike test data for the front cowling, horizontal stabilizer, rear servo, and windshield components for validation purposes.
- Physical articles for testing (Front cowling, horizontal stabilizer, and windshields).

In addition, the University of Alabama in Huntsville acquired 4 main rotor blades for testing purposes. One of these complete blades was shared with NIAR for reverse-engineering purposes.

**Due to the confidential agreement between NIAR and the Industry Partner, the proprietary technical data obtained through this collaboration cannot be shared with the public**. The reverse-engineering process was peer-reviewed by the technical panel of this program and validated for the analysis work presented in Chapter 6.

To build the rotorcraft targets FE models, NIAR followed a physics-based modeling approach, which takes advantage of advances in computational power, the latest computational tools, and years of research in understanding the fundamental physics of the crashworthiness event, generated test-to-test variability data, and verified & validated modeling methodologies. This approach uses the Building Block Approach, as illustrated in Figure 28. The building block approach is the incremental development of analysis and supporting tests, where typically, there is an increase in the size and complexity of the test article and a decrease in the number of supporting tests. To develop this method, it is necessary to understand the underlying physics and corresponding test variability from the coupon to the system level. System-level test results do not drive the definition of the numerical model. Rather, it is driven by a predefined, verified, and validated building block modeling methodology. Following this approach, simulations predict the system level test results within an acceptable scatter band. An objective verification criterion based on understanding the test-to-test variability is used to evaluate the numerical models.

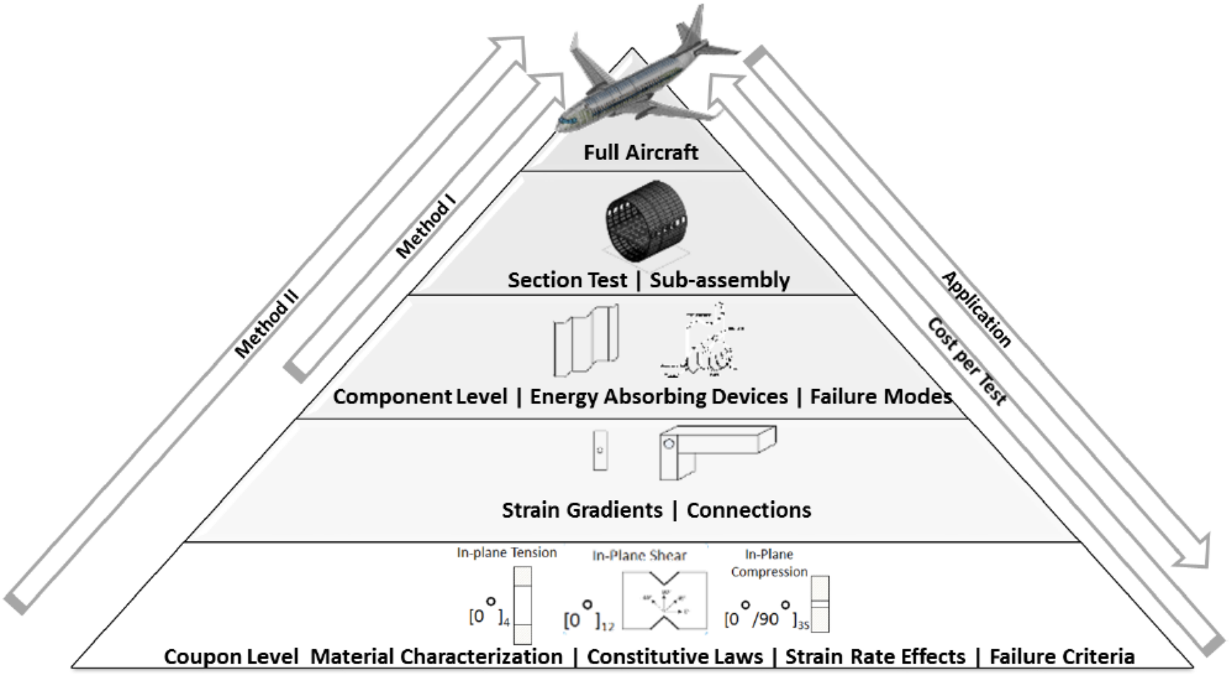


Figure 28. NIAR building block approach.

# 4. FULL-SCALE TEST LEVEL VALIDATION

This chapter presents the work required to validate the rotorcraft structures presented in Chapter 3, specifically, the horizontal stabilizer, the bilayer windshield, and the main rotor blade.

## 4.1 TEST PREPARATION

The full-scale component tests were performed inside a vacuum test chamber at UAH. Rotorcraft targets were installed and positioned relative to the sUAS trajectory to achieve the desired impact location. More detailed information about the test facility and launching system capabilities is discussed in the UAH test report in APPENDIX B.

Unique test fixtures were created for each one of the rotorcraft targets because of their specific geometry and desired impact location. The fixture was divided into two independent sections to facilitate each test setup. A large fixed test frame was designed and anchored to the test chamber and kept common for all the tests. In addition, smaller secondary test fixtures were designed to support each specific target. Details about these fixtures are shown in the following sub-chapters.

### 4.1.1 Fixed Test Frame

The fixed test frame consists of structural steel I-beam members that create a robust structure to facilitate the installation of the individual target fixtures. This fixture was rigidly anchored to the top and bottom of the cylindrical test chamber. Figure 29 illustrates the fixed test frame geometry inside the test chamber and its corresponding CAD geometry.

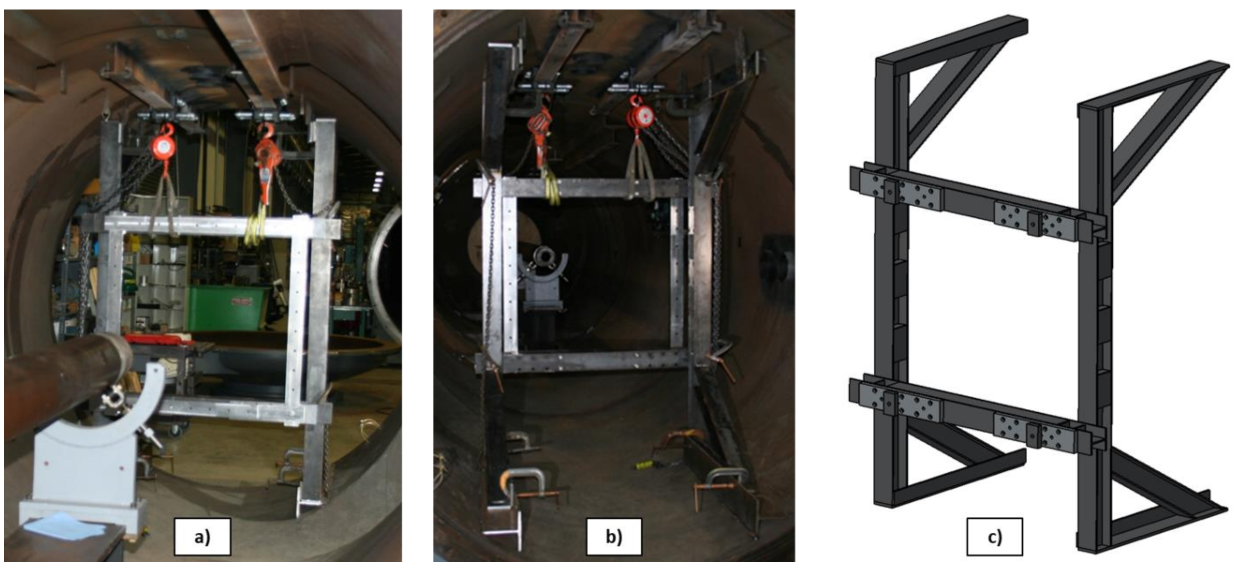


Figure 29. Fixed test frame: a) front view, b) rear view, and c) CAD.

### 4.1.2 Test Matrix

Table 11 summarizes the information of the tests selected for the analysis work.

Table 11. Full-scale test matrix.

| Test Reference | Target | Nominal Velocity | Test Velocity |
|---|---|---|---|
| 21-90 | Horizontal Stabilizer | 90.03 m/s (175 knots) | 92.6 m/s (180 knots) |
| 21-134 | Windshield | 25.72 m/s (50 knots) | 25.7 m/s (50 knots) |
| 21-127 | Windshield | 90.03 m/s (175 knots) | 90 m/s (175 knots) |
| 21-143 | Windshield | 154.3 m/s (300 knots) | 149.2 m/s (290 knots) |
| 21-125 | Blade | 218.6 m/s (425 knots) | 221.6 m/s (430.7 knots) |
| 21-126 | Blade | 218.6 m/s (425 knots) | 227.1 m/s (441.4 knots) |

## 4.2 HORIZONTAL STABILIZER TEST

This chapter presents the validation of the horizontal stabilizer FEM by replicating the physical test 21-90 (see Table 11) conducted as part of this research (APPENDIX B). The Industry Partner provided the physical test article and the design data necessary to create the FEM model (geometry, BOM, and previous bird strike test data for validation).

### 4.2.1 Test Article

The test article consists of a section of the horizontal stabilizer section clamped on both ends with a thick aluminum plate to represent a rigid boundary condition. Figure 30 shows the top and bottom views of the horizontal stabilizer test article as received.

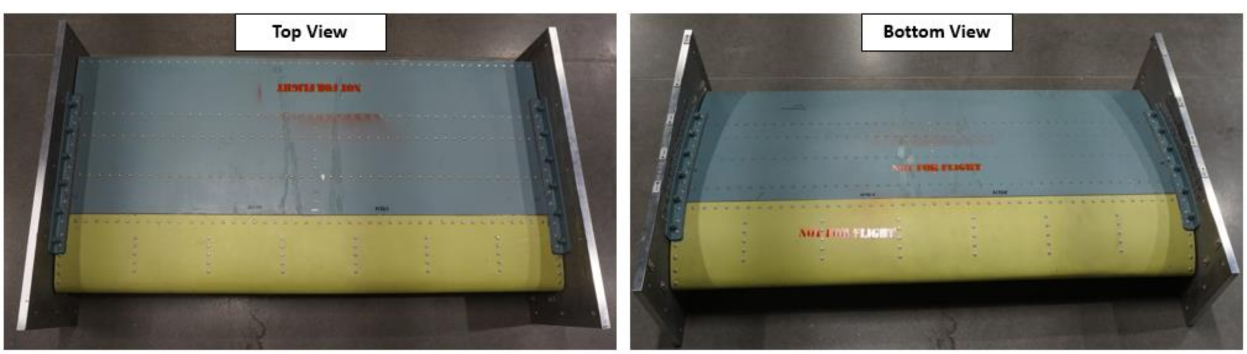


Figure 30. Horizontal stabilizer test article.

The geometry of the horizontal stabilizer was provided by the Industry Partner as introduced in Chapter 0. Figure 31 depicts the CAD of the horizontal stabilizer test article and its overall dimensions.

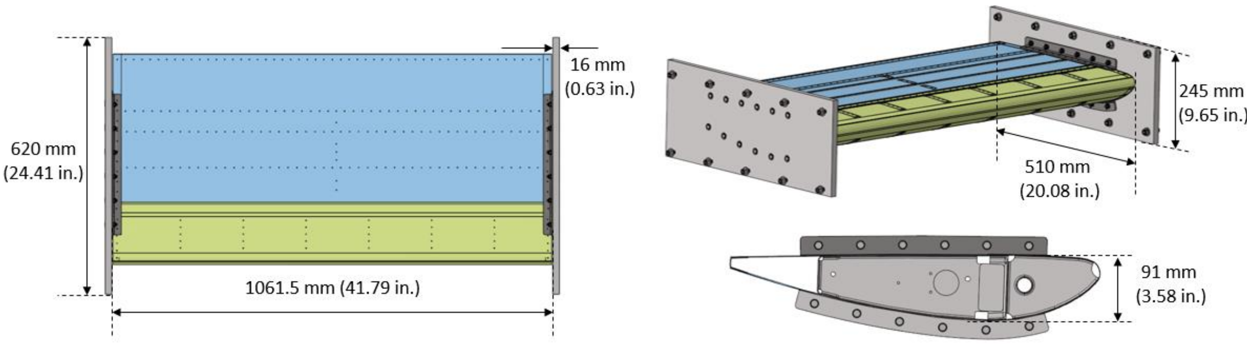


Figure 31. Horizontal stabilizer CAD.

<u>4.2.2 Test Fixture</u>

The horizontal stabilizer test fixture is divided into two sub-assemblies: the fixed test frame (introduced in Chapter 4.1) and the horizontal stabilizer test fixture. Figure 32 presents the CAD and discretization of the horizontal stabilizer test fixture.

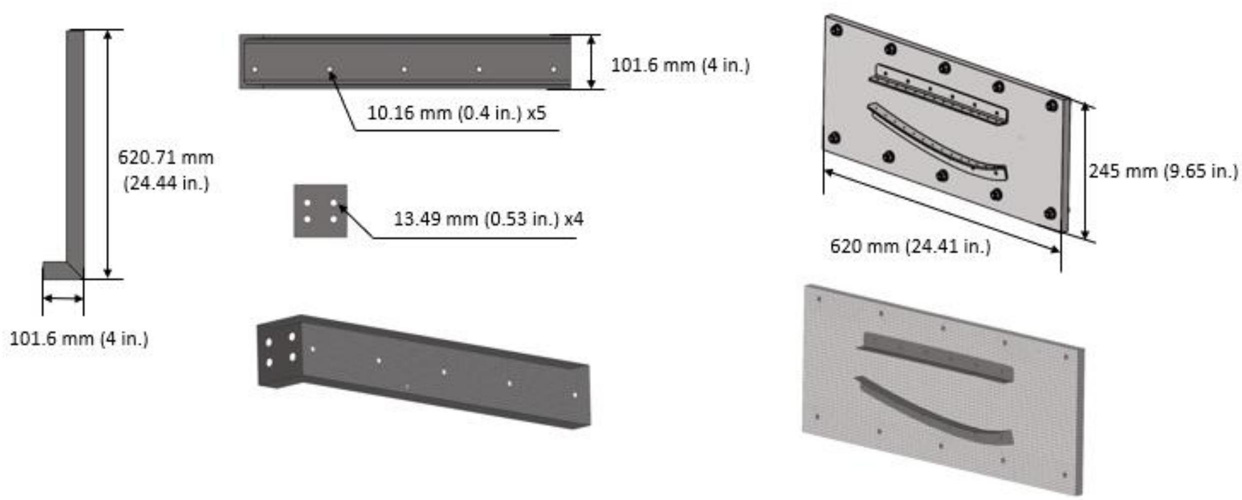


Figure 32. Horizontal stabilizer test fixture – CAD and mesh.

Figure 33 compares the physical and CAD geometry of the test assembly. The CAD highlights the L-shaped members in green color, indicating the region where the fixed test fame and the horizontal stabilizer fixture come together. The L-shaped brackets were attached to the horizontal stabilizer with five steel bolts along the larger bracket face. The shorter face of the L-shaped members was connected to the rigid fixture using four steel bolts. All the L-shaped bracket bolts (numerical model and physical test article) were preloaded with a torque of 108.5 N-m (80 ft-lbf).

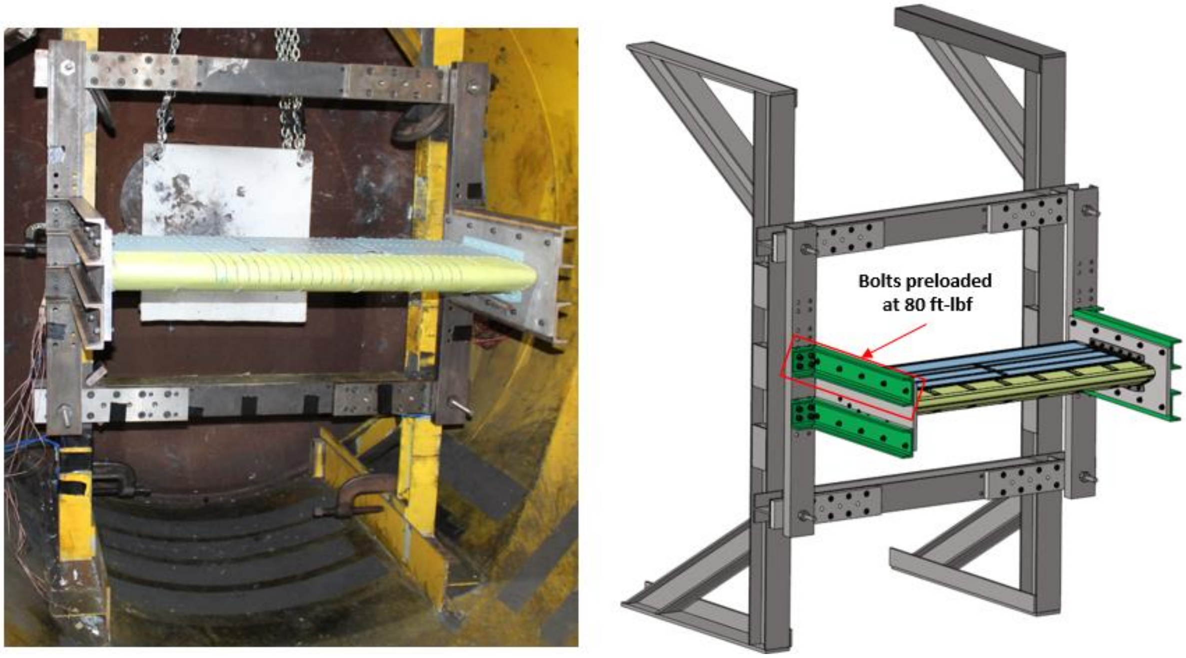


Figure 33. Horizontal stabilizer test fixture (left) and CAD fixture (right).

4.2.3 Test Instrumentation

The following instrumentation was used during the horizontal stabilizer test:

I. High-speed cameras
   Three high-speed video cameras were set up to record the impact event from different angles. The camera's recording frequency was 40,000 frames per second. Camera 1 was positioned above the upper surface of the horizontal stabilizer (top view). Camera 2 was located on the side of the fixture, perpendicular to the shot line (side view). Finally, camera 3 was positioned at an oblique angle with respect to the front of the horizontal stabilizer (isometric view). Figure 34 presents the sketch of the location of the high-speed camera.

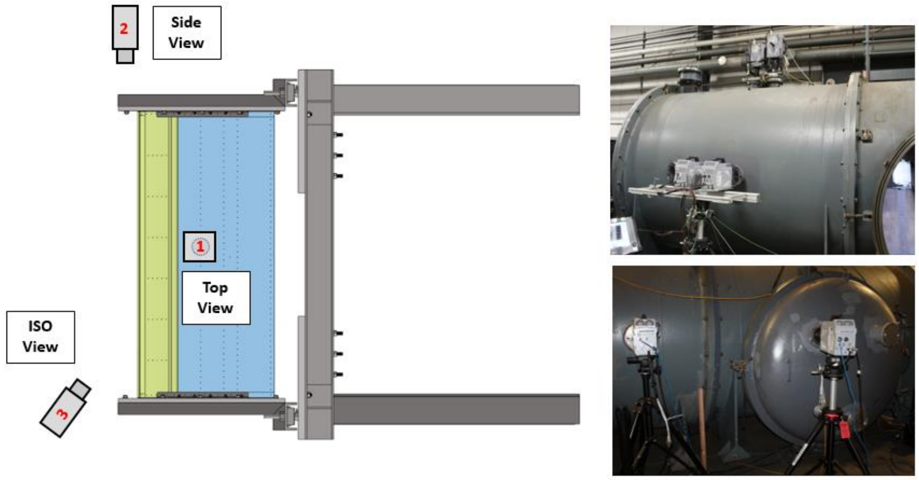


Figure 34. Horizontal stabilizer test instrumentation – High-speed cameras.

II. Load cells

Four compression load cells were installed in the test fixture to collect load time history data during the impact event. The load cells were attached to the rigid fixture and preloaded at 35,585 N (8,000 lbf). All load history data was sampled at 1MHz. Figure 35 shows the location of the four load cells in the test fixture.

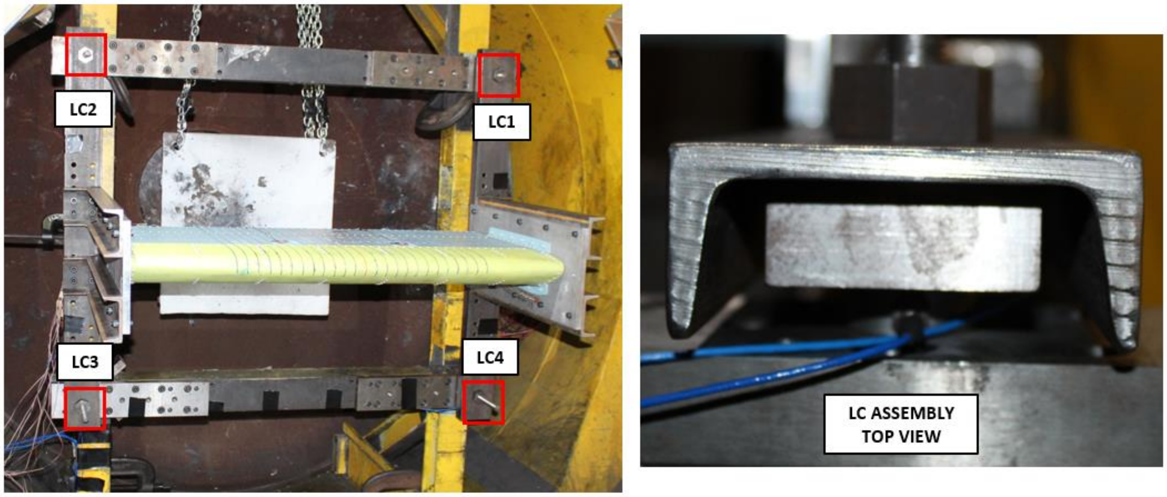


Figure 35. Horizontal stabilizer test instrumentation – Load cells.

III. Strain gages

Four strain gages were positioned on the skin of the horizontal stabilizer: two on the upper skin surfaces and two on the lower skin surface. Strain history data was sampled at 1 MHz. Figure 36 shows the location of the strain gages.

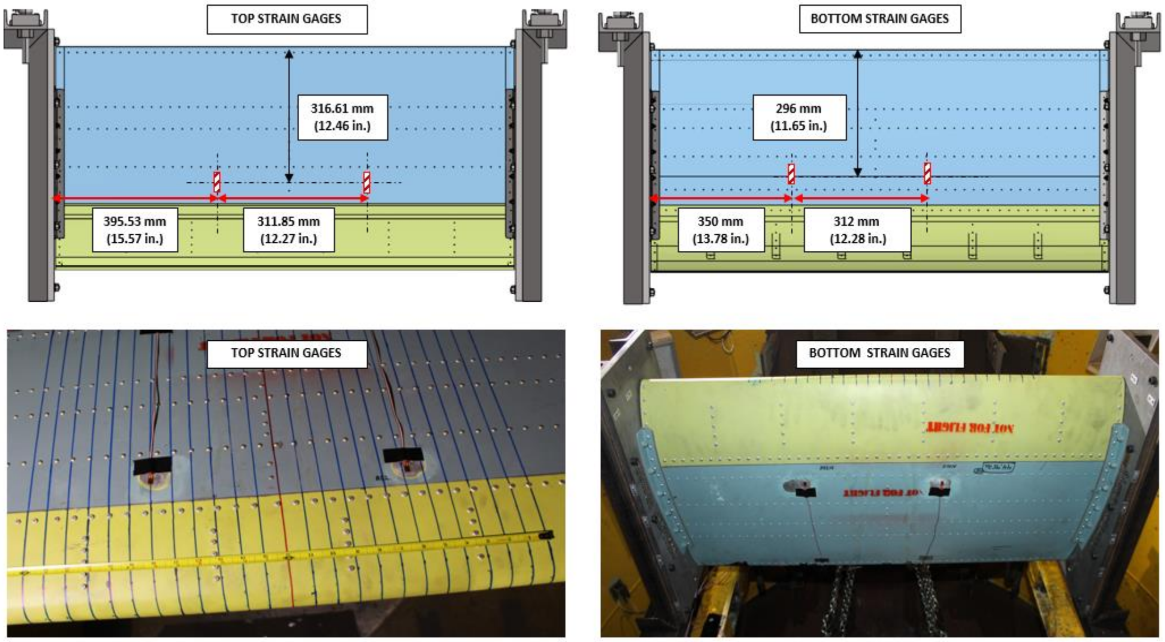


Figure 36. Horizontal stabilizer test instrumentation – Strain gages.

4.2.4 FEM Preparation

The FEM sub-assemblies for this test are the horizontal stabilizer test article and the fixed test frame. Figure 37 shows the test sub-assemblies CAD geometry, mesh, and final FEM (boundary conditions and constraints).

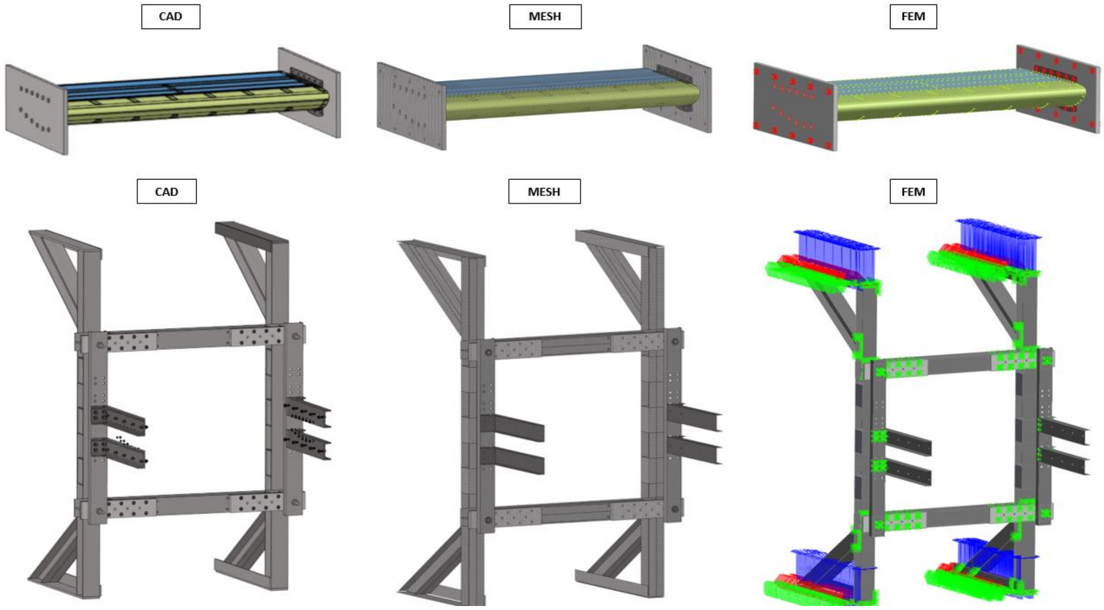


Figure 37. Horizontal stabilizer test FEM: test article (top) and fixed fixture (bottom).

According to the BOM information received, most of the test article was made of aluminum. The bolts connecting the fixture's sub-assemblies were discretized with beam elements connected to the structure through NRBs. A preload of 108.5 N-m (80 ft-lbf) was applied to the beam element to replicate the local stresses at the connection region. Figure 38 shows the beam and NRB connection method used in the FEM.

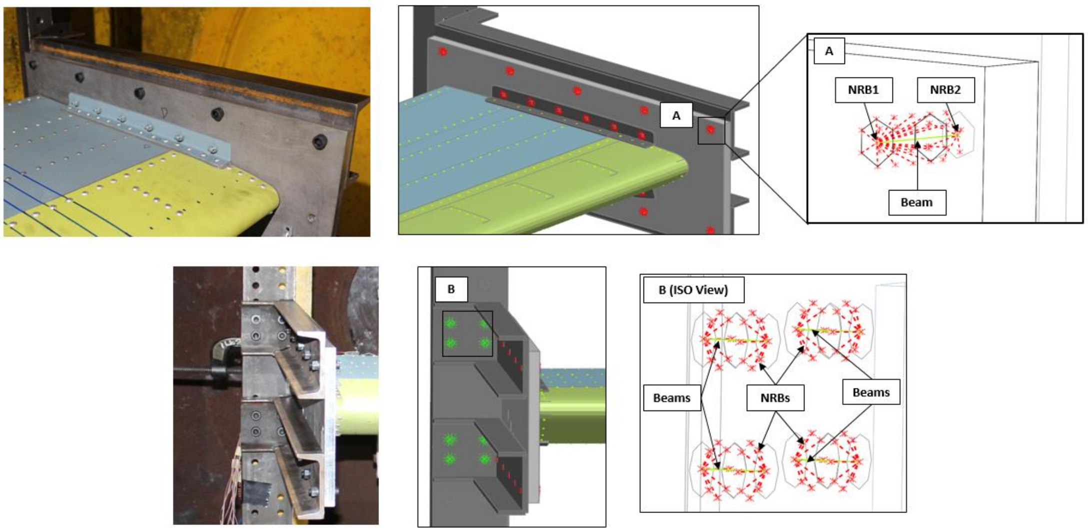


Figure 38. Horizontal stabilizer test FEM – Fixture connections.

Figure 39 illustrates the coordinate system orientation defined for the strain gage elements. These coordinate systems were oriented to match the physical strain gages.

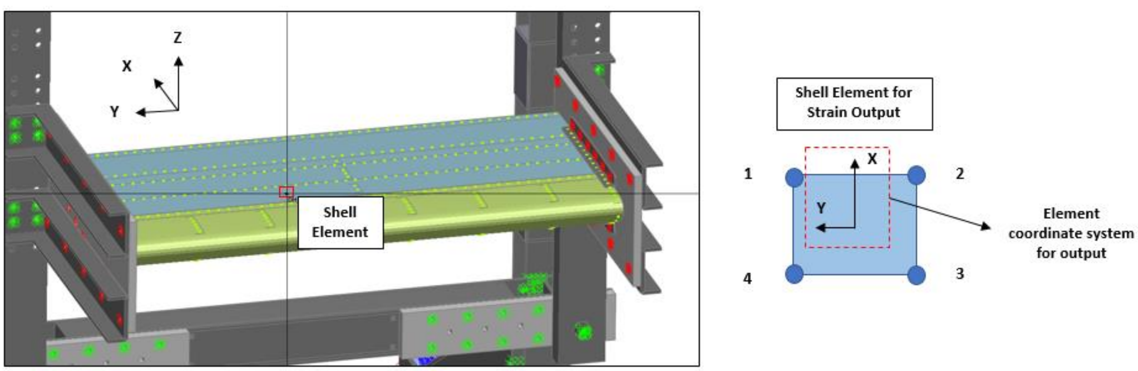


Figure 39. Horizontal stabilizer test FEM – Strain gage.

To capture the interaction between all the components in the model, a **CONTACT_AUTOMATIC_SINGLE_SURFACE* was defined. In addition, the upper and lower flanges of the fixed fixture were constrained in all three axes using a Single Point Constraint (SPC) definition. Figure 40 shows the test setup and the FEM setup.

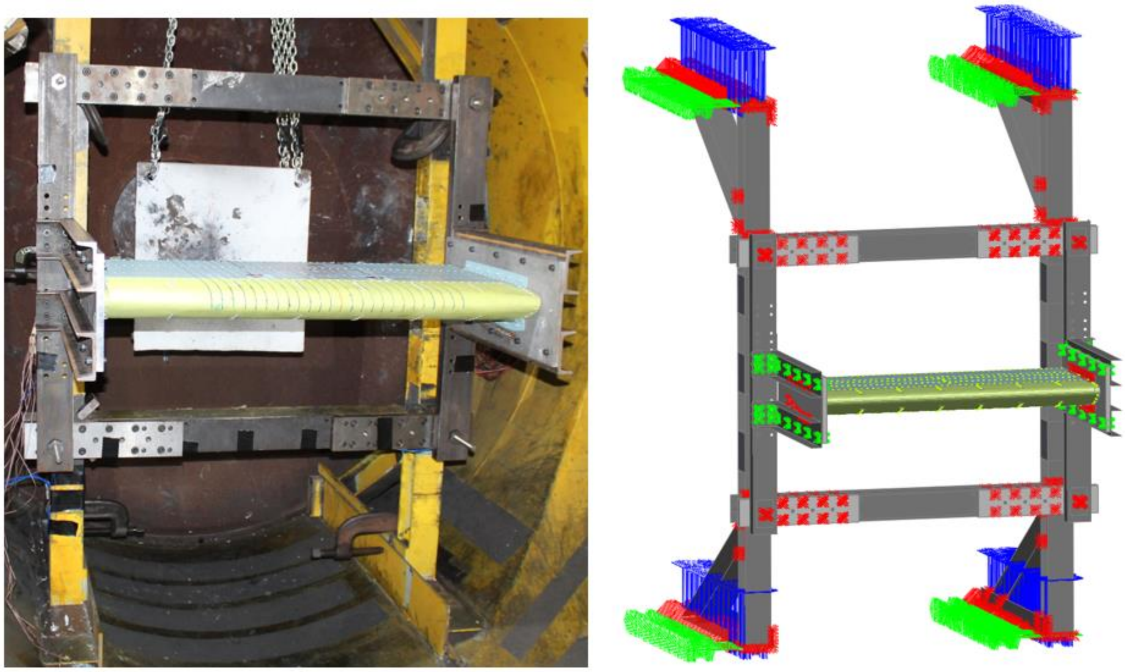

Figure 40. Horizontal stabilizer test setup (left) and FEM setup (right).

4.2.5 FEM Validation

The quadcopter legs and camera gimbal were removed to improve the stability of the UAS launch during the physical test because of their small mass and stiffness. This resulted in a total UAS mass of 0.93 kg (2.06 lb.) The FEM was updated to replicate the test article. Figure 41 compares the test article with the UAS FEM.

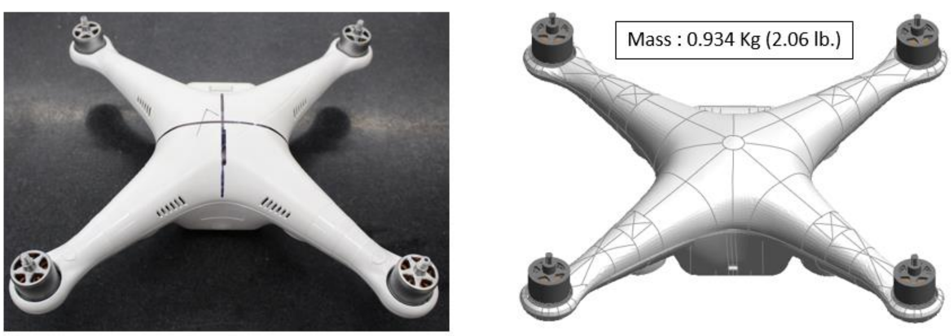


Figure 41. Horizontal stabilizer test – UAS projectile (left) and modified UAS FEM (right).

The modified UAS FEM was oriented and positioned based on the test documentation. Figure 42 compares impact location and UAS orientation between the test article and the numerical model just before impact.

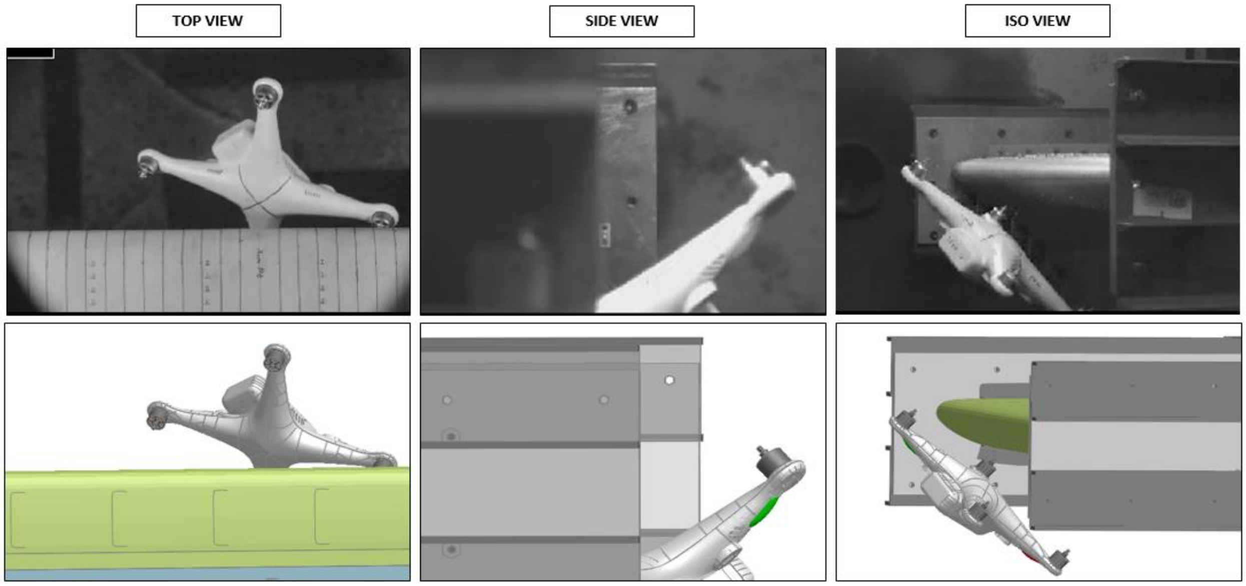


Figure 42. Horizontal stabilizer test – UAS orientation comparison.

The test recorded a UAS velocity before the impact of 180 knots. The same initial velocity was applied to the FEM along the impact direction. Figure 43 illustrates the simulation model configuration and indicates the location of the UAS in space according to the test data. A **CONTACT_ERODING_SINGLE_SURFACE* contact was defined between the UAS and the horizontal stabilizer. In addition, a gravity load was prescribed to act on the FEM during the simulation.

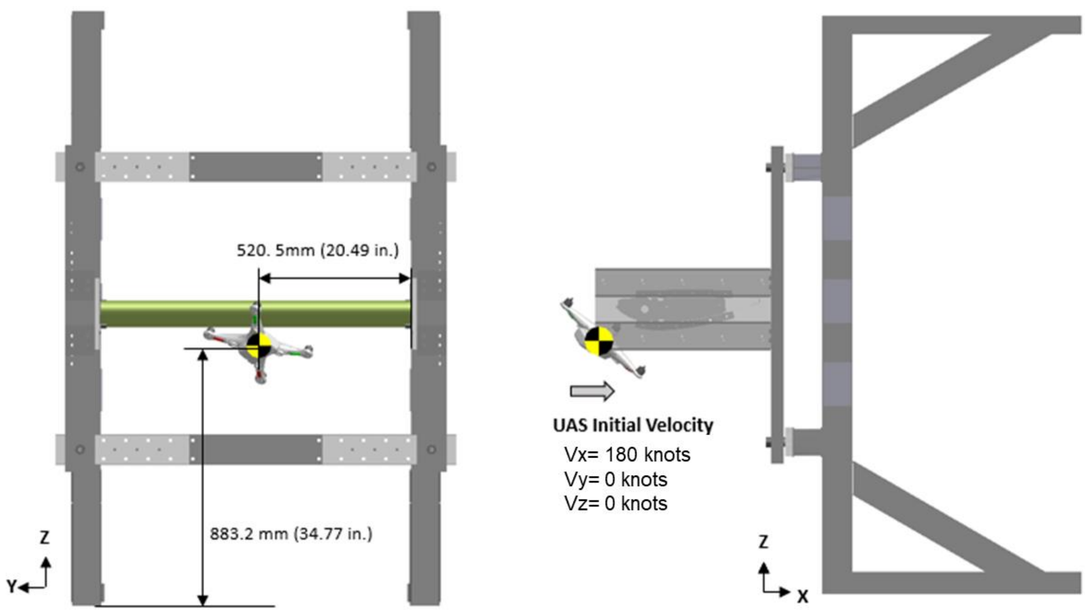


Figure 43. Horizontal stabilizer test FEM setup.

Figure 44 and Figure 45 compare the top and isometric views, respectively. The figures present the initial simulation frame, the first contact between the UAS and the target, and the instant when the motor fractures the leading edge skin. Again, the simulation kinematics show a good correlation with the test.

The results in Figure 46 show a good correlation between the physical test and the numerical analysis. The numerical model properly captures the cracking of the leading edge skin and penetration of the UAS motor through the skin opening observed in the test. The length of the skin damage is very similar: 76.2 mm on the physical article and 72 mm on the numerical model.

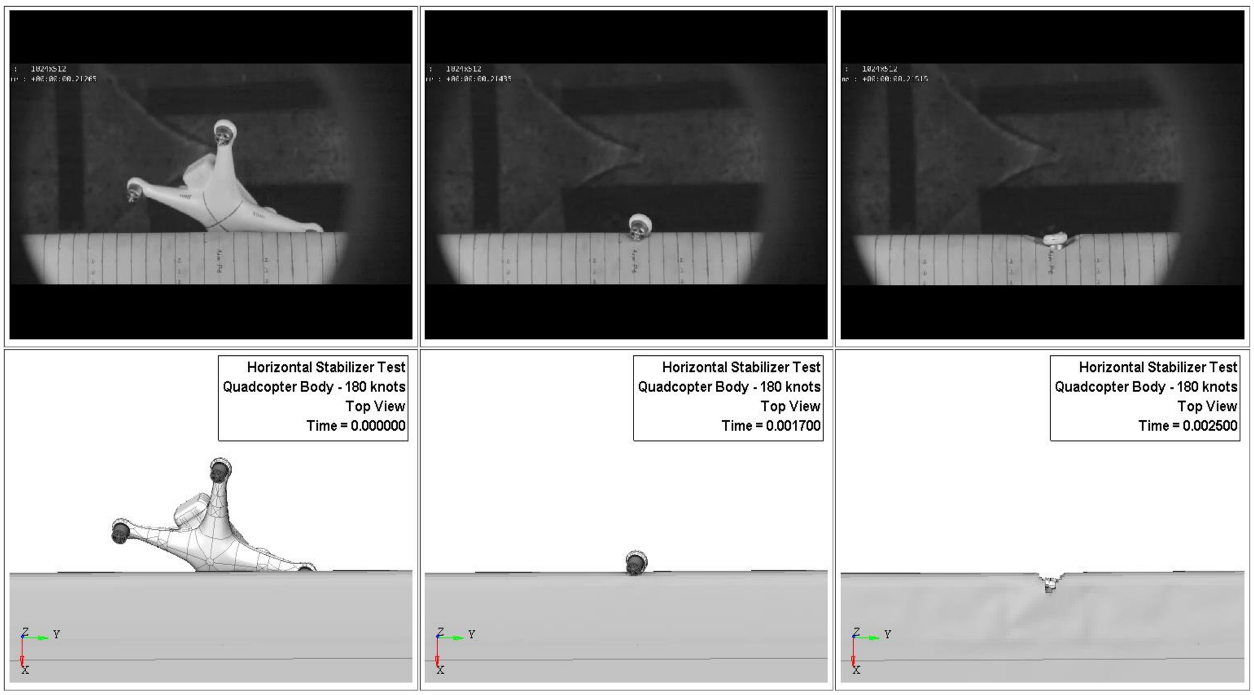


Figure 44. Top view comparison of the horizontal stabilizer impact at t=0 s (left), t=0.0017 s (center), and t=0.0025 s (right).

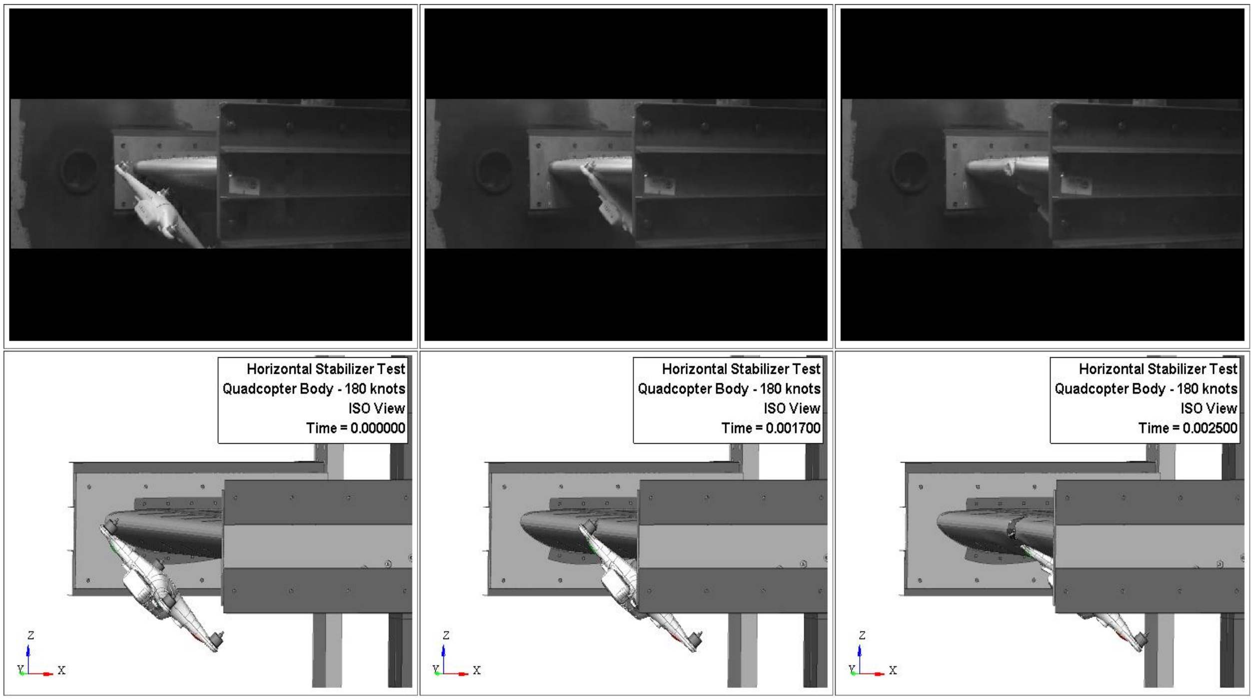


Figure 45. Isometric view comparison of the horizontal stabilizer impact at t= 0 s (left), t=0.0017 s (center), and t=0.0025 s (right).

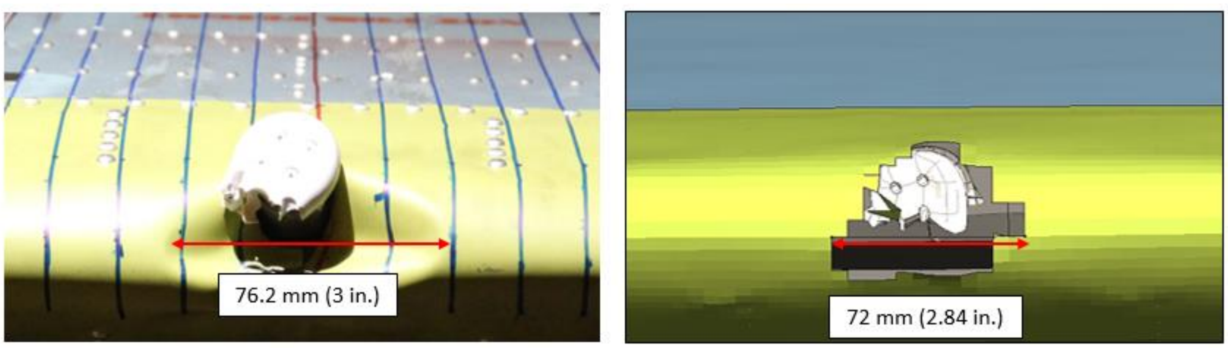


Figure 46. Horizontal stabilizer damage compares the test (left) and FEM (right).

Figure 47 compares the test load history data with the simulation output. The end of contact asymptote indicates the last instant of contact of the UAS with the horizontal stabilizer. The test load history channels show a good correlation with the simulation results. The bottom right test load cell was not considered for the comparison due to bad readings, and it is shown as non-available (N/A) in Figure 47. Consequently, Figure 47 indicates the bottom right test load cell data as non-available (N/A). Figure 48 compares the test strain history data with the simulation output showing an appropriate level of correlation for most of the strain data time history. The values on the vertical axis are not shown for confidential reasons.

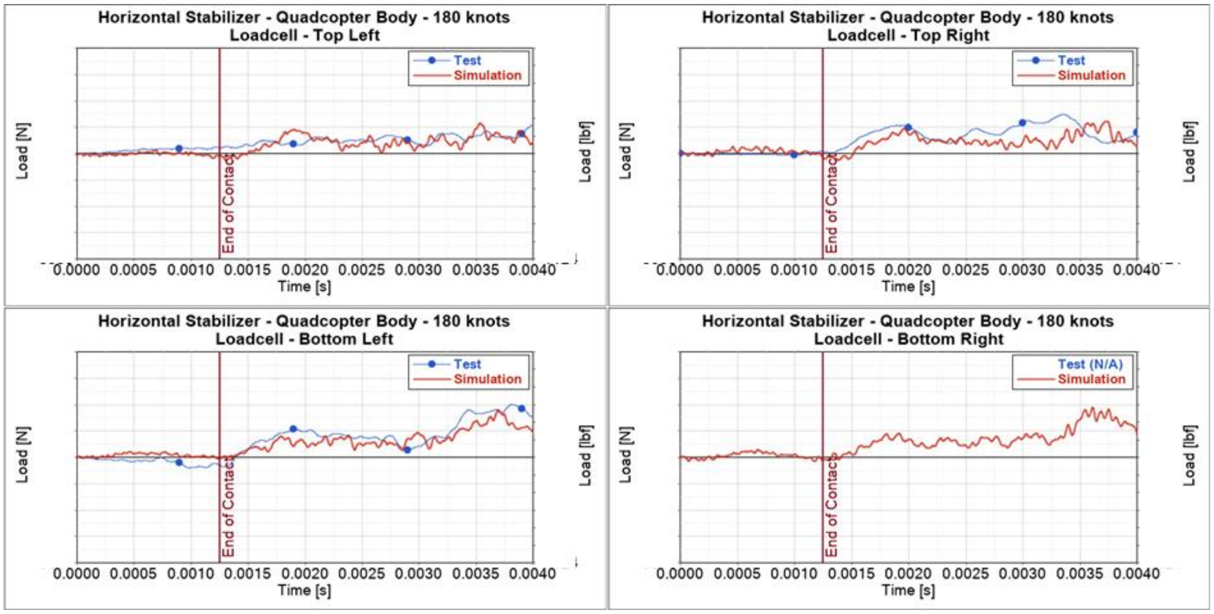


Figure 47. Horizontal stabilizer test – Load cell data validation.

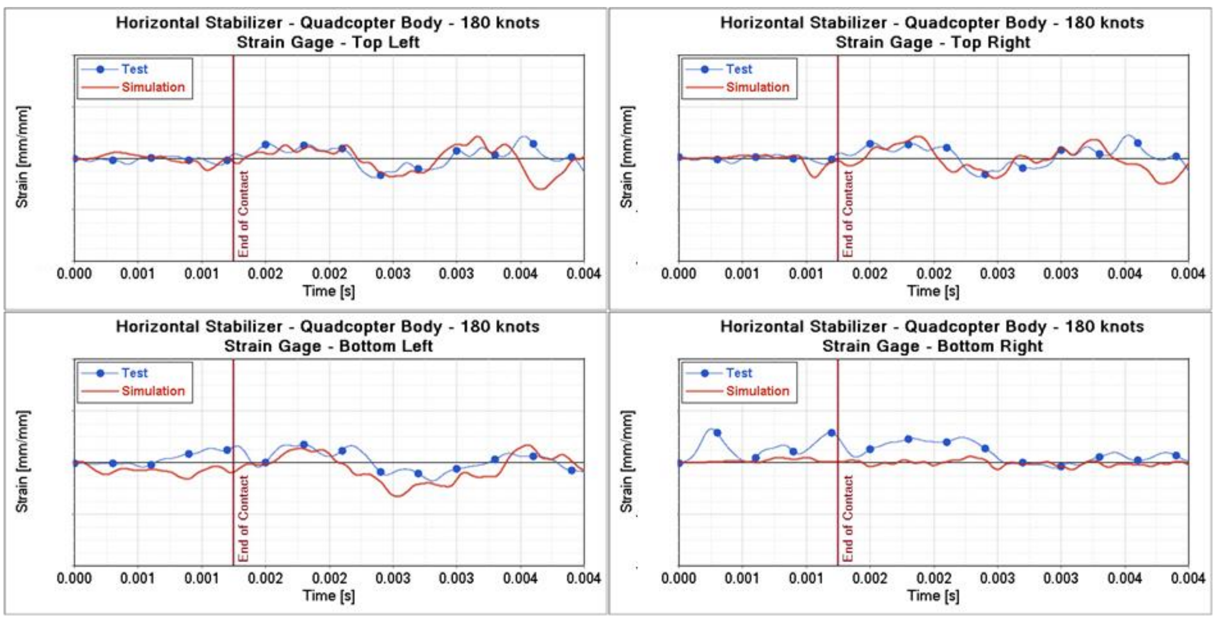


Figure 48. Horizontal stabilizer test – Strain gage data validation.

## 4.3 WINDSHIELD TEST

This chapter presents the validation of the windshield FEM by replicating the physical tests (see Table 11) conducted as part of this research (APPENDIX B). The Industry Partner provided the physical test article and the design data necessary to create the FEM model (geometry, BOMs, and previous bird strike test data for validation). The following sub-chapters summarize the preparation of the test, the FEM setup, and the comparison with the test results. Due to the confidential nature of the collaboration with the Industry Partner, the content discussed only provides a general overview of the windshield properties.

### 4.3.1 Test Article

The Industry Partner supplied a set of bilayer windshields for Part 29 [15] rotorcraft. The bilayer windshield consists of an outer glass layer and an inner polyurethane layer. Both layers are surrounded by a composite frame that attaches to the helicopter cockpit frame. Figure 49 shows one of the windshield physical articles obtained for testing.

Figure 49. Windshield test article.

### 4.3.2 Test Fixture

To properly support the windshield, a test fixture was created and attached to the fixed test frame presented in Chapter 4.1.1. The test fixture was built using a set of light aluminum Minitech struts. These struts allow the assembly of irregular geometries and capture the complex curvature of the windshield under consideration. Figure 50 shows the windshield test fixture geometry.

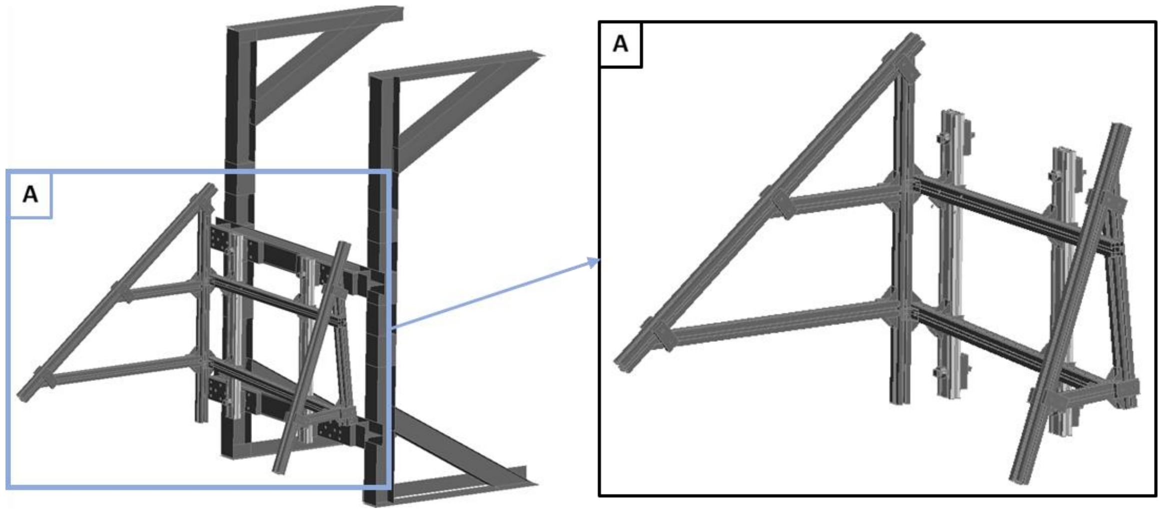


Figure 50. Windshield test fixture.

4.3.3 Test Instrumentation

The windshield test included the following instrumentation:

I. High-speed cameras
Three high-speed video cameras were set up to record the impact event from different angles. The camera's recording frequency was 40,000 frames per second. Camera 1 was positioned above the windshield (top view). Camera 2 was located on the side of the fixture, perpendicular to the shot line (side view). Finally, camera 3 was positioned at an oblique angle with respect to the front of the windshield (isometric view). Figure 51 shows the sketch of the high-speed camera's location with respect to the windshield.

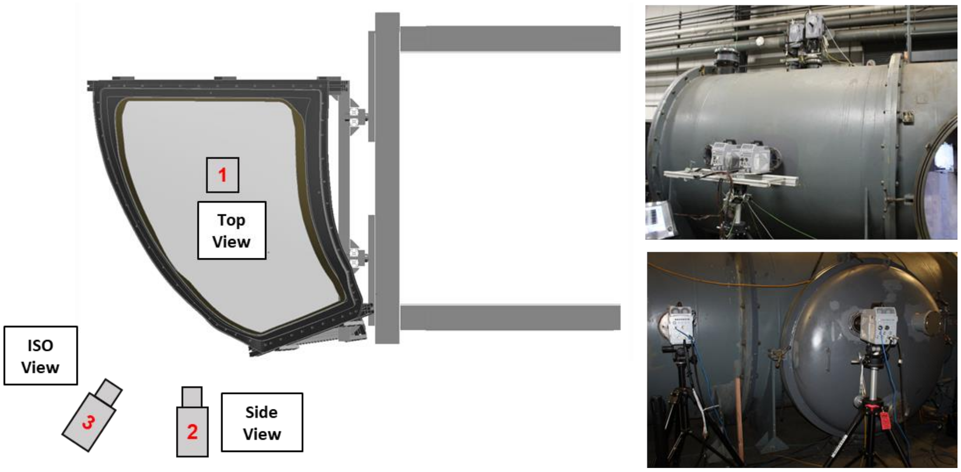


Figure 51. Windshield test instrumentation – High-speed cameras.

II. Load cells

Four compression load cells were installed in the test fixture to collect load time history data during the impact event. The load cells were attached to the rigid fixture and preloaded at 35,585 N (8,000 lbf). All load history data was sampled at 1MHz. Figure 52 shows the location of the four load cells in the test fixture.

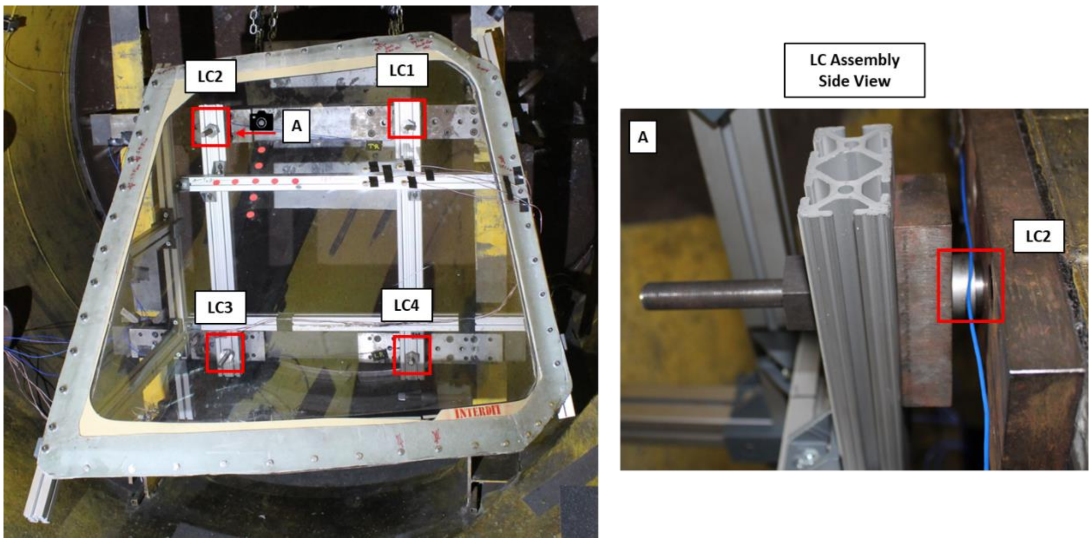


Figure 52. Windshield test instrumentation – Load cells.

III. Strain gages

Four strain gages were positioned on the outer surface of the windshield. Strain history data was sampled at 1 MHz. Figure 53 shows the location of the strain gages on the windshield.

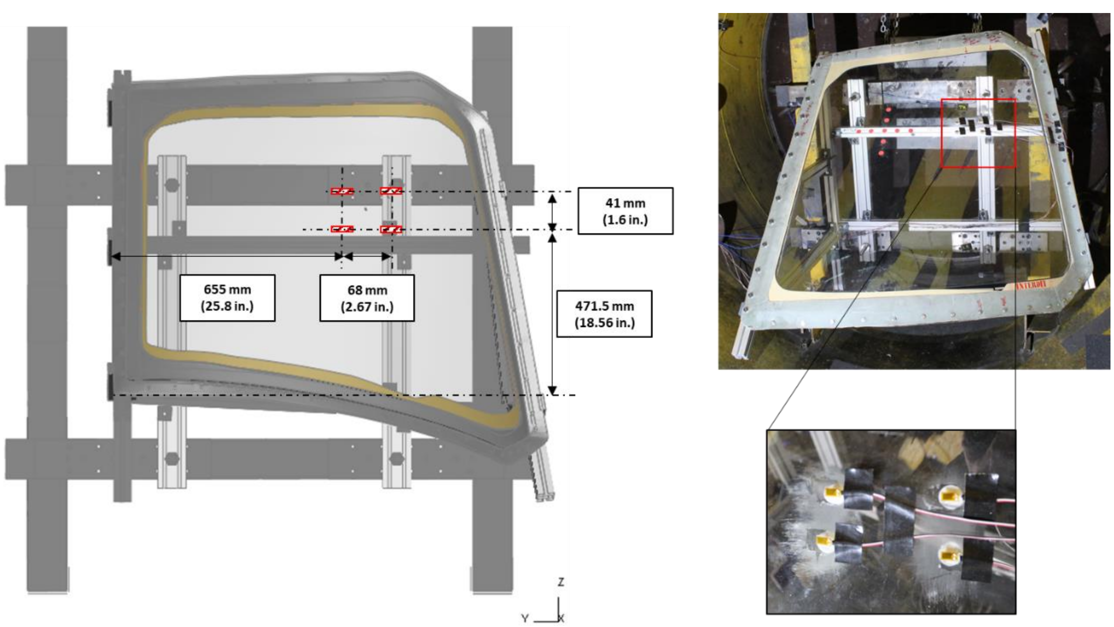


Figure 53. Windshield test instrumentation – Strain gages.

4.3.4 FEM Preparation

The FEM sub-assemblies for this test are the windshield test article (proprietary data provided by Industry Partner), the windshield test fixture (see Chapter 4.3.2), and the fixed test frame (see Chapter 4.1). The fixed test frame is made of structural steel, while most of the windshield test fixtures are built using aluminum Minitech struts. All fasteners surrounding the windshield and connecting the Minitech structure were modeled with beam elements connected to the structure through NRBs. A preload of 108.5 N-m (80 ft-lbf) was applied to the beam elements to replicate the local stresses at the connection region. Furthermore, fixed boundary conditions of the test frame were modeled by means of SPC applied at the upper and lower ends of the FEM in all directions. Figure 54 illustrates the windshield test FEM, highlighting the fastener connections and fixed boundary conditions.

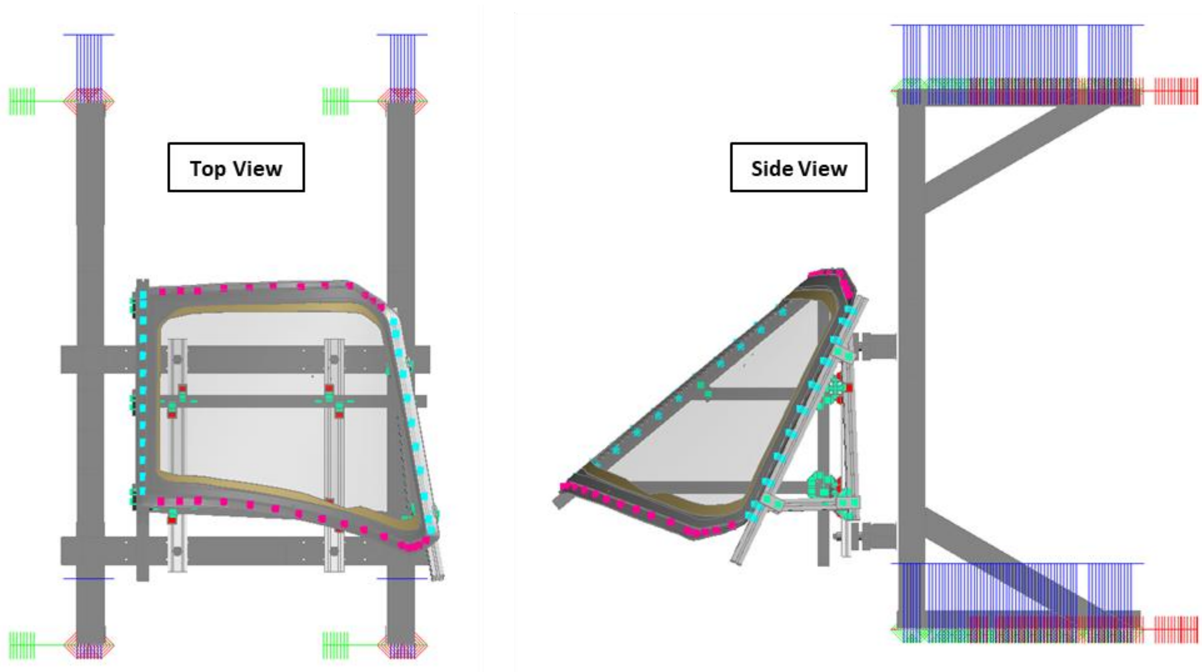


Figure 54. Windshield FEM setup.

To capture the interaction between all the components in the model, a **CONTACT_AUTOMATIC_SINGLE_SURFACE* card was defined. Figure 40 shows the test setup and the FEM setup side by side.

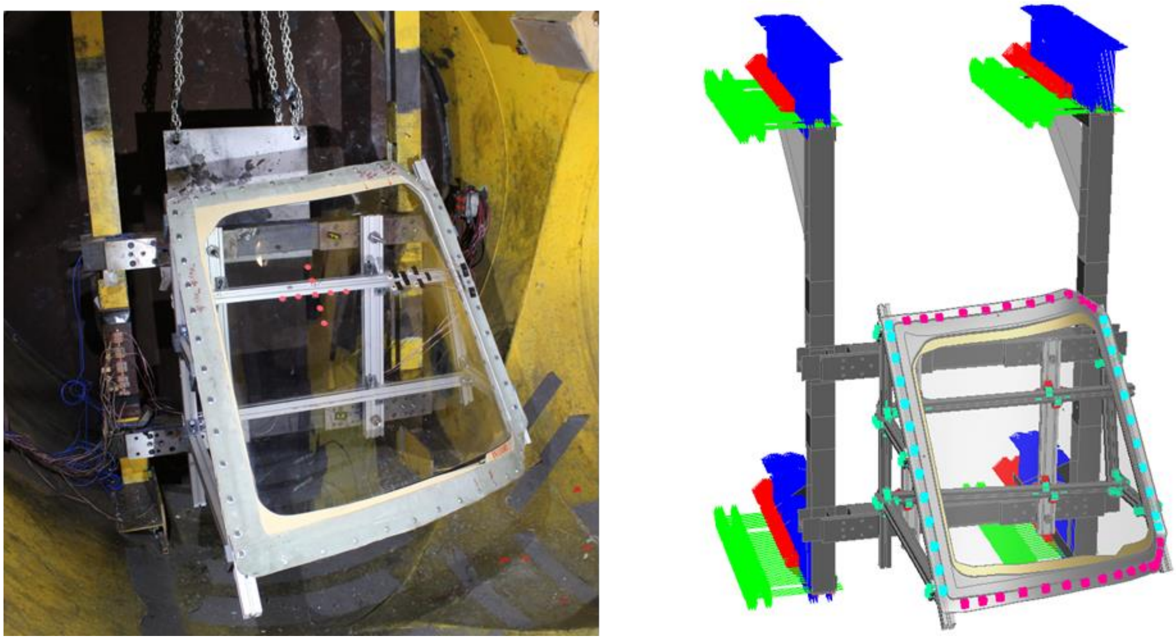

Figure 55. Windshield test setup (left) and FEM setup (right).

### 4.3.5 FEM Validation

Three tests were conducted to validate the behavior of the windshield at different impact velocities (50, 175, and 300 knots). These velocities were determined by estimating the relative velocity of an airborne rotorcraft collision with a UAS. The highest velocity was chosen according to the maximum speed found in the literature for Part 27 [12] and Part 29 [13] rotorcraft in the current market. Due to the limitations of the test-launching system and to improve the stability and accuracy of the tests, the quadcopter legs and camera gimbal were removed. This resulted in a total UAS body mass of 0.97 kg (2.06 lb.). As on the previous test, FEM was updated to replicate the test article accurately.

Due to limitations on the recorded test data, the windshield and UAS FEM validation was done qualitatively by comparing the test and analysis kinematics and the overall damage on the test article. Strain gages debonded for the 175 and 300 knots cases and did not provide a meaningful reading for the lower 50 knots case. In addition, the load cell data was significantly noisy and did not provide relevant data for validation purposes. Finally, the test fixture holding the windshield was made out of different struts that might have contributed to this issue by not representing a stiff enough structure to properly transfer the loads to the load cells.

- <u>50 Knots Impact</u>

Figure 56 shows the test article used for the 50 knots impact test. The UAS body FEM was oriented and positioned following the impact location documented during the test. Figure 57 illustrates the orientation and location of the UAS before impact.


Figure 56. Windshield test article – 50 knots test.

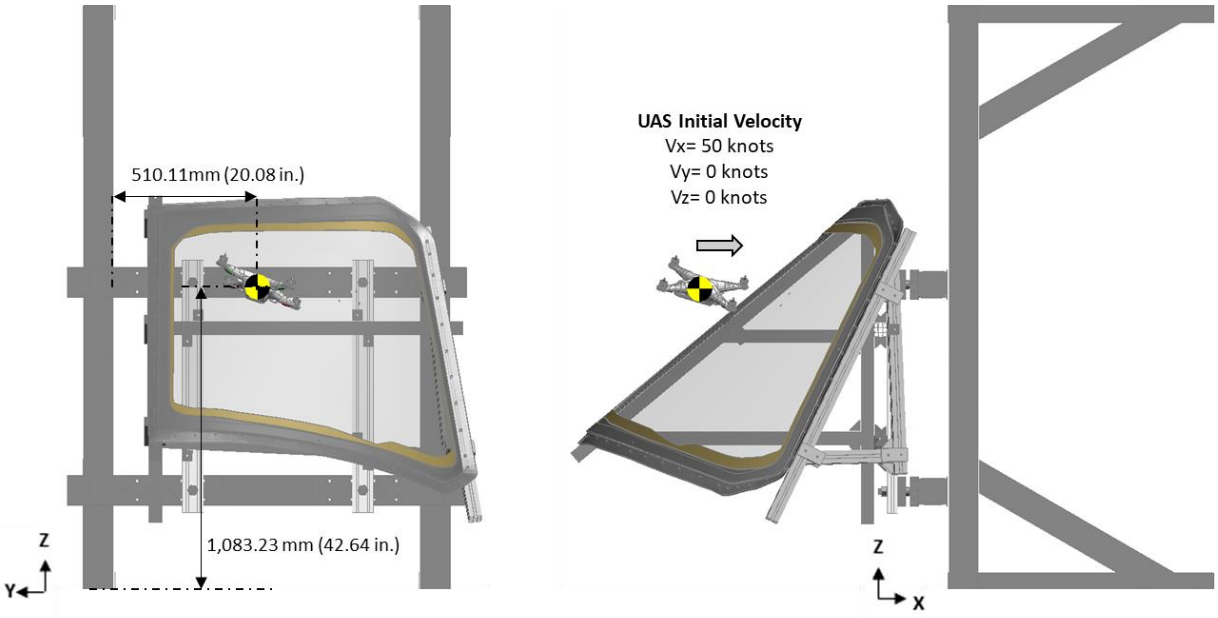


Figure 57. Windshield test FEM setup – 50 knots test.

In addition, Figure 58 compares the initial frame of the test video and the simulation with the available camera views and confirms the orientation of the UAS with respect to the windshield.

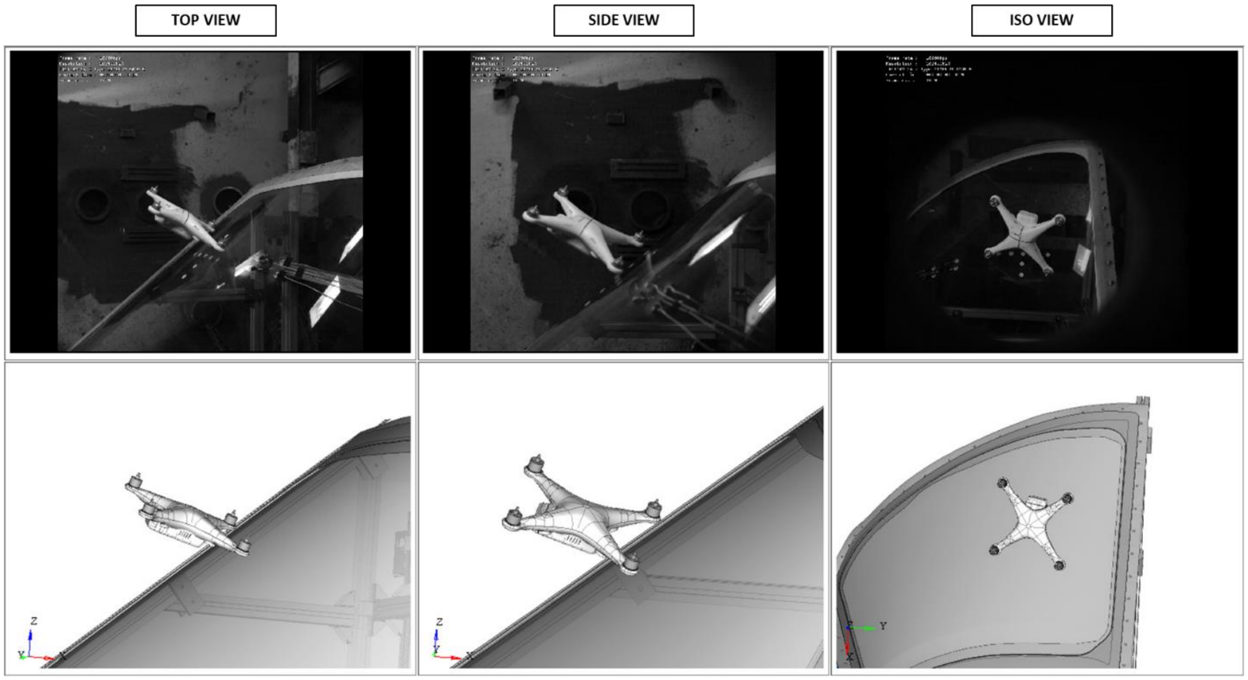


Figure 58. Windshield impact test at 50 knots – UAS orientation.

Figure 59 and Figure 60 compare the test and analysis results for both the isometric and top kinematics. Figure 61 compares the windshield damage observed in the test article and the analysis results. Numerical model results show similar kinematics to those observed during the test, with the UAS sliding on the windshield surface without significant damage. Post-test evaluation of the windshield only identified small surface scratches similar to those observed on the numerical model (minor element erosion on the top layer surface).

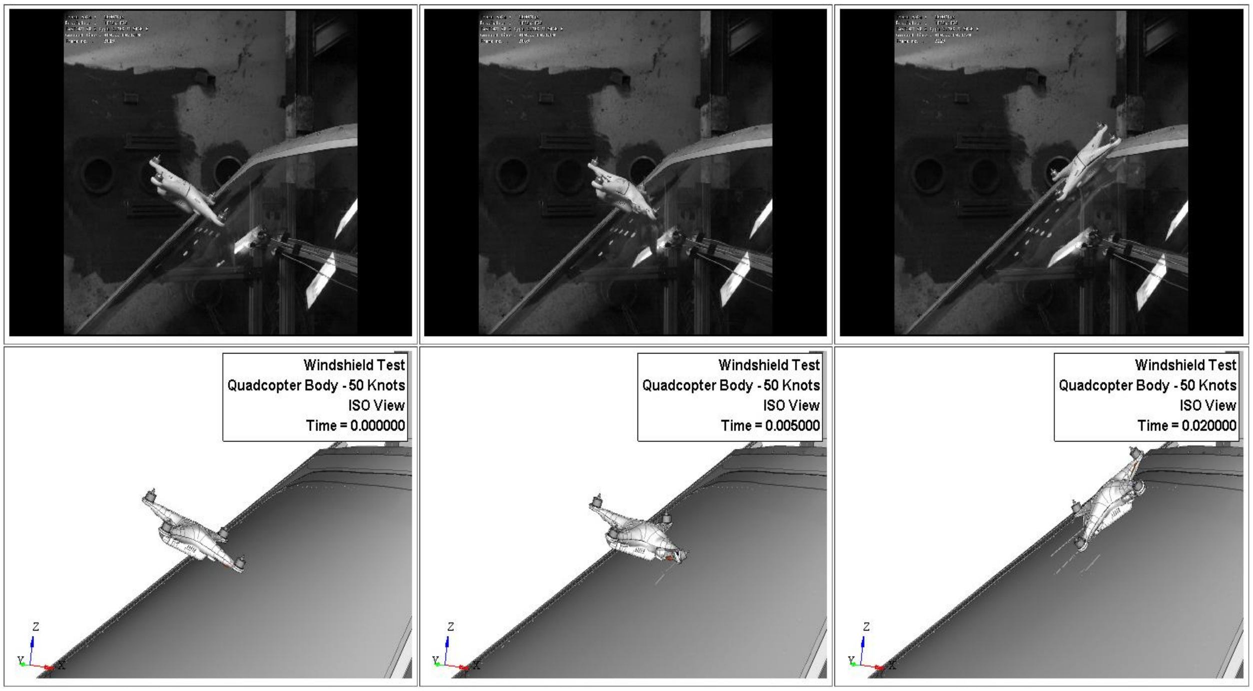


Figure 59. Isometric view comparison of the 50 knots windshield impact at t=0 s (left), t=0.005 s (center), and t=0.02 s (right).

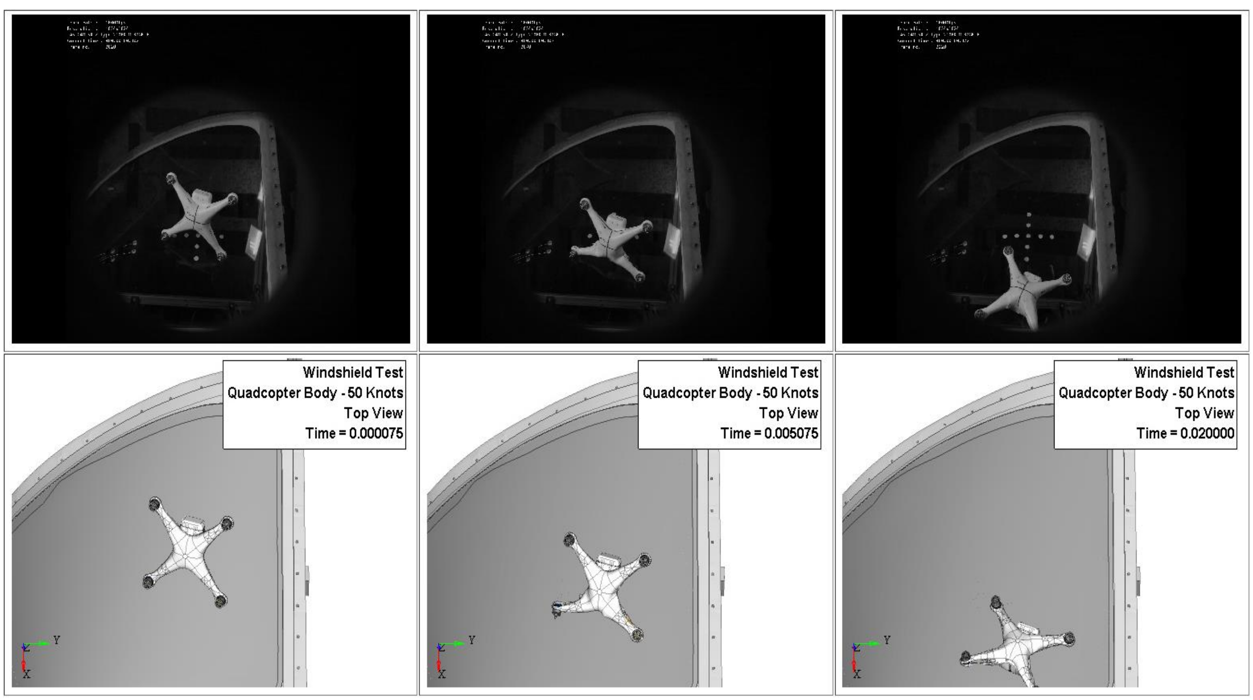


Figure 60. Top view comparison of the 50 knots windshield impact at t=0 s (left), t=0.005 s (center), and t=0.02 s (right).

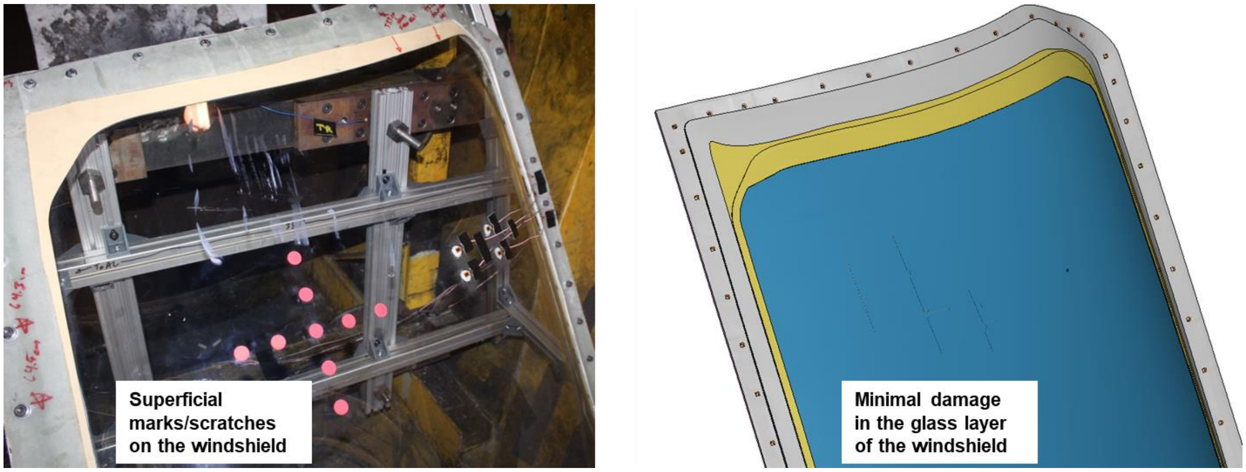


Figure 61. Windshield test at 50 knots – Damage comparison

- 175 Knots Impact

Figure 62 shows the test article used for the 175 knots impact test. The UAS body FEM was oriented and positioned following the impact location documented during the test. Figure 63 illustrates the orientation and location of the UAS before impact.

Figure 62. Windshield test article – 175 knots test.

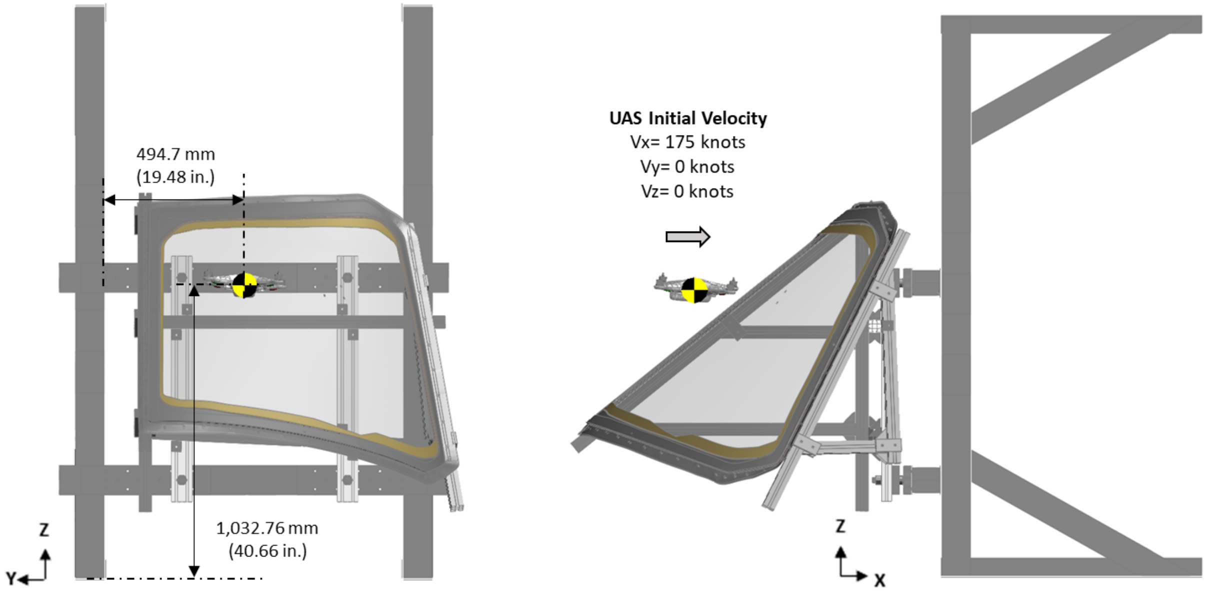


Figure 63. Windshield test FEM setup – 175 knots test.

In addition, Figure 64 compares the initial frame of the test video and the simulation with the available camera views and confirms the orientation of the UAS with respect to the windshield.


Figure 64. Windshield impact test at 175 knots – UAS orientation.

Figure 65 and Figure 66 compare the test and simulation results for both the isometric and top views, respectively. Figure 67 compares the windshield damage observed in the test article and the analysis results. Again, the test and analysis show a good correlation. The numerical model correlates the level of damage observed on the windshield during the test with significant cracking and shattering but without complete failure of the inner layer. The numerical results also show very similar UAS deformation to that observed in the test.

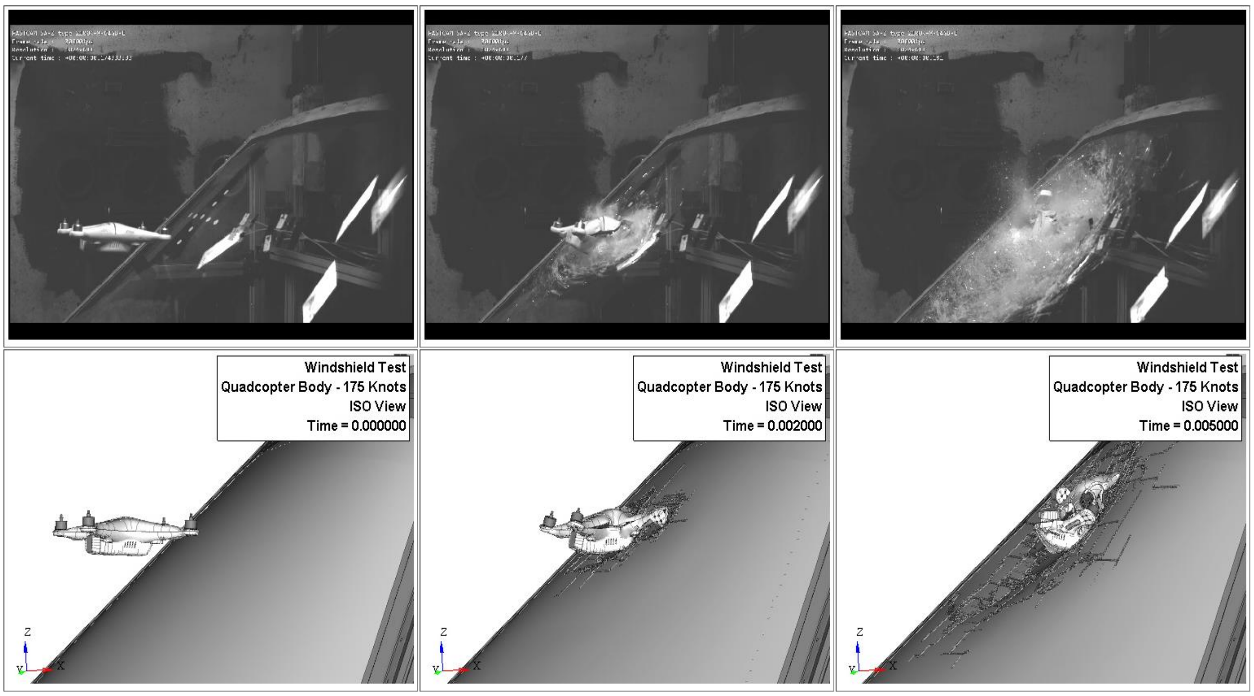


Figure 65. Isometric view comparison of the 175 knots windshield impact at t=0 s (left), t=0.002 s (center), and t=0.005 s (right).

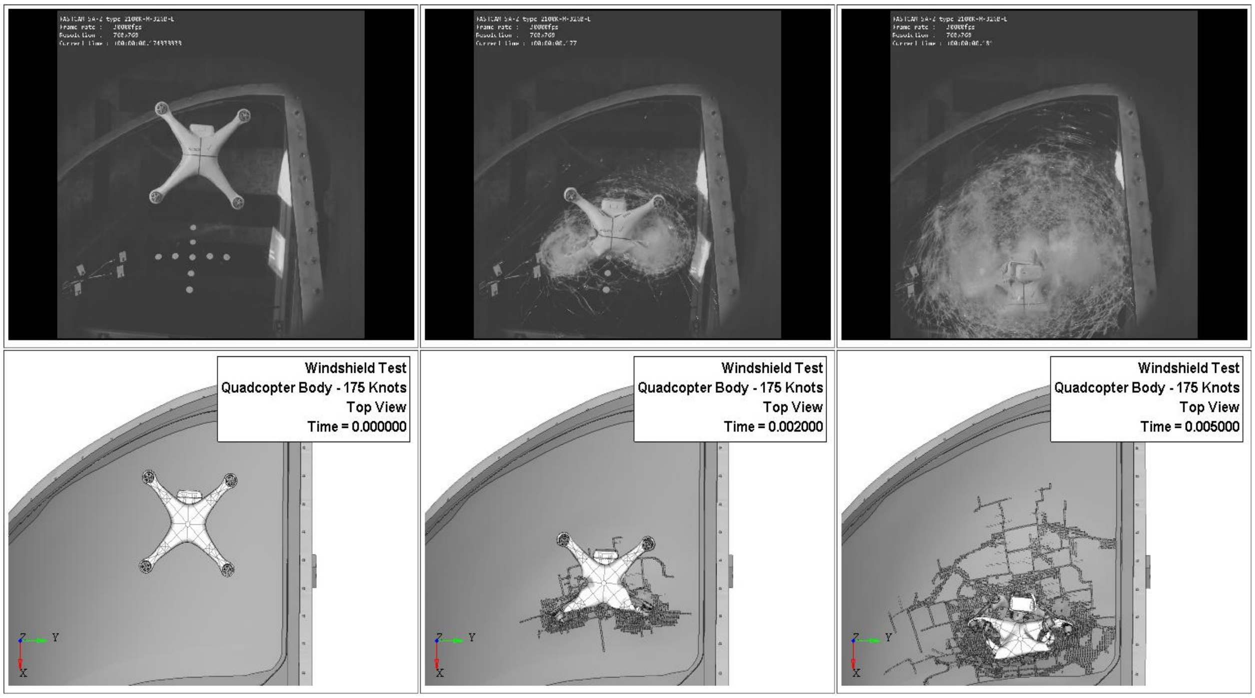


Figure 66. Top view comparison of the 175 knots windshield impact at t=0 s (left), t=0.002 s (center), and t=0.005 s (right).

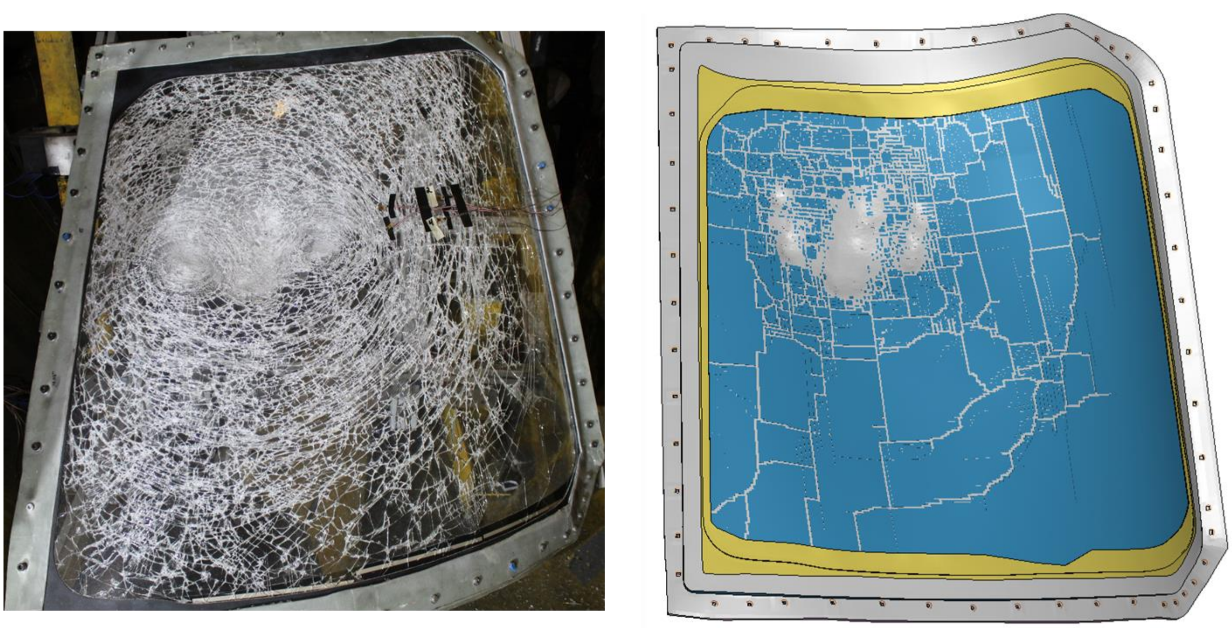

Figure 67. Windshield test at 175 knots – Damage comparison.

- <u>300 Knots Impact</u>

Figure 68 shows the test article used for the 300 knots impact test. The UAS body FEM was oriented and positioned following the impact location documented during the test. Figure 69 illustrates the orientation and location of the UAS before impact.


Figure 68. Windshield test article – 300 knots test.

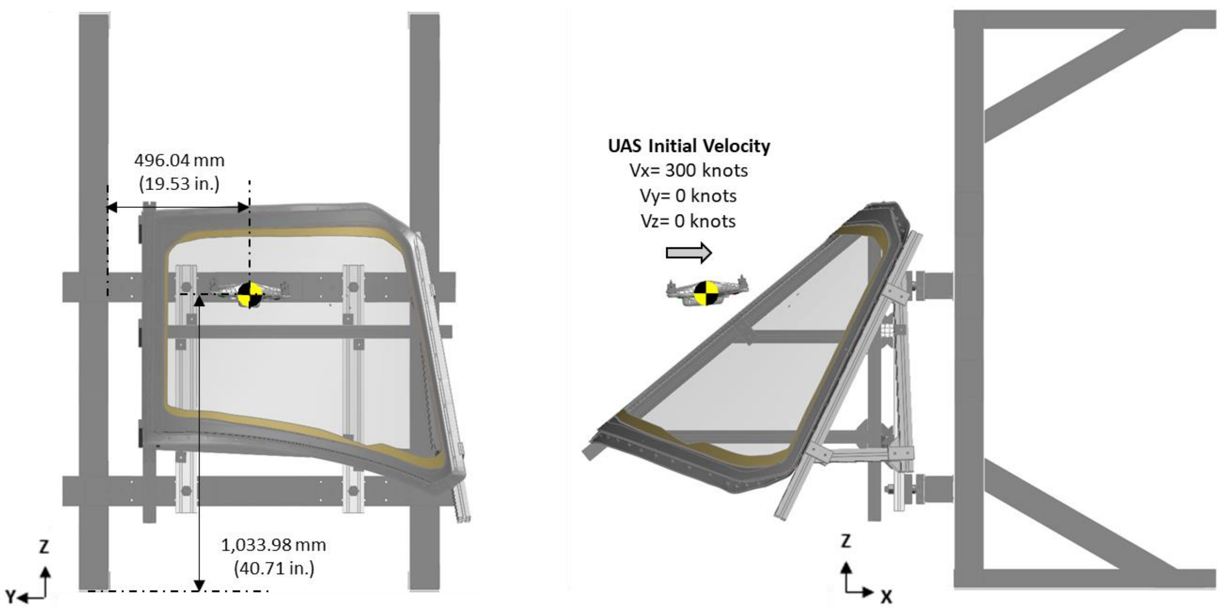


Figure 69. Windshield test FEM setup – 300 knots test.

In addition, Figure 70 compares the initial frame of the test video and the simulation with the available camera views and confirms the orientation of the UAS with respect to the windshield.

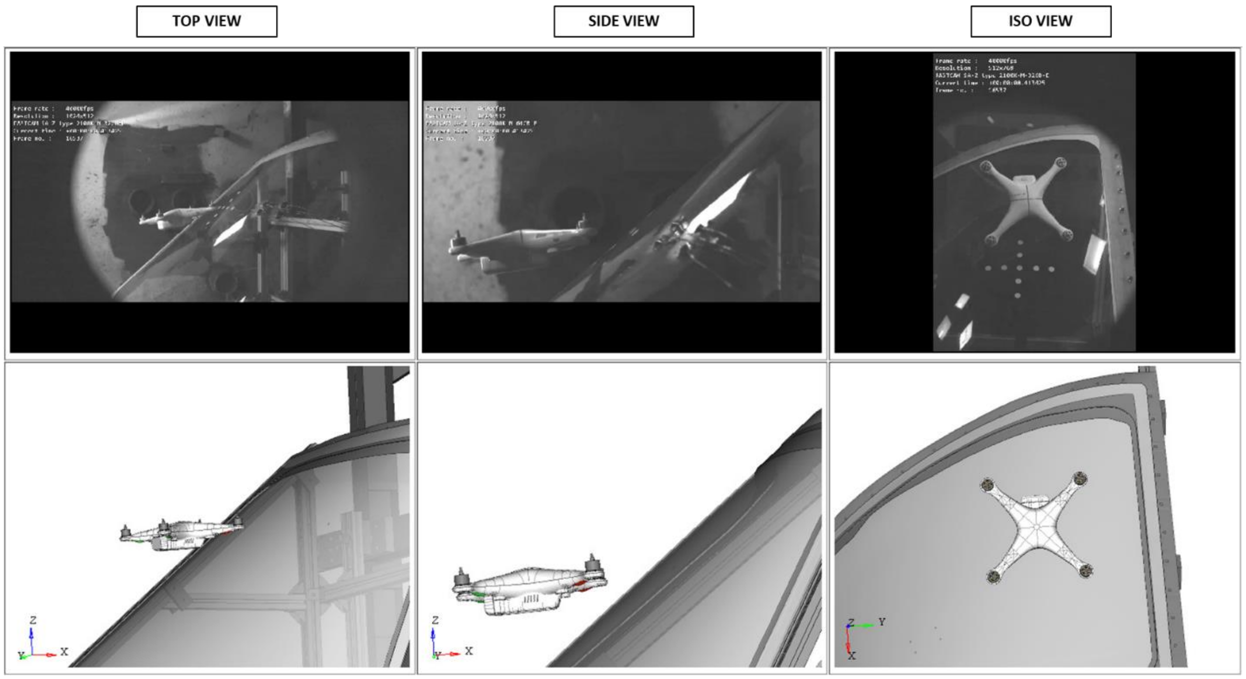


Figure 70. Windshield impact test at 300 knots – UAS orientation.

Figure 71 and Figure 72 present the comparison between the test and simulation results for both the isometric and top views, respectively. Figure 73 compares the windshield damage observed in the test article and the analysis results. The numerical model correlates with the kinematics and test results as with the previous test conditions. The model is capable of capturing the significant shattering and cracking observed on the windshield and the failure of the inner layer. The model can also capture the penetration of the UAS battery into the cockpit as observed during the physical test.

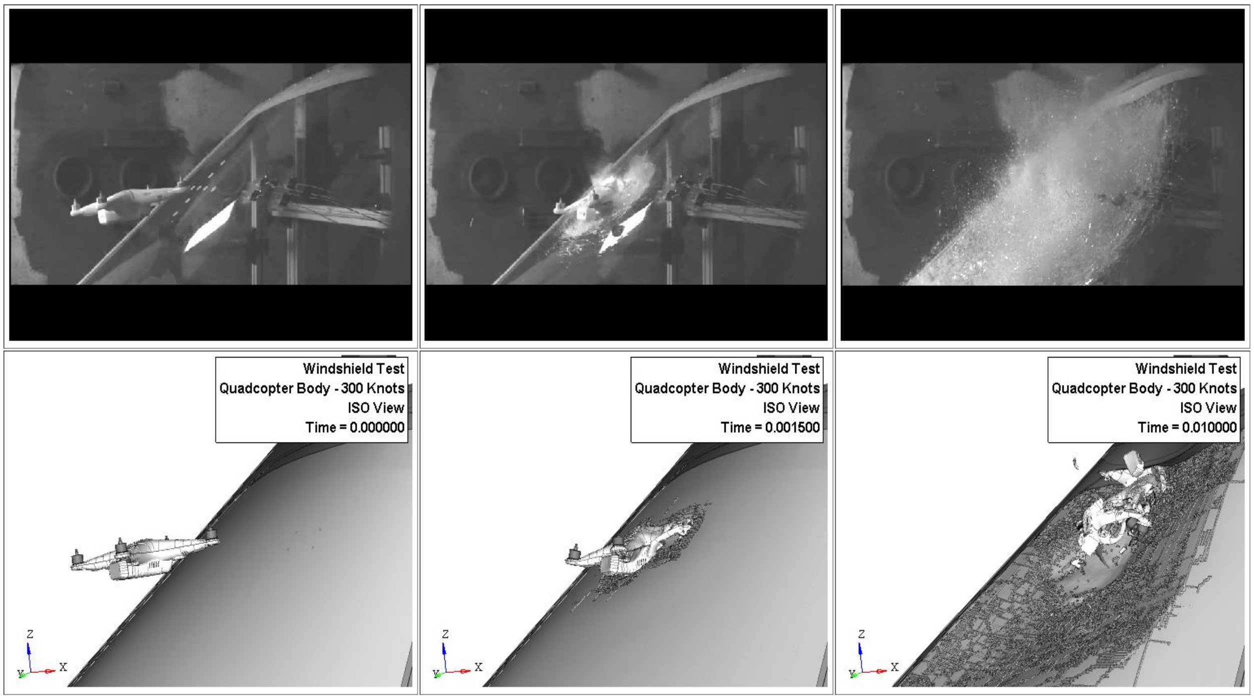


Figure 71. Isometric view comparison of the 300 knots windshield impact at t=0 s (left), t=0.0015 s (center), and t=0.01 s (right).

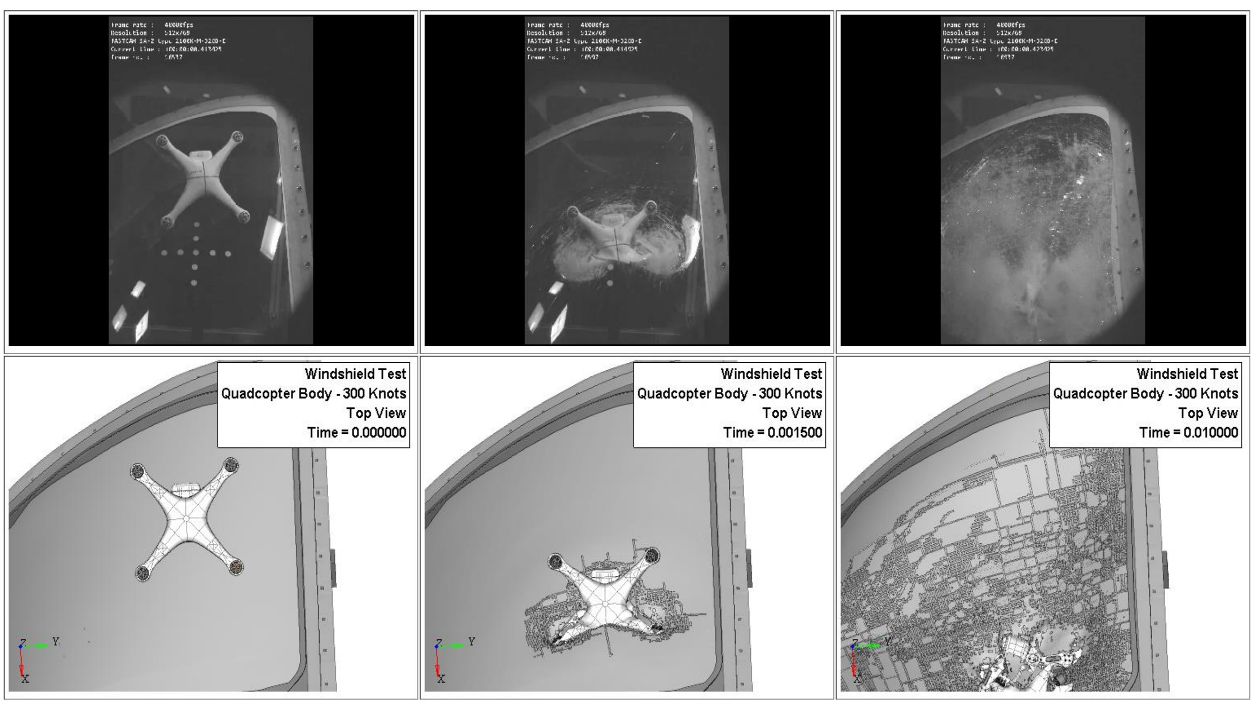


Figure 72. Top view comparison of the 300 knots windshield impact at t=0 s (left), t=0.0015 s (center), and t=0.01 s (right).

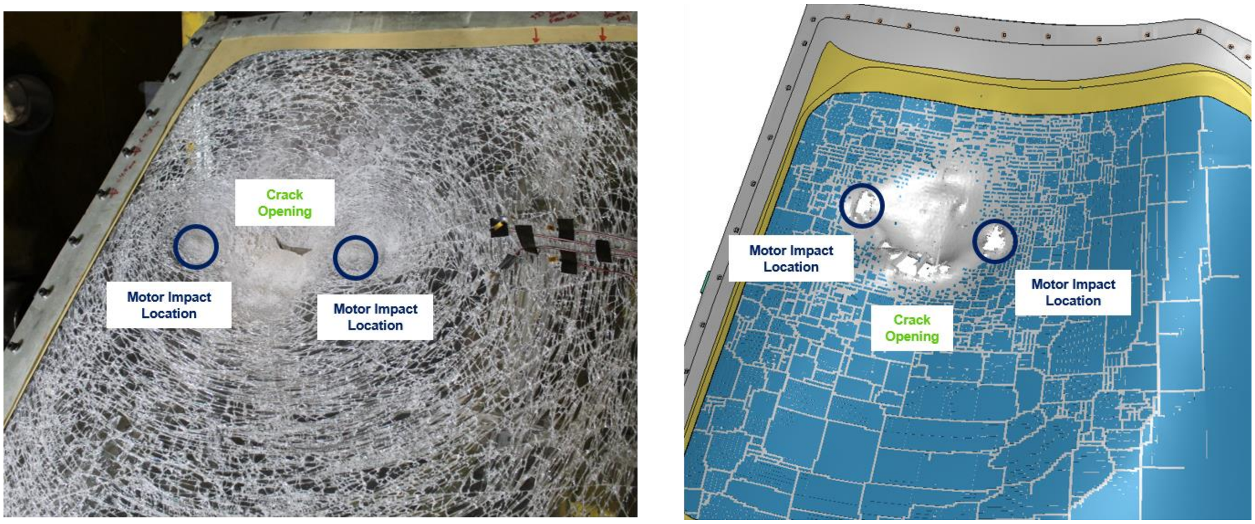


Figure 73. Windshield test at 300 knots – Damage comparison.

## 4.4 BLADE TEST

As introduced in Table 11, two-blade sections were impacted in a vertical configuration to ensure contact between the UAS and the blade. These tests are referred to as tests 21-125 and 21-126. Because the test chamber dimensions were smaller than the size of the full rotor blade, a section of the blade was selected for both tests. Figure 74 shows the blade section distribution and indicates the location test article (Section 4) used for testing.

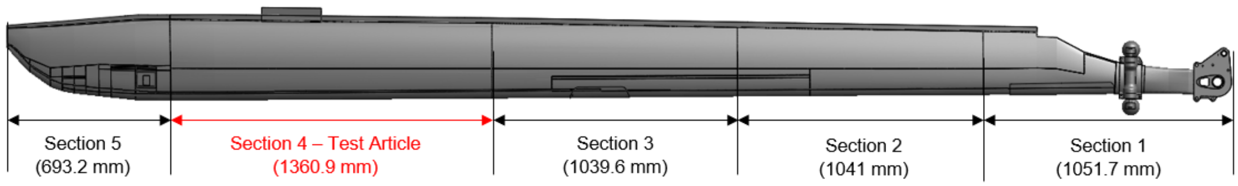


Figure 74. Main rotor blade section distribution – Test section 4.

### 4.4.1 Vertical Configuration Test Setup

The vertical test fixture is divided into two sub-assemblies: the fixed test frame (see section 4.1.1) and the blade test fixture. The blade test fixture consists of eight 3D printed ABS shims, four steel L-brackets, two c-channel beams, eight long steel clamping bolts with their corresponding aluminum bushings, and other connecting steel bolts used to secure the L-brackets.

Figure 75 shows the blade test fixture and full vertical test fixture setup. The blade test fixture connects with a fixed test frame at the preloaded load cells region. Chapter 4.4.2 discusses the details of the load cell locations.

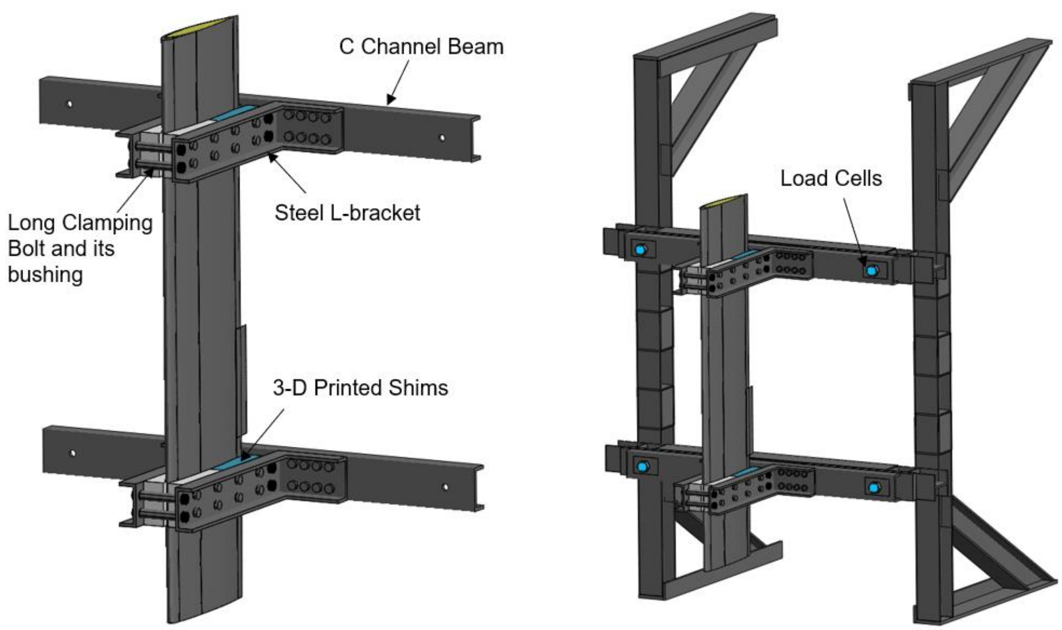


Figure 75. Blade test fixture (left) and full vertical test fixture (right)

4.4.2  Test Instrumentation

The blade section test included the following instrumentation:

I. High-speed cameras
Four high-speed video cameras were set up to record the impact event from different angles. The camera's recording frequency was 40,000 frames per second. Camera 1 was positioned above the upper surface of the horizontal stabilizer (top view). Cameras 2 and 3 were located on the side of the fixture, perpendicular to the shot line (side view). Finally, camera 4 was positioned at an oblique angle with respect to the front of the horizontal stabilizer (ISO view). Figure 76 shows the sketch of the high-speed camera's location with respect to the blade section.

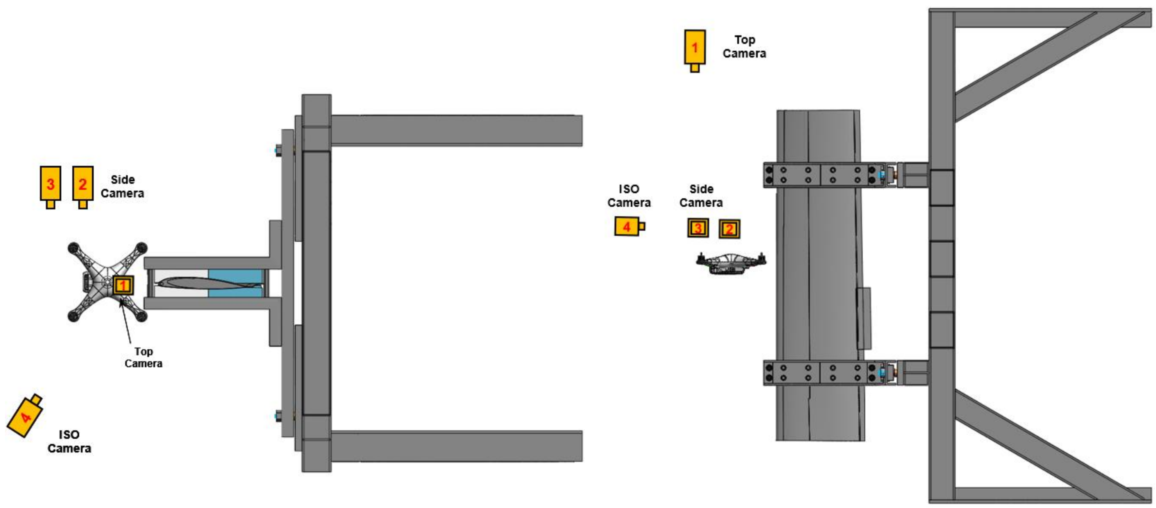


Figure 76. Blade test instrumentation – High-speed cameras.

II. Load cells
Four compression load cells were installed in the test fixture to collect load time history data during the impact event. The load cells were attached to the rigid fixture and preloaded at 35,585 N (8,000 lbf). All load history data was sampled at 1MHz. Figure 52 shows the location of the four load cells in the test fixture.

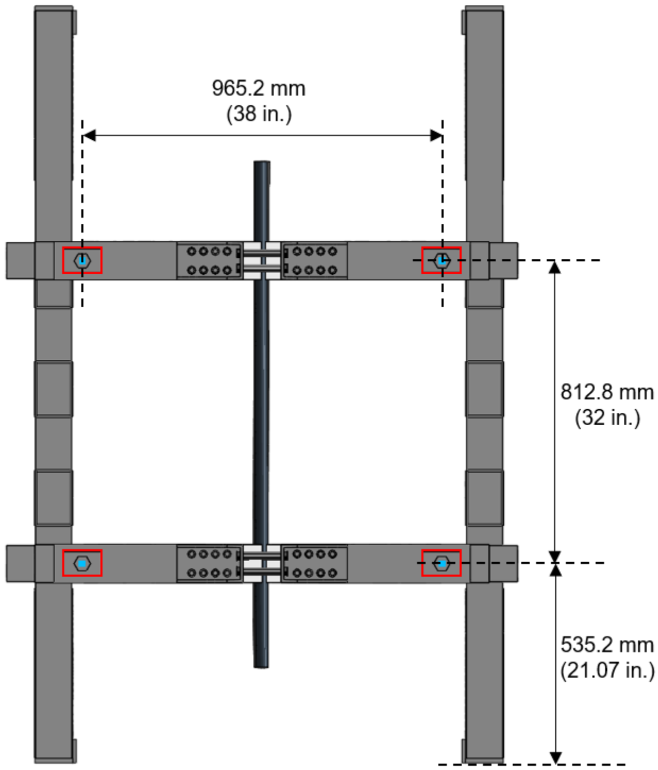


Figure 77. Blade test instrumentation – Load cells.

III. Strain gages

The strain gages were positioned on the outer surface of the blade skin. Strain history data was sampled at 1 MHz. Figure 78 and Figure 79 show the location and orientation of the strain gages for Test 21-125 and Test 21-126, respectively.

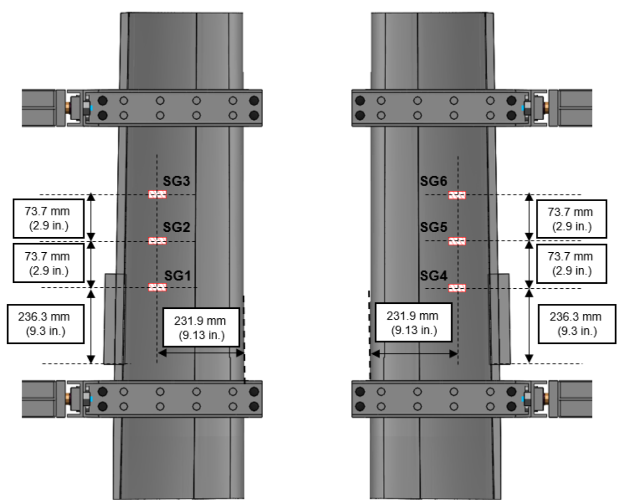


Figure 78. Blade test instrumentation – Strain gages for Test 21-125.

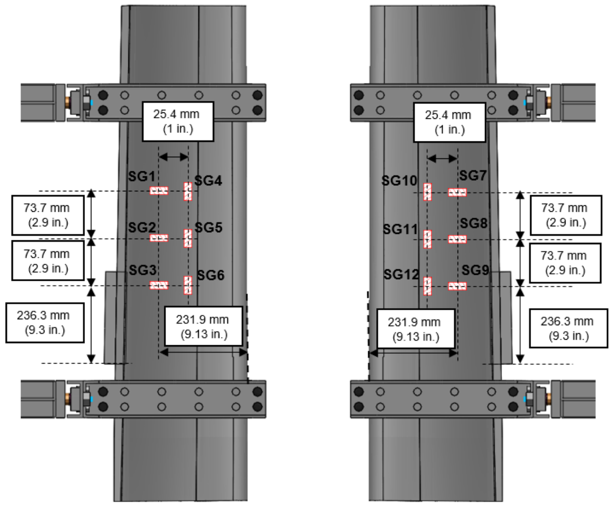


Figure 79. Blade test instrumentation – Strain gages for Test 21-126.

### 4.4.3 FEM Preparation

The UAS was positioned and oriented according to the test documentation in APPENDIX B. The nominal impact was defined at 218.64 m/s (425 knots). The nominal impact location was selected at the center of the blade section. Figure 80 shows the FEM setup of the blade test.

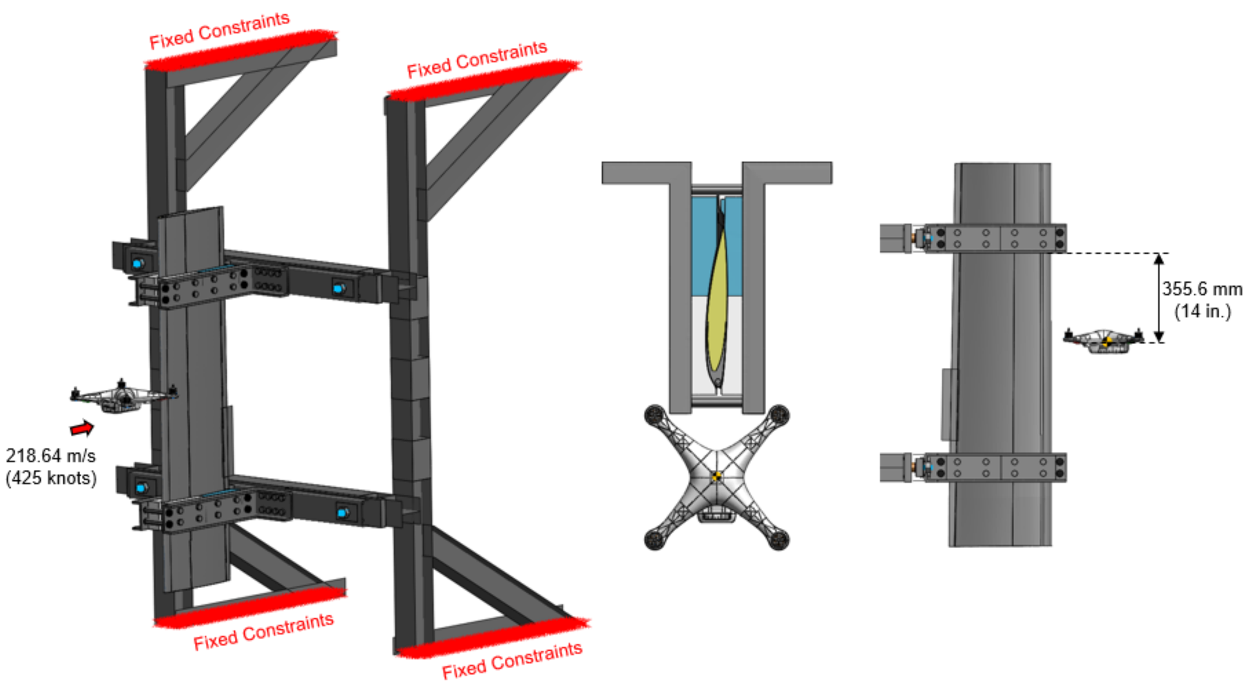


Figure 80. Blade section 4 test – FEM setup.

To capture the appropriate boundary conditions of the test, the FEM setup includes the fasteners' preload documented in the test reports (APPENDIX B). Figure 81 shows the fasteners' preload applied in the simulation model.

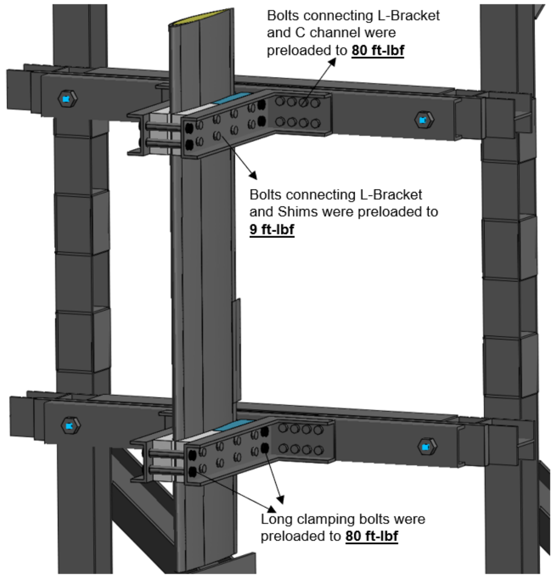


Figure 81. Blade section 4 test – Fasteners preload.

To capture the blade failure modes observed in the tests, the FEM setup implements **AUTOMATIC_SURFACE_TO_SURFACE_TIEBREAK* contacts with calibrated failure normal and shear stress at the following interfaces:

- Foam and mid-blade composite skin
- Lead rod and LE resin
- Trailing edge composites skins

The metallic LE skin and resin interface was defined with shared nodes. Figure 82 identifies the components of the section 4 test specimen.

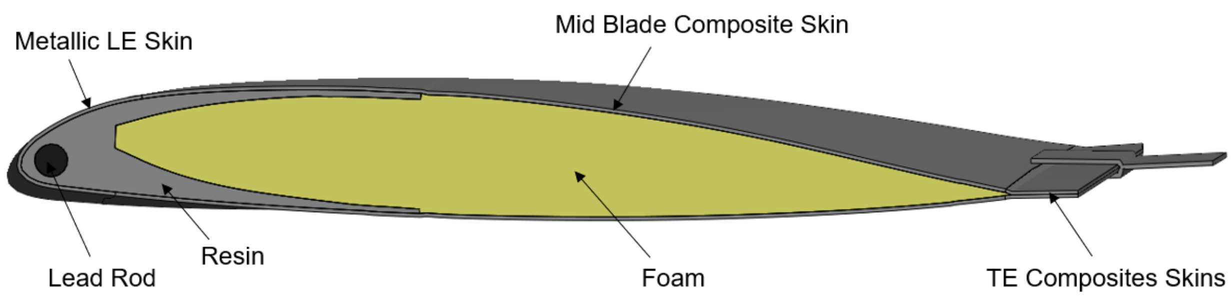


Figure 82. Blade section 4 – Components identification.

4.4.4 Test 21-125 FEM Validation

Following Test 21-125 documentation, the UAS was assigned an initial velocity of 221.59 m/s (430.7 knots). Its orientation was adjusted to a pitch of 33 degrees, a roll of 0 degrees, and a yaw of 41 degrees. The impact location with respect to the UAS center of gravity (CG) was 314.65 mm (12.38 inches) measured from the bottom of the upper bracket, as indicated in Figure 83. This resulted in a deviation of 41.15 mm (1.62 inches) from the nominal impact location.

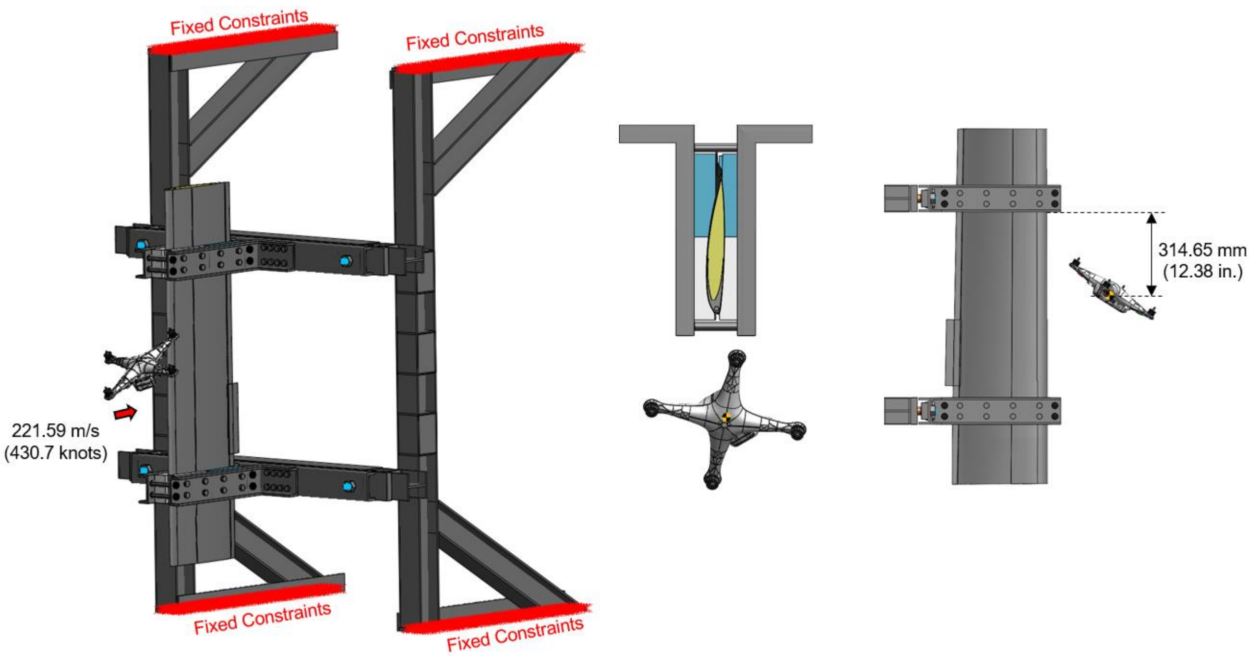


Figure 83. Test 21-125 simulation setup.

Figure 84 to Figure 86 show the isometric, side, and top view kinematics comparison, respectively. These figures present the three instances of the impact event: start of the impact, mid-impact instant, and end of the impact.

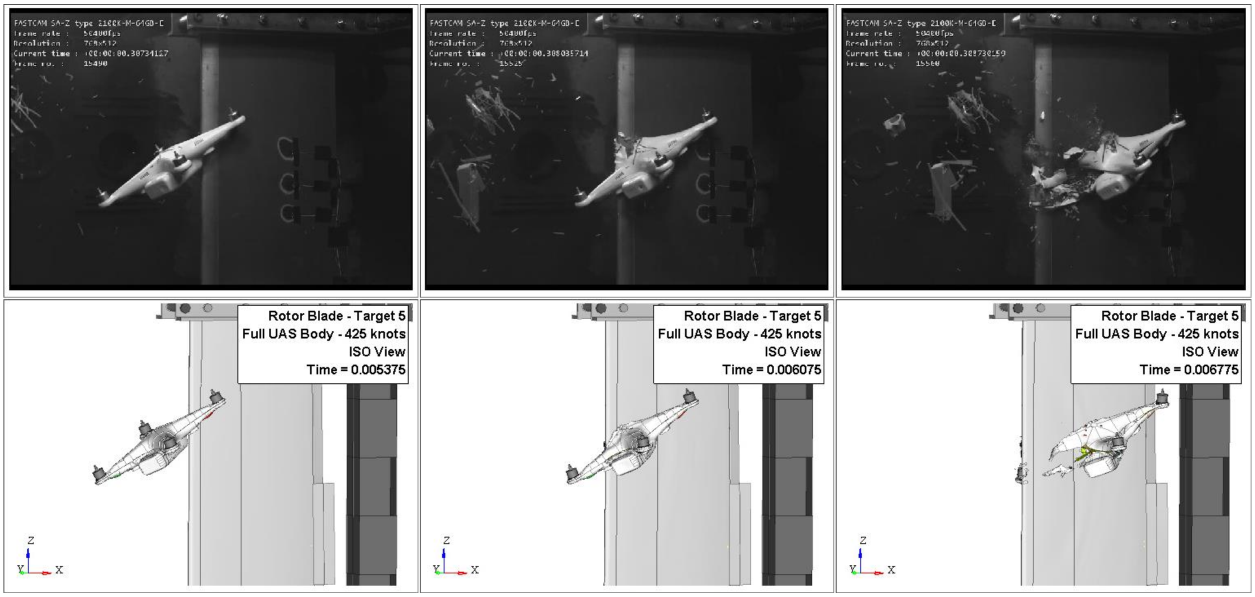


Figure 84. Test 21-125 isometric view kinematics comparison.

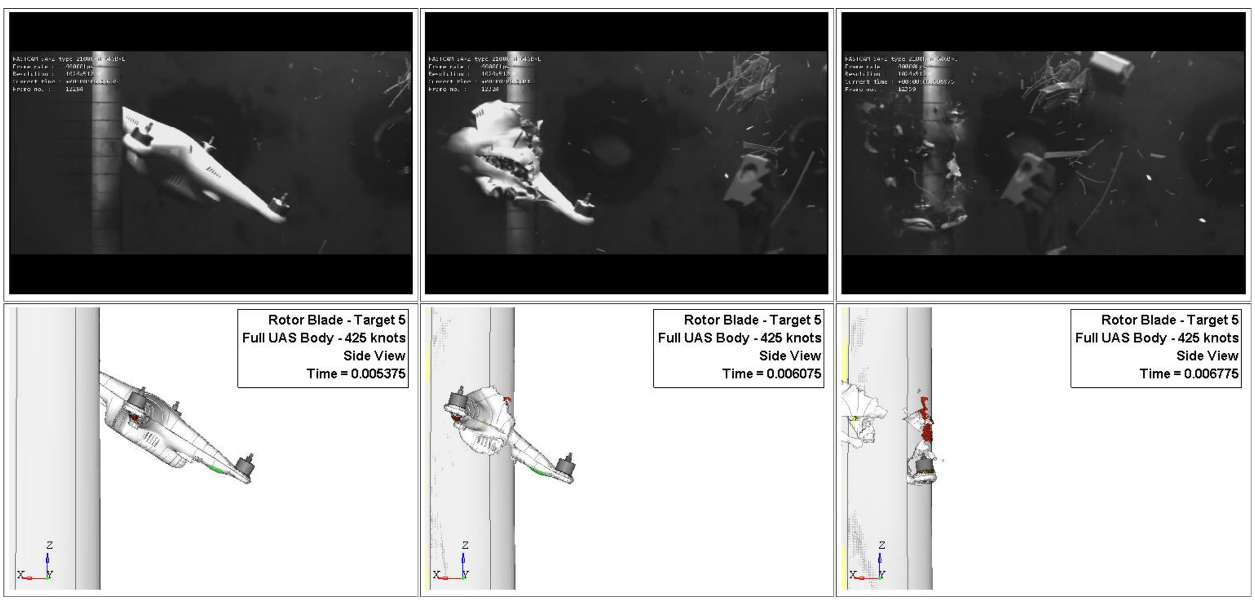


Figure 85. Test 21-125 side view kinematics comparison.

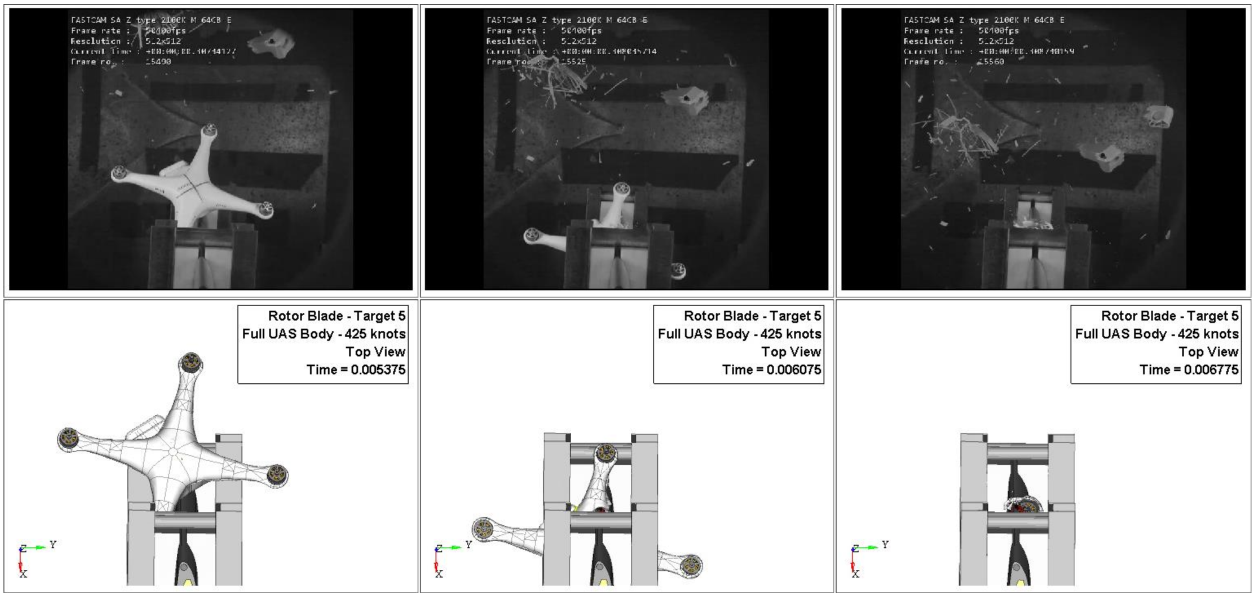


Figure 86. Test 21-125 top view kinematics comparison.

The FEM validation did not compare the load cells data due to the missing documentation on the boundary conditions of the shims. These components allowed relative displacement of the blade, complicating the replication of this behavior in the simulation. It is recommended to use a more rigid connection in future experiments to preserve the quality of the load history data.

The strain gages data was compared with the simulation strain outputs. The simulation and test strain outputs show good correlation, indicating similar strain magnitude and behavior. Figure 87 compares the test strain gage data and the simulation. Strain gage 4 data was affected by the impact of the UAS; this data has not been included in the comparison. The values on the vertical axis are not shown for confidential reasons.

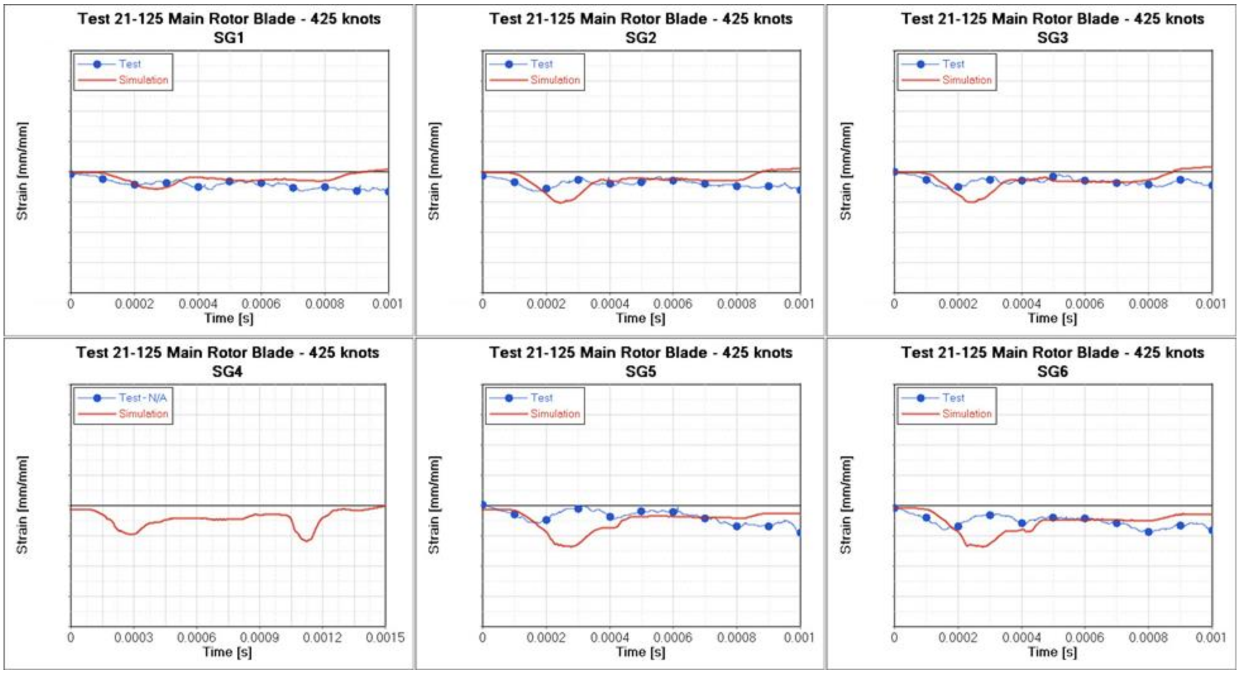


Figure 87. Test 21-125 SGs 1 to 6 simulation and test correlation

The post-test examination of the test article revealed two areas of damage in the blade section: the leading edge and the inside of the blade. Figure 88 shows the dent on the test article's leading edge and the damage observed in the simulation. Although the FEM does not have a noticeable dent as in the test, the effective plastic strain contour indicates permanent deformation in the impact area.

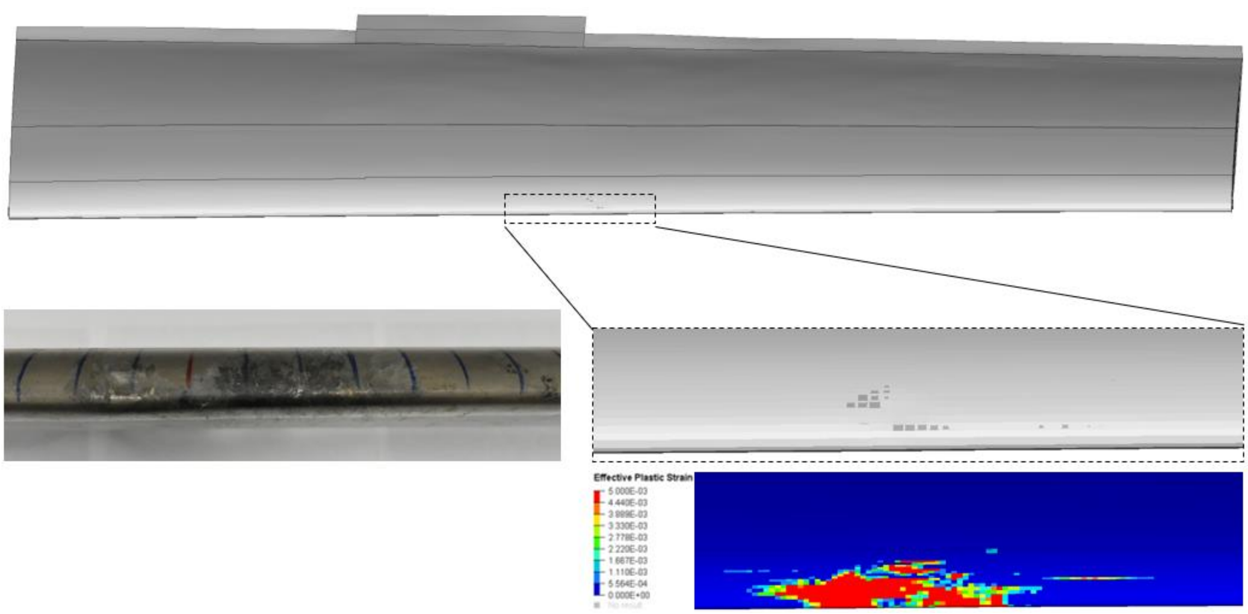


Figure 88. Test 21-125 blade leading edge damage.

NIAR dissected the Test 21-125 blade section into three pieces to examine the damage inside the test specimen. Figure 89 shows the post-test blade dissection. The inboard direction points towards the blade root, whereas the outboard direction points towards the blade tip. Figure 90 presents the cross-section between cuts #1 and #2 in the outboard direction, indicating that the skin was debonded from the foam.

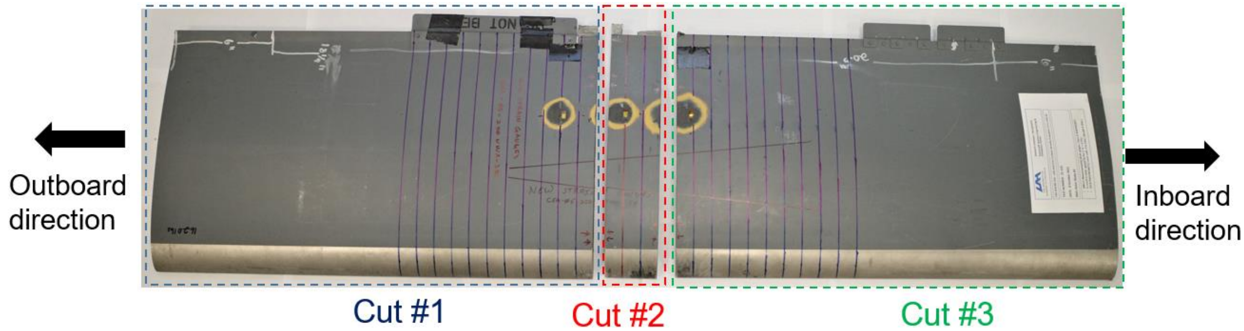


Figure 89. Test 21-125 blade specimen dissection.

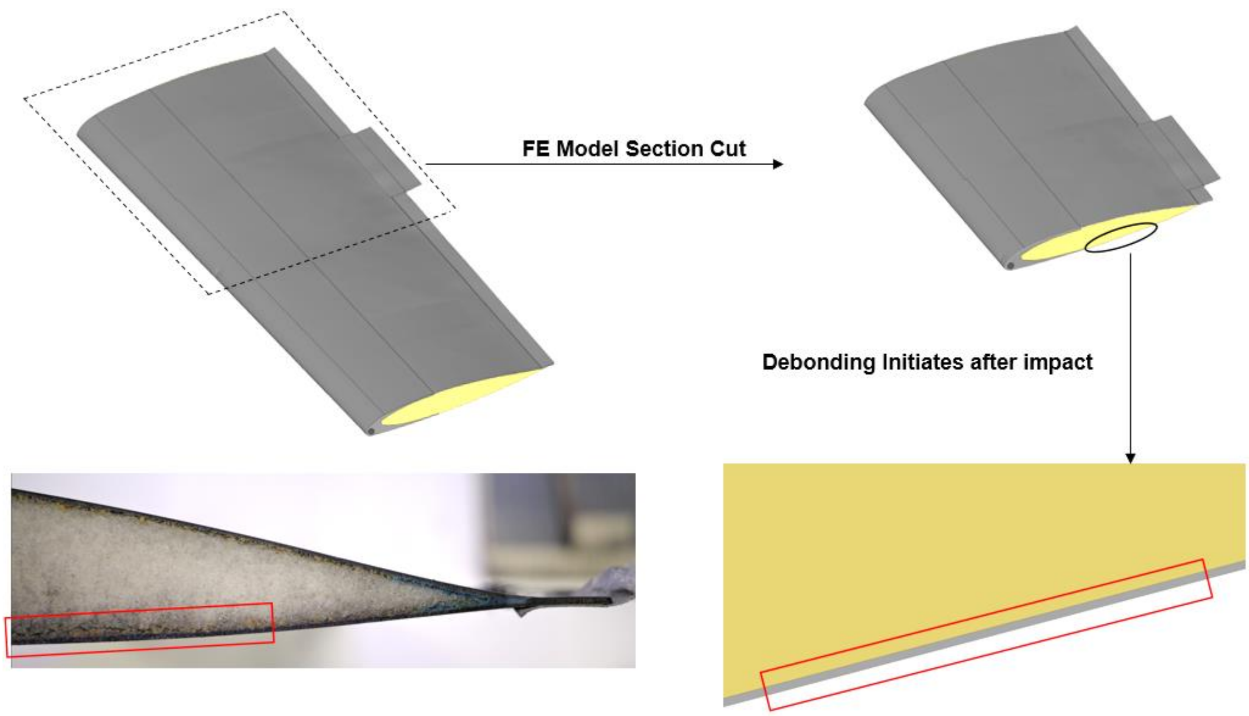


Figure 90. Test 21-125 blade skin debonding.

### 4.4.5 Test 21-126 FEM Validation

Following Test 21-126 documentation, the UAS was assigned an initial velocity of 227.07 m/s (441.4 knots). Its orientation was adjusted to a pitch of 12 degrees, a roll of 0 degrees, and a yaw of 8 degrees. The impact location with respect to the UAS CG was 258 mm (10.16 in.) measured from the bottom of the upper bracket, as indicated in Figure 91. This resulted in a deviation of 97.54 mm (3.84 inches) from the nominal impact location.

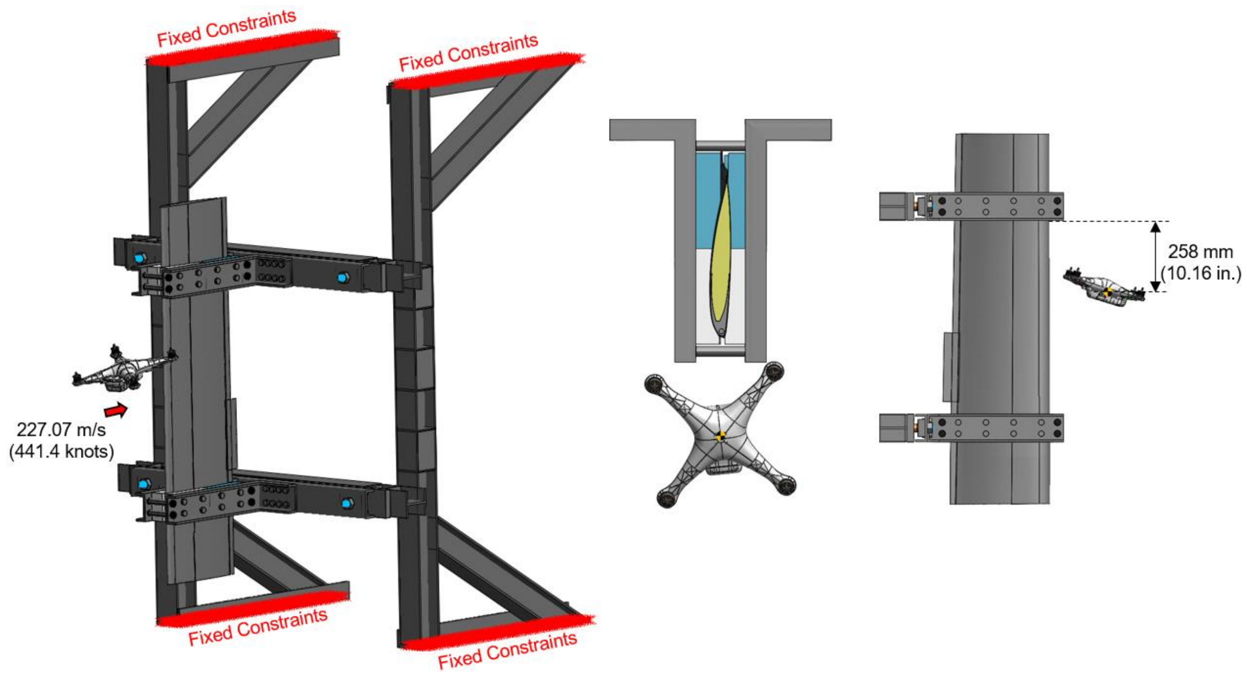


Figure 91. Test 21-126 simulation setup.

Figure 92 through Figure 94 show the isometric, side, and top view kinematics comparison, respectively. These figures present the three instances of the impact event: start of the impact, mid-impact instant, and end of the impact.

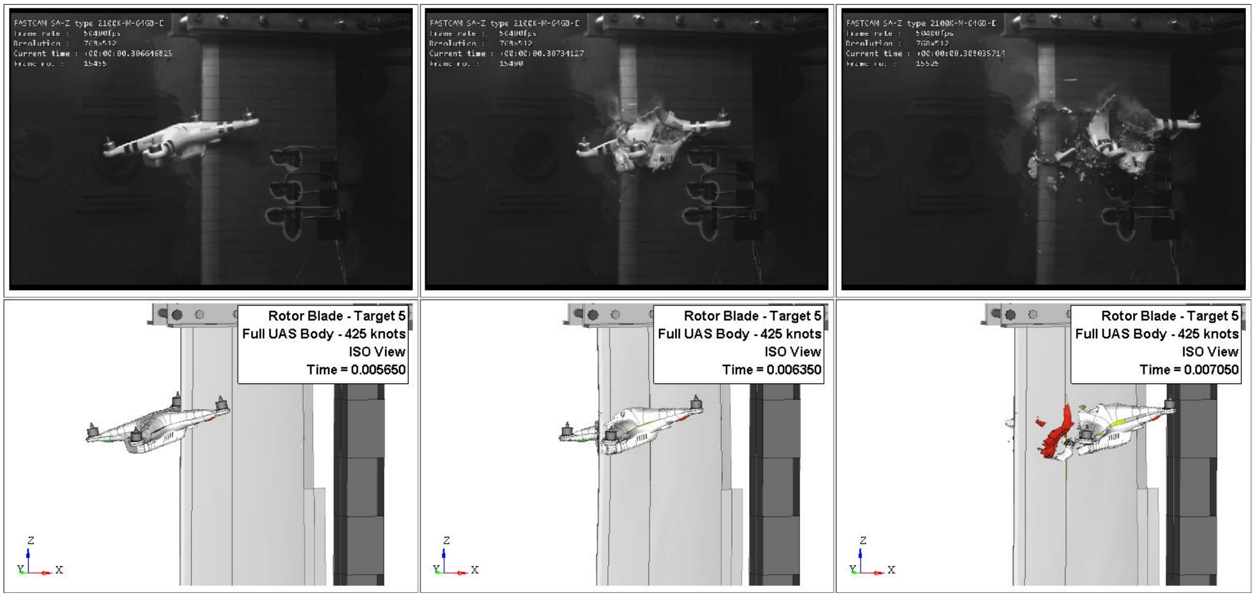


Figure 92. Test 21-126 isometric view kinematics comparison.

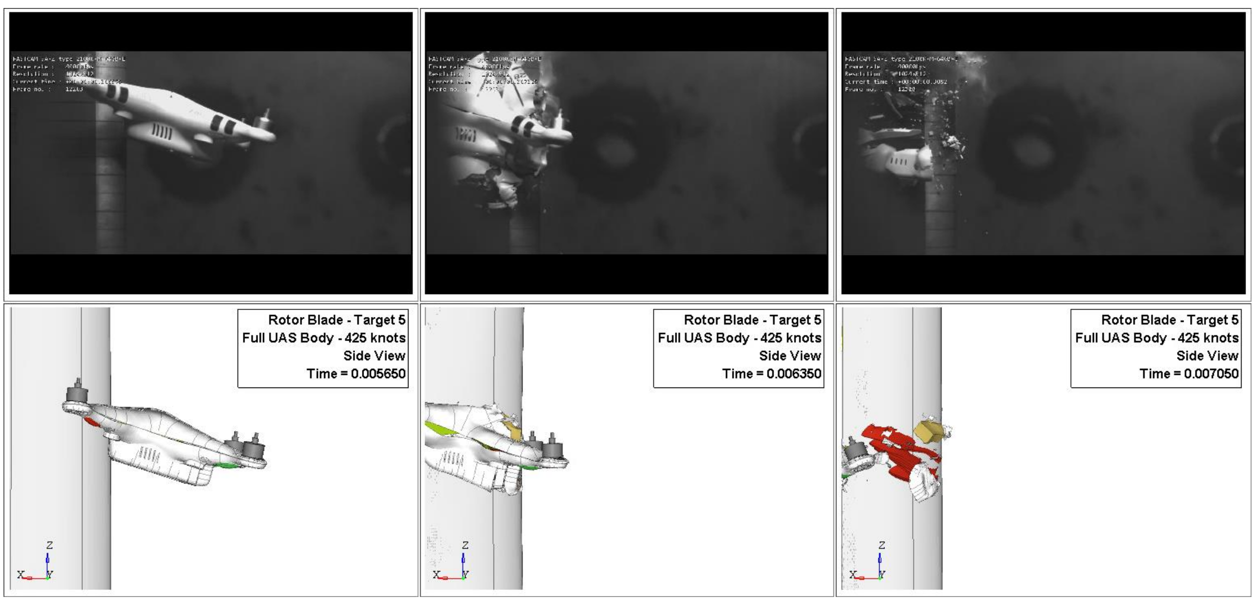


Figure 93. Test 21-126 side view kinematics comparison.

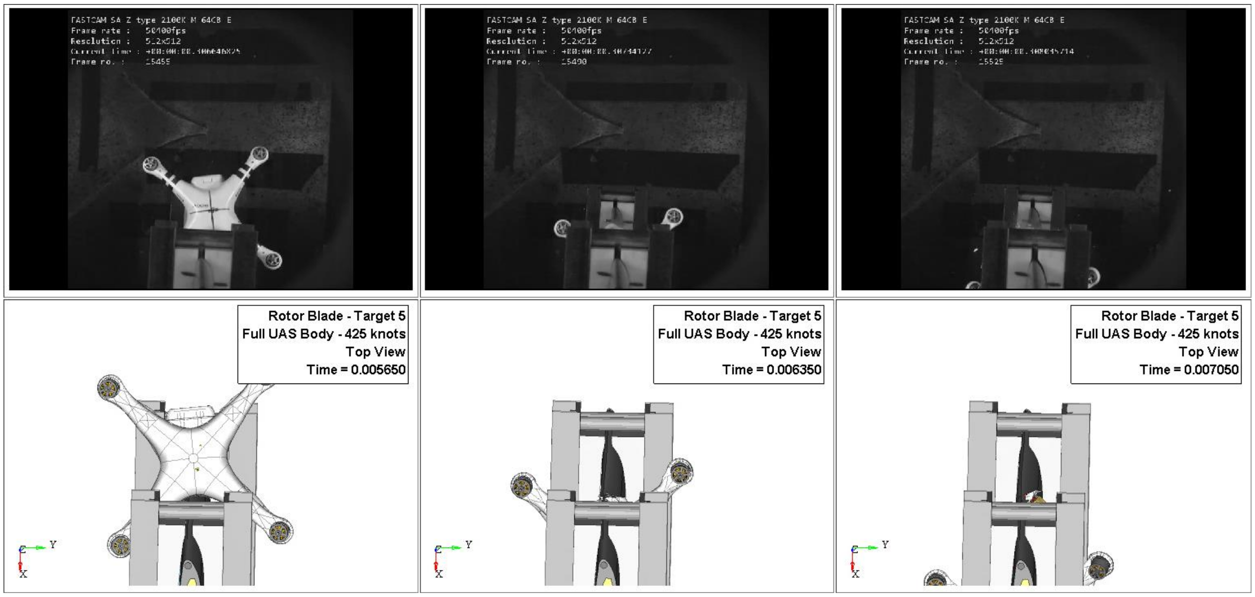


Figure 94. Test 21-126 top view kinematics comparison.

The FEM validation did not compare the load cells data due to the missing documentation on the boundary conditions of the shims. These components allowed relative displacement of the blade, complicating the replication of this behavior in the simulation. It is recommended to use a more rigid connection in future experiments to preserve the quality of the load history data.

The strain gages data was compared with the simulation strain outputs. Due to the low impact location and the side where the debris scratches the blade (see Figure 92), strain gages 9 and 12 (see chapter 4.4.2) data were damaged by the UAS and have not been considered for the comparison. The rest of the simulation and test strain outputs show good correlation, indicating similar strain magnitude and behavior the closer the impact location is to the gage. Strain gages 7, 8, 10 and 11 are located in the face of the blade that suffers a more direct impact from the UAS, and therefore, they capture closely the strain wave. Figure 95 and Figure 96 present the comparison of the test strain gages data and the simulation. The values on the vertical axis are not shown for confidential reasons.

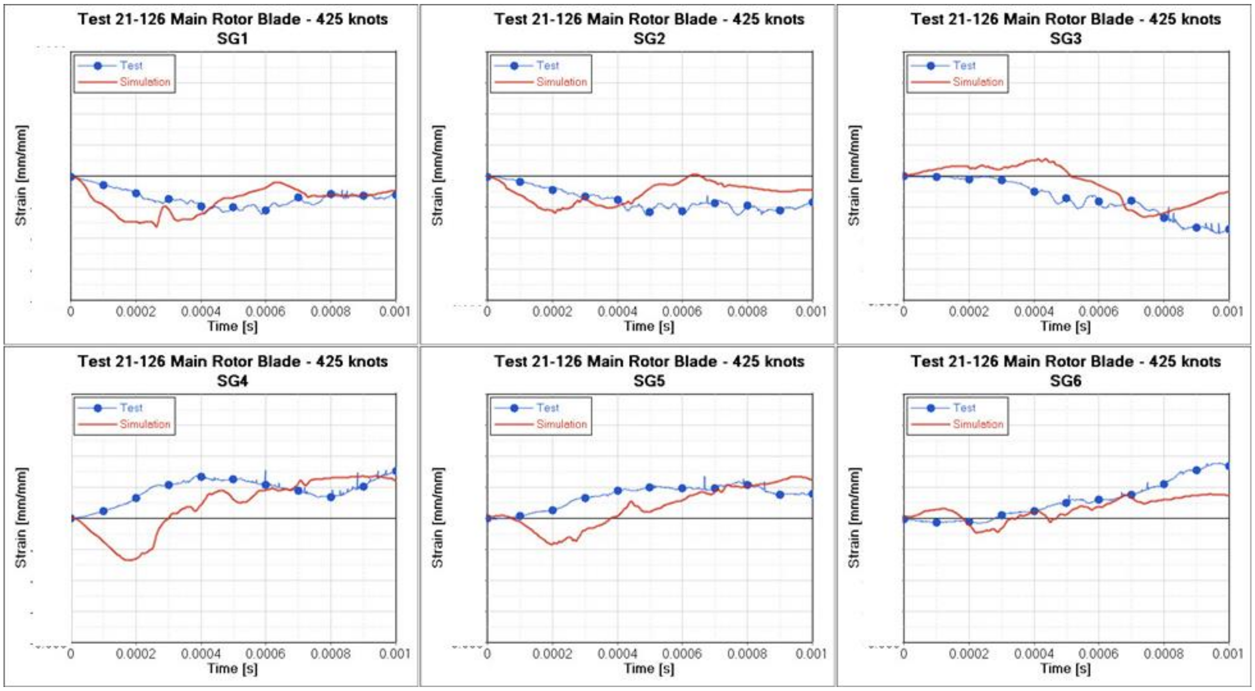


Figure 95. Test 21-126 SGs 1 to 6 simulation and test correlation

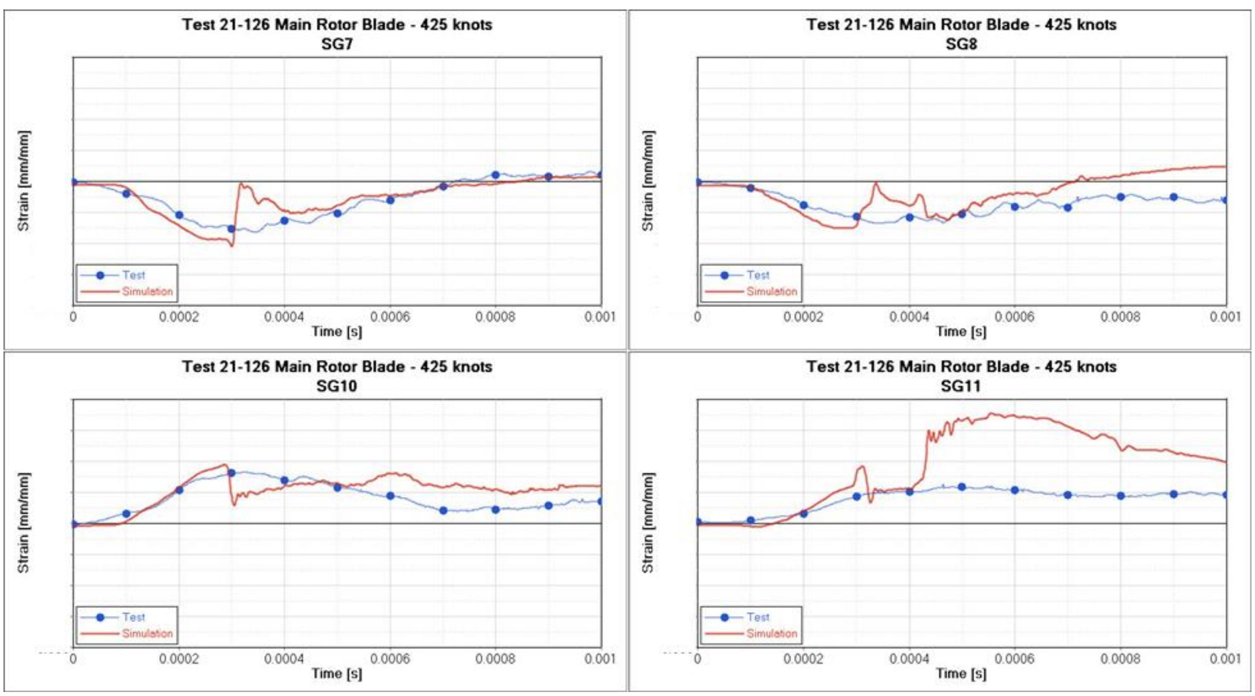


Figure 96. Test 21-126 SGs 7, 8, 10, 11 simulation and test correlation

The post-test examination of the test article revealed two areas of damage in the blade section: the leading edge and the inside of the blade. Figure 97 shows a small dent on the test article’s leading edge compared to the damage observed in the simulation. Although the FEM does not have a noticeable dent as in the test, the effective plastic strain contour indicates permanent deformation in the impact area.

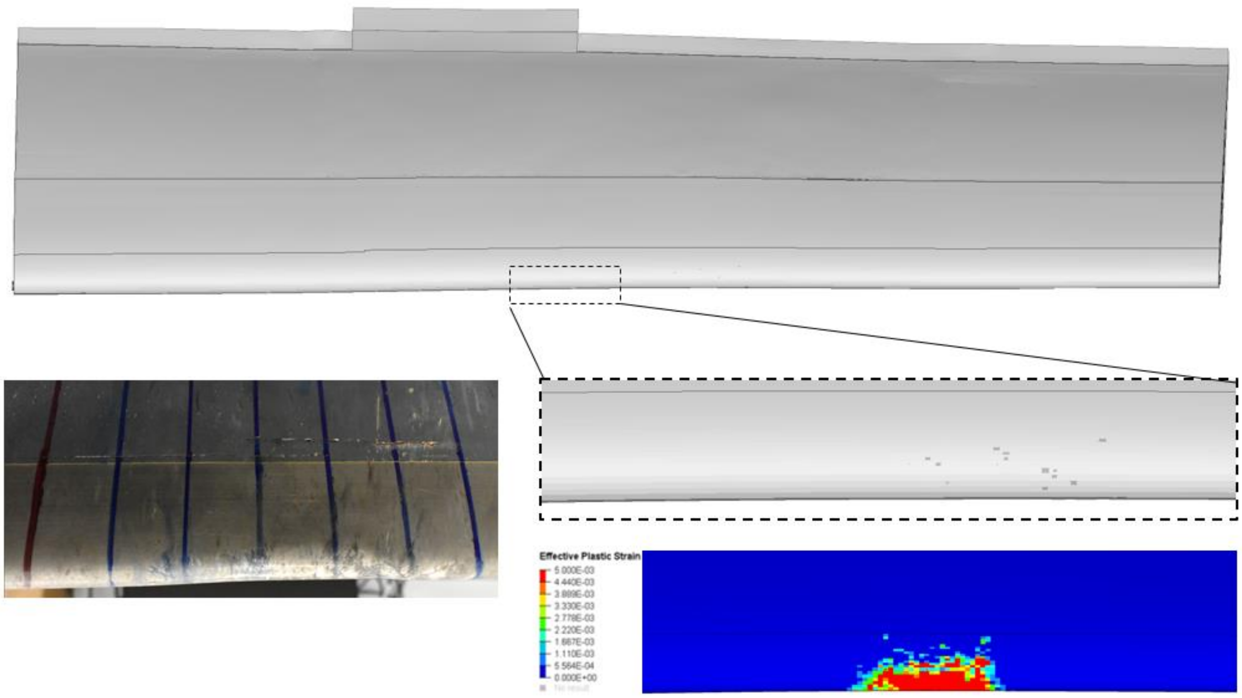


Figure 97. Test 21-126 blade leading edge damage.

NIAR dissected the Test 21-126 blade section into two pieces to examine the damage inside the test specimen. Figure 98 shows the post-test blade dissection. The inboard direction points towards the blade root, whereas the outboard direction points towards the blade tip. Figure 99 presents the cross-section between cuts #1 and #2 in the outboard direction, indicating that the skin was debonded from the foam in the test and the simulation. In addition, Figure 100 shows the trailing edge skin debonding, which was also captured by the simulation.

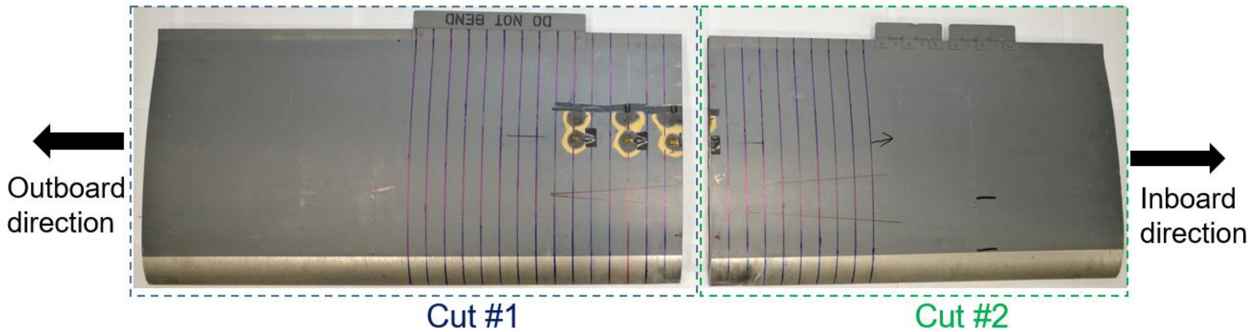


Figure 98. Test 21-126 dissected blade.

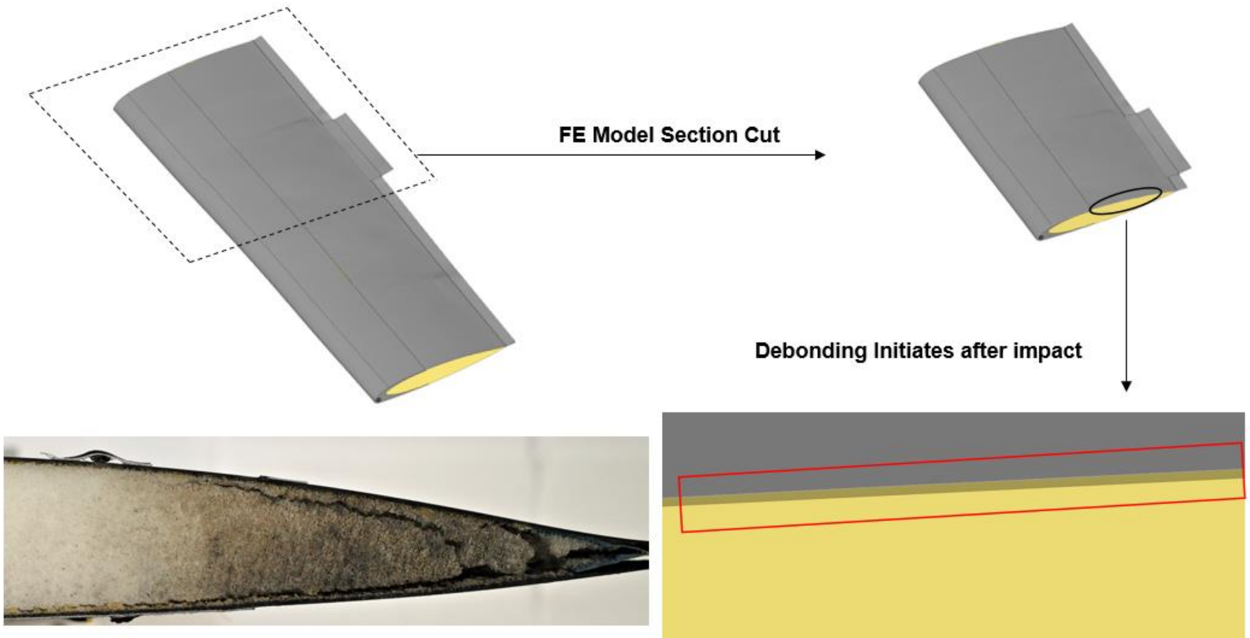


Figure 99. Test 21-126 blade skin debonding.

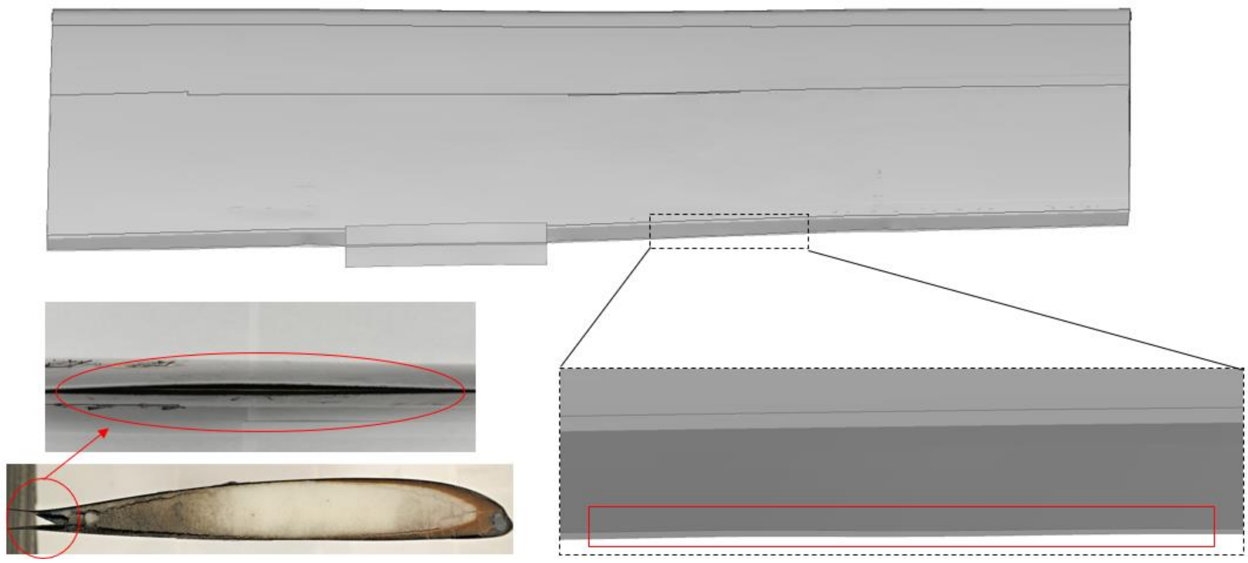

Figure 100. Test 21-126 trailing edge skin debonding.

### 4.4.6 FEM Recommendations

To minimize the challenges experienced when replicating the rotor blade tests through the simulation, the following recommendations will have to be considered for future studies:

1. Load cells must be positioned closer to the blade impact location, reducing the amount of structure between the impact location and the load reading region, facilitating the correlation efforts.
2. Rigid shims to facilitate the setup of the test conditions in the simulation.

## 5. MID-AIR COLLISION ANALYSIS

This chapter discusses the conditions defined for the collision analysis between sUAS and rotorcraft. The damage severity criterion used to determine the severity level is presented in Chapter 5.2. This severity criterion is the same previously defined and used for the original airborne collision work on A3 [2].

### 5.1 IMPACT CONDITIONS DEFINITION

This study focuses on the collision between sUAS (2.7 lb. and 4.0 lb.) and representative rotorcraft airframes. Due to the dimensional constraints of the UAS models, only two impact locations were feasible for most target areas. The only exception was the rear servo, for which only one impact location was determined. The rotorcraft impact locations selected for each target area are introduced in Figure 101 through Figure 107.

Because of the relatively larger dimensions for the rotorcraft components compared to the sUAS, it was feasible to evaluate them as independent structures as done in previous airborne collision studies [2]. Therefore, the collision analysis between sUAS and rotorcraft presented in this report was conducted by applying an initial velocity only to the sUAS model, while the rotorcraft target was fixed through a rigid boundary condition. Consequently, the following variables are considered for the current study:

- Aircraft Type: Rotorcraft
- UAS Configuration: Quadcopter and Fixed-Wing
- UAS Mass: 2.7 and 4.0 lb.
- Aircraft Velocity: 0, 75, and 150 knots
- sUAS Velocity: 39 knots
- Impact Relative Velocity: 39, 114, and 189 knots
- Rotor RPM: 383 RPM
- Impact Areas: Horizontal stabilizer location 1 (center), Horizontal stabilizer location 2 (tip), Rear servo, Cowling location 1 (top left), Cowling location 2 (center), Windshield location 1 (center), Windshield location 2 (top inner), Main rotor blade

The following special considerations were accounted for in this study:

1. The same impact location was maintained for both UAS models (2.7 quadcopter and 4.0 fixed-wing).
2. All impacts were considered for the worst-case scenario with the sUAS moving at maximum speed (39 knots).
3. Relative impact velocity was applied to the sUAS.
4. The aircraft target areas were modeled individually and rigidly constrained at the structural interface.

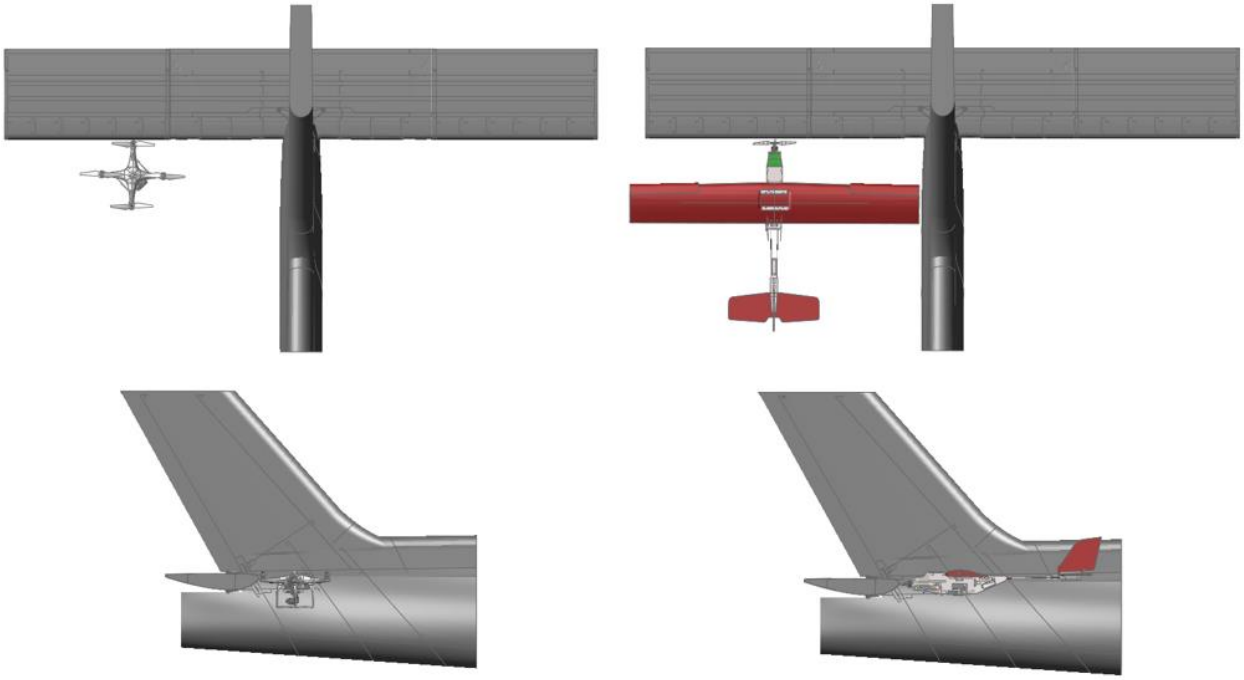

Figure 101. Rotorcraft horizontal stabilizer location 1.

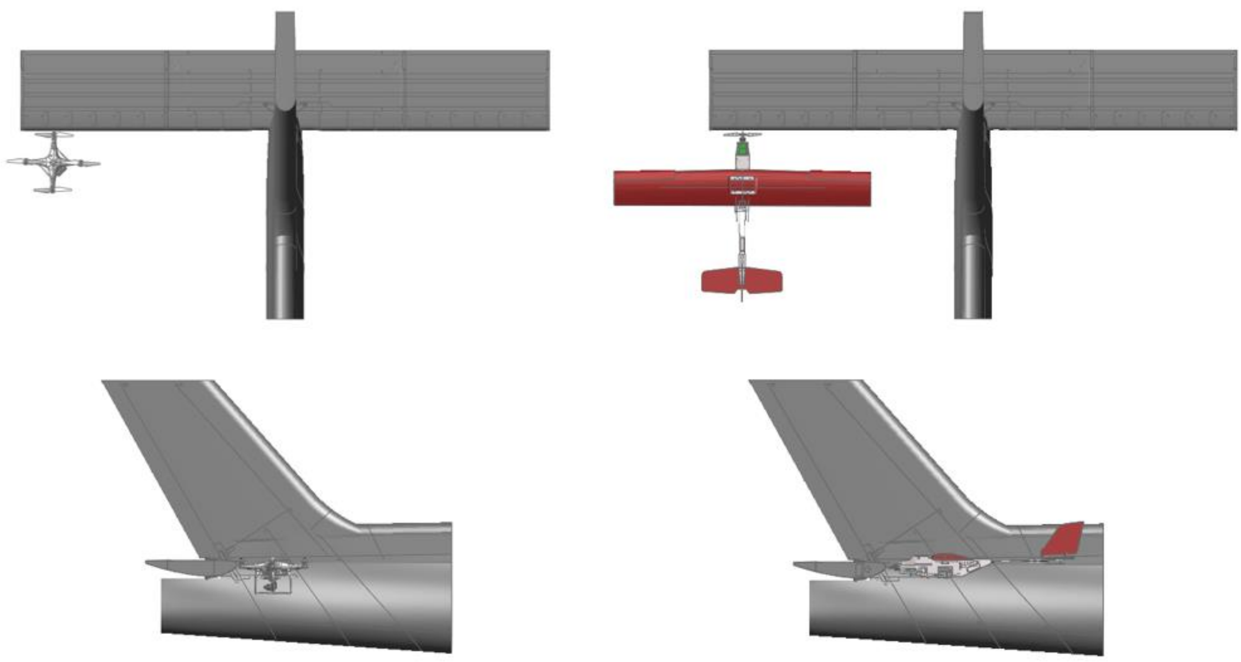

Figure 102. Rotorcraft horizontal stabilizer location 2.

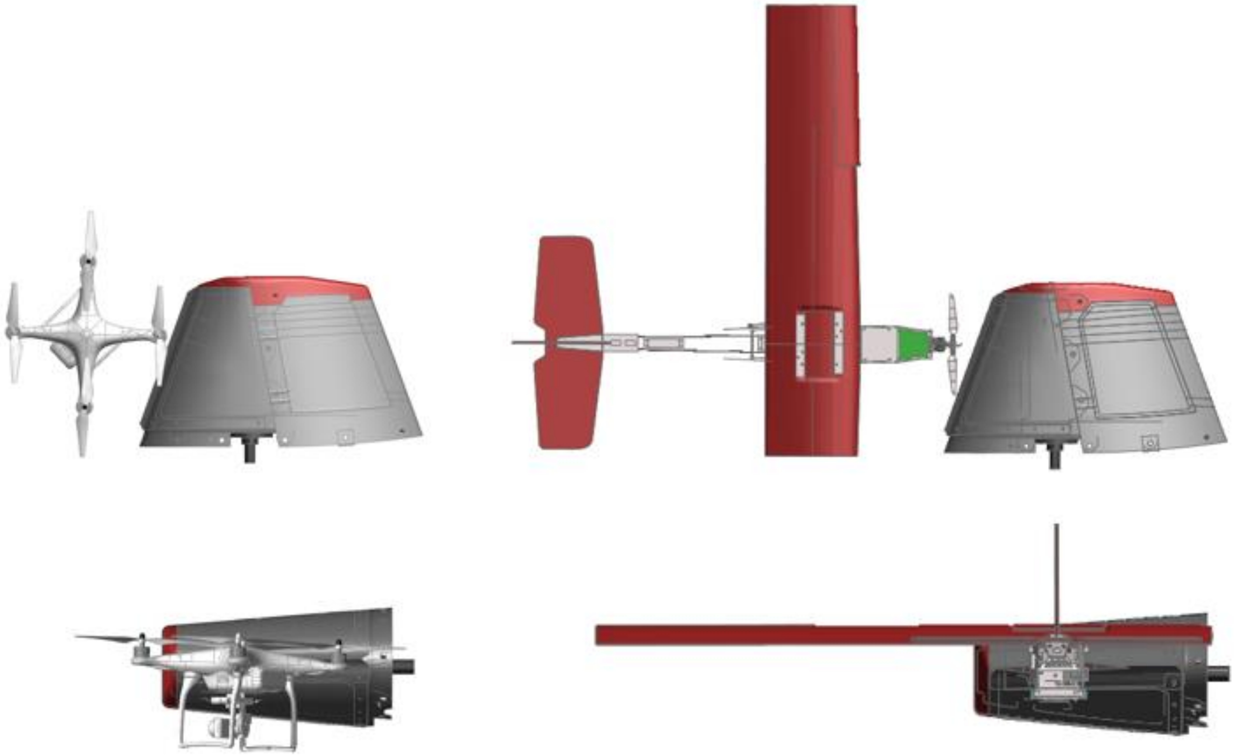

Figure 103 Rotorcraft rear servo location 1.

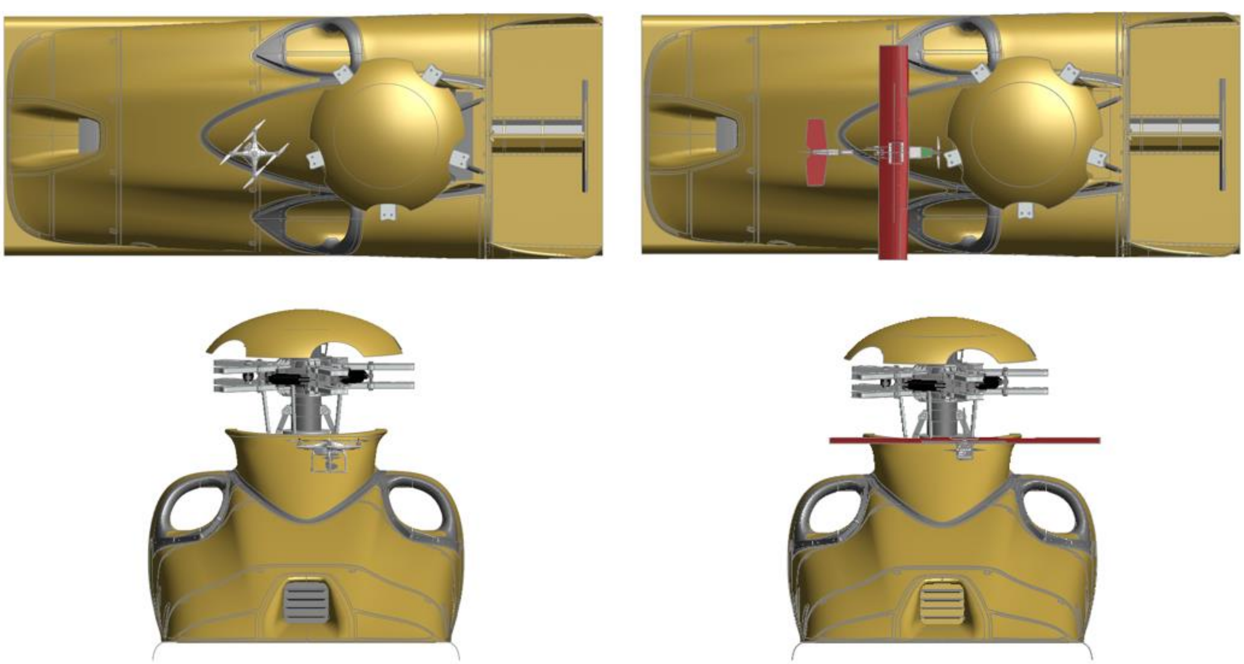

Figure 104. Rotorcraft cowling location 1.

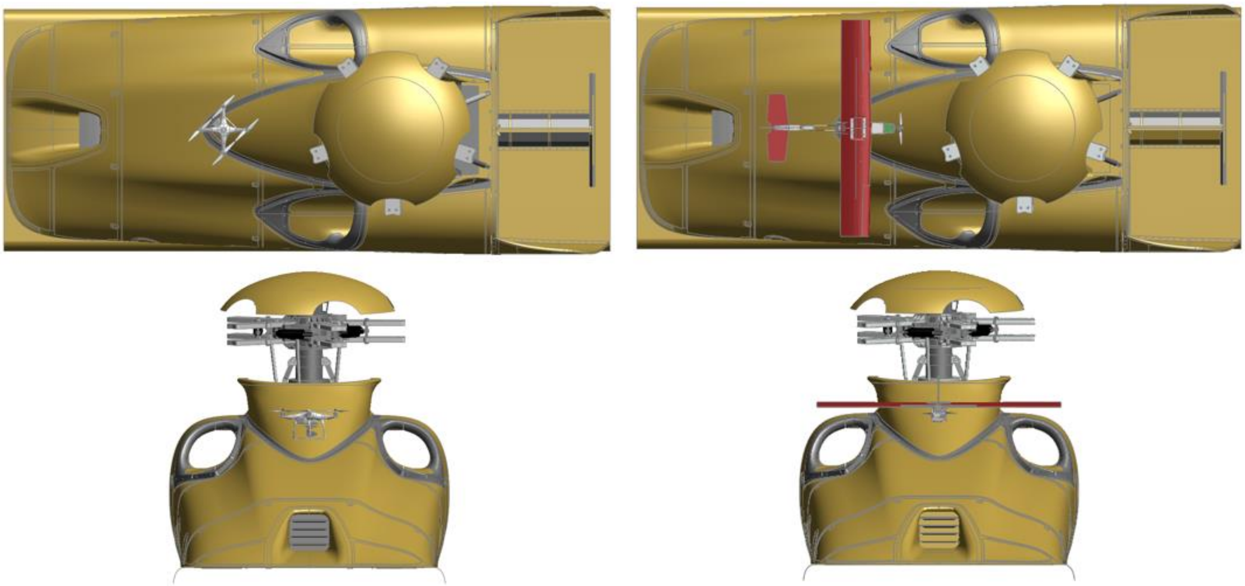

Figure 105. Rotorcraft cowling location 2.

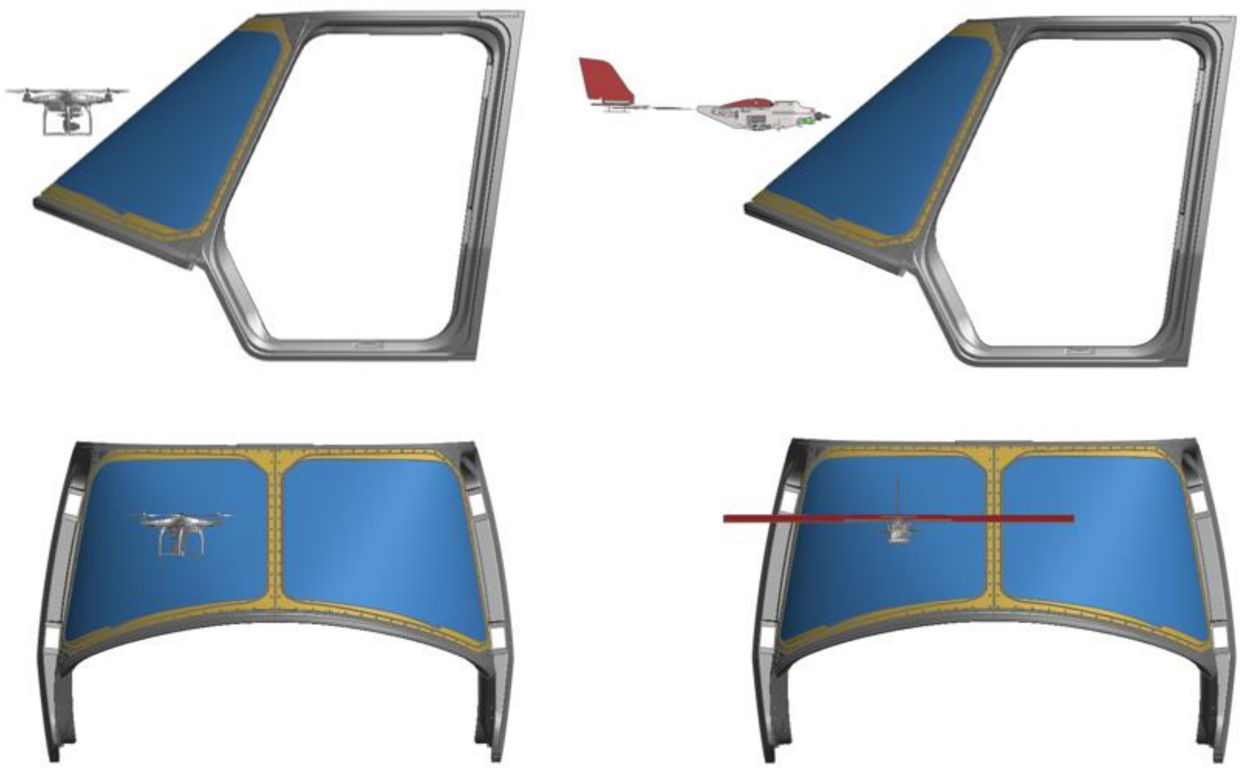

Figure 106. Rotorcraft windshield location 1.

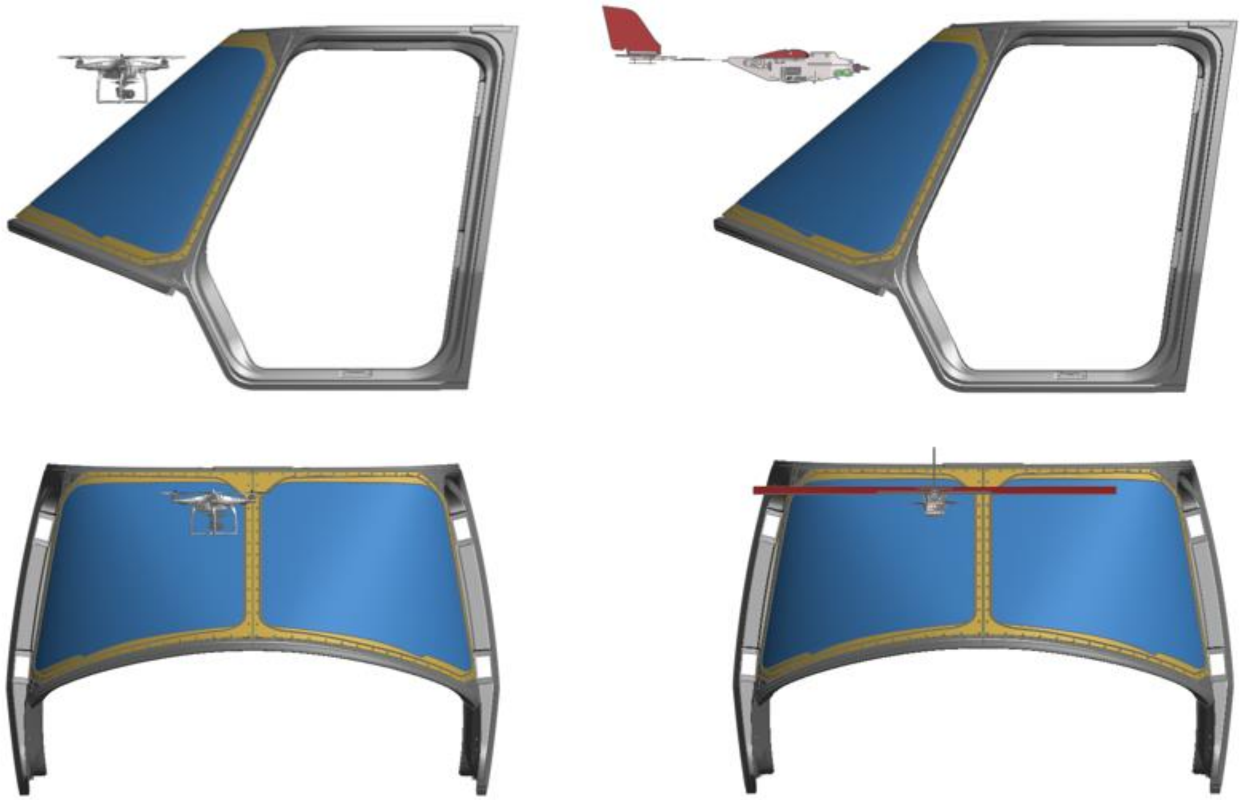

Figure 107. Rotorcraft windshield location 2.

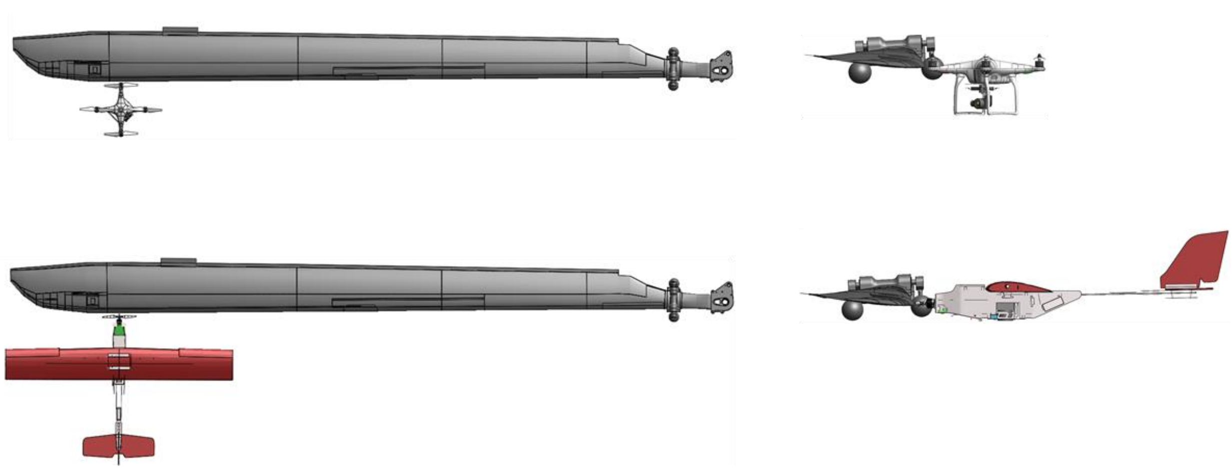

Figure 108. Rotorcraft main rotor blade location 1.

### 5.1.1 Impact Velocity

The rotorcraft velocity at impact was defined based on literature data [31] and pilot feedback. The Part 29 rotorcraft cruise velocity preparation is documented in the performance specifications [31] as 150 knots. Two more velocities were considered for the analysis: a hover velocity of 0 knots and a medium velocity of 75 knots. According to the sUAS research performed under task A3 [2] the maximum velocity for the 2.7 lb. is 39 knots. To compare severity levels between UAS architectures, the same velocity was considered for the 4.0 lb. fixed-wing sUAS.

During the simulation setup process, for each impact velocity case (hover, medium, and cruise), the sUAS was assigned the relative velocity of the impact at the start of the simulation.

### 5.1.2 Impact Conditions

Whenever possible, lessons learned from the A3 and A14 programs were used to expedite the analysis work performed under this study. Accordingly, the impact location and orientation sensitivity studies documented in Volume II [5] apply to the current work.

In consequence, the following indications were considered for this work:

- UAS center of gravity was aligned with the first point of contact at impact to cause the most damage to the target.
- UAS quadcopter model was oriented to impact with one motor first as done in previous airborne collision work Task A3 [5].
- On leading edge structures, the UAS impacted in between ribs, facilitating the possibility of skin perforation and penetration inside the airframe.

### 5.1.3 Load Case Name Convention

This research's broad spectrum of FE model combinations and parameters requires a code to identify the simulated impact conditions according to the UAS, aircraft type, target component, and local impact positions.

Impact conditions were coded using seven characters (ABij-CDE):

- A – Distinguishes aircraft; for this study, the Rotorcraft is denoted (R)
- Bij – Distinguishes between UAS Type and Size:
    - Quadcopter-2.7 lb. (Q2.7)
    - Fixed Wing-4.0 lb. (F4.0)
- C – Distinguishes between impact areas:
    - Cowling (C)
    - Horizontal Stabilizer (H)
    - Rear Servo (R)
    - Windshield (W)
    - Blade (B)
- D – Distinguishes between impact location (1 and 2)
- E - Distinguishes between velocity categories associated with the rotorcraft:
    - Hover – 0 kts (H)
    - Medium – 75 kts (M)
    - Cruise – 150 kts (C)

Example RQ2.7-C1C

- Rotorcraft
- Quadcopter – 2.7 lb.
- Cowling
- Impact Location #1
- Cruise velocity – 150 kts

### 5.1.4 Simulation Matrix

Table 12 and Table 13 present the simulation matrix for the 2.7 lb. quadcopter and 4.0 lb. fixed-wing sUAS against the rotorcraft components, respectively.

Table 12. Simulation matrix of rotorcraft components and 2.7 lb. quadcopter.

| | Rotorcraft and Quadcopter 2.7 lb. Impact (RQ2.7) | | | | | | | | | | | | | | | | | | | | | | | |
|---|---|---|---|---|---|---|---|---|---|---|---|---|---|---|---|---|---|---|---|---|---|---|---|---|
| | H-Stabilizer Location 1 and 2 | | | | | | Rear Servo | | | Cowling Location 1 and 2 | | | | | | Windshield Location 1 and 2 | | | | | | Main Rotor Blade | | |
| Case | RQ2.7-H1H | RQ2.7-H1M | RQ2.7-H1C | RQ2.7-H2H | RQ2.7-H2M | RQ2.7-H2C | RQ2.7-R1H | RQ2.7-R1M | RQ2.7-R1C | RQ2.7-C1H | RQ2.7-C1M | RQ2.7-C1C | RQ2.7-C2H | RQ2.7-C2M | RQ2.7-C2C | RQ2.7-W1H | RQ2.7-W1M | RQ2.7-W1C | RQ2.7-W2H | RQ2.7-W2M | RQ2.7-W2C | RQ2.7-B1H | RQ2.7-B1M | RQ2.7-B1C |

Table 13. Simulation matrix of rotorcraft components and 4.0 lb. fixed-wing.

| | Rotorcraft and Fixed Wing 4.0 lb. Impact (RF4.0) | | | | | | | | | | | | | | | | | | | | | | | |
|---|---|---|---|---|---|---|---|---|---|---|---|---|---|---|---|---|---|---|---|---|---|---|---|---|
| | H-Stabilizer Location 1 and 2 | | | | | | Rear Servo | | | Cowling Location 1 and 2 | | | | | | Windshield Location 1 and 2 | | | | | | Main Rotor Blade | | |
| Case | RF4.0-H1H | RF4.0-H1M | RF4.0-H1C | RF4.0-H2H | RF4.0-H2M | RF4.0-H2C | RF4.0-R1H | RF4.0-R1M | RF4.0-R1C | RF4.0-C1H | RF4.0-C1M | RF4.0-C1C | RF4.0-C2H | RF4.0-C2M | RF4.0-C2C | RF4.0-W1H | RF4.0-W1M | RF4.0-W1C | RF4.0-W2H | RF4.0-W2M | RF4.0-W2C | RF4.0-B1H | RF4.0-B1M | RF4.0-B1C |

## 5.2 DAMAGE CATEGORY DEFINITION

A set of criteria was defined to categorize the damage level, as shown in Table 14. This criterion was developed under task A3 program [2] and applied to airframe structures.

Simulations with the least visible damage are categorized as Level 1, corresponding to minimal localized damage such as surface dents. Damage category Level 2 represents significant visible damage to the external surface of the aircraft with some internal component damage but no skin rupture. The third category, Level 3, describes impact events where the aircraft's outer surface is compromised in a way that could allow the ingress of foreign objects into the airframe, with some damage to the substructure. Finally, Level 4 indicates damage that includes all preceding aspects, extensive damage to internal components, and possibly compromising damage to the primary structure.

Table 14. Damage level categories.

| Severity | Description | Example |
|---|---|---|
| **Level 1** | • The airframe is undamaged.<br>• Small deformations. | 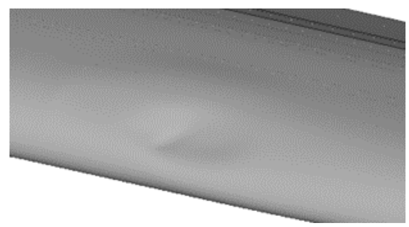 |
| **Level 2** | • Extensive permanent deformation on external surfaces.<br>• Some deformation in internal structure.<br>• No failure of the skin. | 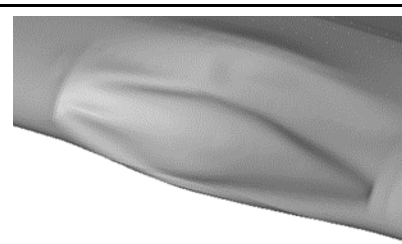 |
| **Level 3** | • Skin fracture.<br>• Penetration of at least one component into the airframe. | 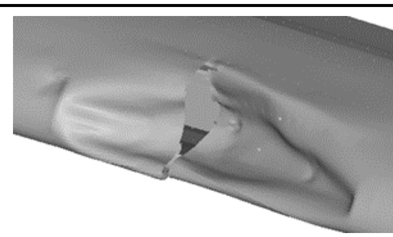 |
| **Level 4** | • Penetration of UAS into airframe and failure of the primary structure. | 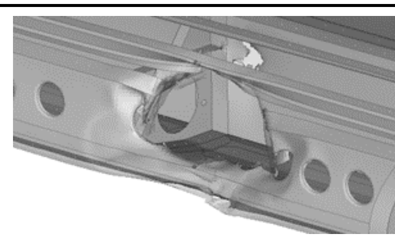 |

Table 15 describes the damage level categories that classify the damage caused to a rotorcraft blade by a UAS airborne collision in four levels.

Table 15. Damage level categories for the rotorcraft blade.

| Severity | Description |
|---|---|
| **Level 1** | • Blade undamaged<br>• Scratches or small dents on a rotor blade<br>• No crack initiation |
| **Level 2** | • Large dents on a rotor blade<br>• Visible cracking of a rotor blade<br>• Skin debonding |
| **Level 3** | • Significant material loss leading to an imbalance on a single blade<br>• No crack initiation at the blade root or hub |
| **Level 4** | • Complete rotor blade failure |

5.2.1 Fire Risk

The risk of fire associated with damaged Lithium-ion Polymer (LiPo) type batteries is addressed for each simulation based on the trends observed during the component ballistic tests performed in the A3 research [2]. Note that the label "Fire Risk" indicates a potential outcome rather than an impending event due to the qualitative nature of the assessment. Further studies and physical testing into this phenomenon would be required to determine any additional severity. Table 16 explains the fire risk criterion.

Table 16. Risk of battery fire.

| Fire Risk | Description | Example |
|---|---|---|
| **Yes** | • UAS (including the battery) penetrates the airframe.<br>• The battery deforms but stays undamaged.<br>• Physical tests showed that partly damaged batteries created heat and sparks. | 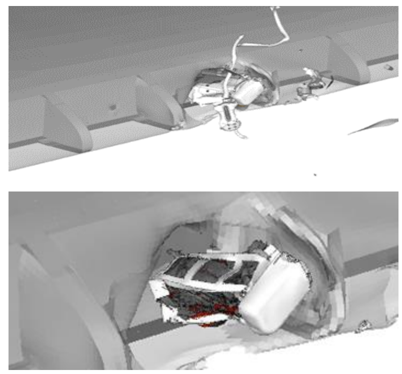 |
| **No** | • The UAS does not penetrate the airframe. | 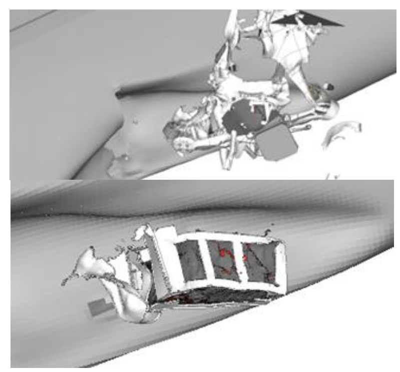 |
| **No** | • UAS (including the battery) penetrates the airframe.<br>• The battery sustains significant damage, destroying its cells.<br>• Physical tests showed that completely damaged batteries did not create heat and sparks. | 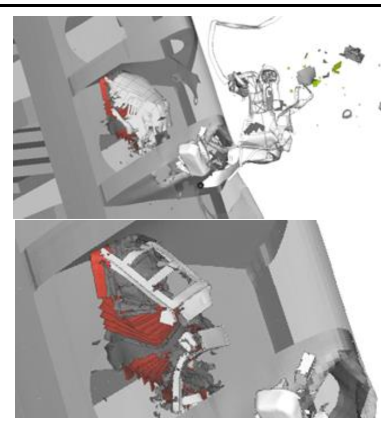 |

## 6. MID-AIR COLLISION DAMAGE ASSESSMENT

### 6.1 QUADCOPTER 2.7 LB.

This chapter presents the results of the airborne collision studies for the 2.7 lb. UAS quadcopter and the rotorcraft components. The target impact areas introduced in Chapter 5 are the front cowling, horizontal stabilizer, rear servo, windshield, and main rotor blade. Figure 109 illustrates the highest damage severity level observed on each target. In general, it can be noticed that the damage sustained by the rotorcraft component increases with the impact velocity. For example, the horizontal stabilizer shows level 4 damage at cruise speed. The front cowling location 1 impact at cruise speed shows level 3 damage to the cowling and level 1 to the rotor shaft structure (secondary impact). The rear servo, windshield, and blade cases have level 2 damage at cruise speed. Table 17 summarizes the damage severity level evaluation and fire risk assessment of the 2.7 lb. quadcopter impact cases.

Table 17 also includes the damage severity assessment of the tail rotor according to the findings from testing. As shown in APPENDIX B, the component level test results indicate the probability of a level 4 damage. Further work will be required in the future to conduct full-scale tests or simulation of the tail rotor.

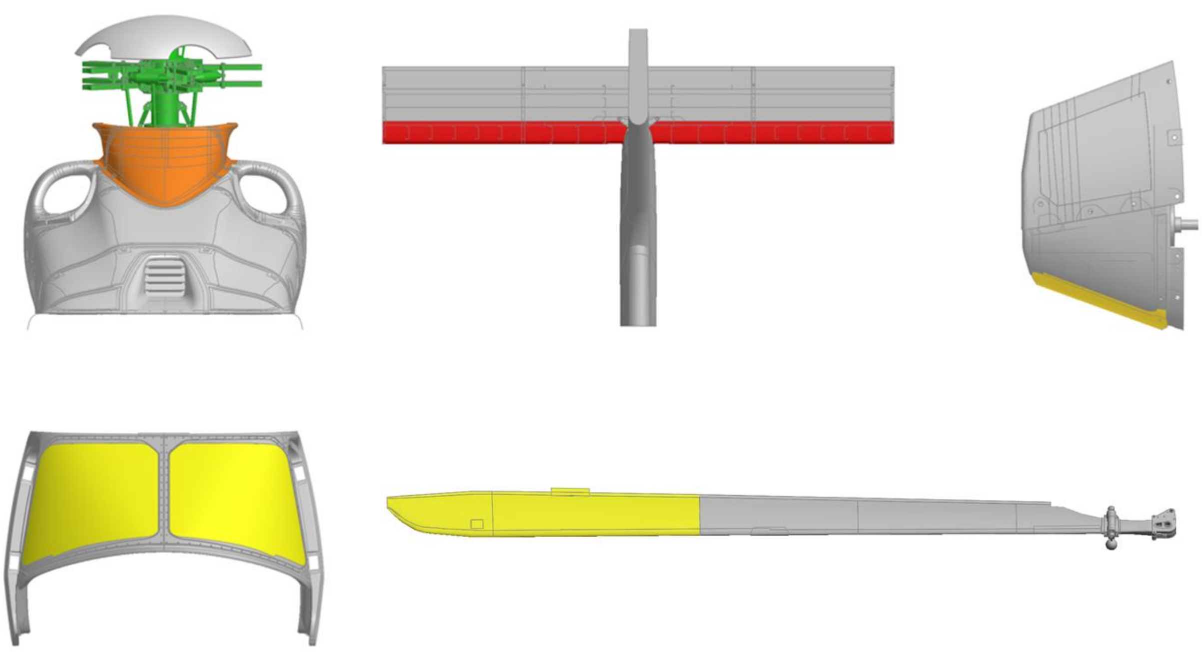

Figure 109. Summary of impact severity levels – Rotorcraft targets and quadcopter 2.7 lb. (RQ2.7).

Table 17. RQ2.7 mid-air collision simulation assessment – damage severity levels and fire risk.

| | | Case | Severity | Fire Risk |
|---|---|---|---|---|
| Mid-air collision Rotorcraft and Quadcopter 2.7 lb. (RQ2.7) | Front Cowling (Locations 1 and 2) | RQ2.7-C1H | Level 1 | No |
| | | RQ2.7-C1M | Level 2 | No |
| | | RQ2.7-C1C | Level 3 | No |
| | | RQ2.7-C2H | Level 1 | No |
| | | RQ2.7-C2M | Level 2 | No |
| | | RQ2.7-C2C | Level 2 | No |
| | Horizontal Stabilizer (Locations 1 and 2) | RQ2.7-H1H | Level 1 | No |
| | | RQ2.7-H1M | Level 3 | No |
| | | RQ2.7-H1C | Level 4 | No |
| | | RQ2.7-H2H | Level 1 | No |
| | | RQ2.7-H2M | Level 3 | No |
| | | RQ2.7-H2C | Level 4 | No |
| | Rear Servo | RQ2.7-R1H | Level 1 | No |
| | | RQ2.7-R1M | Level 1 | No |
| | | RQ2.7-R1C | Level 2 | No |
| | Windshield (Locations 1 and 2) | RQ2.7-W1H | Level 2 | No |
| | | RQ2.7-W1M | Level 2 | No |
| | | RQ2.7-W1C | Level 2 | No |
| | | RQ2.7-W2H | Level 1 | No |
| | | RQ2.7-W2M | Level 2 | No |
| | | RQ2.7-W2C | Level 2 | No |
| | Blade | RQ2.7-B1H | Level 2 | No |
| | | RQ2.7-B1M | Level 2 | No |
| | | RQ2.7-B1C | Level 2 | No |
| | *Tail Rotor | - | Level 4 | No |

Note: *Based on limited Component Level Testing

### 6.1.1 Cowling

The front cowling was impacted with the 2.7 lb. quadcopter model at two locations on the chimney surface. Location 1 was selected based on recommendations provided by the Industry Partner for bird strike analysis (proprietary data) and was chosen for the UAS to impact the center of the chimney resulting in a greater chance of secondary impact with the main rotorcraft rotor. The UAS impacts both cowling locations at three different velocities (hover, medium, and cruise), as explained in Chapter 5.1.2. According to the nomenclature defined in Chapter 5.1.1, location 1 cases are named RQ2.7-C1H, RQ2.7-C1M, and RQ2.7-C1C. Similarly, location 2 cases are RQ2.7-C2H, RQ2.7-C2M, and RQ2.7-C2C.

A fixed boundary condition on the lower part of the cowling was used to constrain the complete model. The impact velocity was determined by adding the UAS maximum speed and the rotorcraft speed. The resultant relative velocity was applied to the UAS body. Furthermore, the rotor assembly spun at an angular velocity of 298.5 rpm, according to the information specified by the Industry Partner for this 5-blade rotorcraft. A gravity body load was prescribed during the simulation to act on the UAS and the cowling.

- Location 1

Figure 110 shows the configuration corresponding to the location 1 case. Again, the UAS was oriented to impact with one motor first to cause the most damage to the structure (conservative analysis).

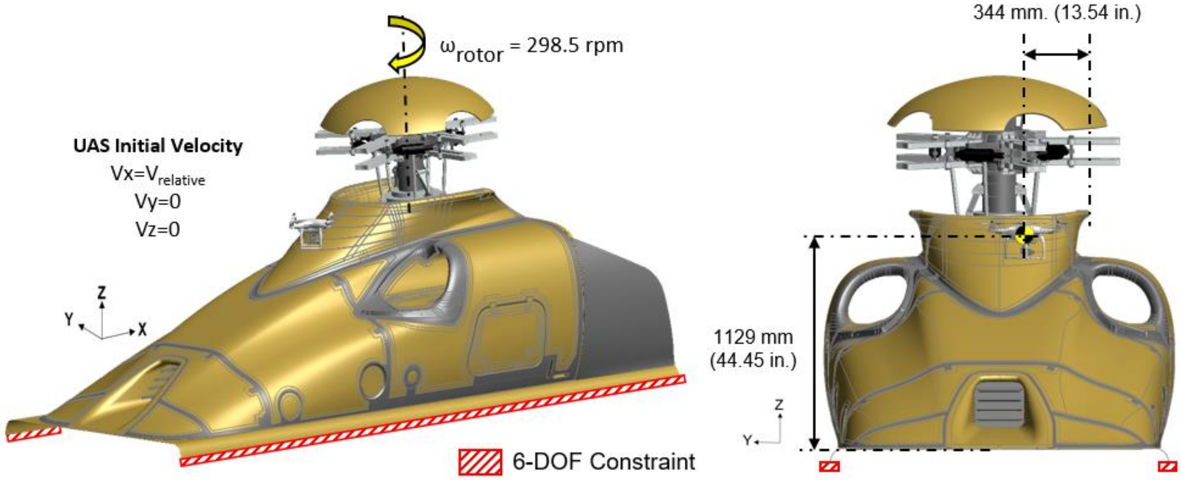


Figure 110. UAS quadcopter impact location 1 – Front cowling.

Figure 111 presents the isometric and side views of the simulation's last instant for the three velocity iterations. Cases are presented from lowest (left) to highest velocity (right). The UAS was deflected towards the rotor shaft assembly after colliding with the cowling surface.

Figure 112 shows the damage observed on the chimney (upper images) and the rotor shaft assembly (lower images). The chimney sustains more damage as the impact velocity increases. RQ2.7-C1H shows no damage to the honeycomb structure. RQ2.7-C1M indicates damage to the honeycomb (core crushing) and no failure of the composite skin. RQ2.7-H1C captures damage to the honeycomb and failure of the skin at the chimney's upper free edge. Thus, RQ2.7-C1H damage severity is level 1, RQ2.7-C1M of level 2, and RQ2.7-C1C of level 3.

The rotor shaft assembly presents no damage due to secondary impacts of the UAS debris. Therefore, the rotor shaft assembly damage severity was level 1 in all three cases.

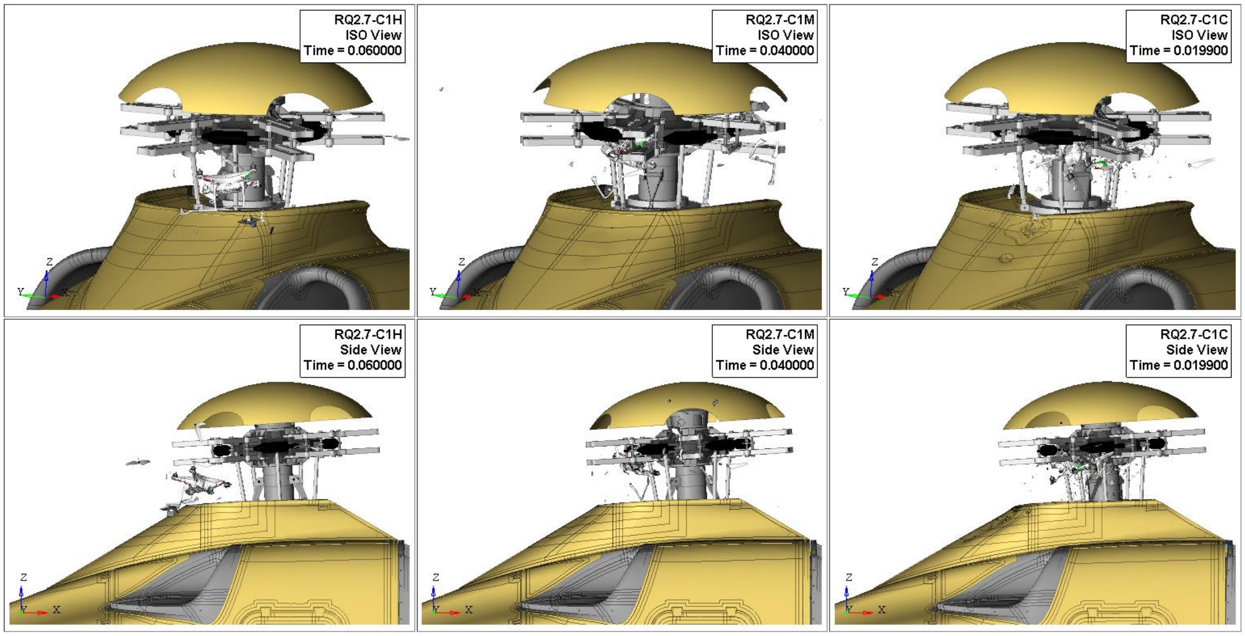


Figure 111. The final time of impact for RQ2.7-C1H, RQ2.7-C1M and RQ2.7-C1C (left to right).

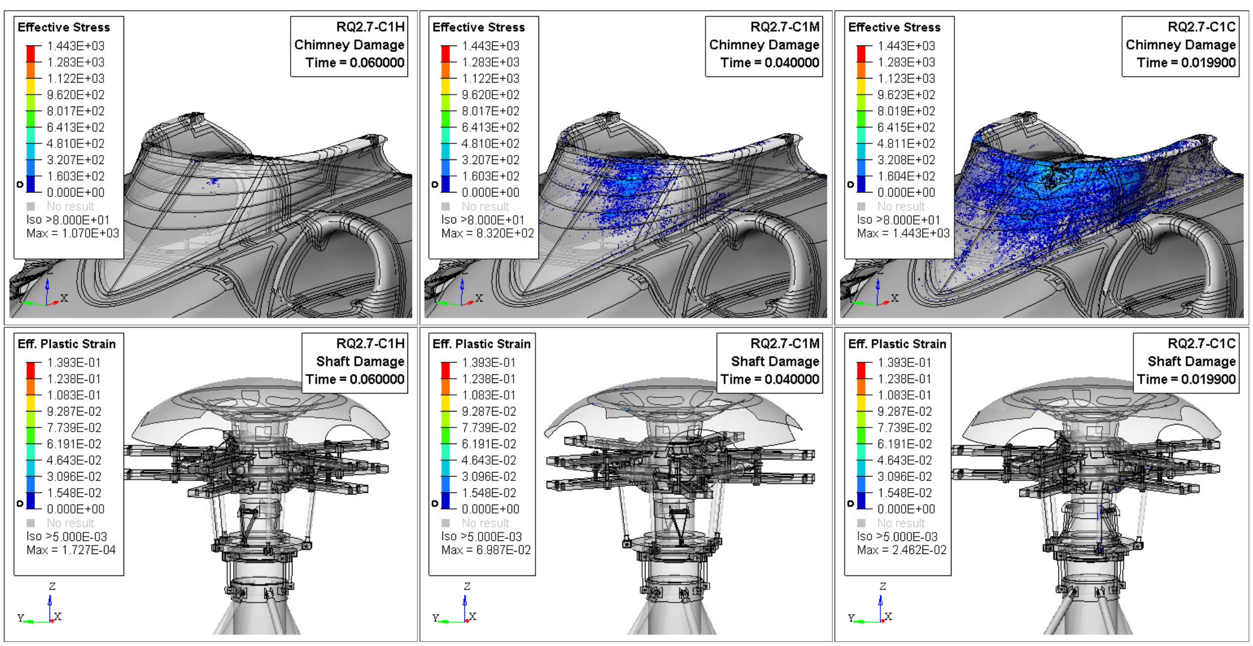


Figure 112. Chimney and rotor shaft damage for RQ2.7-C1H, RQ2.7-C1M and RQ2.7-C1C (left to right).

- <u>Location 2</u>

Figure 114 shows the configuration corresponding to the location 1 case. Again, the UAS was oriented to impact with one motor first to cause the most damage to the structure.

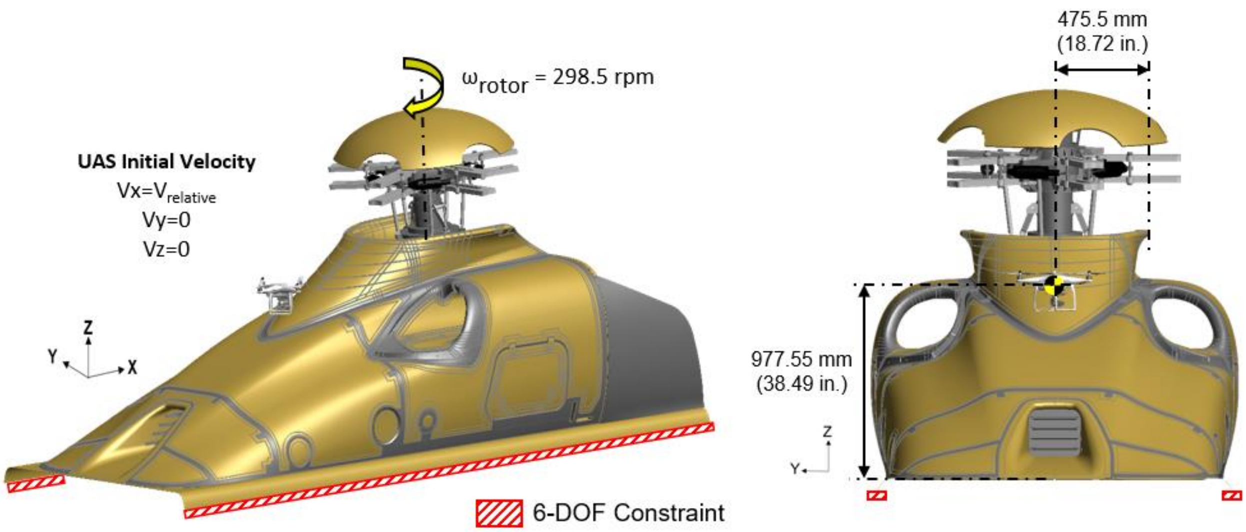


Figure 113. UAS quadcopter impact location 2 – Front cowling.

Figure 114 presents the isometric and side views of the simulation's last instant for the three velocity iterations. Cases are presented from lowest (left) to highest velocity (right). The UAS was deflected towards the rotor shaft assembly after colliding with the cowling surface.

Figure 115 shows the damage observed on the chimney (upper images) and the rotor shaft assembly (lower images). The chimney sustains more damage as the impact velocity increases. RQ2.7-C2H shows no damage to the honeycomb structure. RQ2.7-C2M and RQ2.7-H2C indicate damage to the honeycomb and no failure of the composite skin, showing more honeycomb damage for the cruise velocity. Thus, RQ2.7-C2H damage severity has been determined at level 1, and RQ2.7-C2M and RQ2.7-C2C damage severity is level 2.

The rotor shaft assembly presents no damage due to the secondary impact of the UAS debris. Therefore, the rotor shaft assembly damage severity was level 1 in all three cases.

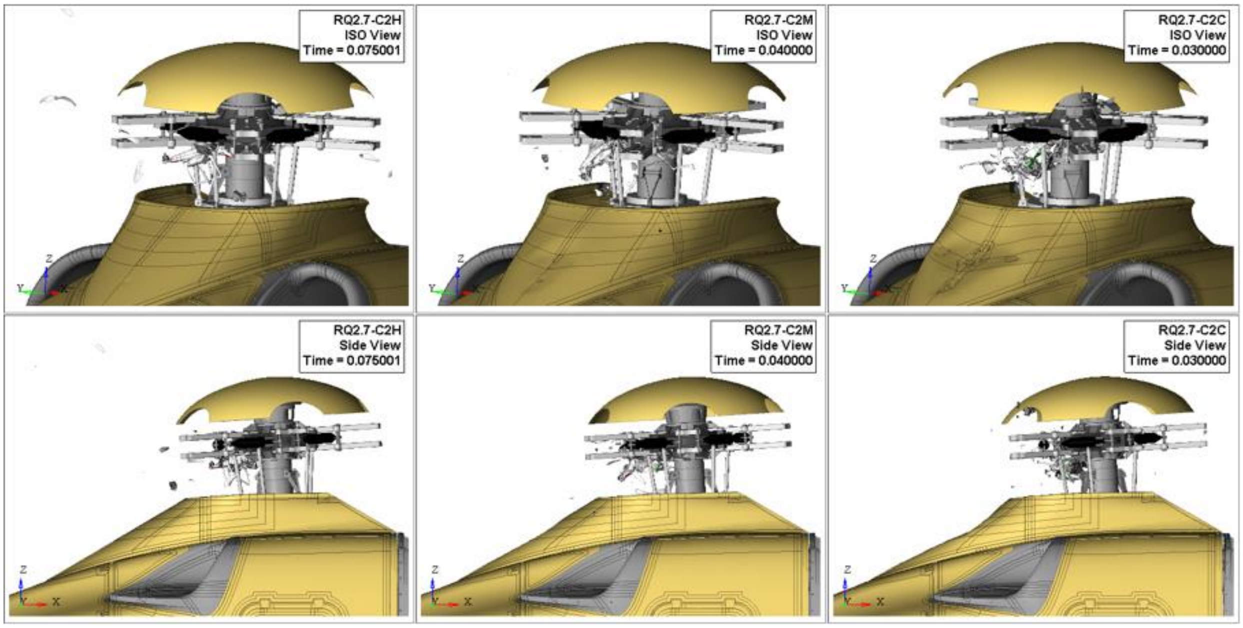


Figure 114. The final time of impact for RQ2.7-C2H, RQ2.7-C2M, and RQ2.7-C2C (left to right).

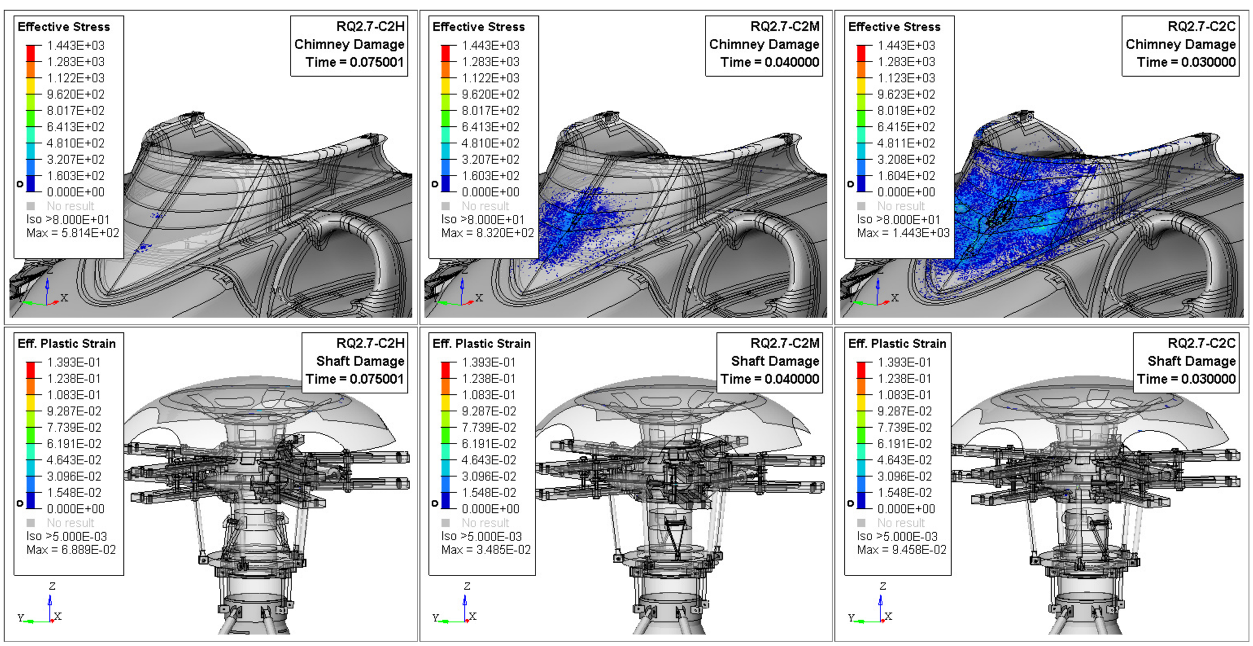


Figure 115. Chimney and rotor shaft damage for RQ2.7-C2H, RQ2.7-C2M, and RQ2.7-C2C (left to right).

6.1.2 Horizontal Stabilizer

The horizontal stabilizer was subjected to impact with the 2.7 lb. quadcopter model at two different leading-edge locations. Location 1 was selected in the middle of the horizontal stabilizer's leading edge. Location 2 was defined at the tip of the stabilizer to increase the moment arm. The UAS impacts both locations at three different velocities (hover, medium, and cruise), as discussed in Chapter 5.1.2. According to the nomenclature defined in Chapter 5.1.1, location 1 cases are named RQ2.7-H1H, RQ2.7-H1M, and RQ2.7-H1C. Similarly, location 2 cases are RQ2.7-H2H, RQ2.7-H2M, and RQ2.7-H2C.

A fixed boundary condition at the tail cone fuselage frame was used to constrain the complete model. The impact velocity was determined by adding the UAS maximum speed and the rotorcraft speed. The resultant relative velocity was applied to the UAS body. A gravity body load was prescribed during the simulation to act on the UAS and the horizontal stabilizer.

- Location 1

Figure 116 shows the impact configuration corresponding to location 1 cases. The UAS was oriented to impact with one motor first to cause the most damage to the airframe.

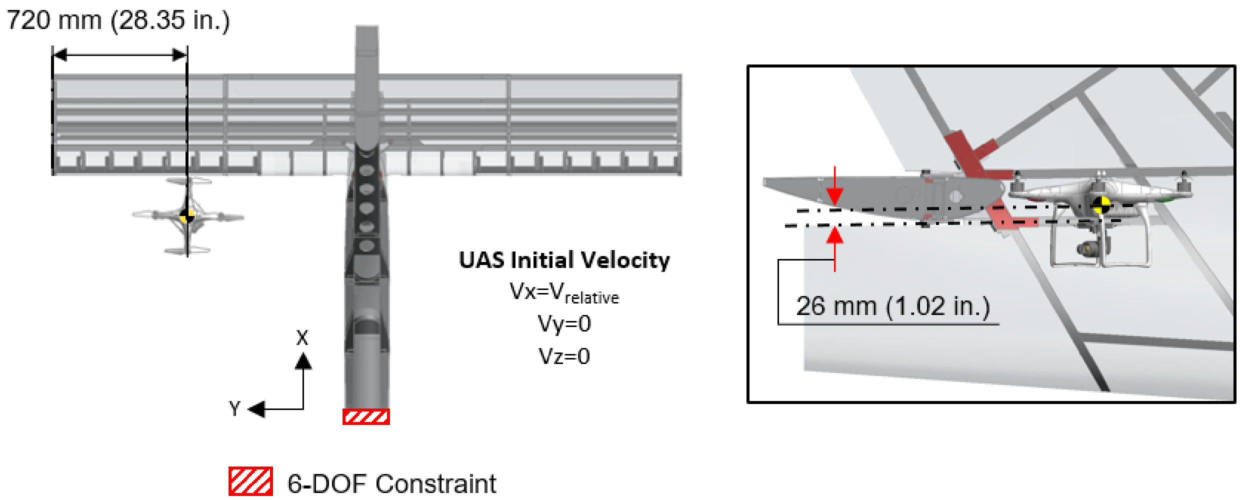


Figure 116. UAS quadcopter impact location 1 – Horizontal stabilizer.

Figure 117 shows the isometric and side views of the simulation's last instant for the three velocity iterations. Cases are presented from lowest (left) to highest velocity (right). In all three cases, the stabilizer rotates backward due to the UAS collision. The simulation also predicts the spring back motion of the stabilizer, which returned to its initial position after the impact.

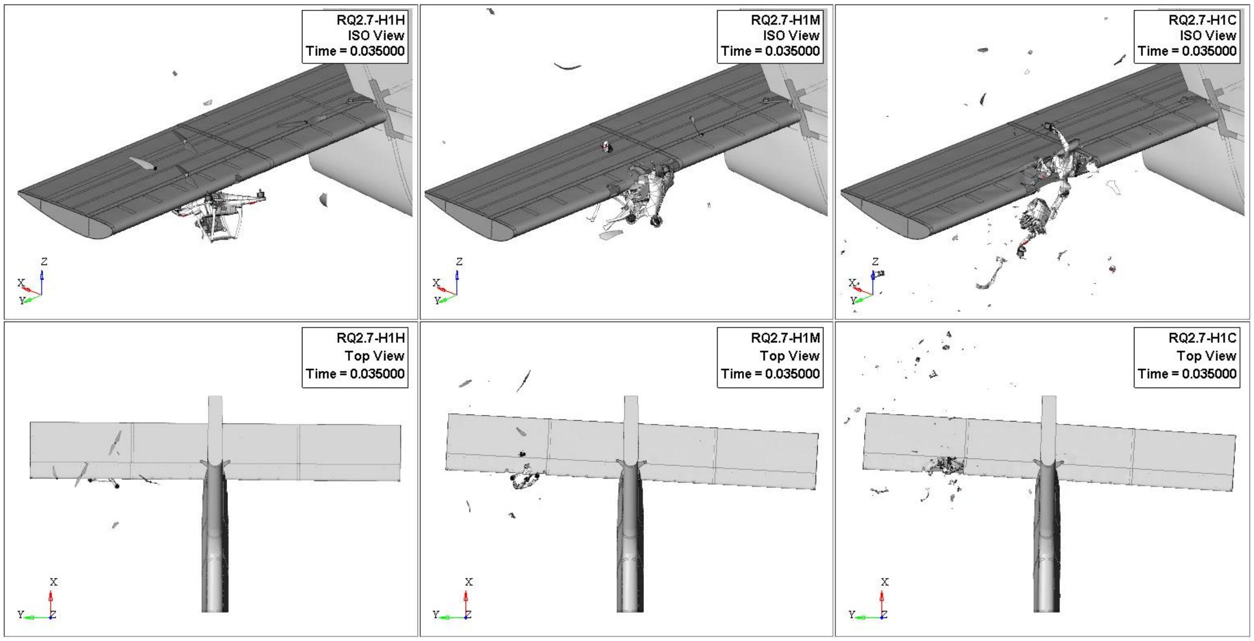


Figure 117. The final time of impact for RQ2.7-H1H, RQ2.7-H1M and RQ2.7-H1C (left to right).

Figure 118 shows the permanent deformation of the horizontal stabilizer's skin (upper images) and the internal components (lower images). The horizontal stabilizer assembly sustains more damage as the impact velocity increases. RQ2.7-H1H shows little damage to the skin and none to the internal components. RQ2.7-H1M presents rupture of the skin and permanent deformation at the closest nose rib. RQ2.7-H1C has a larger opening of the leading edge skin and indicates permanent deformation to the spar, which is considered a primary structural member. Thus, RQ2.7-H1H has a damage severity of level 1, RQ2.7-H1M has a damage severity of level 3, and RQ2.7-H1C is classified as level 4.

In addition, due to the backward deflection of the horizontal stabilizer during the impact, some permanent deformation was observed in the root region of the horizontal stabilizer, where the airframe is connected to the rest of the tail. The deformation was located near the large bolts that secure the stabilizer's connection and increase with the velocity of the impact. Figure 119 depicts the effective plastic strain of the horizontal stabilizer's root region.

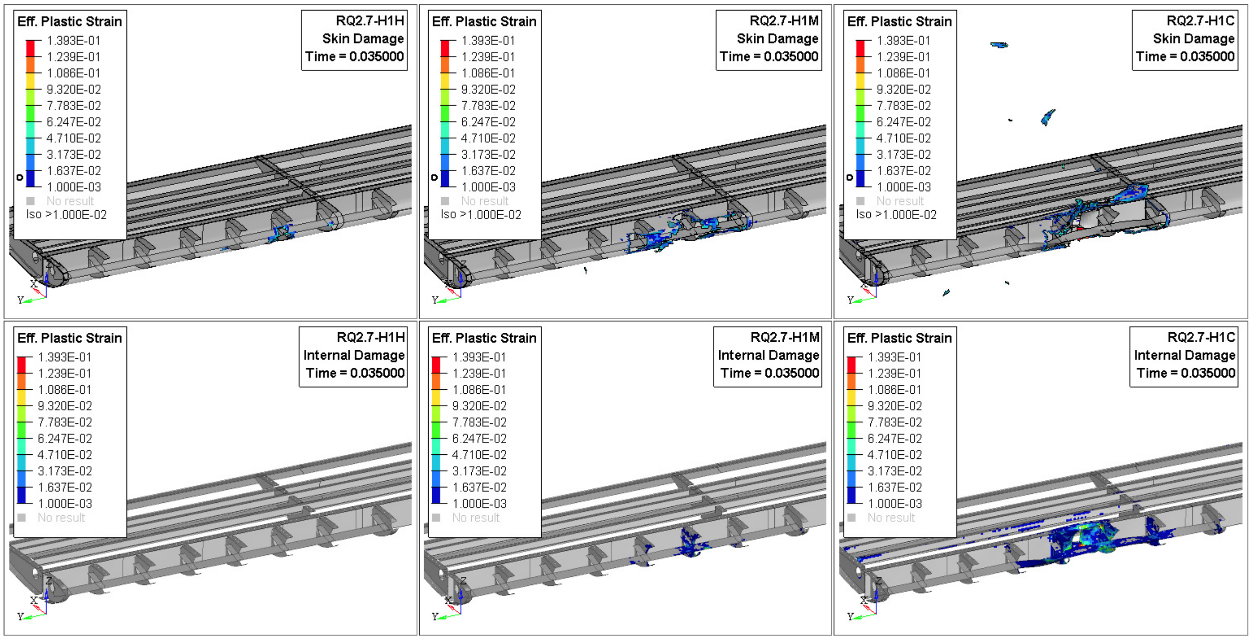


Figure 118. Skin and internal structures plastic strain for RQ2.7-H1H, RQ2.7-H1M and RQ2.7-H1C (left to right).

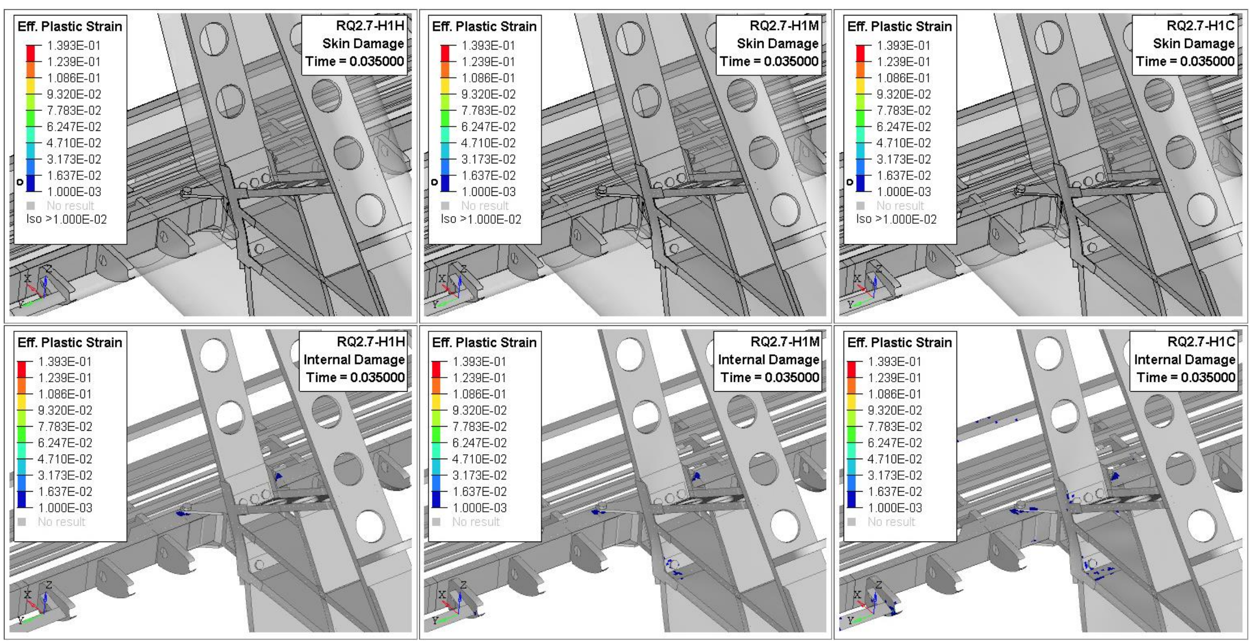


Figure 119. Skin and internal structures plastic strain at the tail root for RQ2.7-H1H, RQ2.7-H1M and RQ2.7-H1C (left to right).

- Location 2

Figure 120 shows the impact configuration corresponding to location 2 cases. The UAS was oriented to impact with one motor first to cause the most damage to the airframe.

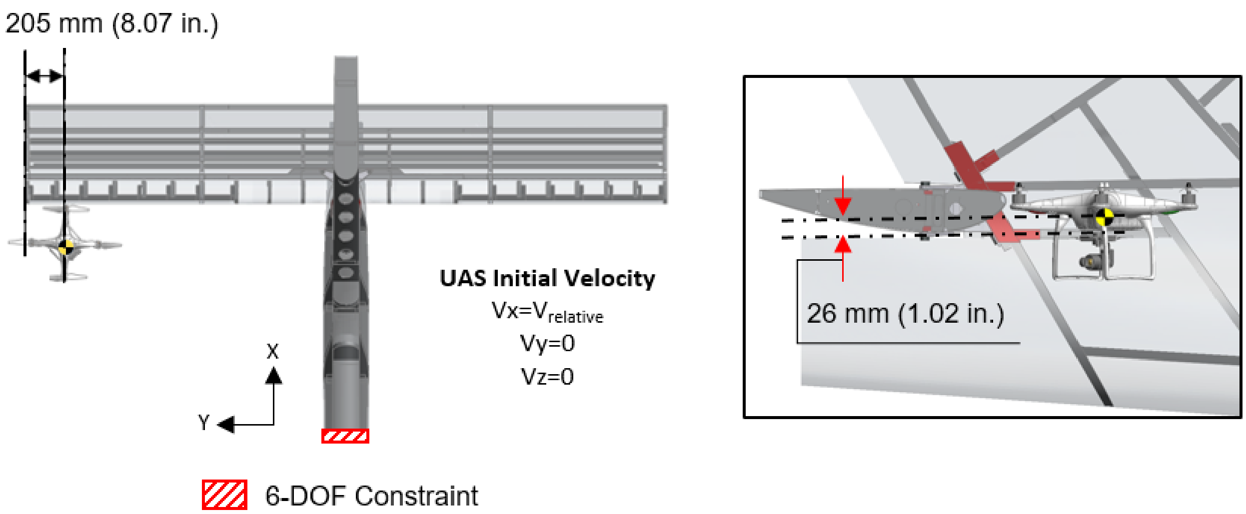


Figure 120. UAS quadcopter impact location 2 – Horizontal stabilizer.

Figure 121 shows the isometric and side views of the simulation's last instant for the three velocity iterations. Cases are presented from lowest (left) to highest velocity (right). In all three cases, the stabilizer rotates backward due to the UAS collision. The simulation also predicts the spring back motion of the stabilizer, which returned to its initial position after the impact.

Figure 122 shows the permanent deformation of the horizontal stabilizer's skin (upper images) and the internal components (lower images). The horizontal stabilizer assembly sustains more damage as the impact velocity increases. RQ2.7-H2H shows little damage to the skin and none to the internal components. RQ2.7-H2M presents rupture of the skin and permanent deformation of the closest nose ribs. RQ2.7-H2C has a larger opening of the leading edge skin and indicates permanent spar deformation, a primary structural member. Thus, RQ2.7-H2H has a damage severity of level 1, RQ2.7-H2M has a damage severity of level 3, and RQ2.7-H2C is classified as level 4.

In addition, due to the backward deflection of the horizontal stabilizer during the impact, some permanent deformation was observed in the root region of the horizontal stabilizer, where the airframe is connected to the rest of the tail. The deformation was located near the large bolts that secure the stabilizer's connection and increase with the velocity of the impact. Figure 123 depicts the effective plastic strain of the horizontal stabilizer's root region.

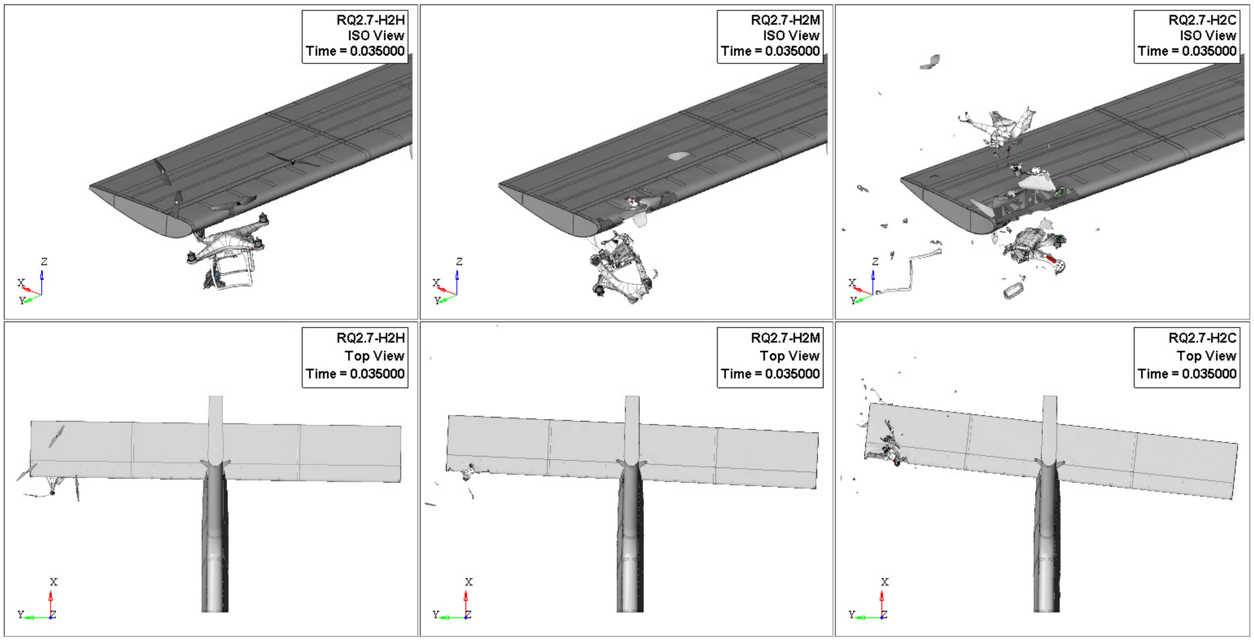


Figure 121. The final impact time for RQ2.7-H2H, RQ2.7-H2M, and RQ2.7-H2C (left to right).

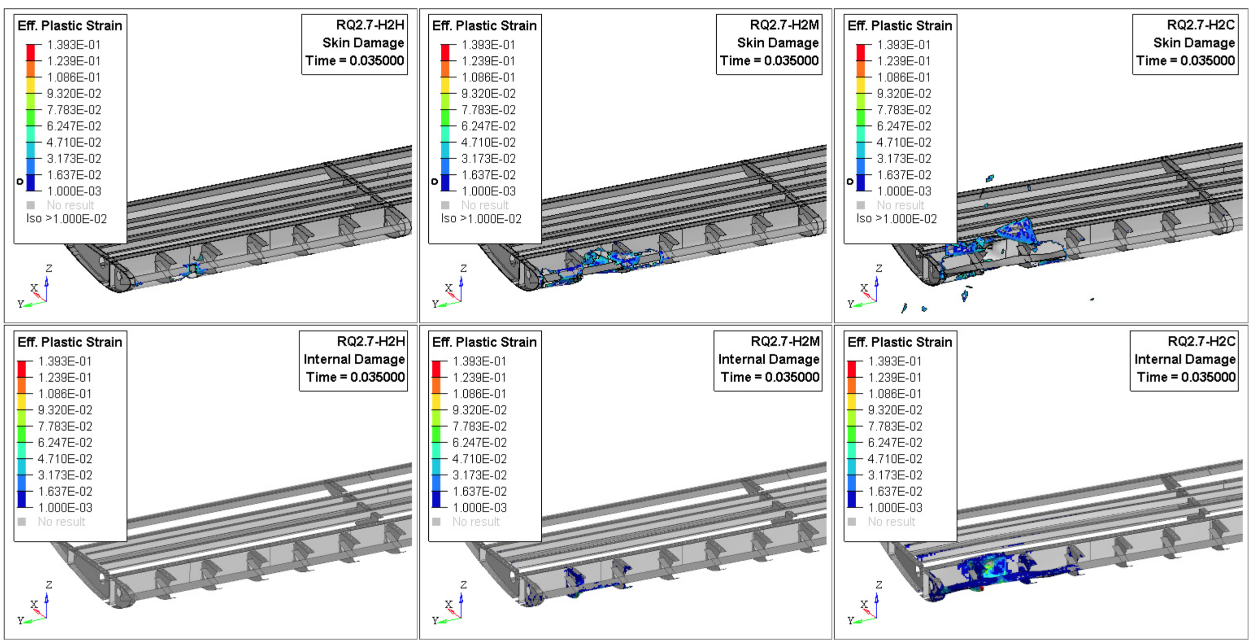


Figure 122. Skin and internal structures plastic strain for RQ2.7-H2H, RQ2.7-H2M, and RQ2.7-H2C (left to right).

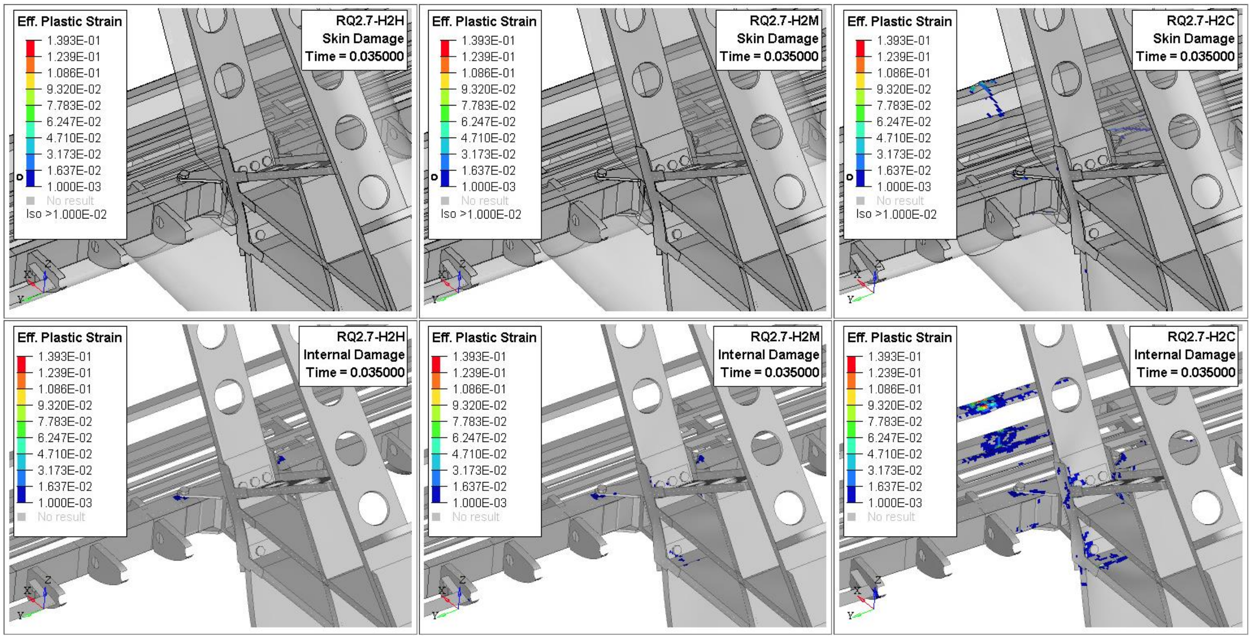

Figure 123. Skin and internal structures plastic strain at the tail root for RQ2.7-H2H, RQ2.7-H2M, and RQ2.7-H2C (left to right).

### 6.1.3 Rear Servo

The rear servo was subjected to impact with the 2.7 lb. quadcopter UAS model. The impact location was selected based on the bird strike data provided by the Industry (proprietary data). The UAS impacts the front leading-edge at three different velocities (hover, medium, and cruise), as discussed in Chapter 5.1.2. According to the nomenclature defined in Chapter 5.1.1, the rear servo cases are named RQ2.7-R1H, RQ2.7-R1M, and RQ2.7-R1C.

A fixed boundary condition at the servo root area was used to constrain the complete model. The impact velocity was determined by adding the UAS maximum speed and the rotorcraft speed. The resultant relative velocity was applied to the UAS body. A gravity body load was prescribed during the simulation to act on the UAS and the rear servo.

Figure 124 shows the analysis setup corresponding to the only rear servo impact location. The UAS was oriented to impact with one motor first to cause the most damage possible.

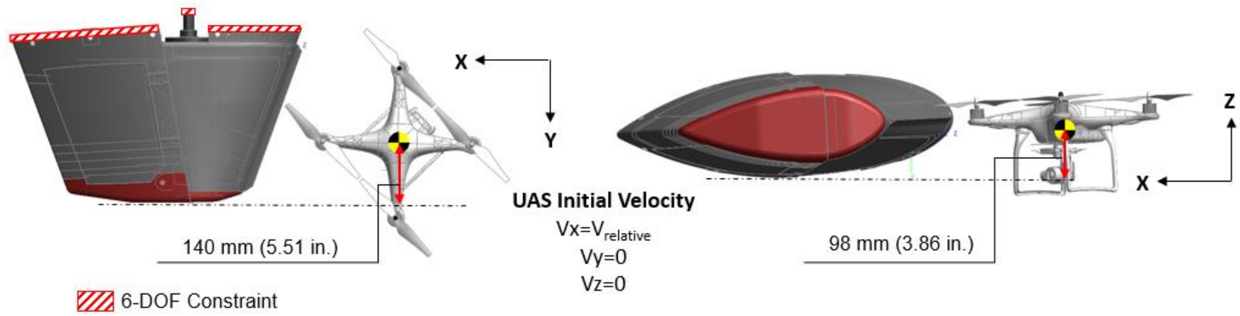


Figure 124. UAS quadcopter critical impact location 1 – Rear servo.

Figure 125 shows the isometric and side views of the simulation's last instant for the three velocity iterations. Again, cases are presented from lowest (left) to highest velocity (right). Again, the rear servo could sustain the impact with the quadcopter, and no indications of failure of the leading edge skin were observed.

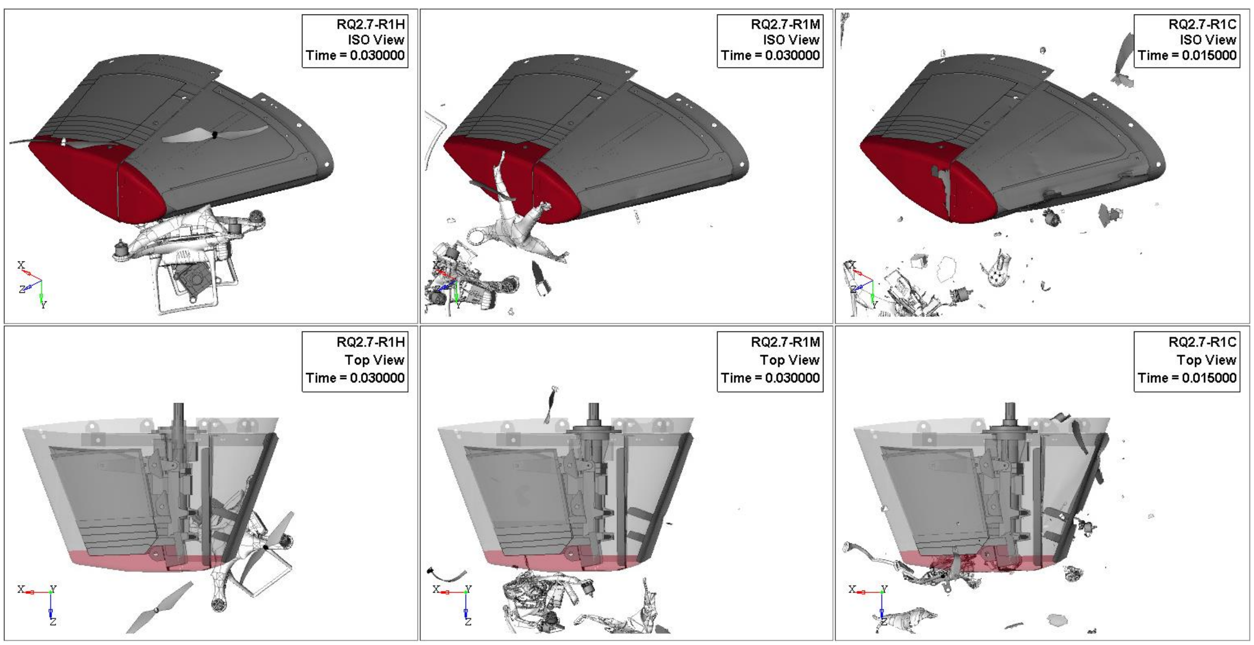


Figure 125. The final time of impact for RQ2.7-R1H, RQ2.7-R1M and RQ2.7-R1C (left to right).

Figure 126 shows the damage to the servo skin (upper images) and the internal structure (lower images). RQ2.7-R1H shows no permanent deformation of the skin and internal structure. Likewise, RQ2.7-R1M indicates little permanent deformation to the skin and internal structure. However, RQ2.7-R1C presents large skin permanent deformation and localized damage to the nose ribs. Thus, RQ2.7-H1H and RQ2.7-H1M have a damage severity of level 1 and RQ2.7-H1C of level 2.

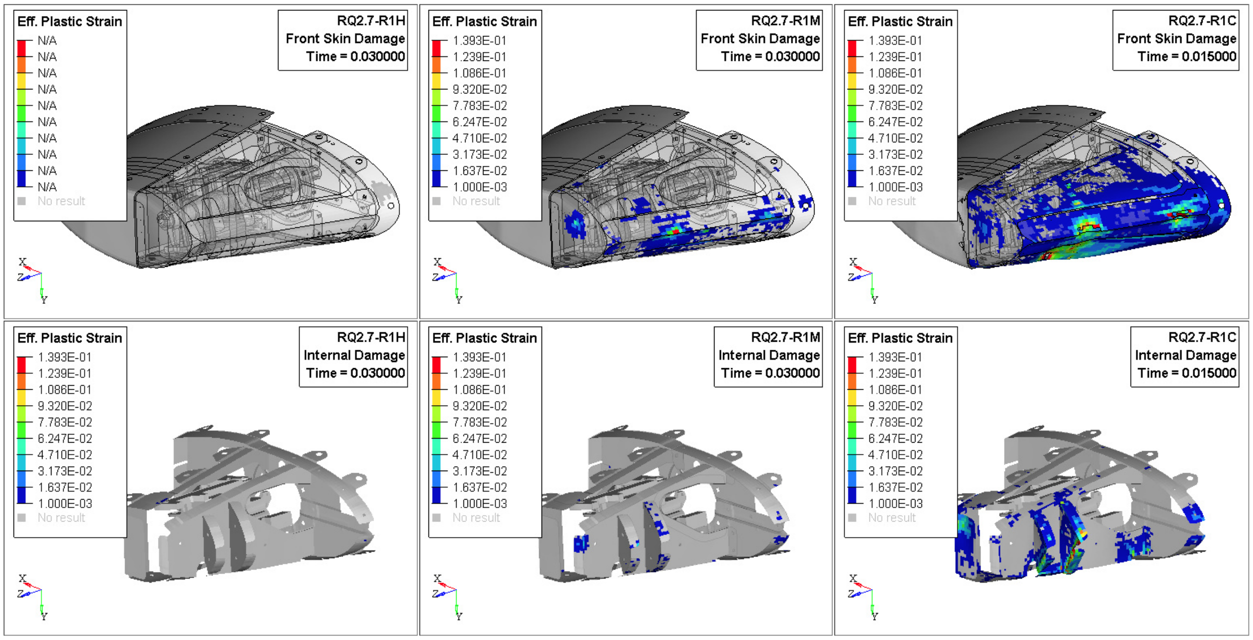


Figure 126. Skin and internal structures plastic strain for RQ2.7-R1H, RQ2.7-R1M and RQ2.7-R1C (left to right).

### 6.1.4 Windshield

The bilayer windshield was impacted by the 2.7 lb. quadcopter at two different locations. Location 1 was defined at the center of the windshield, while location 2 was selected closer to the frame, near the top right corner of the windshield. The UAS impacts both windshield locations at three different velocities (hover, medium, and cruise), as introduced in Chapter 5.1.2. According to the nomenclature defined in Chapter 5.1.1, location 1 cases are named RQ2.7-W1H, RQ2.7-W1M, and RQ2.7-W1C. Similarly, location 2 cases are RQ2.7-W2H, RQ2.7-W2M, and RQ2.7-W2C.

A fixed boundary condition at the rear and lower end of the frame was used to constrain the complete model. Also, the composite frame's lower front end was constrained along the vertical direction based on the feedback provided by Industry Partner. The impact velocity was determined by adding the UAS maximum speed and the rotorcraft speed. The resultant relative velocity was applied to the UAS body. A gravity body load was prescribed during the simulation to act on the UAS and the windshield.

- Location 1

Figure 127 shows the impact configuration corresponding to location 1. The UAS was oriented to impact with one motor first to cause the most damage to the windshield.

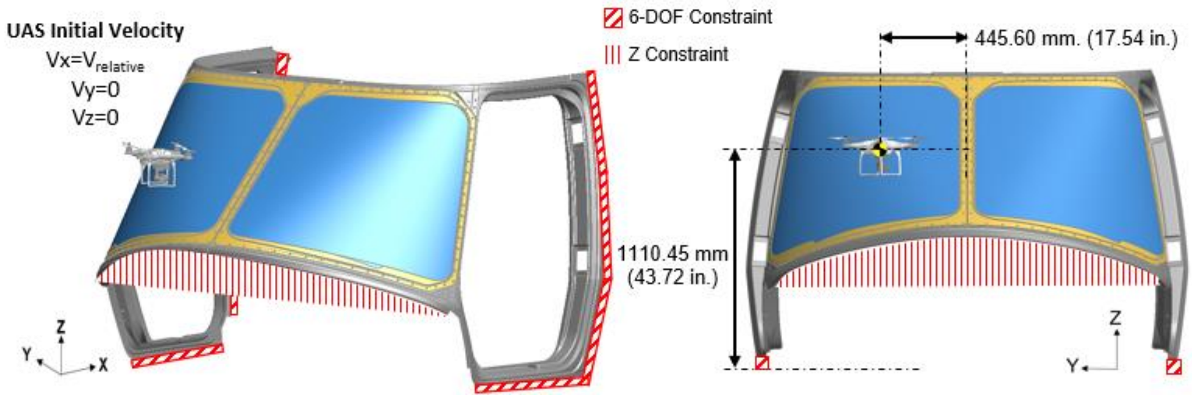


Figure 127. UAS quadcopter impact location 1 – Windshield.

Figure 128 shows the isometric and side views of the simulation's last instant for the three velocity iterations. Figure 129 presents the front and rear windshield view of the simulation's last frame. The images present the lowest (left) cases to the highest velocity (right). The rear view indicates that none of the UAS components penetrated the windshield.

Figure 130 depicts the damage to the outer (upper images) and the inner (lower images) windshield layers for the location 1 impact cases. The windshield shows more damage as the velocity increases. RQ2.7-W1H contains a localized scratch on the outer layer. RQ2.7-W1M shows shattering of the windshield outer layer and partial damage to the inner layer. RQ2.7-W1C captured a larger shattering of the outer layer, which propagated to the entire surface of the windscreen. There is also damage to the inner layer. The UAS did not penetrate the cockpit in any of the cases. Thus, RQ2.7-W1H, RQ2.7-W1M and RQ2.7-W1C have a damage severity of level 2.

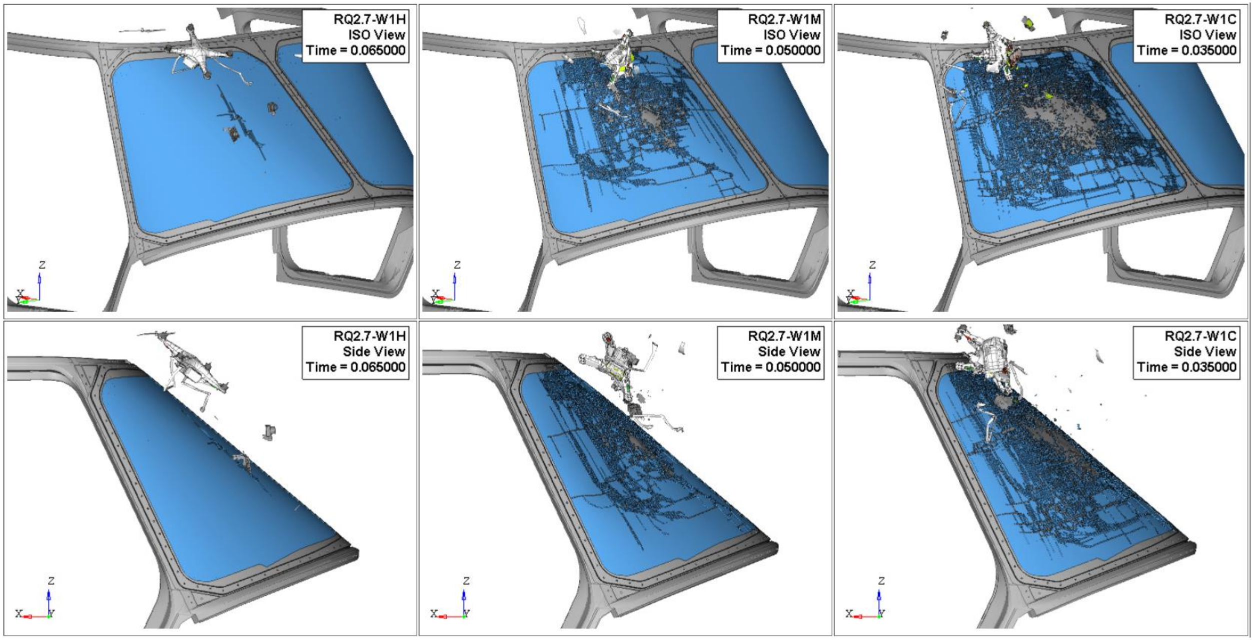


Figure 128. The final time of impact for RQ2.7-W1H, RQ2.7-W1M and RQ2.7-W1C (left to right) – Isometric and side views.

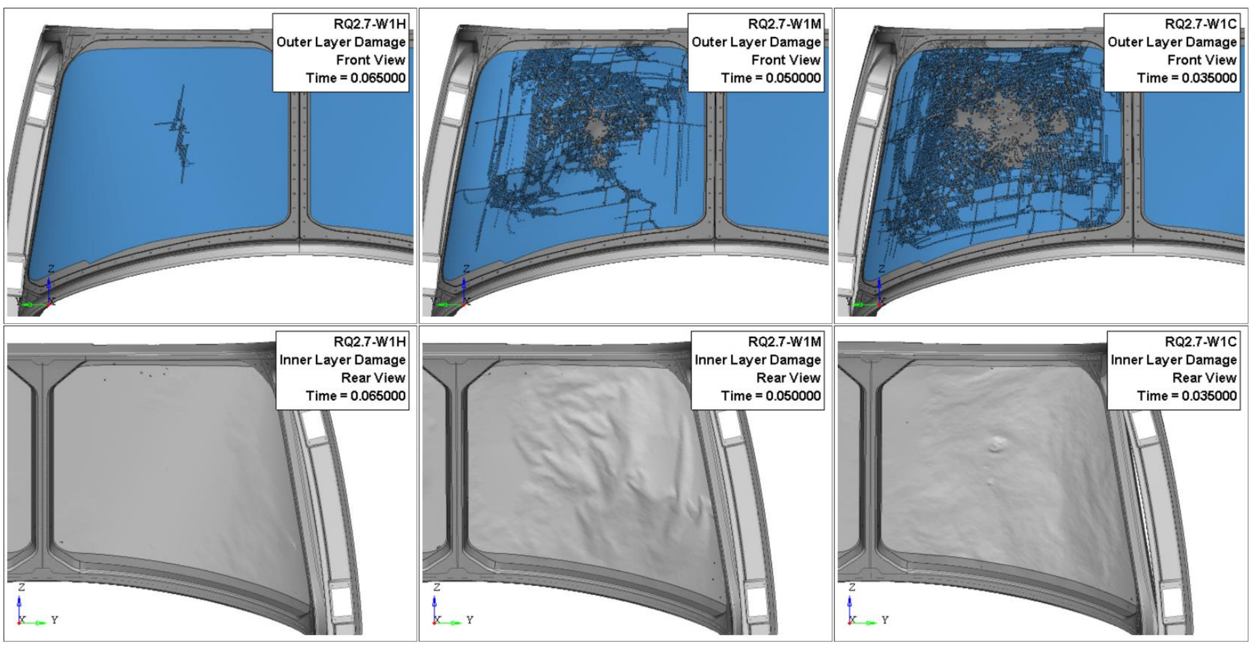


Figure 129. The final time of impact for RQ2.7-W1H, RQ2.7-W1M and RQ2.7-W1C (left to right) – Front and rear view.

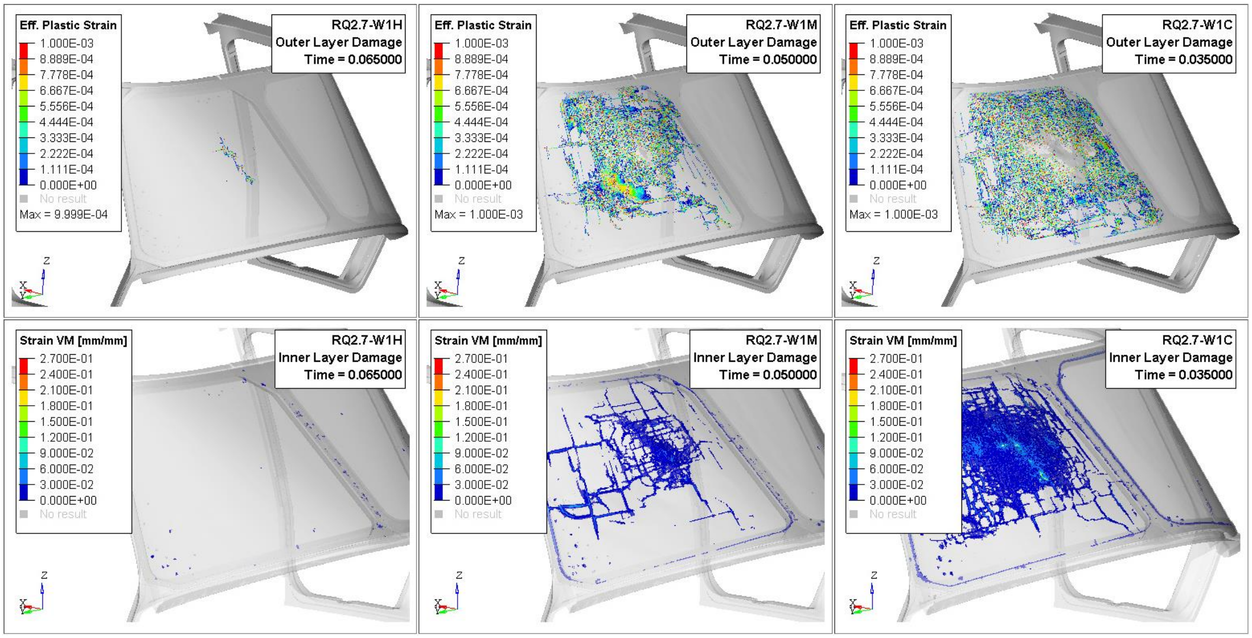


Figure 130. Outer and inner layer damage for RQ2.7-W1H, RQ2.7-W1M and RQ2.7-W1C (left to right).

- Location 2

Figure 131 shows the impact configuration corresponding to location 2. The UAS was oriented to impact with one motor first to cause the most damage to the windshield.

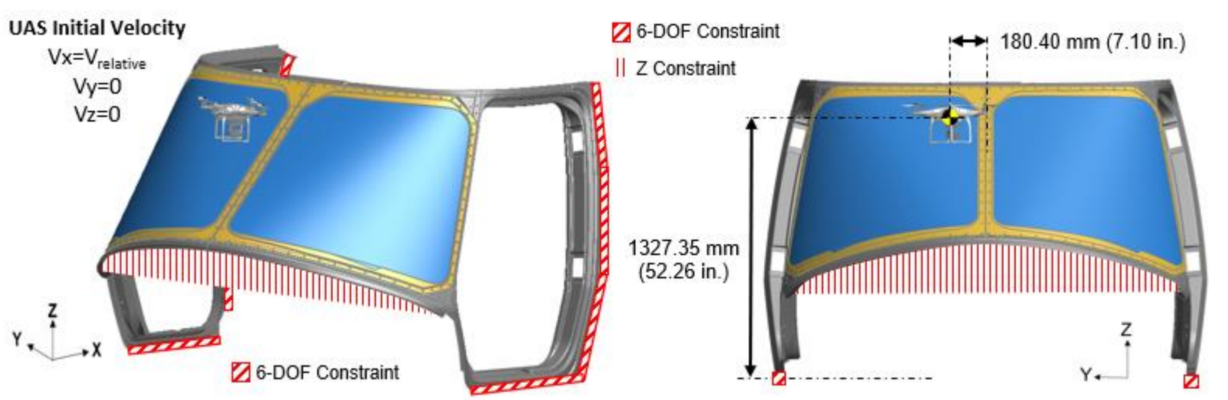


Figure 131. UAS quadcopter impact location 2 – Windshield.

Figure 132 shows the isometric and side views of the simulation's last instant for the three velocity iterations. Figure 133 presents the front and rear windshield view of the simulation's last frame. The images present the lowest (left) cases to the highest velocity (right). The rear view indicates that none of the UAS components penetrated the windshield.

Figure 134 depicts the damage to the outer (upper images) and the inner (lower images) windshield layers for the location 2 impact cases. The windshield shows more damage as the velocity increases. RQ2.7-W2H contains a small localized scratch on the outer layer near the impact location with the UAS. RQ2.7-W2M shows shattering of the upper area of the windshield outer layer and damage to the inner layer. RQ2.7-W2C captured a larger shattering of the outer layer, which propagated to the middle and upper region of the windscreen. There is also damage to the inner layer. The UAS did not penetrate the cockpit in any of the cases. Thus, RQ2.7-W2H damage severity has been determined of level 1. RQ2.7-W2M and RQ2.7-W2C captured damage severity of level 2.

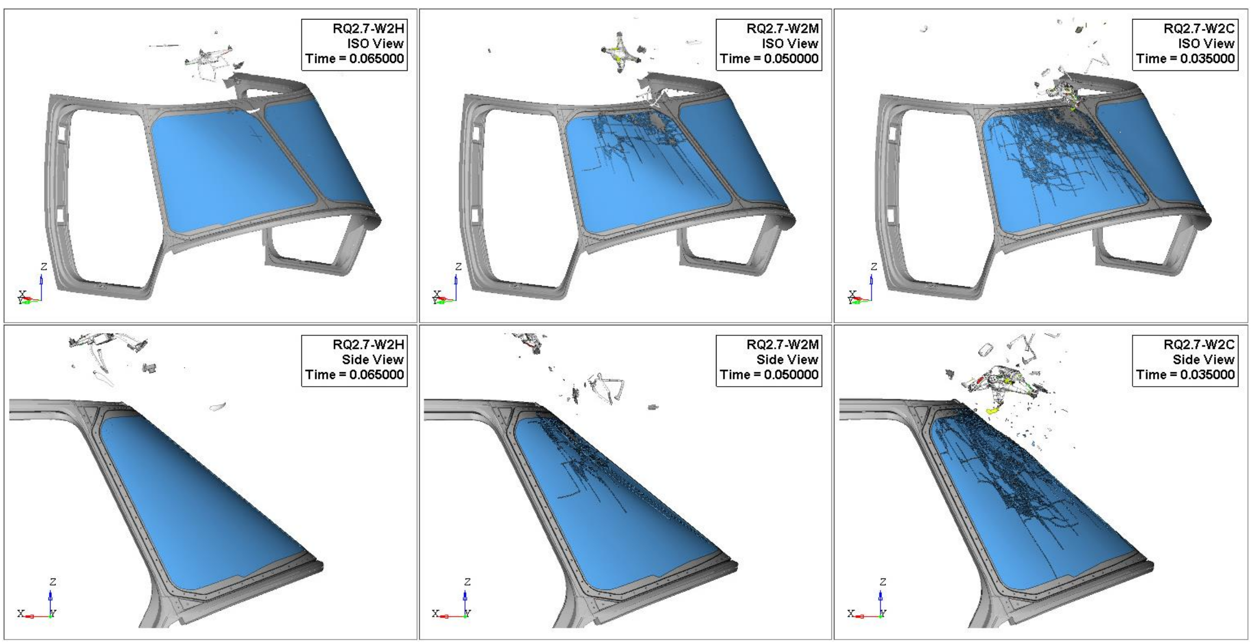


Figure 132. The final time of impact for RQ2.7-W2H, RQ2.7-W2M, and RQ2.7-W2C (left to right) – Isometric and side views.

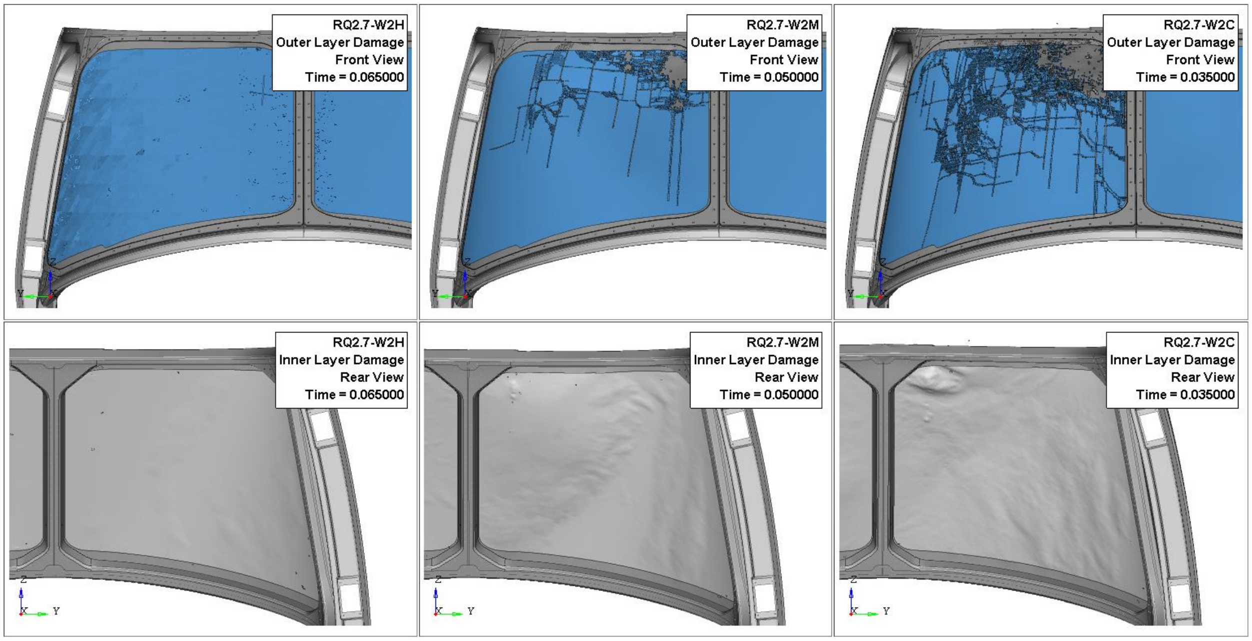


Figure 133. The final time of impact for RQ2.7-W2H, RQ2.7-W2M, and RQ2.7-W2C (left to right) – Front and rear views.

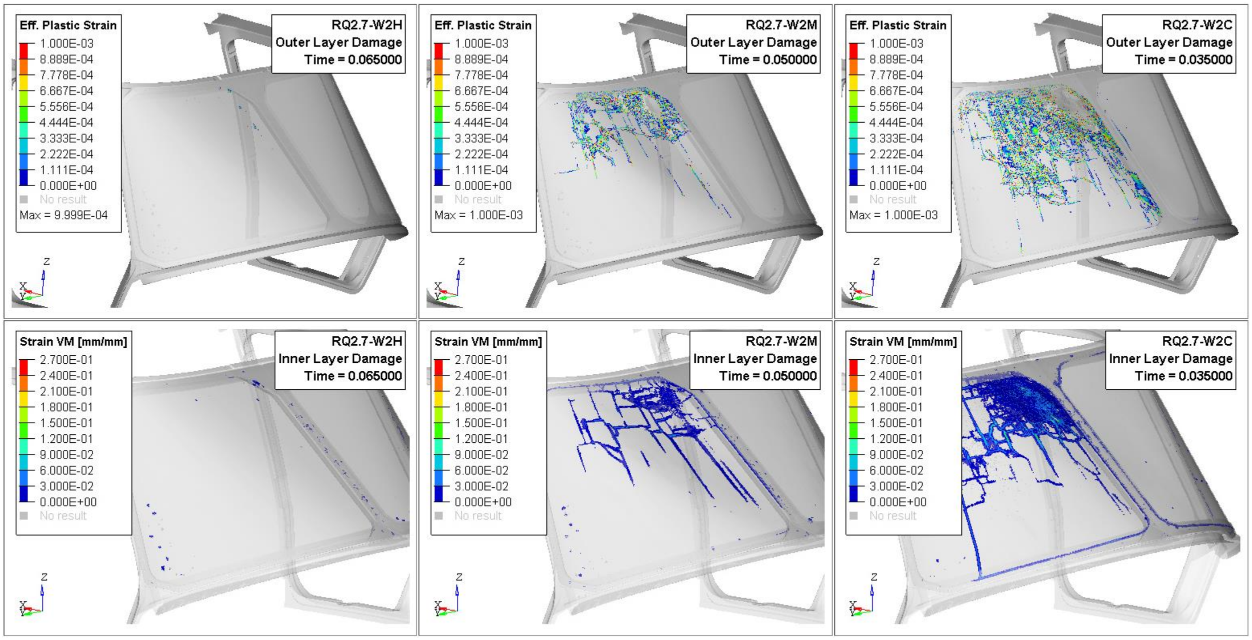


Figure 134. Outer and inner layer damage for RQ2.7-W2H, RQ2.7-W2M, and RQ2.7-W2C (left to right).

### 6.1.5 Main Rotor Blade

The rotor blade leading edge was subjected to impact with the 2.7 lb. quadcopter model at a location near the blade tip. Location 1 was selected based on the probability of the impact occurrence with a high-speed rotating blade. The UAS impacts the blade leading edge at three different velocities (hover, medium, and cruise), as explained in Chapter 5.1.2. According to the nomenclature defined in Chapter 5.1.1, location 1 cases are named RQ2.7-B1H, RQ2.7-B1M, and RQ2.7-B1C.

The blade root handle was connected to a revolute joint. The revolute joint was constrained in 5-DOF, allowing rotation only about the vertical axis (z-axis). The impact velocity was determined by adding the UAS maximum speed and the rotorcraft speed. The resultant relative velocity was applied to the UAS. Furthermore, the rotor blade spun at an angular velocity of 383 rpm, which is representative of this type of helicopter. A gravity body load was prescribed during the simulation to act on the UAS and the blade. Also, the simulation implemented all the blade contact definitions validated at the full-scale test level in Chapter 4.

Figure 135 shows the impact configuration corresponding to location 1. The UAS was oriented to impact with one motor first to cause the most damage to the structure.

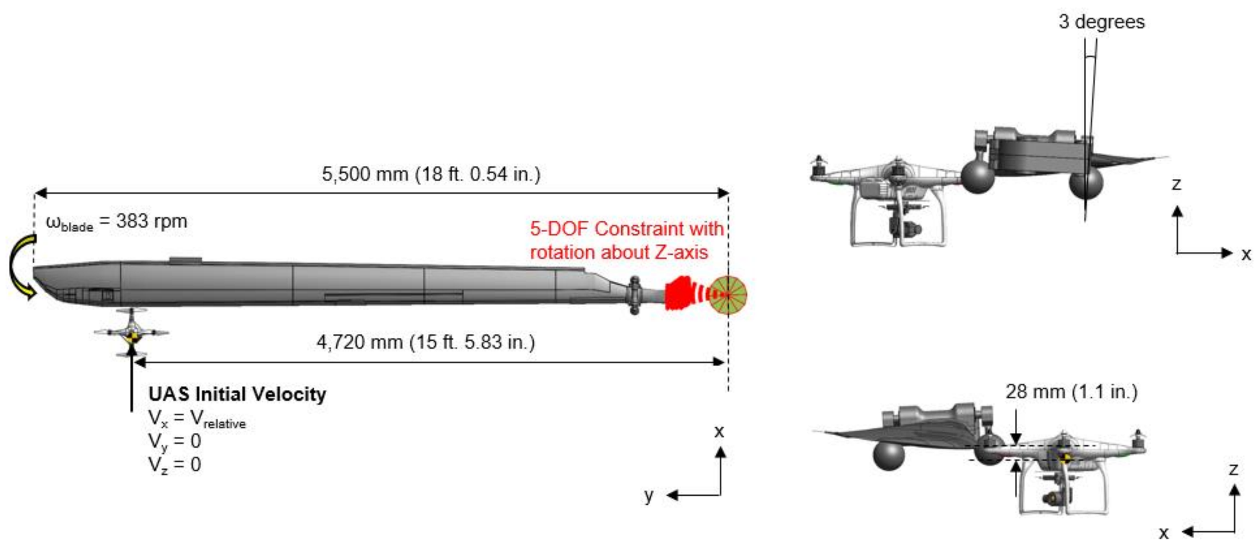


Figure 135. UAS quadcopter impact location 1 – Main rotor blade.

Figure 136 presents the isometric and top views of the simulation's last instant for the three velocity iterations. Cases are presented from lowest (left) to highest velocity (right). The UAS was sliced and broken into pieces during the collision with the blade's leading edge.

Figure 137 shows the damage observed on the blade leading edge (upper images) and the blade cross-section at the impact location (lower images). RQ2.7-B1H shows the minimal damage to the leading edge and debonding of the skin close to the trailing edge. RQ2.7-B1M and RQ2.7-B1C present deeper leading edge indentations that indicate more damage to the leading edge as the impact velocity increases. Moreover, skin debonding was noticed in the Medium and Cruise cases. It is important to note that the skin debonding was observed in the physical tests presented in Chapter 4.4. The large-scale simulation cases capture this behavior in agreement with the test results; however, due to the limitations of the FE model to capture this type of interface interaction after the initiation of the skin separation, the size and propagation of the skin separation must be treated as a conservative approach. Thus, based on the damage severity described in Table 15, all three cases have a damage severity of level 2.

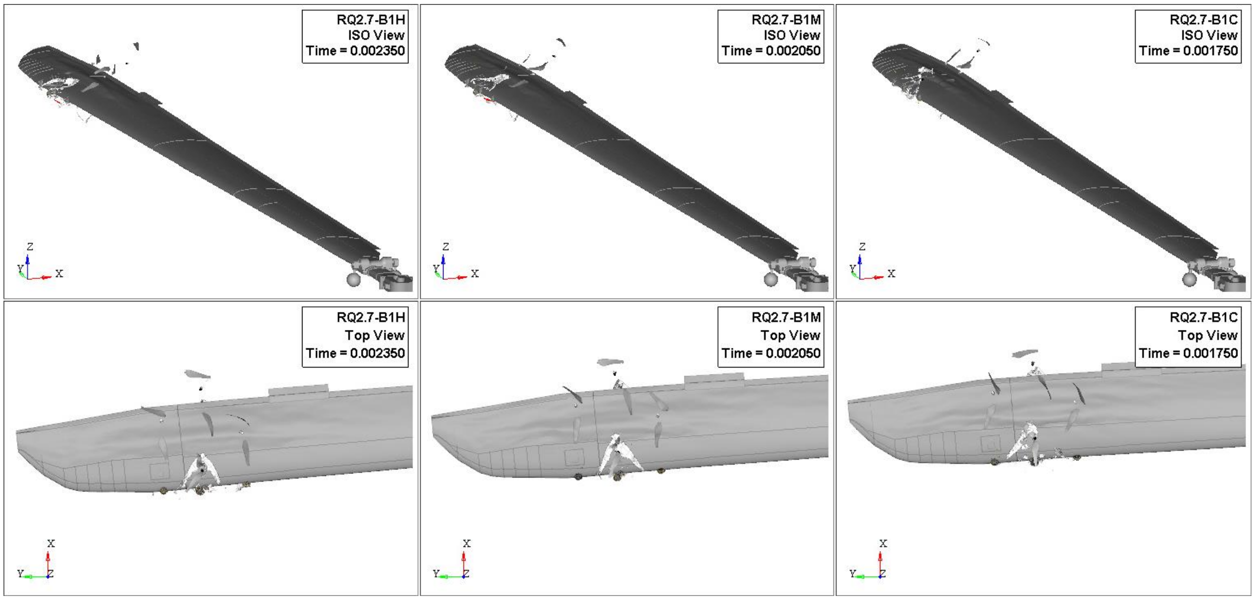


Figure 136. The final time of impact for RQ2.7-B1H, RQ2.7-B1M and RQ2.7-B1C (left to right).

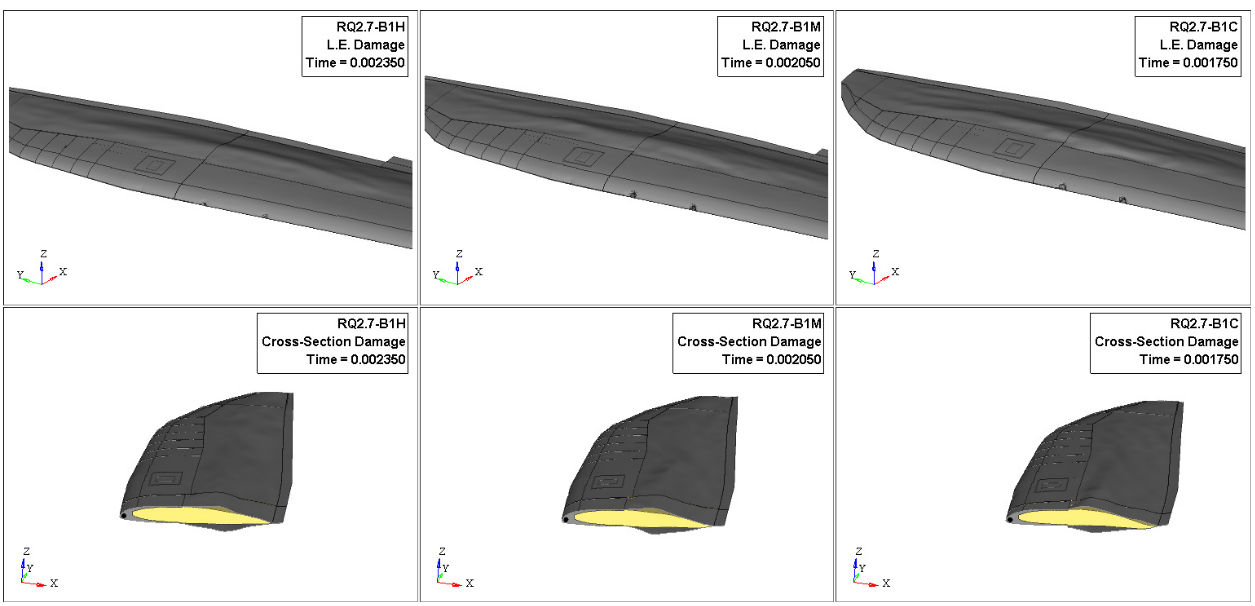


Figure 137. Leading-edge and cross-section damage for RQ2.7-B1H, RQ2.7-B1M and RQ2.7-B1C (left to right).

## 6.2 FIXED WING 4.0 LB.

This chapter presents the results of the airborne collision studies for the 4.0 lb. UAS fixed-wing and the rotorcraft components. The target impact areas introduced in Chapter 5 are the front cowling, horizontal stabilizer, rear servo, windshield, and main rotor blade. Figure 138 illustrates the highest damage severity level observed on each target. In general, it can be noticed that the damage sustained by the rotorcraft component increases with the impact velocity. For example, the horizontal stabilizer and windshield cases captured level 4 damage at cruise speed. The front cowling location 1 impact at cruise speed shows level 3 damage to the cowling and level 1 to the rotor shaft structure (secondary impact). The rear servo and the blade cases have level 2 damage at cruise speed. Table 18 summarizes the damage severity level evaluation and fire risk assessment of the 4.0 lb. fixed-wing impact cases.

Table 18 also includes the damage severity assessment of the tail rotor according to the findings from testing. As shown in APPENDIX B, the component level test results indicate the probability of a level 4 damage. Further work will be required in the future to conduct full-scale tests or simulation of the tail rotor.

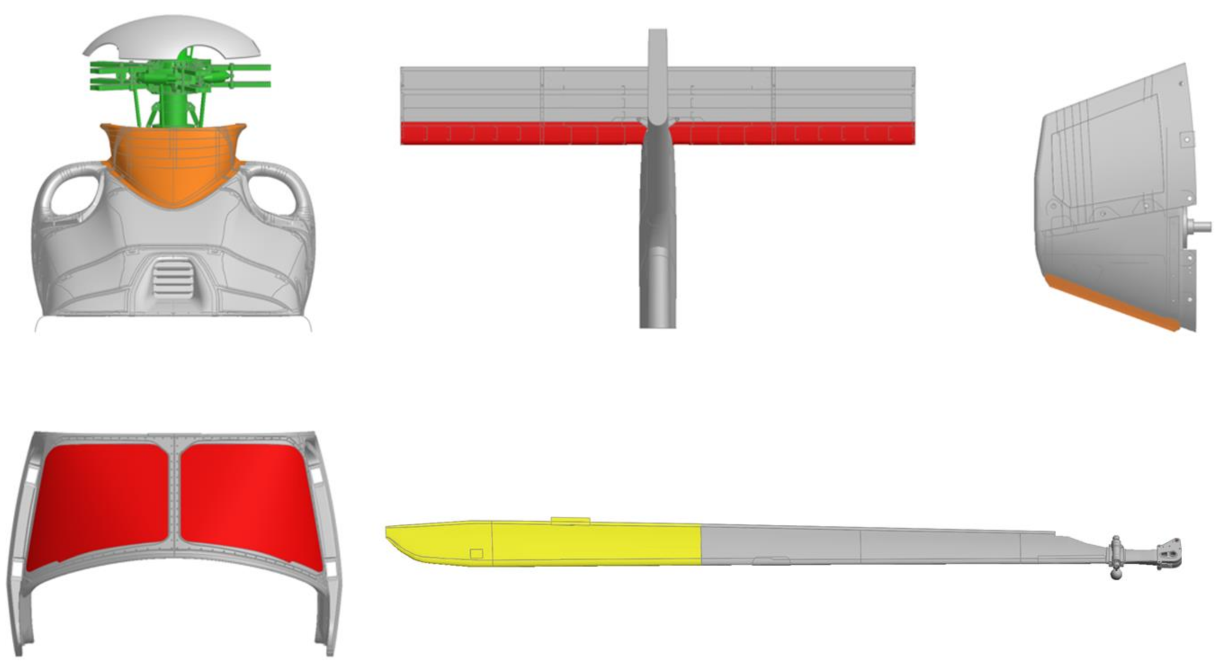

Figure 138. Summary of impact severity levels – Rotorcraft targets and fixed-wing 4.0 lb. (RF4.0).

Table 18. RF4.0 mid-air collision simulation assessment – damage severity levels and fire risk.

<table>
<tr><th></th><th></th><th>Case</th><th>Severity</th><th>Fire Risk</th></tr>
<tr><td rowspan="25">Mid-air collision Rotorcraft and Fixed-Wing 4.0 lb. (RF4.0)</td><td rowspan="6">Front Cowling (Locations 1 and 2)</td><td>RF4.0-C1H</td><td>Level 2</td><td>No</td></tr>
<tr><td>RF4.0-C1M</td><td>Level 2</td><td>No</td></tr>
<tr><td>RF4.0-C1C</td><td>Level 3</td><td>No</td></tr>
<tr><td>RF4.0-C2H</td><td>Level 2</td><td>No</td></tr>
<tr><td>RF4.0-C2M</td><td>Level 2</td><td>No</td></tr>
<tr><td>RF4.0-C2C</td><td>Level 3</td><td>No</td></tr>
<tr><td rowspan="6">Horizontal Stabilizer (Locations 1 and 2)</td><td>RF4.0-H1H</td><td>Level 2</td><td>No</td></tr>
<tr><td>RF4.0-H1M</td><td>Level 3</td><td>No</td></tr>
<tr><td>RF4.0-H1C</td><td>Level 4</td><td>Yes</td></tr>
<tr><td>RF4.0-H2H</td><td>Level 2</td><td>No</td></tr>
<tr><td>RF4.0-H2M</td><td>Level 3</td><td>No</td></tr>
<tr><td>RF4.0-H2C</td><td>Level 4</td><td>Yes</td></tr>
<tr><td rowspan="3">Rear Servo</td><td>RF4.0-R1H</td><td>Level 1</td><td>No</td></tr>
<tr><td>RF4.0-R1M</td><td>Level 2</td><td>No</td></tr>
<tr><td>RF4.0-R1C</td><td>Level 3</td><td>No</td></tr>
<tr><td rowspan="6">Windshield (Locations 1 and 2)</td><td>RF4.0-W1H</td><td>Level 2</td><td>No</td></tr>
<tr><td>RF4.0-W1M</td><td>Level 4</td><td>No</td></tr>
<tr><td>RF4.0-W1C</td><td>Level 4</td><td>Yes</td></tr>
<tr><td>RF4.0-W2H</td><td>Level 2</td><td>No</td></tr>
<tr><td>RF4.0-W2M</td><td>Level 4</td><td>No</td></tr>
<tr><td>RF4.0-W2C</td><td>Level 4</td><td>Yes</td></tr>
<tr><td rowspan="3">Blade</td><td>RF4.0-B1H</td><td>Level 2</td><td>No</td></tr>
<tr><td>RF4.0-B1M</td><td>Level 2</td><td>No</td></tr>
<tr><td>RF4.0-B1C</td><td>Level 2</td><td>No</td></tr>
<tr><td>*Tail Rotor</td><td>-</td><td>Level 4</td><td>No</td></tr>
</table>

Note: *Based on limited Component Level Testing

### 6.2.1 Cowling

The front cowling was impacted with the 4.0 lb. fixed-wing model at two locations on the chimney surface. Location 1 was selected based on recommendations provided by the Industry Partner for bird strike analysis (proprietary data). Location 2 was chosen for the UAS to impact the chimney's center, resulting in a greater chance of secondary impact with the main rotorcraft rotor. The UAS impacts both cowling locations at three different velocities (hover, medium, and cruise), as explained in Chapter 5.1.2. According to the nomenclature defined in Chapter 5.1.1, location 1 cases are named RF4.0-C1H, RF4.0-C1M, and RF4.0-C1C. Similarly, location 2 cases are RF4.0-C2H, RF4.0-C2M, and RF4.0-C2C.

A fixed boundary condition on the lower part of the cowling was used to constrain the complete model. The impact velocity was determined by adding the UAS maximum speed and the rotorcraft speed. The resultant relative velocity was applied to the UAS body. Furthermore, the rotor assembly spun at an angular velocity of 298.5 rpm, according to the information specified by the Industry Partner for this 5-blade rotorcraft. A gravity body load was prescribed during the simulation to act on the UAS and the cowling.

- Location 1

Figure 139 shows the configuration corresponding to the location 1 case. The UAS was oriented to impact with one motor first to cause the most damage to the structure.

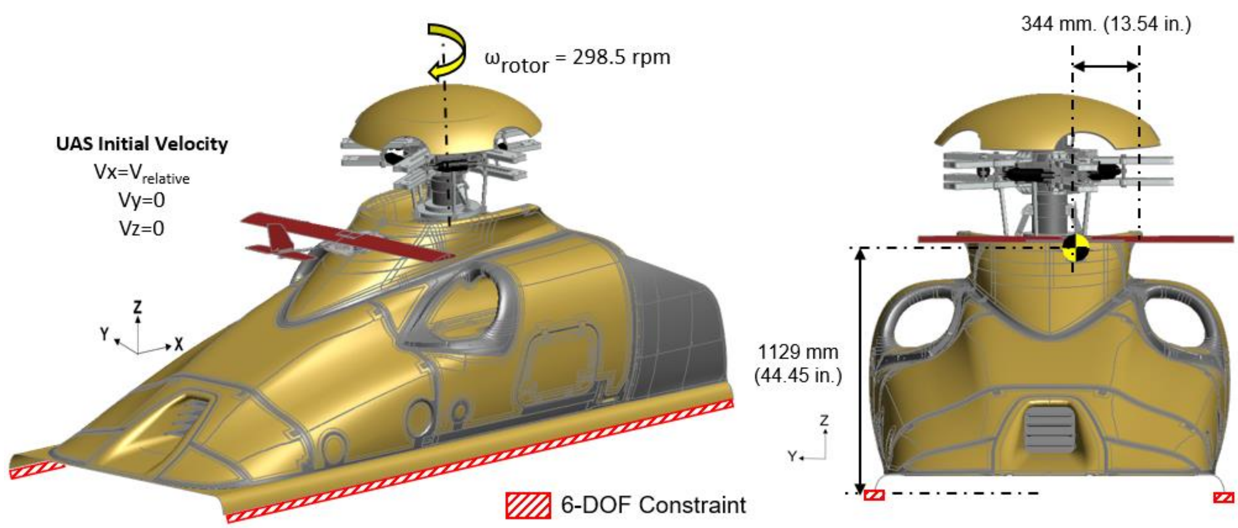


Figure 139. UAS fixed-wing critical impact location 1 – Front cowling.

Figure 139 presents the isometric and side views of the simulation’s last instant for the three velocity iterations. Cases are presented from lowest (left) to highest velocity (right). The UAS was deflected towards the rotor shaft assembly after colliding with the cowling surface.

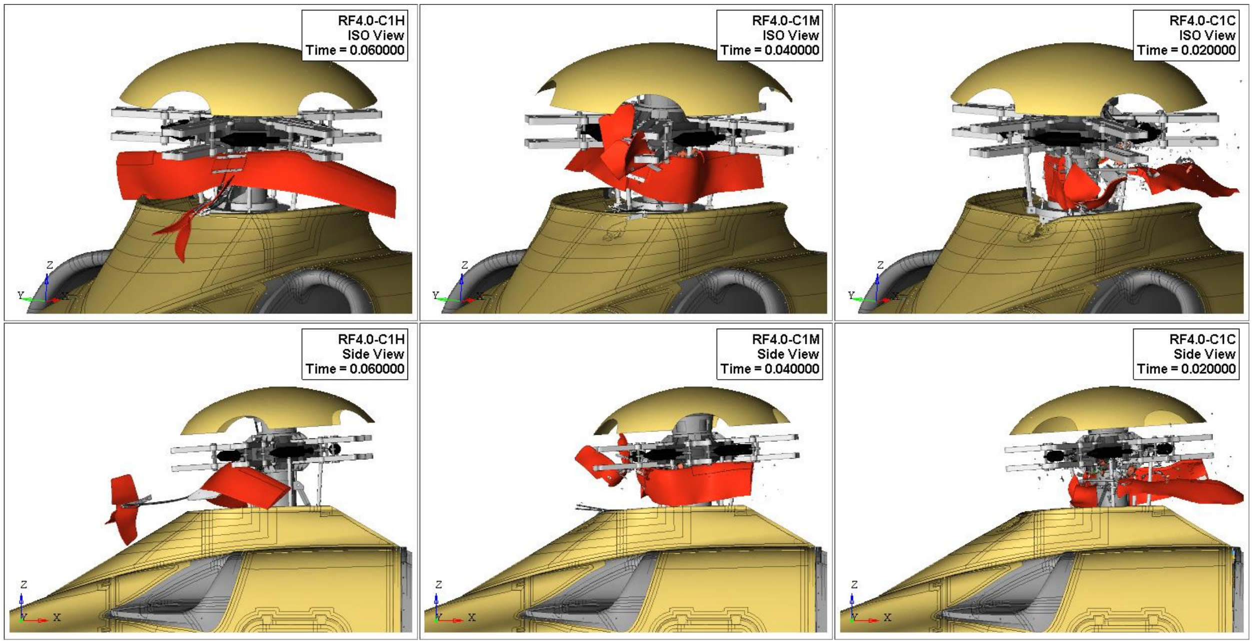


Figure 140. The final time of impact for RF4.0-C1H, RF4.0-C1M and RF4.0-C1C (left to right).

Figure 141 shows the damage observed on the chimney (upper images) and the rotor shaft assembly (lower images). The chimney sustains more damage as the impact velocity increases. RF4.0-C1H shows no damage to the honeycomb structure (core crushing). RF4.0-C1M indicates damage to the honeycomb and no failure of the composite skin. RF4.0-H1C captures damage to the honeycomb and failure of the skin at the chimney’s upper free edge. Thus, RF4.0-C1H and RF4.0-C1M have damage severity of level 2 and RF4.0-C1C of level 3.

Regarding the rotor shaft's secondary impact, RF4.0-C1C shows little permanent deformation to one of the rotor pitch links. Therefore, the secondary impact damage severity to the rotor was classified as level 1 for RF4.0-C1H and RF4.0-C1M, and level 2 for RF4.0-C1C

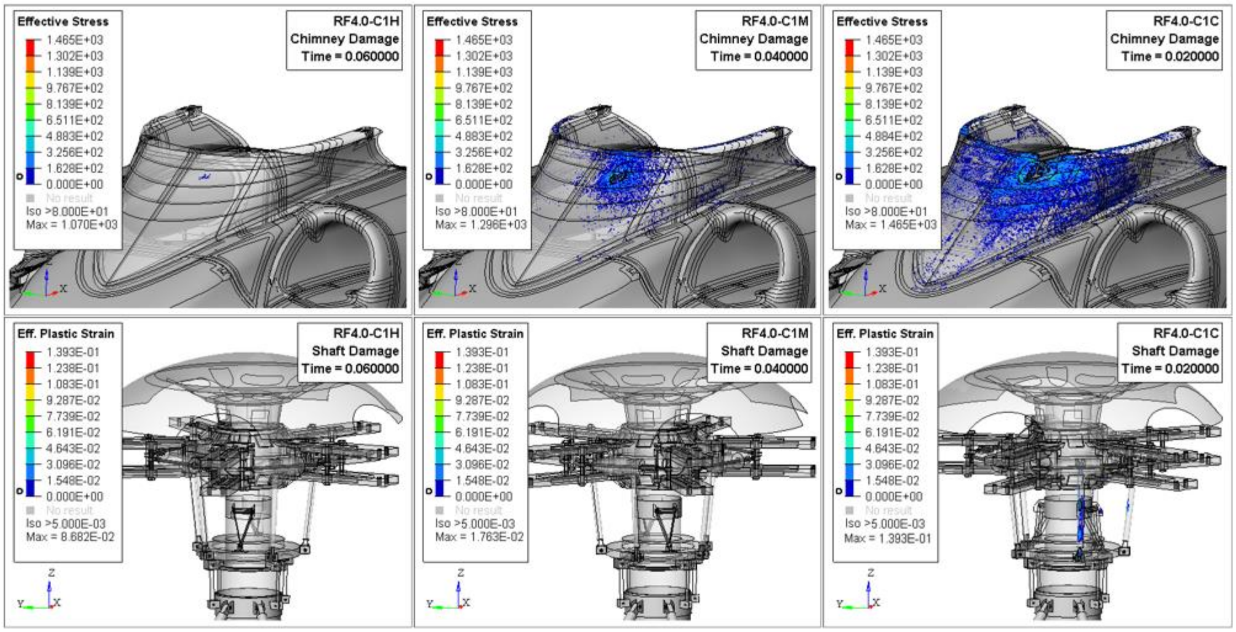


Figure 141. Chimney and rotor shaft damage for RF4.0-C1H, RF4.0-C1M and RF4.0-C1C (left to right).

- <u>Location 2</u>

Figure 142 shows the configuration corresponding to the location 2 cases. The UAS was oriented to impact with one motor first to cause the most damage to the structure.

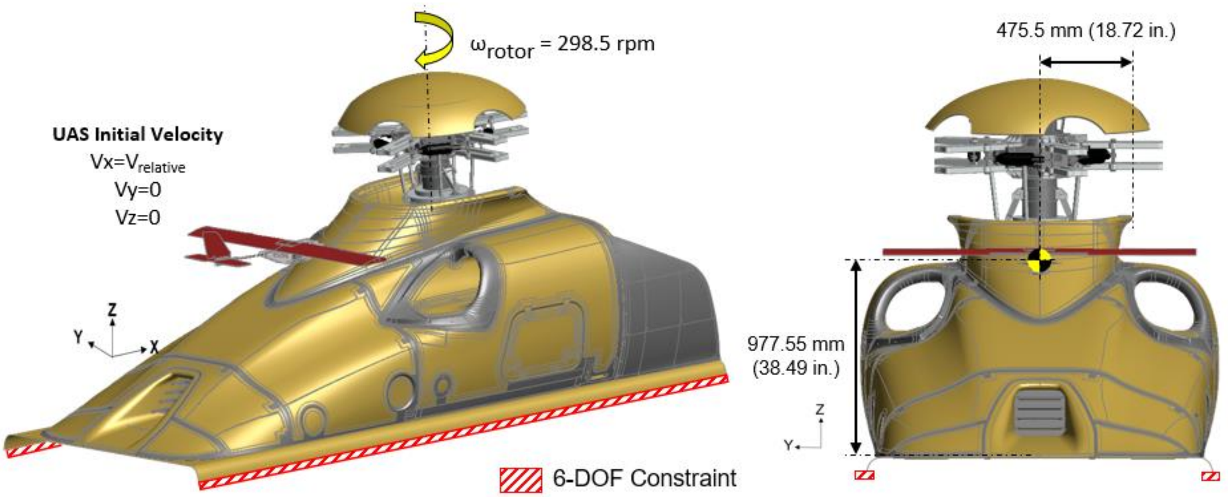


Figure 142. UAS Fixed-wing impaction location 2 – Front cowling.

Figure 143 presents the isometric and side views of the simulation's last instant for the three velocity iterations. Cases are presented from lowest (left) to highest velocity (right). The UAS was deflected towards the rotor shaft assembly after colliding with the cowling surface.

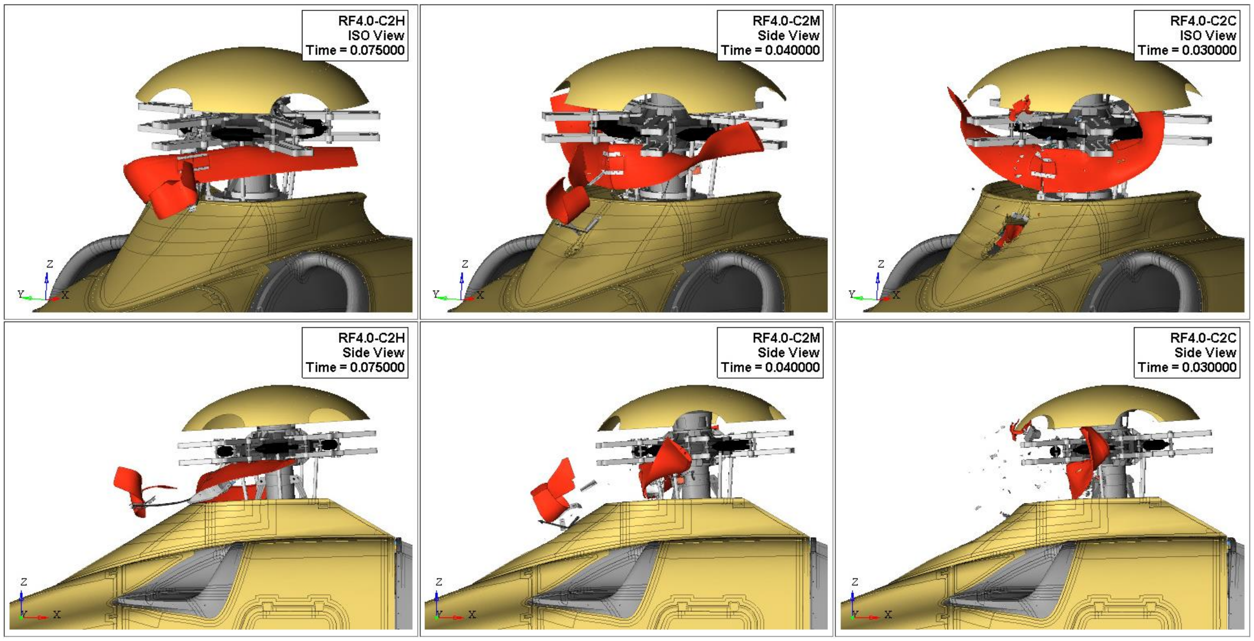


Figure 143. The final time of impact for RF4.0-C2H, RF4.0-C2M, and RF4.0-C2C (left to right).

Figure 144 shows the damage observed on the chimney (upper images) and the rotor shaft assembly (lower images). The chimney sustains more damage as the impact velocity increases. RF4.0-C2H indicates no damage to the honeycomb (core crushing) skin and a small permanent deformation concentration in the impact region. RF4.0-C2M shows the honeycomb's failure and the composite skin's permanent deformation. RF4.0-C2C captures failure of the honeycomb and composite skin, resulting in the opening of a large crack in the chimney. In addition, some UAS body debris, such as camera fragments and shattered PCB material, penetrated the inside volume confined by the chimney. Thus, RF4.0-C2H and RF4.0-C2M have damage severity of level 2 and RF4.0-C2C has damage severity of level 3. The cruise speed case was determined as level 3 because the chimney is not the primary structure.

Furthermore, the rotor shaft assembly did not sustain damage in any impact cases. Hence, RF4.0-C2H, RF4.0-C2M, and RF4.0-C2C secondary impact of the UAS with the shaft presented damage severity of level 1.

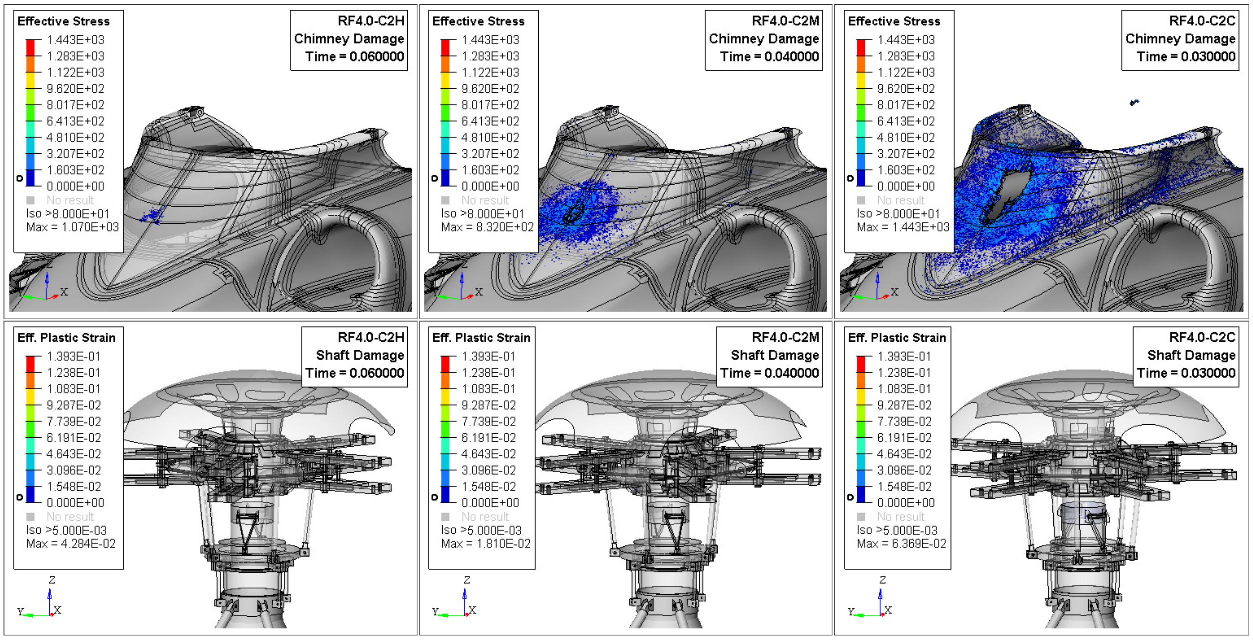


Figure 144. Chimney and rotor shaft damage for RF4.0-C2H, RF4.0-C2M, and RF4.0-C2C (left to right).

### 6.2.2 Horizontal Stabilizer

The horizontal stabilizer was subjected to impact with the 4.0 lb. fixed-wing model at two different leading-edge locations. Location 1 was selected in the middle of the horizontal stabilizer's leading edge. Location 2 was defined at the tip of the stabilizer to increase the moment arm. The UAS impacts both locations at three different velocities (hover, medium, and cruise), as discussed in Chapter 5.1.2. According to the nomenclature defined in Chapter 5.1.1, location 1 cases are named RF4.0-H1H, RF4.0-H1M, and RF4.0-H1C. Similarly, location 2 cases are RF4.0-H2H, RF4.0-H2M, and RF4.0-H2C.

A fixed boundary condition at the tail cone fuselage frame was used to constrain the complete model. The impact velocity was determined by adding the UAS maximum speed and the rotorcraft speed. The resultant relative velocity was applied to the UAS body. A gravity body load was prescribed during the simulation to act on the UAS and the horizontal stabilizer.

- Location 1

Figure 110 shows the impact configuration corresponding to location 1 cases. The UAS was oriented to impact with one motor first to cause the most damage to the airframe.

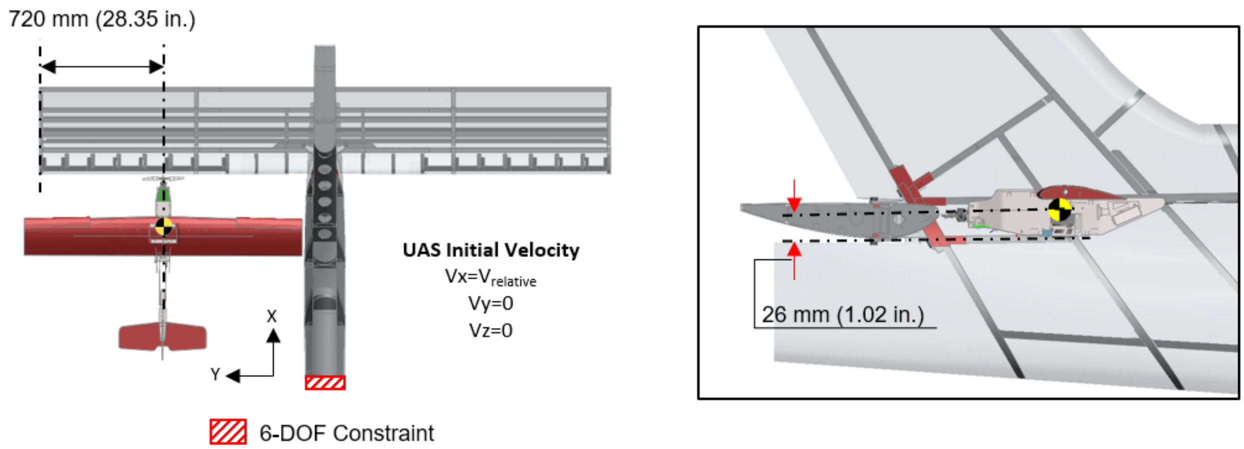


Figure 145. UAS fixed-wing critical impact location 1 – Horizontal stabilizer.

Figure 145 shows the isometric and side views of the simulation's last instant for the three velocity iterations. Cases are presented from lowest (left) to highest velocity (right). In all three cases, the stabilizer rotates backward due to the UAS collision. The simulation also predicts the spring back motion of the stabilizer, which returned to its initial position after the impact.

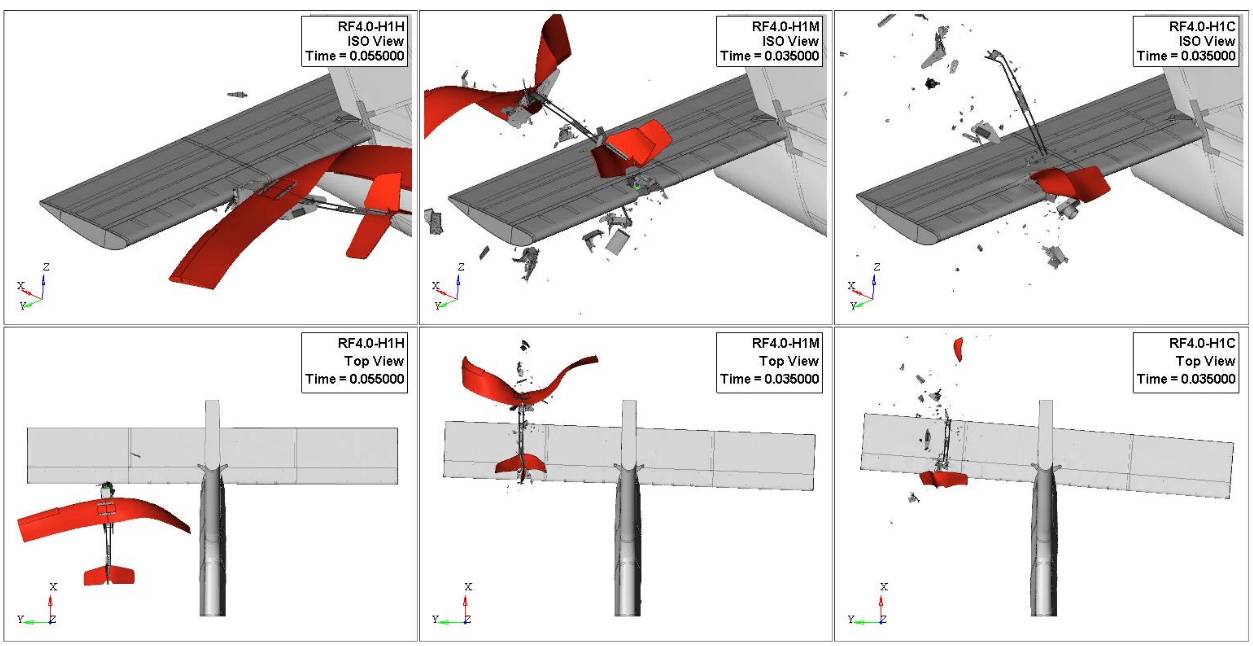


Figure 146. The final time of impact for RF4.0-H1H, RF4.0-H1M and RF4.0-H1C (left to right).

Figure 146 shows the permanent deformation of the horizontal stabilizer's skin (upper images) and the internal components (lower images). The horizontal stabilizer assembly sustains more damage as the impact velocity increases. RF4.0-H1H shows little damage to the skin and none to the internal components. RF4.0-H1M presents rupture of the skin and permanent deformation at the closest nose rib. RF4.0-H1C has a larger opening of the leading edge skin and shows a hole on the main spar's web, a primary structural member. Thus, RF4.0-H1H has a damage severity of level 2, RF4.0-H1M has a damage severity of level 3, and RF4.0-H1C is classified as level 4. Due to the penetration of the UAS battery into the airframe, there is risk of fire for RF4.0-H1C.

In addition, due to the backward deflection of the horizontal stabilizer during the impact, permanent deformation was observed in the root region of the horizontal stabilizer, where the airframe is connected to the rest of the tail. The deformation was located near the large bolts that secure the stabilizer's connection and increase with the velocity of the impact. Figure 148 depicts the effective plastic strain of the horizontal stabilizer's root region.

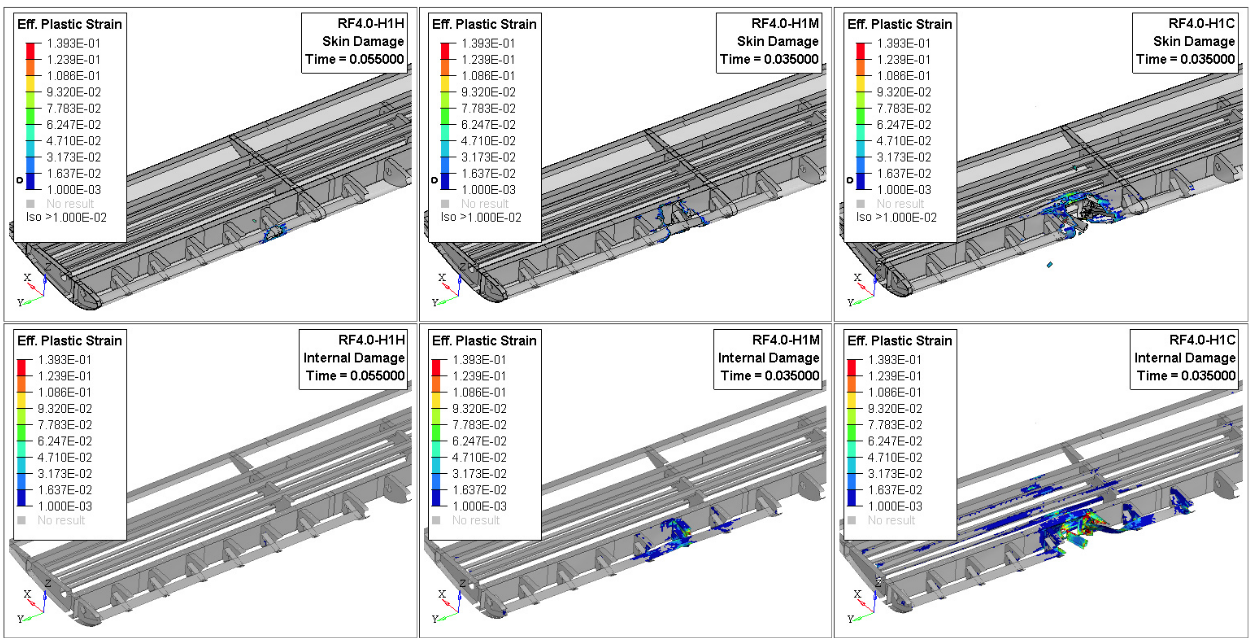


Figure 147. Skin and internal structures plastic strain for RF4.0-H1H, RF4.0-H1M and RF4.0-H1C (left to right).

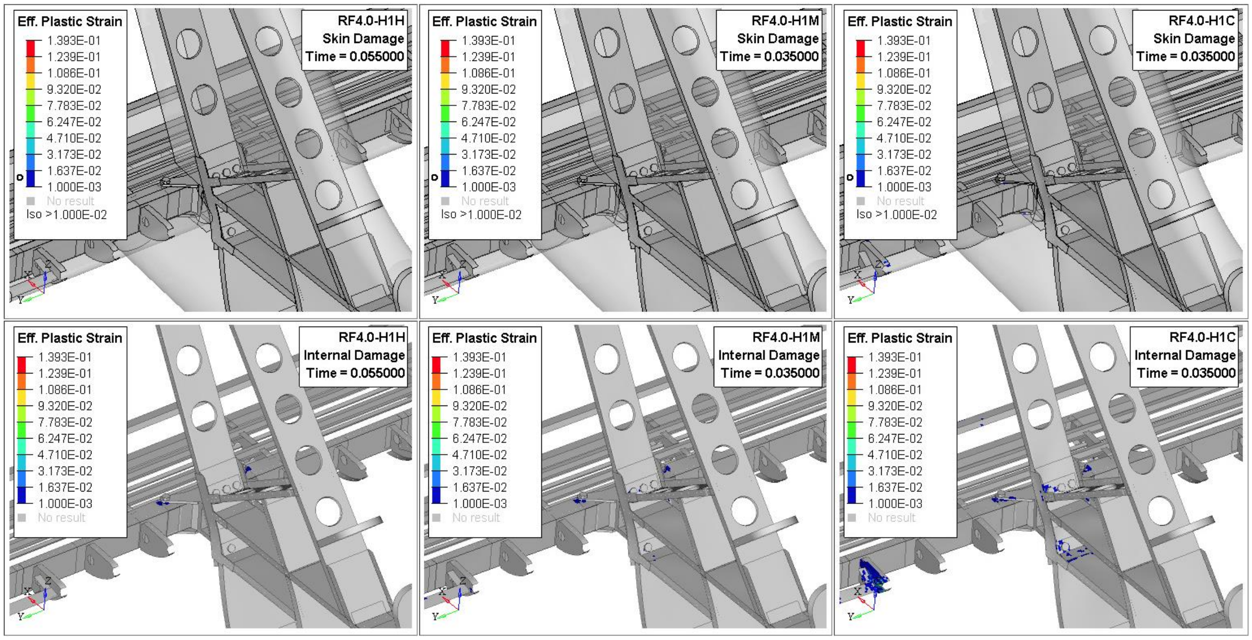


Figure 148. Skin and internal structures plastic strain at the tail root for RF4.0-H1H, RF4.0-H1M and RF4.0-H1C (left to right).

- <u>Location 2</u>

Figure 149 shows the impact configuration corresponding to location 2 cases. The UAS was oriented to impact with one motor first to cause the most damage to the airframe.

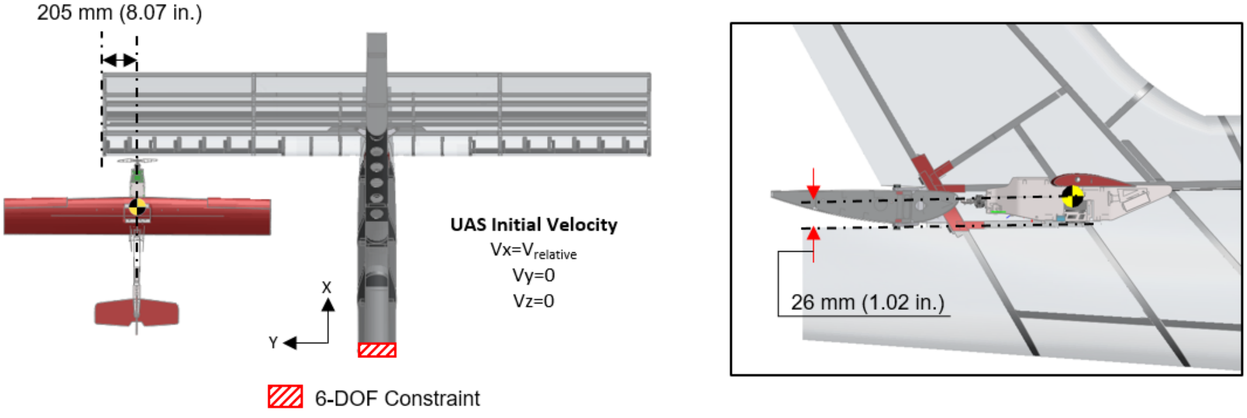


Figure 149. UAS fixed-wing critical impact location 2 – Horizontal stabilizer.

Figure 150 shows the isometric and side views of the simulation's last instant for the three velocity iterations. Cases are presented from lowest (left) to highest velocity (right). In all three cases, the stabilizer rotates backward due to the UAS collision. The simulation also predicts the spring back motion of the stabilizer, which returned to its initial position after the impact.

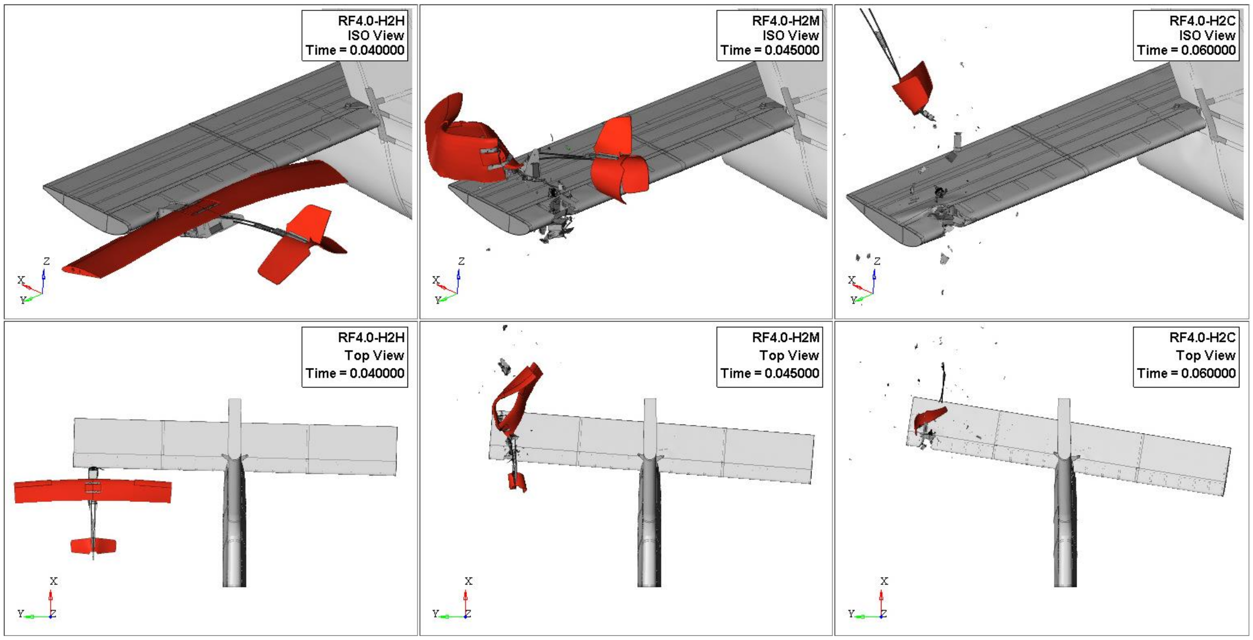


Figure 150. The final time of impact for RF4.0-H2H, RF4.0-H2M, and RF4.0-H2C (left to right).

Figure 151 shows the permanent deformation of the horizontal stabilizer's skin (upper images) and the internal components (lower images). The horizontal stabilizer assembly sustains more damage as the impact velocity increases. RF4.0-H2H shows a small perforation of the leading edge skin and no damage to the internal components. RF4.0-H2M presents rupture of the skin and permanent deformation of the closest nose ribs. RF4.0-H2C has a large opening of the leading edge skin, permanent deformation to the spar, and failure of the spar's web, a primary structural member. Thus, RF4.0-H2H has a damage severity of level 2, RF4.0-H2M has a damage severity of level 3, and RF4.0-H2C is classified as level 4. Due to the penetration of the UAS battery into the airframe, there is risk of fire for RF4.0-H2C.

In addition, due to the backward deflection of the horizontal stabilizer during the impact, some permanent deformation was observed in the root region of the horizontal stabilizer, where the airframe is connected to the rest of the tail. The deformation was located near the large bolts that secure the stabilizer's connection and increase with the velocity of the impact. The cruise velocity impact contains the most permanent deformation in this area. Figure 152 depicts the effective plastic strain of the horizontal stabilizer's root region.

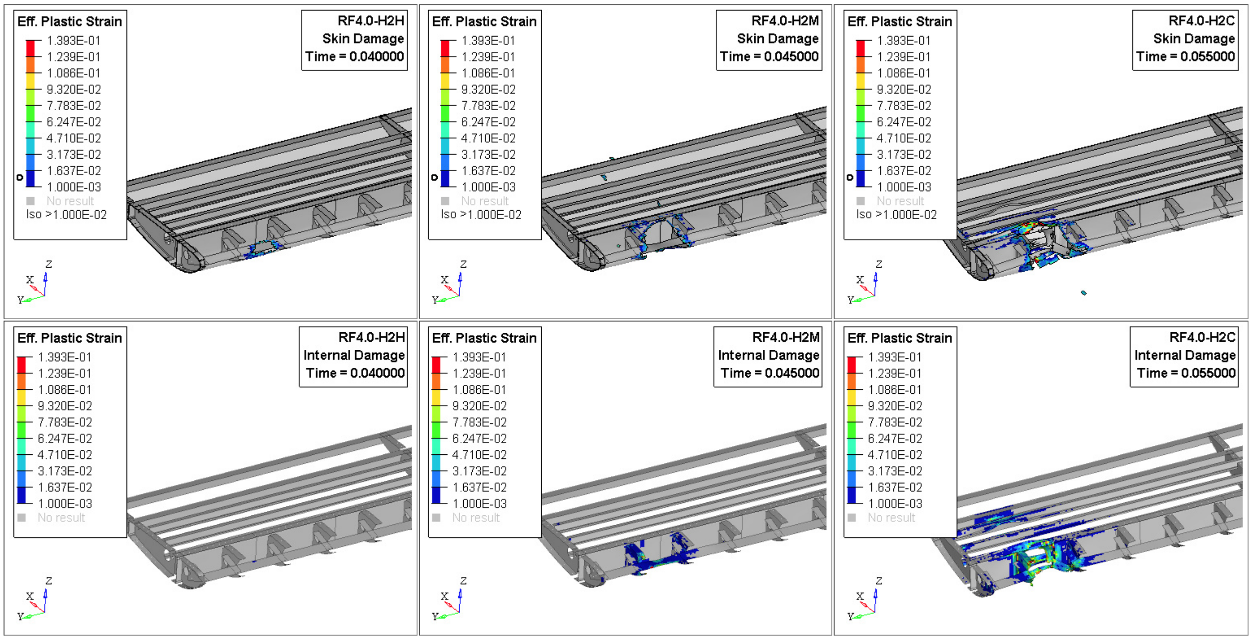


Figure 151. Skin and internal structures plastic strain for RF4.0-H2H, RF4.0-H2M, and RF4.0-H2C (left to right).

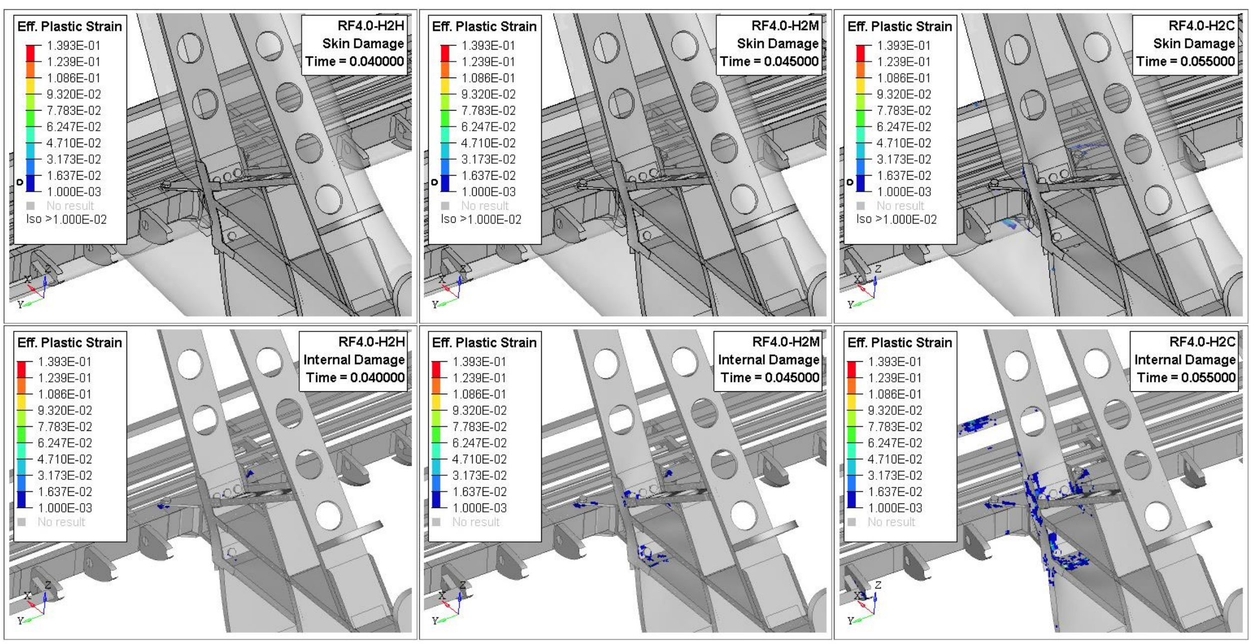


Figure 152. Skin and internal structures plastic strain at the tail root for RF4.0-H2H, RF4.0-H2M, and RF4.0-H2C (left to right).

### 6.2.3 Rear Servo

The rear servo was subjected to impact with the 4.0 lb. fixed-wing UAS model. The impact location was selected based on the bird strike data provided by the Industry Partner (proprietary data). The UAS impacts the front leading-edge at three different velocities (hover, medium, and cruise), as discussed in Chapter 5.1.2. According to the nomenclature defined in Chapter 5.1.1, the rear servo cases are named RF4.0-R1H, RF4.0-R1M, and RF4.0-R1C.

The 4.0 lb. UAS wing span was larger than the rear servo width. Also, the rear servo is attached to the tail of the helicopter. This observation highlights the spatial constraint for the fixed-wing model to impact the servo in a horizontal flight condition because the UAS wing would interfere with the helicopter fuselage. The following assumption was made to establish a comparison between the damage caused by the 2.7 lb. quadcopter model at the same impact location and maintaining a conservative worst-case scenario approach: the 4.0 lb. UAS wing was trimmed to prevent interference between the UAS and the helicopter geometry. The total mass of the UAS was re-adjusted by adding non-structural mass to account for the removed elements mass, keeping the UAS MTOW at 4.0 lb. It must be noted that the damage evaluation obtained through this exercise will be a worst-case level, guaranteeing that other impact configurations with this UAS will result in the same or lesser damage severity. Figure 153 depicts the details of the wing trimming assumption.

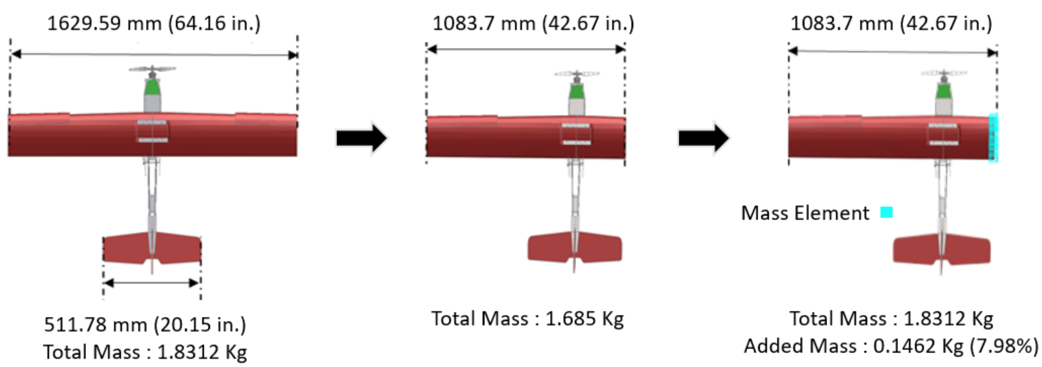


Figure 153. F4.0 UAS simplification of the right-wing for the rear servo impact analysis.

A fixed boundary condition at the servo root area was used to constrain the complete model. The impact velocity was determined by adding the UAS maximum speed and the rotorcraft speed. The resultant relative velocity was applied to the UAS body. A gravity body load was prescribed during the simulation to act on the UAS and the rear servo.

Figure 154 shows the analysis setup corresponding to the only rear servo impact location. The UAS was oriented to impact with one motor first to cause the most damage possible.

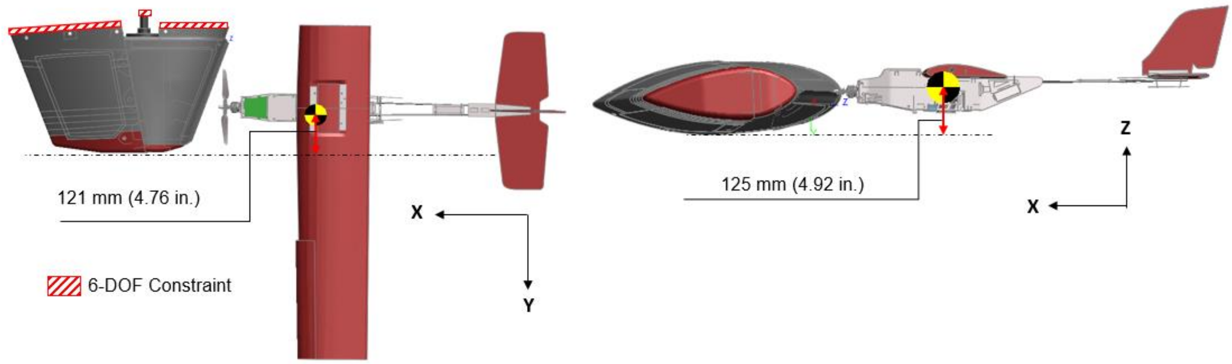


Figure 154. UAS fixed-wing impact location 1 – Rear servo.

Figure 155 shows the isometric and side views of the simulation's last instant for the three velocity iterations. Cases are presented from lowest (left) to highest velocity (right). Again, the rear servo could sustain the impact with the quadcopter, and no indications of failure of the leading edge skin were observed.

Figure 156 shows the damage to the servo skin (upper images) and the internal structure (lower images). RF4.0-R1H shows no permanent deformation of the skin and internal structure. Likewise, RF4.0-R1M indicates little permanent deformation to the skin and internal structure. However, RF4.0-R1C presents large skin permanent deformation and localized damage to the nose ribs. Thus, RF4.0-H1H has a damage severity of level 1, RF4.0-H1M achieved level 2, and RF4.0-H1C reached level 3.

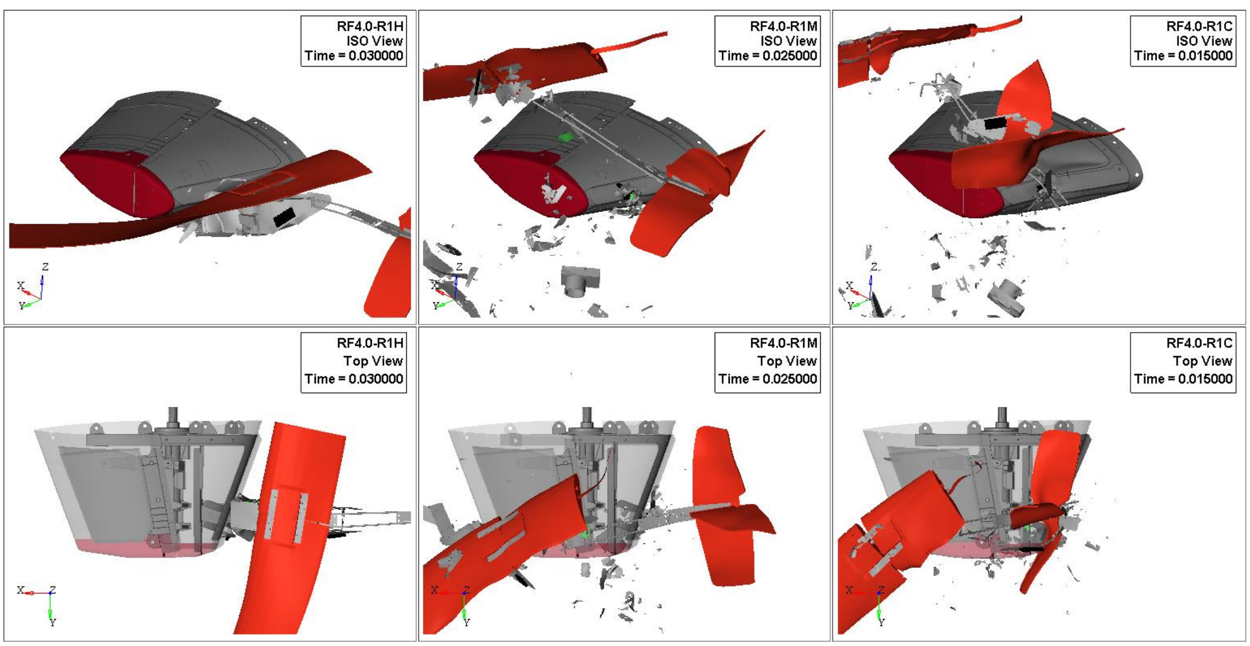


Figure 155. The final time of impact for RF4.0-R1H, RF4.0-R1M and RF4.0-R1C (left to right).

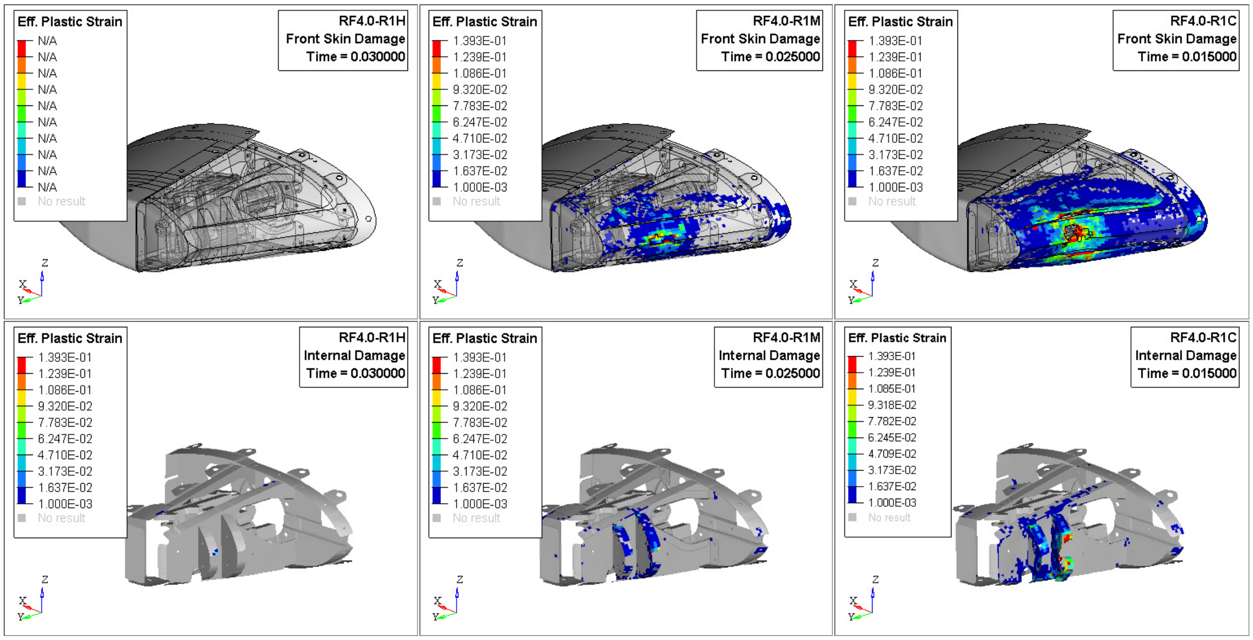


Figure 156. Skin and internal structures plastic strain for RF4.0-R1H, RF4.0-R1M and RF4.0-R1C (left to right).

### 6.2.4 Windshield

The bilayer windshield was subjected to impact with the 4.0 lb. fixed-wing at two different locations. Location 1 was defined at the center of the windshield, while location 2 was selected closer to the frame, near the top right corner of the windshield. The UAS impacts both windshield locations at three different velocities (hover, medium, and cruise), as introduced in Chapter 5.1.2. According to the nomenclature defined in Chapter 5.1.1, location 1 cases are named RF4.0-W1H, RF4.0-W1M, and RF4.0-W1C. Similarly, location 2 cases are RF4.0-W2H, RF4.0-W2M, and RF4.0-W2C.

A fixed boundary condition at the rear and lower end of the frame was used to constrain the complete model. Also, the composite frame's lower front end was constrained along the vertical direction based on the feedback provided by Industry Partner. The impact velocity was determined by adding the UAS maximum speed and the rotorcraft speed. The resultant relative velocity was applied to the UAS body. A gravity body load was prescribed during the simulation to act on the UAS and the windshield.

- Location 1

Figure 157 shows the impact configuration corresponding to location 1. The UAS was oriented to impact with one motor first to cause the most damage to the windshield.

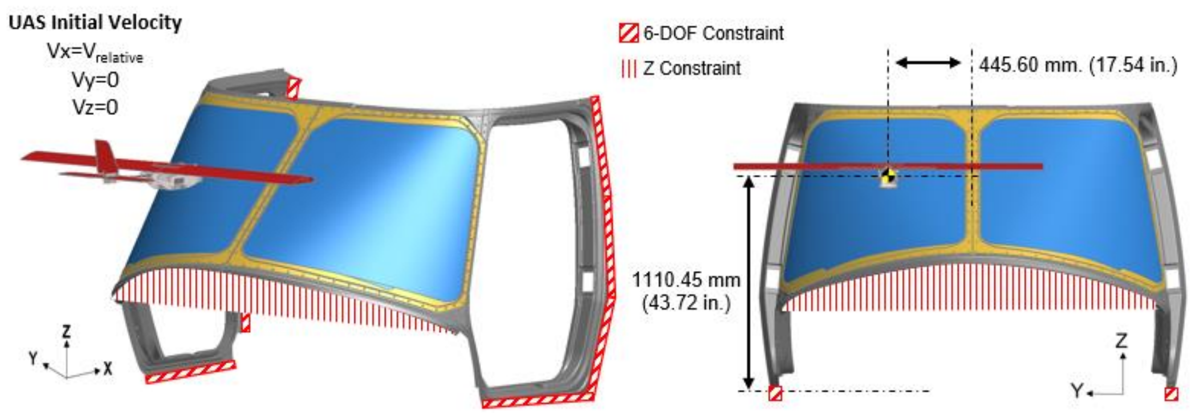


Figure 157. UAS fixed-wing impact location 1 – Windshield.

Figure 158 shows the isometric and side views of the simulation's last instant for the three velocity iterations. Figure 159 presents the front and rear windshield view of the simulation's last frame. The images present the lowest (left) cases to the highest velocity (right). The rear view indicates that the UAS perforated the windscreen at cruise velocity.

Figure 160 depicts the damage to the outer (upper images) and the inner (lower images) windshield layers for the location 1 impact cases. The windshield shows more damage as the velocity increases. RF4.0-W1H contains a localized scratch on the outer layer. RF4.0-W1M indicates shattering propagating along the windshield and a small perforation on the layers that opened a hole through the windshield. RF4.0-W1C captured a larger shattering of the outer layer, which propagated to the entire surface of the windscreen.

Moreover, the bilayer windshield was perforated by the UAS, creating an opening in the windscreen. The battery and other UAS debris entered the cockpit in RF4.0-W1C case. Thus, RF4.0-W1H has a damage severity of level 2. RF4.0-W1M and RF4.0-W1C have damage severity of level 4.

Due to the penetration of the UAS battery into the cockpit, there is risk of fire for RF4.0-W1C.

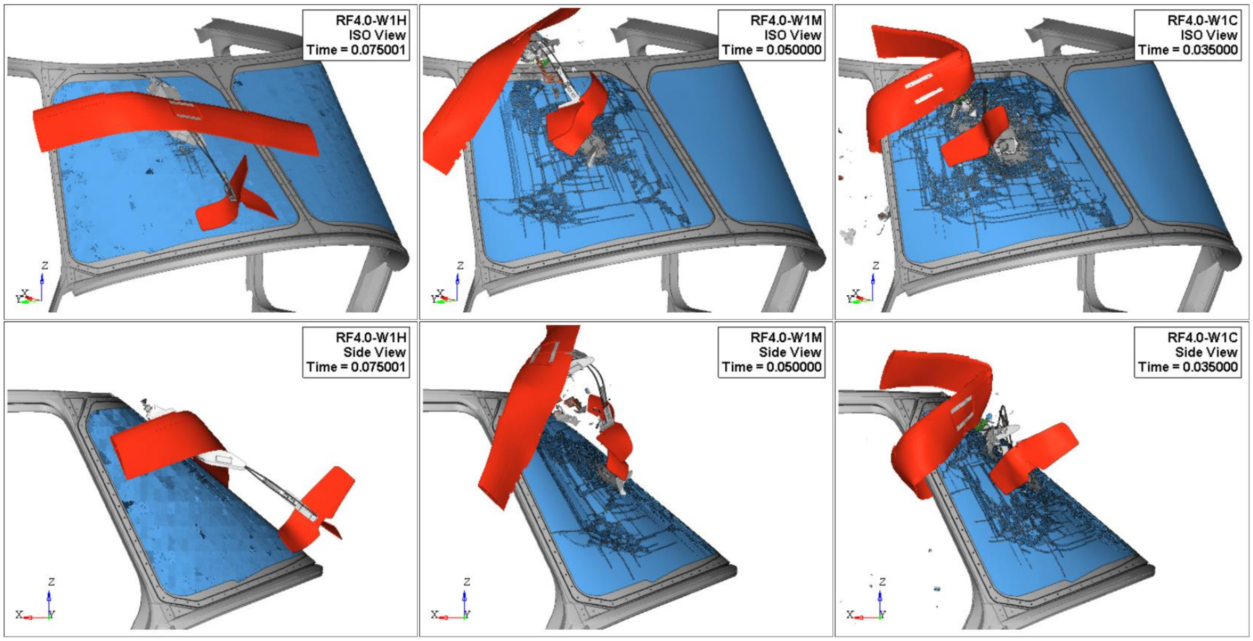


Figure 158. The final time of impact for RF4.0-W1H, RF4.0-W1M and RF4.0-W1C (left to right) – Isometric and side views.

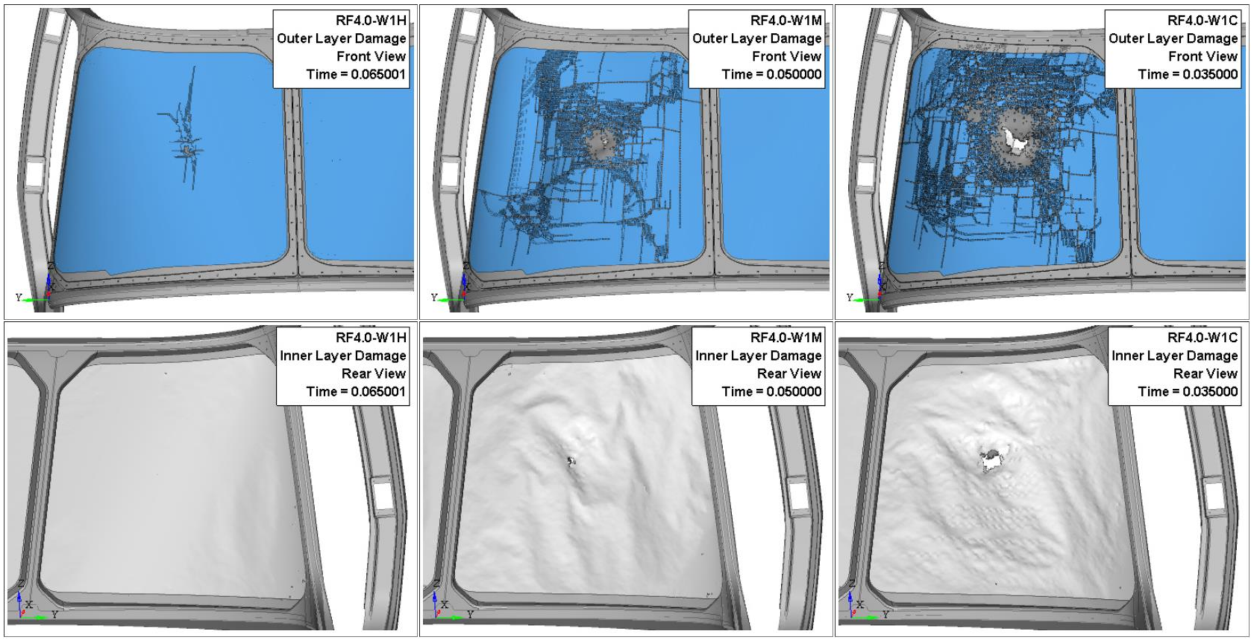


Figure 159. The final time of impact for RF4.0-W1H, RF4.0-W1M and RF4.0-W1C (left to right) – Front and rear views.

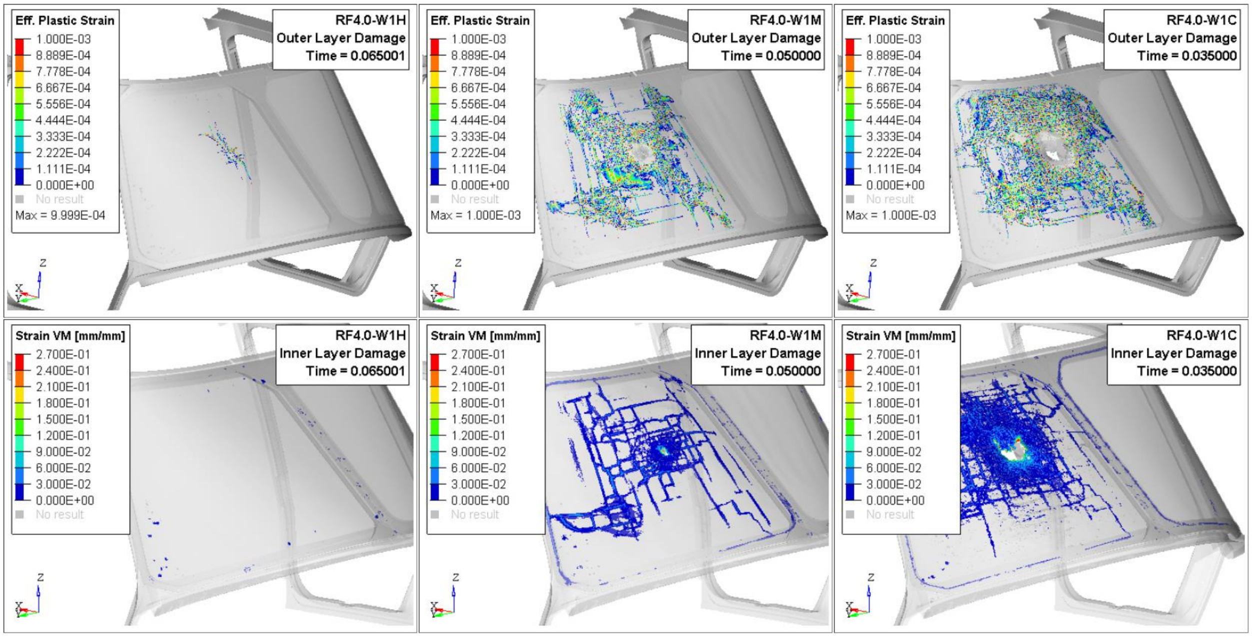


Figure 160. Outer and inner layer damage for RF4.0-W1H, RF4.0-W1M and RF4.0-W1C (left to right).

- Location 2

Figure 161 shows the impact configuration corresponding to location 2. The UAS was oriented to impact with one motor first to cause the most damage to the windshield.

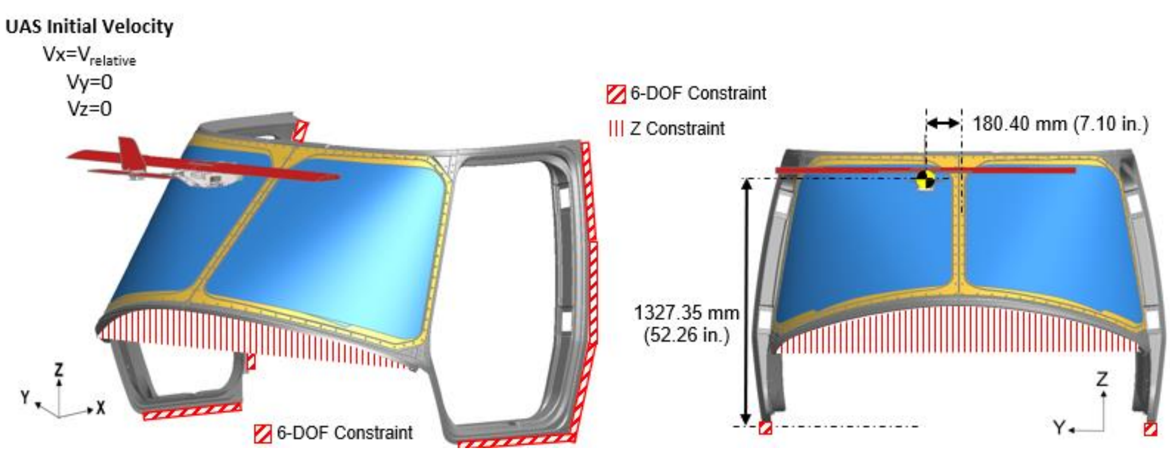


Figure 161. UAS fixed-wing impact location 2 – Windshield.

Figure 162 shows the isometric and side views of the simulation's last instant for the three velocity iterations. Figure 163 presents the front and rear windshield view of the simulation's last frame. The images present the lowest (left) cases to the highest velocity (right). The rear view indicates that the UAS perforated the windscreen at cruise velocity.

Figure 164 depicts the damage to the outer (upper images) and the inner (lower images) windshield layers for the location 2 impact cases. The windshield shows more damage as the velocity increases. RQ2.7-W2H contains a small localized scratch on the outer layer near the impact location with the UAS. RF4.0-W2M shows shattering of the top-center corner of the windshield, indicating failure of the outer and inner layers, resulting in a small hole through the windshield. RF4.0-W2C captured a larger shattering of the outer layer, which propagated to the rest of the windscreen. There is also damage and perforation to the inner layer. The UAS did not penetrate the cockpit for RF4.0-W2H and RF4.0-W2M cases. The battery and other UAS debris entered the cockpit in RF4.0-W2C case. Thus, RF4.0-W2H damage severity has been determined of level 2. RF4.0-W2M and RF4.0-W2C captured damage severity of level 4.

Due to the penetration of the UAS battery into the cockpit, there is risk of fire for RF4.0-W2C.

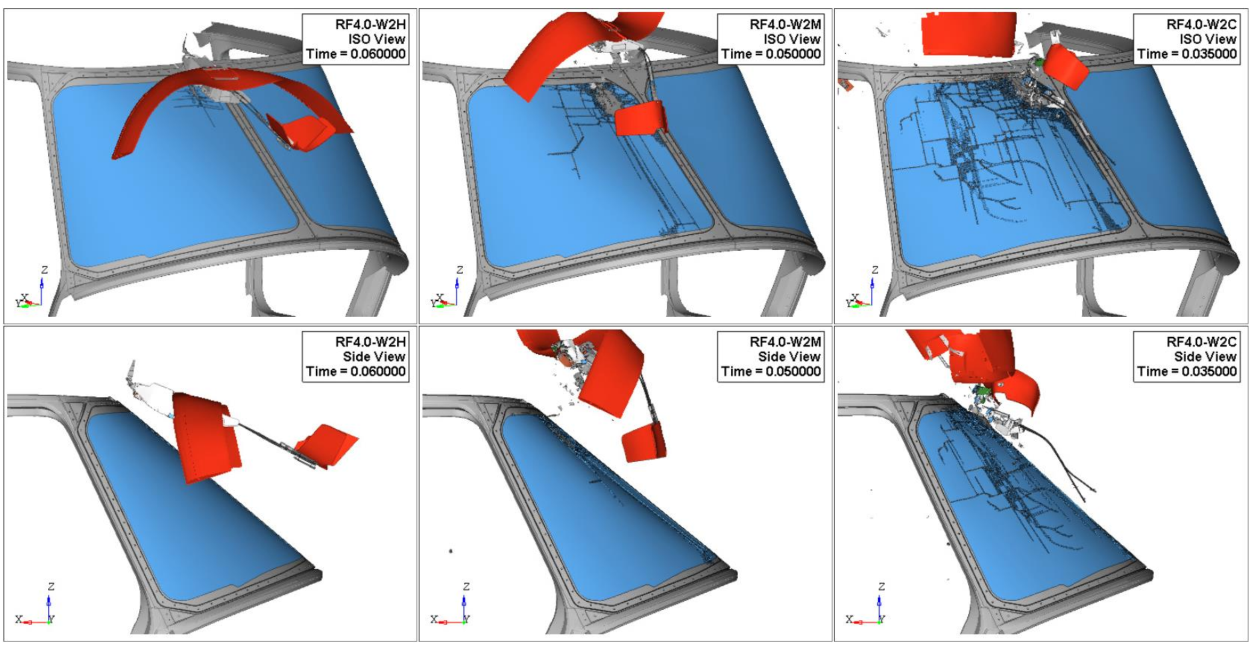


Figure 162. The final time of impact for RF4.0-W2H, RF4.0-W2M, and RF4.0-W2C (left to right) – Isometric and side views.

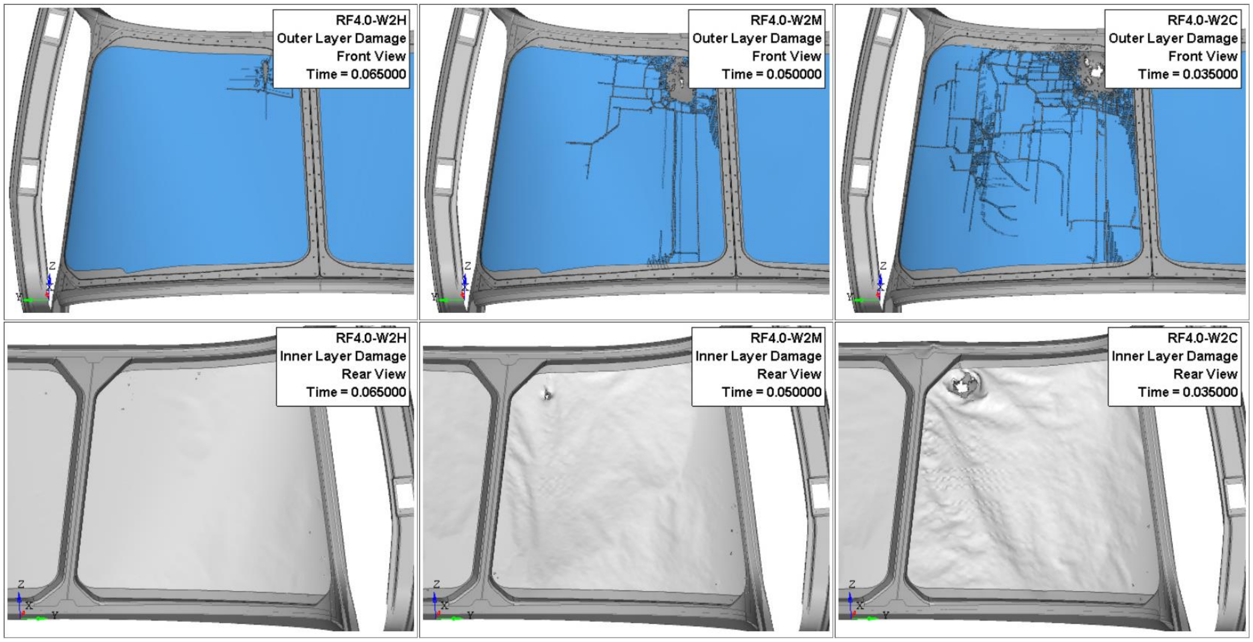


Figure 163. The final time of impact for RF4.0-W2H, RF4.0-W2M, and RF4.0-W2C (left to right) – Front and rear views.

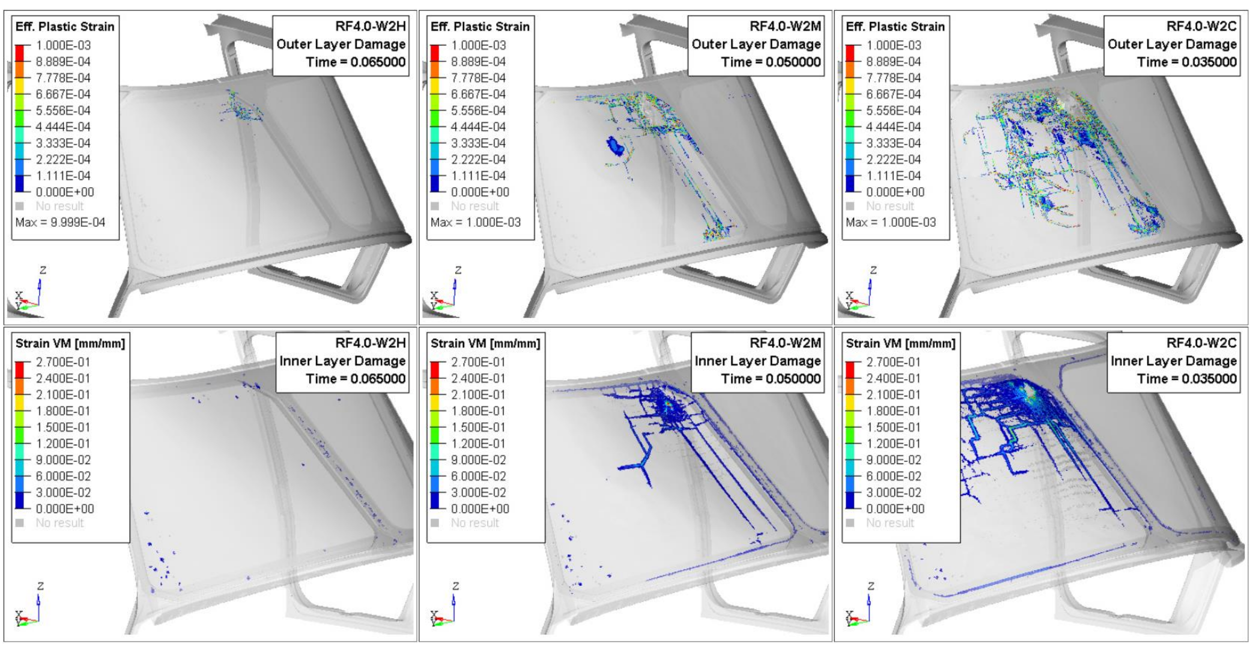


Figure 164. Outer and inner layer damage for RF4.0-W2H, RF4.0-W2M, and RF4.0-W2C (left to right).

### 6.2.5 Main Rotor Blade

The rotor blade leading edge was subjected to impact with the 4.0 lb. fixed-wing model at a location near the blade tip. Location 1 was selected based on the probability of the impact occurrence with a high-speed rotating blade. The UAS impacts the blade leading edge at three different velocities (hover, medium, and cruise), as explained in Chapter 5.1.2. According to the nomenclature defined in Chapter 5.1.1, location 1 cases are named RF4.0-B1H, RF4.0-B1M, and RF4.0-B1C.

The blade root handle was connected to a revolute joint. The revolute joint was constrained in 5-DOF, allowing rotation only about the vertical axis (z-axis). The impact velocity was determined by adding the UAS maximum speed and the rotorcraft speed. The resultant relative velocity was applied to the UAS. Furthermore, the rotor blade spun at an angular velocity of 383 rpm, which is representative of this type of helicopter. A gravity body load was prescribed during the simulation to act on the UAS and the blade. Also, the simulation implemented all the blade contact definitions validated at the full-scale test level in Chapter 4.

Figure 165 shows the impact configuration corresponding to location 1. The UAS was oriented to impact with one motor first to cause the most damage to the structure.

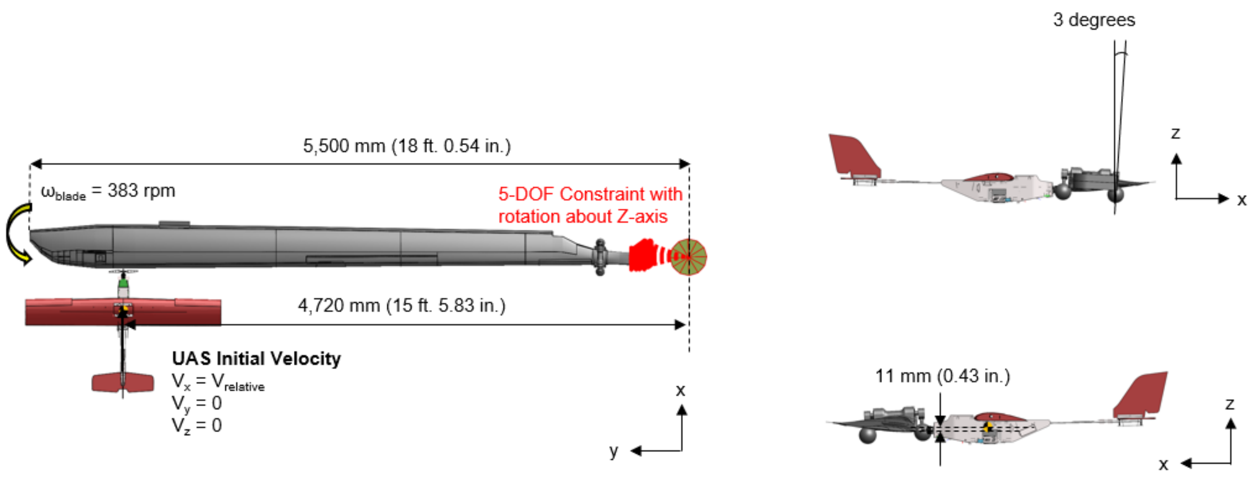


Figure 165. UAS fixed-wing critical impact location 1 – Front cowling.

Figure 166 presents the isometric and top views of the simulation's last instant for the three velocity iterations. Cases are presented from lowest (left) to highest velocity (right). The UAS was sliced and broken into pieces during the collision with the blade's leading edge.

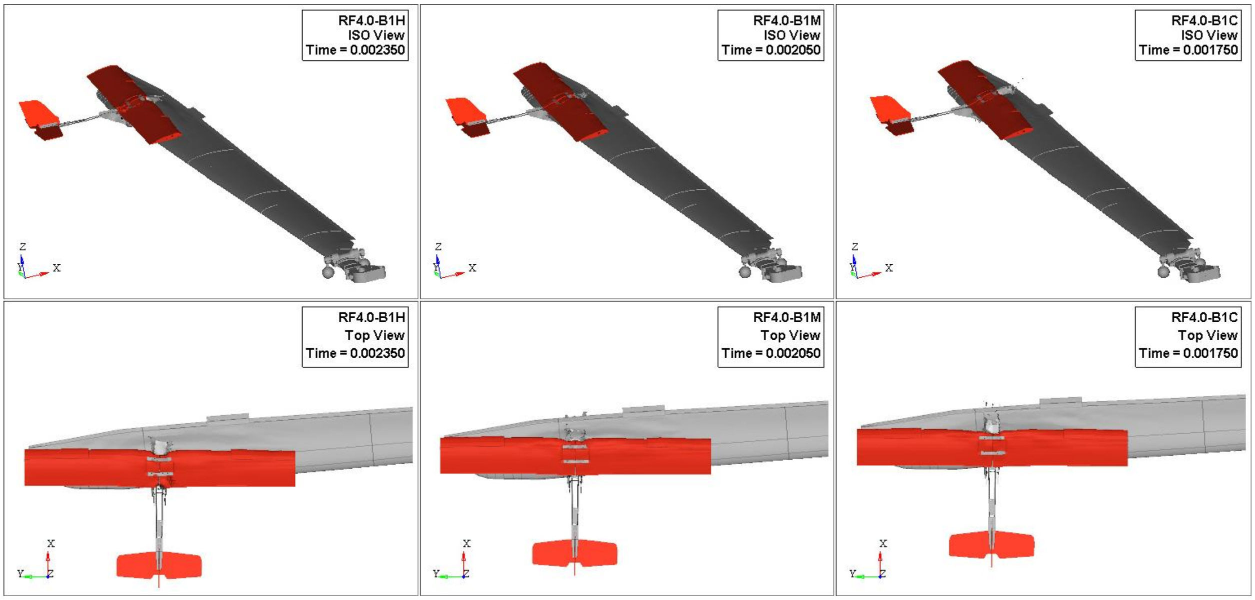


Figure 166. The final time of impact for RF4.0-B1H, RF4.0-B1M and RF4.0-B1C (left to right).

Figure 167 shows the damage observed on the blade leading edge (upper images) and the impact location cross-sections (lower images). RF4.0-B1H shows a medium-sized dent to the leading edge, while RF4.0-B1M and RF4.0-B1C present deeper dents, indicating larger damage as the impact velocity increases. All three cases have localized debonding between the skin and foam interface. It is important to note that the skin debonding was observed in the physical tests presented in Chapter 4.4. The large-scale simulation cases capture this behavior in agreement with the test results; however, due to the limitations of the FE model to capture this type of interface interaction after the initiation of the skin separation, the size and propagation of the skin separation must be treated as a conservative approach. Thus, based on the damage severity described in Table 15, all three cases have a damage severity of level 2.

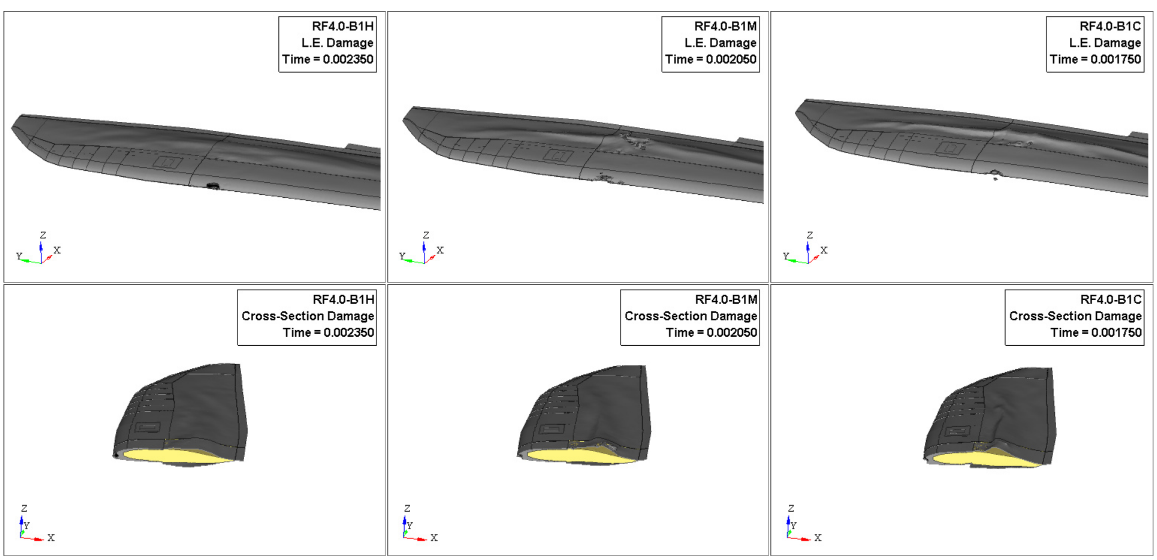


Figure 167. Leading-edge and cross-section damage for RF4.0-B1H, RF4.0-B1M and RF4.0-B1C (left to right).

## 7. CONCLUSIONS

The effect of an airborne collision between an sUAS and a crewed aircraft is a concern to the public and government officials at all levels. The ASSURE group has performed and has ongoing research to assess the damage of sUAS airborne collisions to aircraft using FE advanced virtual models. These are some of the completed research programs concerning this subject:

- Airborne Collision Phase I (Task A3) [2] (Volume I): sUAS (mass range: 2.7 to 8 lb. architectures: Quadcopter and Fixed Wing) impacts on Narrow Body Commercial Aircraft and Business Jets operating under FAR 25 requirements [10]
- Airborne Collision Phase I research extension (Task A30) [32]: Large sUAS (mass range: 10 to 55 lb. architectures: Quadcopter and Fixed Wing) impacts on Narrow Body Commercial Aircraft and Business Jets operating under FAR 25 requirements [10]
- Airborne Collision Phase II research extension [33]: Large sUAS (mass range: 10 to 55 lb. architectures: Quadcopter and Fixed Wing) impacts on General Aviation aircraft operating under FAR 23 requirements [11]

Task A16 studies focus on the collision between sUAS and a Part 29 rotorcraft. NIAR has developed and validated advanced virtual models of representative rotorcraft structures that could be subjected to mid-air collision and are critical for flight safety. The structures under consideration are the front cowling, horizontal stabilizer, rear servo, windshield, and main rotor blade. Access to these targets' proprietary information and physical test articles was possible due to the collaboration with an Industry Partner. Creating advanced virtual models facilitates analyzing and evaluating several impact conditions without conducting full-scale physical testing. The UAS models selected for this work were developed during Task A3 [2]: 2.7 lb. quadcopter [5] and 4.0 lb. fixed-wing [6]. Additional component-level test experiments were performed in this research program to extend the validation of the FEM for mid-air airborne collisions up to 500 knots. With all FEM validated, an analysis matrix of 42 impact cases was defined to evaluate the damage severity of airborne collisions between sUAS and rotorcraft.

The severity evaluation criterion follows the guidelines of the ASSURE Airborne Collision Phase I program [2]. The lowest damage category, Level 1, generally corresponds to minimal localized damage. The next category, Level 2, represents significant visible damage to the external surface of the aircraft with some internal component damage but with no appreciable skin rupture. The third category, Level 3, describes impact events where the aircraft's outer surface is compromised in a way that could allow the ingress of foreign objects into the airframe, with some damage to the substructure. Finally, Level 4 indicates extensive damage to internal components and possibly compromising part of the primary structure. The risk of fire associated with damaged LiPo-type batteries was addressed for each simulation based on the trends observed during component-level ballistic testing and the particular kinematics of a given impact scenario. Note that the label “Fire Risk” indicates a potential outcome rather than an impending event due to the qualitative nature of the assessment. Further studies and physical testing into this phenomenon would be required to determine any additional severity (see Table 14 and Table 16).

It should be noted that the orientation of the sUAS with respect to the targets’ impact area was selected using a conservative approach, aligning the center of gravity of the sUAS normal to the aircraft impact area. The models generated in this program could be used in the future to assess the effect of the sUAS impact area offset and orientation on the severity classification of the impact event.

Table 19. Damage severity evaluation criteria.

| Severity | Airframe Damage Description | Blade Damage Description |
|---|---|---|
| Level 1 | The airframe is undamaged.<br>Small deformations. | Blade undamaged.<br>Scratches of small dents on a rotor blade.<br>No crack initiation. |
| Level 2 | Extensive permanent deformation on external surfaces.<br>Some deformation in internal structure.<br>No Skin Failure. | Large dents on a rotor blade.<br>Visible cracking of a rotor blade.<br>Skin debonding. |
| Level 3 | Skin fracture.<br>Penetration of at least one component into the airframe. | Significant material loss leading to an imbalance on a single blade.<br>No crack initiation at the blade root or hub. |
| Level 4 | Penetration of UAS into airframe and failure of the primary structure. | Complete rotor blade failure. |

The results of the 48 impact scenarios, which correspond to the 2.7 lb. quadcopter and 4.0 lb. fixed-wing, are summarized in Table 20 and Table 21, respectively. In addition, Figure 168 and Figure 169 illustrate the highest severity level observed on each target's impact location for the 2.7 lb. quadcopter and 4.0 lb. fixed-wing cases, respectively. As the results indicate, the following parameters affect the severity classification of the impact event:

1. There is a clear trend with the increase of sUAS mass and impact velocity on the severity outcome. Less severity for smaller mass sUAS and lower impact velocities.
2. Nonetheless, it should be noted that the architecture and construction of the sUAS could also influence the severity levels:
    a. Fixed Wing architectures, in general, tend to concentrate the loads (alignment of the items of mass in the fuselage axis) on smaller impact areas than quadcopter configurations, creating more severe localized damage to the rotorcraft structure.
    b. Fixed Wing configurations with a puller propeller/motor configuration will create more severe damage than pusher propeller motor configurations.
3. From a severity level point of view, the most critical impact locations are in the horizontal stabilizer, followed by the windshield, cowling, the main rotor blade, and the rear servo.

Since the UAS models selected for this program were also used for Task A3 work [5] [6], and the damage observed during the component validation studies using bird strike results, it can be inferred that a UAS impact against a rotorcraft will be more severe than a bird strike. Furthermore, as discussed in Task A3 [2], UAS impacts with a similar quadcopter and fixed-wing configuration to the model selected are likely to cause more damage than bird strikes of equivalent energy. This is due to the hard-bodied mechanical construction of the UAS, its high-dense rigid materials, and the discrete distribution of masses within the UAS architecture.

The findings from this research may be used to conservatively define airborne hazard severity thresholds for collisions between sUAS (2.7 lb. Quadcopter and 4.0 Fixed Wing) and Part 29 [13] rotorcraft.

Table 20. RQ2.7 mid-air collision simulation assessment – damage severity levels and fire risk.

| | | Case | Severity | Fire Risk |
|---|---|---|---|---|
| Mid-air collision Rotorcraft and Quadcopter 2.7 lb. (RQ2.7) | Front Cowling (Locations 1 and 2) | RQ2.7-C1H | Level 1 | No |
| | | RQ2.7-C1M | Level 2 | No |
| | | RQ2.7-C1C | Level 3 | No |
| | | RQ2.7-C2H | Level 1 | No |
| | | RQ2.7-C2M | Level 2 | No |
| | | RQ2.7-C2C | Level 2 | No |
| | Horizontal Stabilizer (Locations 1 and 2) | RQ2.7-H1H | Level 1 | No |
| | | RQ2.7-H1M | Level 3 | No |
| | | RQ2.7-H1C | Level 4 | No |
| | | RQ2.7-H2H | Level 1 | No |
| | | RQ2.7-H2M | Level 3 | No |
| | | RQ2.7-H2C | Level 4 | No |
| | Rear Servo | RQ2.7-R1H | Level 1 | No |
| | | RQ2.7-R1M | Level 1 | No |
| | | RQ2.7-R1C | Level 2 | No |
| | Windshield (Locations 1 and 2) | RQ2.7-W1H | Level 2 | No |
| | | RQ2.7-W1M | Level 2 | No |
| | | RQ2.7-W1C | Level 2 | No |
| | | RQ2.7-W2H | Level 1 | No |
| | | RQ2.7-W2M | Level 2 | No |
| | | RQ2.7-W2C | Level 2 | No |
| | Blade | RQ2.7-B1H | Level 2 | No |
| | | RQ2.7-B1M | Level 2 | No |
| | | RQ2.7-B1C | Level 2 | No |
| | *Tail Rotor | - | Level 4 | No |

Note: *Based on limited Component Level Testing

Table 21. RF4.0 mid-air collision simulation assessment – damage severity levels and fire risk.

| | | Case | Severity | Fire Risk |
|---|---|---|---|---|
| Mid-air collision Rotorcraft and Fixed-Wing 4.0 lb. (RF4.0) | Front Cowling (Locations 1 and 2) | RF4.0-C1H | Level 2 | No |
| | | RF4.0-C1M | Level 2 | No |
| | | RF4.0-C1C | Level 3 | No |
| | | RF4.0-C2H | Level 2 | No |
| | | RF4.0-C2M | Level 2 | No |
| | | RF4.0-C2C | Level 3 | No |
| | Horizontal Stabilizer (Locations 1 and 2) | RF4.0-H1H | Level 2 | No |
| | | RF4.0-H1M | Level 3 | No |
| | | RF4.0-H1C | Level 4 | Yes |
| | | RF4.0-H2H | Level 2 | No |
| | | RF4.0-H2M | Level 3 | No |
| | | RF4.0-H2C | Level 4 | Yes |
| | Rear Servo | RF4.0-R1H | Level 1 | No |
| | | RF4.0-R1M | Level 2 | No |
| | | RF4.0-R1C | Level 3 | No |
| | Windshield (Locations 1 and 2) | RF4.0-W1H | Level 2 | No |
| | | RF4.0-W1M | Level 4 | No |
| | | RF4.0-W1C | Level 4 | Yes |
| | | RF4.0-W2H | Level 2 | No |
| | | RF4.0-W2M | Level 4 | No |
| | | RF4.0-W2C | Level 4 | Yes |
| | Blade | RF4.0-B1H | Level 2 | No |
| | | RF4.0-B1M | Level 2 | No |
| | | RF4.0-B1C | Level 2 | No |
| | *Tail Rotor | - | Level 4 | No |

Note: *Based on limited Component Level Testing

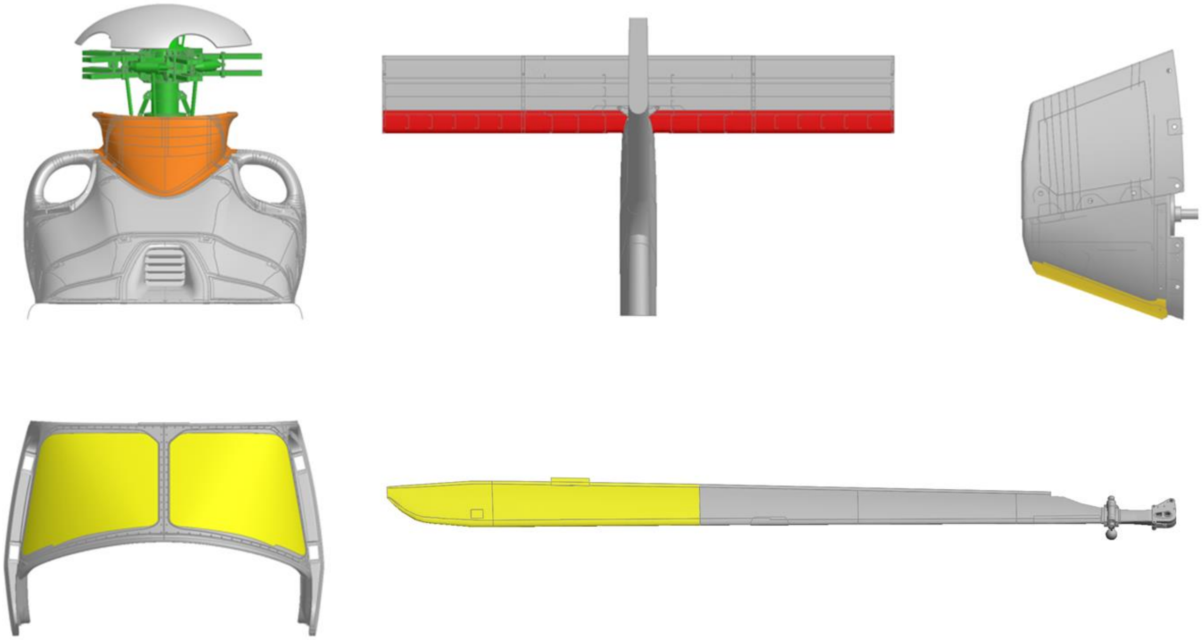

Figure 168. Summary of impact severity levels – Rotorcraft targets and quadcopter 2.7 lb. (RQ2.7).

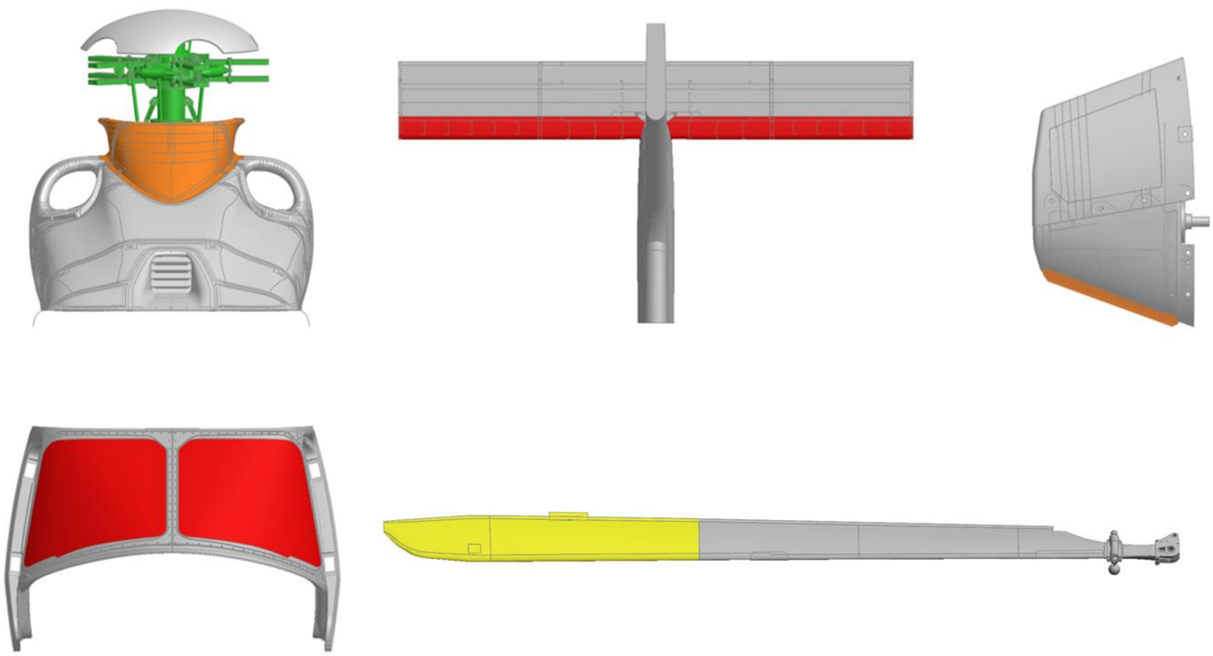

Figure 169. Summary of impact severity levels – Rotorcraft targets and fixed-wing 4.0 lb. (RF4.0).

## 7.1 FUTURE RESEARCH

The following items could be addressed in future airborne collision studies:

1. Develop a helicopter operational outcome table associated with the various impact severity levels. For example, the maximum current severity level of 4 only captures damage to the primary structure but does not determine whether the rotorcraft can land with the damage or if the damage creates a catastrophic failure.
2. Expand the evaluation criteria to identify possible flight-critical systems failures due to the impact event
3. "Fire Risk" indicates a potential outcome rather than an impending event due to the qualitative nature of the assessment. Further studies and physical testing into this phenomenon would be required to determine any additional severity criteria.
4. Study the effect of the impact offset on the severity classification for critical impact conditions. The current evaluation criteria may be conservative since the alignment and the orientation of the sUAS impact are defined to introduce maximum damage to the structure.
5. Study the effect of frangibility and items of mass location with respect to the sUAS center of gravity. Research shows that the alignment of stiffer components and items of mass results in larger severity levels. However, additional research is needed to quantify the specific effect regarding collision damage severity level.
6. Evaluate sUAS configurations up to 55 lbs.
7. Study the influence of the main rotor downwash over the sUAS impact trajectory.

## 8. REFERENCES


[1] "The Economic Impact of Unmanned Aircraft Systems Integration in the United States", AUVSI's, 2013. Web link [accessed 07/27/2021]: https://www.auvsi.org/our-impact/economic-report

[2] Olivares G., et al., "UAS Airborne Collision Severity Evaluation. Executive Summary – Structural Evaluation", ASSURE Report, 2017.

[3] "Unmanned Aircraft Systems", FAA Aerospace Forecasts, 2021. Web link [accessed 07/27/2021]:https://www.faa.gov/data_research/aviation/aerospace_forecasts/media/Unmanned_Aircraft_Systems.pdf

[4] Olivares, G., Gomez, L. and Marco, R., "Volume VII – UAS Airborne Collision Severity Evaluation – 14 CFR Part 23 General Aviation", Federal Aviation Administration, Report DOT/FAA/AR-XX/XX, 2022.

[5] Olivares, G., Gomez, L., Espinosa de los Monteros, J., Baldridge, R., Zinzuwadia, C., and Aldag, T., "Volume II – UAS Airborne Collision Severity Evaluation – Quadcopter", Federal Aviation Administration, Report DOT/FAA/AR-XX/XX, 2017.

[6] Olivares, G., Lacy, T., Kota, K., Ricks, T., Jayakody, N., Gomez, L., Espinosa de los Monteros, J., and Baldridge, R., "Volume III – UAS Airborne Collision Severity Evaluation – Fixed Wing", Federal Aviation Administration, Report DOT/FAA/AR-XX/XX, 2017.

[7] Public Law 112-95, Section 331(8)

[8] FAA Advisory Circular AC 107-2, "Small Unmanned Aircraft System (sUAS)", Washington, DC, 2016.

[9] Micro Unmanned Aircraft Systems Aviation Rulemaking Committee, "ARC Recommendations Final Report", 2016.

[10] U.S. Code of Federal Regulations, Title 14, Part 25, "Airworthiness standards: transport category airplanes", Washington, DC, U.S. Government Publishing Office, 2016.

[11] U.S. Code of Federal Regulations, Title 14, Part 23, "Airworthiness standards: normal category airplanes", Washington, DC, U.S. Government Publishing Office, 2016.

[12] U.S. Code of Federal Regulations, Title 14, Part 27, "Airworthiness standards: normal category rotorcraft", Washington, DC, U.S. Government Publishing Office, 2016.

[13] U.S. Code of Federal Regulations, Title 14, Part 29, "Airworthiness standards: transport category rotorcraft", Washington, DC, U.S. Government Publishing Office, 2016.

[14] Range Safety Group, Range Commanders Council, "Range Safety Criteria for Unmanned Air Vehicles", Document 323-99, 2001.

[15] Lum, C. W., and Waggoner, B., "A Risk Based Paradigm and Model for Unmanned Aerial Systems in the National Airspace", *Infotech@Aerospace Conferences*, 2011-1424, AIAA, St. Louis, MO, 2011.

[16] Dalamagkidis, K., Valavanis, K., and Piegl, L. A., *On Integrating Unmanned Aircraft Systems into the National Airspace System*, 2nd ed., Springer Netherlands, 2012.

[17] McGeer, T., “Aerosonde Hazard Estimation”, The Insitu Group, 1994.

[18] Civil Aviation Safety Authority, “Potential Damage Assessment of a Mid-Air Collision with a Small UAV”, Technical Report, 2013.

[19] Fraser, C. S. R., and Donnithorne-Tait, D., “An Approach to the Classification of Unmanned Aircraft”, *26th International Conference on Unmanned Air Vehicle Systems 2011*, Bristol, UK, 2011, pp. 157-211.

[20] Marshall, M. M., Anderson, E. E., and Tighe, D. E., “A Literature Review in Support of TCRG 14-05: UAS Systems Safety Criteria”, Draft Report, FAA Award 14-G-007, 2015.

[21] Jimenez, H., Mavris, D., Hoffman, D., Mines, J., and O’Sullivan, S., “A Survey of Evaluation Methods for Unmanned Aircraft Risk and Safety to Third Parties”, Report, Federal Aviation Administration, 2015.

[22] FAA COE Task: A11LUAS.COE.7 .2 UAS Airborne Collision Severity Evaluation.

[23] Olivares, G., Gomez, L., Espinosa de los Monteros, J., Baldridge, R., and Marco, R., “Annex B NIAR Final Report Task A14: UAS Ground Collision Severity Evaluation 2017-2018”, Federal Aviation Administration, Report DOT/FAA/AR-XX/XX, 2019.

[24] Azzedine, D. et al., “Drone Impact Assessment on Aircraft Structure: Flat Plate Testing and Analysis”, National Research Council Canada, Report CR-GTL-2020-0053, 2020.

[25] Olivares, G., Gomez, L., Ly, H., and Marco, R., “Task A17: UAS Engine Ingestion Severity Evaluation”, Federal Aviation Administration, Report DOT/FAA/AR-XX/XX, 2022.

[26] “LS-DYNA Theory Manual”, *LS-DYNA R8.0 User Manual*, Livermore Software Technology Corporation, 2015.

[27] “LS-DYNA Keywords User’s Manual”, *LS-DYNA R8.0 User Manual Vol. I*, Livermore Software Technology Corporation, 2015.

[28] Hashin, Z. and Rotem, A., “A Fatigue Failure Criterion for Fiber Reinforced Materials”, Journal of Composite Materials, 1973.

[29] “LS-DYNA Keywords User’s Manual – Material Models”, *LS-DYNA R8.0 User’s Manual Vol. II*, Livermore Software Technology Corporation, 2015.

[30] MMPDS-09, *Metallic Material Properties Development, and Standardization (MMPDS)*, Chapter 9, Ed. 7, Battelle Memorial Institute, 2014.

[31] Jackson, P., *Jane’s All the World’s Aircraft 2007-2008*, Jane’s Information Group, 2007.

[32] Olivares, G., Gomez, L., Baldridge, R., Marco, R., Ly, H., “Large sUAS Airborne Collision Severity Evaluation with 14 CFR 25 Aircraft - ATO Office of Safety”, Federal Aviation Administration, Report DOT/FAA/AR-XX/XX, 2020.

[33] Olivares, G., Gomez, L., Zinzuwadia, C., Surya Kadiyala, S., Marco, R., “Analysis of Collision Severity between Small Unmanned Aircraft Systems and Fixed Wing, General Aviation Aircraft”, Federal Aviation Administration, Report DOT/FAA/AR-XX/XX, 2021.

APPENDIX A – COMPONENT LEVEL TEST

## A.1 TEST 01 – BATTERY AT 500 KNOTS – SHARP EDGE

Test 01 consists of the impact of battery A with the sharp aluminum edge at a nominal velocity of 257.2 m/s (500 knots). Two iterations were carried out to evaluate data repeatability. For kinematics comparison, NIAR has identified iteration 1 as the repetition with the least deviation regarding the nominal test requirements. All batteries were fully charged previous to the test.

An initial velocity of 262.73 m/s (510.7 knots) was applied to the battery A FEM, which corresponds to the velocity recorded for repetition 1 in the test documentation (APPENDIX B).

Figure 170 through Figure 173 show the comparison of the kinematics between the test and simulation at four different instances of the impact event.

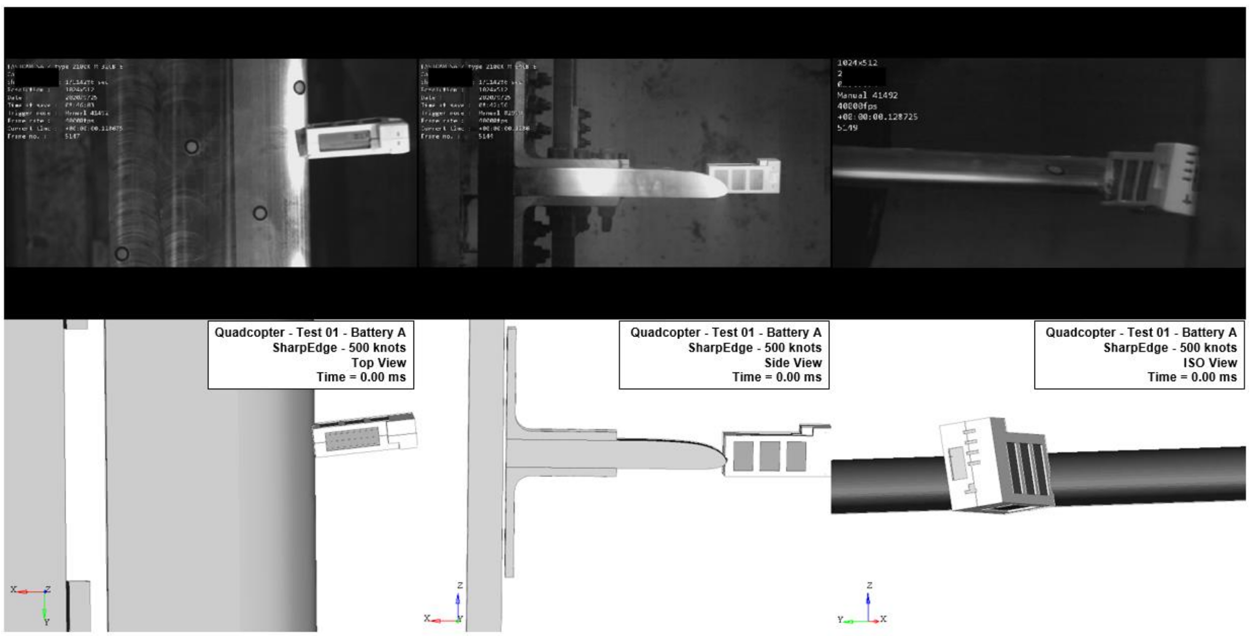


Figure 170. Comparison for battery A impact on sharp edge at 262.73 m/s (510.7 knots) at t = 0.00 ms (beginning of contact).

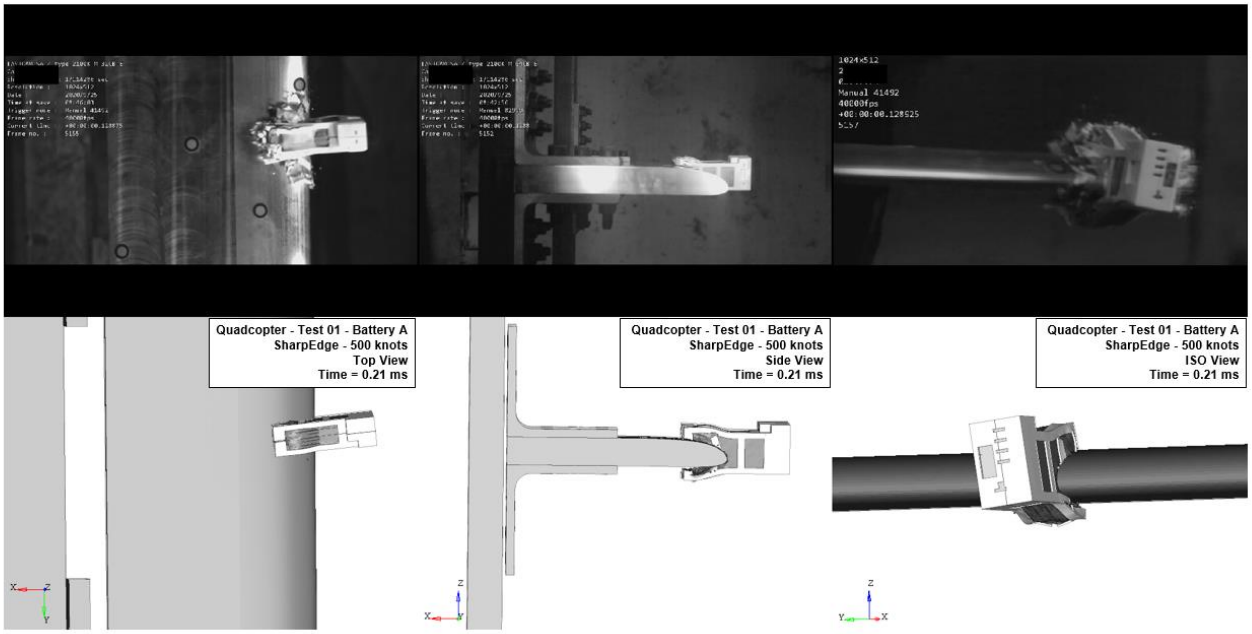


Figure 171. Comparison for battery A impact on sharp edge at 262.73 m/s (510.7 knots) at t = 0.21 ms.

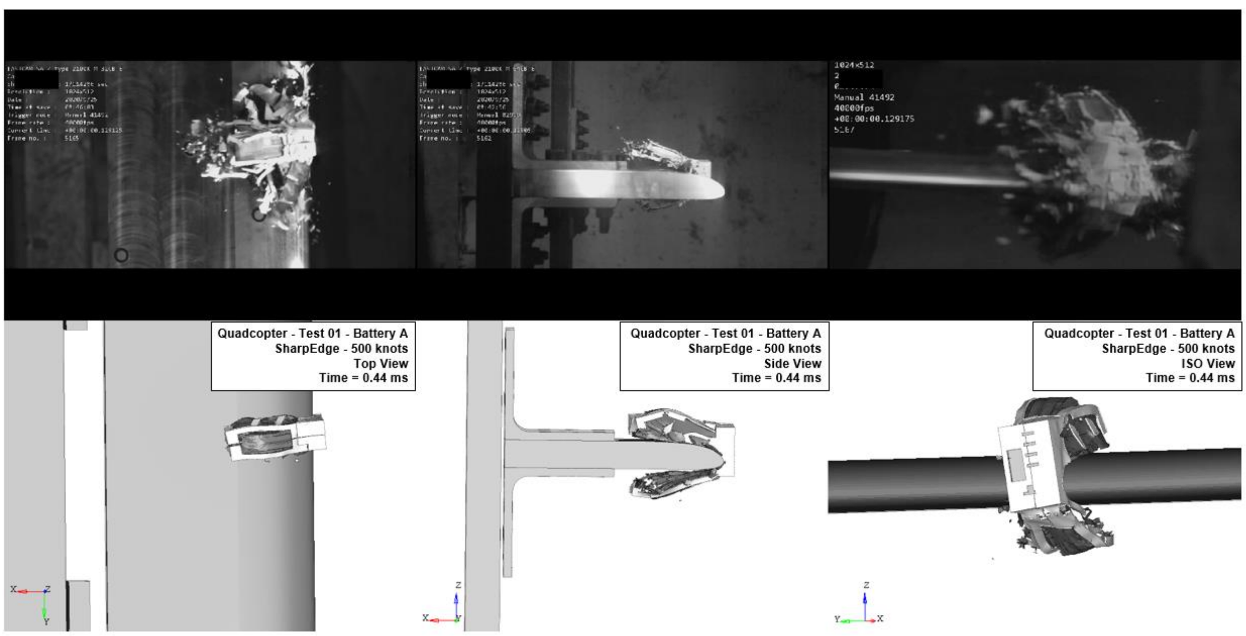


Figure 172. Comparison for battery A impact on sharp edge at 262.73 m/s (510.7 knots) at t = 0.44 ms.

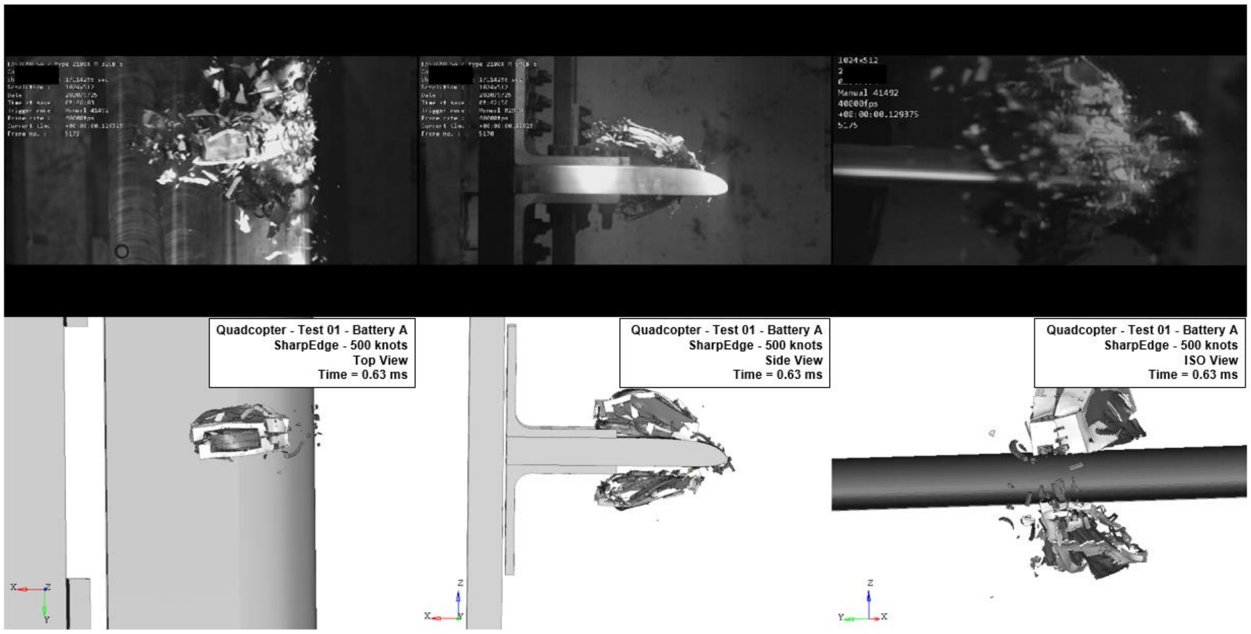


Figure 173. Comparison for battery A impact on sharp edge at 262.73 m/s (510.7 knots) at t = 0.63 ms (end of contact).

Figure 174 compares the load-time history of both test repetitions and the simulation load output. All the curves were filtered with a low-pass filter of 15,000 Hz. The top-load cells were not considered for the comparison due to out-of-normal readings during the test. This is indicated as non-available (N/A) in Figure 174. The load data shows good repeatability for tests and simulation and confirms the good correlation of the FEM. The values on the vertical axis are not shown for confidential reasons.

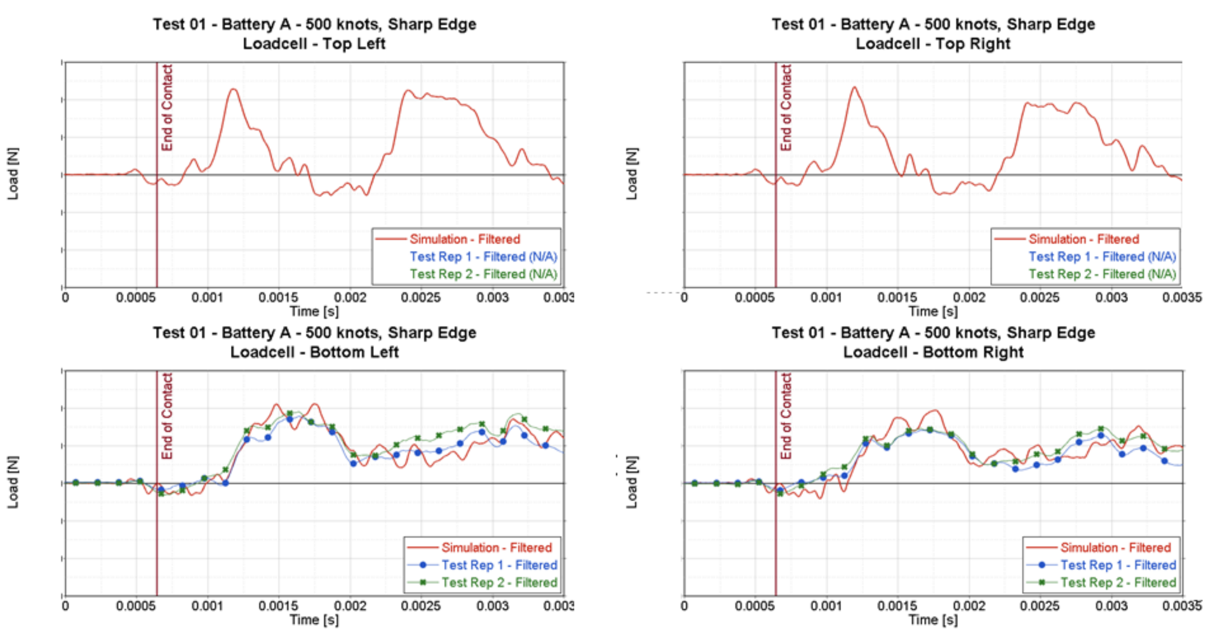


Figure 174. Load cell history data validation for battery A impact on sharp edge at 262.73 m/s (510.7 knots).

## A.2 TEST 02 – BATTERY AT 500 KNOTS – 1.6 MM AL PANEL

Test 02 consists of the impact of battery A with the 1.6 mm (0.063″) aluminum panel at a nominal velocity of 257.2 m/s. Two iterations were carried out to evaluate data repeatability. For kinematics comparison, NIAR has identified iteration 2 as the repetition with the least deviation regarding the nominal test requirements. All batteries were fully charged previous to the test.

An initial velocity of 257.56 m/s (500.6 knots) was applied to the battery A FEM, corresponding to the velocity recorded for repetition 2 in the test documentation (APPENDIX B).

Figure 175 through Figure 178 show the comparison of the kinematics between the test and simulation at four different instances of the impact event.

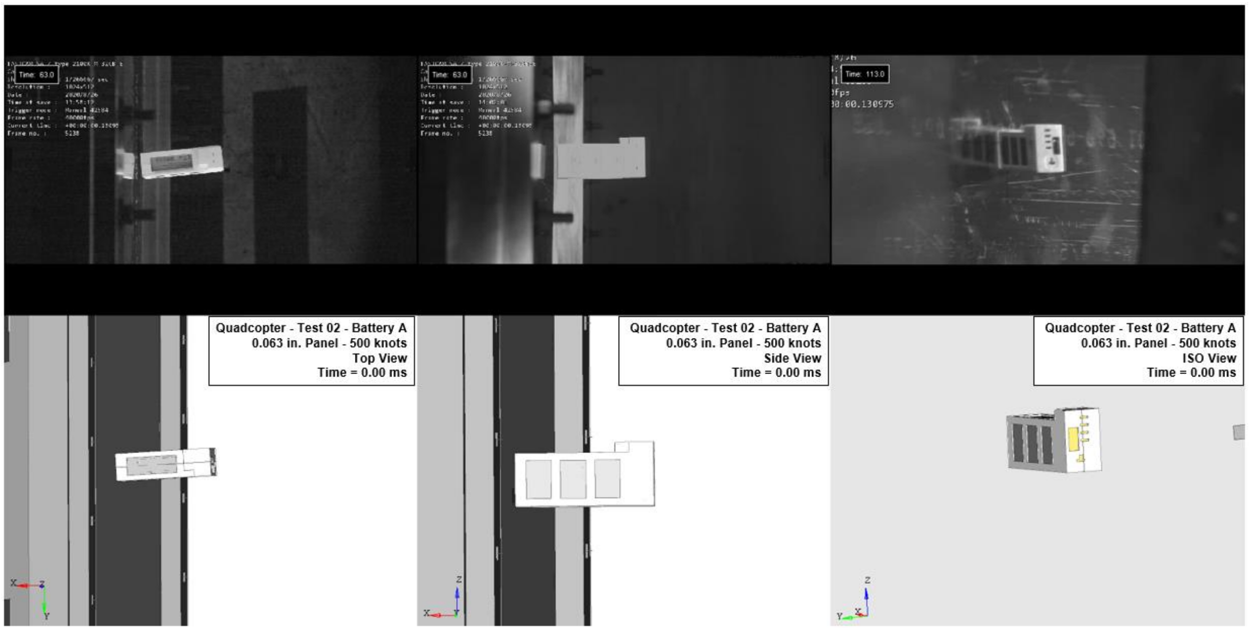


Figure 175. Comparison of battery A impact on 0.063” aluminum panel at 257.56 m/s (500.6 knots) at t = 0.00 ms (beginning of contact).

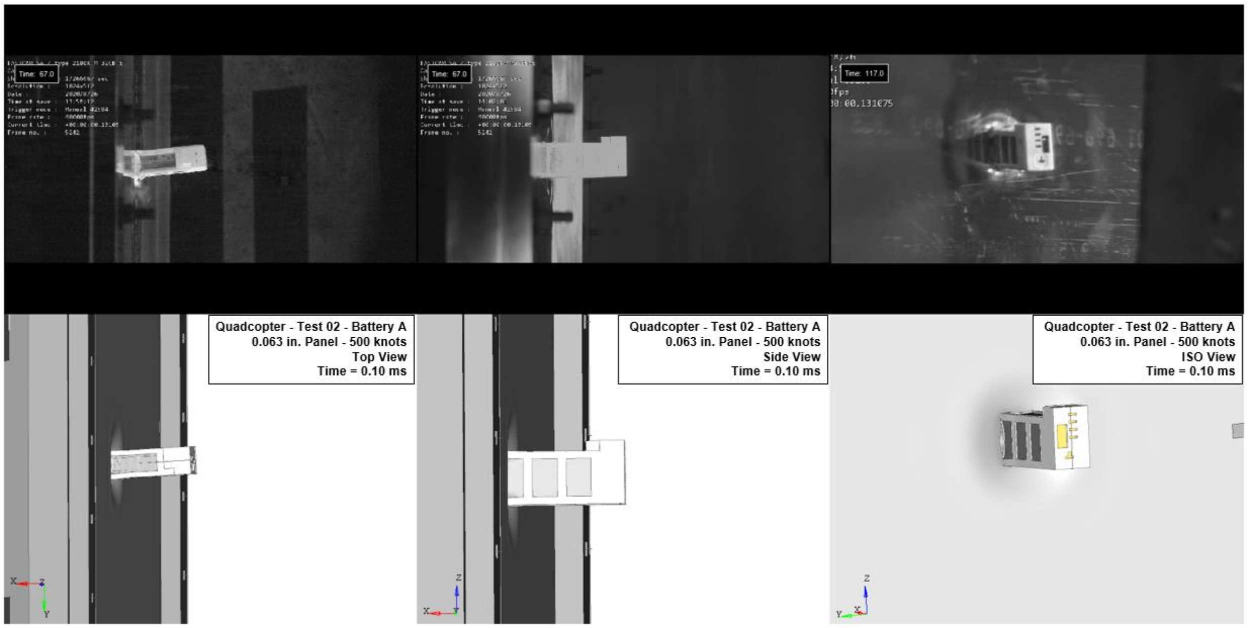


Figure 176. Comparison of battery A impact on 0.063” aluminum panel at 257.56 m/s (500.6 knots) at t = 0.10 ms (panel failure).

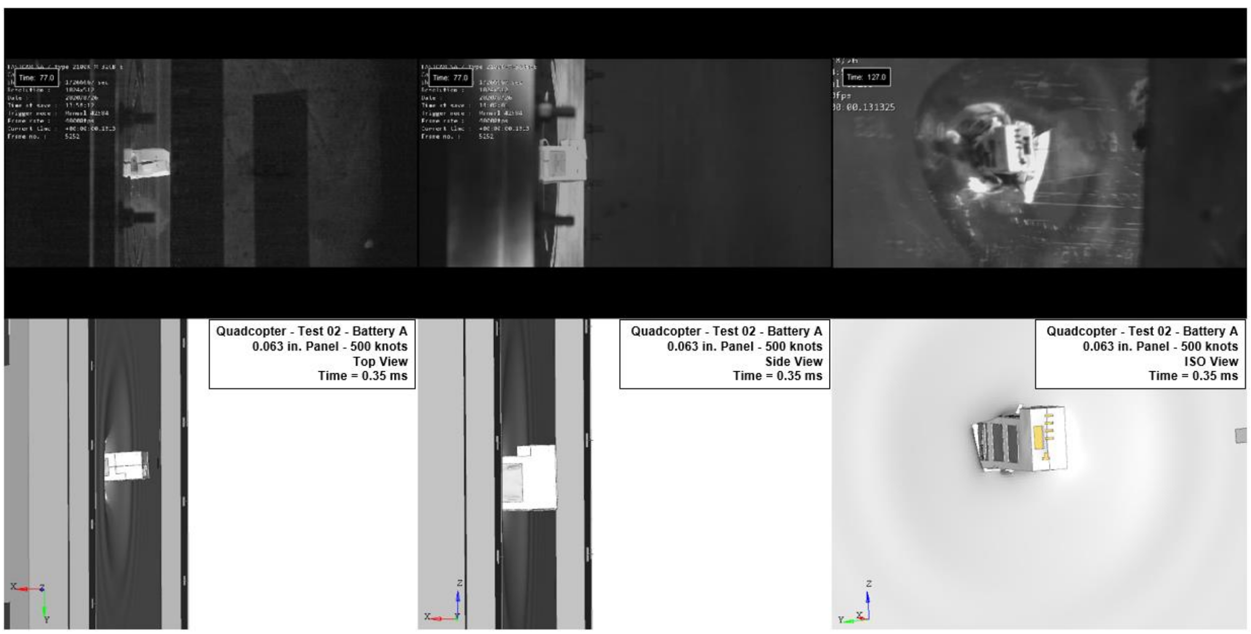


Figure 177. Comparison of battery A impact on 0.063” aluminum panel at 257.56 m/s (500.6 knots) at t = 0.35 ms.

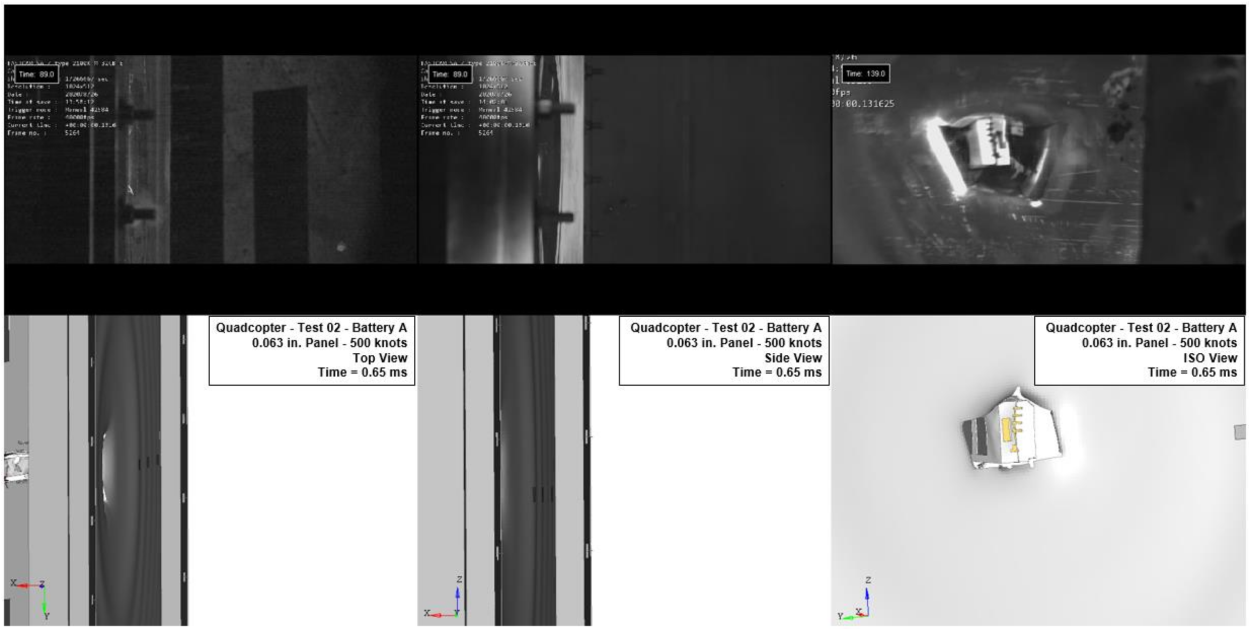


Figure 178. Comparison for battery A impact on 0.063” aluminum panel at 257.56 m/s (500.6 knots) at t = 0.65 ms (end of contact).

Figure 179 compares the simulation and test Y (horizontal) and Z (vertical) direction in-plane deformations and the out-of-plane displacements with a maximum displacement of the aluminum panel.

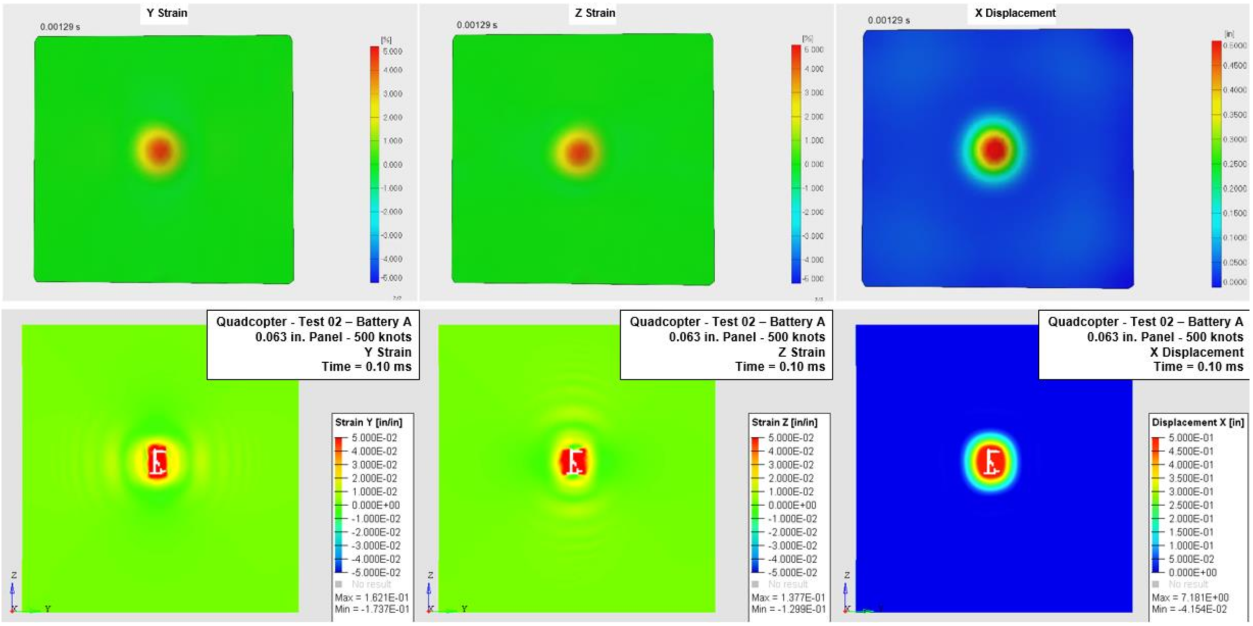


Figure 179. Comparison of test and simulation strains and displacements for battery A impact on 0.063” aluminum panel at 257.56 m/s (500.6 knots) at t = 0.10 ms (maximum displacement).

Figure 180 shows the out-of-plane displacement of the panel during the impact event obtained from the DIC data, and the simulation tracked displacements. The values on the vertical axis are not shown for confidential reasons.

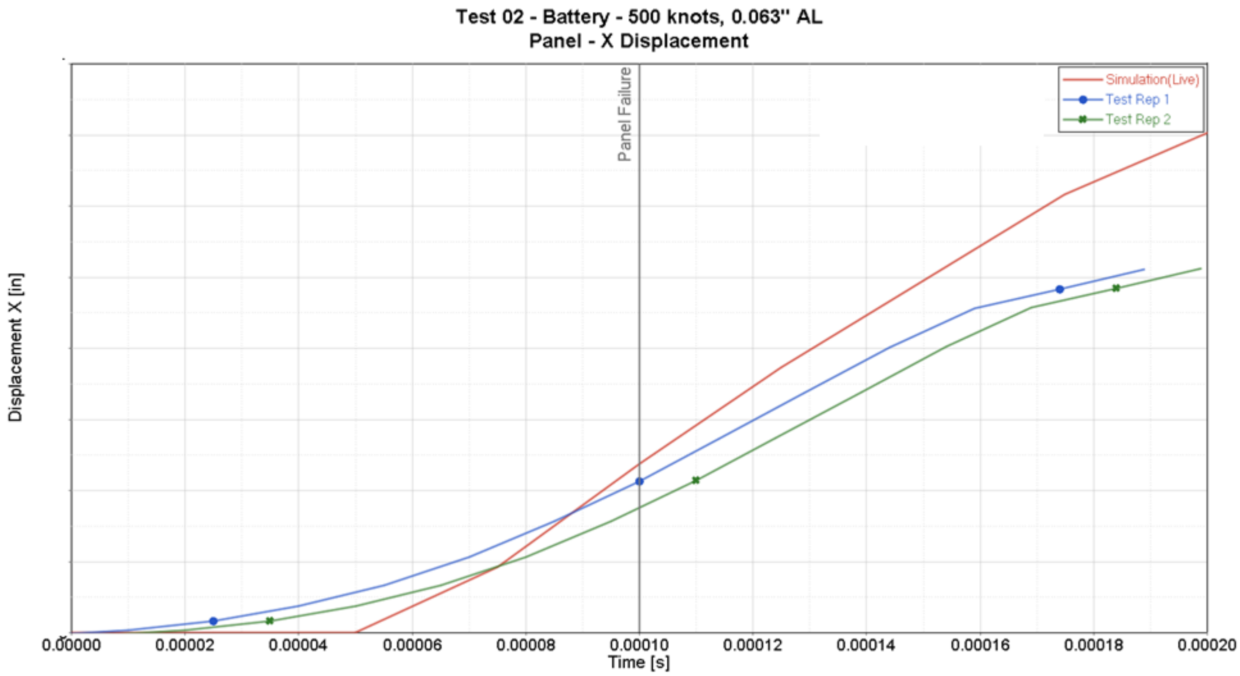


Figure 180. Comparison of the test and simulation out-of-plane displacements for battery A impact on 0.063" aluminum panel at 257.56 m/s (500.6 knots).

The physical panel was scanned after the test to compare the dimensions of the damaged area. Figure 181 compares the panel's damaged area dimensions for the test and simulation. The hole predicted by the simulation shows a similar height but a smaller width dimension. This is due to the eroding nature of the material failure defined in the panel FEM.

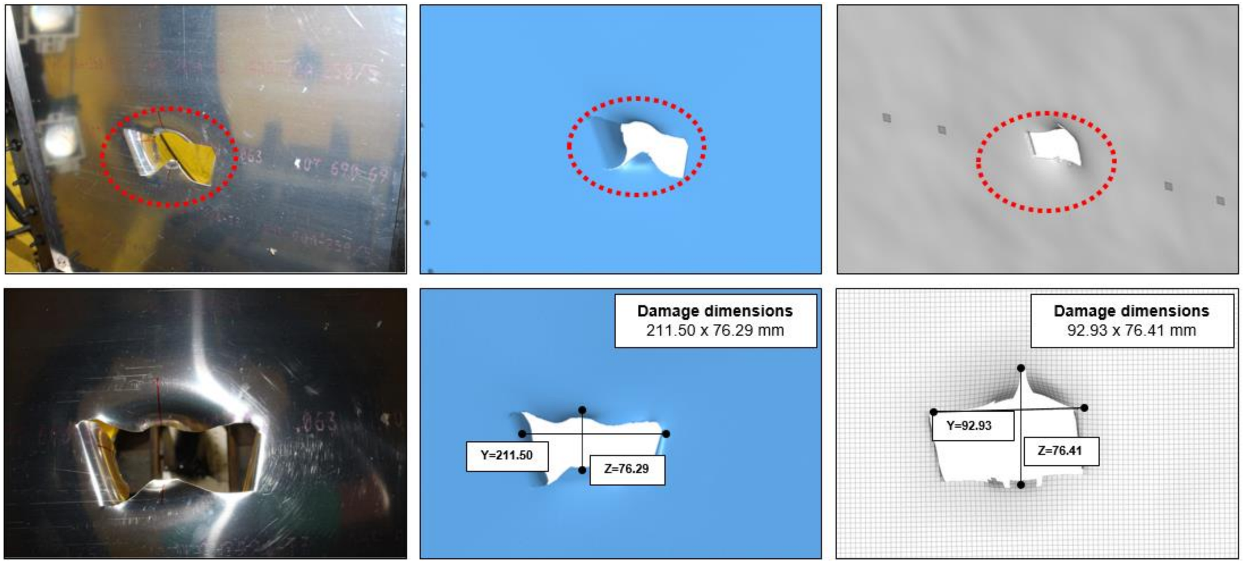


Figure 181. Comparison of the final damage of the panel for the test (left), scan (middle), and simulation (right) of the battery A impact on 0.063” aluminum panel at 257.56 m/s (500.6 knots).

Figure 182 compares the physical and simulation projectile damage. The battery case failed for both physical test and simulation, and the cells were damaged but stayed attached.

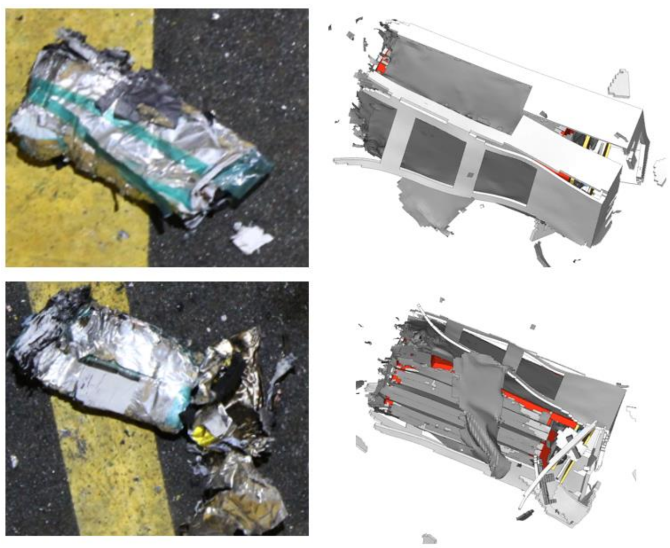

Figure 182. Comparison of the test (left) and simulation (right) projectile damage for battery A impact on 0.063” aluminum panel at 257.56 m/s (500.6 knots).

Figure 183 compares the load-time history of both test repetitions and the simulation load output. All the curves were filtered with a low-pass filter of 15,000 Hz. The load data shows good repeatability for test and simulation and confirms the good correlation up to the end of the contact, marked with an asymptote. However, the post-impact oscillations of the panel deviate from those of the physical test. Figure 184 compares the strain data collected at both test iterations to the simulation strains. The values on the vertical axis are not shown for confidential reasons.

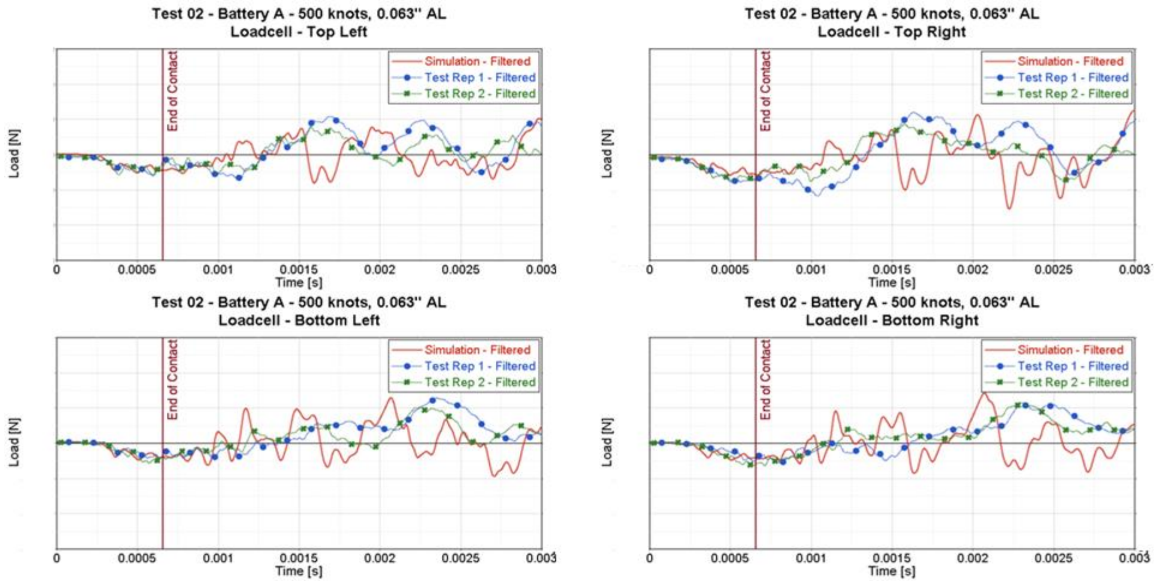


Figure 183. Load cell history data validation for battery A impact on 0.063" aluminum panel at 257.56 m/s (500.6 knots).

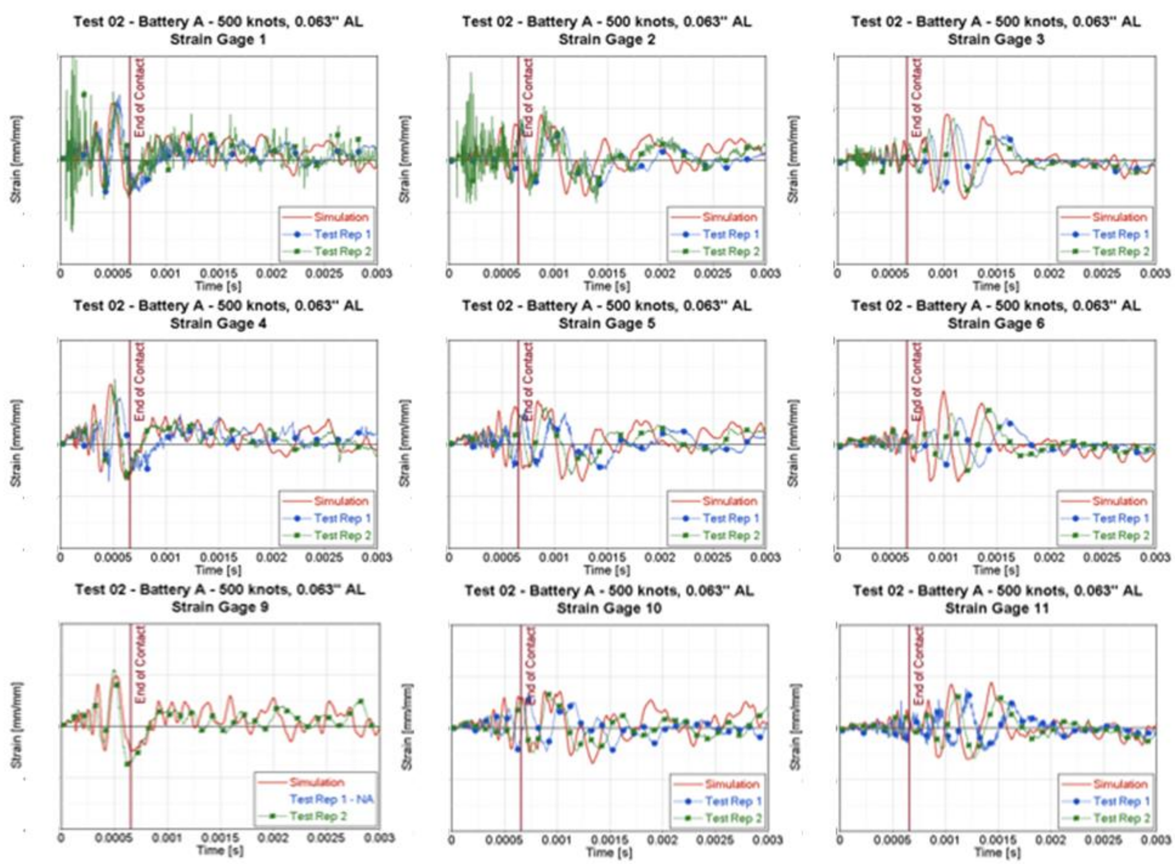


Figure 184. Strain comparison of strain gages 1-6 and 9-11 for battery A impact on 0.063" aluminum panel at 257.56 m/s (500.6 knots).

A.3 TEST 03 – BATTERY AT 500 KNOTS – 6.35 MM AL PANEL

Test 03 consists of the impact of battery A with the 6.35 mm (0.25″) aluminum panel at a nominal velocity of 257.2 m/s (500 knots). Two iterations were carried out to evaluate data repeatability. For iteration 1, a triggering error compromised the data recording. Hence, NIAR has selected iteration 2 for the FEM validation. All batteries were fully charged previous to the test.

An initial velocity of 257.56 m/s (500.6 knots) was applied to the battery A FEM, corresponding to the velocity recorded for repetition 2 in the test documentation (APPENDIX B).

Figure 185 through Figure 188 show the comparison of the kinematics between the test and simulation at four different instances of the impact event.

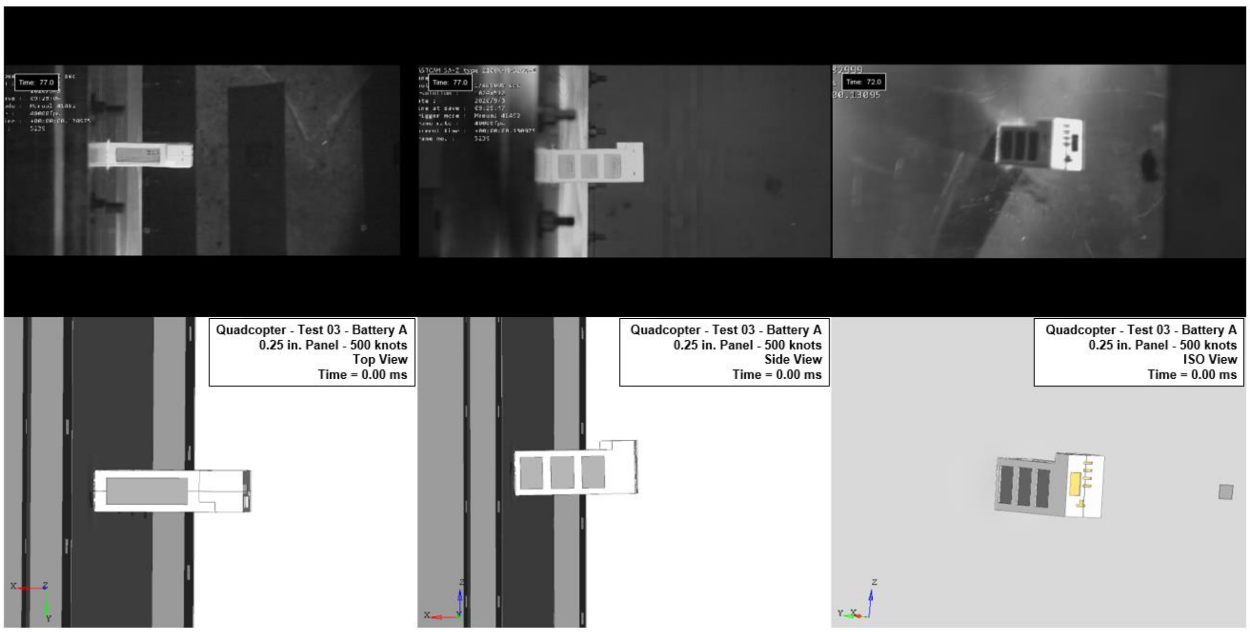


Figure 185. Comparison of battery A impact on 0.25” aluminum panel at 257.56 m/s (500.6 knots) at t = 0.00 ms (beginning of contact).

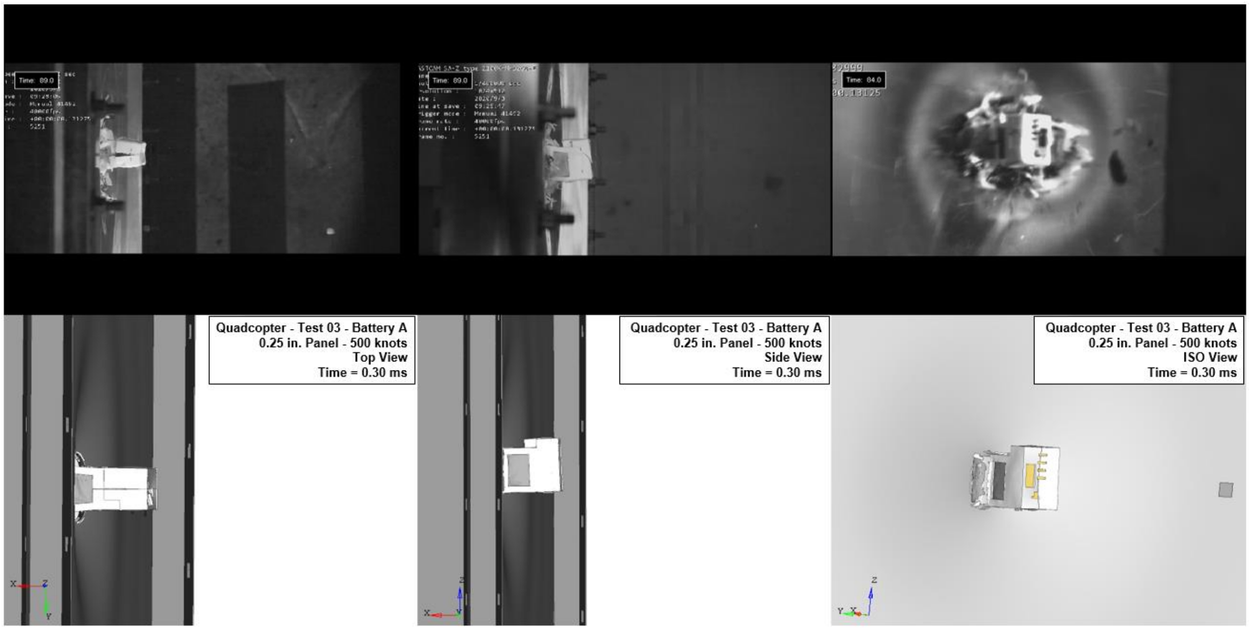


Figure 186. Comparison of battery A impact on 0.25” aluminum panel at 257.56 m/s (500.6 knots) at t = 0.30 ms.

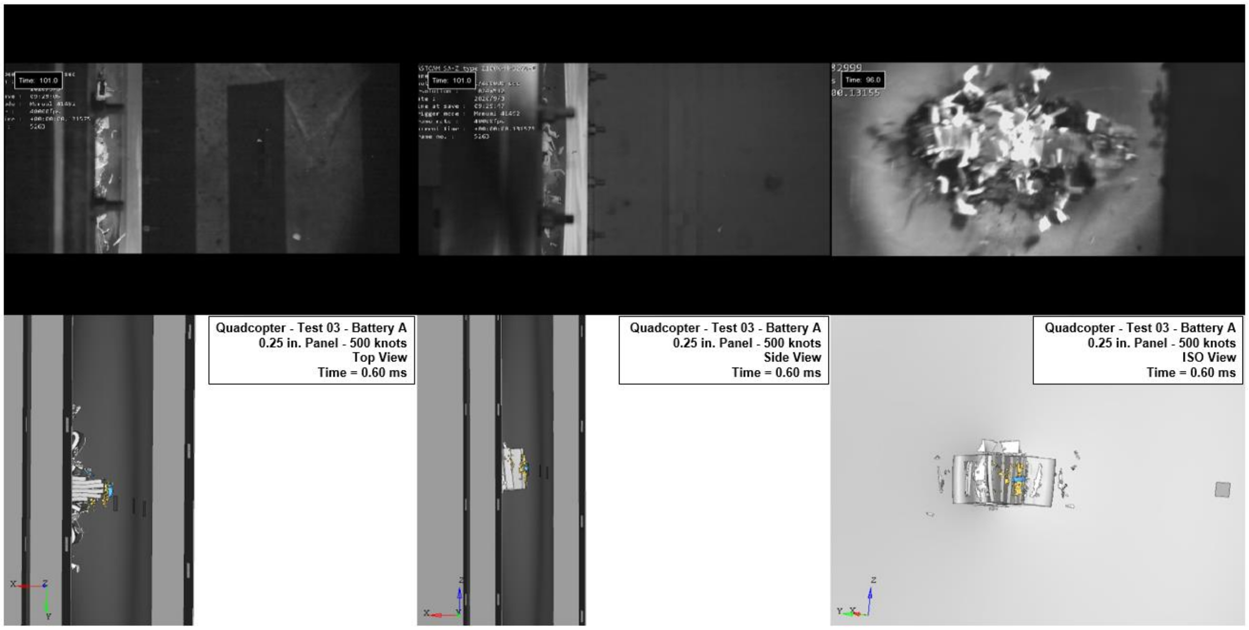


Figure 187. Comparison of battery A impact on 0.25” aluminum panel at 257.56 m/s (500.6 knots) at t = 0.60 ms.

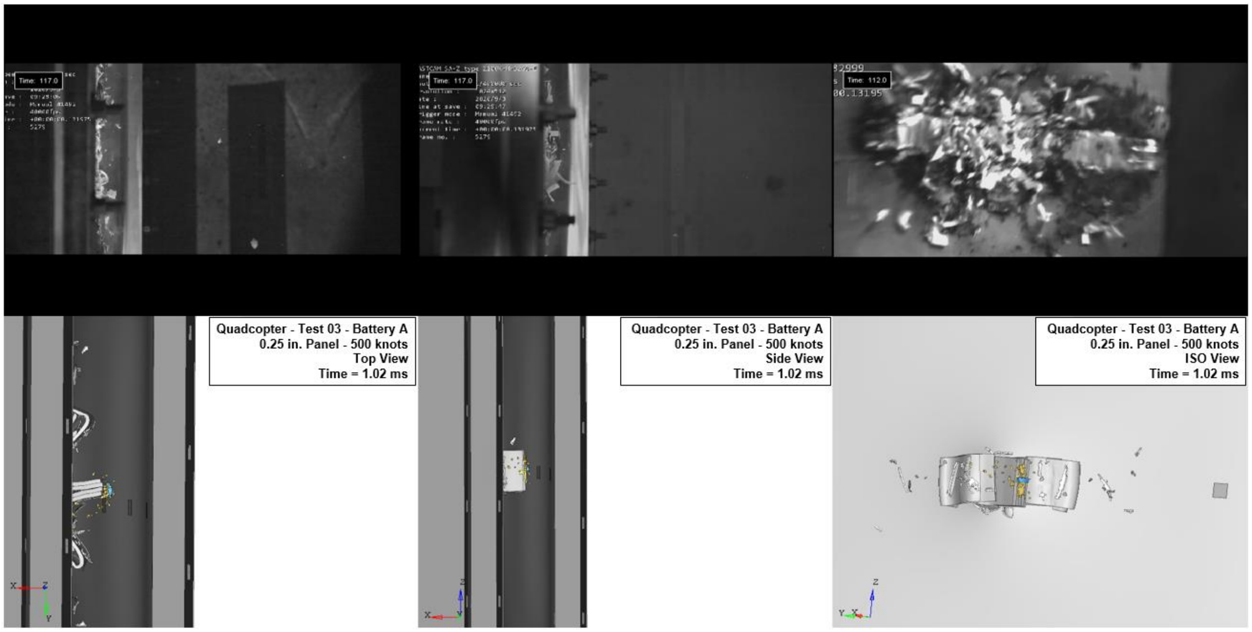


Figure 188. Comparison of battery A impact on 0.25" aluminum panel at 257.56 m/s (500.6 knots) at t = 1.02 ms (end of contact).

Figure 189 compares the simulation and test Y (horizontal) and Z (vertical) direction in-plane deformations and the out-of-plane displacements, for instance, with a maximum displacement of the aluminum panel.

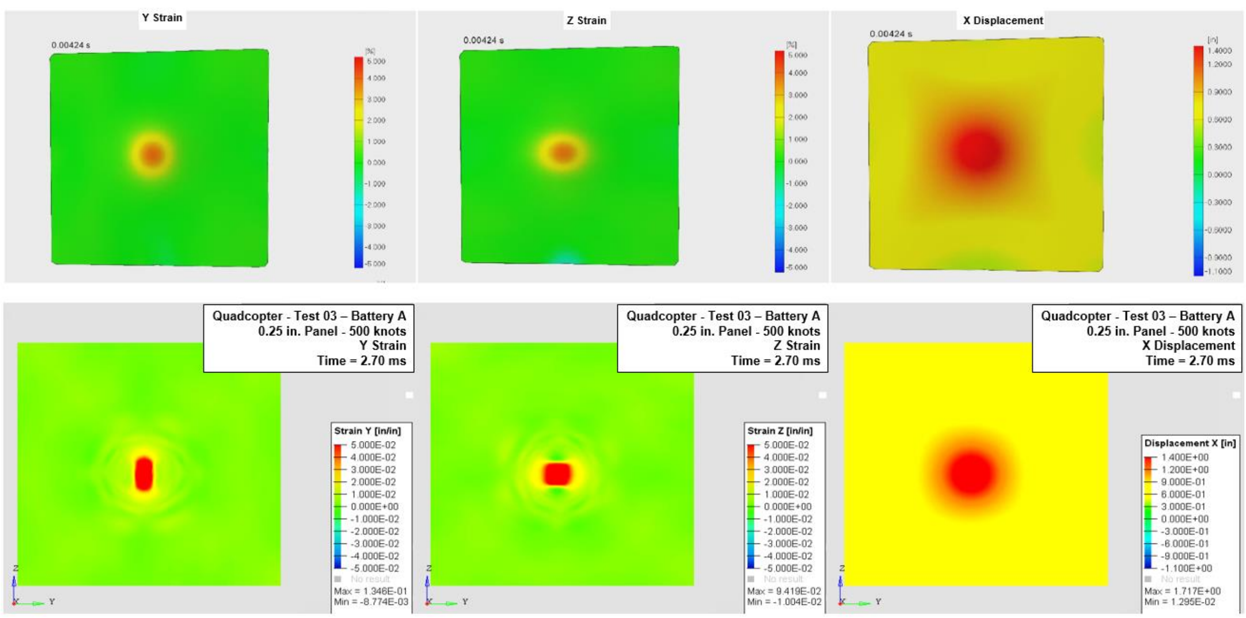


Figure 189. Comparison of test and simulation strains and displacements for battery A impact on 0.25" aluminum panel at 257.56 m/s (500.6 knots) at t = 2.70 ms (maximum displacement).

Figure 190 shows the out-of-plane displacement of the panel during the impact event obtained from the DIC data, and the simulation tracked displacements. The values on the vertical axis are not shown for confidential reasons.

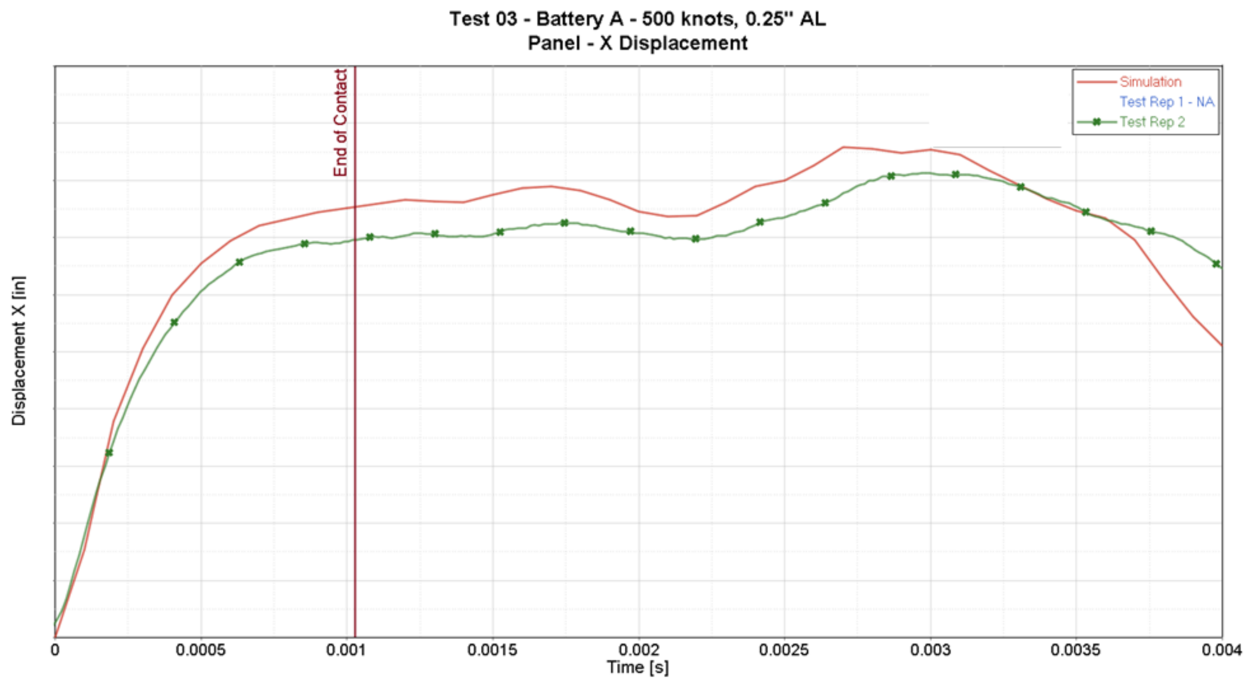


Figure 190. Comparison of the test and simulation out-of-plane displacements for battery A impact on 0.25” aluminum panel at 257.56 m/s (500.6 knots).

The physical panel was scanned after the test to compare the dimensions of the damaged area. Figure 191 compares the panel’s damaged area dimensions for the test and simulation. Again, there is good agreement between the physical test and the predicted panel’s damaged area.

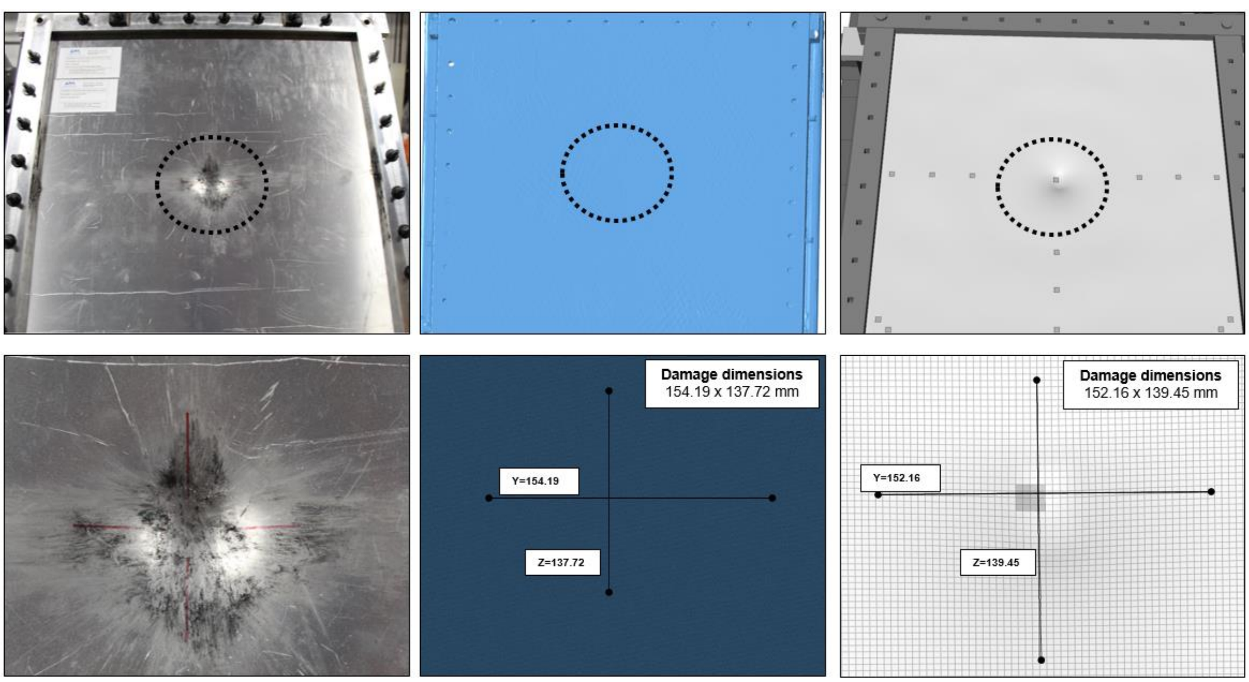


Figure 191. Comparison of the final damage of the panel for the test (left), scan (middle), and simulation (right) of the battery A impact on 0.25” aluminum panel at 257.56 m/s (500.6 knots).

Figure 192 compares the physical and simulation projectile damage. For both physical tests and simulation, the battery was highly damaged.

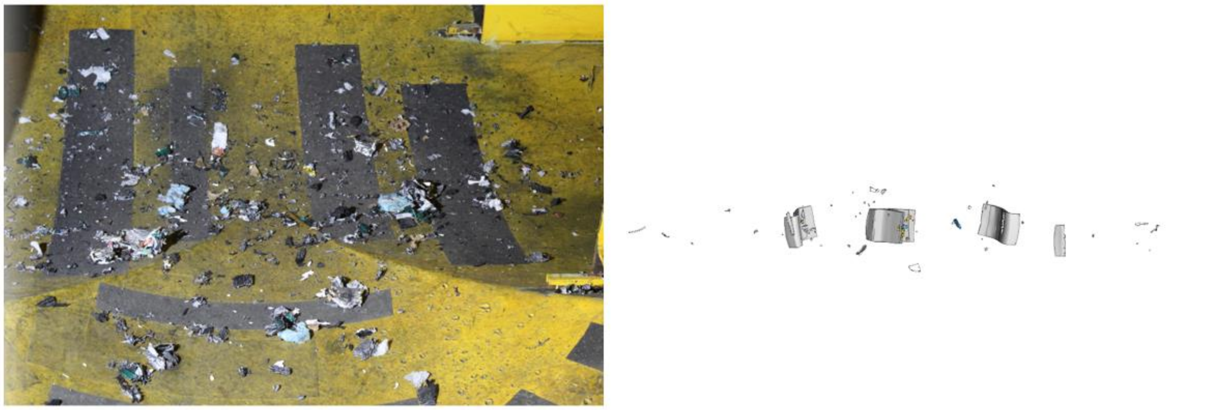

Figure 192. Comparison of the test (left) and simulation (right) projectile damage for battery A impact on 0.25” aluminum panel at 257.56 m/s (500.6 knots).

Figure 193 compares the load-time history of iteration 2 and the simulation load output. All the curves were filtered with a low-pass filter of 15,000 Hz. The repeatability of the data cannot be compared since there is data only for iteration 2. Moreover, iteration 2 load history data shows a good correlation of the FEM. Figure 194 compares the strain data collected at repetition 2 to the simulation strains. The values on the vertical axis are not shown for confidential reasons.

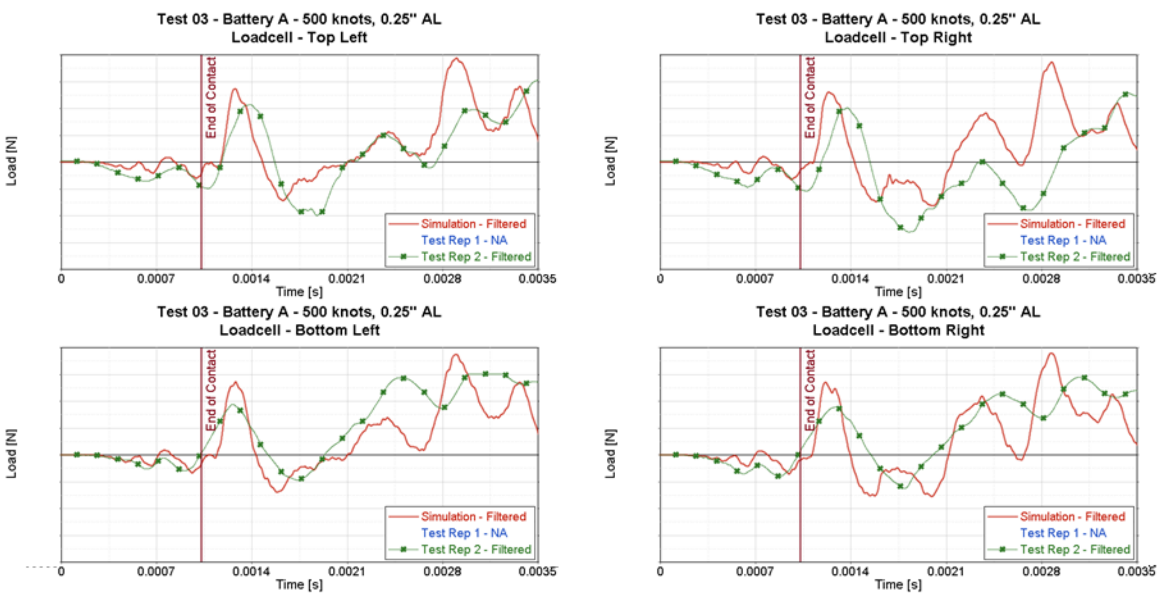


Figure 193. Load cell history data validation for battery A impact on 0.25” aluminum panel at 257.56 m/s (500.6 knots).

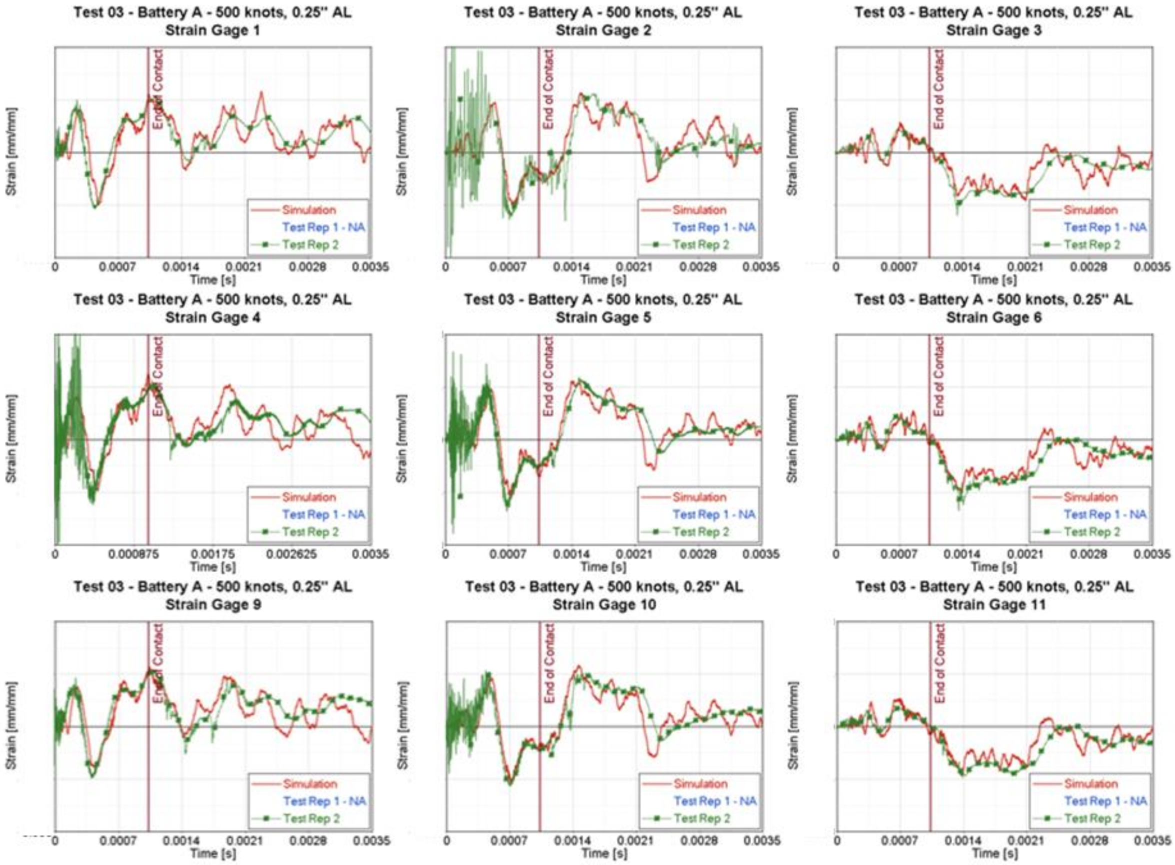


Figure 194. Strain comparison of strain gages 1-6 and 9-11for battery A impacts 0.25" aluminum panel at 257.56 m/s (500.6 knots).

## A.4 TEST 04 – MOTOR AT 500 KNOTS – 1.6 MM AL PANEL

Test 04 consists of the impact of motor A with the 1.6 mm (0.063″) aluminum panel at a nominal velocity of 257.2 m/s (500 knots). Two iterations were carried out to evaluate data repeatability. For kinematics comparison, NIAR has identified iteration 1 as the repetition with the least deviation regarding the nominal test requirements.

An initial velocity of 263.91 m/s (513 knots) was applied to the motor A FEM, corresponding to the velocity recorded for repetition 1 in the test documentation (APPENDIX B).

Figure 195 through Figure 198 show the comparison of the kinematics between the test and simulation at four different instances of the impact event.

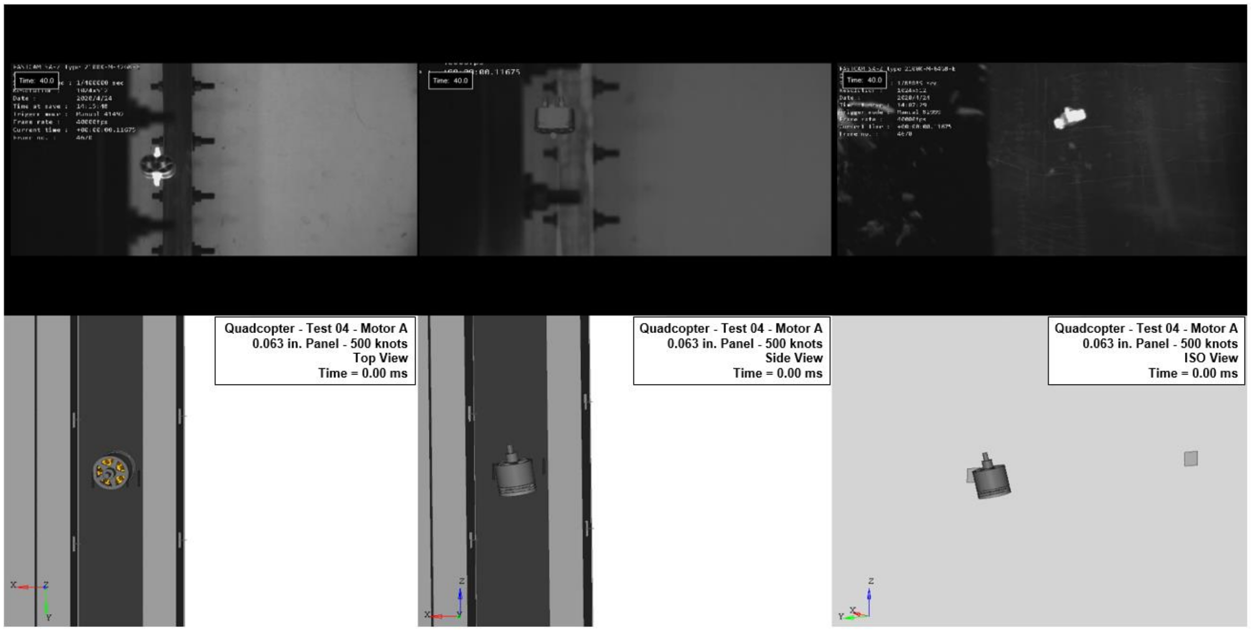


Figure 195. Comparison of motor A impact on 0.063” aluminum panel at 263.91 m/s (513 knots) at t = 0.00 ms (beginning of contact).

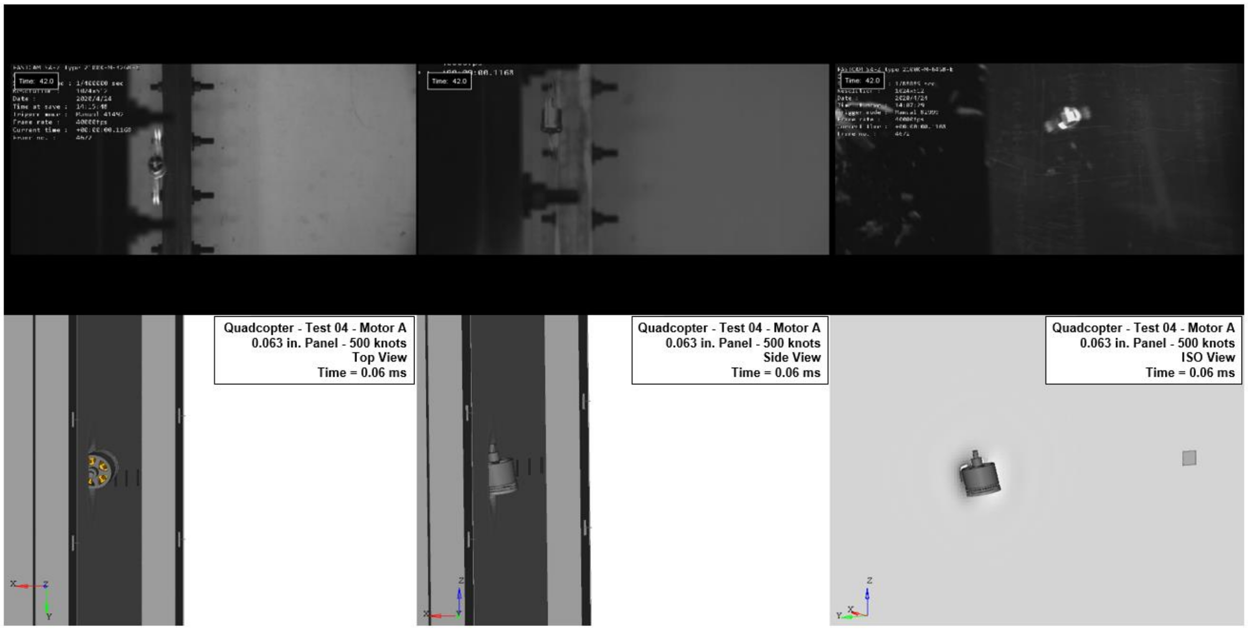


Figure 196. Comparison of motor A impact on 0.063” aluminum panel at 263.91 m/s (513 knots) at t = 0.06 ms (panel failure).

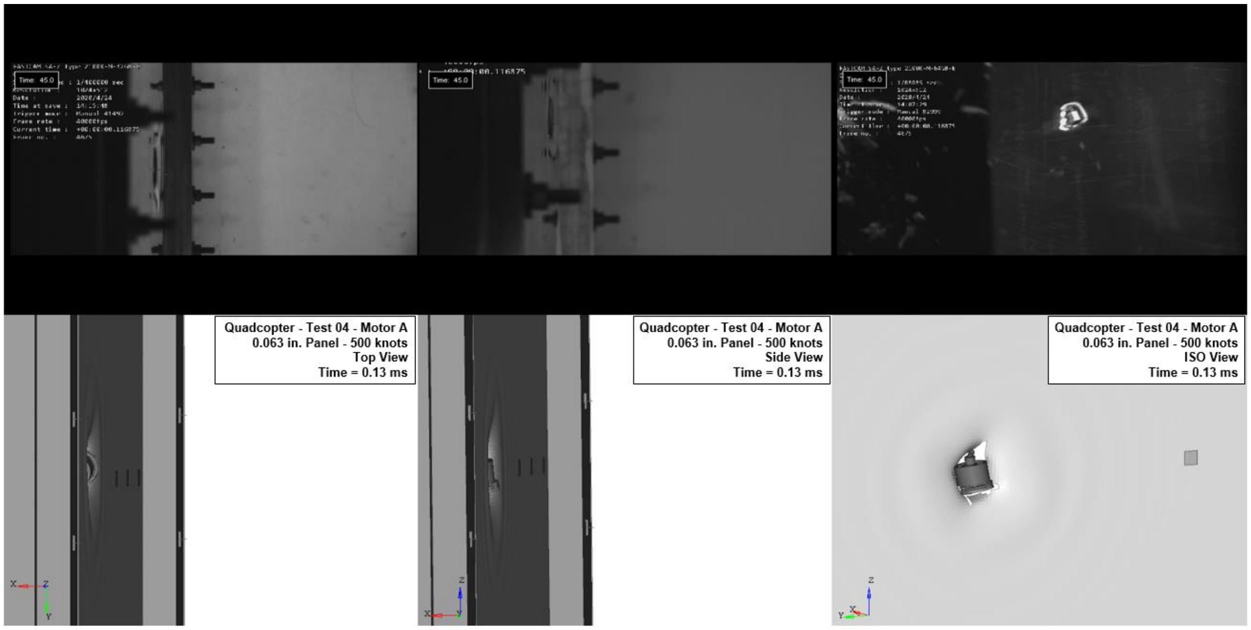


Figure 197. Comparison of motor A impact on 0.063” aluminum panel at 263.91 m/s (513 knots) at t = 0.13 ms.

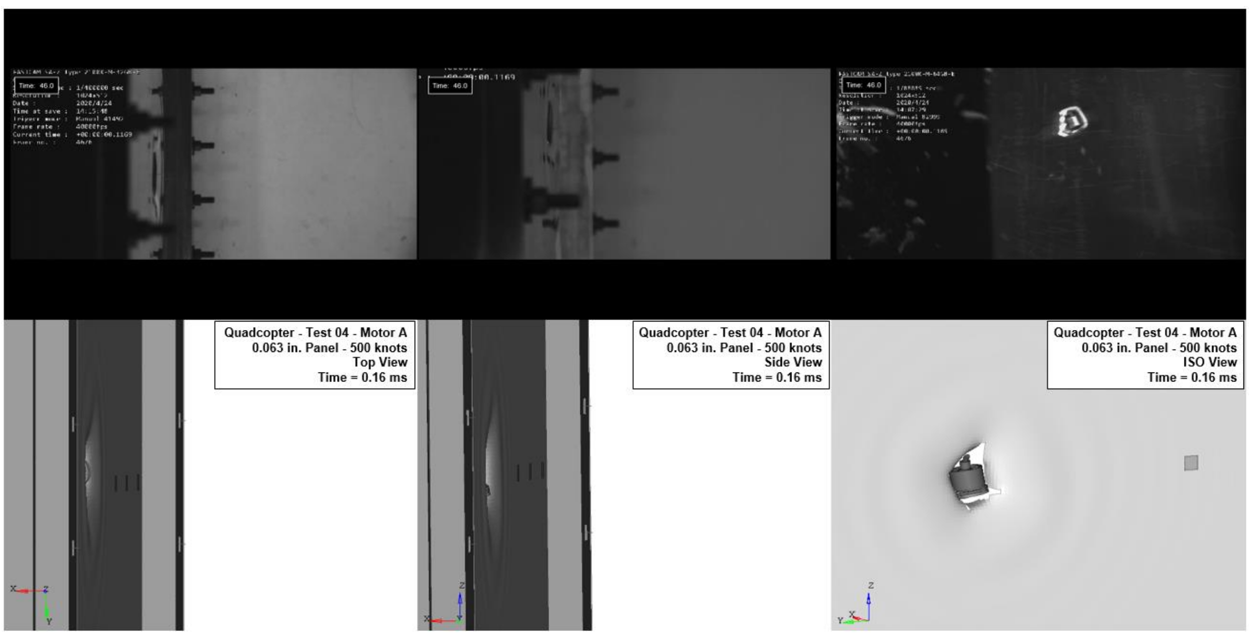


Figure 198. Comparison of motor A impact on 0.063” aluminum panel at 263.91 m/s (513 knots) at t = 0.16 ms.

Figure 199 compares the simulation and test Y (horizontal) and Z (vertical) direction in-plane deformations and the out-of-plane displacements, for instance, with the aluminum panel's maximum displacement. The simulation predicts the panel’s failure before the test, as seen in Figure 199.

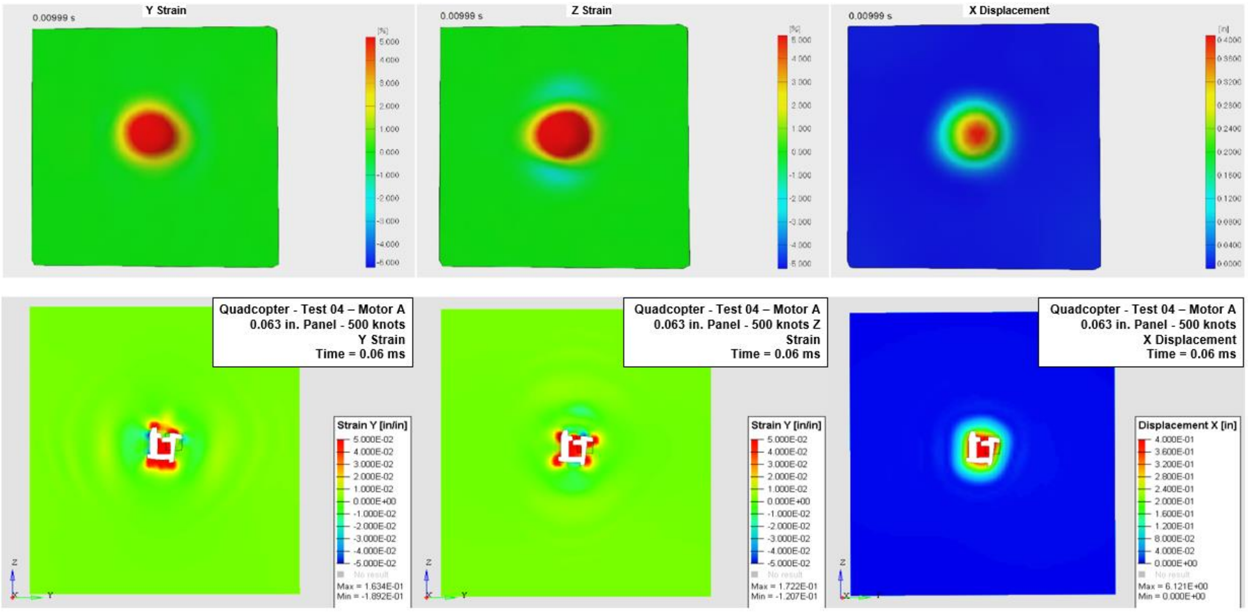


Figure 199. Comparison of test and simulation strains and displacements for motor A impact on 0.063" aluminum panel at 263.91 m/s (513 knots) at t = 0.06 ms (maximum displacement).

Figure 200 shows the out-of-plane displacement of the panel during the impact event obtained from the DIC data, and the simulation tracked displacements. The values on the vertical axis are not shown for confidential reasons.

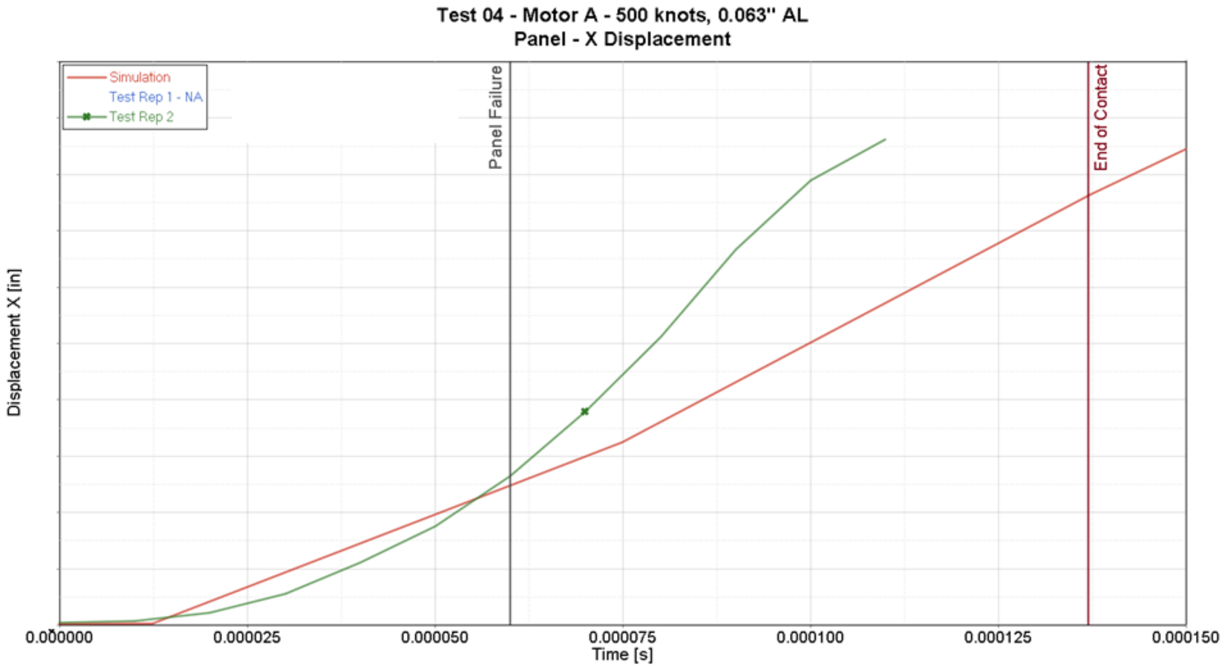


Figure 200. Comparison of the test and simulation out-of-plane displacements for motor A impact on 0.063" aluminum panel at 263.91 m/s (513 knots).

The physical panel was scanned after the test to compare the dimensions of the damaged area. Figure 201 compares the panel's damaged area dimensions for the test and simulation. Again, there is good agreement between the physical test and the predicted panel's damaged area.

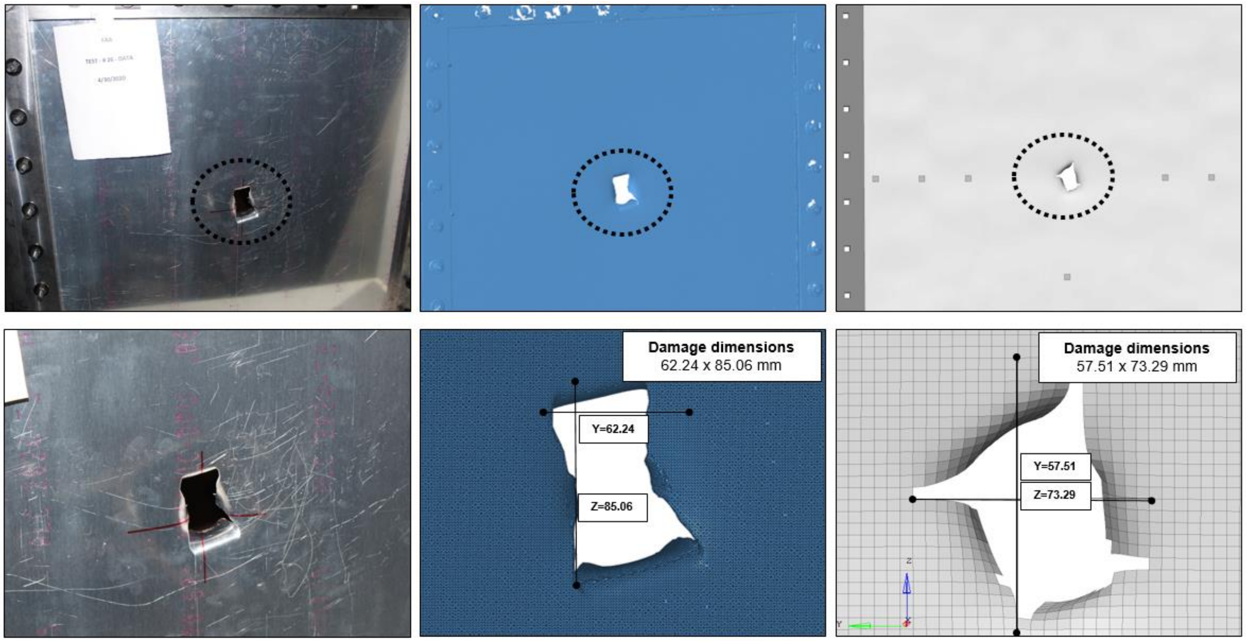


Figure 201. Comparison of the final damage of the panel for the test (left), scan (middle), and simulation (right) of the motor A impact on 0.063" aluminum panel at 263.91 m/s (513 knots).

Figure 202 compares the physical and simulation projectile damage. For both physical tests and simulation, the motor sustained minor damage.

Figure 202. Comparison of the test (left) and simulation (right) projectile damage for motor A impact on 0.063" aluminum panel at 263.91 m/s (513 knots).

Figure 203 compares the load-time history of both test repetitions and the simulation load output. All the curves were filtered with a low-pass filter of 15,000 Hz. The load data shows repeatability of the test and a good correlation of the FEM. Figure 204 compares the strain data collected at both test iterations to the simulation strains. The values on the vertical axis are not shown for confidential reasons.

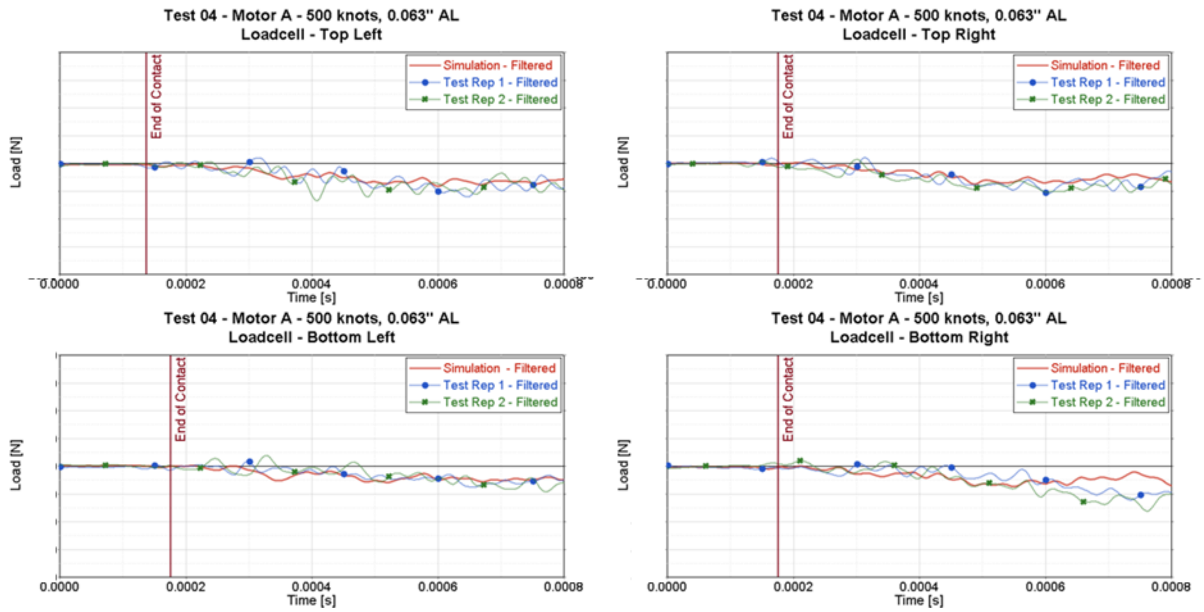


Figure 203. Load cell history data validation for motor A impact on 0.063" aluminum panel at 263.91 m/s (513 knots).

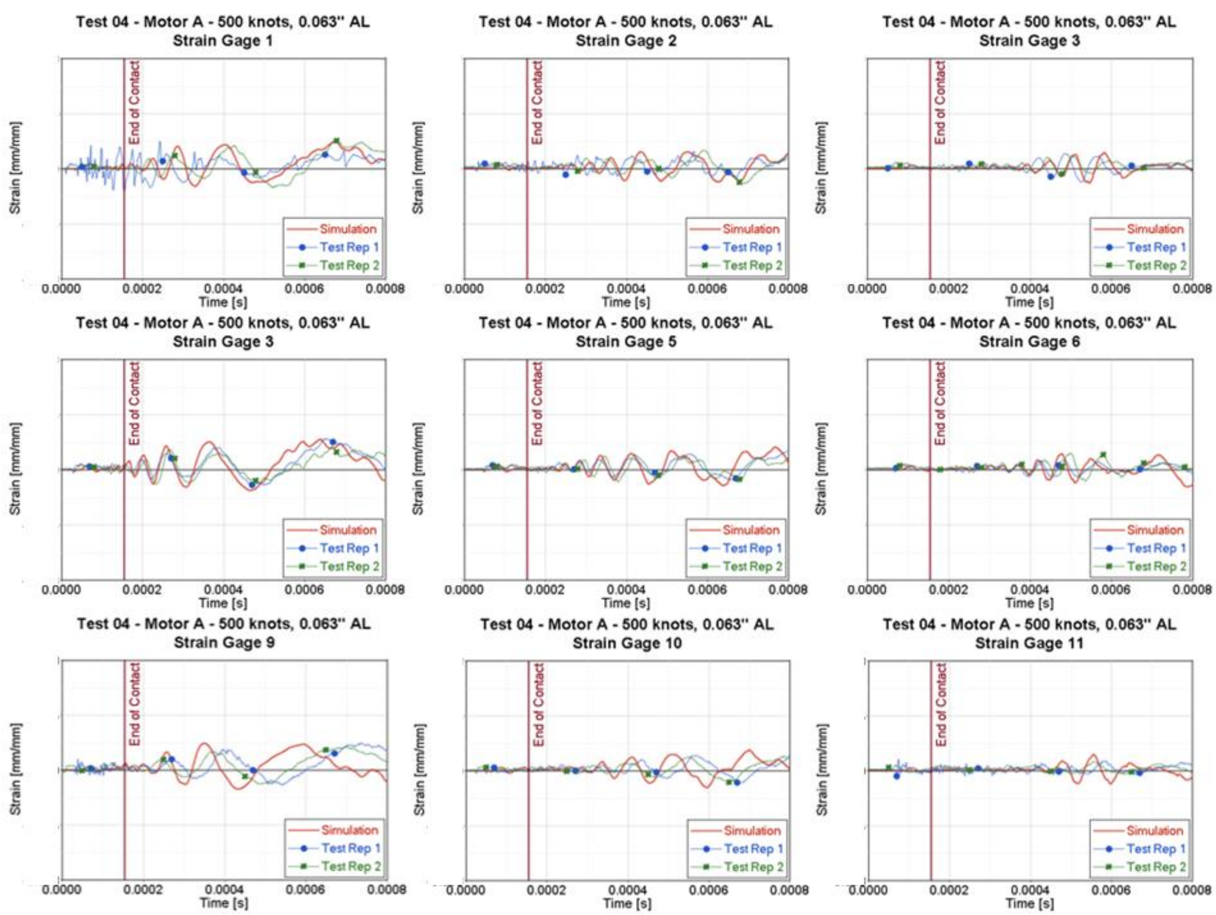


Figure 204. Strain comparison of strain gages 1-6 and 9-11 for motor A impact on 0.063" aluminum panel at 263.91 m/s (513 knots).

A.5 TEST 05 – MOTOR AT 500 KNOTS – 6.35 MM AL PANEL

Test 05 consists of the impact of battery A the 6.35 mm (0.25″) aluminum panel, at a nominal velocity of 257.2 m/s. Two iterations were carried out to evaluate data repeatability. For iteration 2, a triggering error compromised the data recording. Hence, NIAR has selected iteration 1 for the FEM validation.

An initial velocity of 267.51 m/s (520 knots) was applied to the motor A FEM, corresponding to the velocity recorded for repetition 1 in the test documentation (APPENDIX B).

Figure 205 through Figure 208 show the comparison of the kinematics between the test and simulation at four different instances of the impact event.

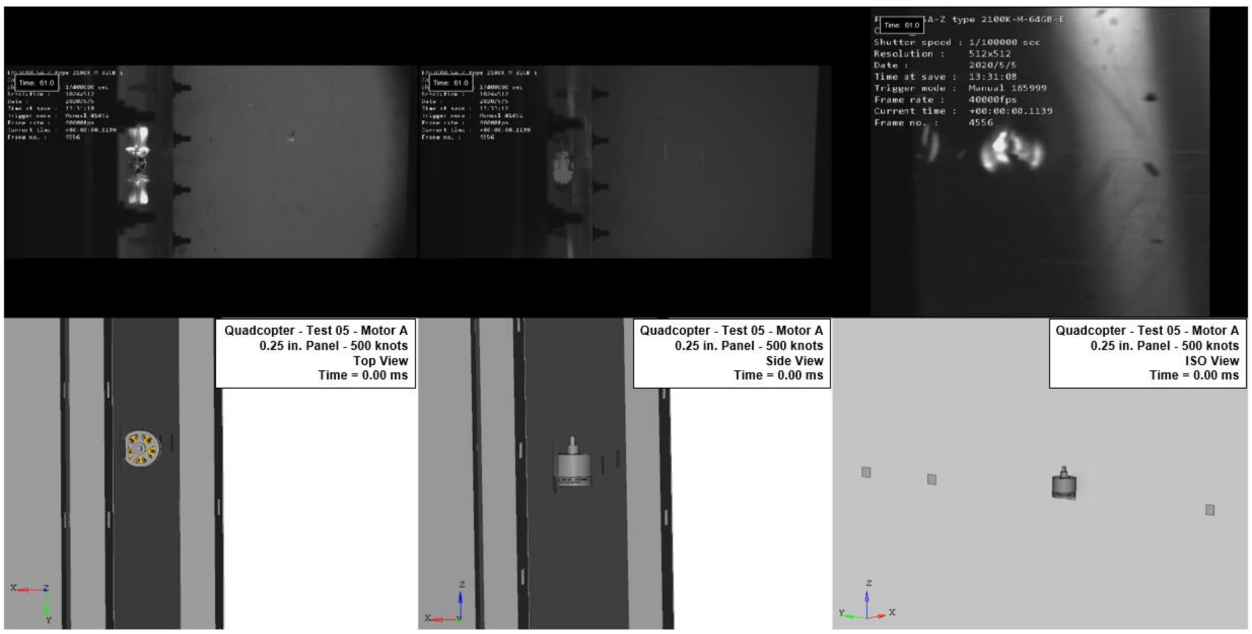


Figure 205. Comparison for motor A impact on 0.25” aluminum panel at 267.51 m/s (520 knots) at t = 0.00 ms (beginning of contact).

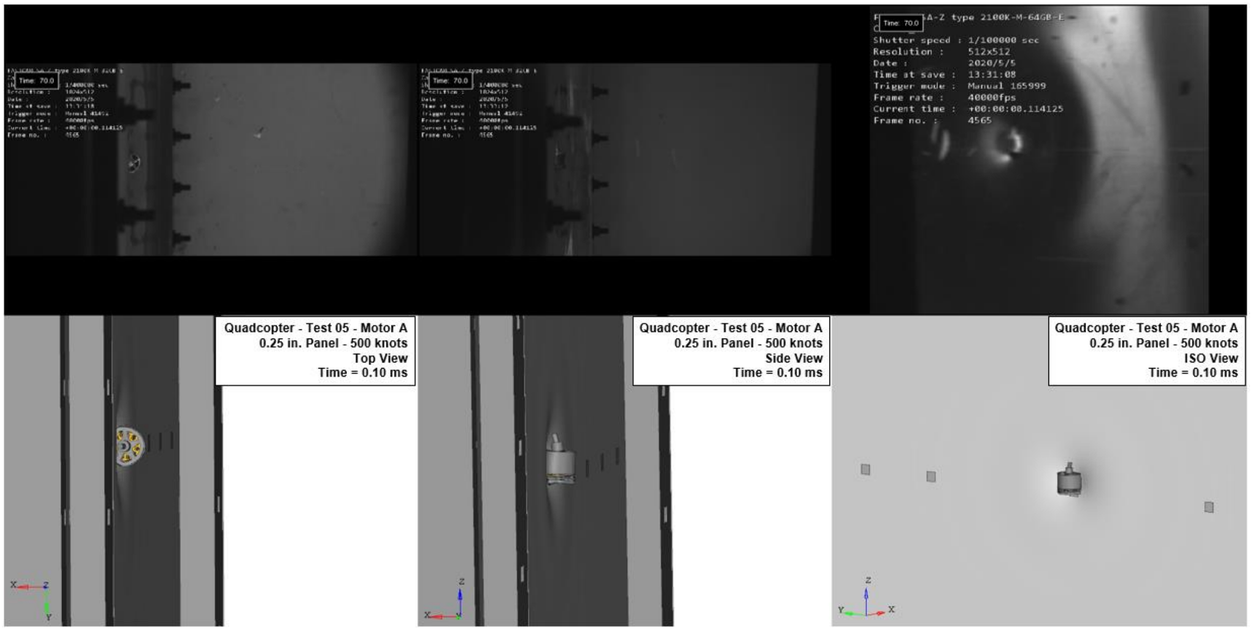


Figure 206. Comparison for motor A impact on 0.25” aluminum panel at 267.51 m/s (520 knots) at t = 0.10 ms.

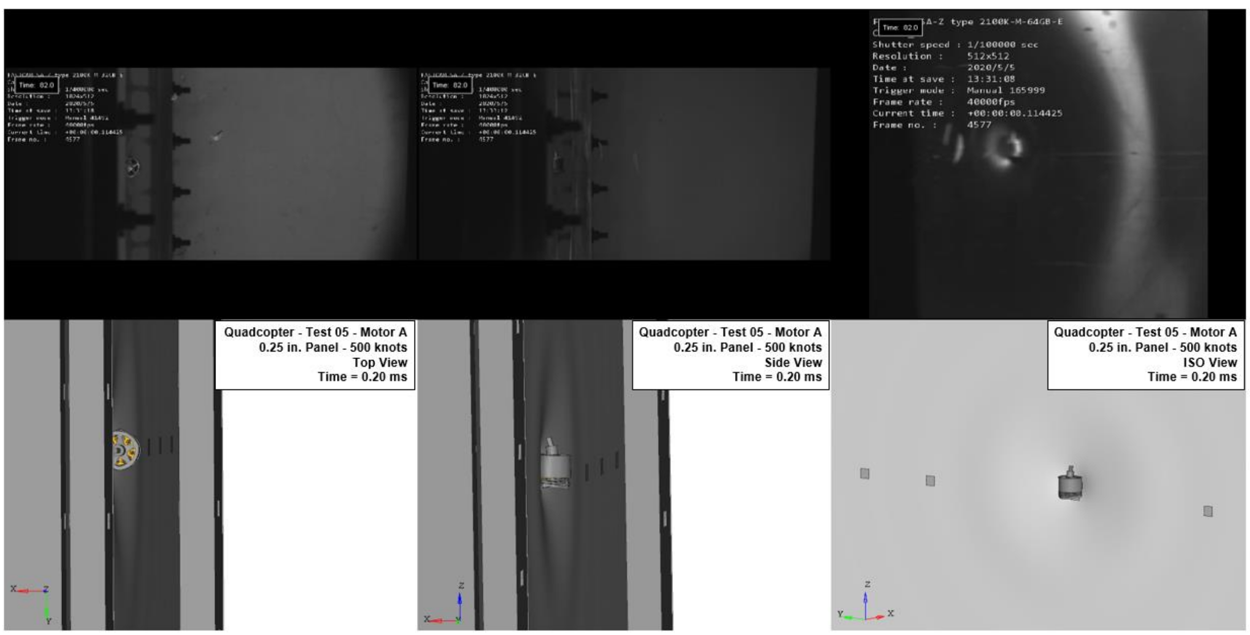


Figure 207. Comparison for motor A impact on 0.25” aluminum panel at 267.51 m/s (520 knots) at t = 0.20 ms.

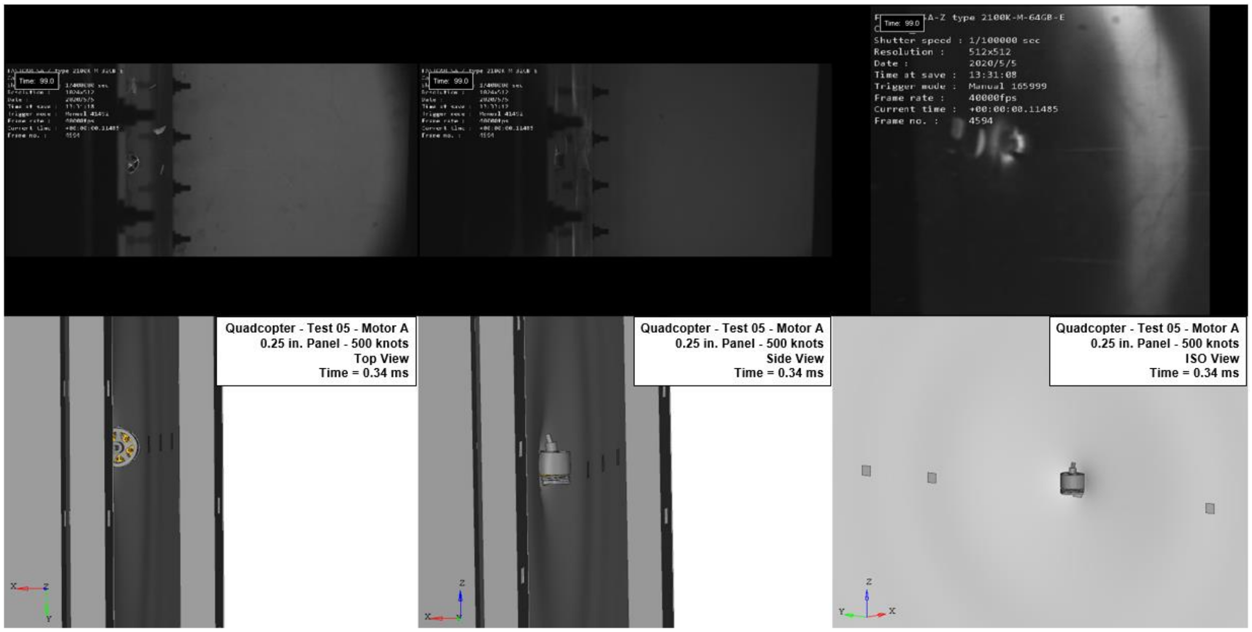


Figure 208. Comparison for motor A impact on 0.25" aluminum panel at 267.51 m/s (520 knots) at t = 0.34 ms (end of contact).

Figure 209 compares the simulation and test Y (horizontal) and Z (vertical) direction in-plane deformations and the out-of-plane displacements with a maximum displacement of the aluminum panel.

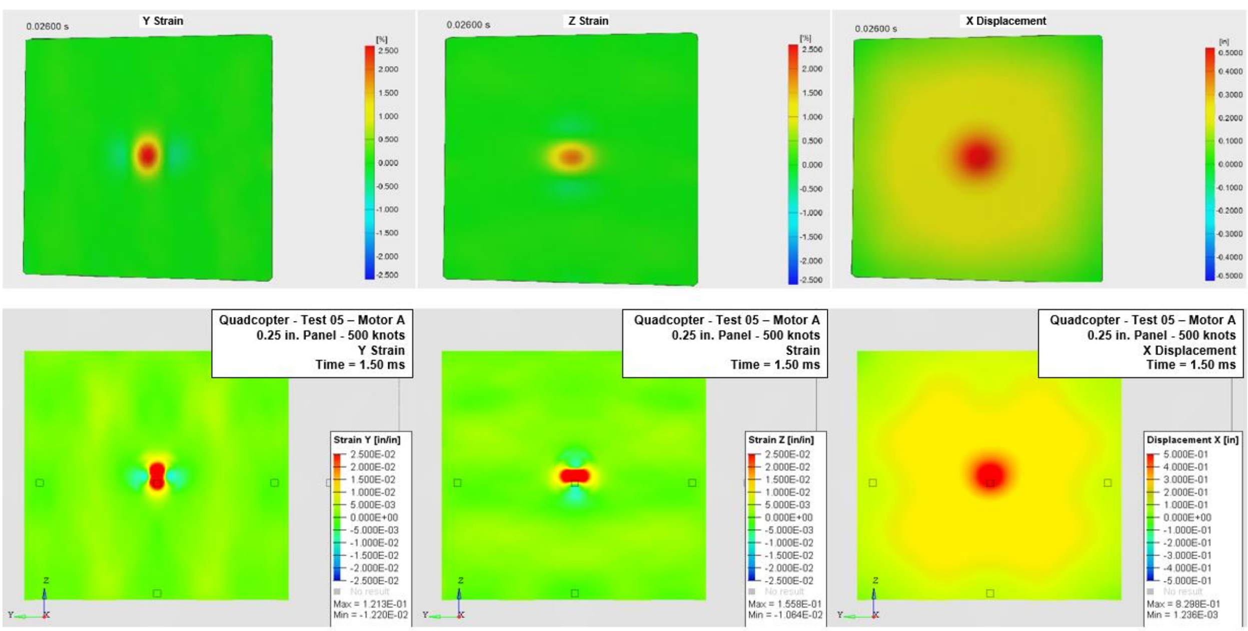


Figure 209. Comparison of test and simulation strains and displacements for motor A impact on 0.25" aluminum panel at 267.51 m/s (520 knots) at t = 1.50 ms (maximum displacement).

Figure 210 shows the out-of-plane displacement of the panel during the impact event obtained from the DIC data, and the simulation tracked displacements. The values on the vertical axis are not shown for confidential reasons.

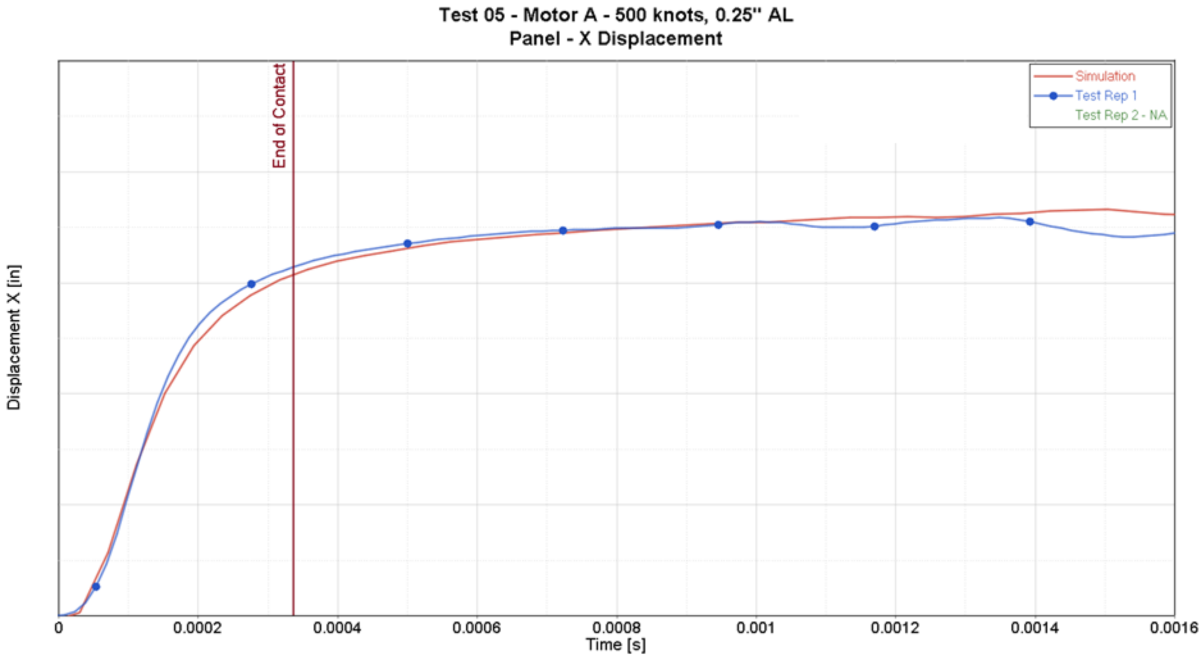


Figure 210. Comparison of the test and simulation out-of-plane displacements for motor A impact on 0.25” aluminum panel at 267.51 m/s (520 knots).

The physical panel was scanned after the test to compare the dimensions of the damaged area. Figure 211 compares the panel’s damaged area dimensions for the test and simulation. Again, there is good agreement between the physical test and the predicted panel’s damaged area.

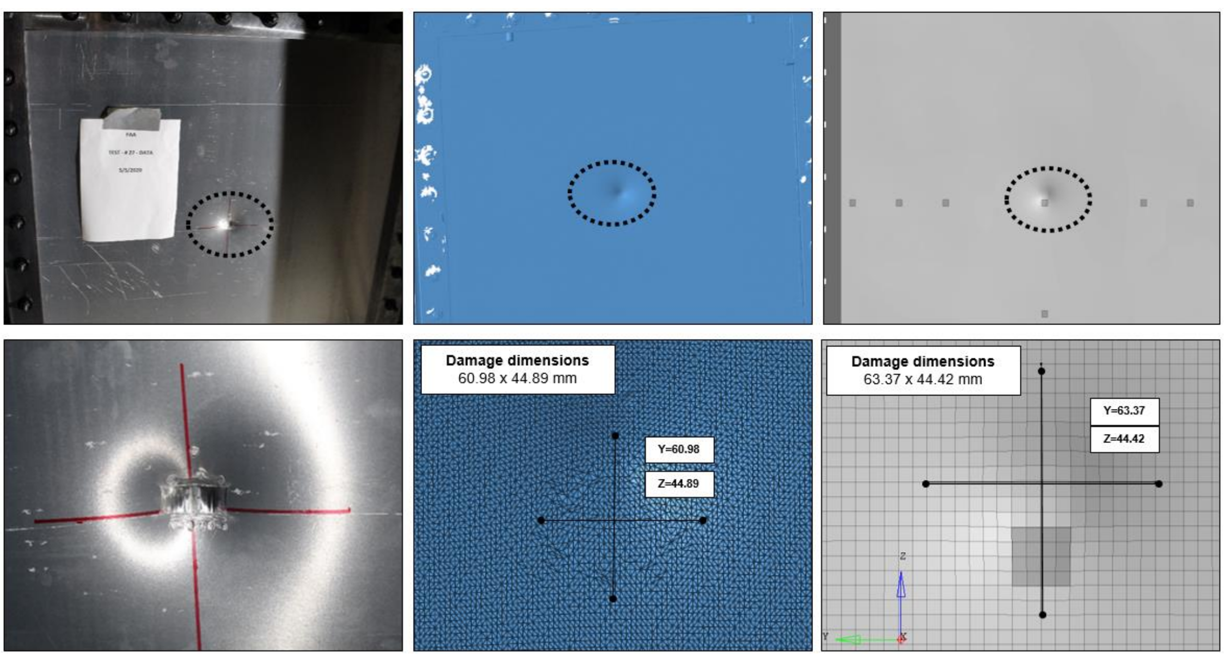


Figure 211. Comparison of the final damage of the panel for the test (left), scan (middle), and simulation (right) of the motor A impact on 0.25” aluminum panel at 267.51 m/s (520 knots).

Figure 212 compares the physical and simulation projectile damage. The motor did not penetrate the panel for both physical test and simulation but was crushed due to the impact.

Figure 212. Comparison of the test (left) and simulation (right) projectile damage for motor A impact on 0.25” aluminum panel at 267.51 m/s (520 knots).

Figure 213 compares the load-time history of both test repetitions and the simulation load output. All the curves were filtered with a low-pass filter of 15,000 Hz. The load data shows good repeatability for test and simulation and confirms the good correlation up to the end of the contact, marked with an asymptote. However, the post-impact oscillations of the panel deviate from those of the physical test. Figure 214 compares the strain data collected at both test iterations to the simulation strains. The values on the vertical axis are not shown for confidential reasons.

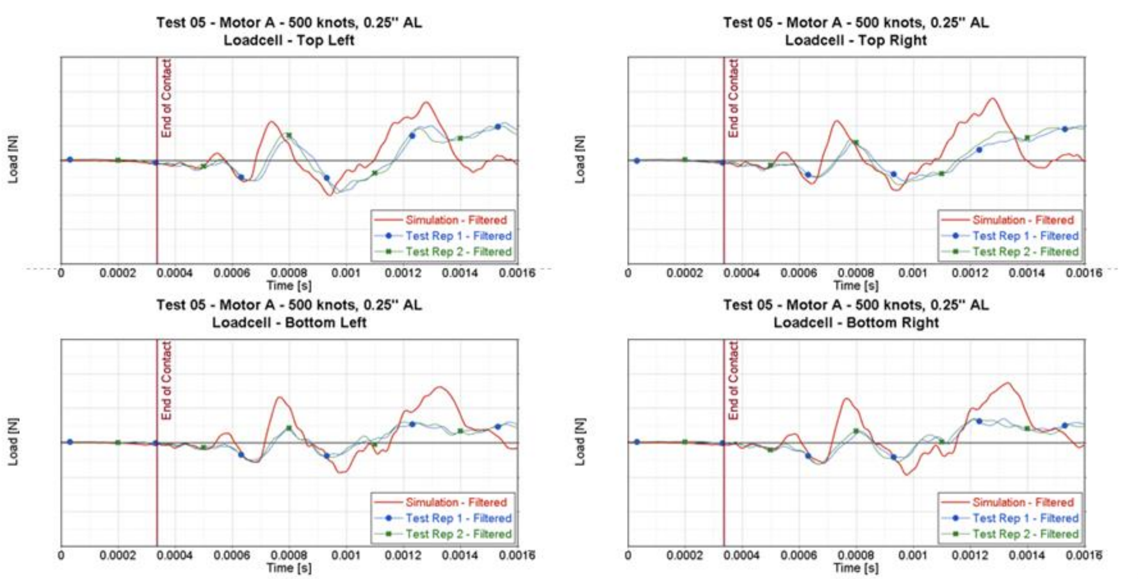


Figure 213. Load cell history data validation for motor A impact on 0.25” aluminum panel at 267.51 m/s (520 knots).

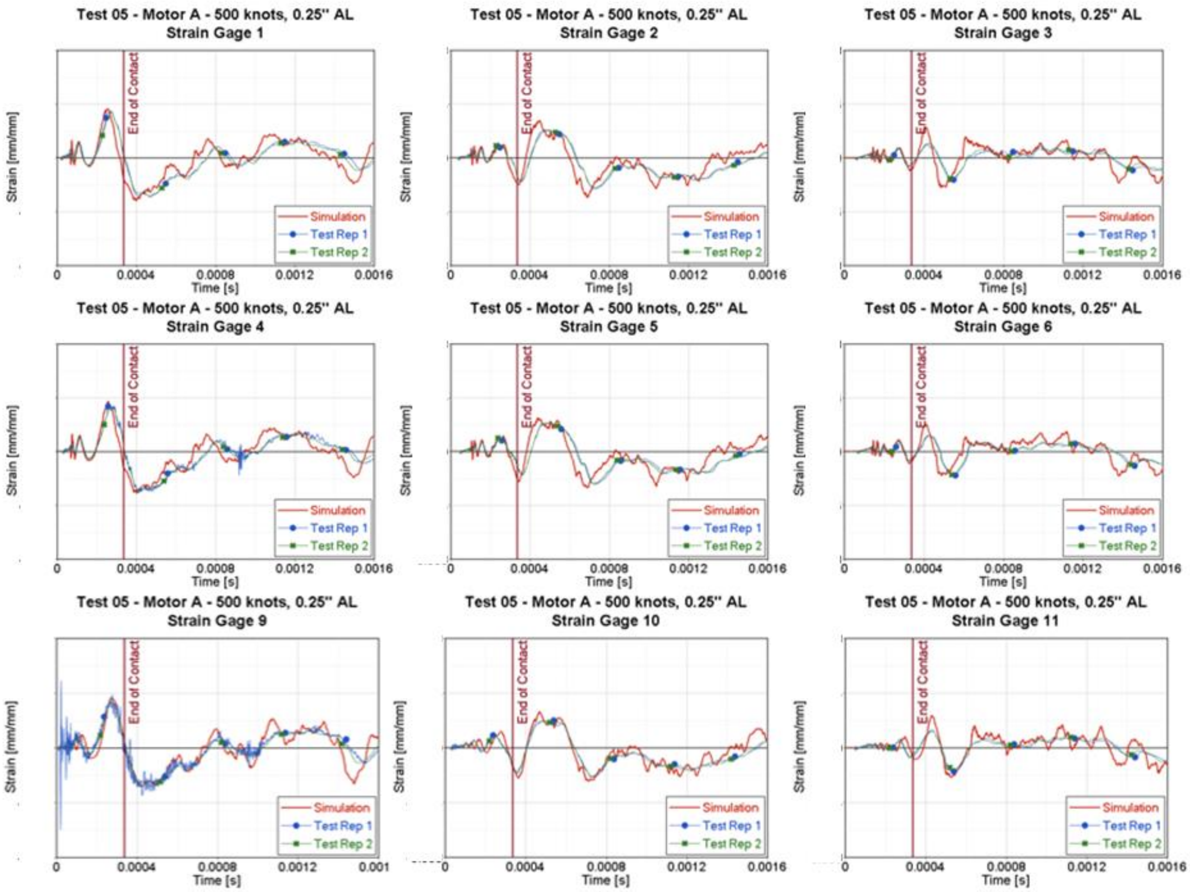


Figure 214. Strain comparison of strain gages 1-6 and 9-11 for motor A impact on 0.25” aluminum panel at 267.51 m/s (520 knots).

## A.6 TEST 06 – CAMERA AT 500 KNOTS – 1.6 MM AL PANEL

Test 06 consists of the impact of the quadcopter camera with the 1.6 mm (0.063″) flat aluminum panel at a nominal velocity of 257.2 m/s (500 knots). Two iterations were carried out to evaluate data repeatability. For kinematics comparison, NIAR has identified iteration 2 as the repetition with the least deviation regarding the nominal test requirements.

An initial velocity of 266.48 m/s (518 knots) was applied to the camera FEM, corresponding to the velocity recorded for repetition 1 in the test documentation (APPENDIX B).

Figure 215 through Figure 218 show the comparison of the kinematics between the test and simulation at four different instances of the impact event.

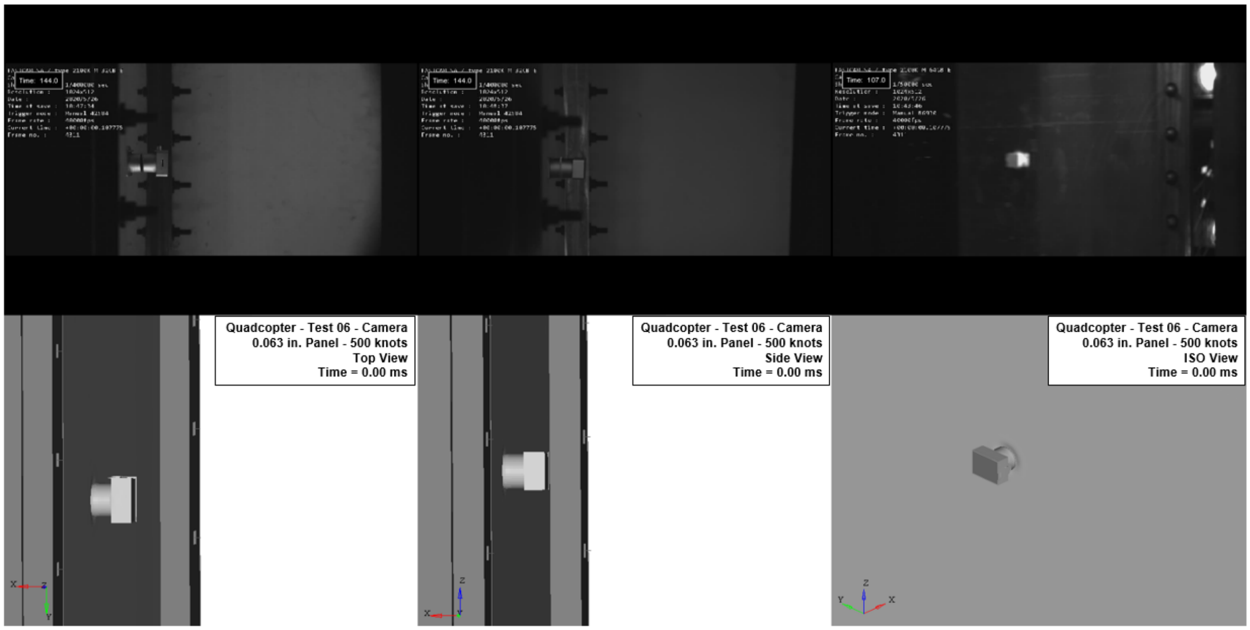


Figure 215. Comparison for camera impact on 0.063” aluminum panel at 266.48 m/s (518 knots) at t = 0.00 ms (beginning of contact).

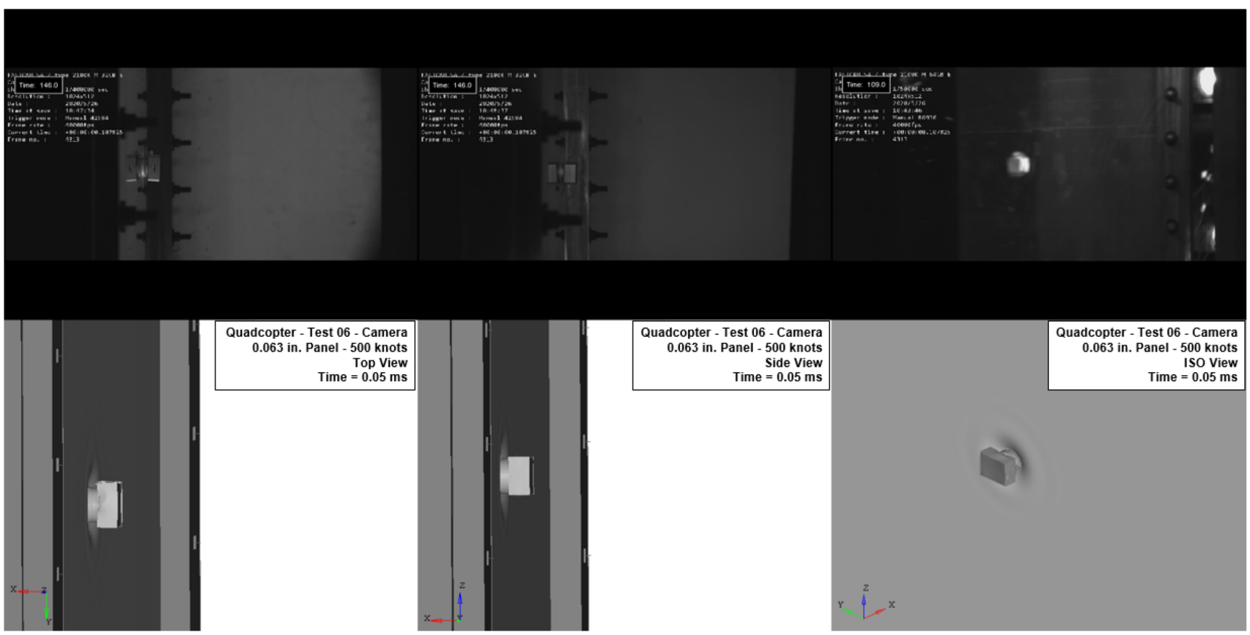


Figure 216. Comparison for camera impact on 0.063” aluminum panel 266.48 m/s (518 knots) at t = 0.05 ms (panel failure).

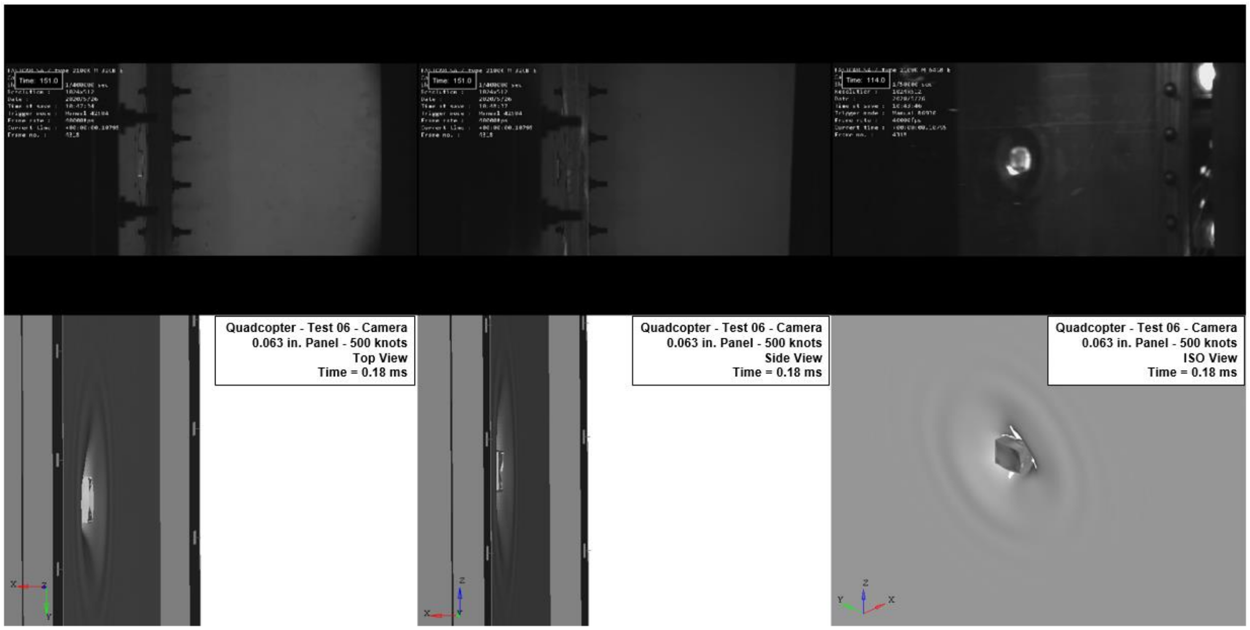


Figure 217. Comparison for camera impact on 0.063” aluminum panel 266.48 m/s (518 knots) at t = 0.18 ms.

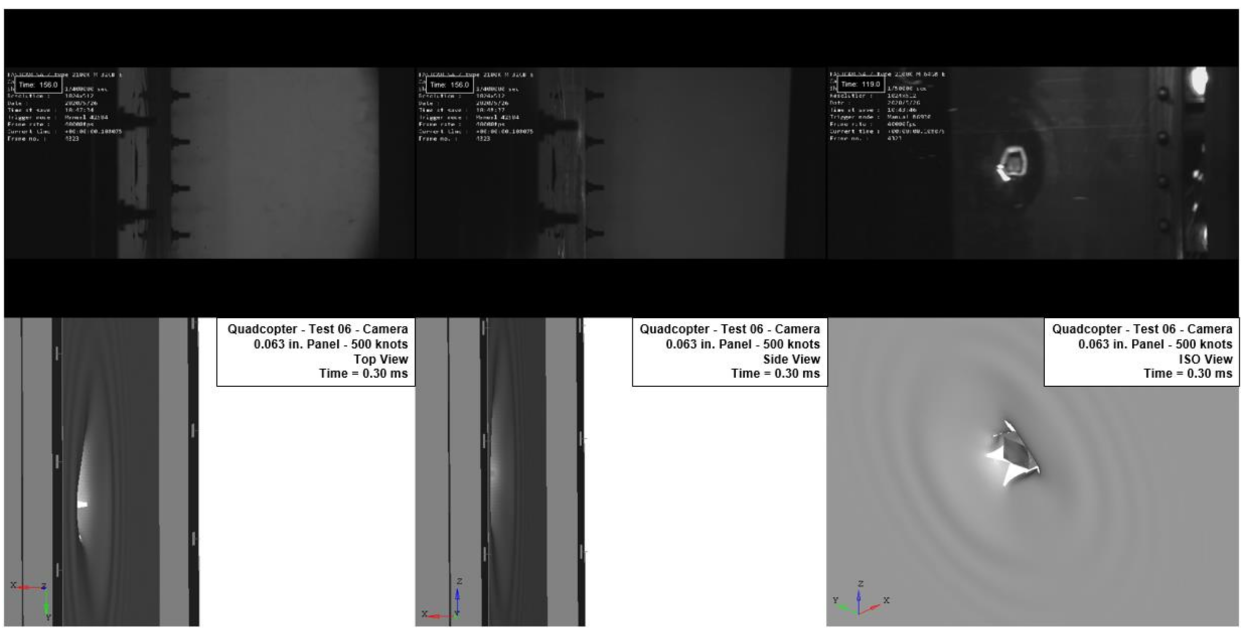


Figure 218. Comparison for camera impact on 0.063” aluminum panel at 266.48 m/s (518 knots) at t = 0.30 ms (end of contact).

Figure 219 compares the simulation and test Y (horizontal) and Z (vertical) direction in-plane deformations and the out-of-plane displacements, for instance, with the aluminum panel's maximum displacement. The simulation predicts the panel’s failure before the test, as seen in Figure 219.

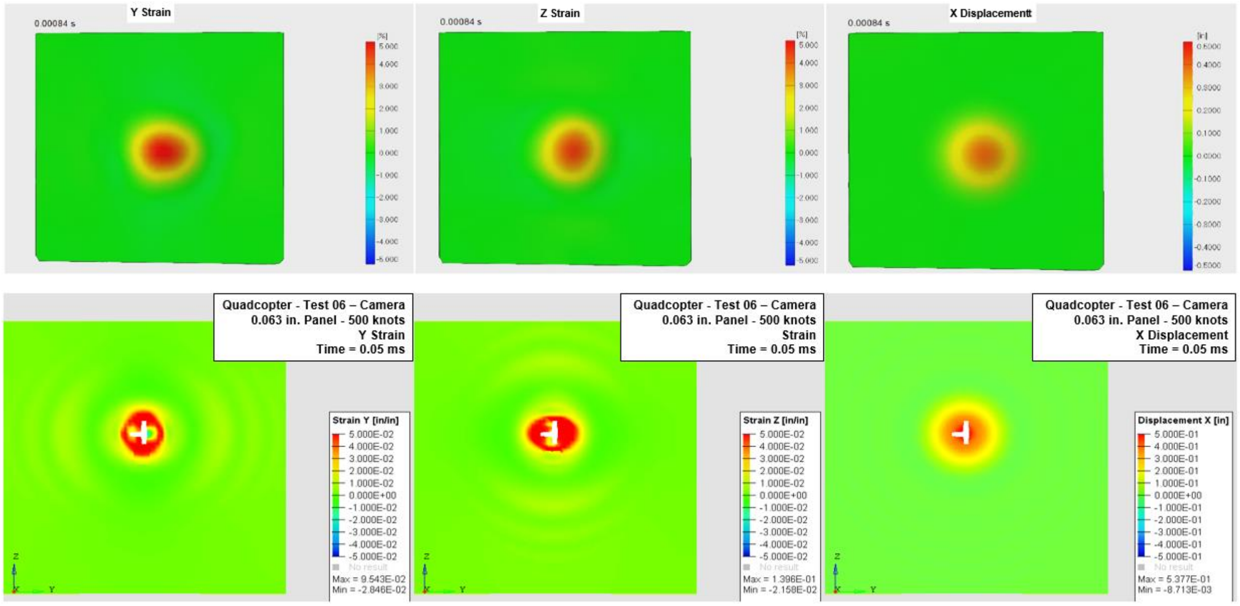


Figure 219. Comparison of test and simulation strains and displacements for camera impact on 0.063" aluminum panel at 266.48 m/s (518 knots) at t = 0.05 ms (maximum displacement).

Figure 220 shows the out-of-plane displacement of the panel during the impact event obtained from the DIC data, and the simulation tracked displacements. The values on the vertical axis are not shown for confidential reasons.

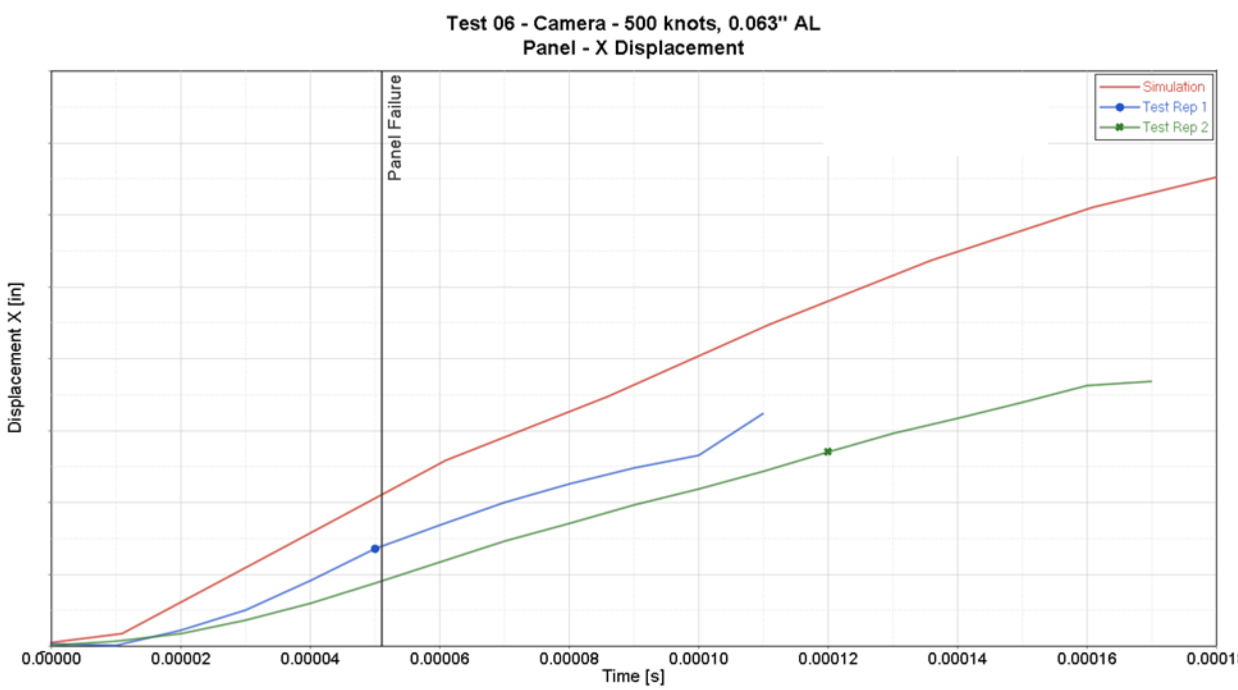


Figure 220. Comparison of the test and simulation out-of-plane displacements for camera impact on 0.063" aluminum panel at 266.48 m/s (518 knots).

The physical panel was scanned after the test to compare the dimensions of the damaged area. Figure 221 compares the panel's damaged area dimensions for the test and simulation. Again, there is good agreement between the physical test and the predicted panel's damaged area.

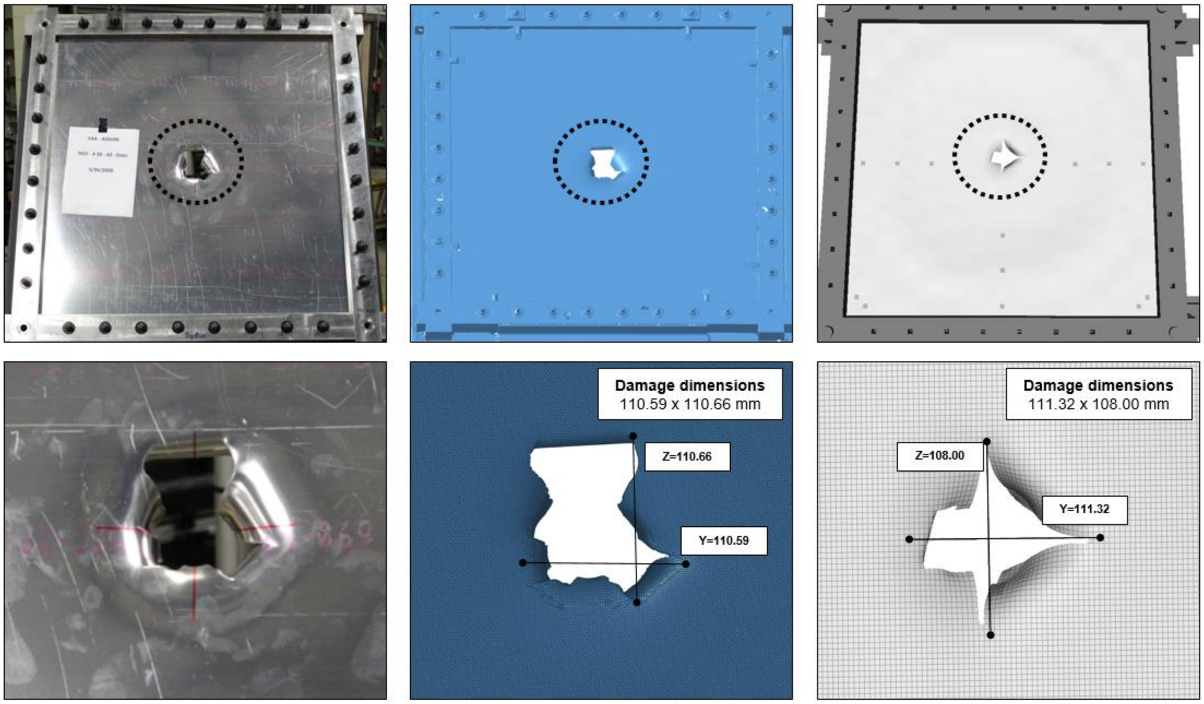


Figure 221. Comparison of the final damage of the panel for the test (left), scan (middle), and simulation (right) for camera impact on 0.063" aluminum panel at 266.48 m/s (518 knots).

Figure 222 compares the physical and simulation projectile damage. Unfortunately, the camera penetrated the panel for physical tests and simulation, splitting it into pieces.

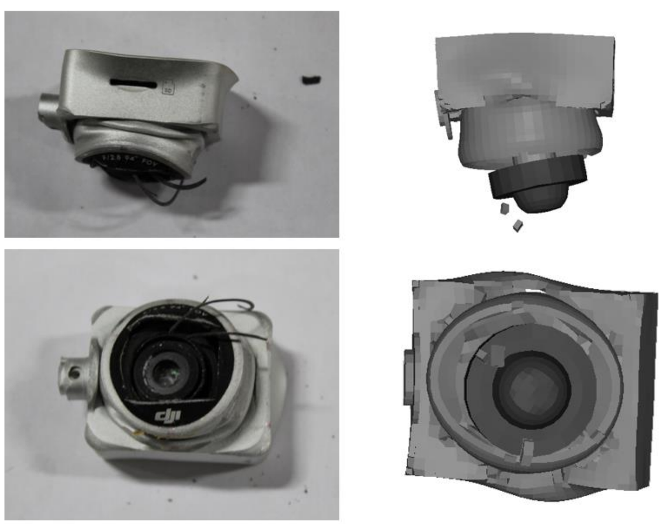

Figure 222. Comparison of the test (left) and simulation (right) projectile damage for camera impact on 0.063" aluminum panel at 266.48 m/s (518 knots).

Figure 223 compares the load-time history of both test repetitions and the simulation load output. Again, all the curves were filtered with a low-pass filter of 15,000 Hz. The load data shows good repeatability for test and simulation and confirms the good correlation up to the end of the contact, marked with an asymptote. However, the post-impact oscillations of the panel deviate from those of the physical test for the top load cell readings. The values on the vertical axis are not shown for confidential reasons.

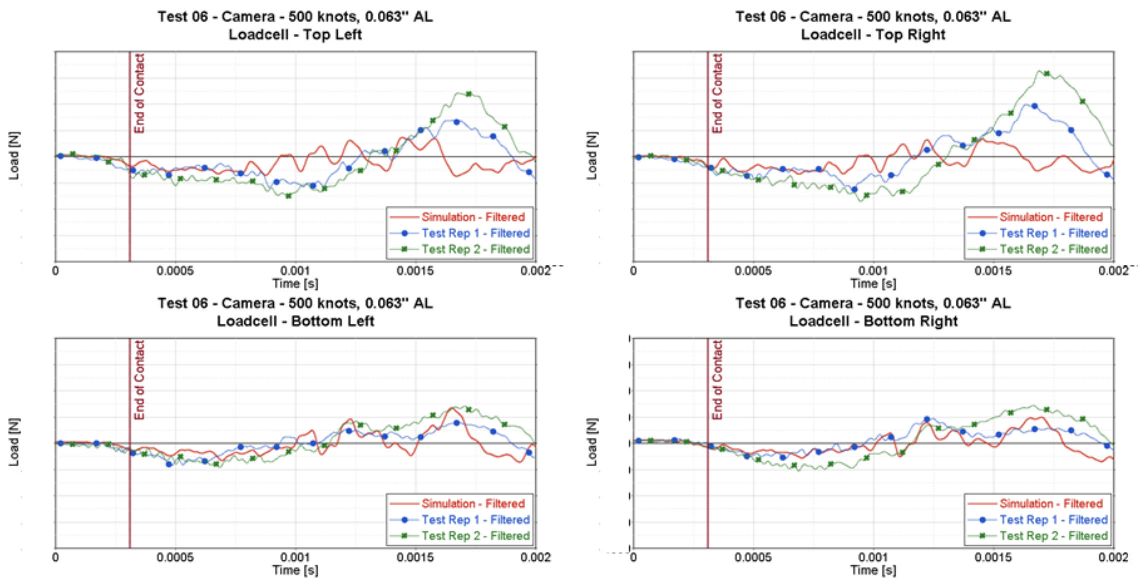


Figure 223. Load cell history data validation for camera impact on 0.063" aluminum panel at 266.48 m/s (518 knots).

Figure 224 compares the strain data collected at both test iterations to the simulation strains. The values on the vertical axis are not shown for confidential reasons.

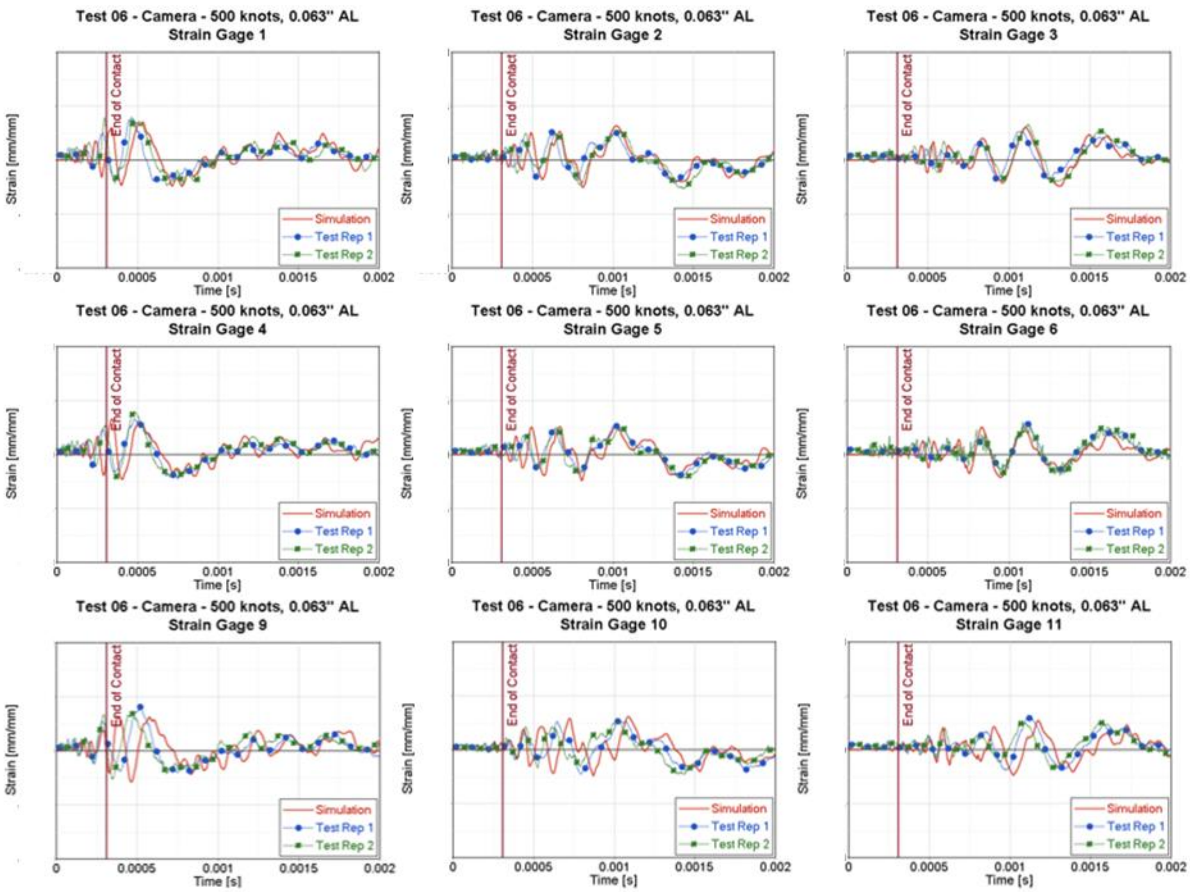


Figure 224. Strain comparison of strain gages 1-6 and 9-11 for camera impact on 0.063" aluminum panel at 266.48 m/s (518 knots).

## A.7 TEST 07 – CAMERA AT 500 KNOTS – 6.35 MM AL PANEL

Test 07 consists of the impact of the quadcopter camera with the 6.35 mm (0.25″) aluminum panel at a nominal velocity of 257.2 m/s (500 knots). Two iterations were carried out to evaluate data repeatability. For kinematics comparison, NIAR has identified iteration 2 as the repetition with the least deviation regarding the nominal test requirements.

An initial velocity of 268.3 m/s (521 knots) was applied to the camera FEM, corresponding to the velocity recorded for repetition 1 in the test documentation (APPENDIX B).

Figure 225 through Figure 228 show the comparison of the kinematics between the test and simulation at four different instances of the impact event.

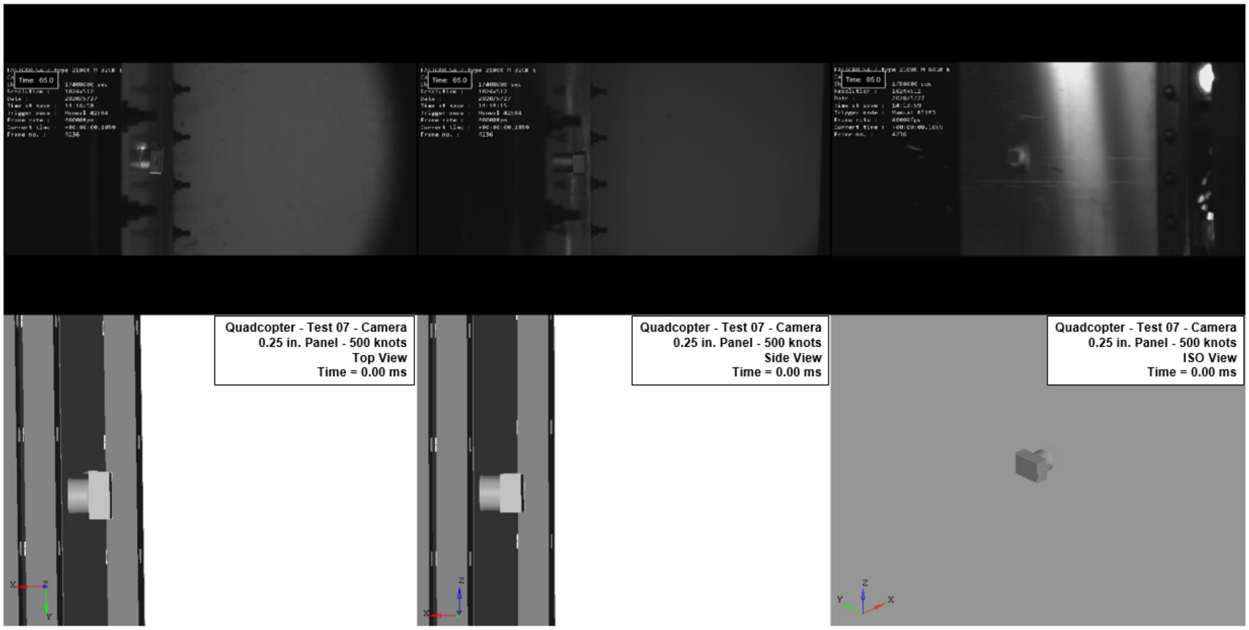


Figure 225. Comparison for camera impact on 0.25” aluminum panel at 268.03 m/s (521 knots) at t = 0.00 ms (beginning of contact).

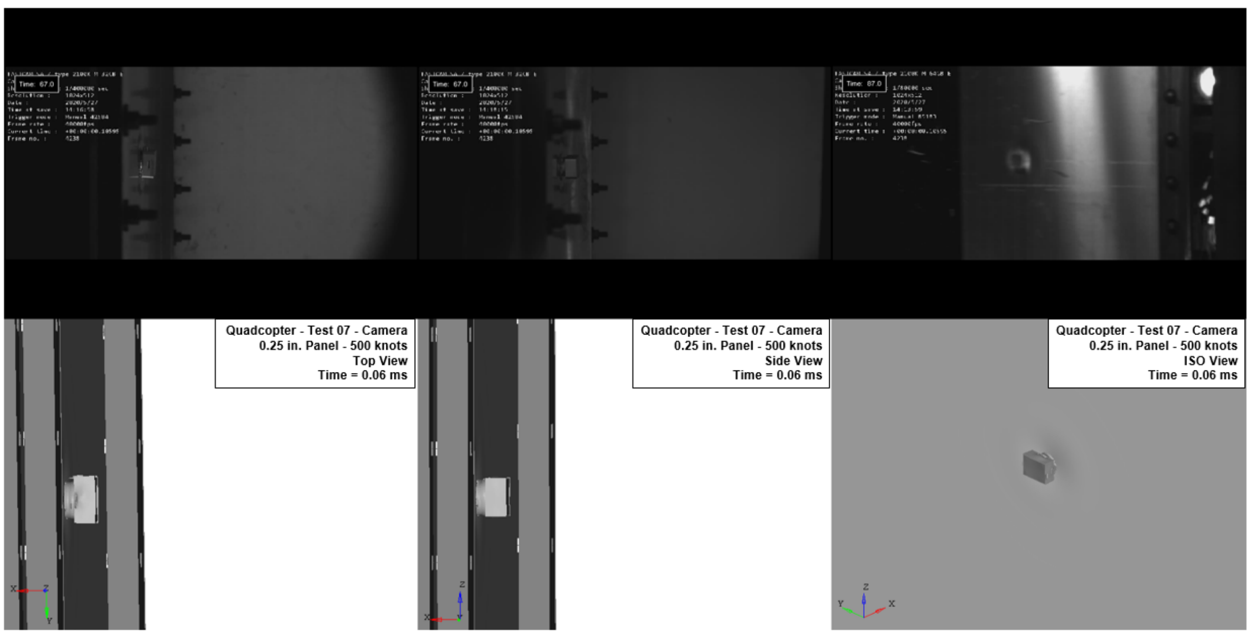


Figure 226. Comparison for camera impact on 0.25” aluminum panel at 268.03 m/s (521 knots) at t = 0.06 ms.

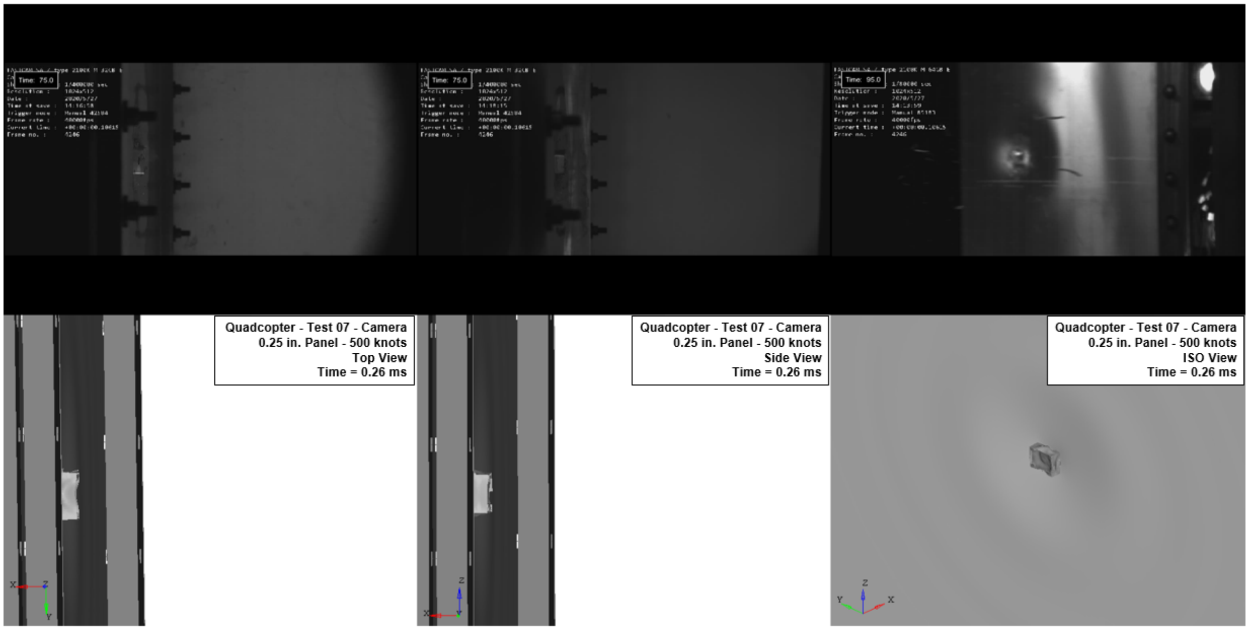


Figure 227. Comparison for camera impact on 0.25” aluminum panel at 268.03 m/s (521 knots) at t = 0.26 ms.

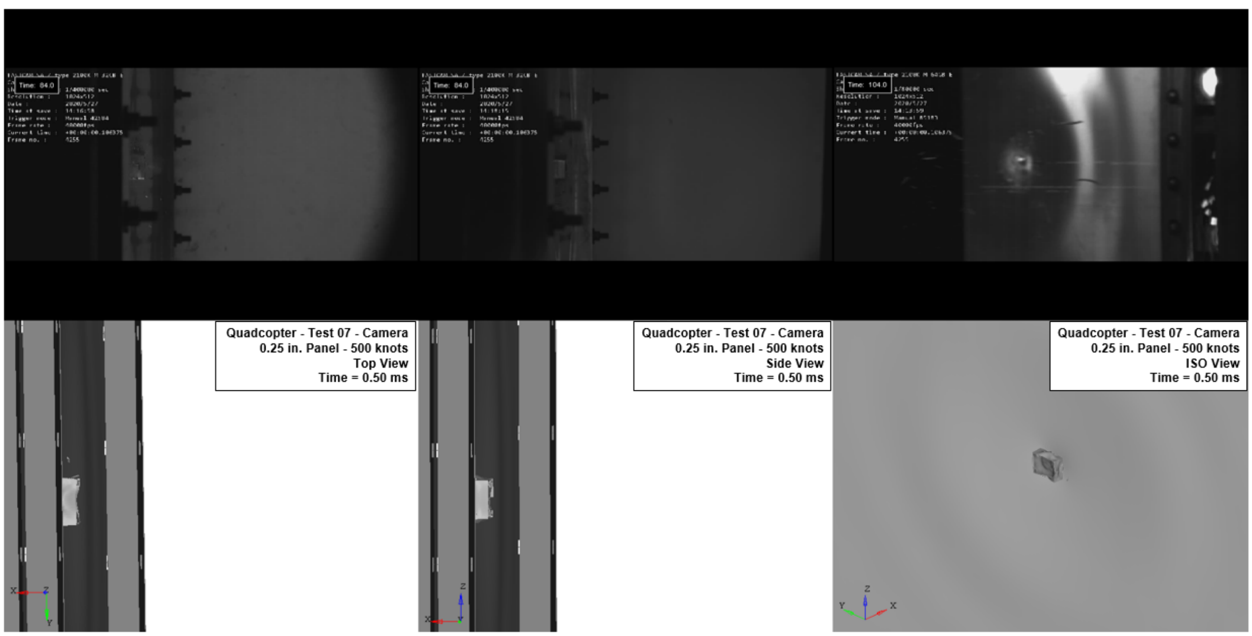


Figure 228. Comparison for camera impact on 0.25” aluminum panel at 268.03 m/s (521 knots) at t = 0.50 ms (end of contact).

Figure 229 compares the simulation and test Y (horizontal) and Z (vertical) direction in-plane deformations and the out-of-plane displacements with a maximum displacement of the aluminum panel.

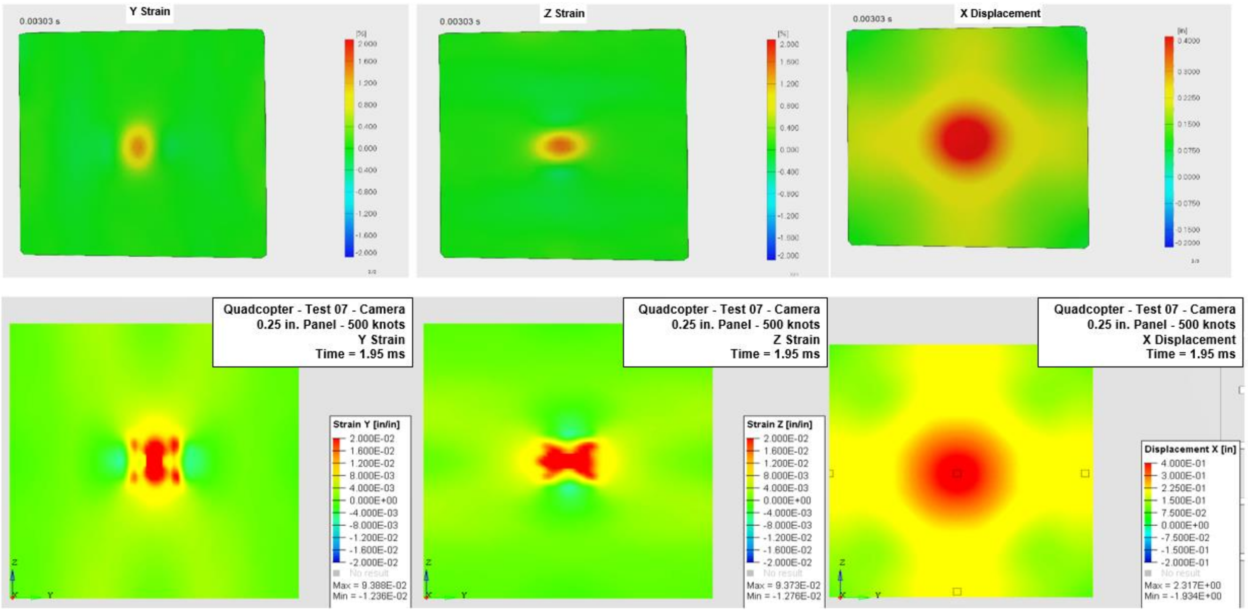


Figure 229. Comparison of test and simulation strains and displacements for camera impact on 0.25" aluminum panel at 268.03 m/s (521 knots) at t = 1.95 ms (maximum displacement).

Figure 230 shows the out-of-plane displacement of the panel during the impact event obtained from the DIC, and the simulation tracked displacements. The values on the vertical axis are not shown for confidential reasons.

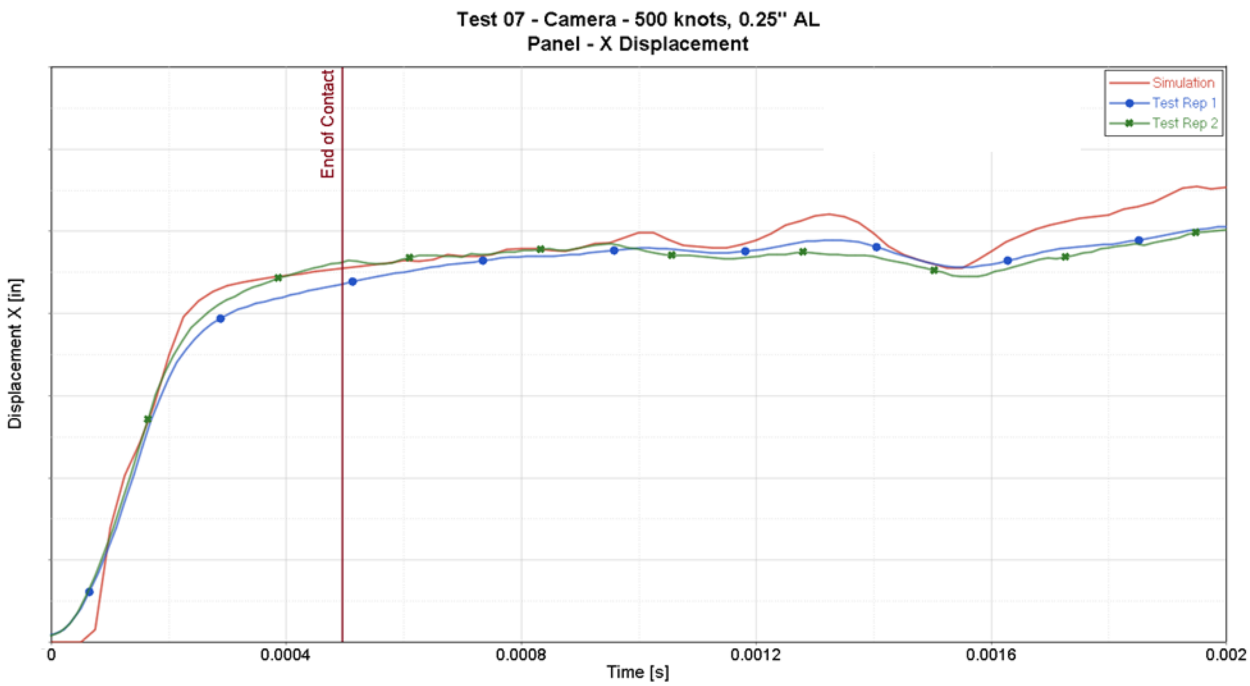


Figure 230. Comparison of the test and simulation out-of-plane displacements for camera impact on 0.25" aluminum panel at 268.03 m/s (521 knots).

The physical panel was scanned after the test to compare the dimensions of the damaged area. Figure 231 compares the panel's damaged area dimensions for the test and simulation. Again, there is good agreement between the physical test and the predicted panel's damaged area.

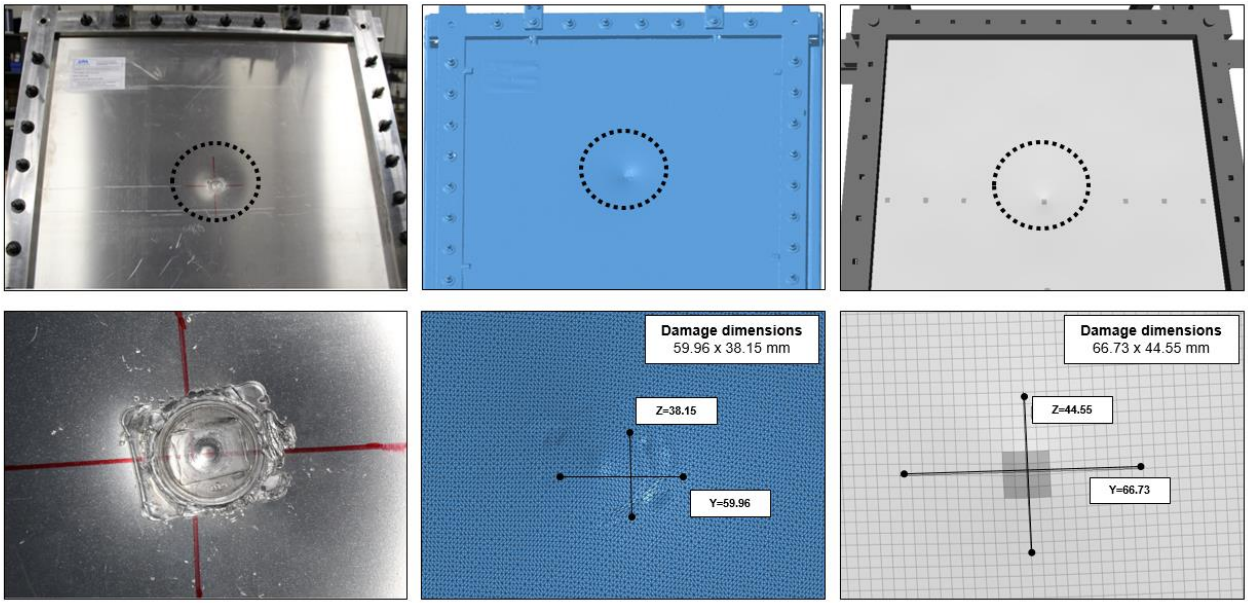


Figure 231. Comparison of the final damage of the panel for the test (left), scan (middle), and simulation (right) for the camera impact on a 0.25" aluminum panel at 268.03 m/s (521 knots).

Figure 232 compares the physical and simulation projectile damage. The camera got crushed during impact for both physical test and simulation and left an indentation on the panel, but it did not penetrate through it.

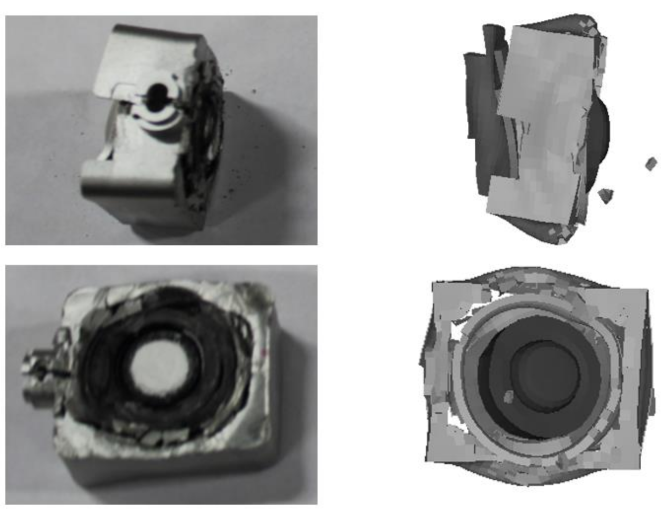

Figure 232. Comparison of the test (left) and simulation (right) projectile damage for camera impact on 0.25" aluminum panel at 268.03 m/s (521 knots).

Figure 233 compares the load-time history of both test repetitions and the simulation load output. All the curves were filtered with a low-pass filter of 15,000 Hz. The load data shows good repeatability for test and simulation and confirms the good correlation of the FEM up to the end of the contact, marked with an asymptote. However, the post-impact oscillations of the panel have some deviation from those of the physical test. The values on the vertical axis are not shown for confidential reasons.

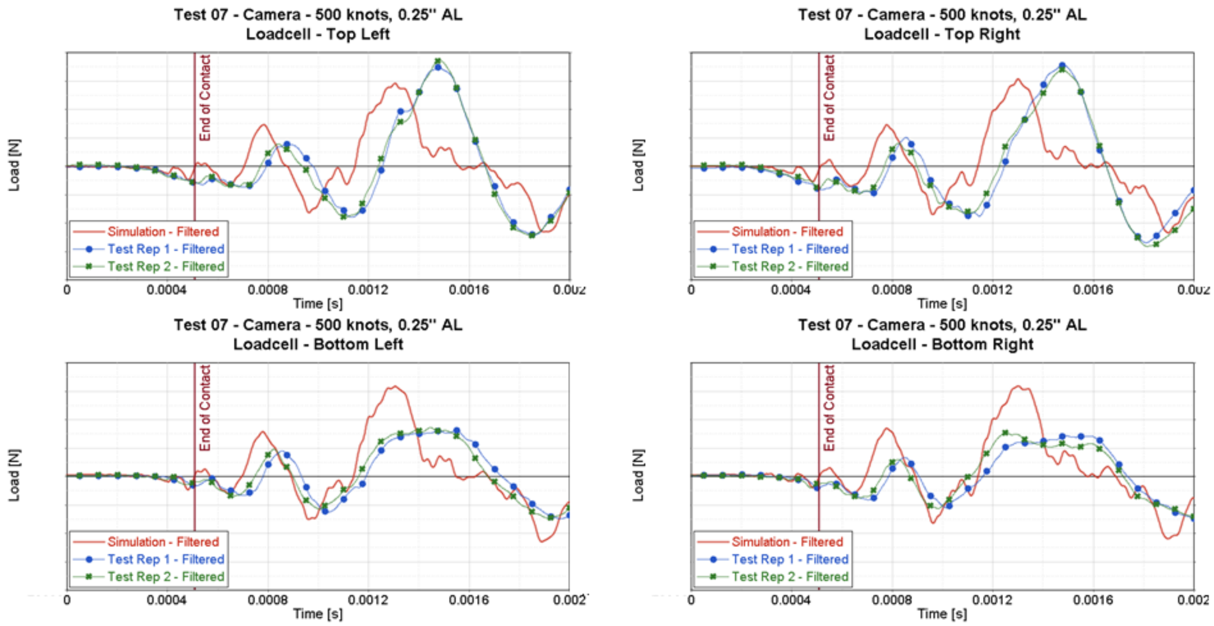


Figure 233. Load cell history data validation for camera impact on 0.25" aluminum panel at 268.03 m/s (521 knots).

Figure 234 compares the strain data collected at both test iterations to the simulation strains. The values on the vertical axis are not shown for confidential reasons.

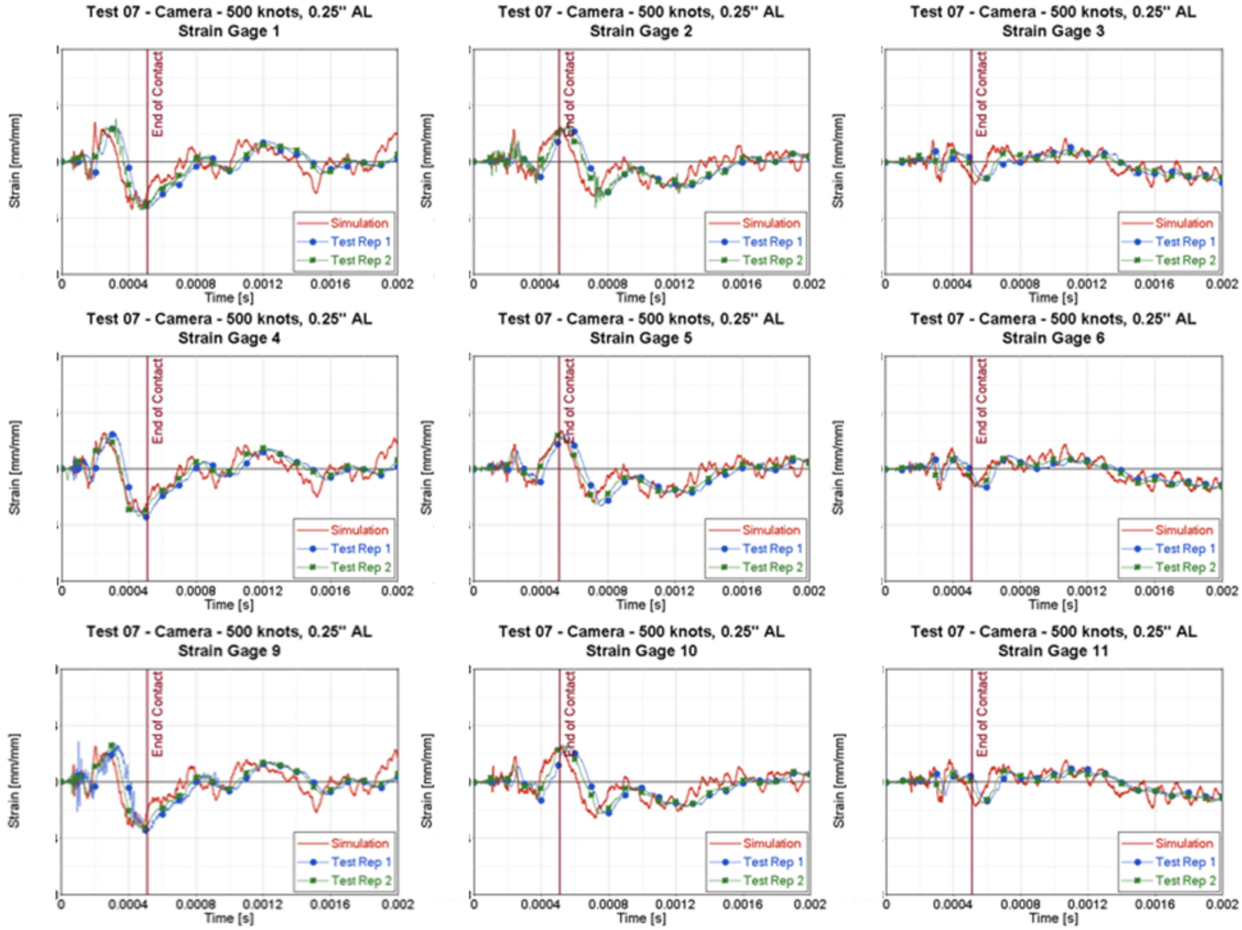


Figure 234. Strain comparison of strain gages 1-6 and 9-11 for camera impact on 0.25" aluminum panel at 268.03 m/s (521 knots).

## A.8 TEST 08 – BATTERY AT 50 KNOTS – 1.6 MM AL PANEL

Test 08 consists of the impact of battery A with a 1.6 mm (0.063") aluminum panel at a nominal velocity of 25.7 m/s (50 knots). Two iterations were carried out to evaluate data repeatability. For iteration 2, a triggering error difficulted the data recording. Hence, NIAR has selected iteration 1 for the FEM validation. All batteries were fully charged previous to the test.

An initial velocity of 26.75 m/s (52 knots) was applied to the battery A FEM, corresponding to the velocity recorded for repetition 2 in the test documentation (APPENDIX B).

Figure 235 through Figure 238 show the comparison of the kinematics between the test and simulation at four different instances of the impact event.

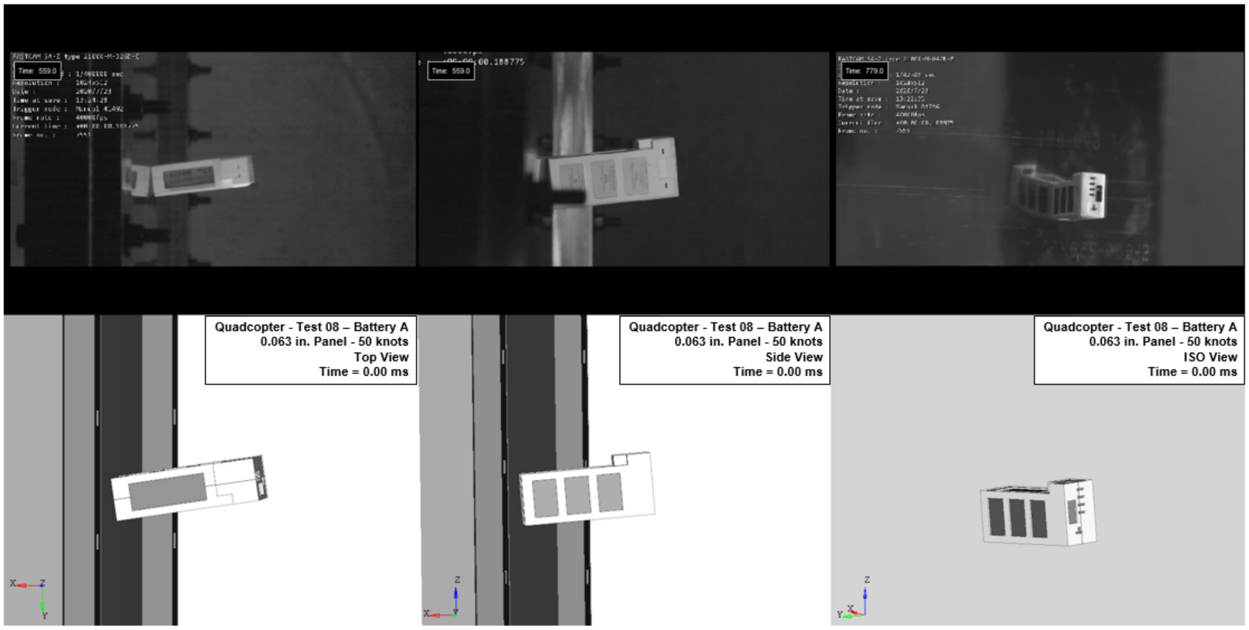


Figure 235. Comparison for battery A impact on 0.063” aluminum panel at 26.75 m/s (52 knots) at t = 0.00 ms (beginning of contact).

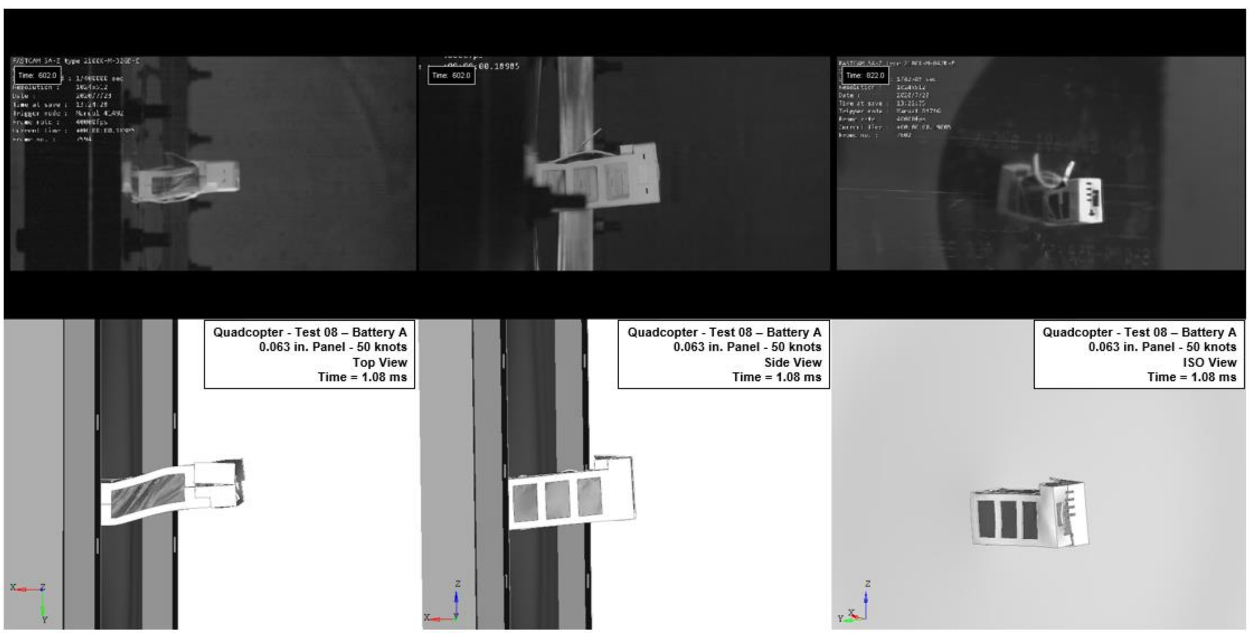


Figure 236. Comparison for battery A impact on 0.063” aluminum panel at 26.75 m/s (52 knots) at t = 1.08 ms.

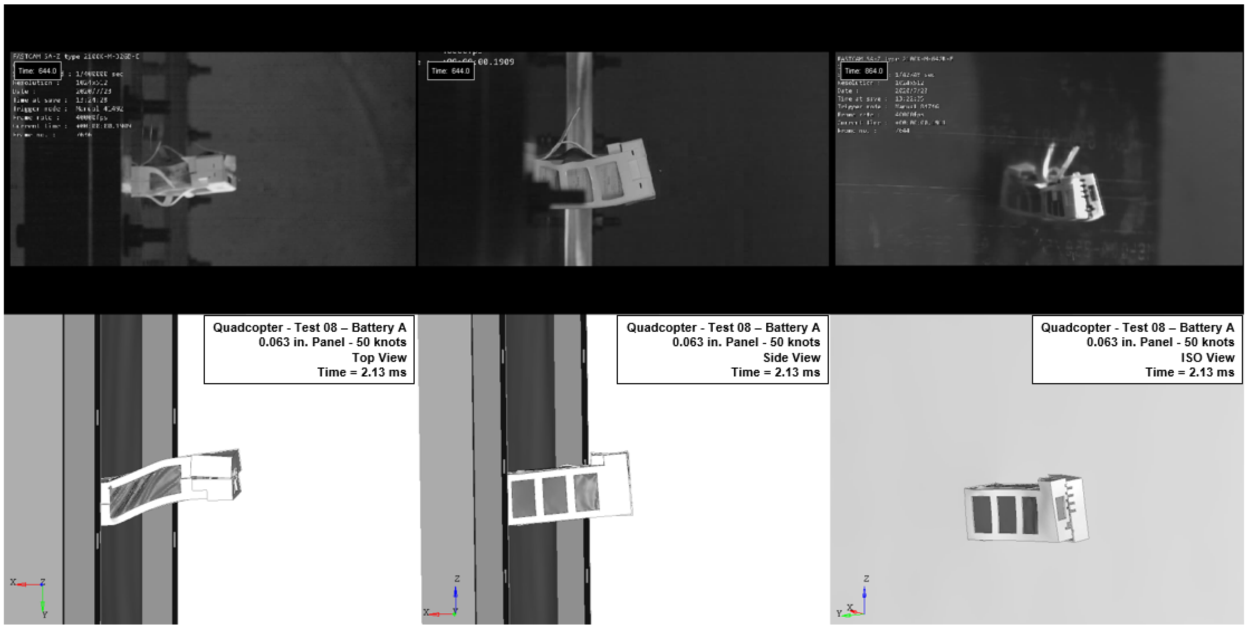


Figure 237. Comparison for battery A impact on 0.063” aluminum panel at 26.75 m/s (52 knots) at t = 2.13 ms.

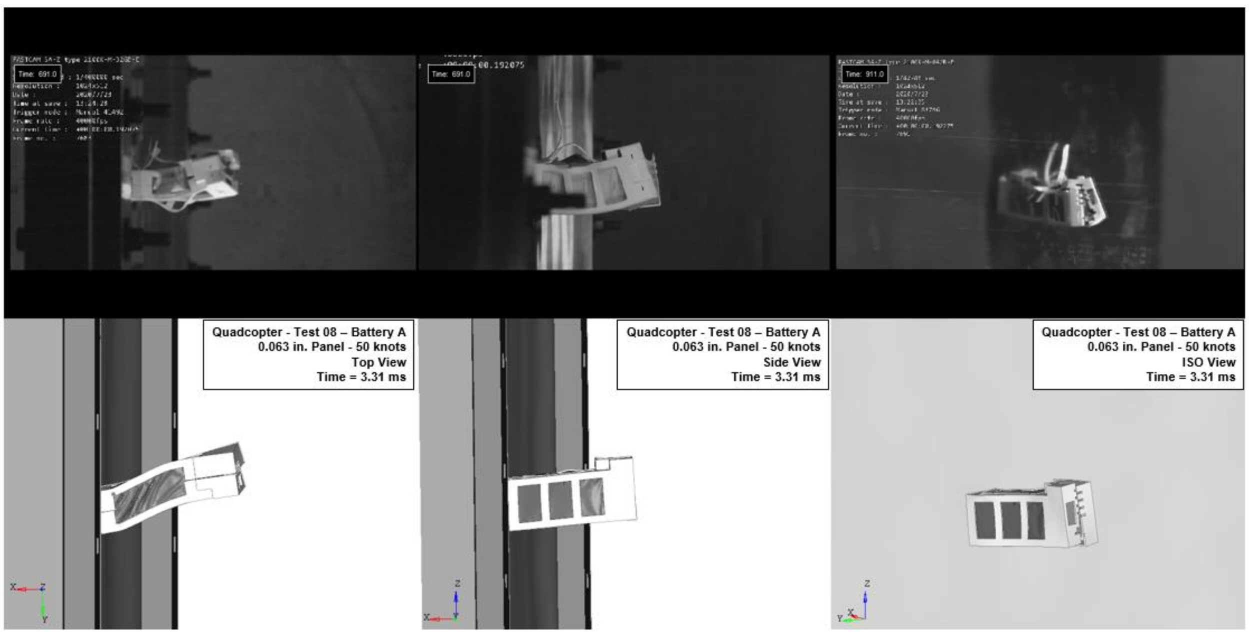


Figure 238. Comparison for battery A impact on 0.063” aluminum panel at 26.75 m/s (52 knots) at t = 3.31 ms (end of contact).

Figure 239 compares the simulation and test Y (horizontal) and Z (vertical) direction in-plane deformations and the out-of-plane displacements, for instance, with a maximum displacement of the aluminum panel.

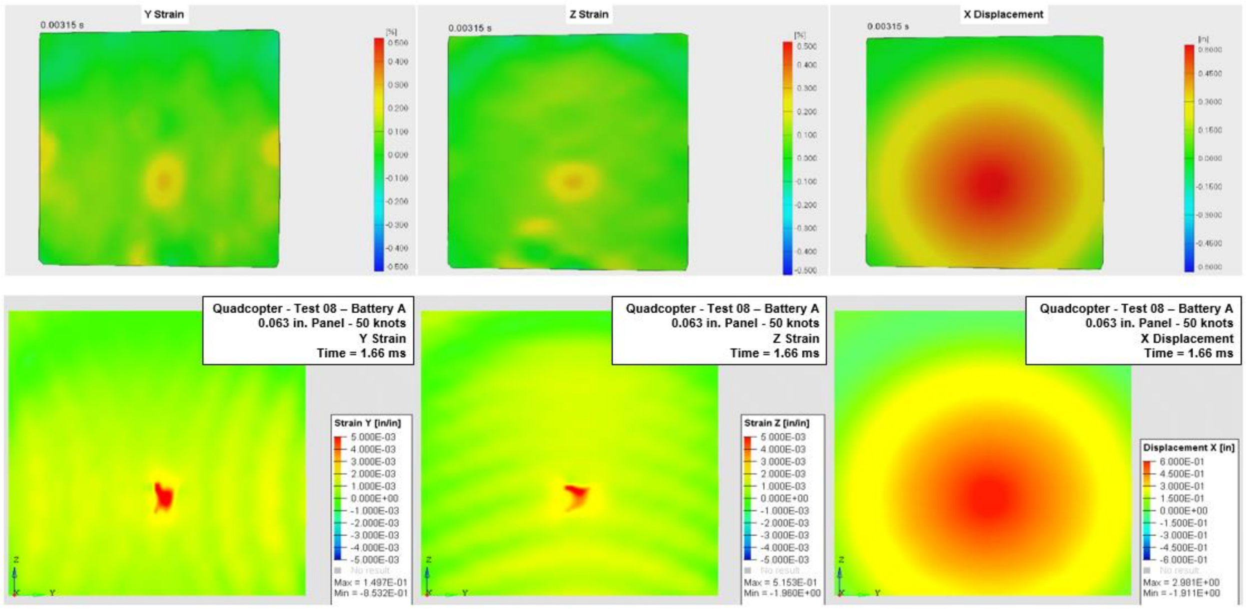


Figure 239. Comparison of test and simulation strains and displacements for battery A impact on 0.063” aluminum panel at 26.75 m/s (52 knots) at t = 1.66 ms (maximum displacement).

Figure 240 shows the out-of-plane displacement of the panel during the impact event obtained from the DIC data, and the simulation tracked displacements. The values on the vertical axis are not shown for confidential reasons.

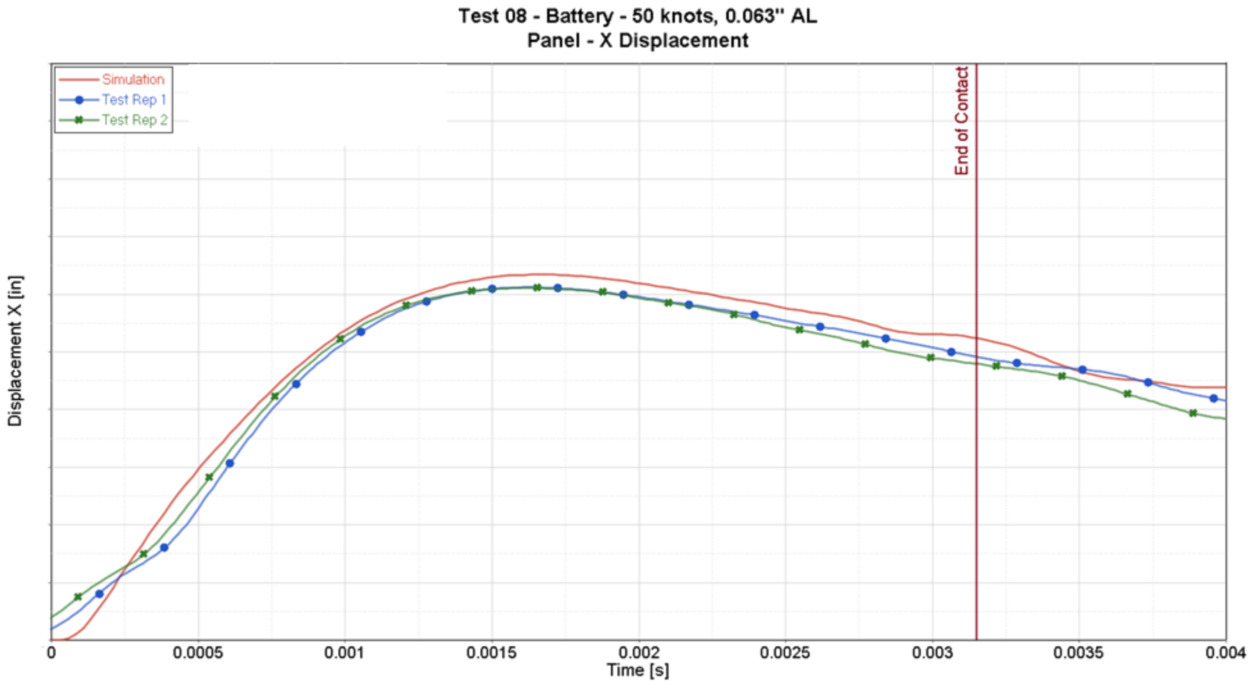


Figure 240. Comparison of the test and simulation out-of-plane displacements for camera impact on 0.25” aluminum panel at 268.03 m/s (521 knots).

The physical panel was scanned after the test to compare the dimensions of the damaged area. Figure 241 compares the panel's damaged area dimensions for the test and simulation. Again, there is good agreement between the physical test and the predicted panel's damaged area.

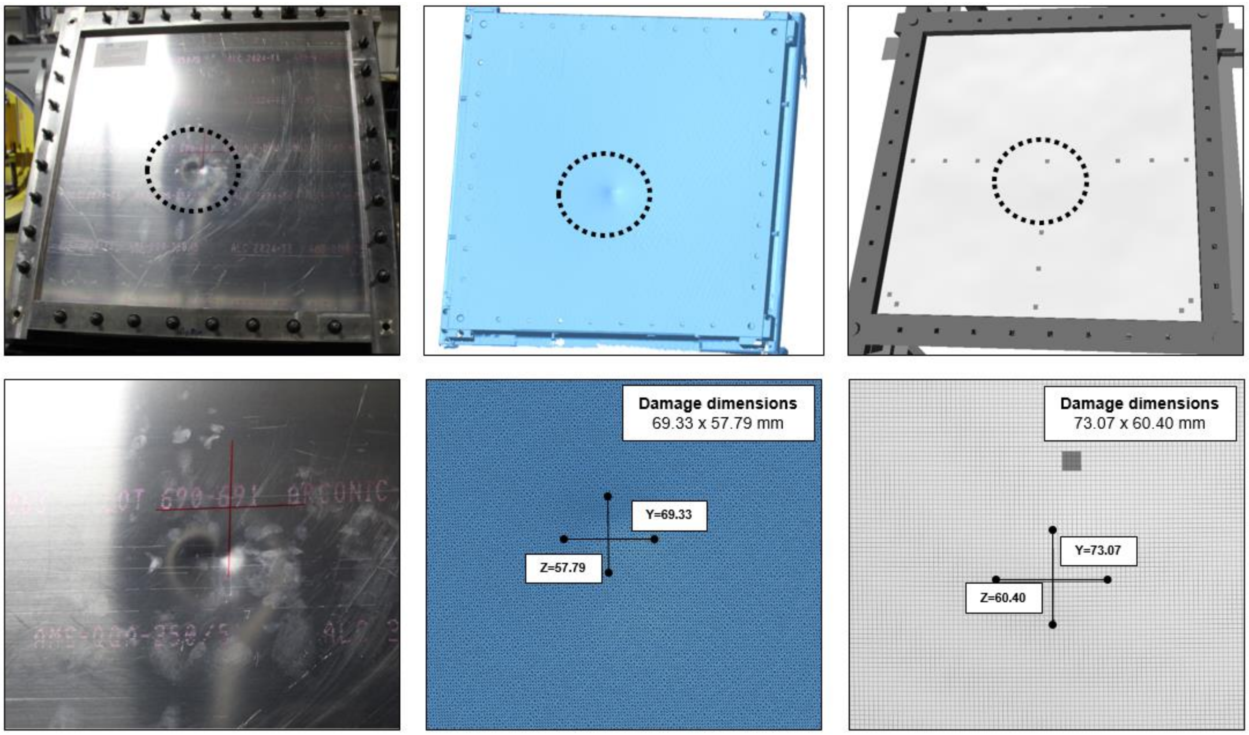


Figure 241. Comparison of the final damage of the panel for the test (left), scan (middle), and simulation (right) for the battery A impact on 0.063" aluminum panel at 26.75 m/s (52 knots).

Figure 242 compares the physical and simulation projectile damage. For both physical test and simulation, the battery case was separated into two pieces with the cell pack attached to one of them. The battery left an indentation on the panel but did not penetrate it.

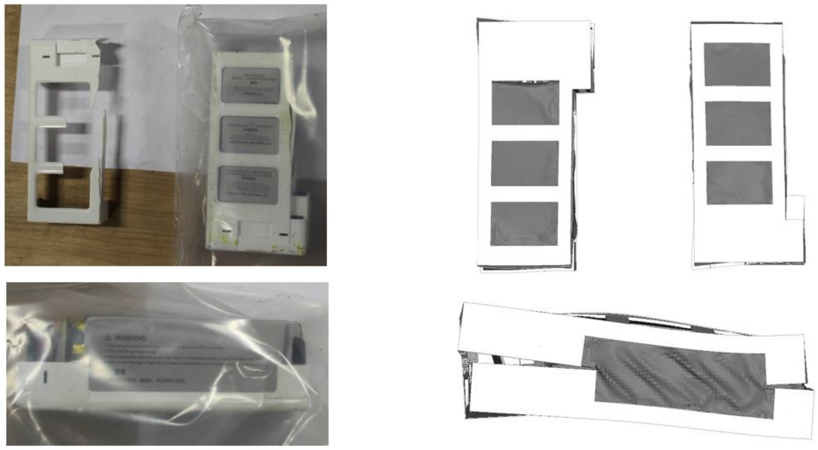

Figure 242. Comparison of the test (left) and simulation (right) projectile damage for battery A impact on 0.063” aluminum panel at 26.75 m/s (52 knots).

Figure 243 compares the load-time history of iteration 2 and the simulation load output. All the curves were filtered with a low-pass filter of 15,000 Hz. The load data shows good repeatability for both tests. The simulation loads correlate well to the test loads, although there are some deviations from the second oscillation. The values on the vertical axis are not shown for confidential reasons.

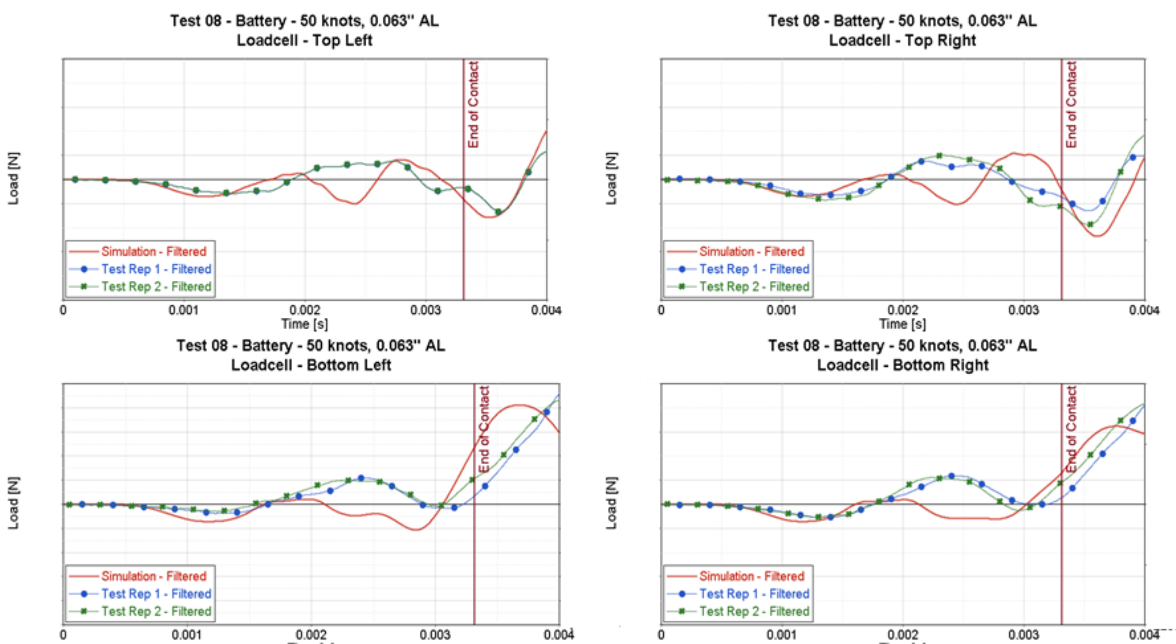


Figure 243. Load cell history data validation for battery A impact on 0.063” aluminum panel at 26.75 m/s (52 knots).

Figure 244 compares the strain data collected at both test iterations to the simulation strains. The values on the vertical axis are not shown for confidential reasons.

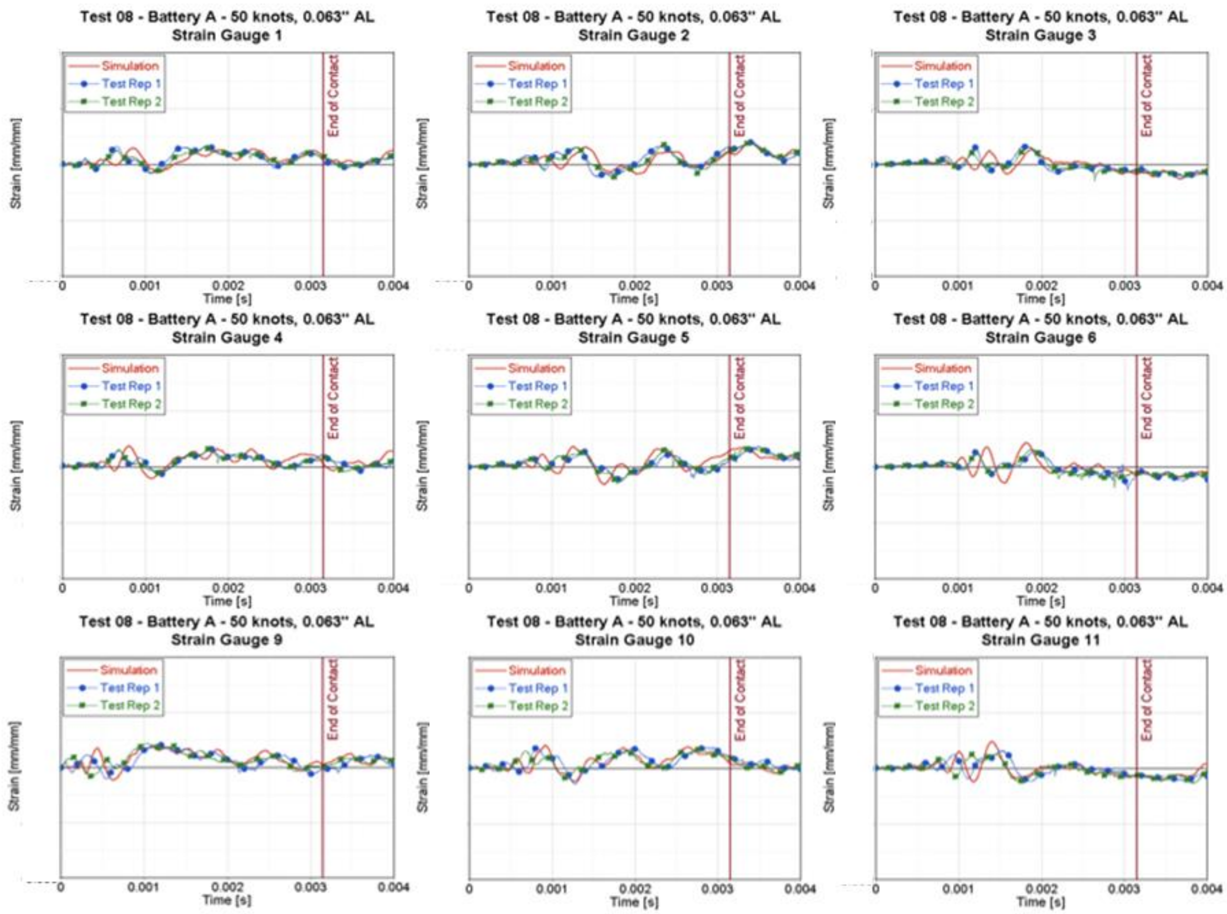


Figure 244. Strain comparison of strain gages 1-6 and 9-11 for battery A impact on 0.063" aluminum panel at 26.75 m/s (52 knots).

A.9 TEST 09 – BATTERY AT 120 KNOTS – 1.6 MM AL PANEL

Test 09 consists of the impact of battery A with a 1.6 mm (0.063″) aluminum panel at a nominal velocity of 61.7 m/s (120 knots). Two iterations were carried out to evaluate data repeatability. For kinematics comparison, NIAR has identified iteration 1 as the repetition with the least deviation regarding the nominal test requirements. All batteries were fully charged previous to the test.

An initial velocity of 62.18 m/s (120.87 knots) was applied to the battery A FEM, corresponding to the velocity recorded for repetition 1 in the test documentation (APPENDIX B).

Figure 245 through Figure 248 show the comparison of the kinematics between the test and simulation at four different instances of the impact event.

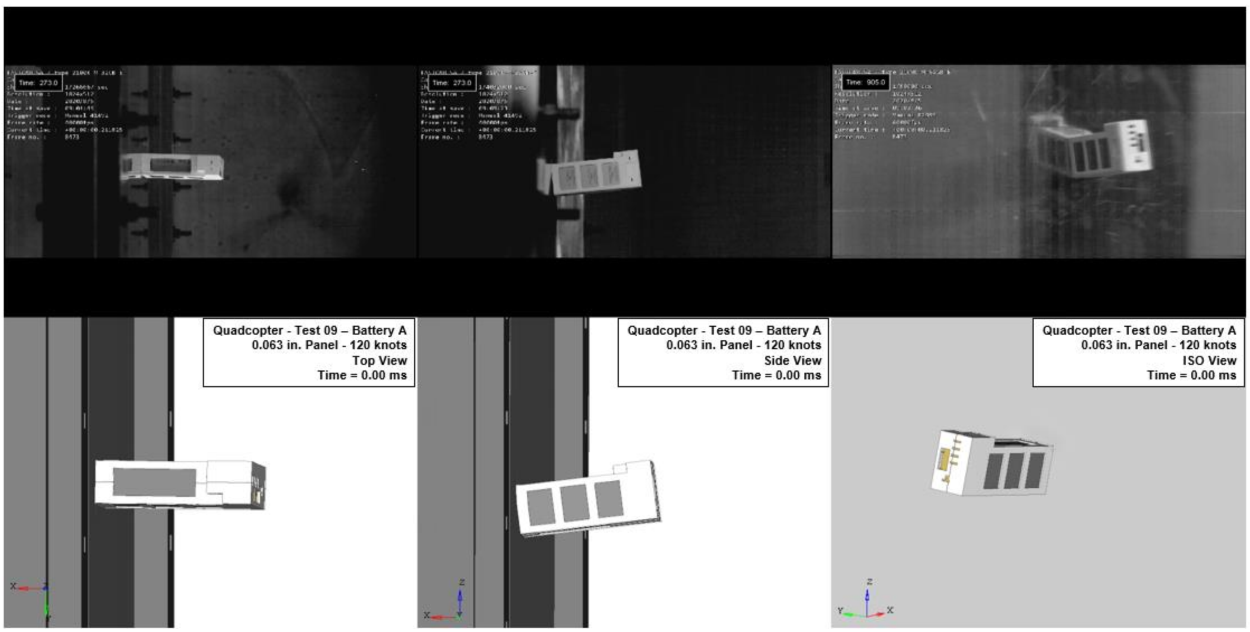


Figure 245. Comparison of battery A impact on 0.063” aluminum panel at 62.18 m/s (120.87 knots) at t = 0.00 ms (beginning of contact).

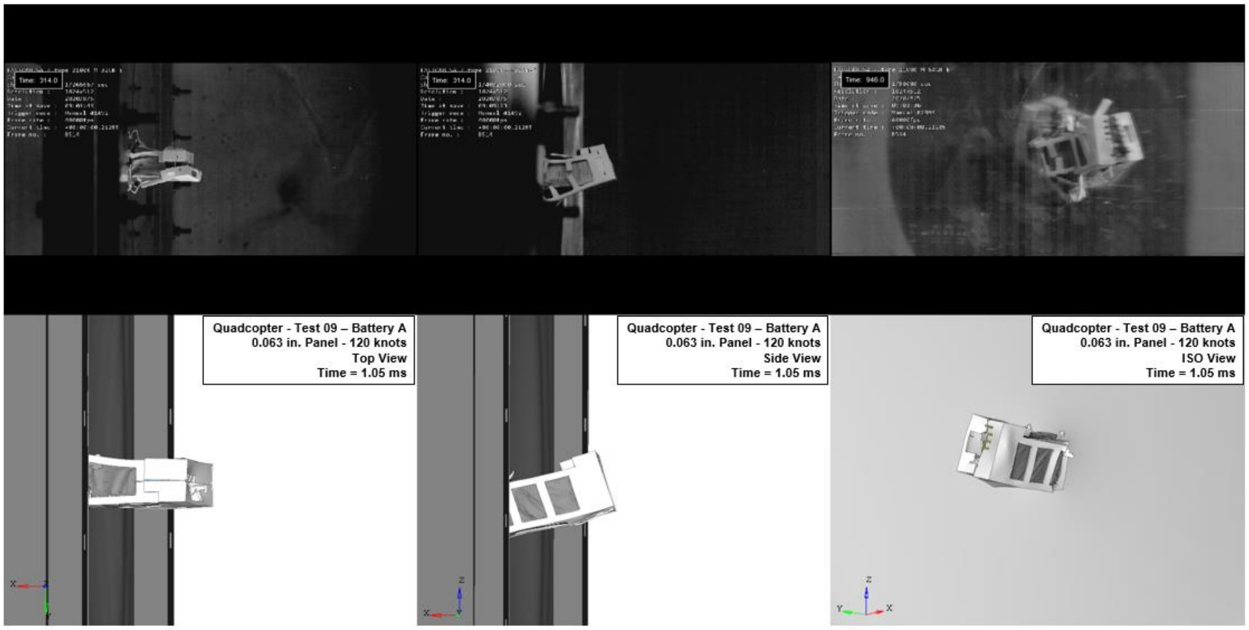


Figure 246. Comparison of battery A impact on 0.063" aluminum panel at 62.18 m/s (120.87 knots) at t = 1.05 ms.

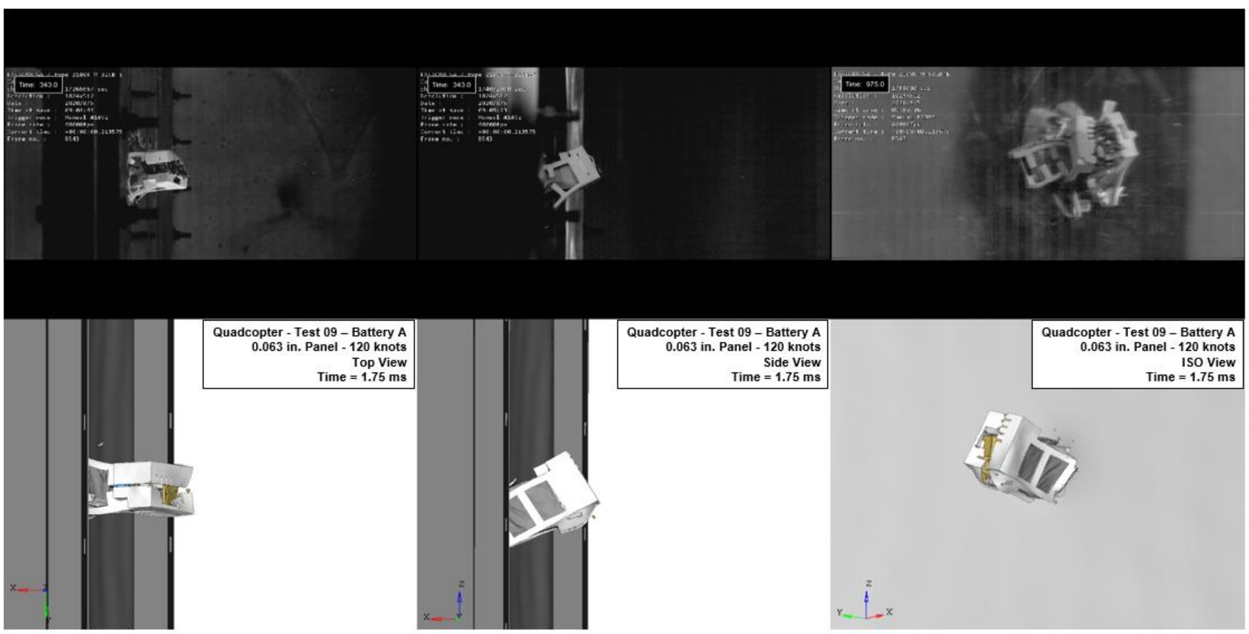


Figure 247. Comparison of battery A impact on 0.063" aluminum panel at 62.18 m/s (120.87 knots) at t = 1.75 ms.

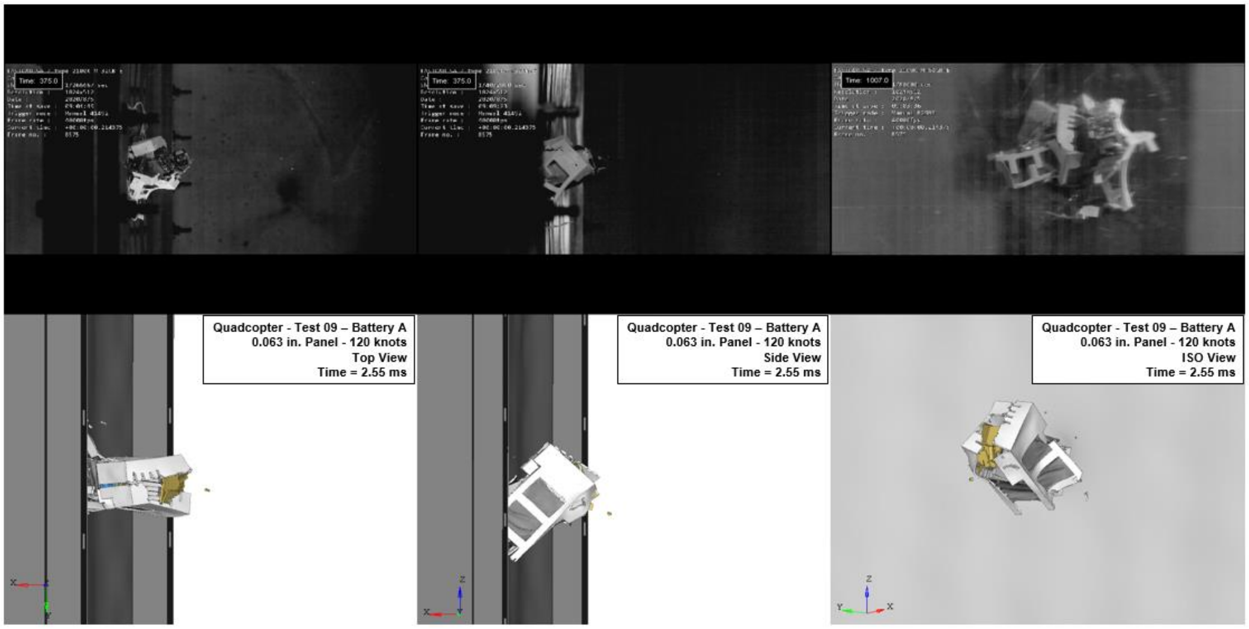


Figure 248. Comparison of battery A impact on 0.063” aluminum panel at 62.18 m/s (120.87 knots) at t = 2.55 ms (end of contact).

Figure 249 compares the simulation and test Y (horizontal) and Z (vertical) direction in-plane deformations and the out-of-plane displacements, for instance, with a maximum displacement of the aluminum panel.

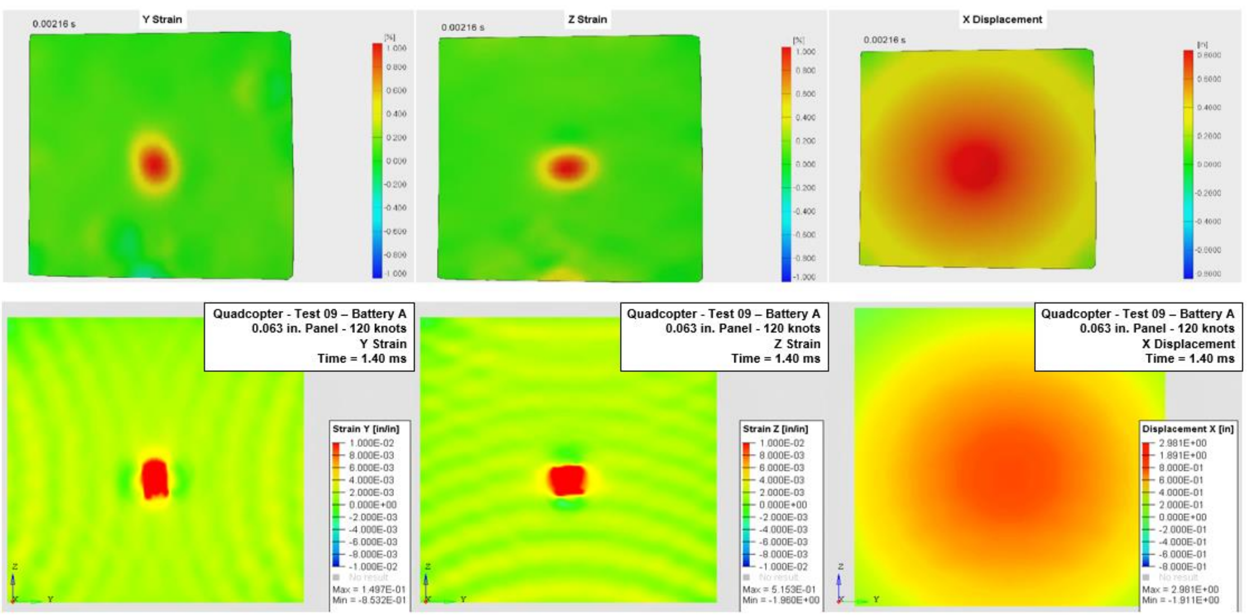


Figure 249. Comparison of test and simulation strains and displacements for battery A impact on 0.063” aluminum panel at 62.18 m/s (120.87 knots) at t = 1.40 ms (maximum displacement).

Figure 250 shows the out-of-plane displacement of the panel during the impact event obtained from the DIC data, and the simulation tracked displacements. The values on the vertical axis are not shown for confidential reasons.

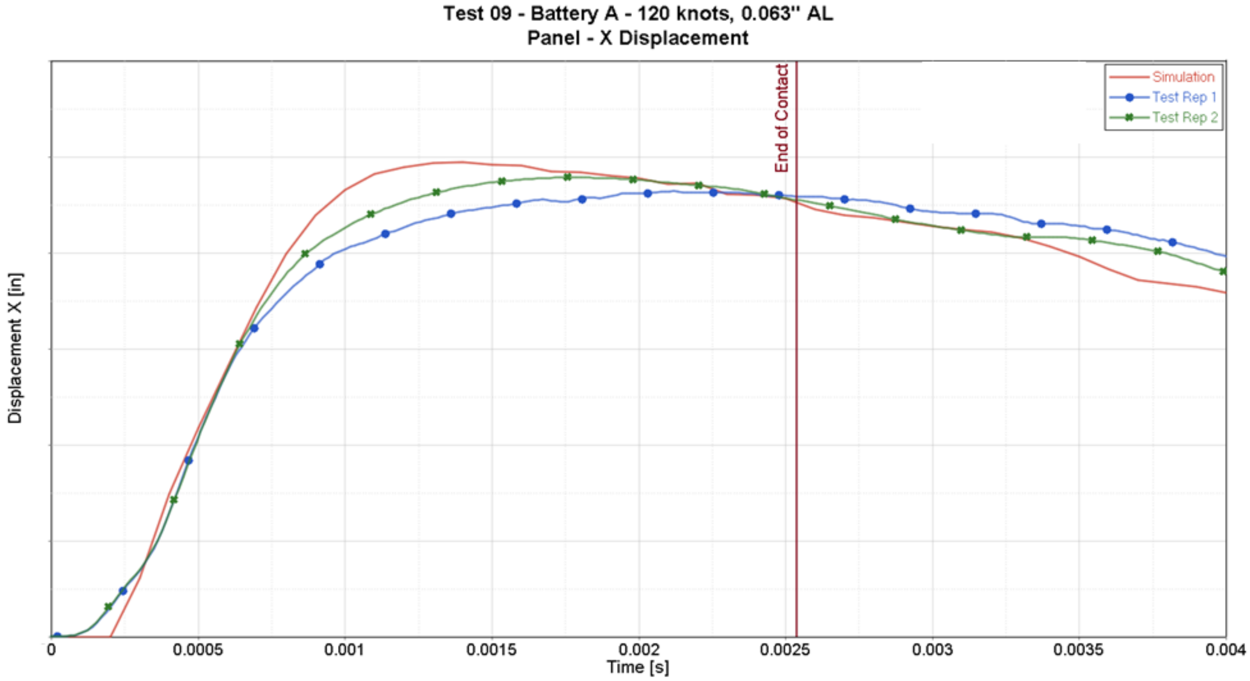


Figure 250. Comparison of the test and simulation out-of-plane displacements for battery A impact on 0.063” aluminum panel at 62.18 m/s (120.87 knots).

The physical panel was scanned after the test to compare the dimensions of the damaged area. Figure 251 compares the panel’s damaged area dimensions for the test and simulation. Again, there is good agreement between the physical test and the predicted panel’s damaged area.

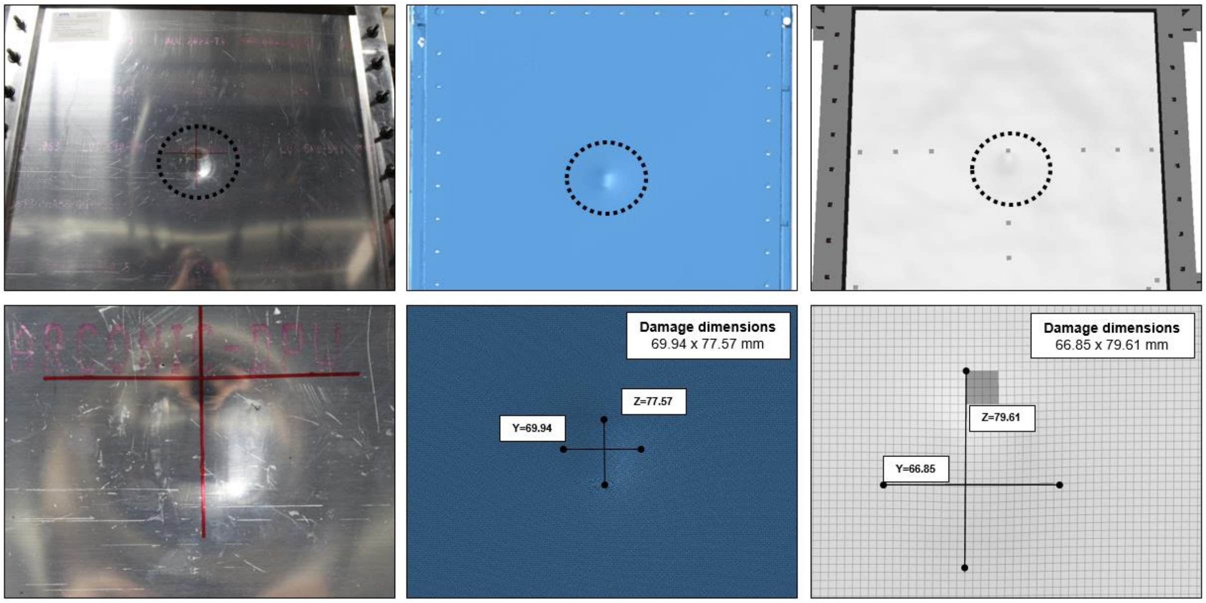


Figure 251. Comparison of the final damage of the panel for the test (left), scan (middle), and simulation (right) for the battery A impact on 0.063” aluminum panel at 62.18 m/s (120.87 knots).

Figure 252 compares the physical and simulation projectile damage. The battery case broke into pieces for both physical test and simulation, and the cells were damaged but stayed attached. The quadcopter battery indented the aluminum panel, but it did not penetrate through it. The battery indicated a “Fire Risk” during the physical test.

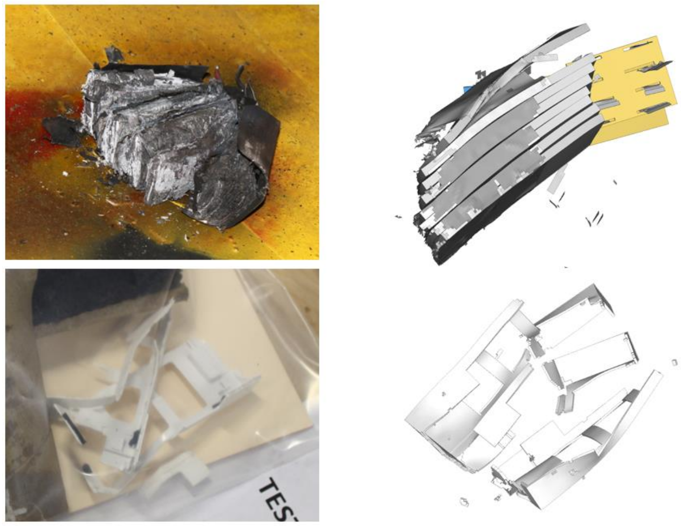

Figure 252. Comparison of the test (left) and simulation (right) projectile damage for battery A impact on 0.063” aluminum panel at 62.18 m/s (120.87 knots).

Figure 253 compares the load-time history of both test repetitions and the simulation load output. All the curves were filtered with a low-pass filter of 15,000 Hz. The load data shows good repeatability for both tests. The simulation loads correlate well to the test loads except for the magnitude of the second oscillation. The values on the vertical axis are not shown for confidential reasons.

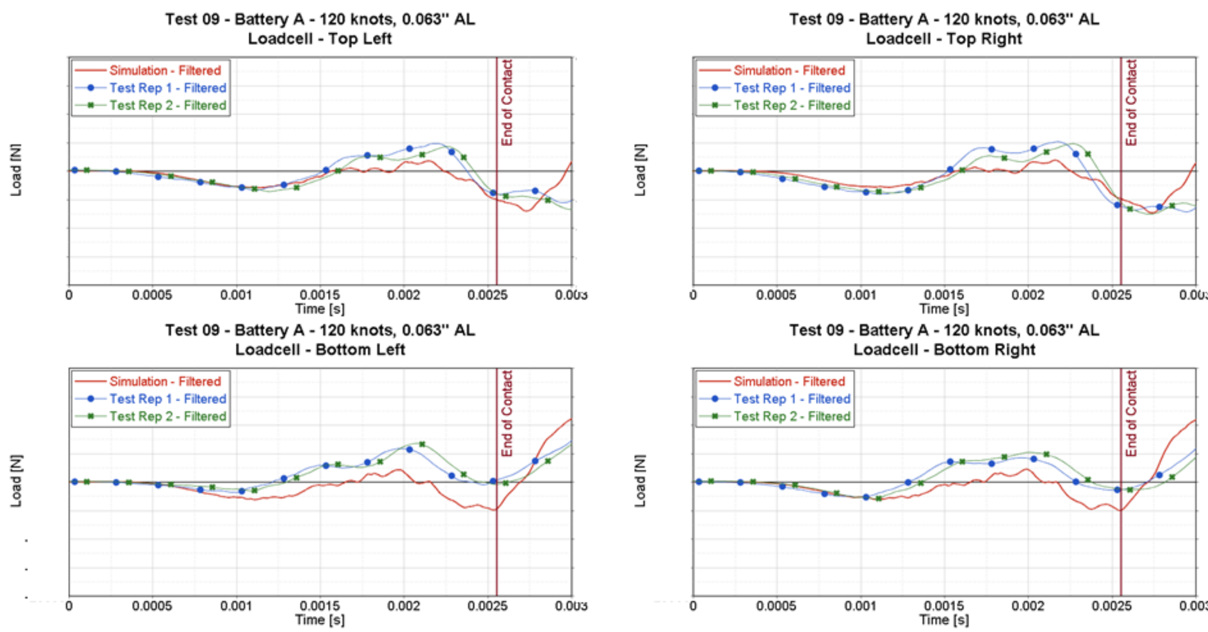


Figure 253. Load cell history data validation for battery A impact on 0.063” aluminum panel at 62.18 m/s (120.87 knots).

Figure 254 compares the strain data collected at iteration 1 to the simulation strains. The values on the vertical axis are not shown for confidential reasons.

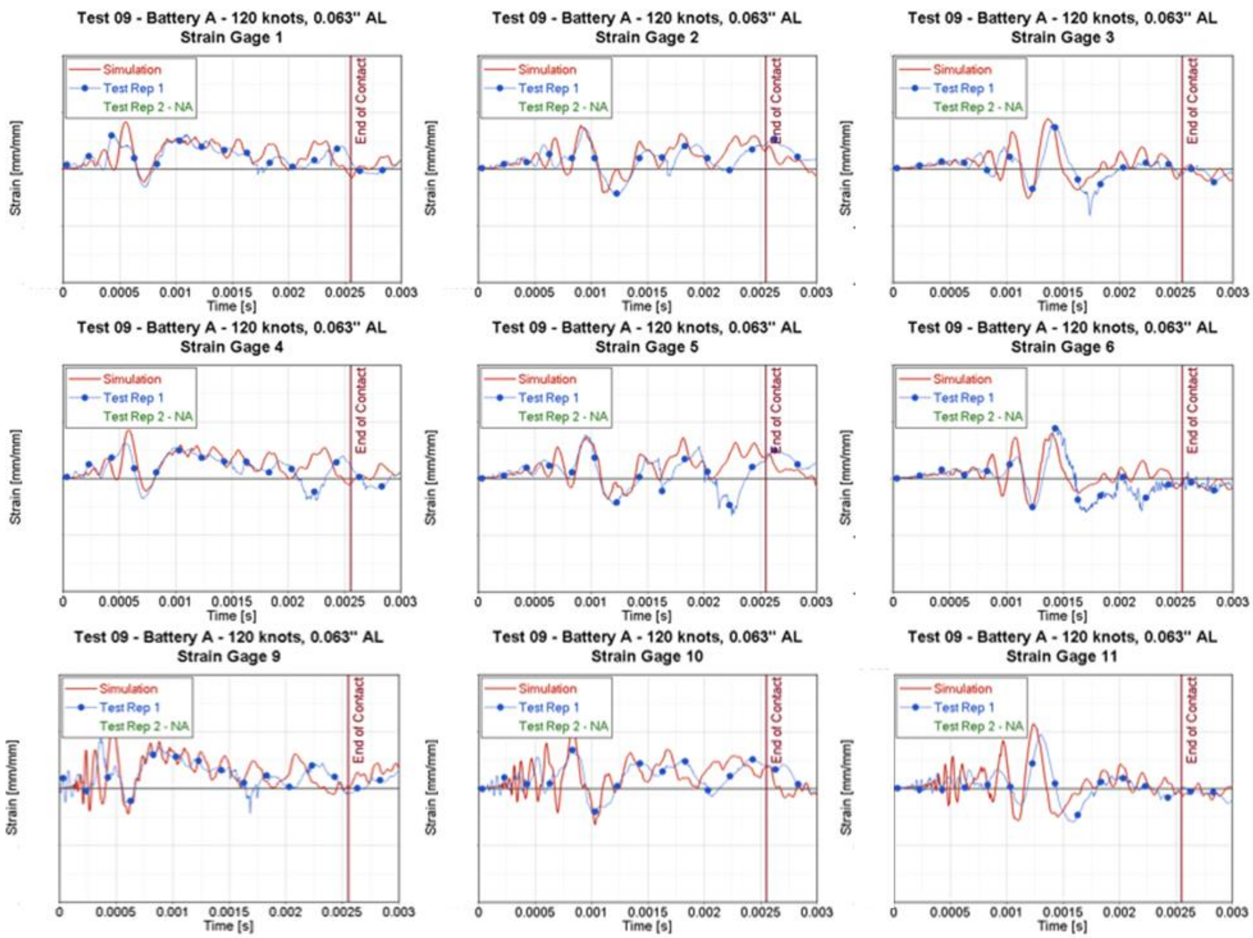


Figure 254. Strain comparison of strain gages 1-6 and 9-11 for battery A impact on 0.063” aluminum panel at 62.18 m/s (120.87 knots).

## A.10 TEST 10 – BATTERY AT 120 KNOTS – 6.35 MM AL PANEL

Test 10 consists of the impact of battery A with a 6.35mm (0.25″) aluminum panel at a nominal velocity of 61.7 m/s (120 knots). Two iterations were carried out to evaluate data repeatability. For kinematics comparison, NIAR has identified iteration 1 as the repetition with the least deviation regarding the nominal test requirements. All batteries were fully charged before the test.

An initial velocity of 59.68 m/s (116.0 knots) was applied to the battery A FEM, corresponding to the velocity recorded for repetition 1 in the test documentation (APPENDIX B).

Figure 255 through Figure 258 show the comparison of the kinematics between the test and simulation at four different instances of the impact event.

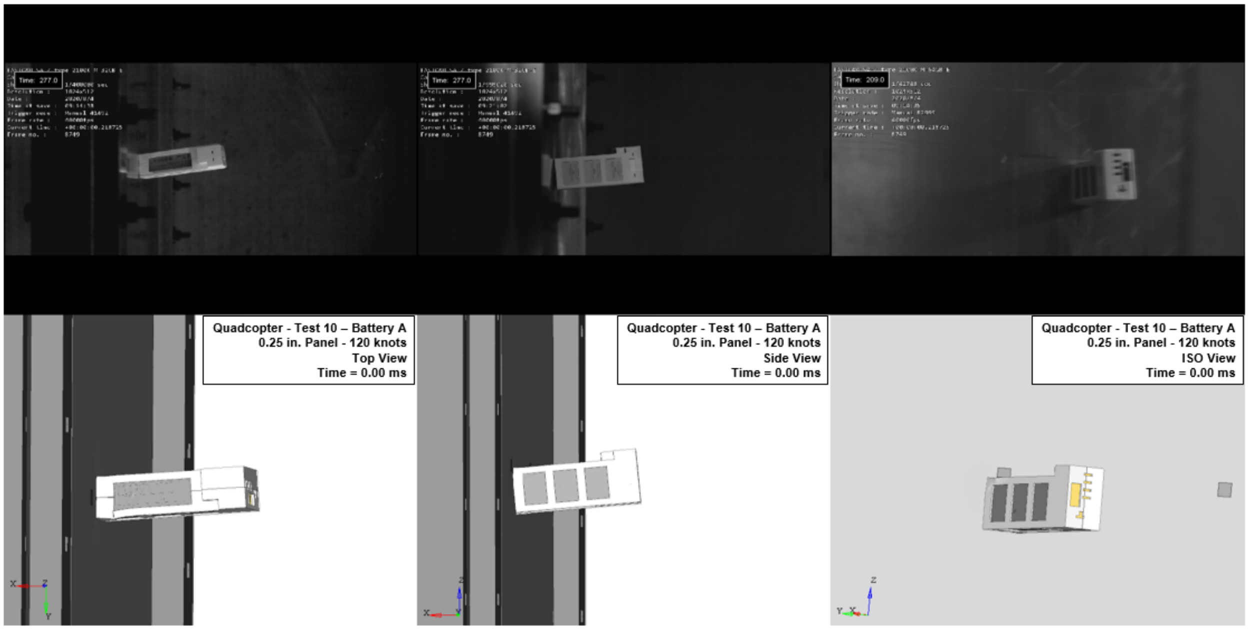


Figure 255. Comparison of battery A impact on 0.25" aluminum panel at 59.68 m/s (116.0 knots) at t = 0.00 ms (beginning of contact).

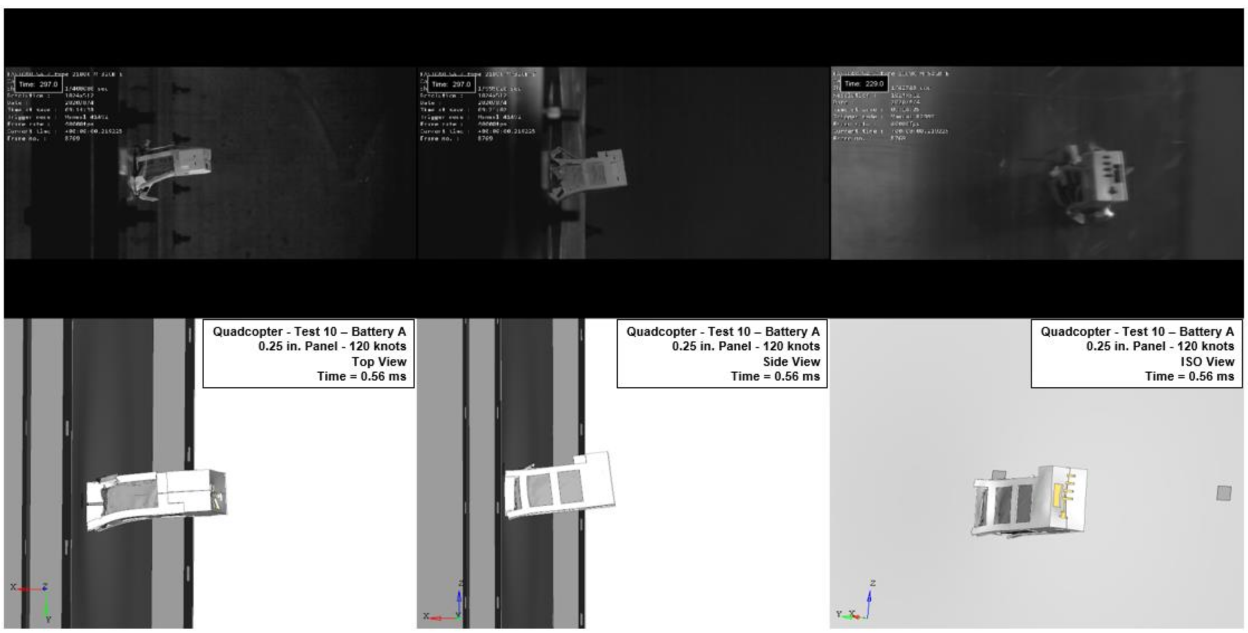


Figure 256. Comparison of battery A impact on 0.25" aluminum panel at 59.68 m/s (116.0 knots) at t = 0.56 ms.

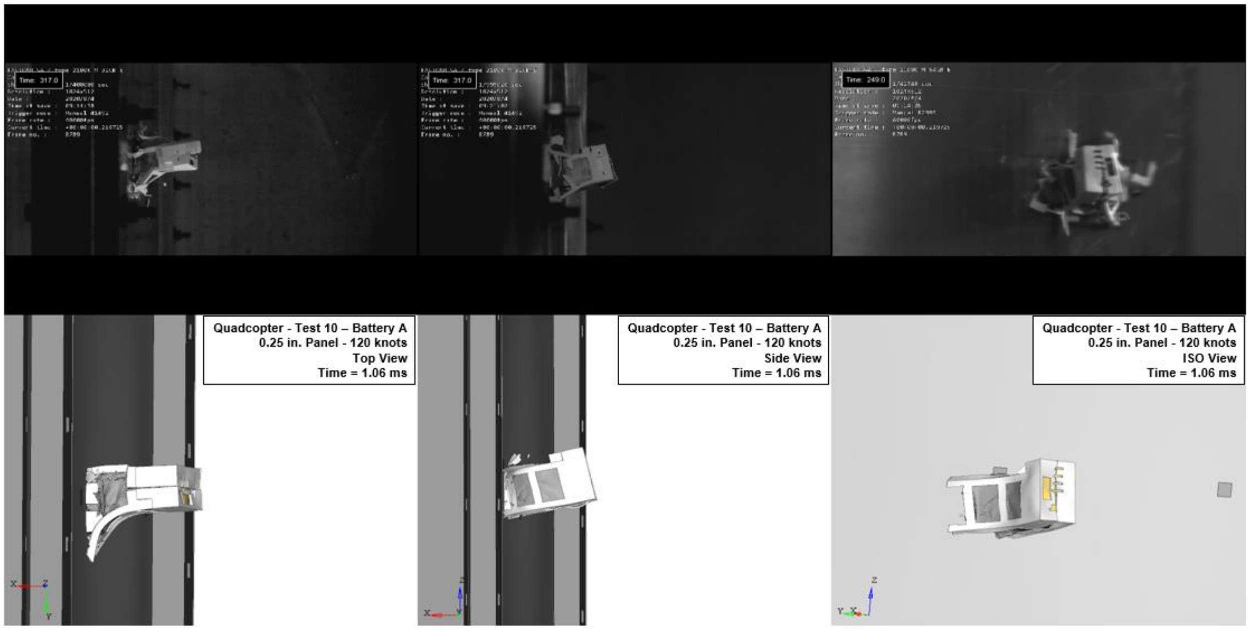


Figure 257. Comparison of battery A impact on 0.25” aluminum panel at 59.68 m/s (116.0 knots) at t = 1.06 ms.

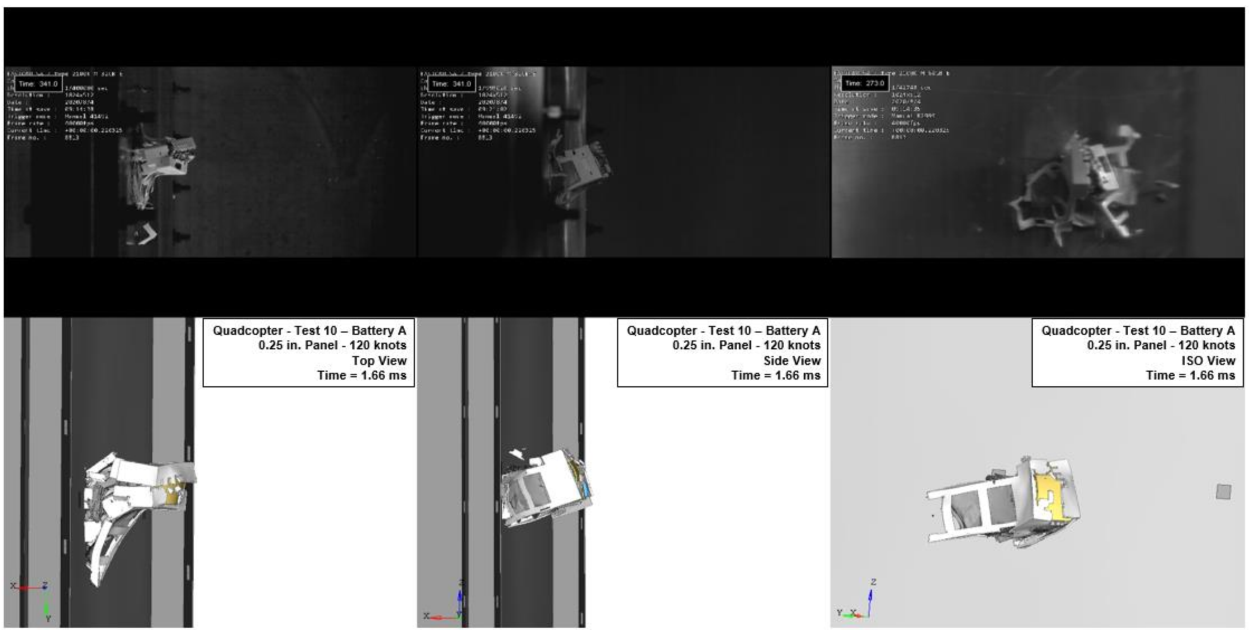


Figure 258. Comparison of battery A impact on 0.25” aluminum panel at 59.68 m/s (116.0 knots) at t = 1.66 ms (end of contact).

Figure 259 compares the simulation and test Y (horizontal) and Z (vertical) direction in-plane deformations as well as the out-of-plane displacements, for instance, with a maximum displacement of the aluminum panel.

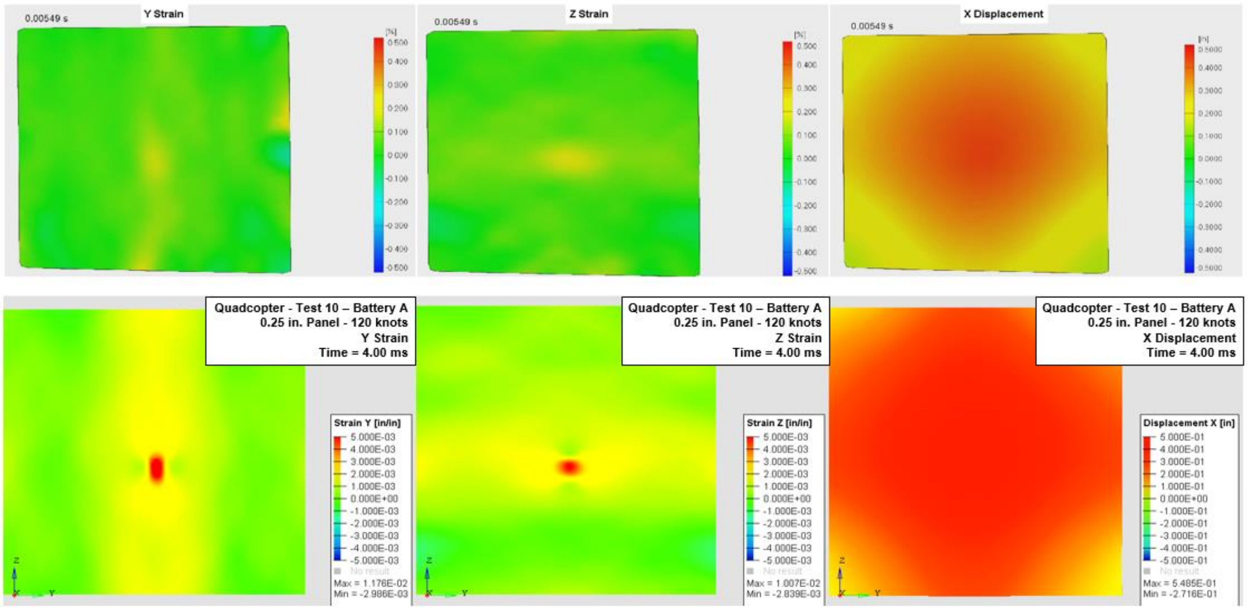


Figure 259. Comparison of test and simulation strains and displacements for battery A impact on 0.25" aluminum panel at 59.68 m/s (116.0 knots) at t = 4.00 ms (maximum displacement).

Figure 260 shows the out-of-plane displacement of the panel during the impact event obtained from the DIC data, and the simulation tracked displacements. The values on the vertical axis are not shown for confidential reasons.

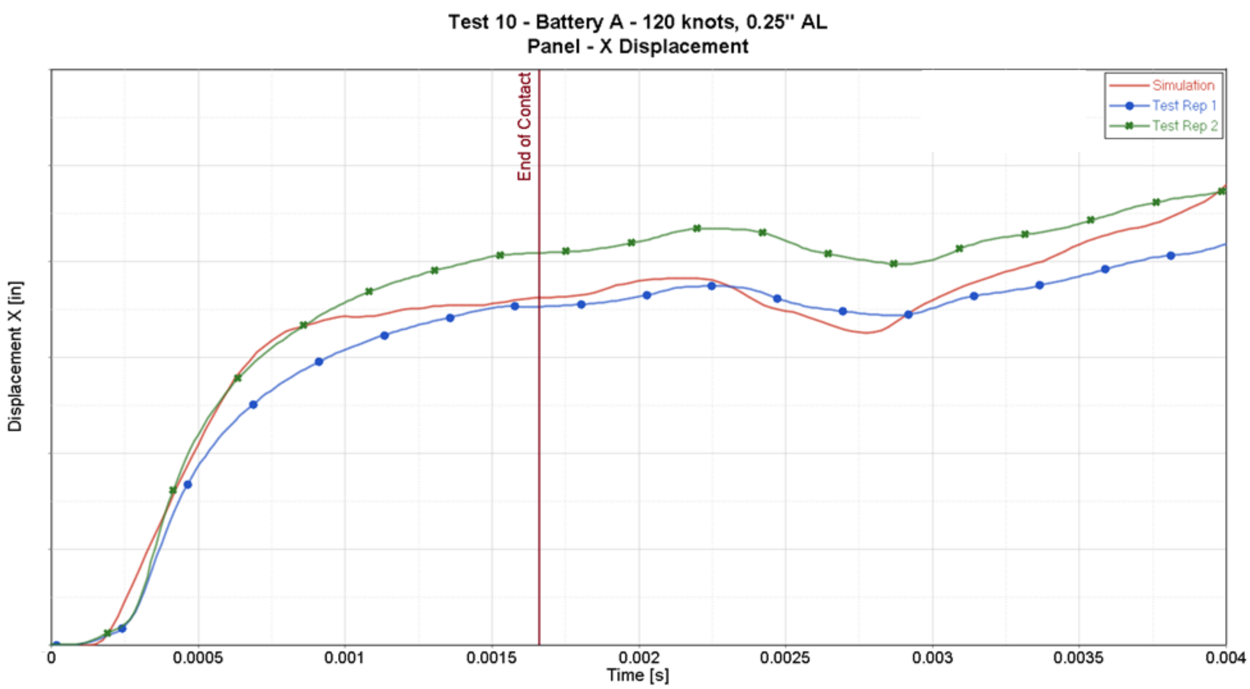


Figure 260. Comparison of the test and simulation out-of-plane displacements for battery A impact on 0.25" aluminum panel at 59.68 m/s (116.0 knots).

The physical panel was scanned after the test to compare the dimensions of the damaged area. Figure 261 compares the panel's damaged area dimensions for the test and simulation. For this case, the simulation predicts a smaller area holding plastic deformation. However, the overall shape is captured.

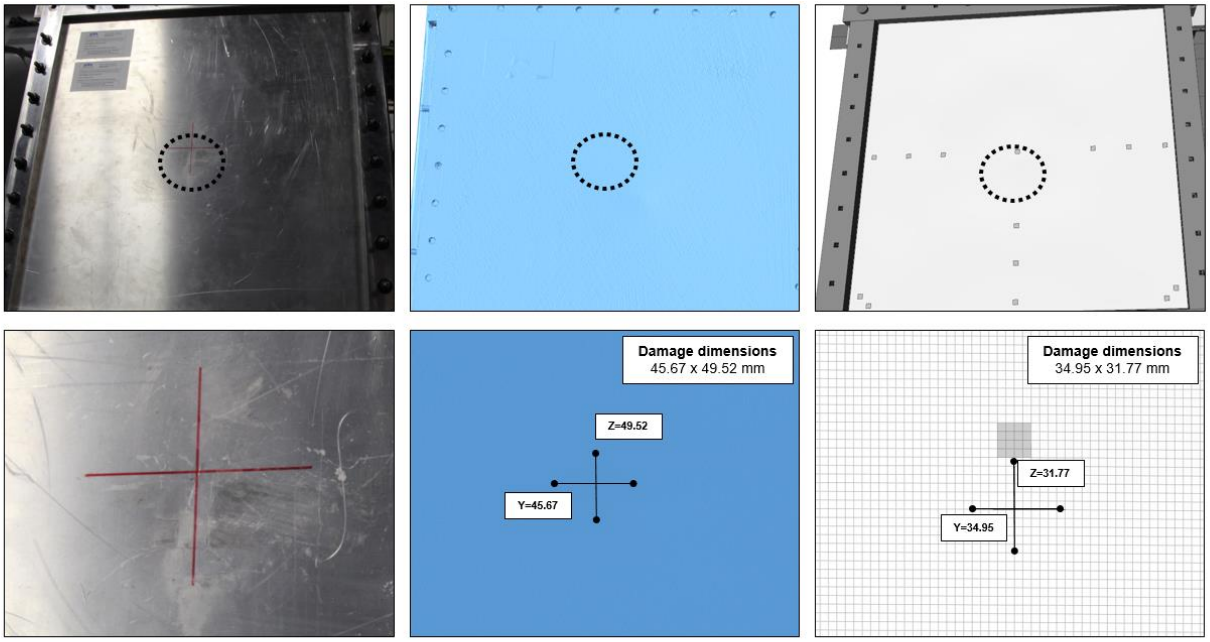


Figure 261. Comparison of the final damage of the panel for the test (left), scan (middle), and simulation (right) for battery A impact on 0.25" aluminum panel at 59.68 m/s (116.0 knots).

Figure 262 compares the physical and simulation projectile damage. The battery case split into fragments for both the physical test and simulation and the battery cells separated into several pieces, some of which showed a "Fire Risk" in the physical test. The battery left a small indentation on the panel but did not penetrate it.


Figure 262. Comparison of the test (left) and simulation (right) projectile damage for battery A impact on 0.25” aluminum panel at 59.68 m/s (116.0 knots).

Figure 263 compares the load-time history of both test repetitions and the simulation load output. All the curves were filtered with a low-pass filter of 15,000 Hz. The load data shows good repeatability for tests and simulation and confirms the good correlation of the FEM. Figure 264 compares the strain data collected at both repetitions to the simulation strains. The values on the vertical axis are not shown for confidential reasons.

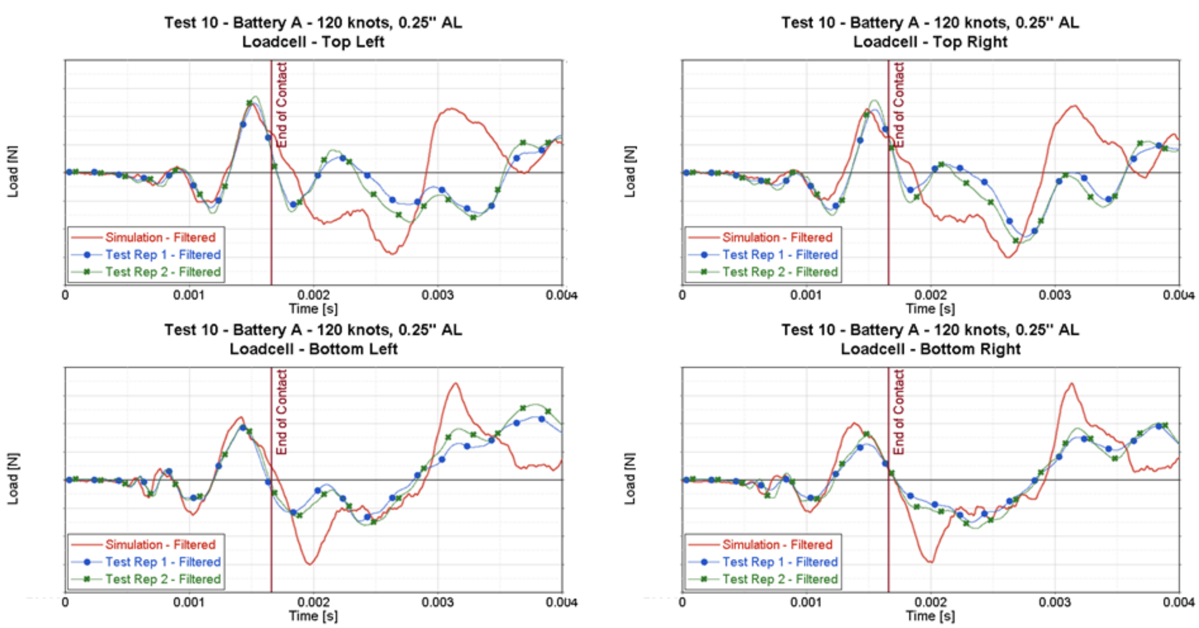


Figure 263. Load cell history data validation for battery A impact on 0.25” aluminum panel at 59.68 m/s (116.0 knots).

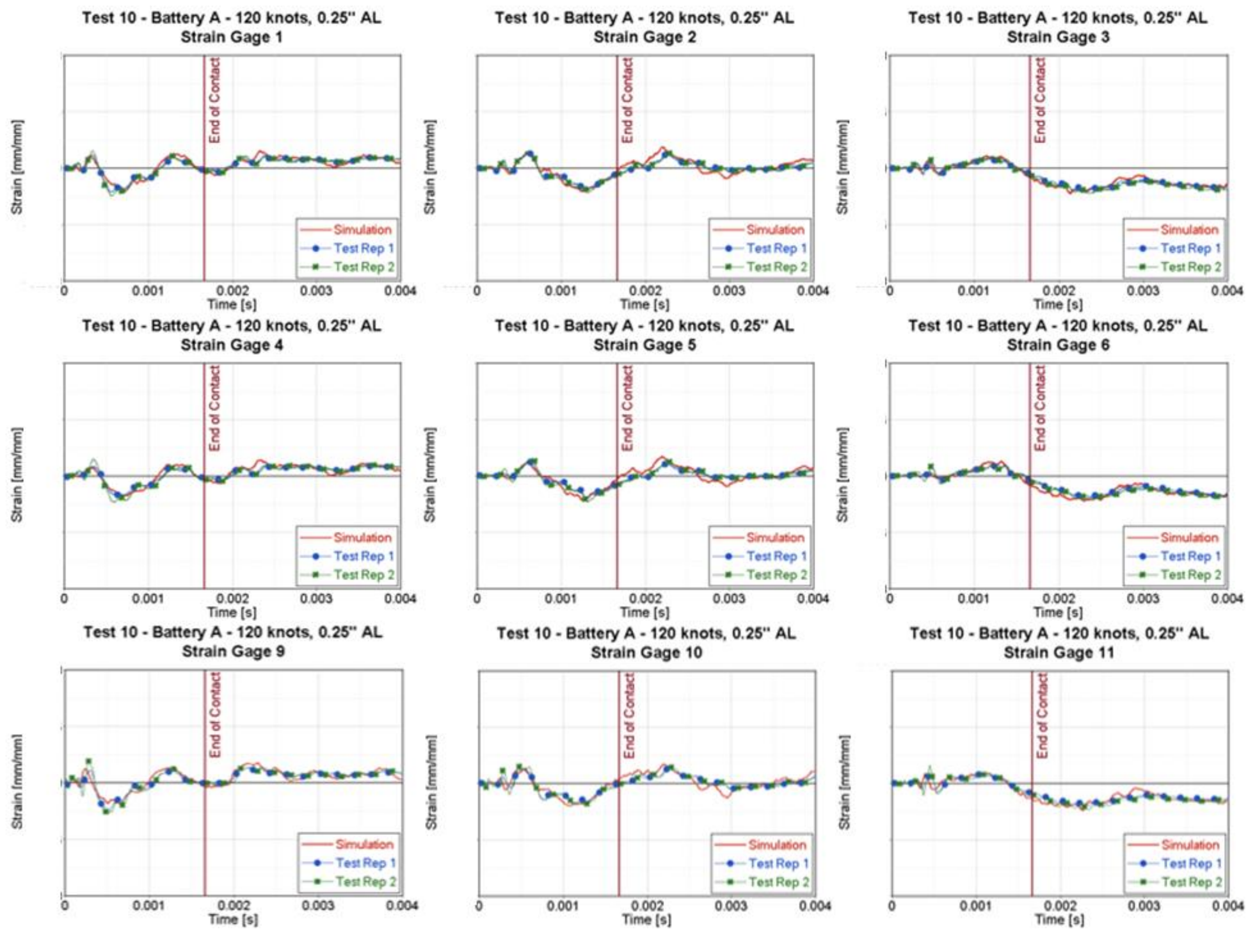


Figure 264. Strain comparison of strain gages 1-6 and 9-11 for battery A impact on 0.25” aluminum panel at 59.68 m/s (116.0 knots).

## A.11 TEST 11 – MOTOR AT 120 KNOTS – 1.6 MM AL PANEL

Test 11 consists of the impact of motor A with the 1.6 mm (0.063″) aluminum panel at a nominal velocity of 61.7 m/s (120 knots). NIAR has identified iteration 1 as the repetition with the least deviation regarding the nominal test requirements.

An initial velocity of 63.79 m/s (124.0 knots) was applied to the motor A FEM, corresponding to the velocity recorded for repetition 1 in the test documentation (APPENDIX B).

Figure 265 through Figure 268 shows the kinematics between the test and simulation at four different instances of the impact event.

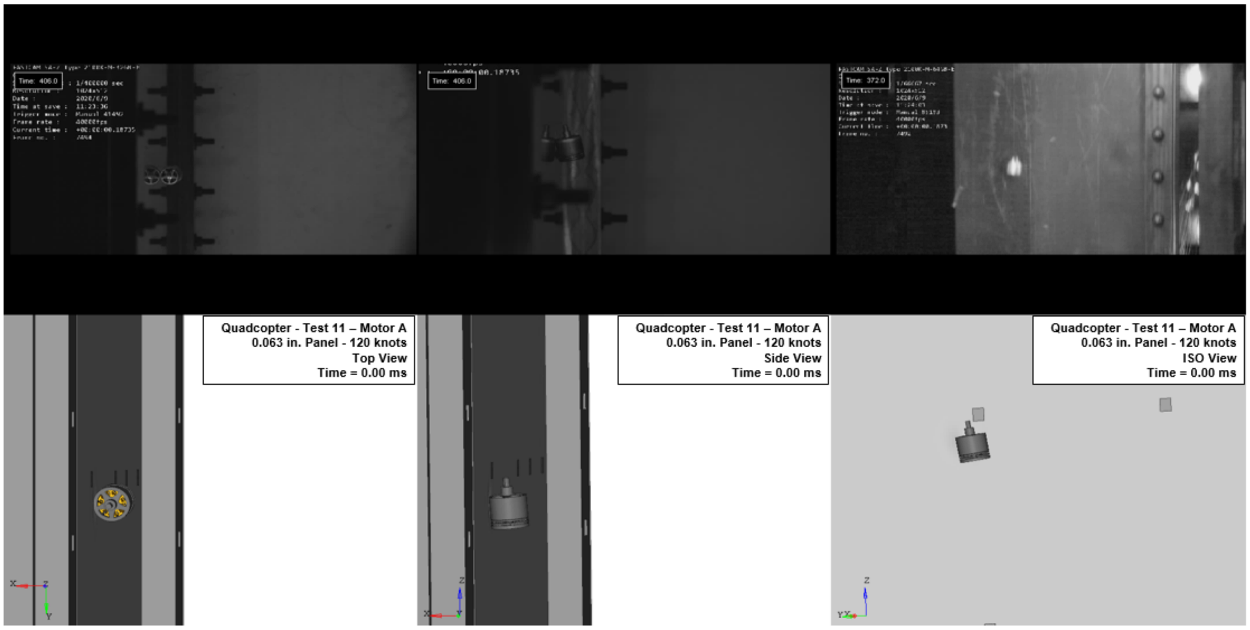


Figure 265. Comparison for motor A impact on 0.063” aluminum panel at 63.79 m/s (124 knots) at t = 0.00 ms (beginning of contact).

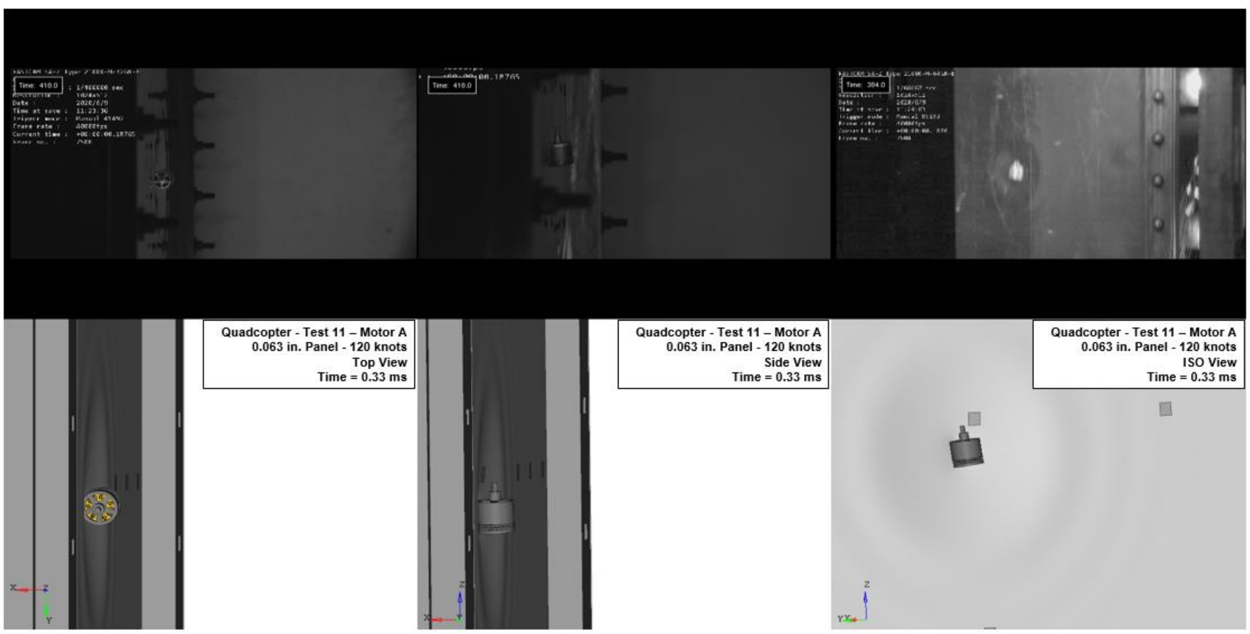


Figure 266. Comparison for motor A impact on 0.063” aluminum panel at 63.79 m/s (124 knots) at t = 0.33 ms.

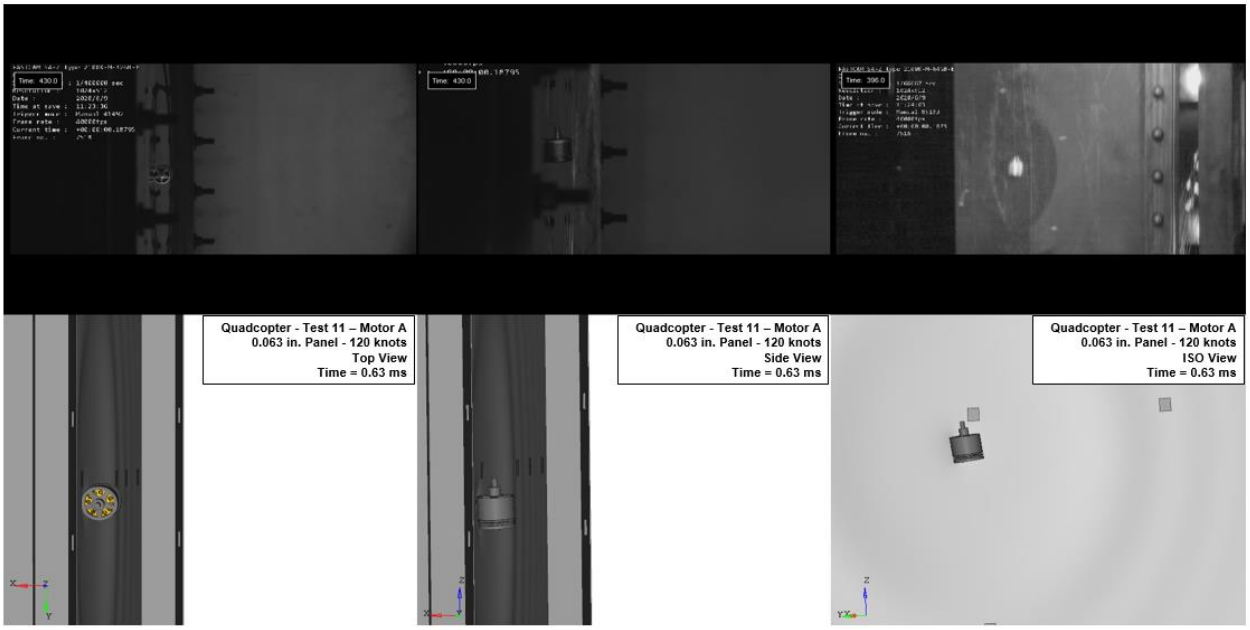


Figure 267 Comparison for motor A impact on 0.063” aluminum panel at 63.79 m/s (124 knots) at t = 0.63 ms.

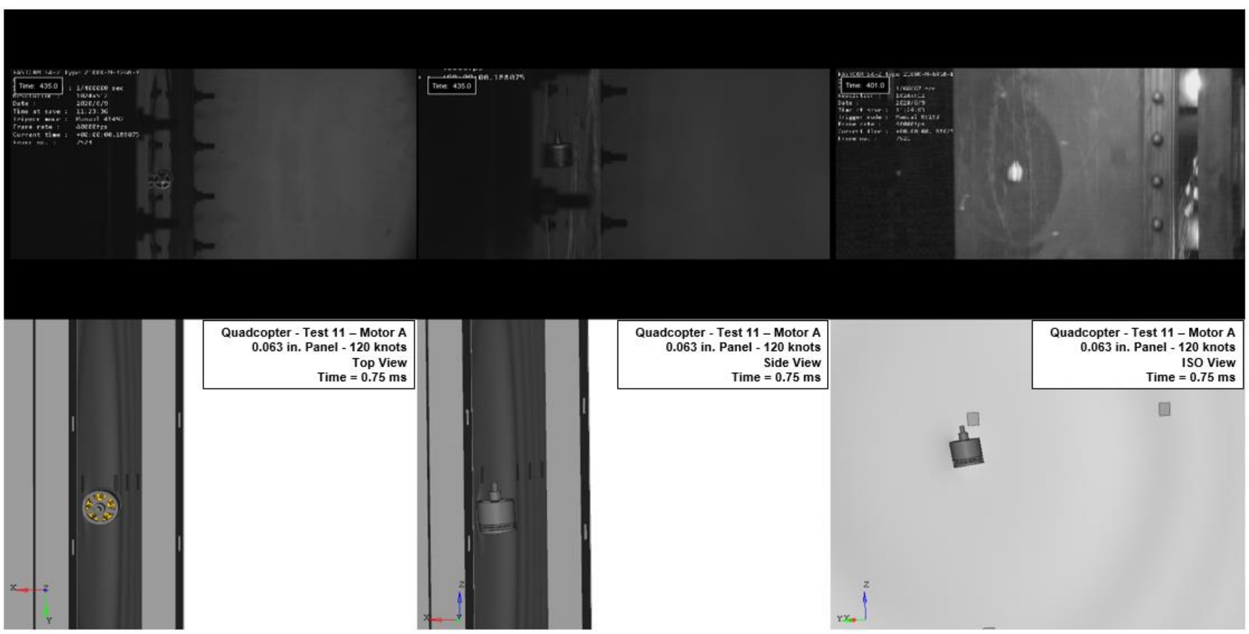


Figure 268 Comparison for motor A impact on 0.063” aluminum panel at 63.79 m/s (124 knots) at t = 0.75 ms (end of contact).

Figure 269 compares the simulation and test Y (horizontal) and Z (vertical) direction in-plane deformations as well as the out-of-plane displacements, for instance, with a maximum displacement of the aluminum panel.

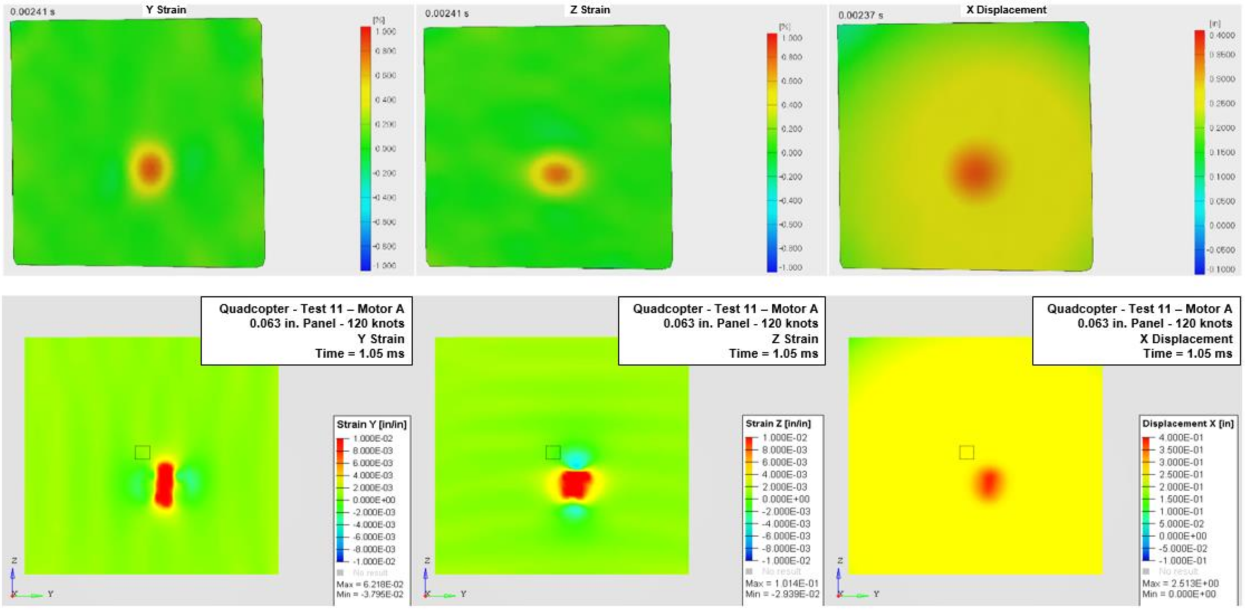


Figure 269 Comparison of test and simulation strains and displacements for motor A impact on 0.063" aluminum panel at 63.79 m/s (124 knots) at t = 1.05 ms (maximum displacement).

Figure 270 shows the out-of-plane displacement of the panel during the impact event obtained from the DIC data, and the simulation tracked displacements. The values on the vertical axis are not shown for confidential reasons.

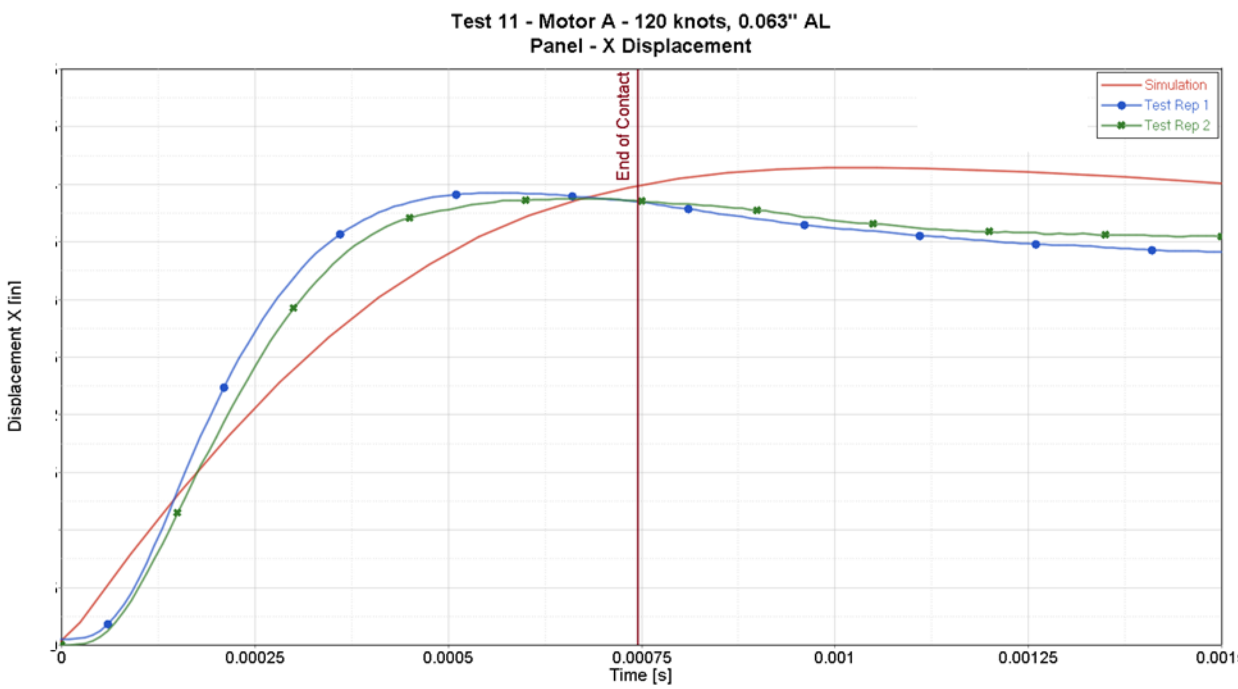


Figure 270. Comparison of the test and simulation out-of-plane displacements for motor A impact on 0.063" aluminum panel at 63.79 m/s (124 knots).

The physical panel was scanned after the test to compare the dimensions of the damaged area. Figure 271 compares the panel's damaged area dimensions for the test and simulation. Again, there is good agreement between the physical test and the predicted panel's damaged area.

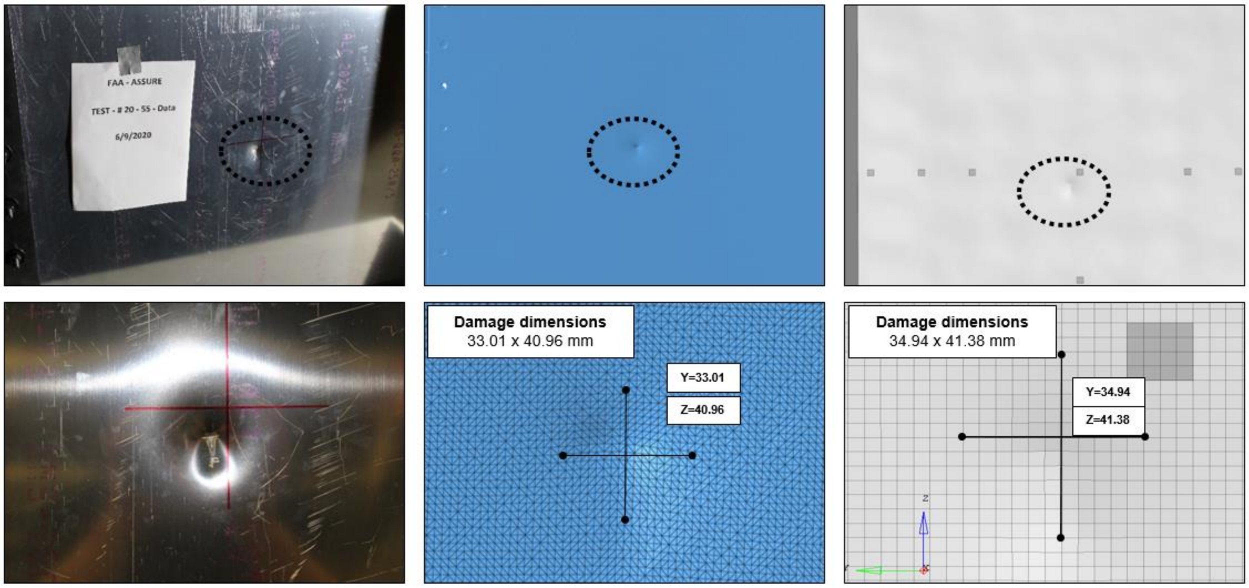


Figure 271. Comparison of the final damage of the panel for the test (left), scan (middle), and simulation (right) for motor A impact on 0.063" aluminum panel at 63.79 m/s (124 knots).

Figure 272 compares the physical and simulation projectile damage. For both physical tests and simulation, the motor sustained minor damage.

Figure 272. Comparison of the test (left) and simulation (right) projectile damage for motor A impact on 0.063" aluminum panel at 63.79 m/s (124 knots).

Figure 273 compares the load-time history of both test repetitions and the simulation load output. Again, all the curves were filtered with a low-pass filter of 15,000 Hz. The load data shows good repeatability for test and simulation and confirms the good correlation of the FEM. Figure 274 compares the strain data collected at both repetitions to the simulation strains. The values on the vertical axis are not shown for confidential reasons.

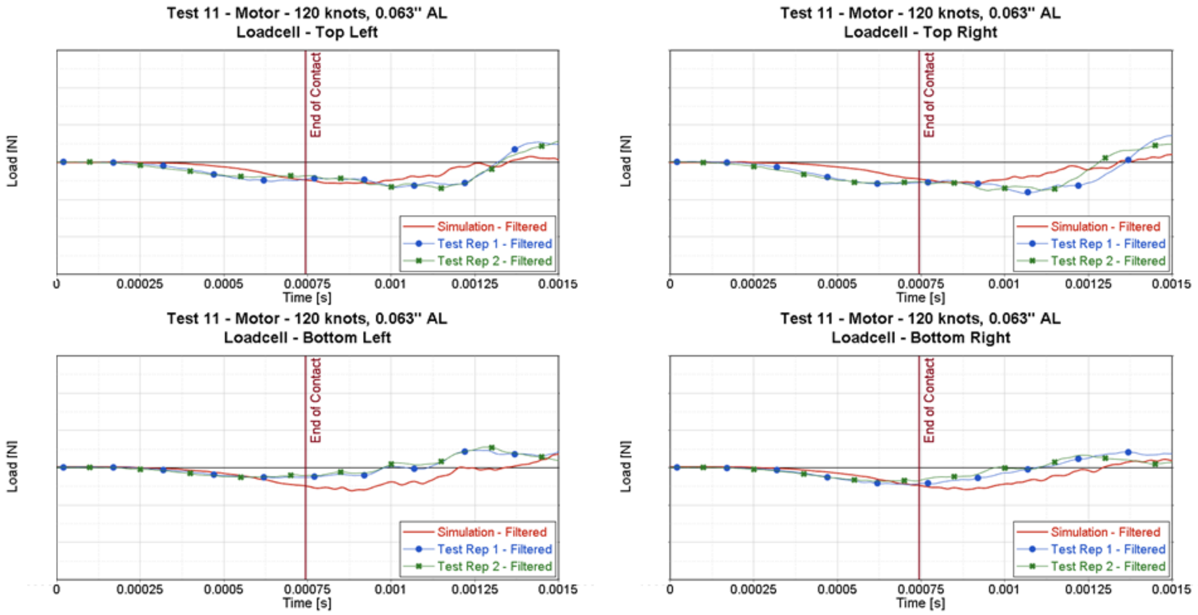


Figure 273. Load cell history data validation for motor A impact on 0.063” aluminum panel at 63.79 m/s (124 knots).

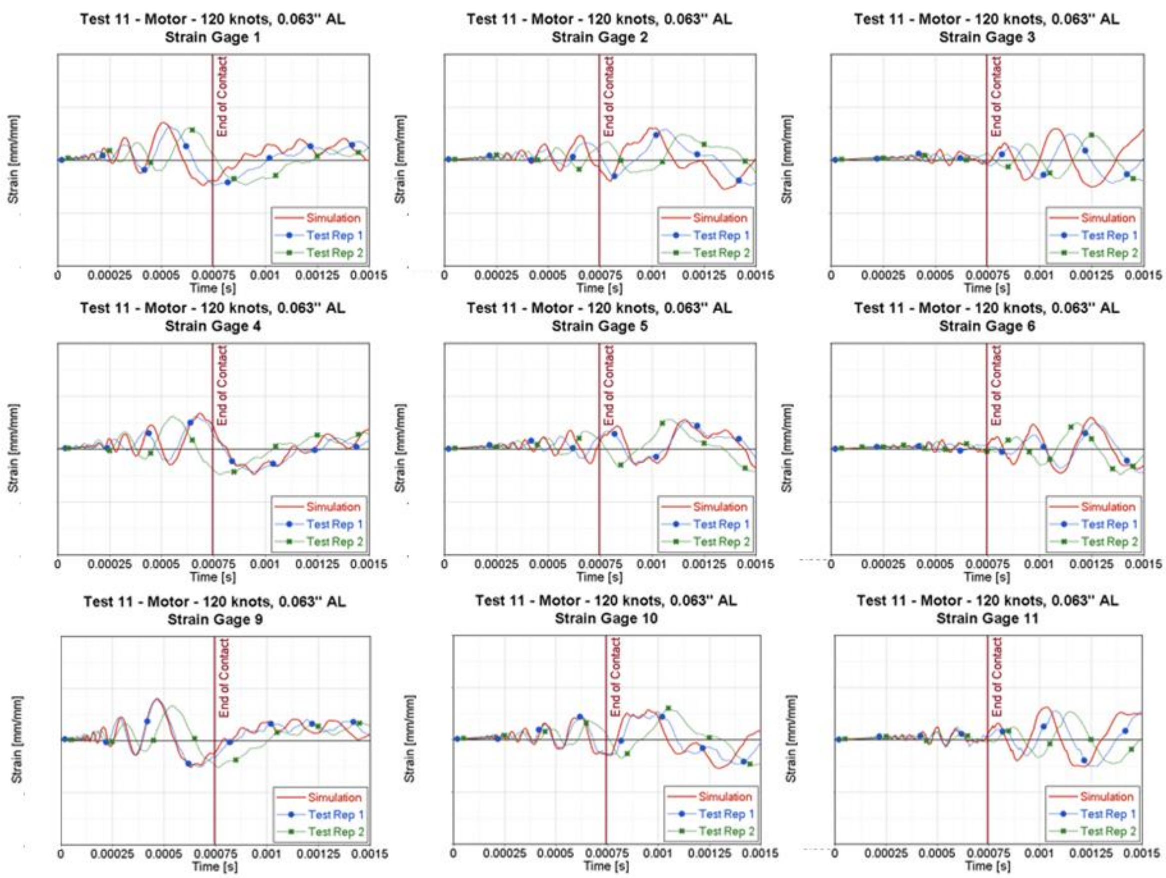


Figure 274. Strain comparison of strain gages 1-6 and 9-11 for motor A impact on 0.063” aluminum panel at 63.79 m/s (124 knots).

## A.12 TEST 12 – MOTOR AT 50 KNOTS – 1.6 MM AL PANEL

Test 12 consists of the impact of motor A with the 1.6 mm (0.063″) aluminum panel at a nominal velocity of 25.7 m/s (50 knots). Two iterations were carried out to evaluate data repeatability. For kinematics comparison, NIAR has identified iteration 1 as the repetition with the least deviation regarding the nominal test requirements.

An initial velocity of 29.32 m/s (57.0 knots) was applied to the motor A FEM, corresponding to the velocity recorded for repetition 1 in the test documentation (APPENDIX B).

Figure 275 through Figure 278 show the comparison of the kinematics between the test and simulation at four different instances of the impact event.

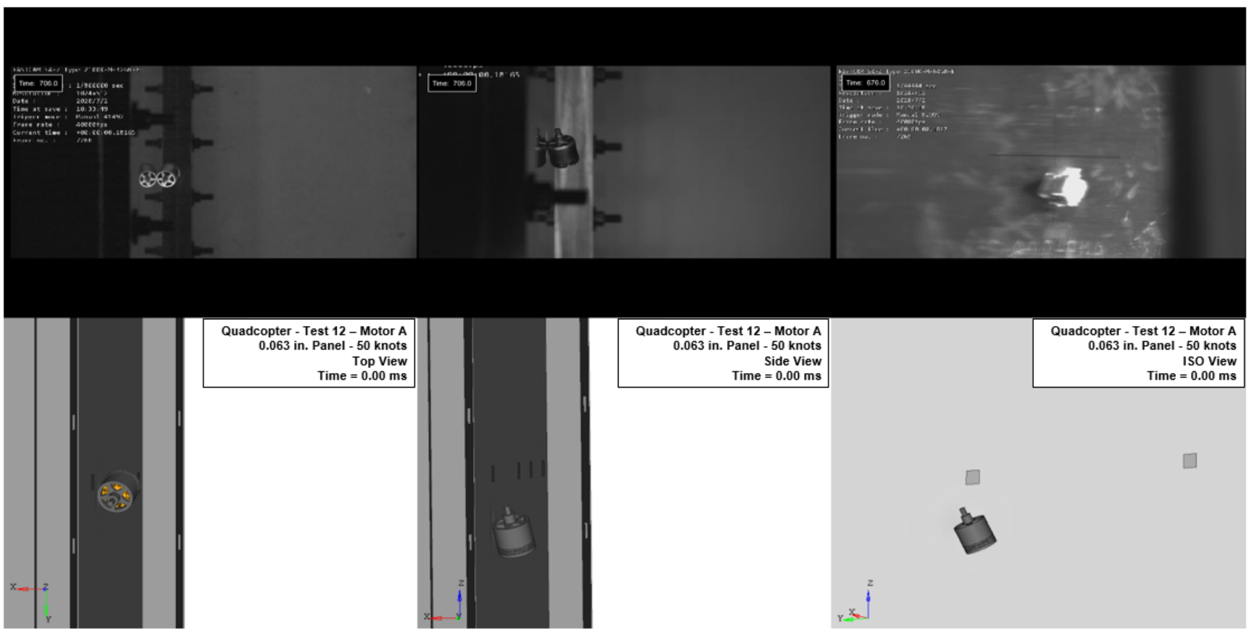


Figure 275. Comparison for motor A impact on 0.063" aluminum panel at 29.32 m/s (57.0 knots) at t = 0.00 ms (beginning of contact).

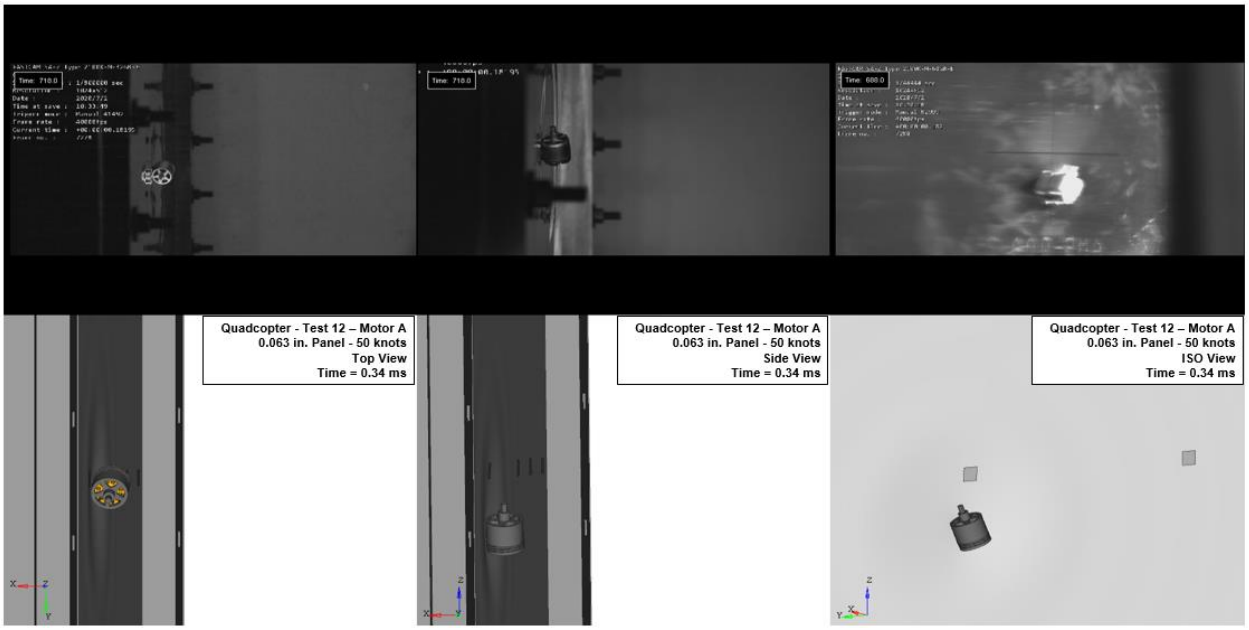


Figure 276. Comparison for motor A impact on 0.063" aluminum panel at 29.32 m/s (57.0 knots) at t = 0.34 ms.

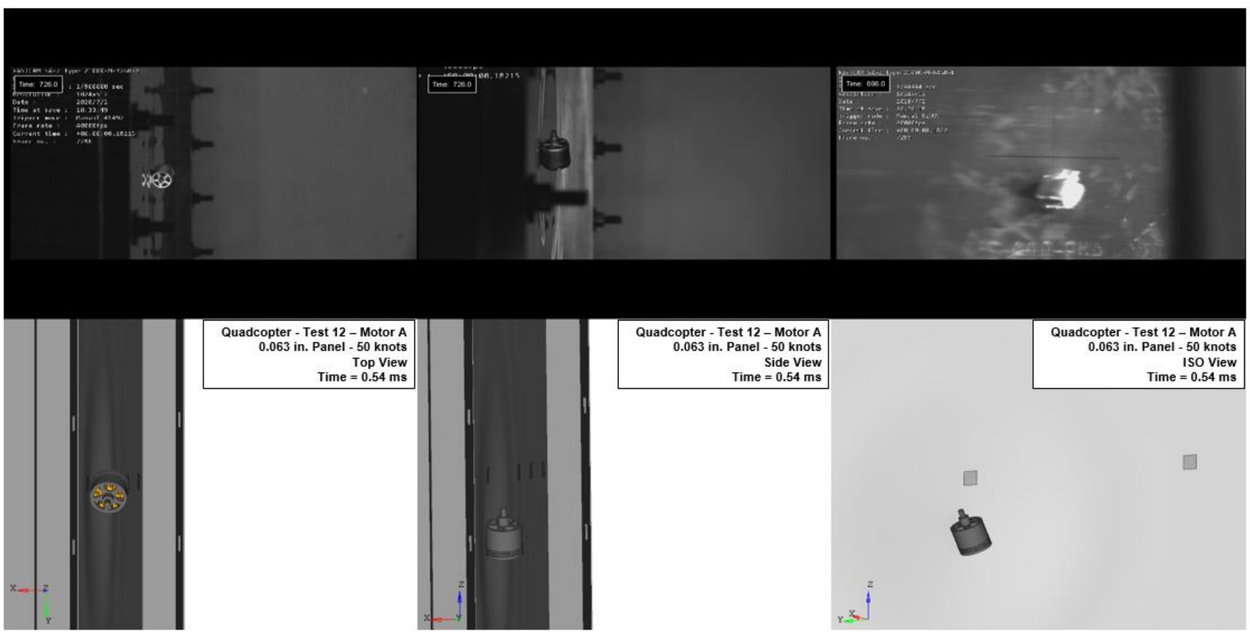


Figure 277 Comparison for motor A impact on 0.063" aluminum panel at 29.32 m/s (57.0 knots) at t = 0.54 ms.

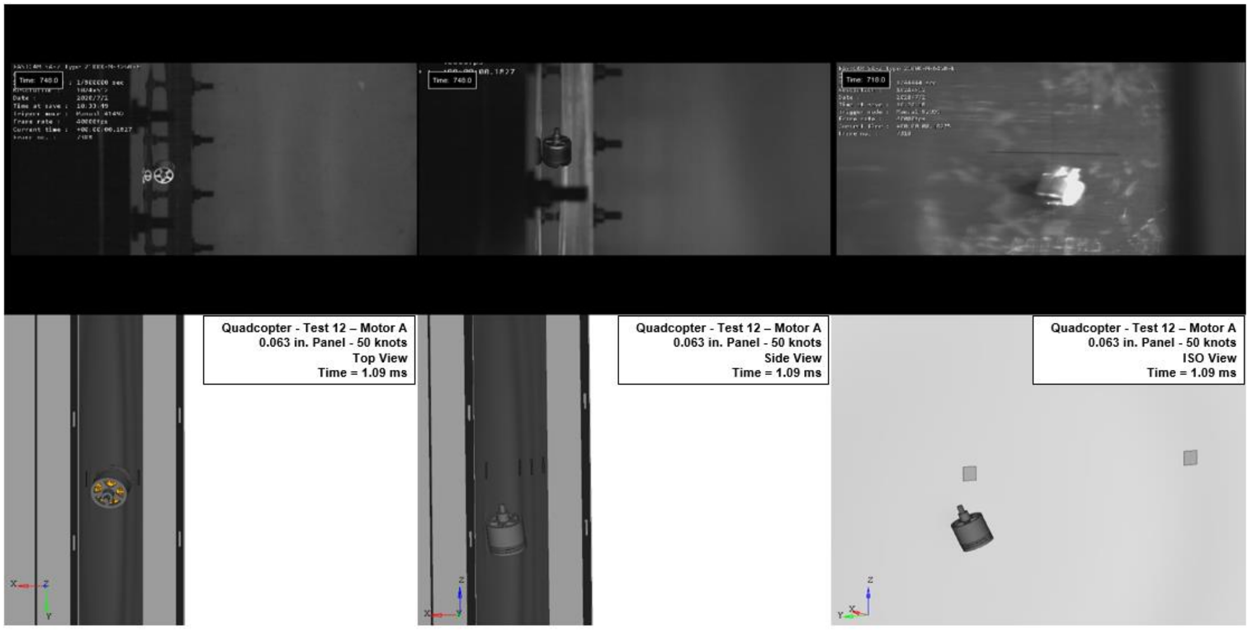


Figure 278 Comparison for motor A impact on 0.063" aluminum panel at 29.32 m/s (57.0 knots) at t = 1.09 ms (end of contact).

Figure 279 compares the simulation and test Y (horizontal) and Z (vertical) direction in-plane deformations and the out-of-plane displacements with a maximum displacement of the aluminum panel.

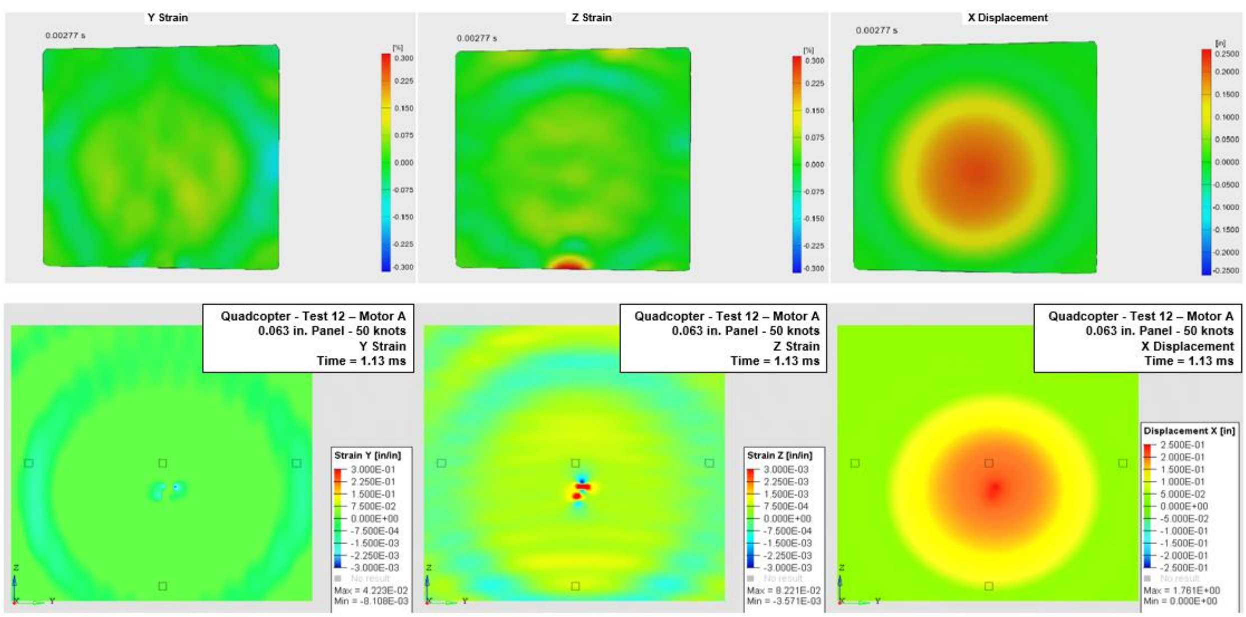


Figure 279. Comparison of test and simulation strains and displacements for motor A impact on 0.063" aluminum panel at 29.32 m/s (57.0 knots) at t = 1.13 ms (maximum displacement).

Figure 280 shows the out-of-plane displacement of the panel during the impact event obtained from the DIC data, and the simulation tracked displacements. The values on the vertical axis are not shown for confidential reasons.

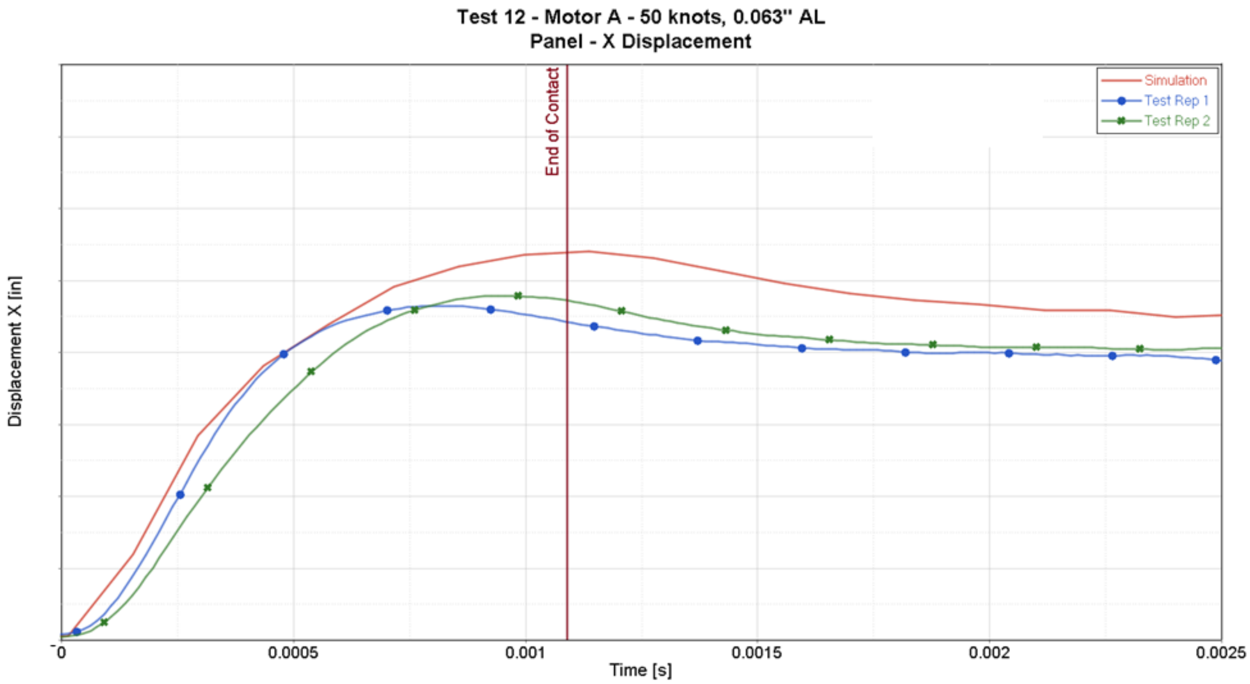


Figure 280. Comparison of the test and simulation out-of-plane displacements for motor A impact on 0.063" aluminum panel at 29.32 m/s (57.0 knots).

The physical panel was scanned after the test to compare the dimensions of the damaged area. Figure 281 compares the panel's damaged area dimensions for the test and simulation. Again, there is good agreement between the physical test and the predicted panel's damaged area.

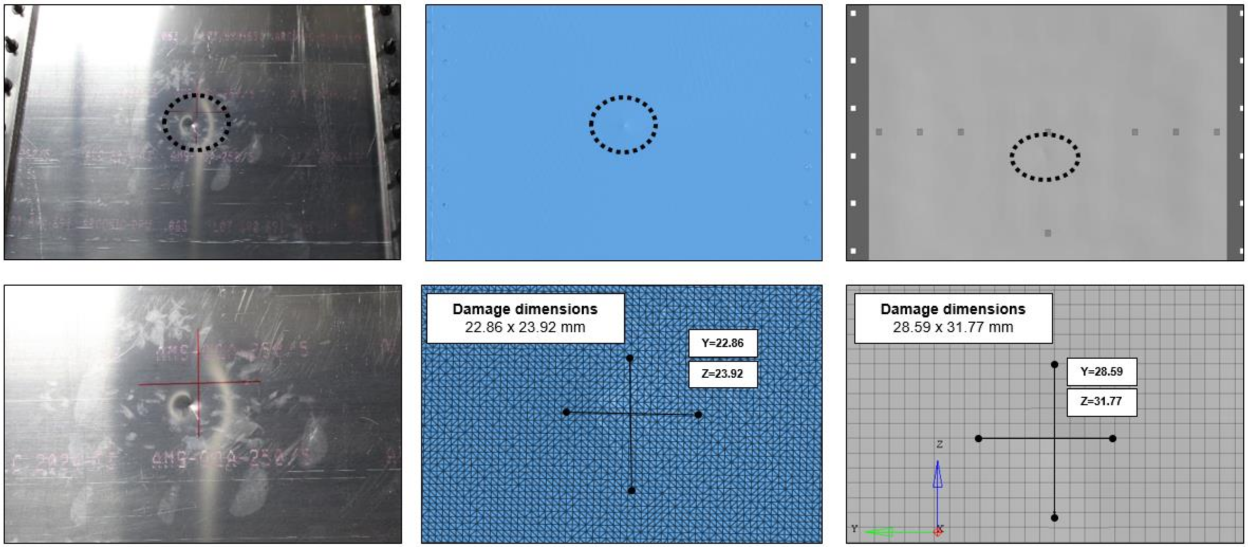


Figure 281. Comparison of the final damage of the panel for the test (left), scan (middle), and simulation (right) for motor A impact on 0.063” aluminum panel at 29.32 m/s (57.0 knots).

Figure 282 compares the physical and simulation projectile damage. For both physical tests and simulation, the motor sustained minor damage.

Figure 282. Comparison of the test (left) and simulation (right) projectile damage for motor A impact on 0.063” aluminum panel at 29.32 m/s (57.0 knots).

Figure 283 compares the load-time history of both test repetitions and the simulation load output. All the curves were filtered with a low-pass filter of 15,000 Hz. The load data shows good repeatability for test and simulation and confirms the good correlation of the FEM up to the end of the contact, which is marked with an asymptote. However, there are some deviations between the test and simulation loads after the contact ends. Figure 284 compares the strain data collected at both repetitions to the simulation strains. The values on the vertical axis are not shown for confidential reasons.

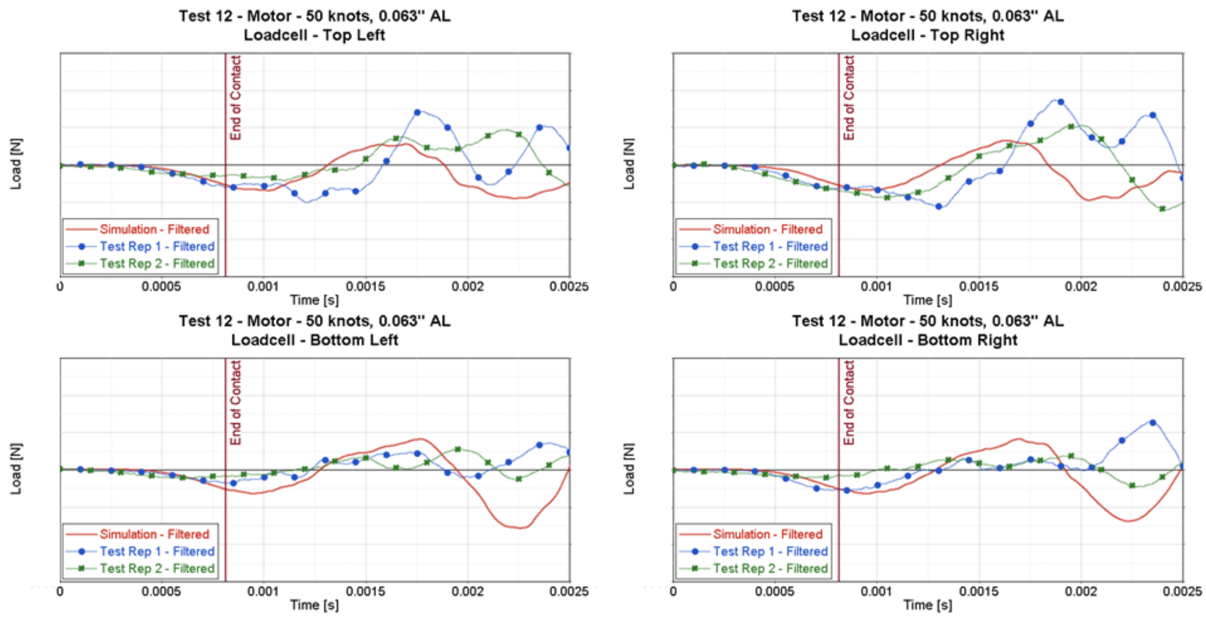


Figure 283. Load cell history data validation for motor A impact on 0.063” aluminum panel at 29.32 m/s (57.0 knots).

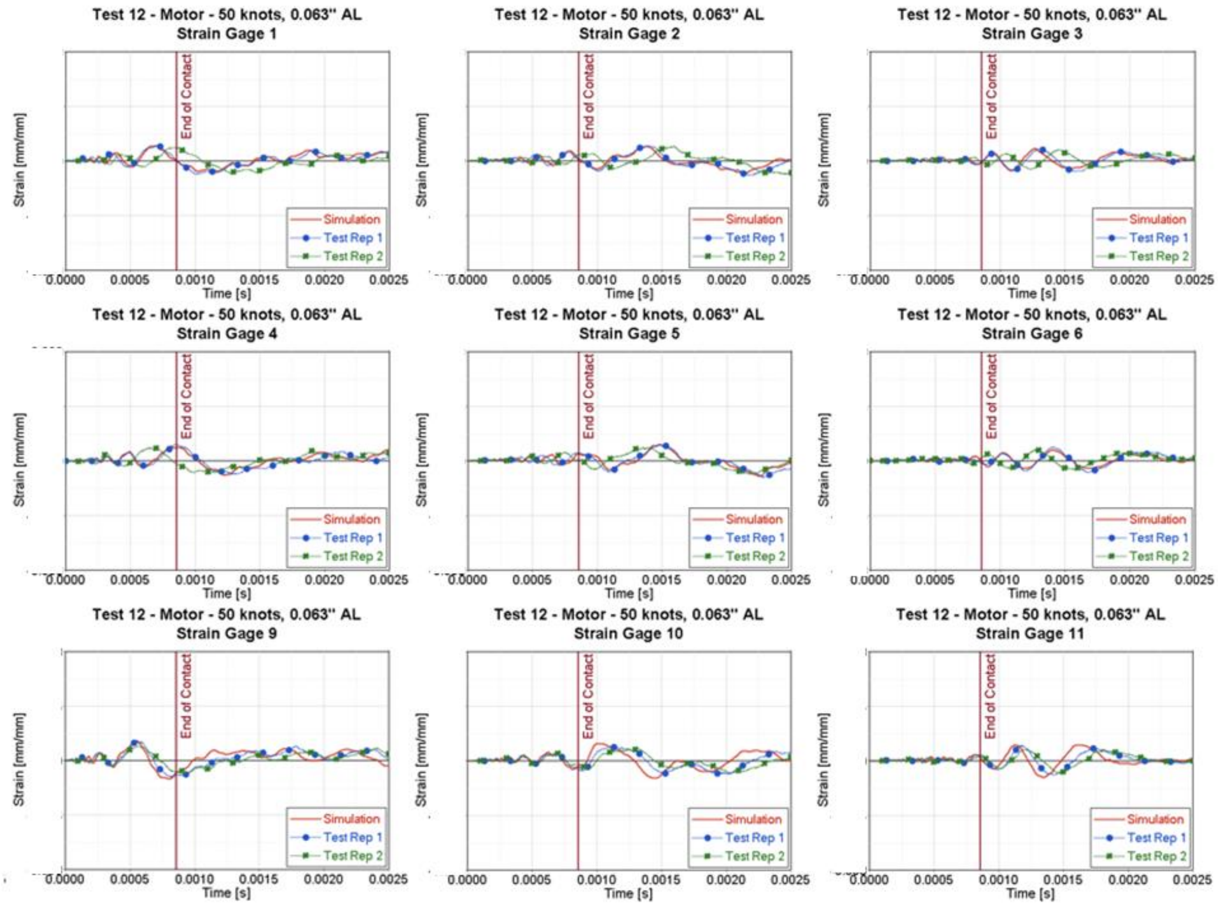


Figure 284. Strain comparison of strain gages 1-6 and 9-11 for motor A impact on 0.063" aluminum panel at 29.32 m/s (57.0 knots).

## A.13 TEST 13 – CAMERA AT 120 KNOTS – 1.6 MM AL PANEL

Test 13 consists of the impact of the quadcopter camera with the 1.6 mm (0.063") aluminum panel at a nominal velocity of 61.7 m/s (120 knots). Two iterations were carried out with the same test conditions but replaced the thin panel from test to test. Repetition 2 had the least deviation from the nominal conditions.

An initial velocity of 63.28 m/s (123.0 knots) was applied to the camera FEM, corresponding to the velocity recorded for repetition 2 in the test documentation (APPENDIX B).

Figure 285 through Figure 288 show the comparison of the kinematics between the test and simulation at four different instances of the impact event.

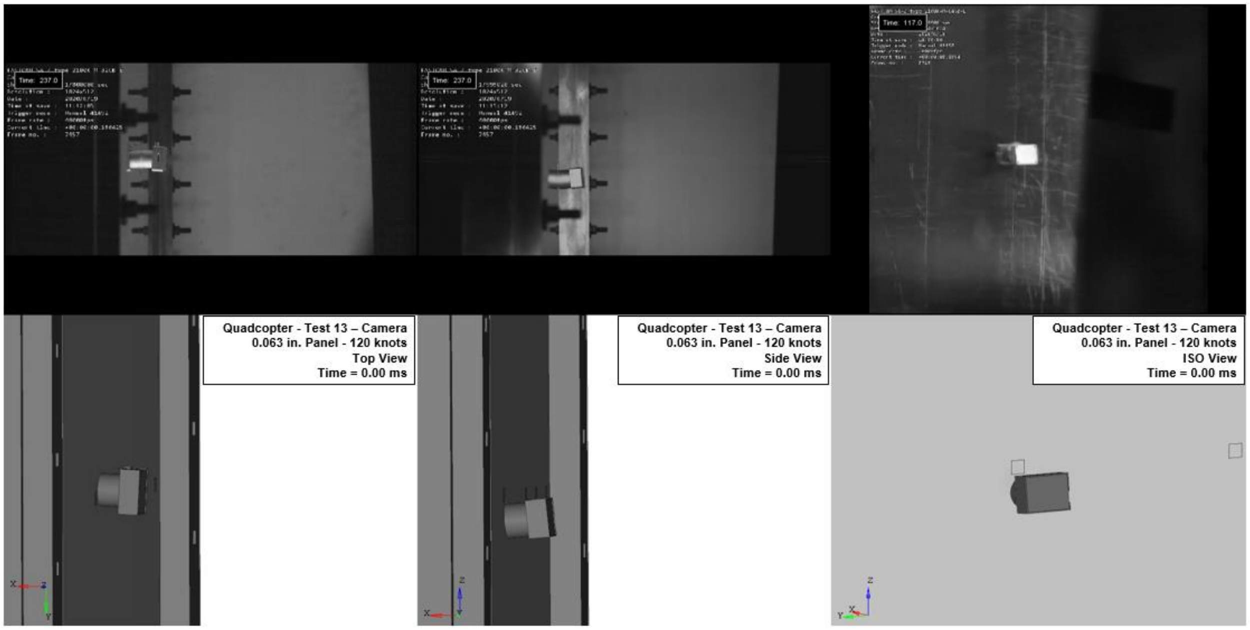


Figure 285. Comparison for camera impact on 0.063" aluminum panel at 63.28 m/s (123.0 knots) at t = 0.00 ms (beginning of contact).

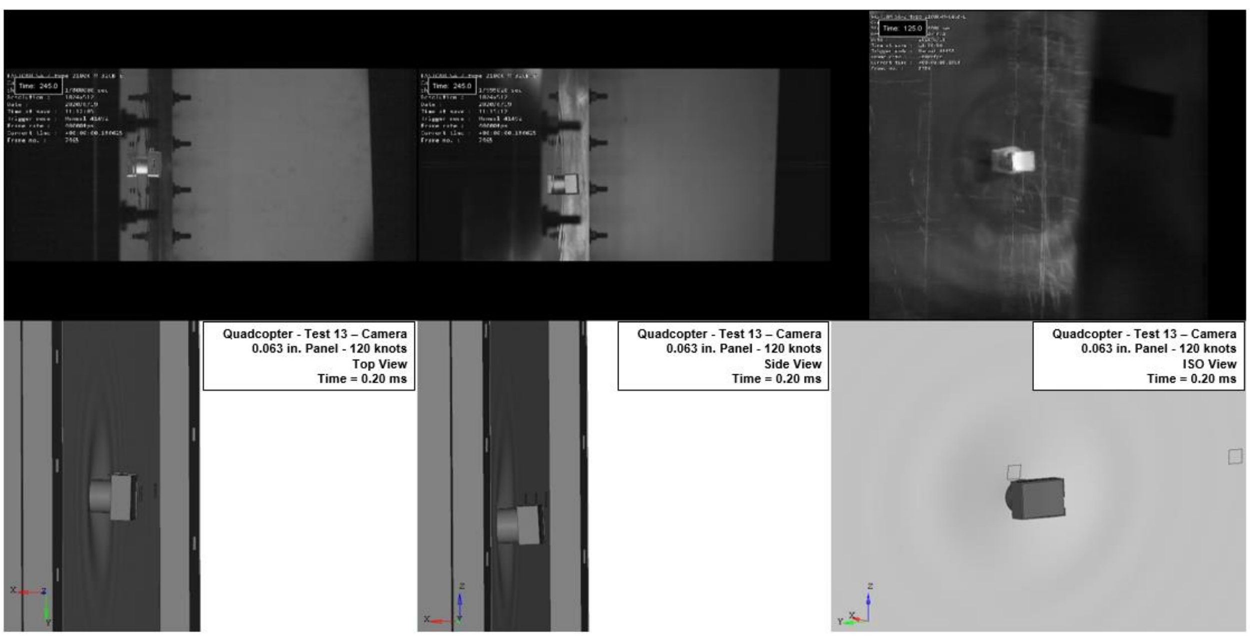


Figure 286. Comparison for camera impact on 0.063" aluminum panel at 63.28 m/s (123.0 knots) at t = 0.20 ms.

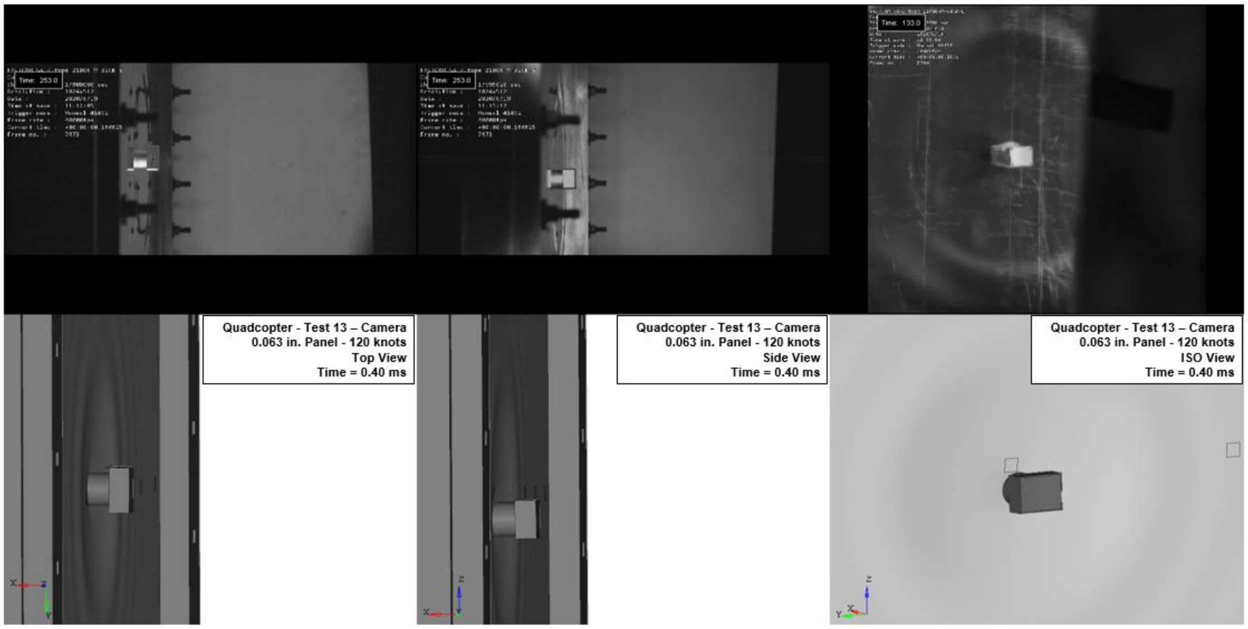


Figure 287 Comparison for camera impact on 0.063” aluminum panel at 63.28 m/s (123.0 knots) at t = 0.40 ms.

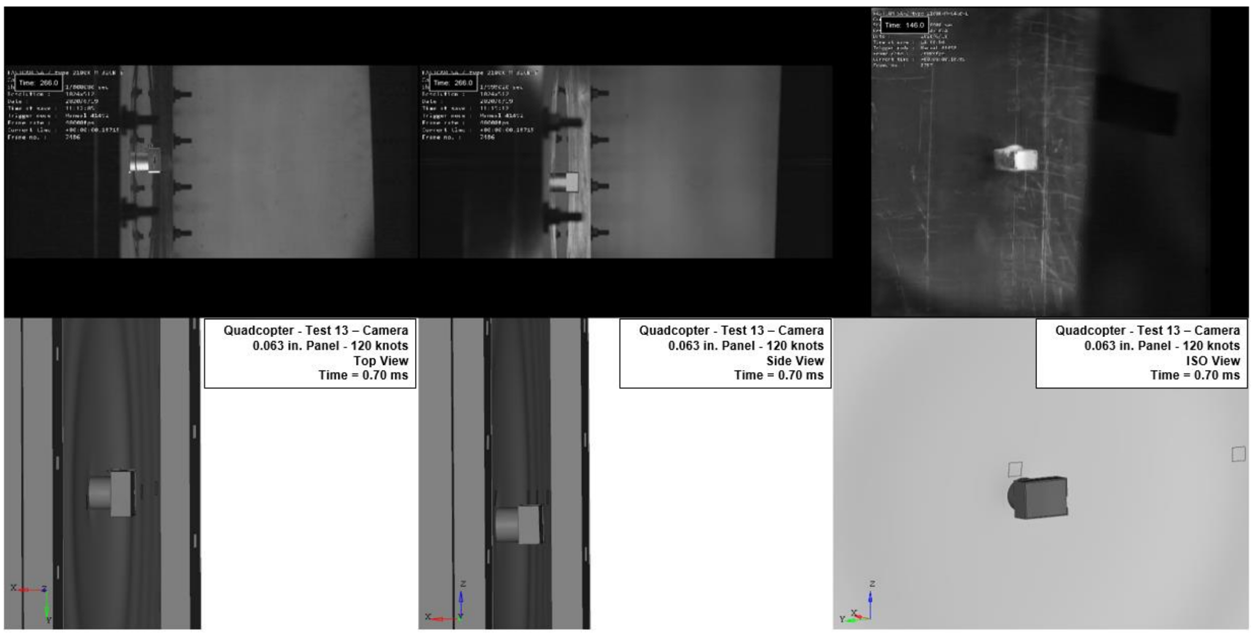


Figure 288 Comparison for camera impact on 0.063” aluminum panel at 63.28 m/s (123.0 knots) at t = 0.70 ms (end of contact).

Figure 289 compares the simulation and test Y (horizontal) and Z (vertical) direction in-plane deformations and the out-of-plane displacements, for instance, with a maximum displacement of the aluminum panel. Figure 290 shows the out-of-plane displacement of the panel during the impact event obtained from the DIC data, and the simulation tracked displacements. The values on the vertical axis are not shown for confidential reasons.

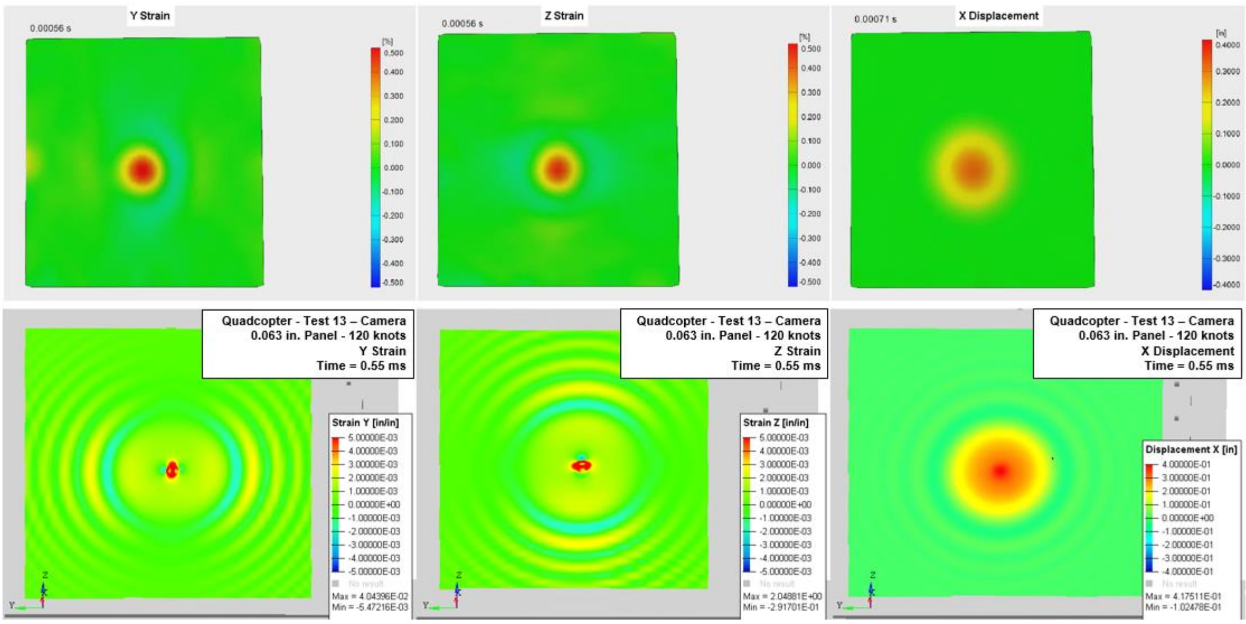


Figure 289. Comparison of test and simulation strains and displacements for camera impact on 0.063” aluminum panel at 63.28 m/s (123.0 knots) at t = 0.55 ms (maximum displacement).

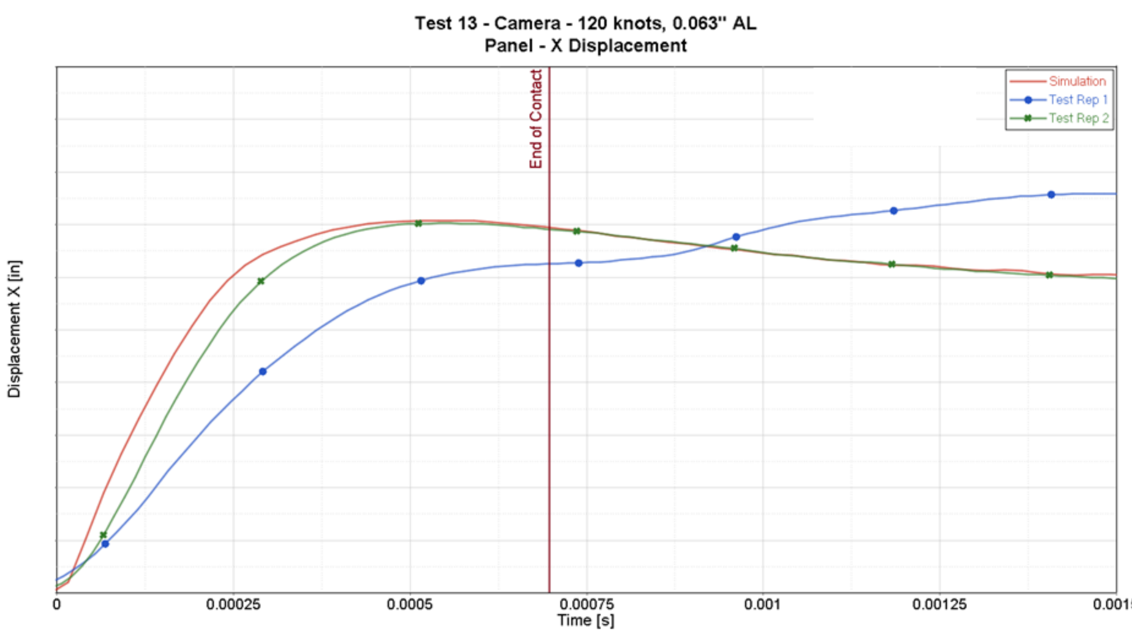


Figure 290. Comparison of the test and simulation out-of-plane displacements for camera impact on 0.063” aluminum panel at 63.28 m/s (123.0 knots).

The physical panel was scanned after the test to compare the dimensions of the damaged area. Figure 291 compares the panel's damaged area dimensions for the test and simulation. Again, there is good agreement between the physical test and the predicted panel's damaged area.

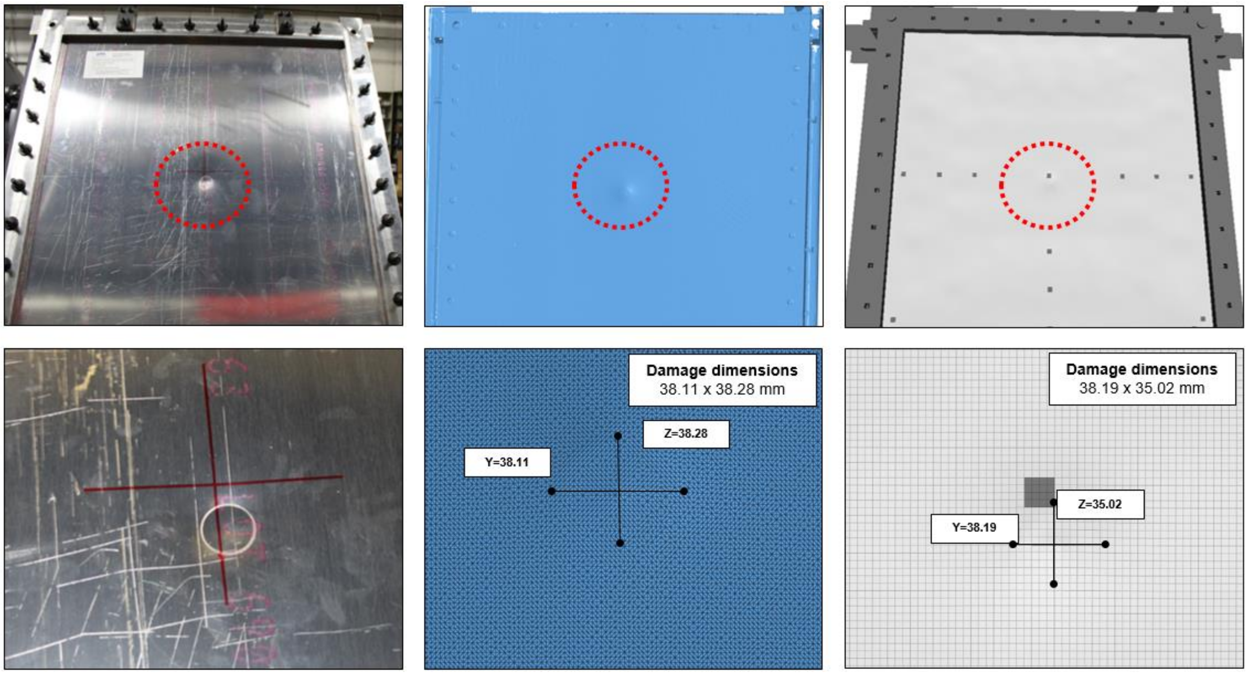


Figure 291. Comparison of the final damage of the panel for the test (left), scan (middle), and simulation (right) for camera impact on 0.063" aluminum panel at 63.28 m/s (123.0 knots).

Figure 292 compares the physical and simulation projectile damage. For both physical tests and simulation, the camera sustained minimal damage.

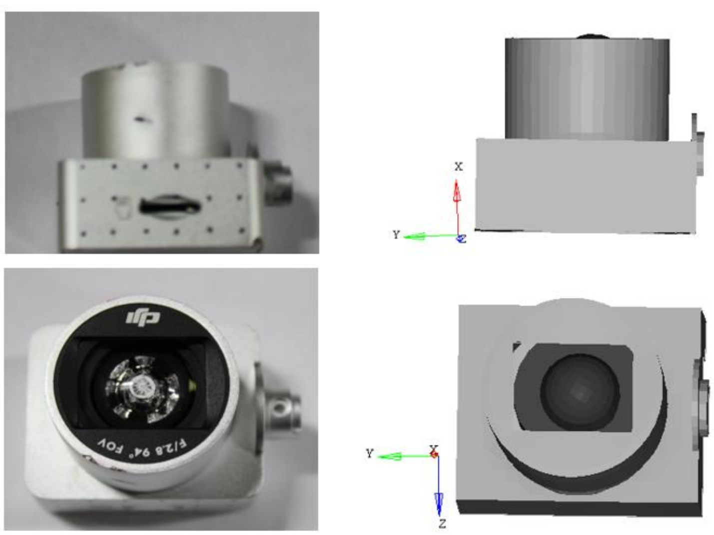


Figure 292. Comparison of the test (left) and simulation (right) projectile damage for camera impact on 0.063" aluminum panel at 63.28 m/s (123.0 knots).

Figure 293 compares the load-time history of both test repetitions and the simulation load output. All the curves were filtered with a low-pass filter of 15,000 Hz. The load data shows good repeatability for tests and simulation and confirms the good correlation of the FEM. Figure 294 compares the strain data collected at both test iterations to the simulation strains. The values on the vertical axis are not shown for confidential reasons.

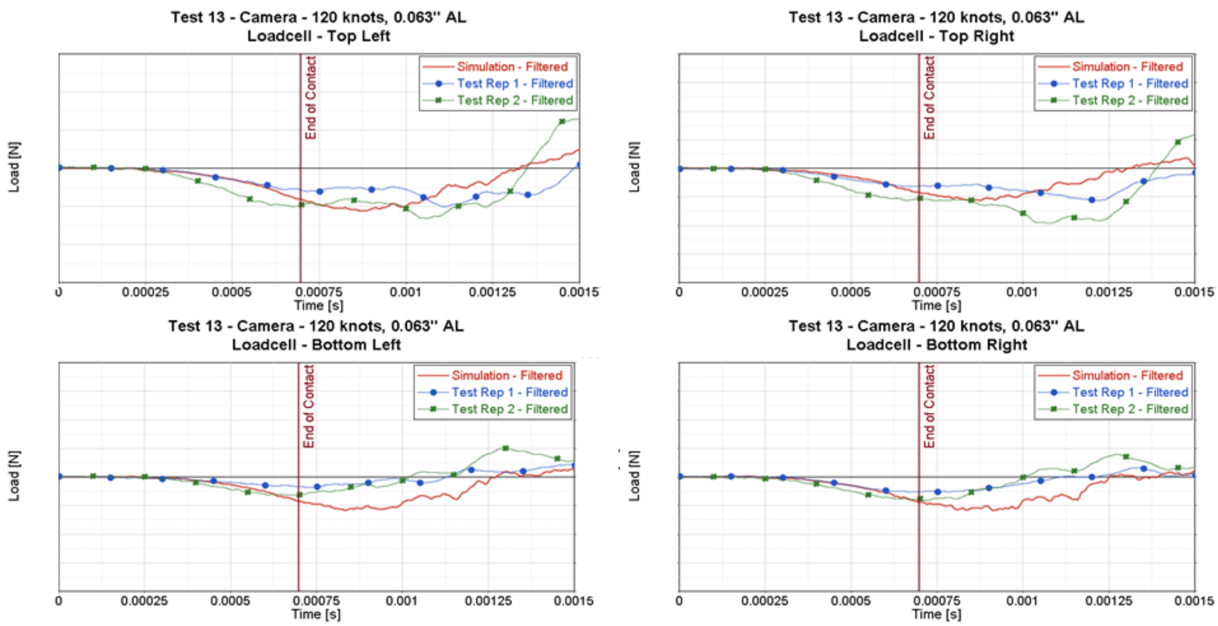


Figure 293. Load cell history data validation for camera impact on 0.063” aluminum panel at 63.28 m/s (123.0 knots).

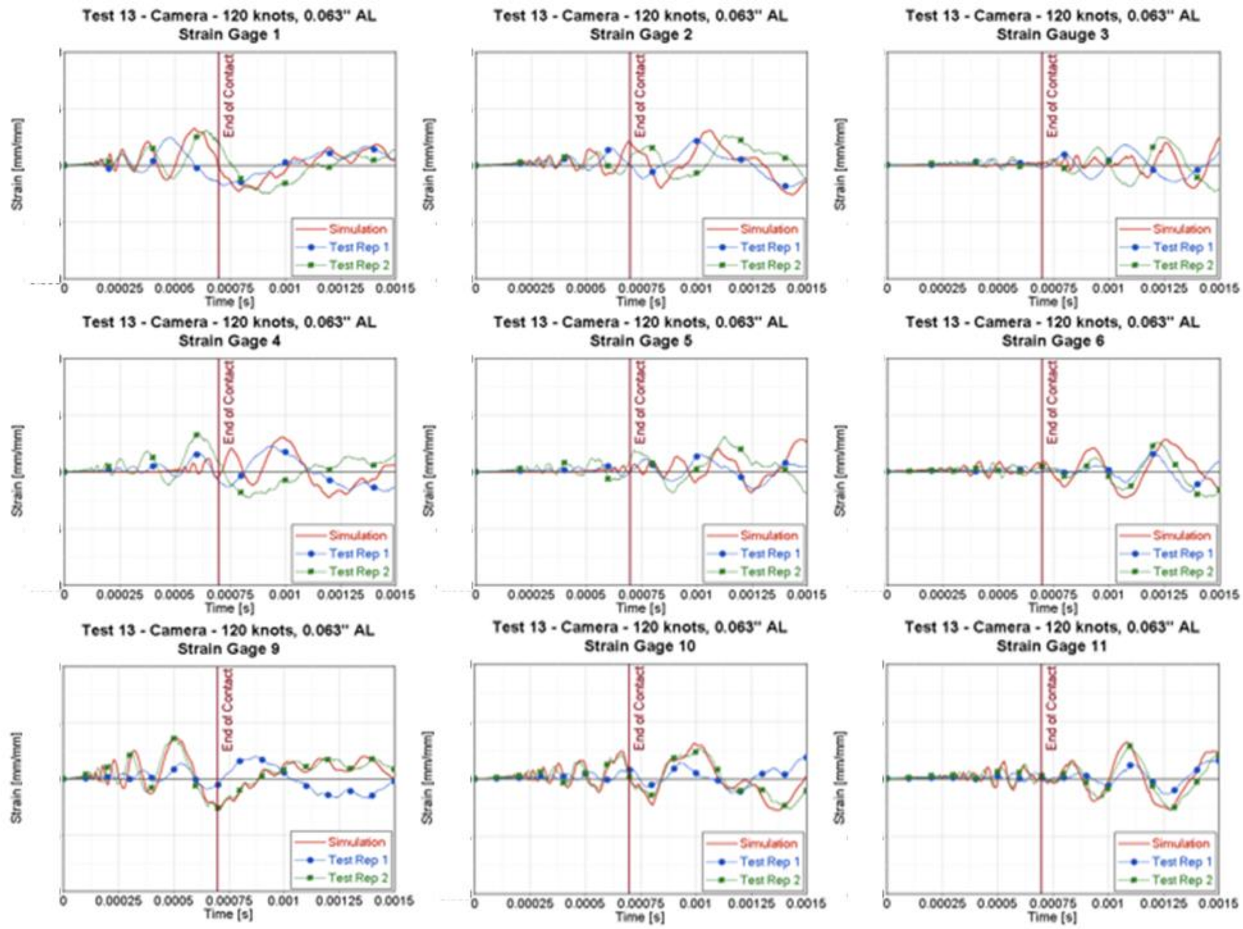


Figure 294. Strain comparison of strain gages 1-6 and 9-11 for camera impact on 0.063” aluminum panel at 63.28 m/s (123.0 knots).

## A.14 TEST 14 – CAMERA AT 50 KNOTS – 1.6 MM AL PANEL

Test 14 consists of the impact of the quadcopter camera with the 1.6 mm (0.063″) aluminum panel at a nominal velocity of 25.7 m/s (50 knots). Two iterations were carried out to evaluate data repeatability. For kinematics comparison, NIAR has identified iteration 1 as the repetition with the least deviation regarding the nominal test requirements.

An initial velocity of 27.27 m/s (53.0 knots) was applied to the camera FEM, corresponding to the velocity recorded for repetition 2 in the test documentation (APPENDIX B).

Figure 295 through Figure 298 show the comparison of the kinematics between the test and simulation at four different instances of the impact event.

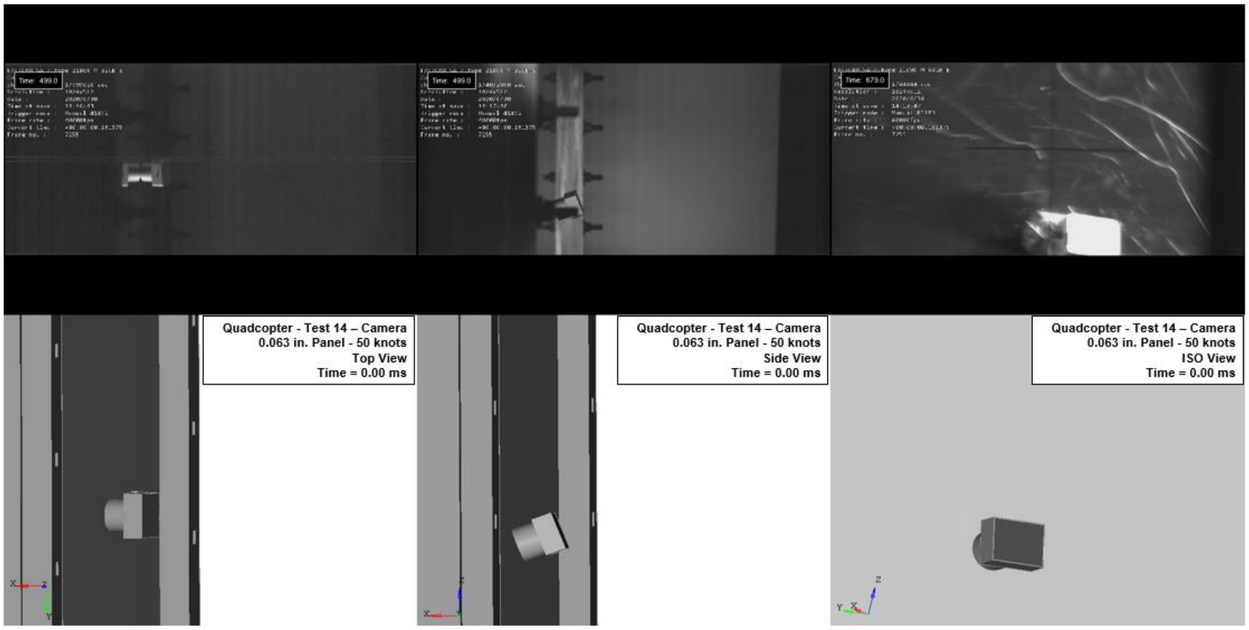


Figure 295. Comparison for camera impact on 0.063" aluminum panel at 27.27 m/s (53.0 knots) at t = 0.00 ms (beginning of contact).

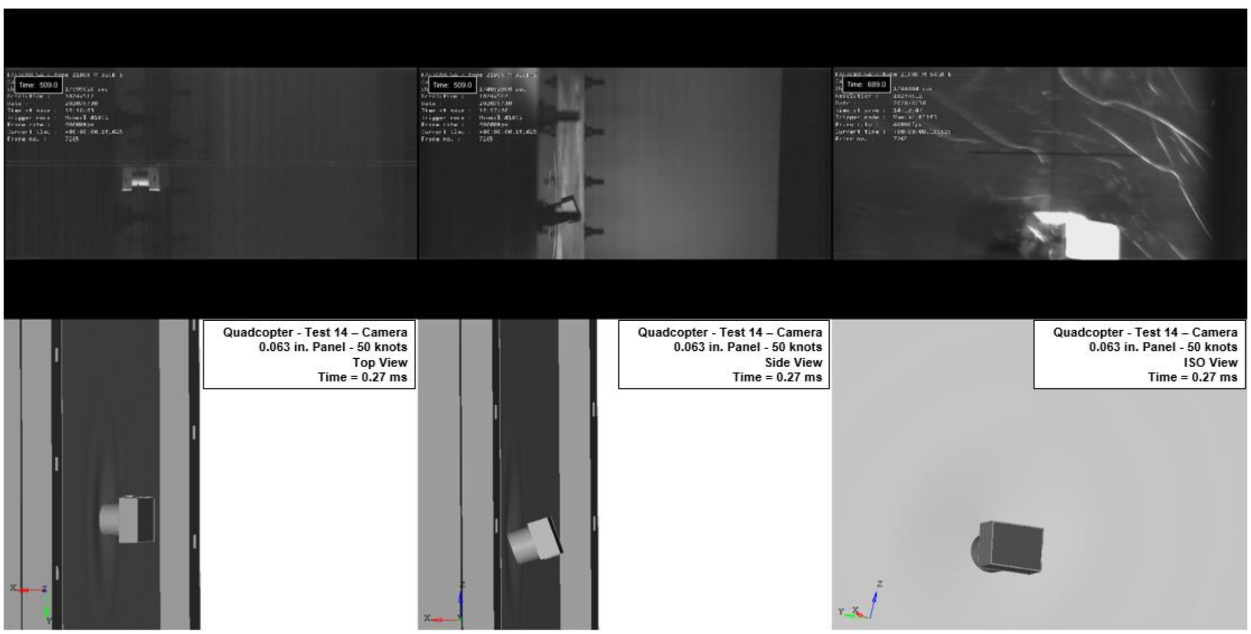


Figure 296. Comparison for camera impact on 0.063" aluminum panel at 27.27 m/s (53.0 knots) at t = 0.27 ms.

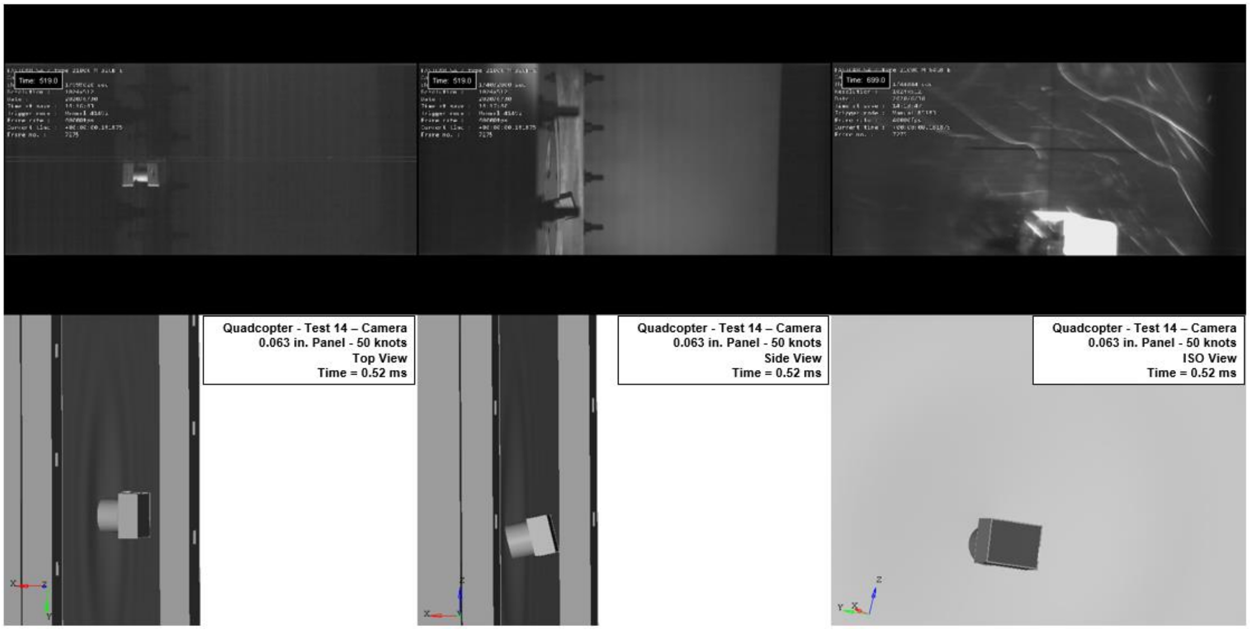


Figure 297 Comparison for camera impact on 0.063” aluminum panel at 27.27 m/s (53.0 knots) at t = 0.52 ms.

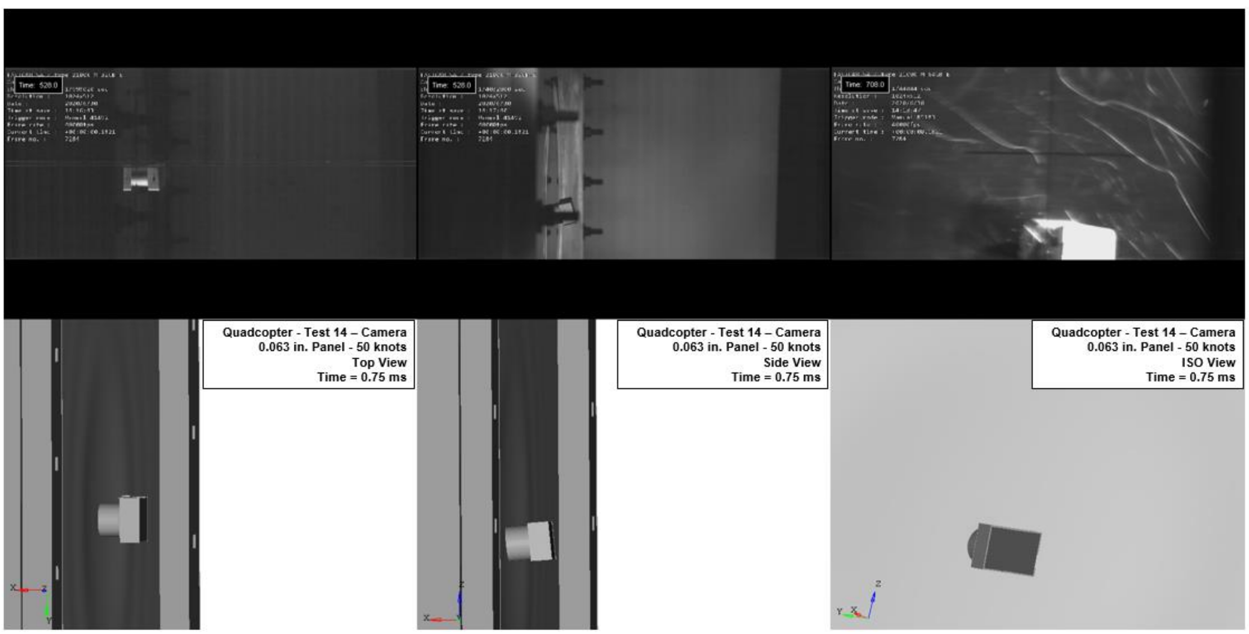


Figure 298 Comparison for camera impact on 0.063” aluminum panel at 27.27 m/s (53.0 knots) at t = 0.75 ms (end of contact).

Figure 299 compares the simulation and test Y (horizontal) and Z (vertical) direction in-plane deformations and the out-of-plane displacements, for instance, with a maximum displacement of the aluminum panel.

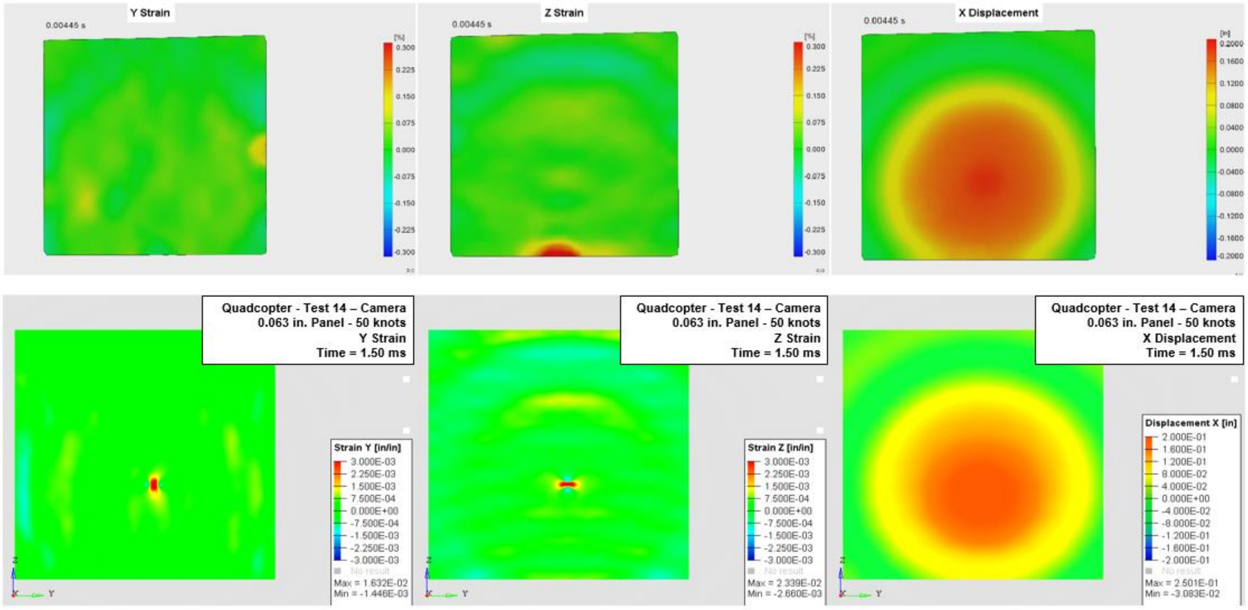


Figure 299. Comparison of test and simulation strains and displacements for camera impact on 0.063” aluminum panel at 27.27 m/s (53.0 knots) at t = 1.50 ms (maximum displacement).

Figure 300 shows the out-of-plane displacement of the panel during the impact event obtained from the DIC data, and the simulation tracked displacements. The values on the vertical axis are not shown for confidential reasons.

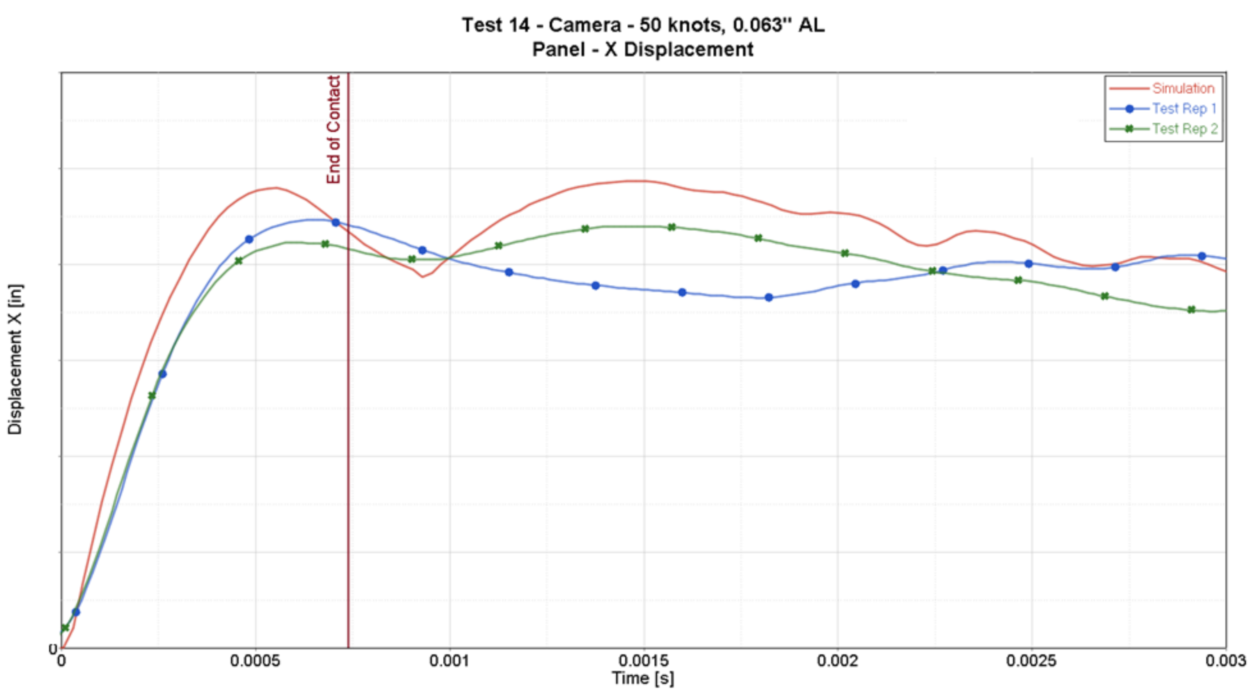


Figure 300. Comparison of the test and simulation out-of-plane displacements for camera impact on 0.063” aluminum panel at 27.27 m/s (53.0 knots).

The physical panel was scanned after the test to compare the dimensions of the damaged area. Figure 301 compares the panel's damaged area dimensions for the test and simulation. There is good agreement between the physical test and the predicted panel's damaged area. Figure 302 compares the physical and simulation projectile damage. For both physical tests and simulation, the camera sustained minor damage.

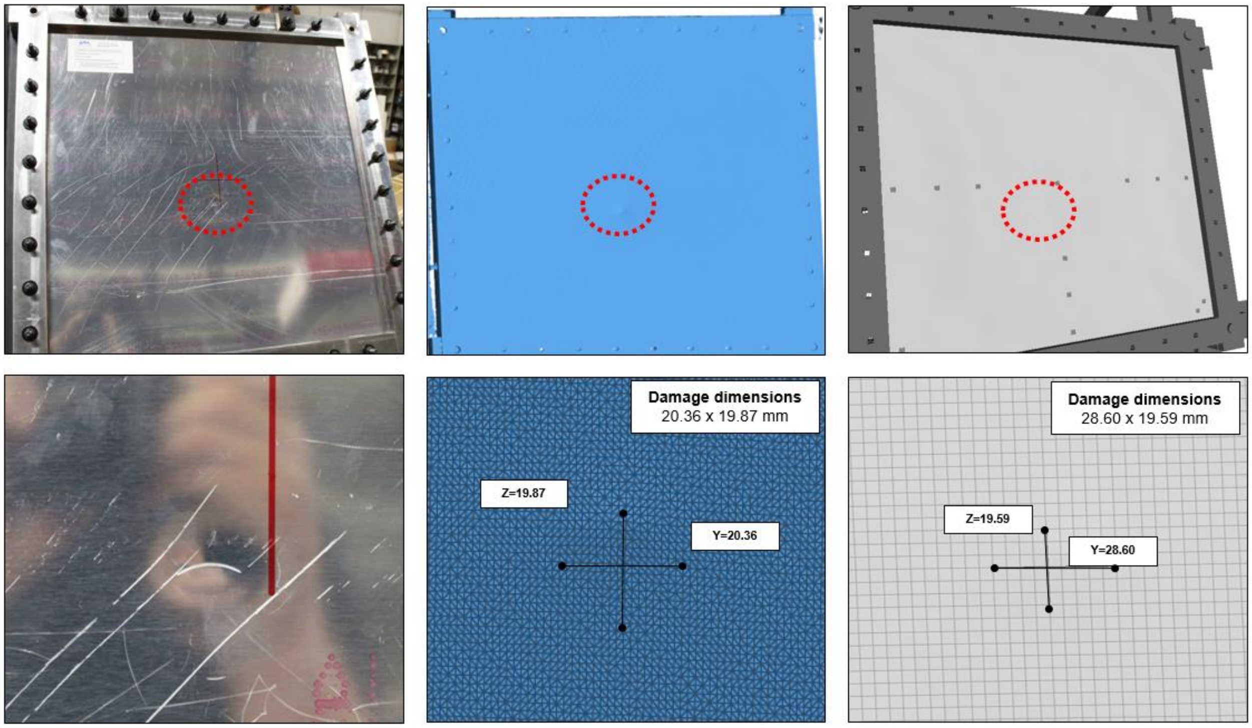


Figure 301. Comparison of the final damage of the panel for the test (left), scan (middle), and simulation (right) for camera impact on 0.063" aluminum panel at 27.27 m/s (53.0 knots).

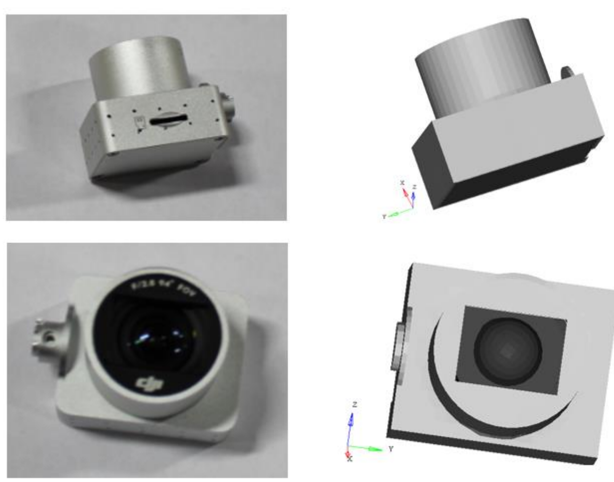

Figure 302. Comparison of the test (left) and simulation (right) projectile damage for camera impact on 0.063" aluminum panel at 27.27 m/s (53.0 knots).

Figure 303 compares the load-time history of both test repetitions and the simulation load output. All the curves were filtered with a low-pass filter of 15,000 Hz. The load data shows good repeatability for test and simulation and confirms the good correlation up to the end of the contact, marked with an asymptote. However, the post-impact oscillations of the panel deviate from those of the physical test. Figure 304 compares the strain data collected at both test iterations to the simulation strains. The values on the vertical axis are not shown for confidential reasons.

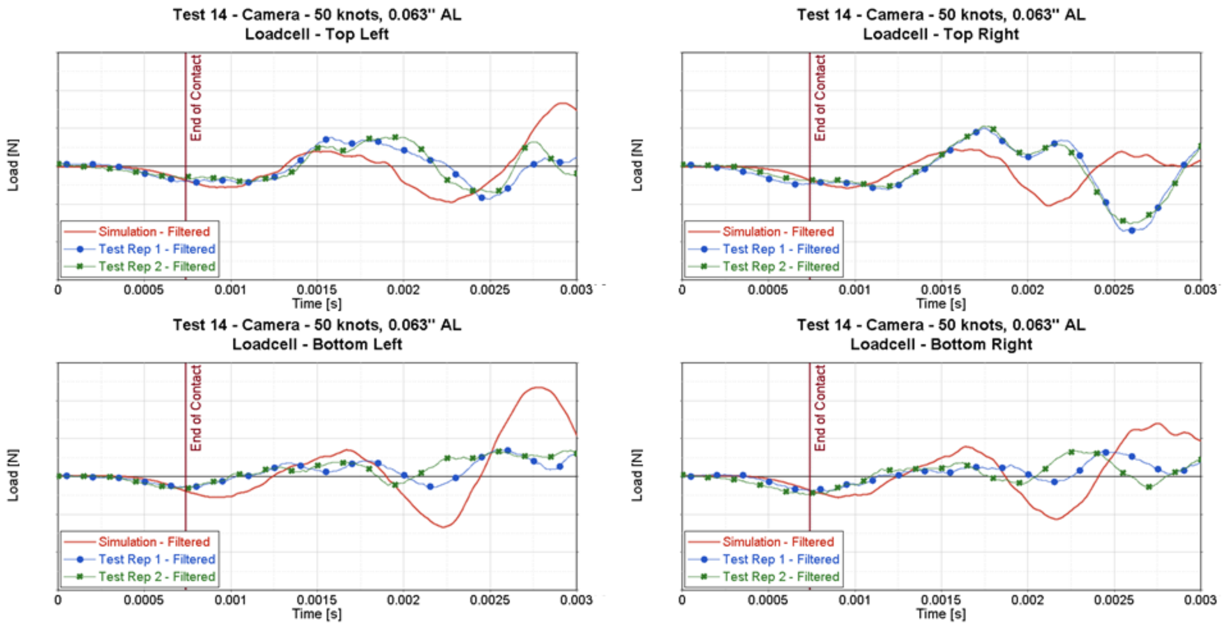


Figure 303. Load cell history data validation for camera impact on 0.063” aluminum panel at 27.27 m/s (53.0 knots).

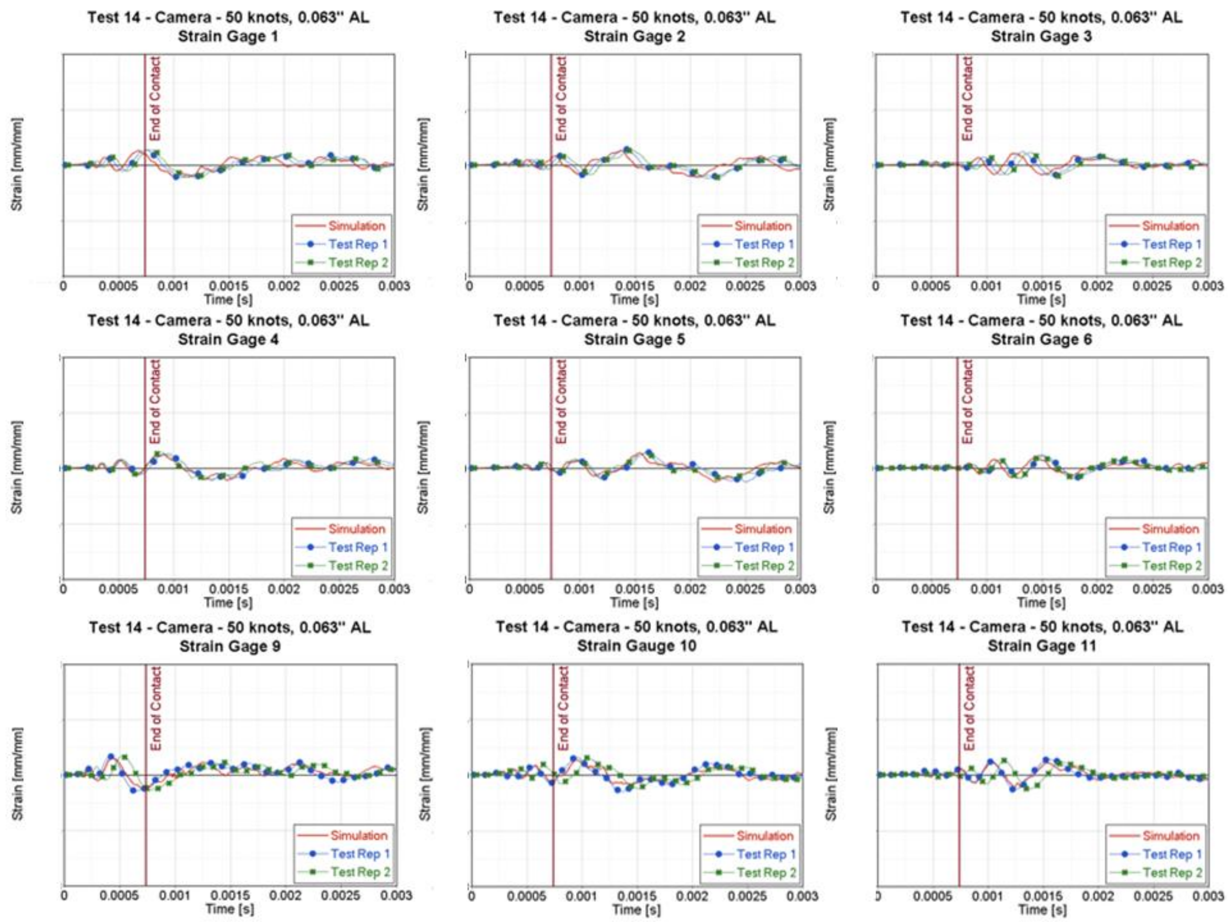


Figure 304. Strain comparison of strain gages 1-6 and 9-11 for camera impact on 0.063” aluminum panel at 27.27 m/s (53.0 knots).

## A.15 TEST 15 – BATTERY AT 500 KNOTS – SHARP EDGE

Test 15 consists of the impact of the fixed-wing battery B with the sharp aluminum edge at a nominal velocity of 257.2 m/s (500 knots). Two iterations were carried out to evaluate data repeatability. For kinematics comparison, NIAR has identified iteration 2 as the repetition with the least deviation regarding the nominal test requirements. All batteries were fully charged previous to the test.

An initial velocity of 256.64 m/s (498.87 knots) was applied to the battery A FEM, which corresponds to the velocity recorded for repetition 2 in the test documentation (APPENDIX B).

Figure 305 through Figure 308 show the comparison of the kinematics between the test and simulation at four different instances of the impact event.

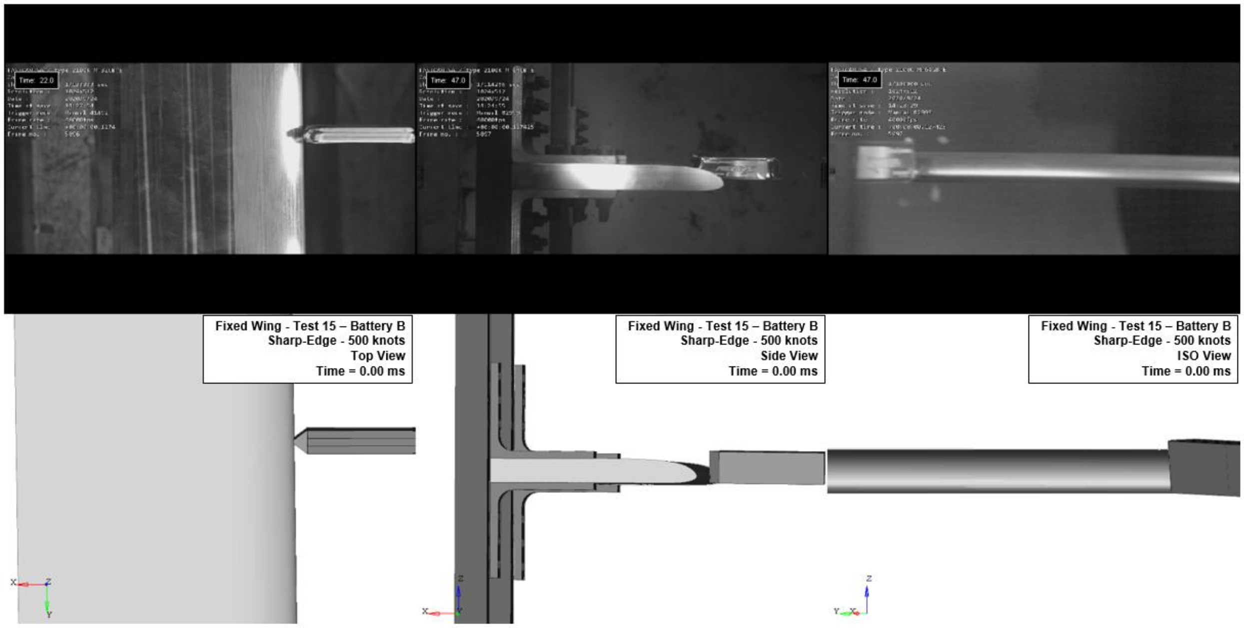


Figure 305. Comparison for battery B impact on sharp edge at 256.64 m/s (498.87 knots) at t = 0.00 ms (beginning of contact).

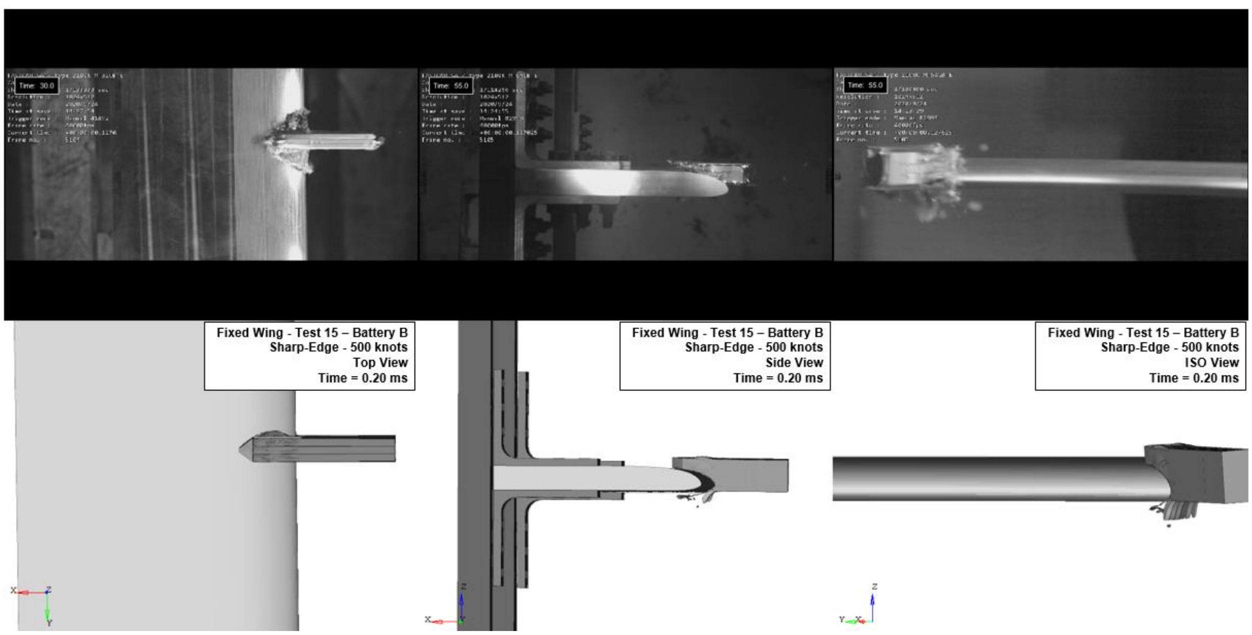


Figure 306. Comparison for battery B impact on sharp edge at 256.64 m/s (498.87 knots) at t = 0.20 ms.

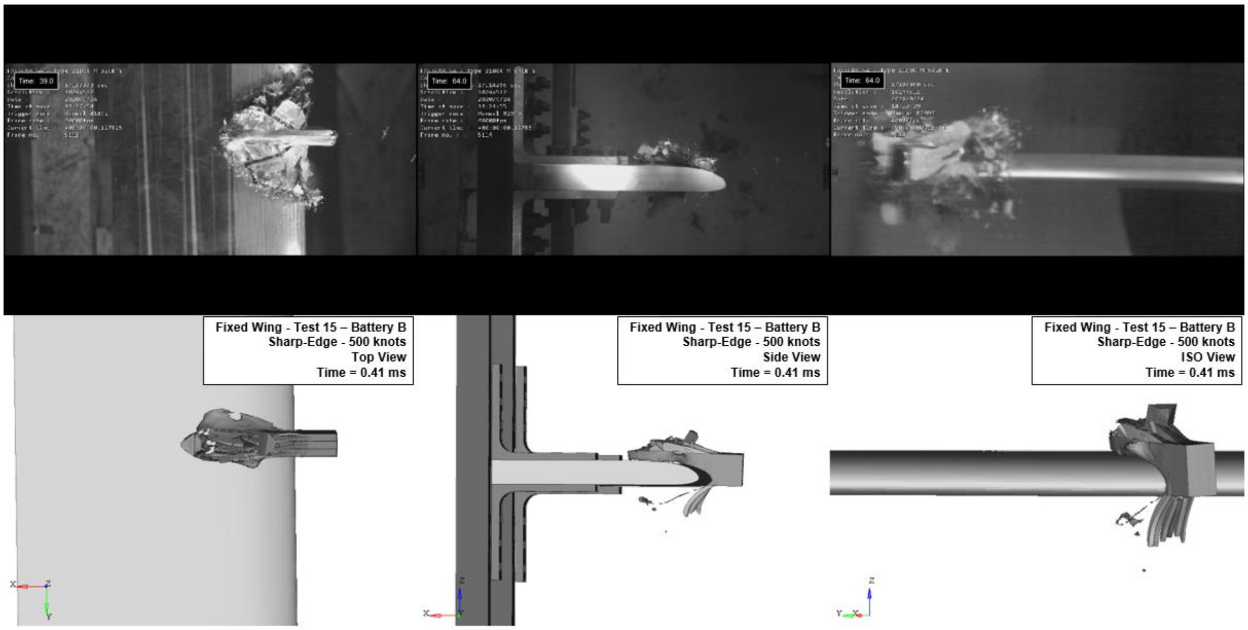


Figure 307 Comparison for battery B impact on sharp edge at 256.64 m/s (498.87 knots) at t = 0.41 ms.

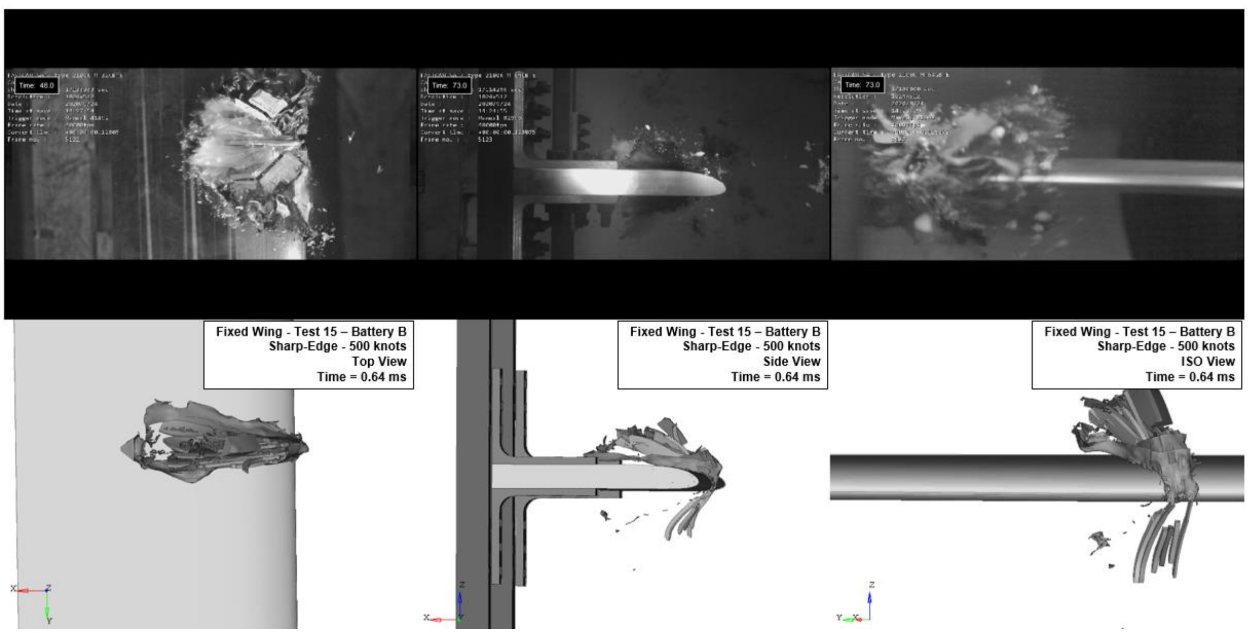


Figure 308 Comparison for battery B impact on sharp edge at 256.64 m/s (498.87 knots) at t = 0.64 ms (end of contact).

Figure 309 compares the load-time history of both test repetitions and the simulation load output. All the curves were filtered with a low-pass filter of 15,000 Hz. The top-load cells were not considered for the comparison due to out-of-normal readings during the test. This is indicated as non-available (N/A) in Figure 309. Nevertheless, the load data shows good repeatability for tests and simulation and confirms the good correlation of the FEM. The values on the vertical axis are not shown for confidential reasons.

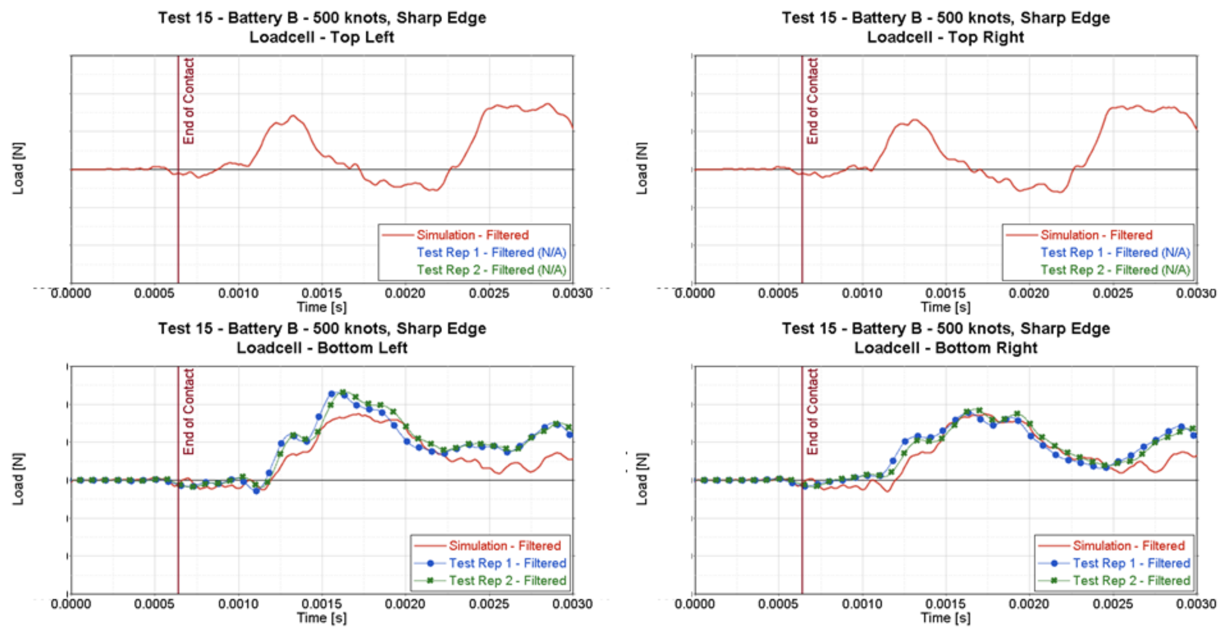


Figure 309. Load cell history data validation for battery B with a sharp edge at 256.64m/s (498.87 knots).

## A.16 TEST 16 – BATTERY AT 500 KNOTS – 1.6 MM AL PANEL

Test 16 consists of the impact of the battery B with the 1.6 mm (0.063″) aluminum panel at a nominal velocity of 257.2 m/s (500 knots). Two iterations were carried out to evaluate data repeatability. For kinematics comparison, NIAR has identified iteration 2 as the repetition with the least deviation regarding the nominal test requirements. All batteries were fully charged previous to the test.

An initial velocity of 256.94 m/s (499.46 knots) was applied to the battery A FEM, which corresponds to the velocity recorded for repetition 2 in the test documentation (APPENDIX B).

Figure 310 through Figure 313 show the comparison of the kinematics between the test and simulation at four different instances of the impact event.

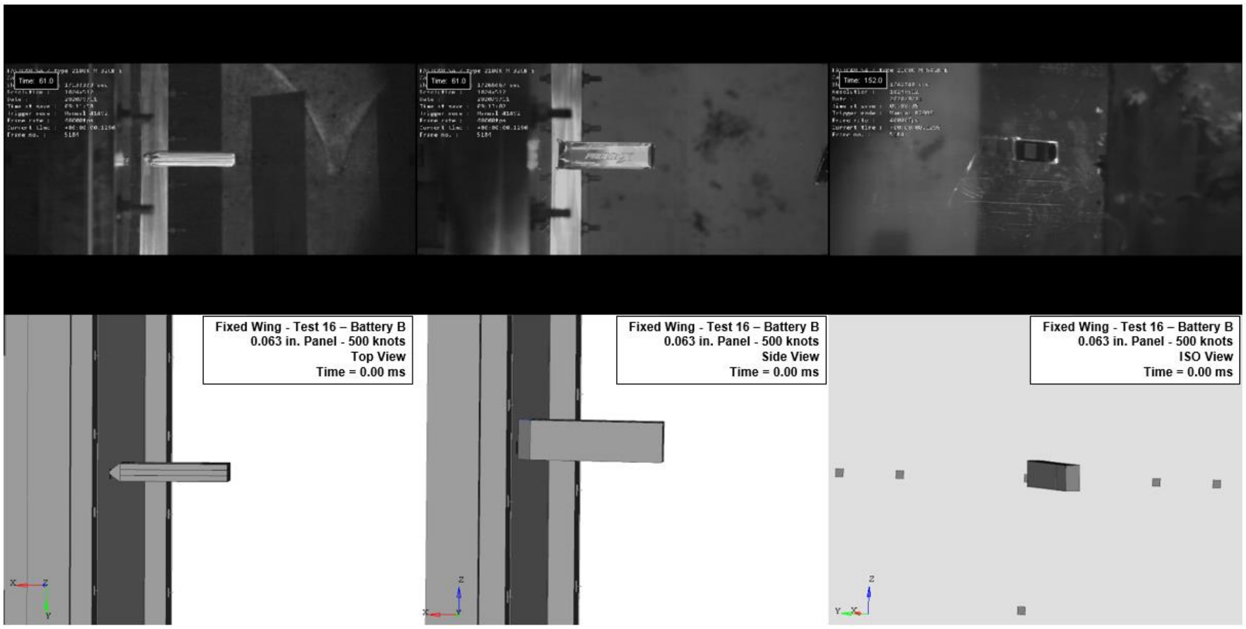


Figure 310. Comparison for battery B impact on 0.063” aluminum panel at 256.94 m/s (499.46 knots) at t = 0.00 ms (beginning of contact).

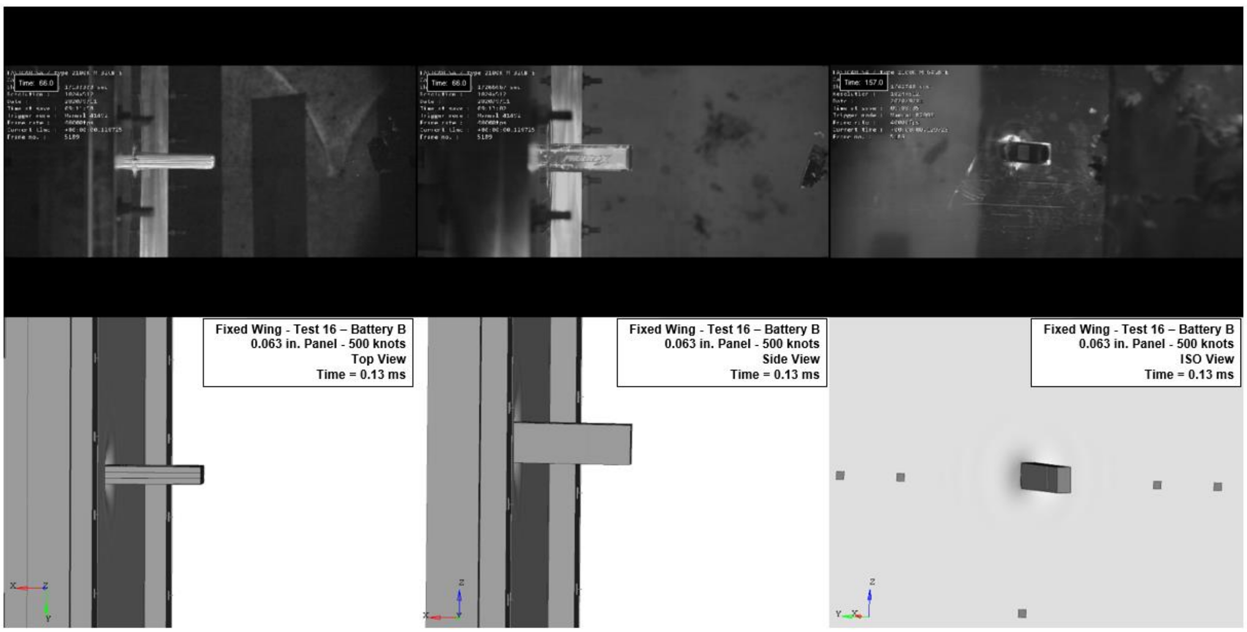


Figure 311. Comparison for battery B impact on 0.063” aluminum panel at 256.94 m/s (499.46 knots) at t = 0.13 ms (panel failure).

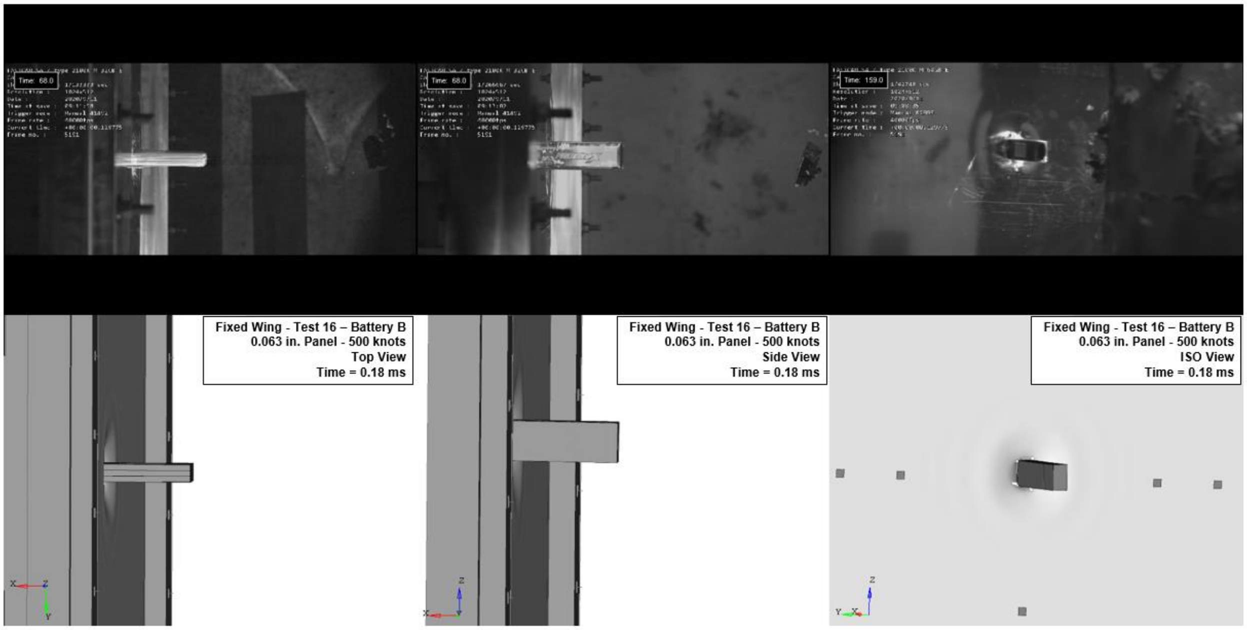


Figure 312 Comparison for battery B impact on 0.063” aluminum panel at 256.94 m/s (499.46 knots) at t = 0.18 ms.

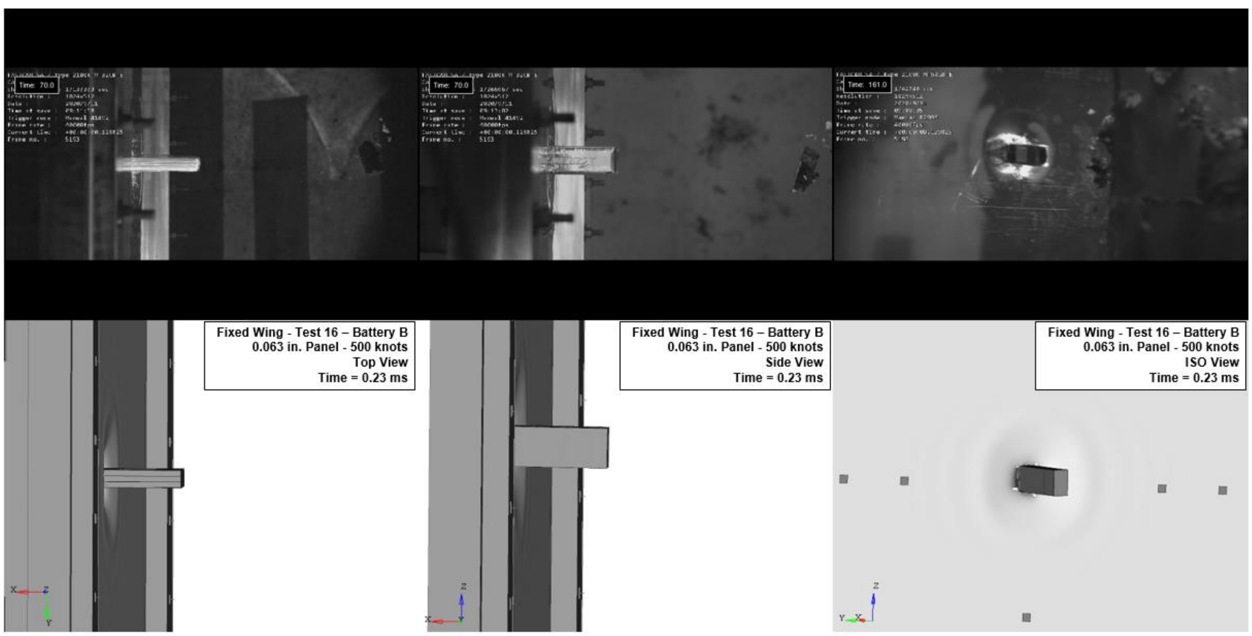


Figure 313 Comparison for battery B impact on 0.063” aluminum panel at 256.94 m/s (499.46 knots) at t = 0.23 ms (end of contact).

Figure 314 compares the test and simulation contour plots for the Y (horizontal) and Z (vertical) in-plane strains and out-of-plane displacements, for instance, with maximum deflection.

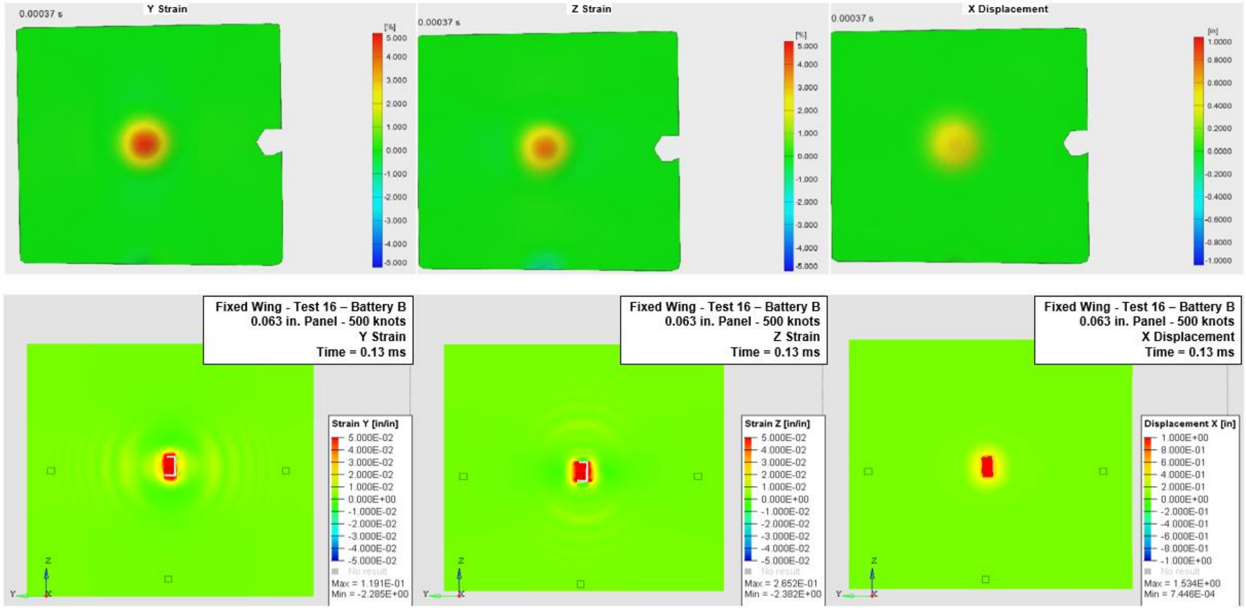


Figure 314. Comparison of test and simulation strains and displacements for battery B impact on 0.063” aluminum panel at 256.94 m/s (499.46 knots) at t = 0.13 ms (maximum displacement).

Figure 315 shows the out-of-plane displacement of the panel over the test period obtained from the DIC data, and the simulation tracked displacements. The values on the vertical axis are not shown for confidential reasons.

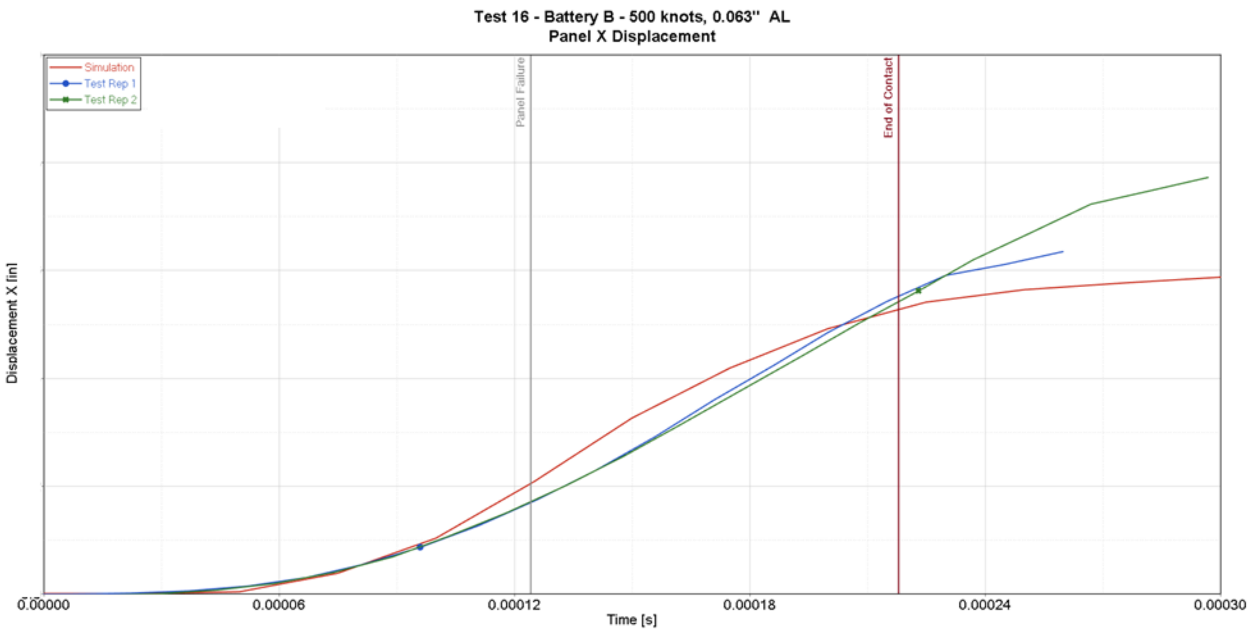


Figure 315. Comparison of the test and simulation out-of-plane displacements for battery B impact on 0.063” aluminum panel at 256.94 m/s (499.46 knots).

The physical panel was scanned after the test to compare the dimensions of the damaged area. Figure 316 compares the panel's damaged area dimensions for the test and simulation. The hole predicted by the simulation shows smaller height and width dimensions. This is due to the eroding nature of the material failure defined in the panel FEM.

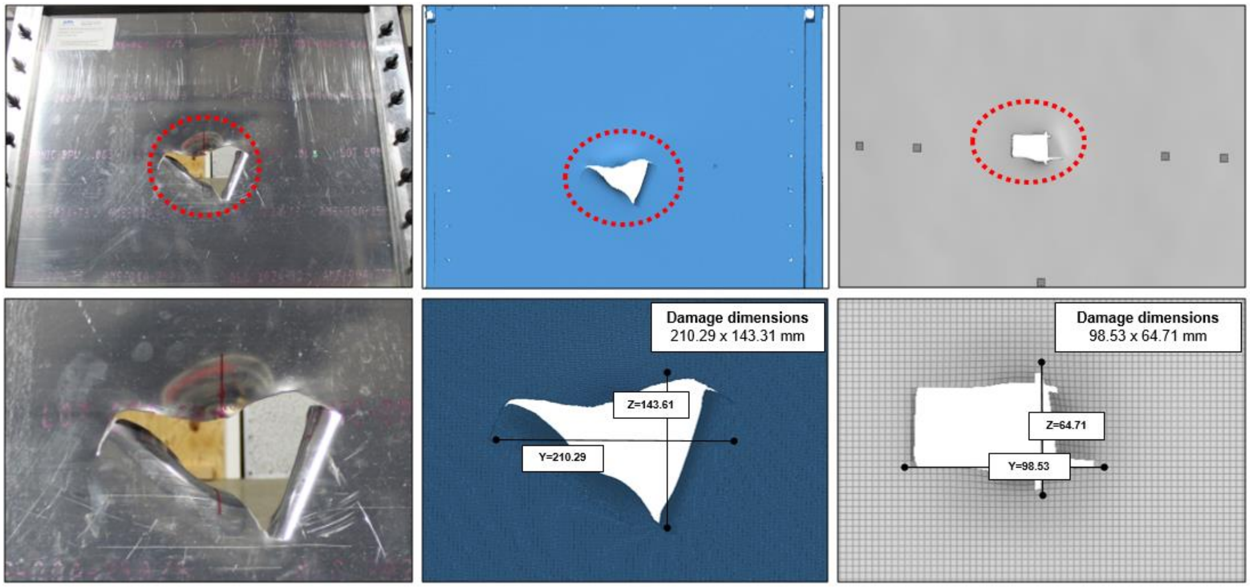


Figure 316. Comparison of the final damage of the panel for the test (left), scan (middle), and simulation (right) for battery B impact on 0.063" aluminum panel at 256.94 m/s (499.46 knots).

Figure 317 compares the physical and simulation projectile damage. The battery penetrated the panel for the physical test and simulation and sustained great damage.

Figure 317. Comparison of the test (left) and simulation (right) projectile damage for battery B impact on 0.063" aluminum panel at 256.94 m/s (499.46 knots).

Figure 318 compares the load-time history of both test repetitions and the simulation load output. All the curves were filtered with a low-pass filter of 15,000 Hz. The load data shows good repeatability for the test and simulation and confirms the good correlation of the FEM. Figure 319 compares the strain data collected at both test iterations to the simulation strains. The values on the vertical axis are not shown for confidential reasons.

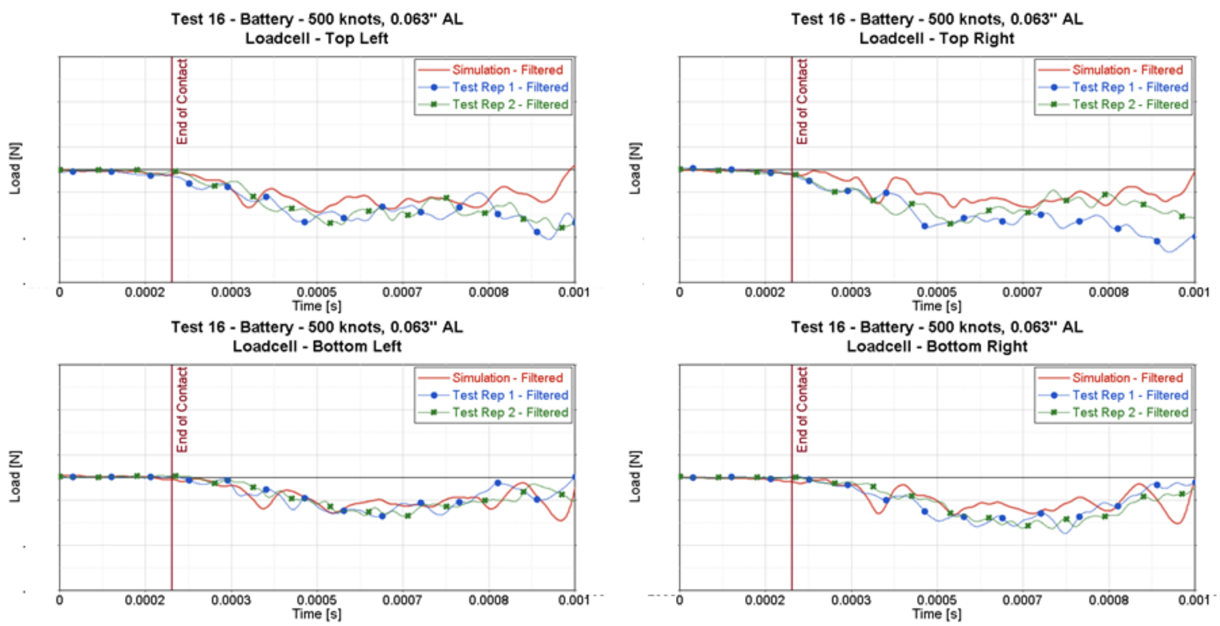


Figure 318. Load cell history data validation for battery B impact 0.063” aluminum panel at 256.94 m/s (499.46 knots).

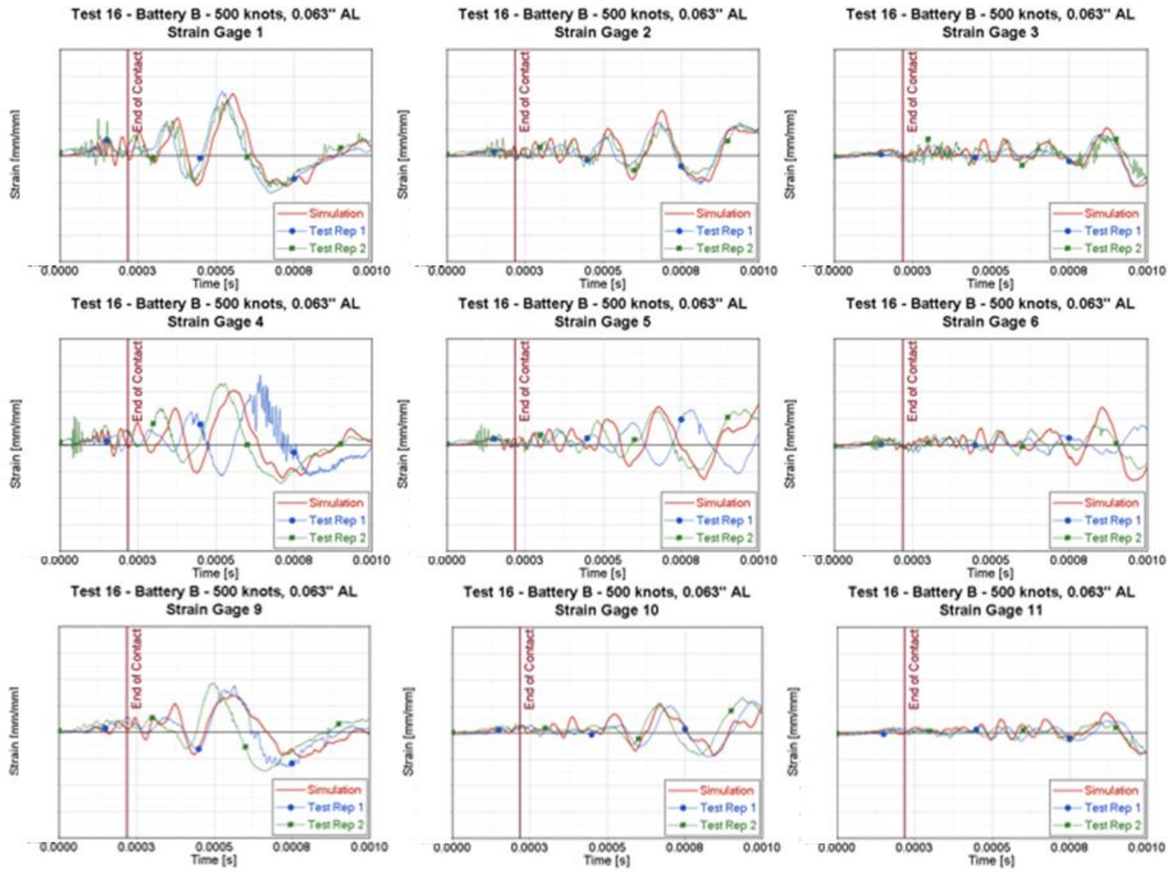


Figure 319. Strain comparison of strain gages 1-6 and 9-11 for battery B impact on 0.063” aluminum panel at 256.94 m/s (499.46 knots).

## A.17 TEST 17 – BATTERY AT 500 KNOTS – 6.35 MM AL PANEL

Test 17 consists of the impact of the fixed-wing battery B with the 6.35 mm (0.25″) aluminum panel at a nominal velocity of 257.2 m/s (500 knots). Two iterations were carried out to evaluate data repeatability. For kinematics comparison, NIAR has identified iteration 2 as the repetition with the least deviation regarding the nominal test requirements. All batteries were fully charged previous to the test.

An initial velocity of 257.84 m/s (501.2 knots) was applied to the battery A FEM, corresponding to the velocity recorded for repetition 2 in the test documentation (APPENDIX B).

Figure 320 through Figure 323 show the comparison of the kinematics between the test and simulation at four different instances of the impact event.

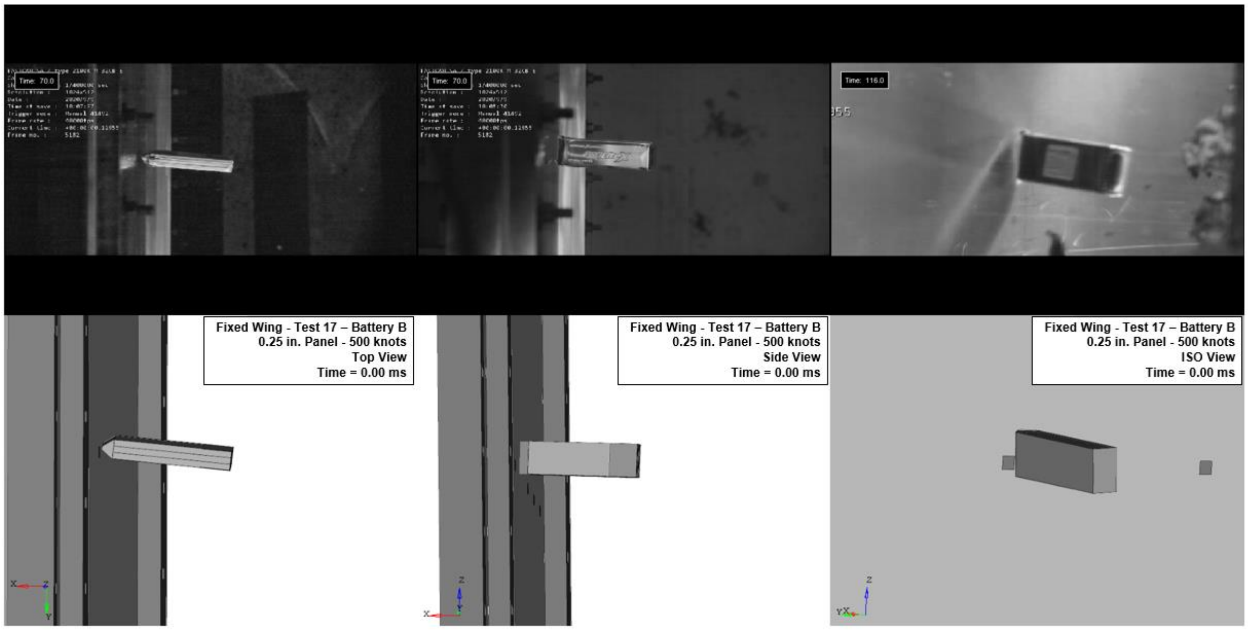


Figure 320. Comparison of battery B impact on 0.25” aluminum panel at 257.84 m/s (501.2 knots) at t = 0.00 ms (beginning of contact).

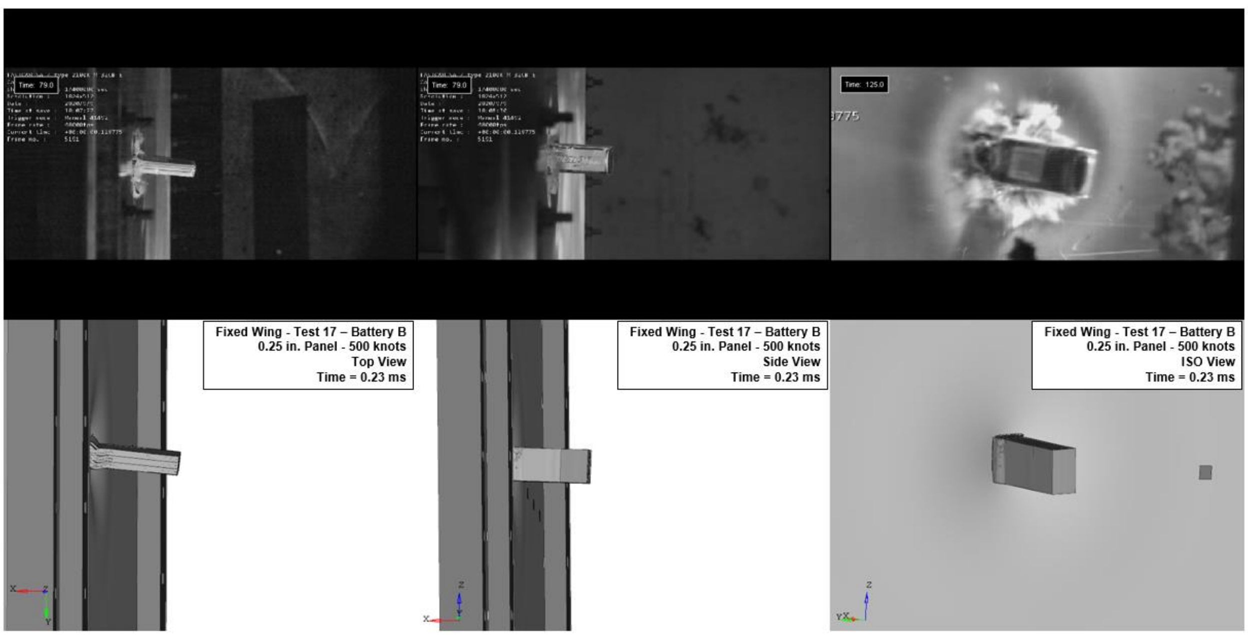


Figure 321. Comparison of battery B impact on 0.25” aluminum panel at 257.84 m/s (501.2 knots) at t = 0.23 ms.

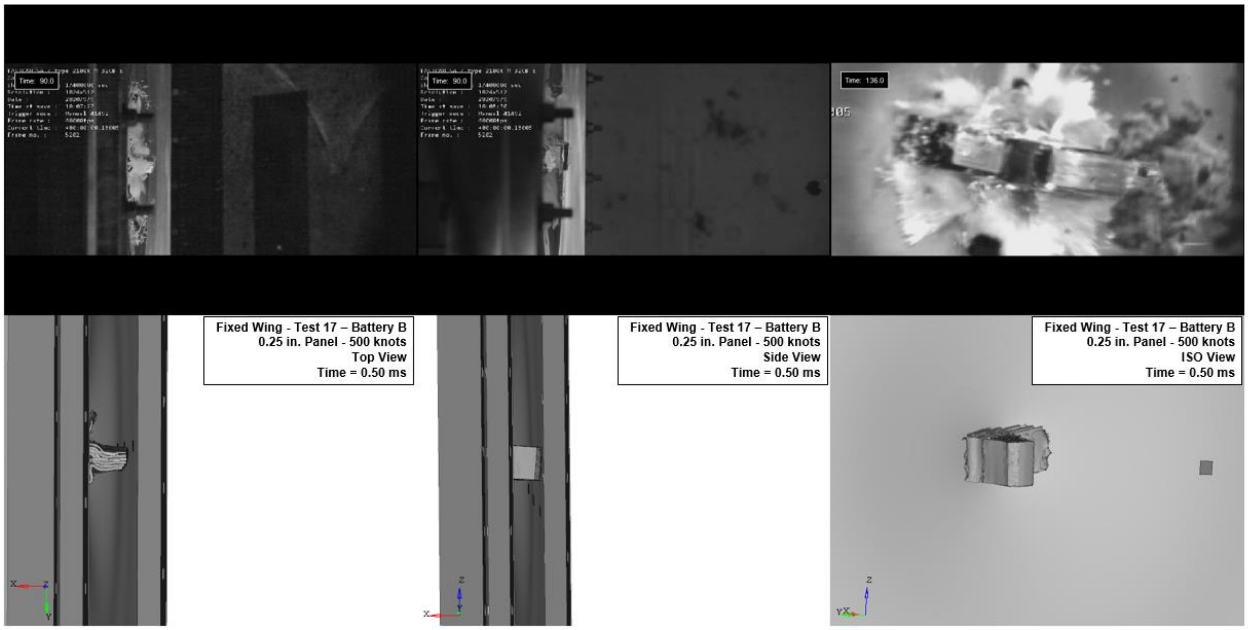


Figure 322 Comparison of battery B impact on 0.25" aluminum panel at 257.84 m/s (501.2 knots) at t = 0.50 ms.

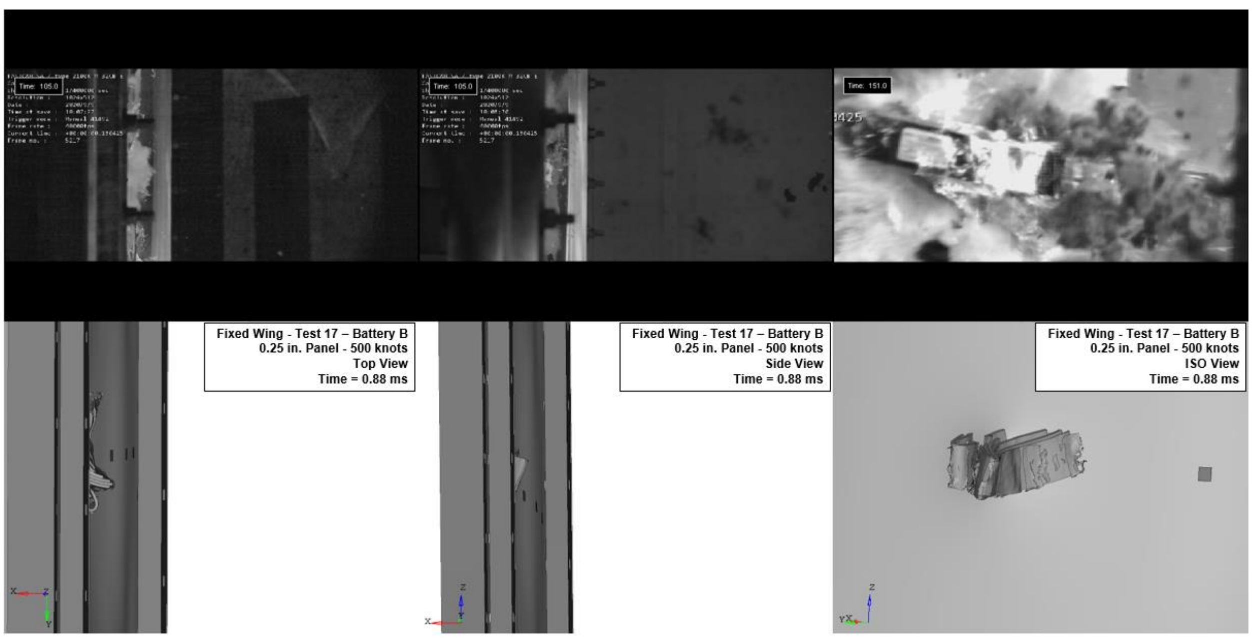


Figure 323 Comparison of battery B impact on 0.25" aluminum panel at 257.84 m/s (501.2 knots) at t = 0.88 ms (end of contact).

Figure 324 compares the simulation and test Y (horizontal) and Z (vertical) direction in-plane deformations and the out-of-plane displacements, for instance, with the aluminum panel's maximum displacement.

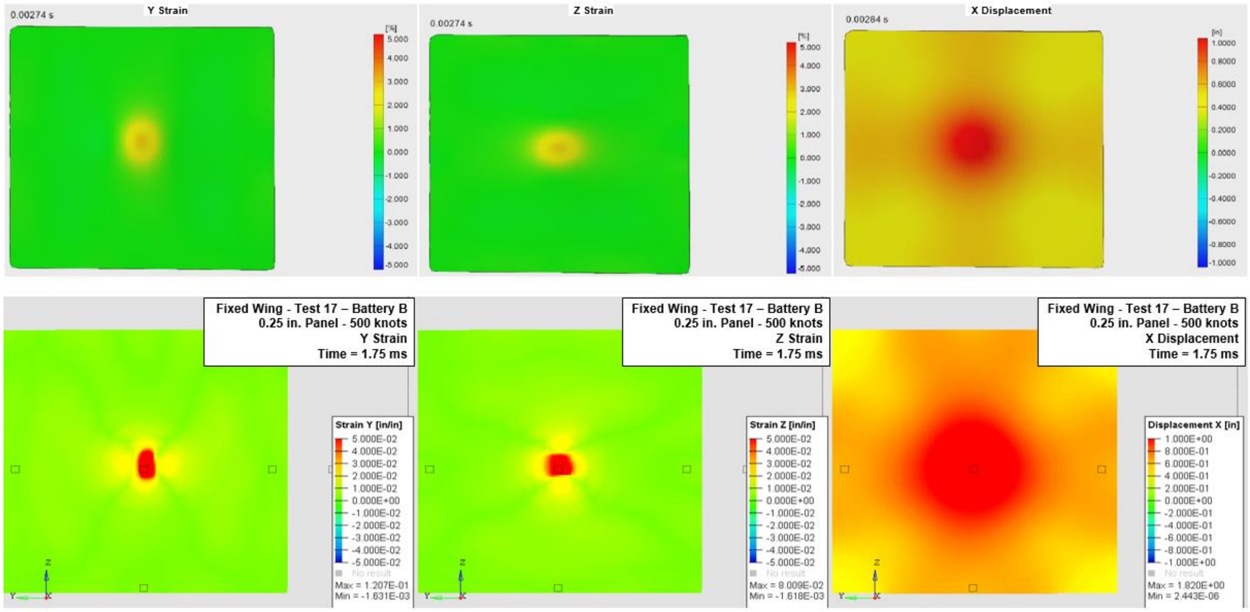


Figure 324. Comparison of test and simulation strains and displacements for battery B impact on 0.25” aluminum panel at 257.84 m/s (501.2 knots) at t = 1.75 ms (maximum displacement).

Figure 325 shows the out-of-plane displacement of the panel over the test period obtained from the DIC data, and the simulation tracked displacements. The values on the vertical axis are not shown for confidential reasons.

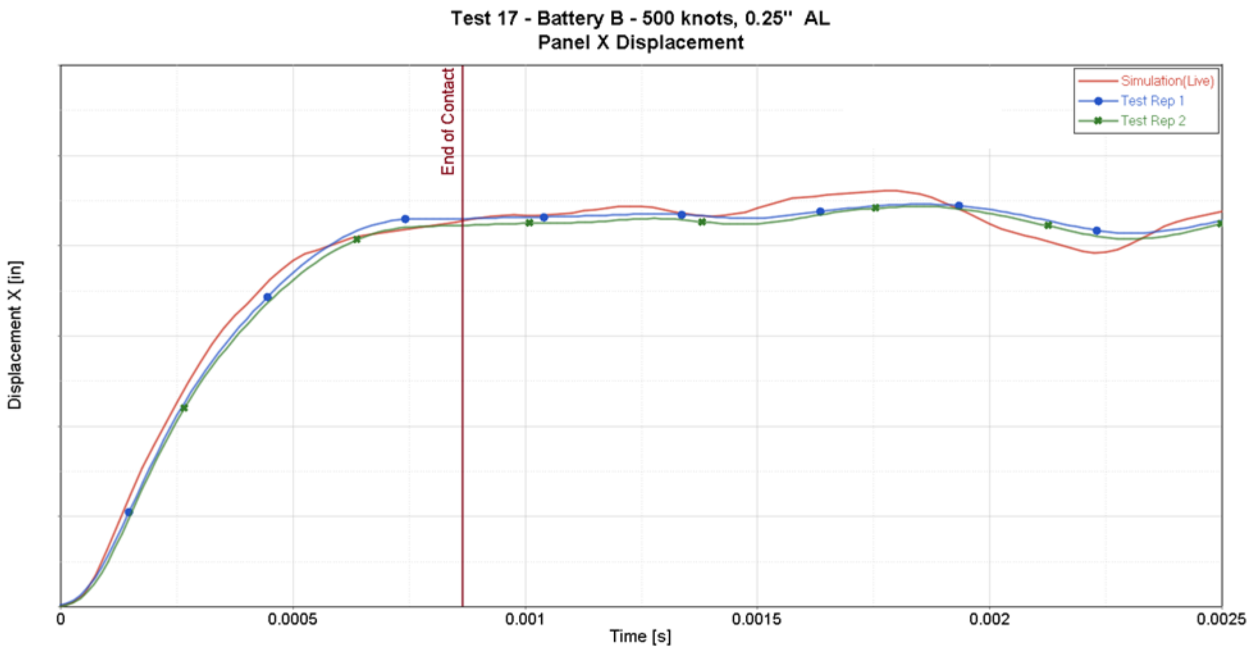


Figure 325. Comparison of the test and simulation out-of-plane displacements for battery B impact on 0.25” aluminum panel at 257.84 m/s (501.2 knots).

The physical panel was scanned after the test to compare the dimensions of the damaged area. Figure 326 compares the panel's damaged area dimensions for the test and simulation. There is good agreement between the physical test and the predicted height of the damaged area, and the simulation predicts a smaller width of the area holding permanent deformation.

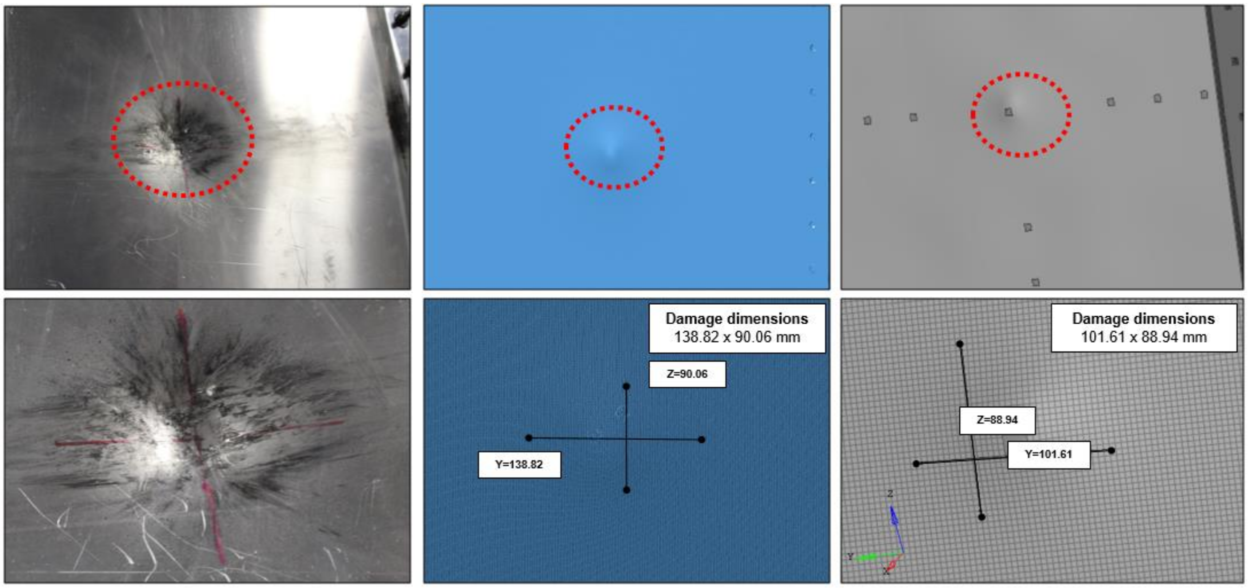


Figure 326. Comparison of the final damage of the panel for the test (left), scan (middle), and simulation (right) for battery B impact on 0.25" aluminum panel at 257.84 m/s (501.2 knots).

Figure 327 compares the physical and simulation projectile damage. For both physical tests and simulation, the battery was highly damaged. The battery left an indentation on the panel but did not penetrate it.

Figure 327. Comparison of the test (left) and simulation (right) projectile damage for battery B impact on 0.25" aluminum panel at 257.84 m/s (501.2 knots).

Figure 328 compares the load-time history of both test repetitions and the simulation load output. All the curves were filtered with a low-pass filter of 15,000 Hz. The load data shows test repeatability and a good correlation of the FEM. Figure 329 compares the strain data collected at both test iterations to the simulation strains. The values on the vertical axis are not shown for confidential reasons.

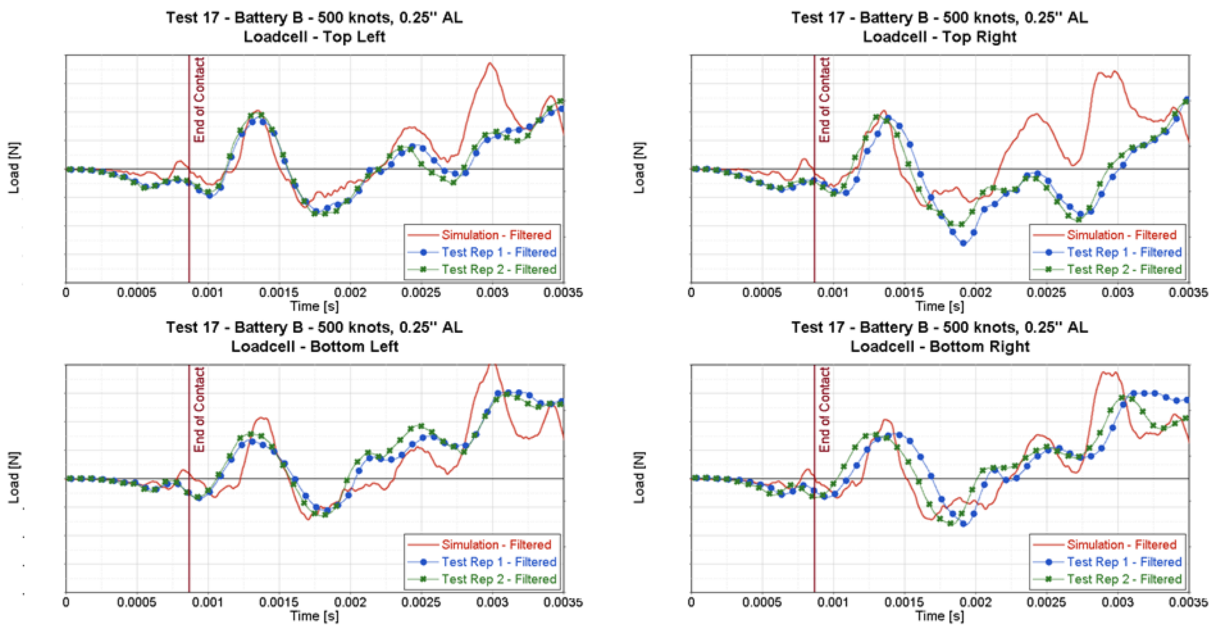


Figure 328. Load cell history data validation for battery B impact on 0.25” aluminum panel at 257.84 m/s (501.2 knots).

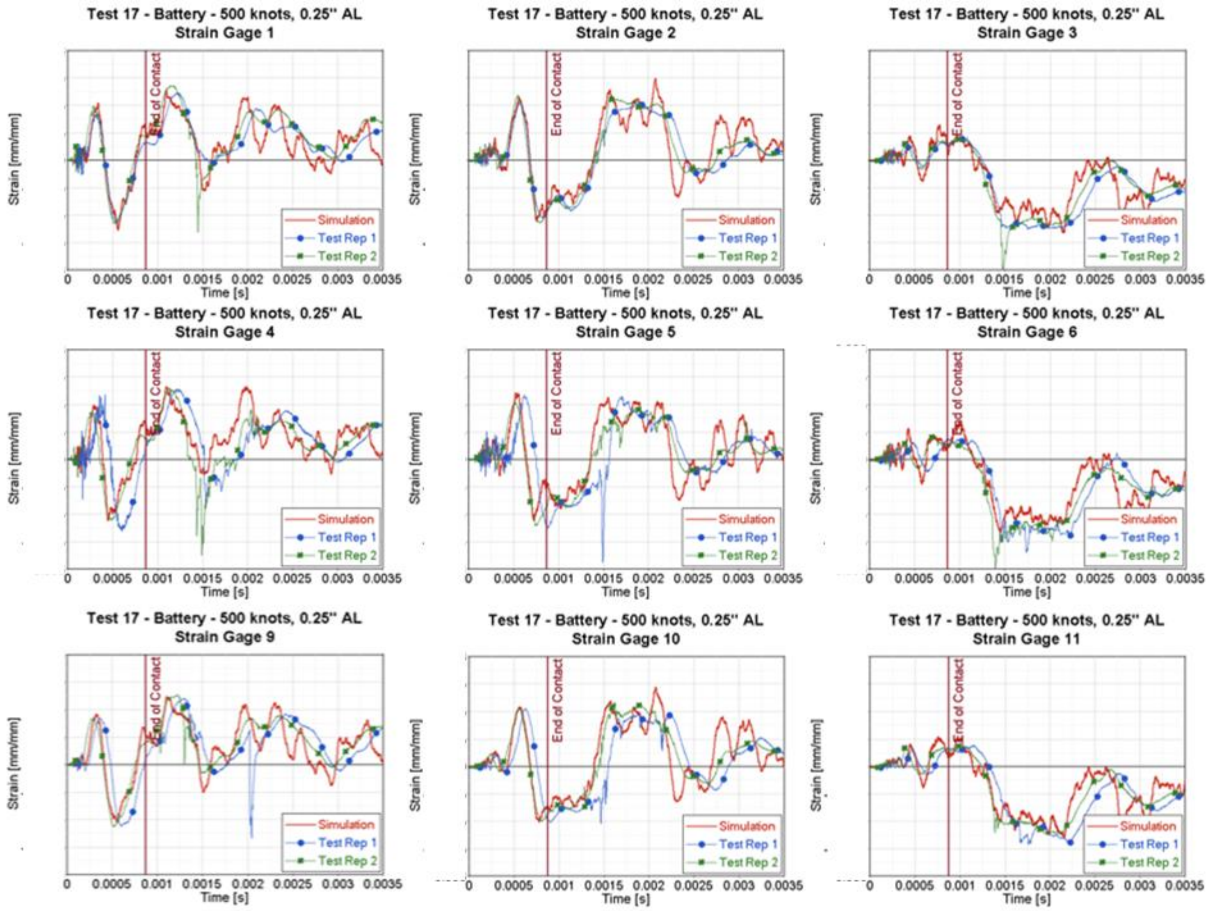


Figure 329. Strain comparison of strain gages 1-6 and 9-11 for battery B impact on 0.25” aluminum panel at 257.84 m/s (501.2 knots).

## A.18 TEST 18 – MOTOR AT 500 KNOTS – 1.6 MM AL PANEL

Test 18 consists of the impact of motor B with the 1.6 mm (0.063″) aluminum panel at a nominal velocity of 257.2 m/s (500 knots). Two iterations were carried out to evaluate data repeatability. For kinematics comparison, NIAR has identified iteration 1 as the repetition with the least deviation regarding the nominal test requirements.

An initial velocity of 271.11 m/s (527 knots) was applied to motor B FEM, corresponding to the velocity recorded for repetition 1 in the test documentation (APPENDIX B).

Figure 330 through Figure 333 show the comparison of the kinematics between the test and simulation at four different instances of the impact event.

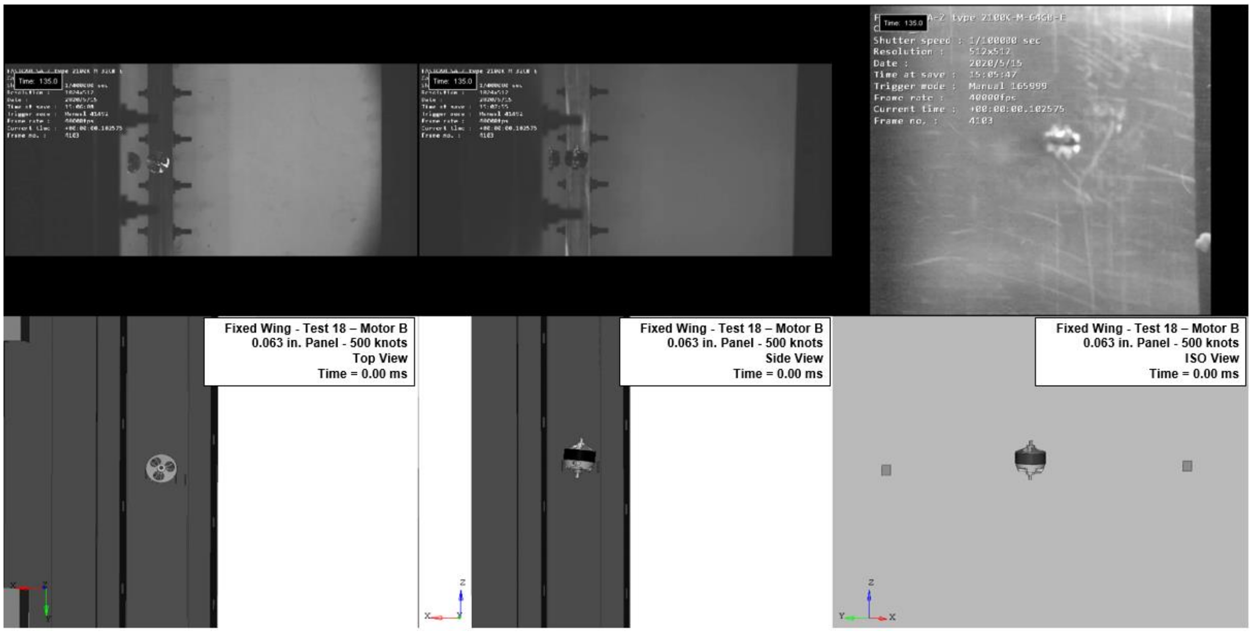


Figure 330. Comparison for motor B impact on 0.063” aluminum panel at 271.11 m/s (527 knots) at t = 0.00 ms (beginning of contact).

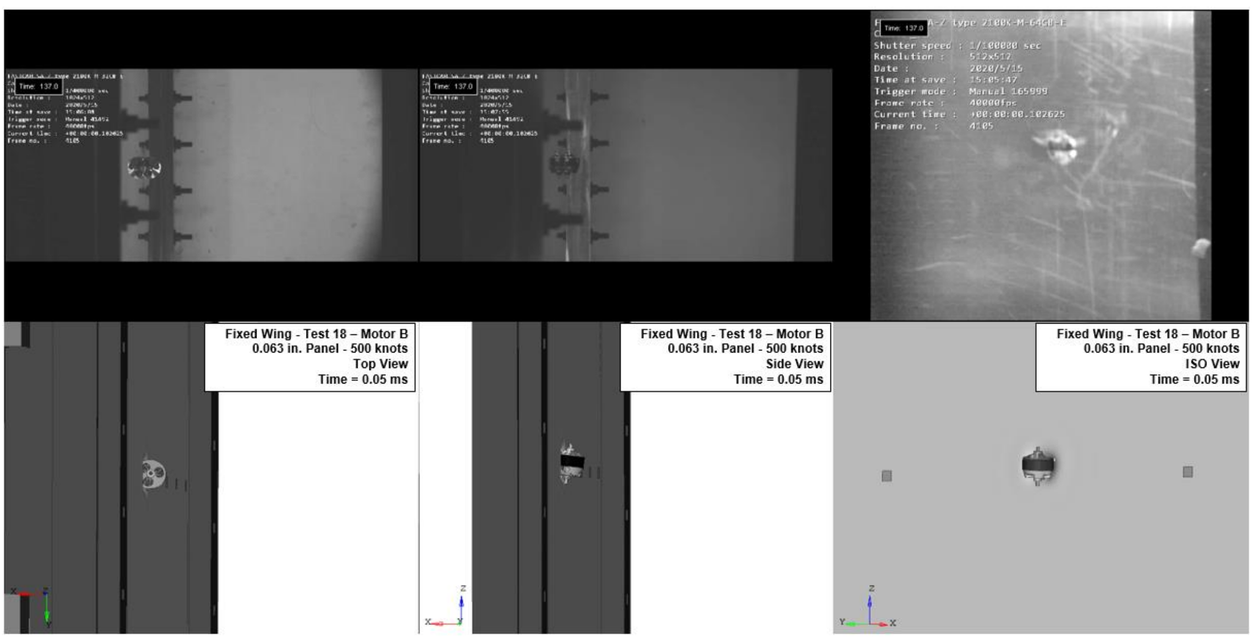


Figure 331. Comparison for motor B impact on 0.063” aluminum panel at 271.11 m/s (527 knots) at t = 0.05 ms (panel failure).

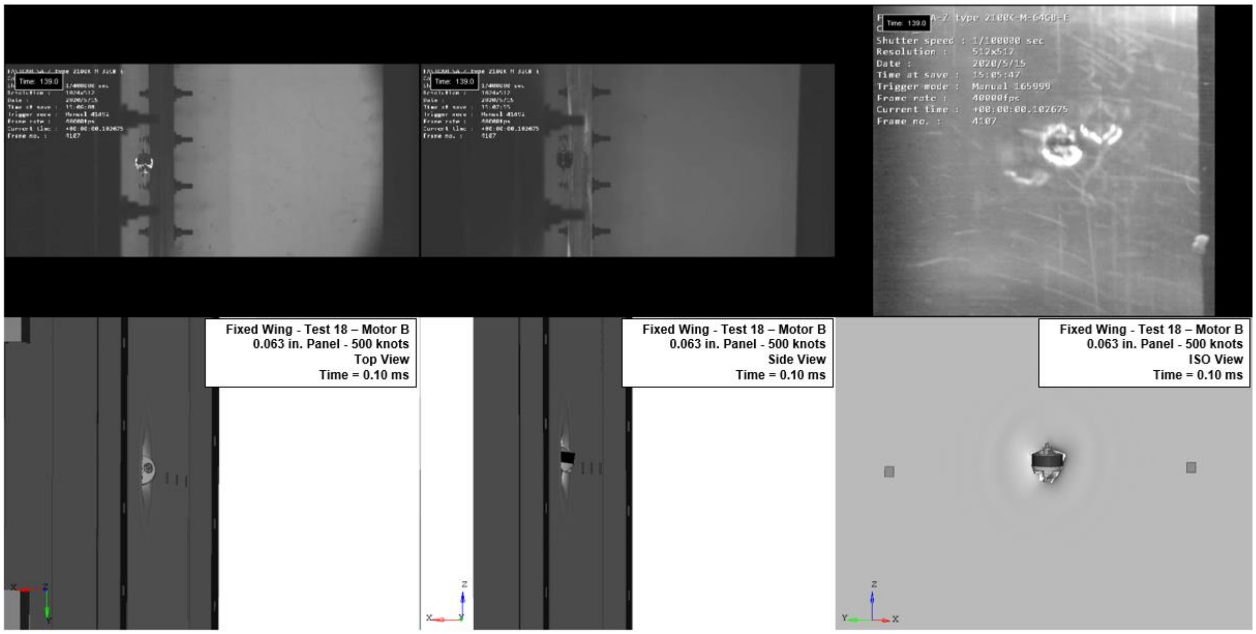


Figure 332 Comparison for motor B impact on 0.063” aluminum panel at 271.11 m/s (527 knots) at t = 0.10 ms.

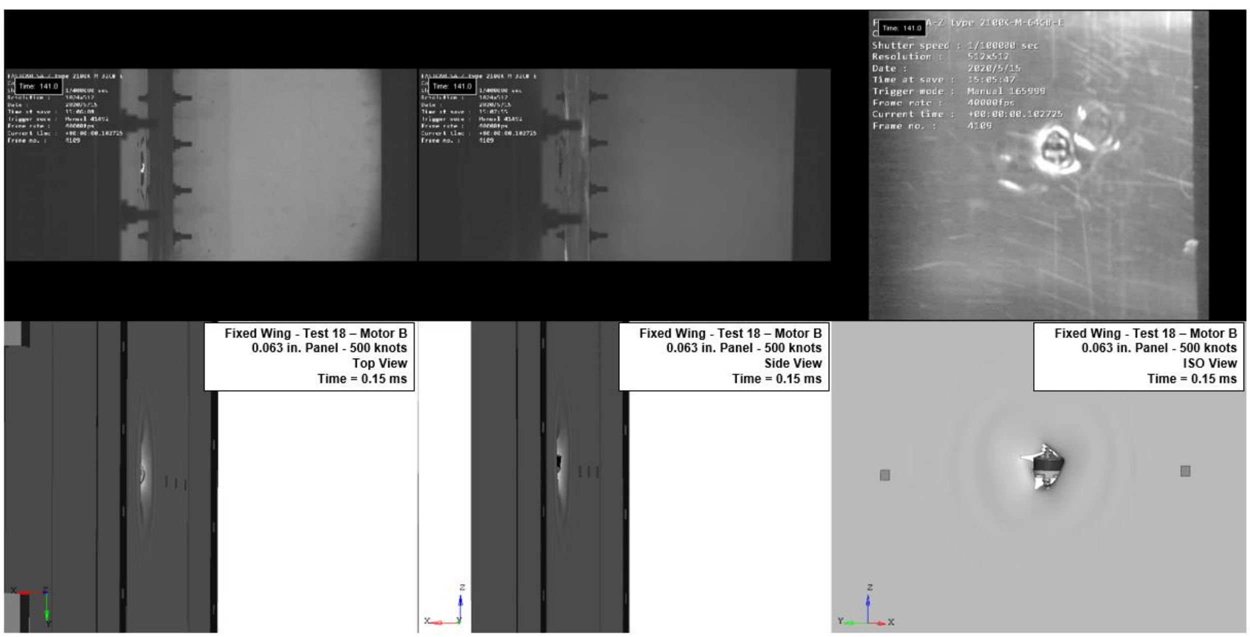


Figure 333 Comparison for motor B impact on 0.063” aluminum panel at 271.11 m/s (527 knots at t = 0.15 ms (end of contact).

Figure 334 compares the simulation and test Y (horizontal) and Z (vertical) direction in-plane deformations and the out-of-plane displacements with a maximum displacement of the aluminum panel.

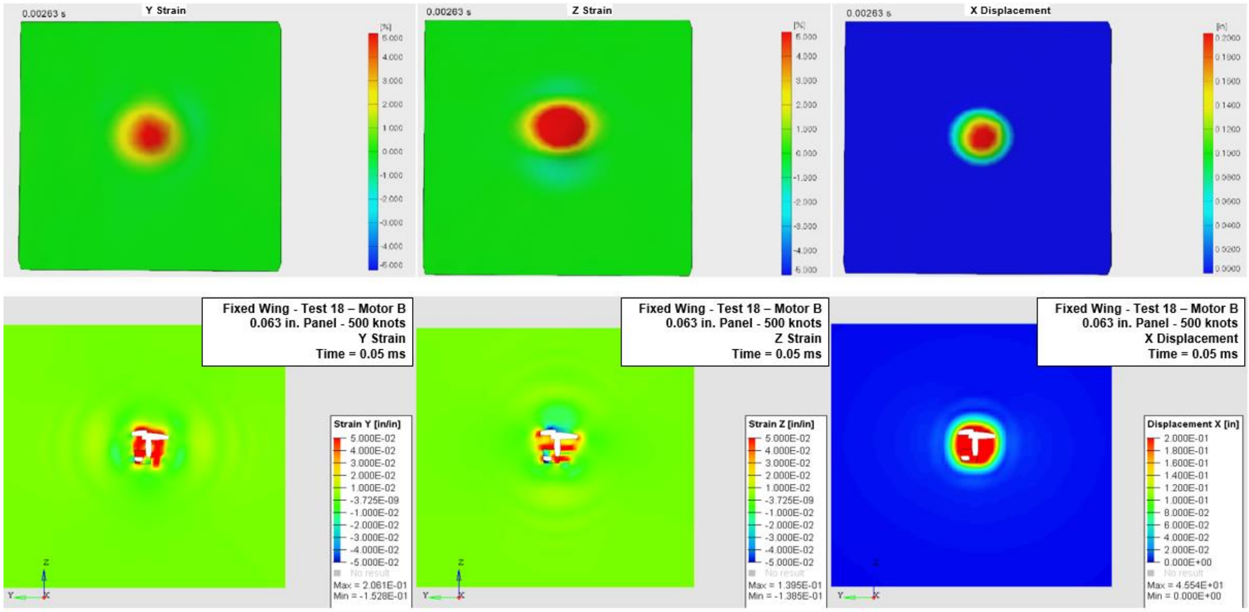


Figure 334. Comparison of test and simulation strains and displacements for motor B impact on 0.063" aluminum panel at 271.11 m/s (527 knots) at t = 0.05 ms (panel failure).

Figure 335 shows the out-of-plane displacement of the panel during the impact event obtained from the DIC data, and the simulation tracked displacements. The values on the vertical axis are not shown for confidential reasons.

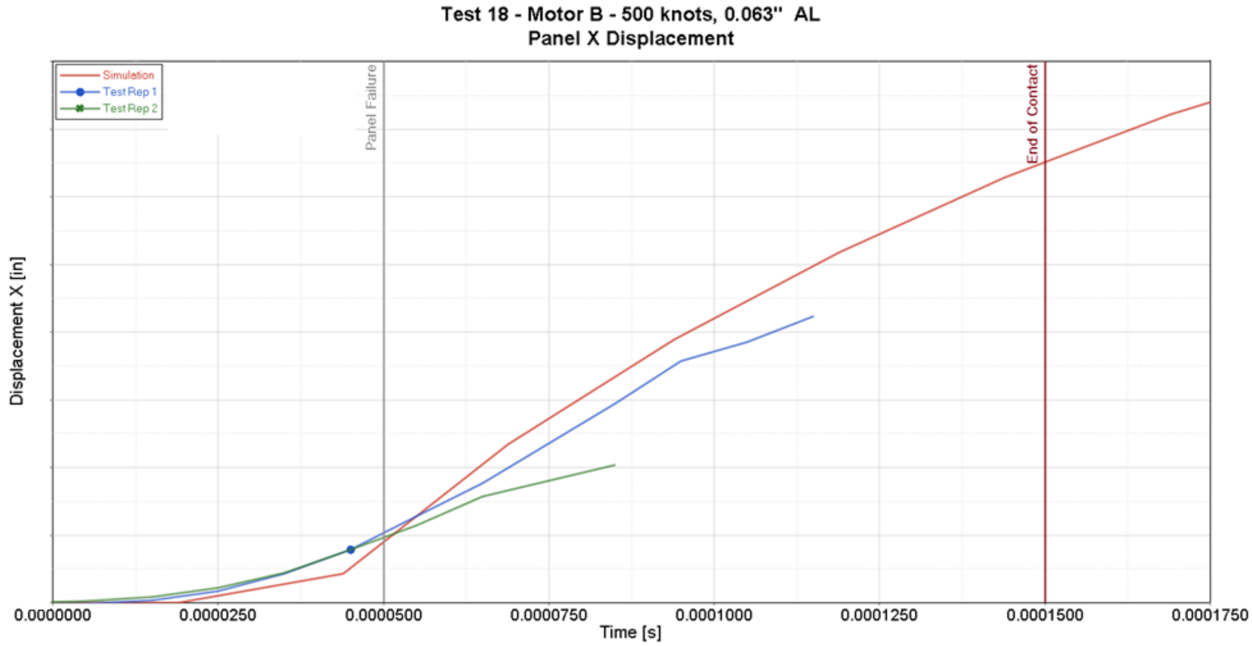


Figure 335. Comparison of the test and simulation out-of-plane displacements for motor B impact on 0.063" aluminum panel at 271.11 m/s (527 knots).

The physical panel was scanned after the test to compare the dimensions of the damaged area. Figure 336 compares the panel's damaged area dimensions for the test and simulation. The hole predicted by the simulation is smaller in the vertical direction and bigger in the horizontal dimension. These differences are due to the eroding nature of the material failure defined in the panel FEM.

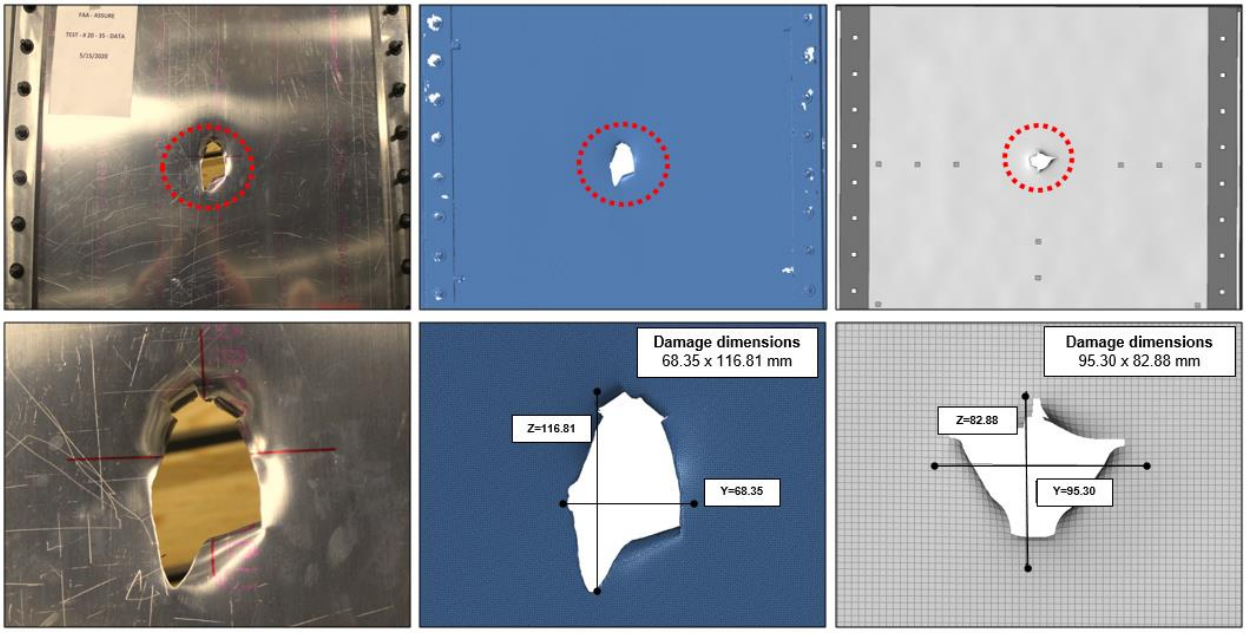


Figure 336. Comparison of the final damage of the panel for the test (left), scan (middle), and simulation (right) for motor B impact on 0.063" aluminum panel at 271.11 m/s (527 knots).

Figure 337 compares the physical and simulation projectile damage. The motor penetrated the panel for both physical test and simulation, but it sustained little damage.

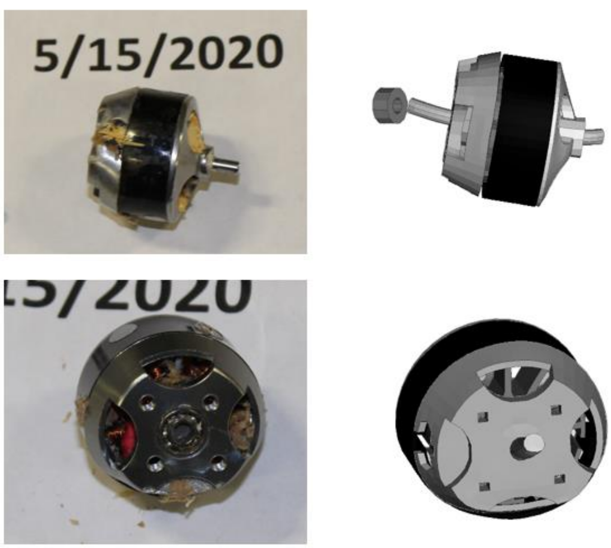


Figure 337. Comparison of the test (left) and simulation (right) projectile damage for motor B impact on 0.063" aluminum panel at 271.11 m/s (527 knots).

Figure 338 compares the load-time history of both test repetitions and the simulation load output. All the curves were filtered with a low-pass filter of 15,000 Hz. The load data shows good repeatability for tests and simulation and confirms the good correlation of the FEM. The values on the vertical axis are not shown for confidential reasons.

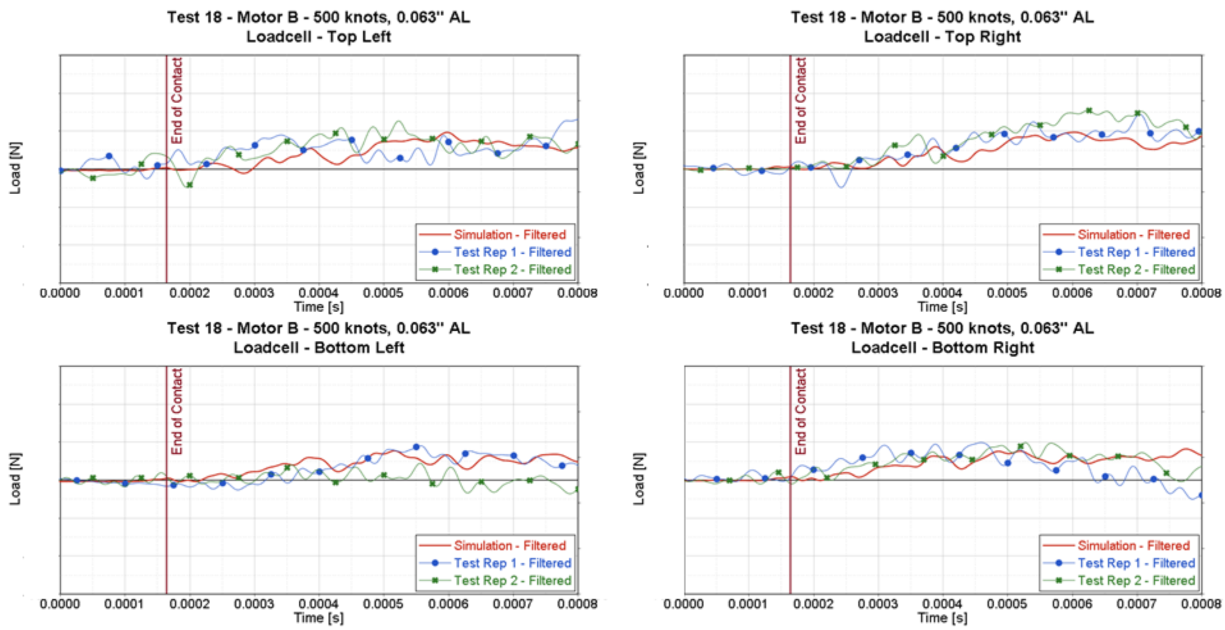


Figure 338. Load cell history data validation for motor B impact on 0.063” aluminum panel at 271.11 m/s (527 knots).

Figure 339 compares the strain data collected at both test iterations to the simulation strains. The simulation has a good correlation to the test strain gages history data. For strain gage 9, there was no data available; hence, the test data is shown as non-available (N/A). The values on the vertical axis are not shown for confidential reasons.

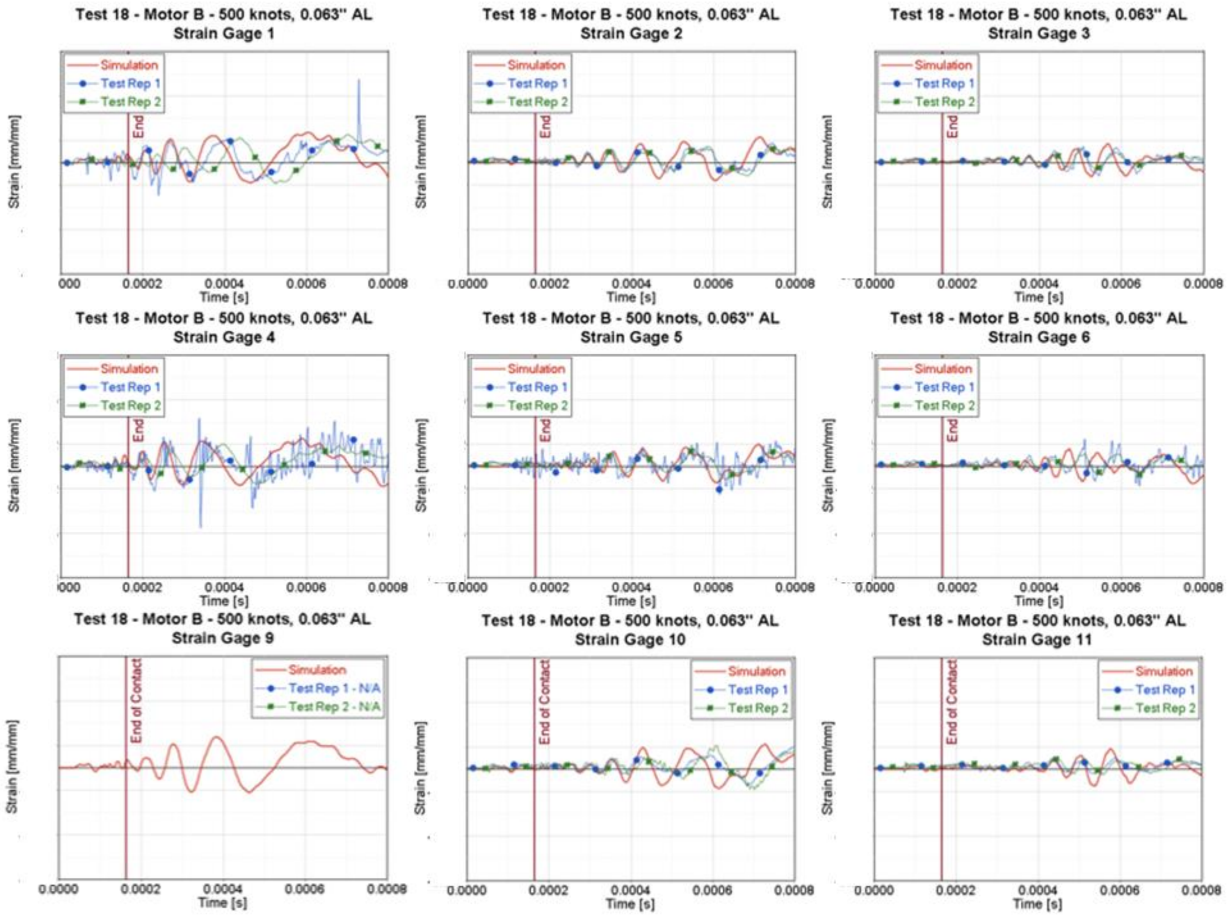


Figure 339. Strain comparison of strain gages 1-6 and 9-11 for motor B impact on 0.063” aluminum panel at 271.11 m/s (527 knots).

## A.19 TEST 19 – MOTOR AT 500 KNOTS – 6.35 MM AL PANEL

Test 19 consists of the impact of motor B with the 6.35 mm (0.25″) aluminum panel at a nominal velocity of 257.2 m/s (500 knots). Two iterations were carried out to evaluate data repeatability. For kinematics comparison, NIAR has identified iteration 2 as the repetition with the least deviation regarding the nominal test requirements.

An initial velocity of 268.80 m/s (522.2 knots) was applied to the motor B FEM, corresponding to the velocity recorded for repetition 2 in the test documentation (APPENDIX B).

Figure 340 through Figure 343 show the comparison of the kinematics between the test and simulation at four different instances of the impact event.

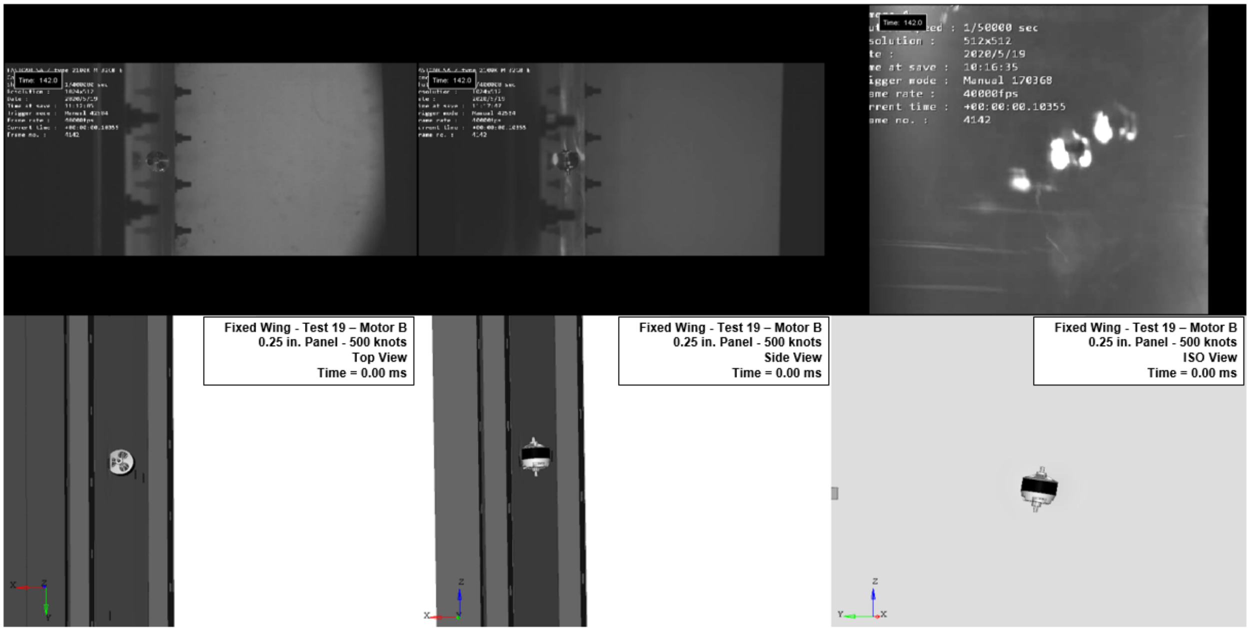


Figure 340. Comparison for motor B impact on 0.25” aluminum panel at 268.80 m/s (522.2 knots) at t = 0.00 ms (beginning of contact).

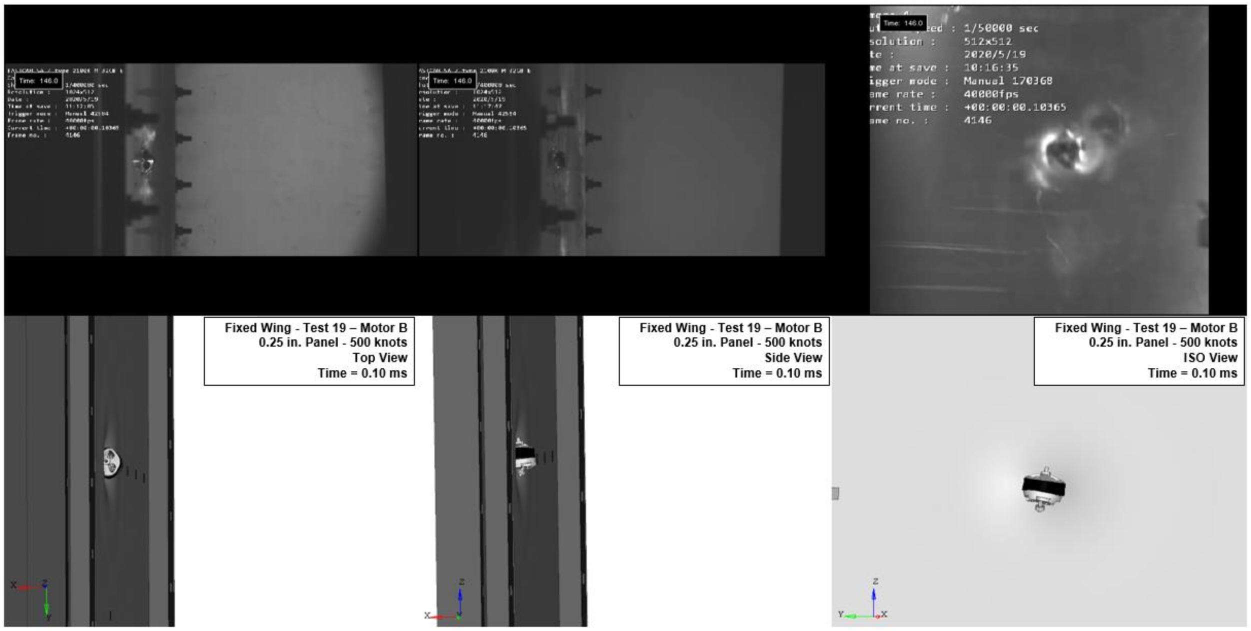


Figure 341. Comparison for motor B impact on 0.25” aluminum panel at 268.80 m/s (522.2 knots) at t = 0.10 ms.

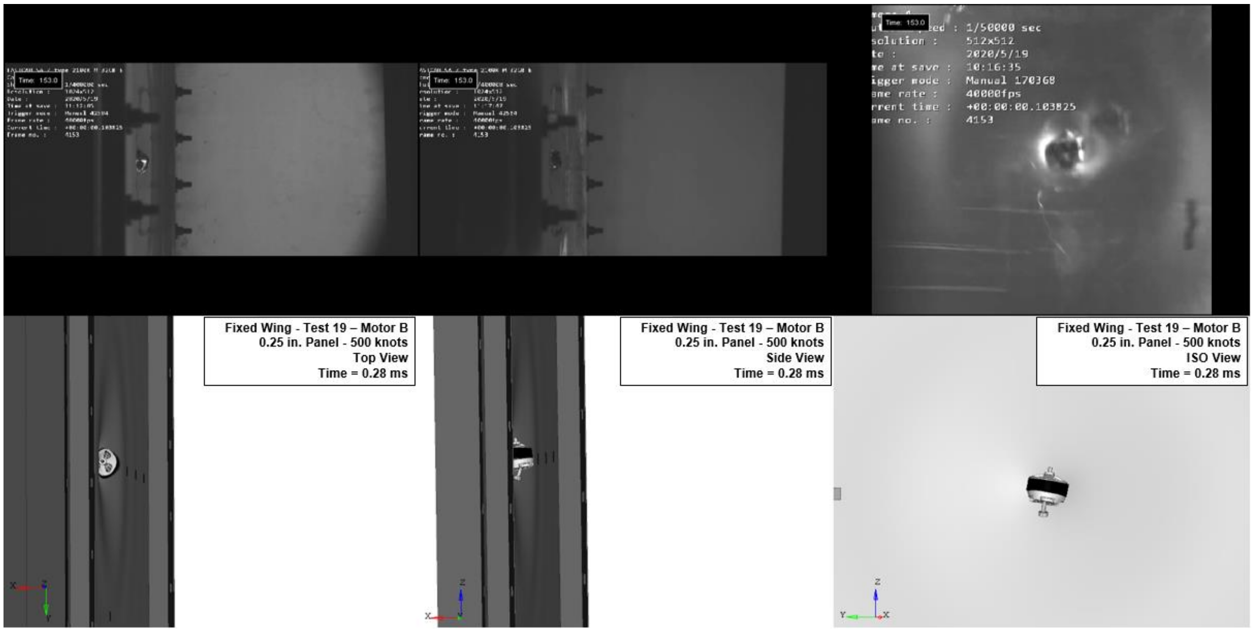


Figure 342 Comparison for motor B impact on 0.25” aluminum panel at 268.80 m/s (522.2 knots) at t = 0.28 ms.

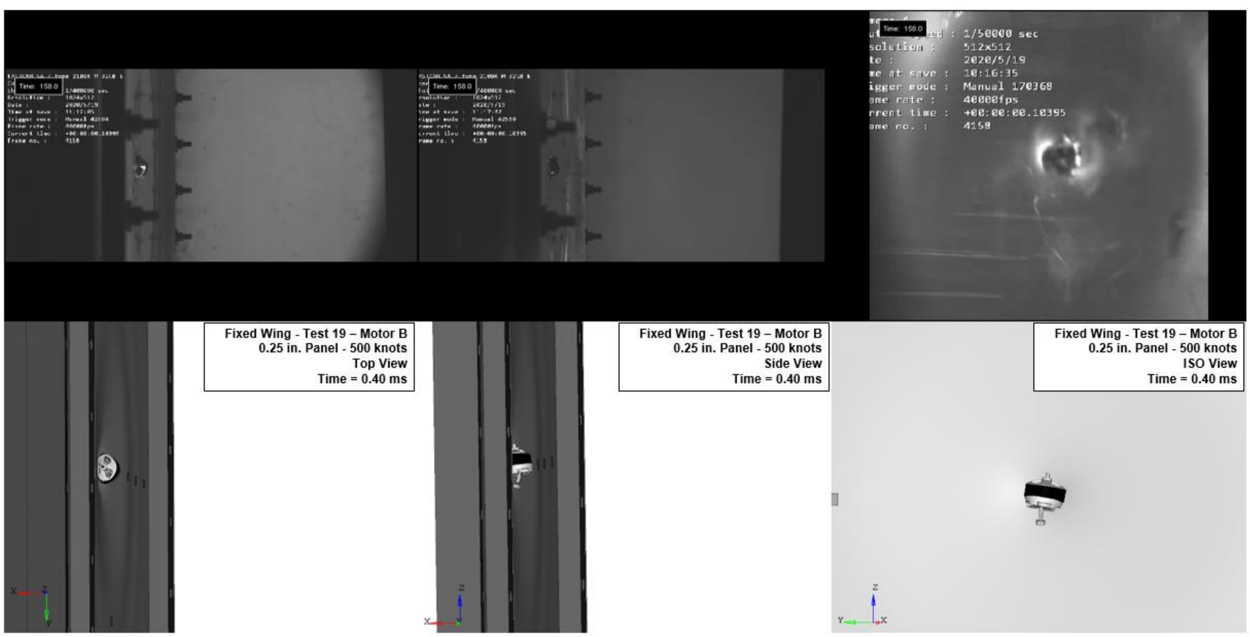


Figure 343 Comparison for motor B impact on 0.25” aluminum panel at 268.80 m/s (522.2 knots) at t = 0.40 ms (end of contact).

Figure 344 compares the simulation and test Y (horizontal) and Z (vertical) direction in-plane deformations and the out-of-plane displacements, for instance, with the aluminum panel's maximum displacement.

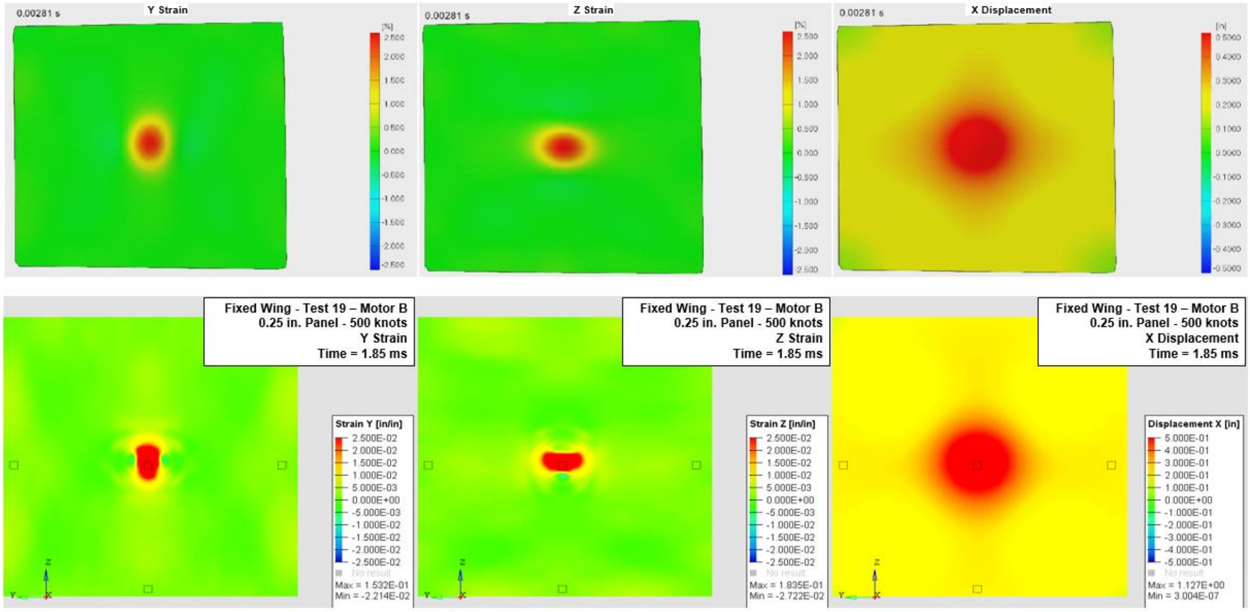


Figure 344. Comparison of test and simulation strains and displacements for motor B impact on 0.25” aluminum panel at 268.80 m/s (522.2 knots) at t = 1.85 ms (maximum displacement).

Figure 345 shows the out-of-plane displacement of the panel during the impact event obtained from the DIC data, and the simulation tracked displacements. The values on the vertical axis are not shown for confidential reasons.

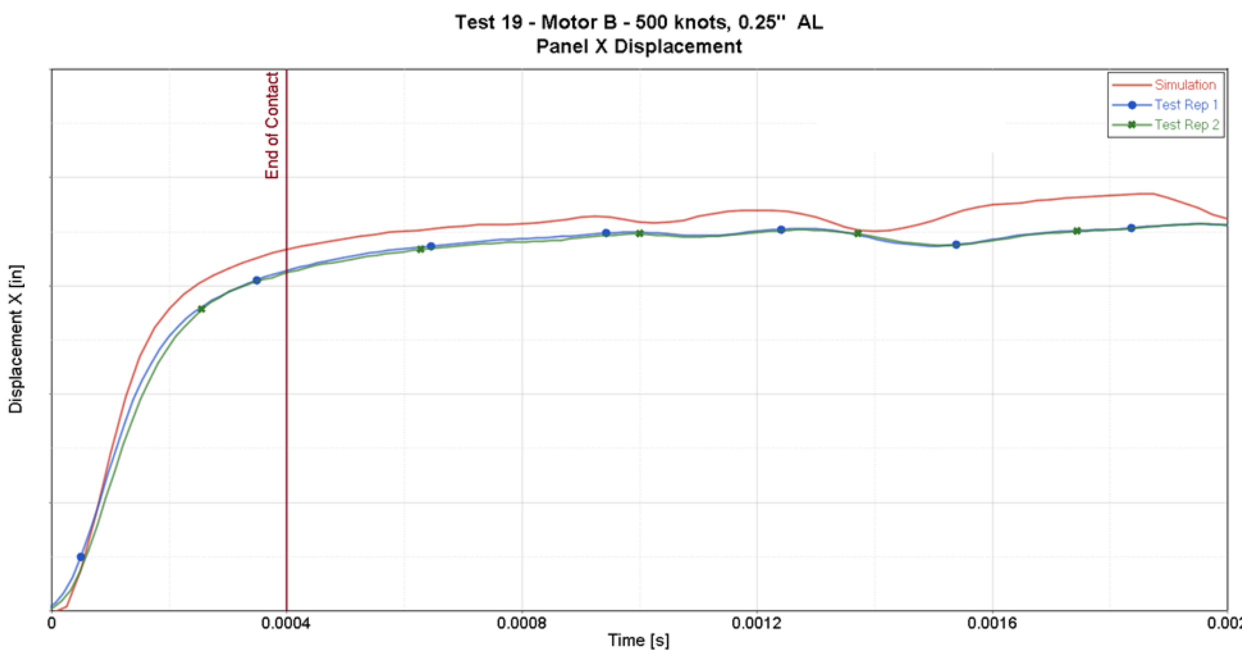


Figure 345. Comparison of the test and simulation out-of-plane displacements for motor B impact on 0.25” aluminum panel at 268.80 m/s (522.2 knots).

The physical panel was scanned after the test to compare the dimensions of the damaged area. Figure 346 compares the panel's damaged area dimensions for the test and simulation. Again, there is good agreement between the physical test and the simulation.

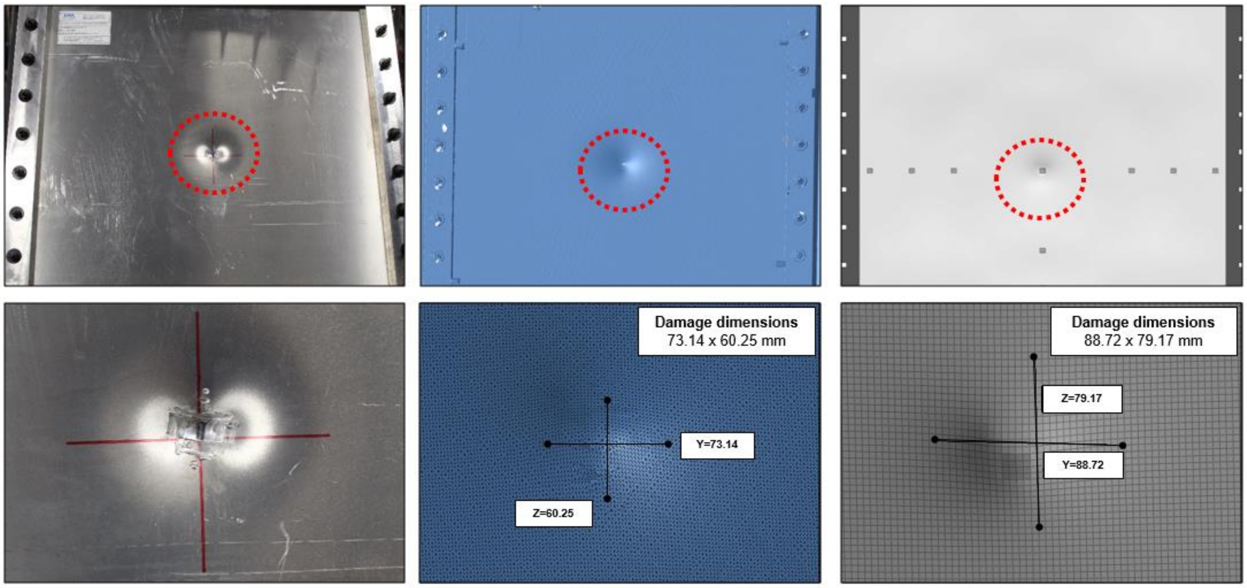


Figure 346. Comparison of the final damage of the panel for the test (left), scan (middle), and simulation (right) for motor B impact on 0.25" aluminum panel at 268.80 m/s (522.2 knots).

Figure 347 compares the physical and simulation projectile damage. The motor did not penetrate the panel for the physical test and simulation, but it held significant plastic deformation due to the impact.

Figure 347. Comparison of the test (left) and simulation (right) projectile damage for motor B impact on 0.25" aluminum panel at 268.80 m/s (522.2 knots).

Figure 348 compares the load-time history of iteration 2 and the simulation load output. All the curves were filtered with a low-pass filter of 15,000 Hz. The repeatability of the data cannot be compared since there is data only for iteration 2. However, iteration 2 load history data confirm the good correlation of the FEM. The values on the vertical axis are not shown for confidential reasons.

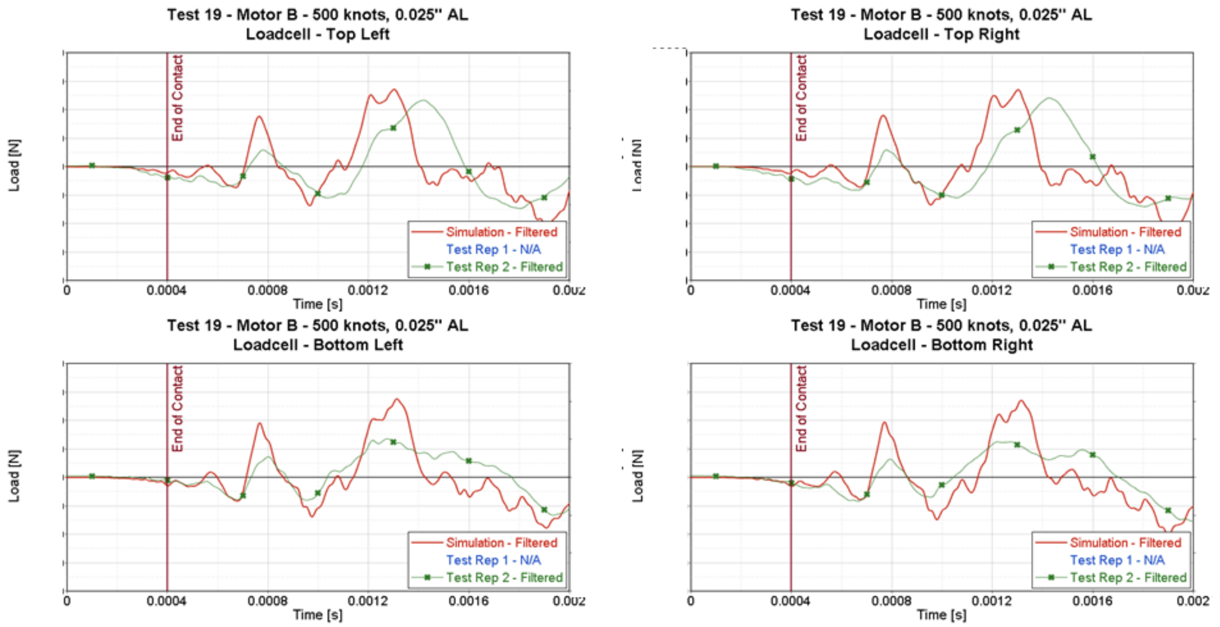


Figure 348. Load cell history data validation for motor B impact on 0.25” aluminum panel at 268.80 m/s (522.2 knots).

Figure 349 compares the strain data collected at both repetitions to the simulation strains. The simulation shows a good correlation to the test strain gages history data. The values on the vertical axis are not shown for confidential reasons.

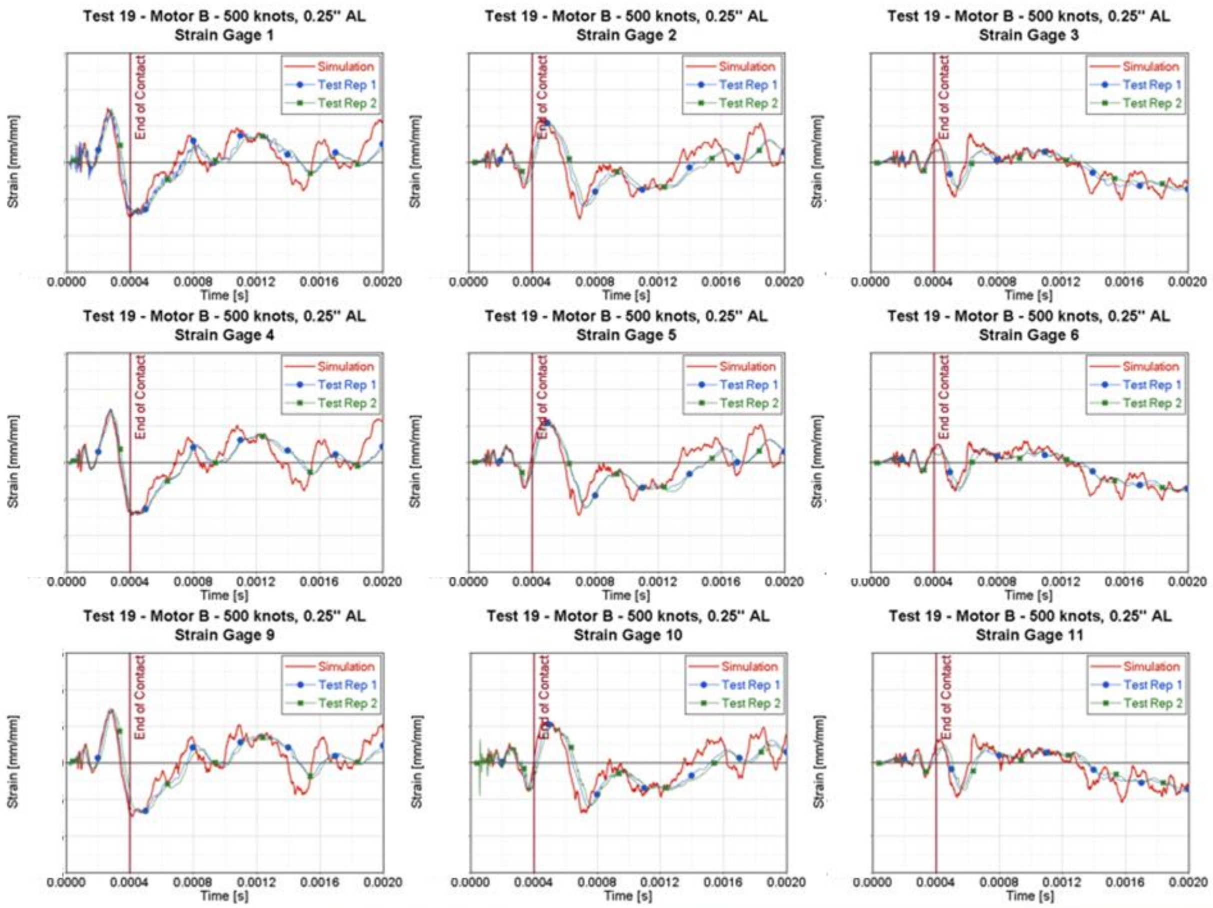


Figure 349. Strain comparison of strain gages 1-6 and 9-11 for motor B impact on 0.25" aluminum panel at 268.80 m/s (522.2 knots).

## A.20 TEST 20 – BATTERY AT 50 KNOTS – 1.6 MM AL PANEL

Test 20 consists of the impact of the battery B with the 1.6 mm (0.063") aluminum panel at a nominal velocity of 25.7 m/s (50 knots). Two iterations were carried out to evaluate data repeatability. For kinematics comparison, NIAR has identified iteration 1 as the repetition with the least deviation regarding the nominal test requirements. All batteries were fully charged before the test.

An initial velocity of 26.75 m/s (52.0 knots) was applied to the battery B FEM, corresponding to the velocity recorded for repetition 1 in the test documentation (APPENDIX B).

Figure 350 through Figure 353 show the comparison of the kinematics between the test and simulation at four different instances of the impact event.

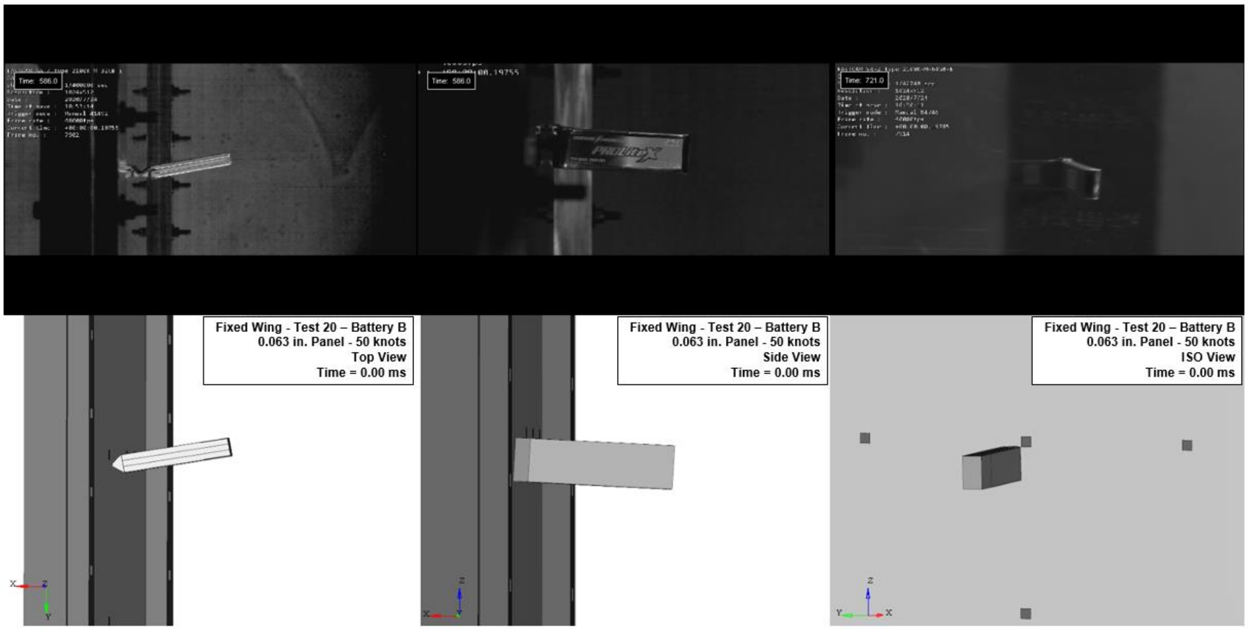


Figure 350. Comparison for battery B impact on 0.063” aluminum panel at 26.75 m/s (52.0 knots) at t = 0.00 ms (beginning of contact).

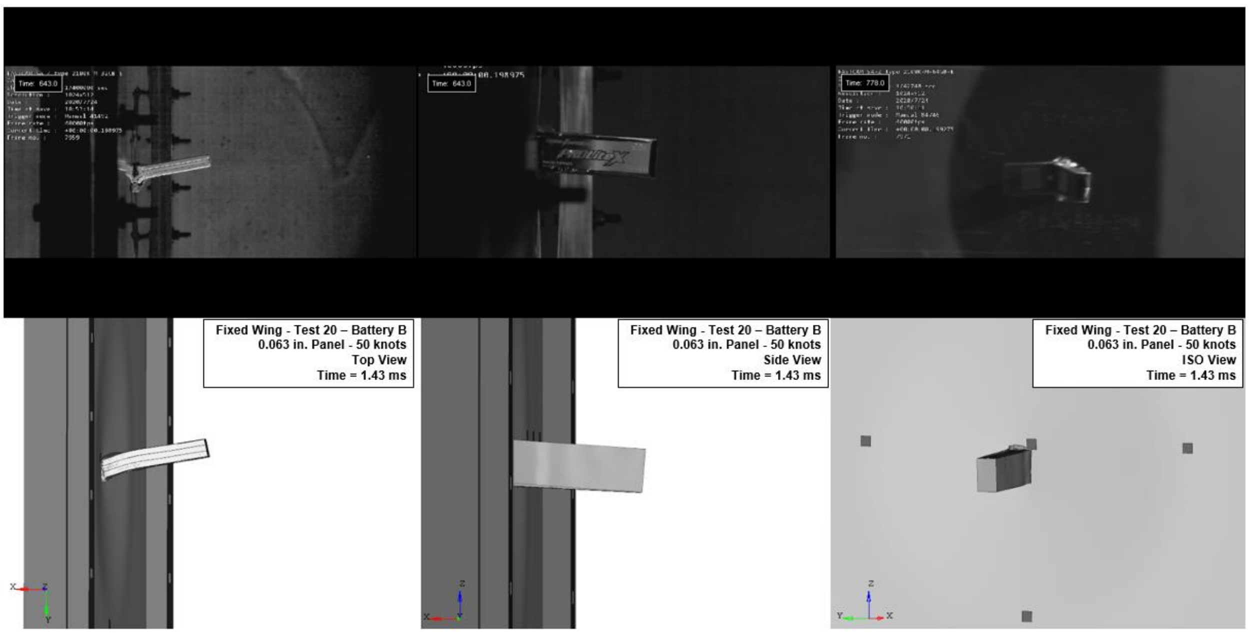


Figure 351. Comparison for battery B impact on 0.063” aluminum panel at 26.75 m/s (52.0 knots) at t = 1.43 ms.

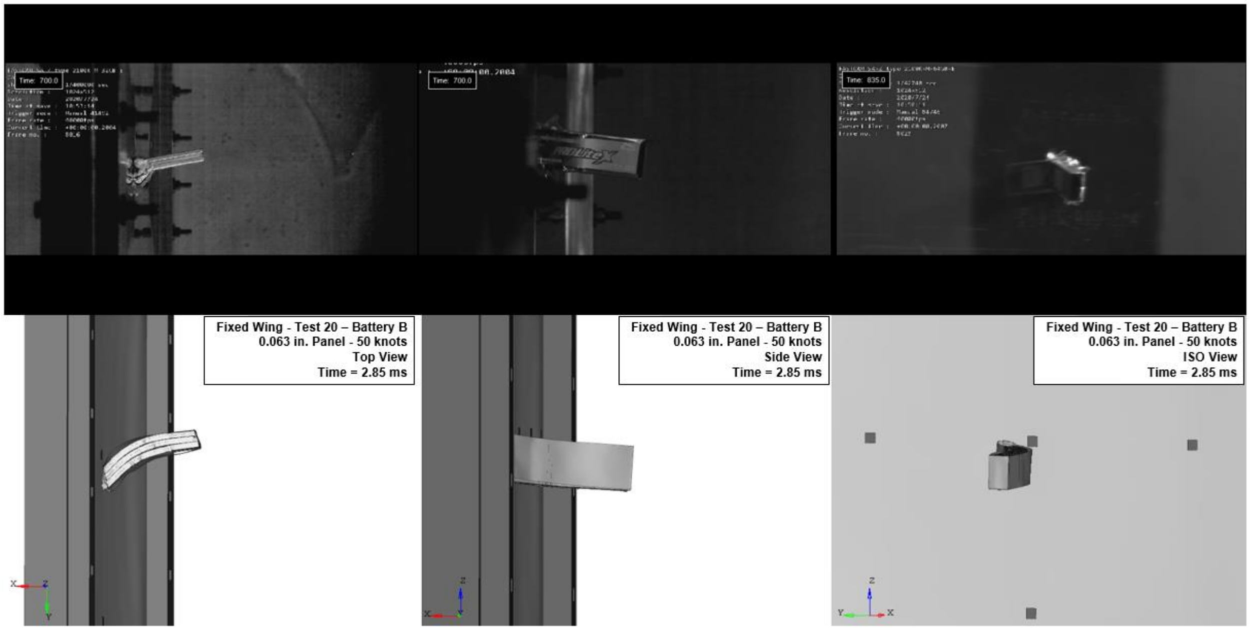


Figure 352 Comparison for battery B impact on 0.063” aluminum panel at 26.75 m/s (52.0 knots) at t = 2.85 ms.

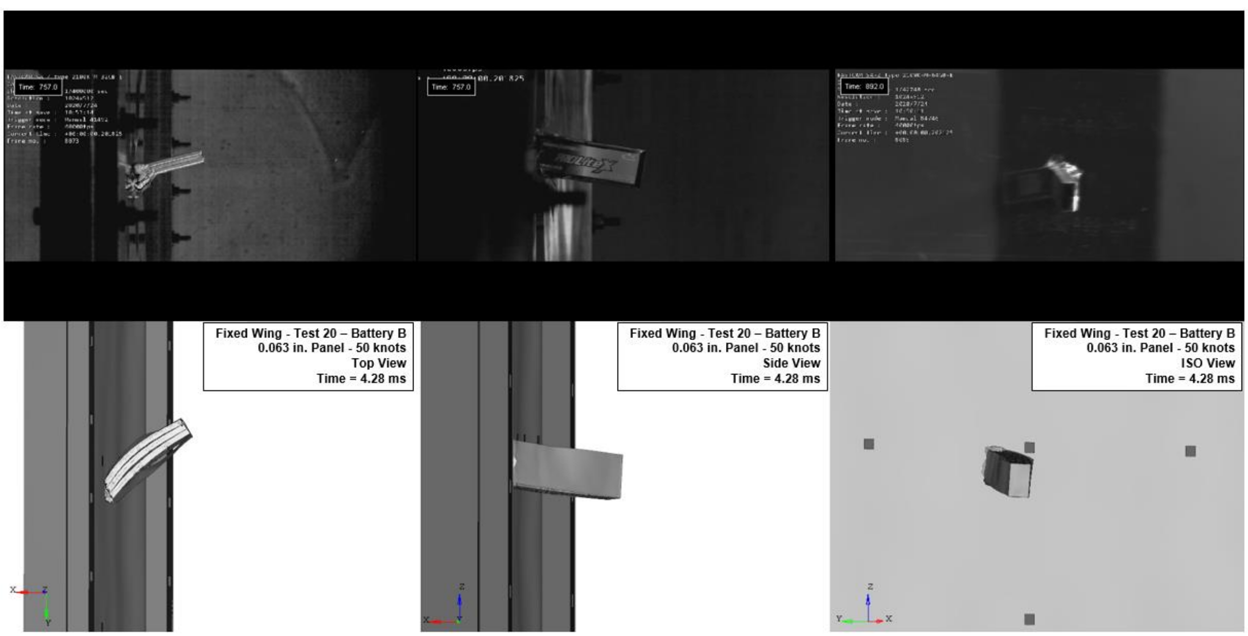


Figure 353 Comparison for battery B impact on 0.063” aluminum panel at 26.75 m/s (52.0 knots) at t = 4.28 ms (end of contact).

Figure 354 compares the simulation and test Y (horizontal) and Z (vertical) direction in-plane deformations and the out-of-plane displacements, for instance, with a maximum displacement of the aluminum panel.

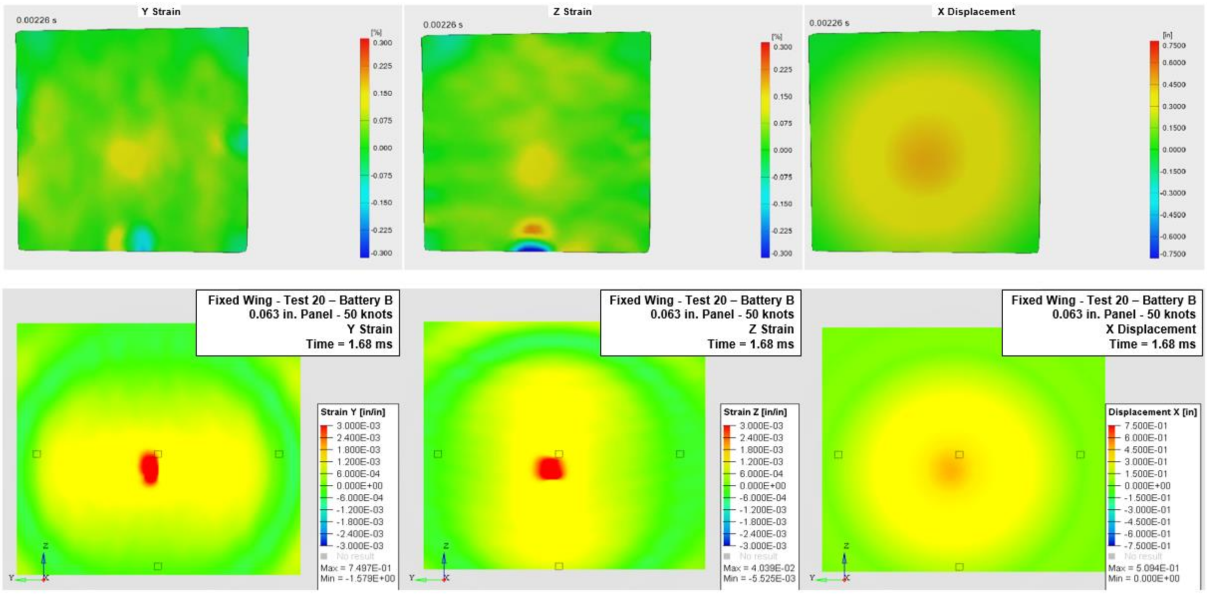

Figure 354. Comparison of test and simulation strains and displacements for battery B impact on 0.063” aluminum panel at 26.75 m/s (52.0 knots) at t = 1.50 ms (maximum displacement).

Figure 355 shows the out-of-plane displacement of the panel during the impact event obtained from the DIC data, and the simulation tracked displacements. The values on the vertical axis are not shown for confidential reasons.

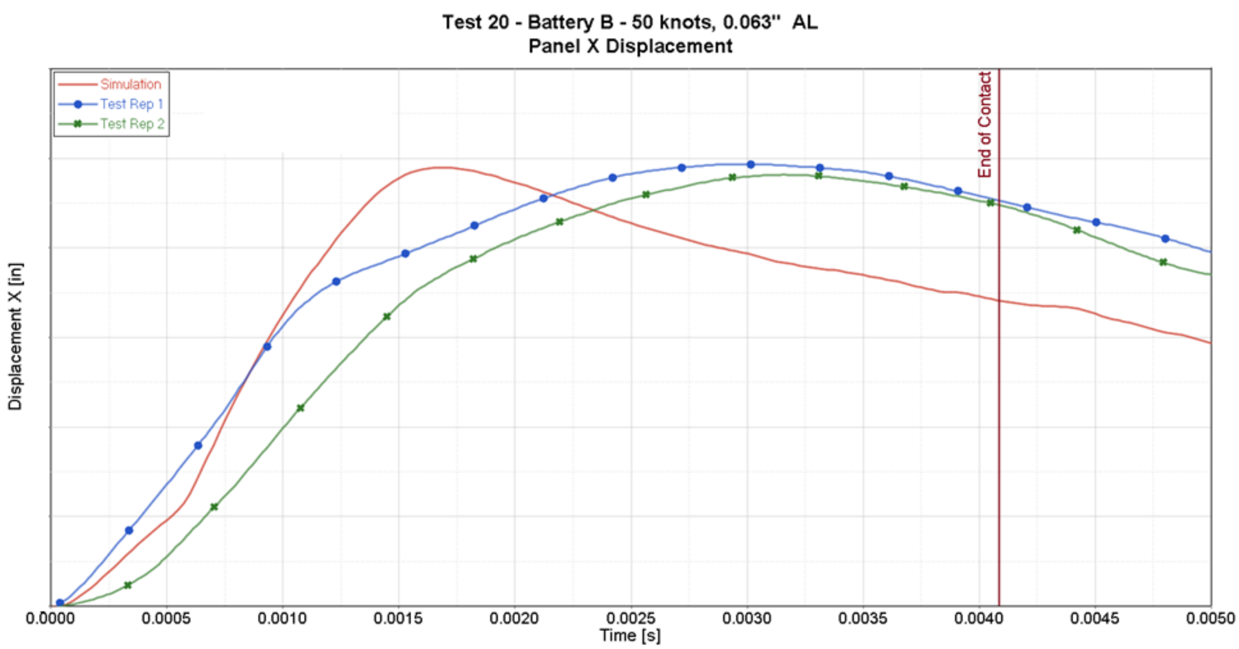


Figure 355. Comparison of the test and simulation out-of-plane displacements for battery B impact on 0.063” aluminum panel at 26.75 m/s (52.0 knots).

The physical panel was scanned after the test to compare the dimensions of the damaged area. Figure 356 compares the panel’s damaged area dimensions for the test and simulation. The panel

FEM overestimates the permanent deformation. This is due to the conservative assumptions in the battery B FEM.

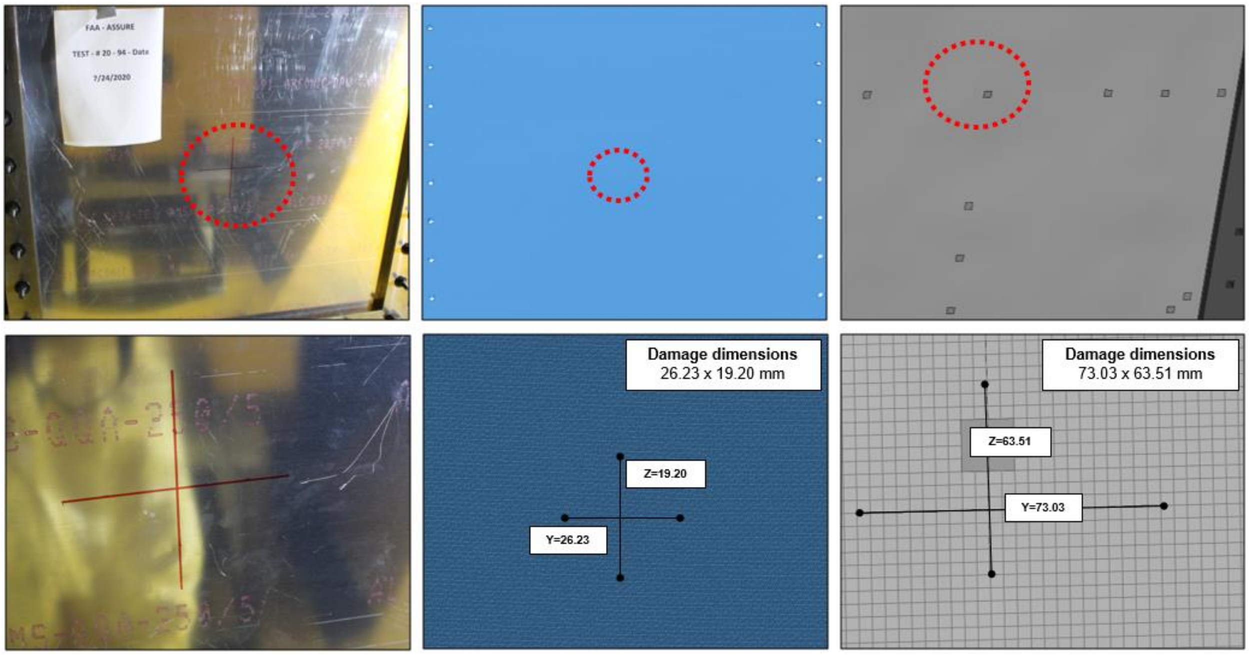


Figure 356. Comparison of the final damage of the panel for the test (left), scan (middle), and simulation (right) for battery B impact on 0.063” aluminum panel at 26.75 m/s (52.0 knots).

Figure 357 compares the physical and simulation projectile damage. The battery was partially damaged for the physical tests and simulation due to the impact, but the cells stayed attached with some plastic deformation.

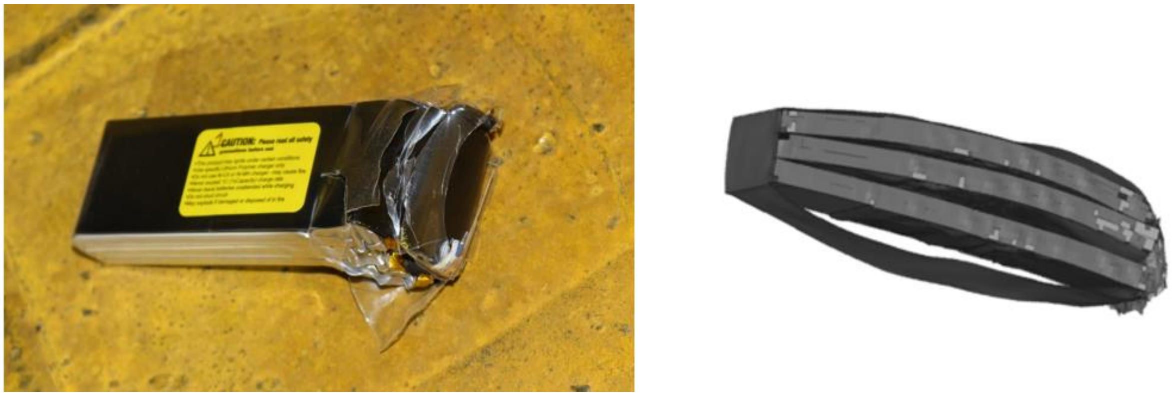

Figure 357. Comparison of the test (left) and simulation (right) projectile damage for battery B impact on 0.063” aluminum panel at 26.75 m/s (52.0 knots).

Figure 358 compares the load-time history of both test repetitions and the simulation load output. All the curves were filtered with a low-pass filter of 15,000 Hz. The load data shows good repeatability for test and simulation and confirms the good correlation of the FEM for the bottom load readings. The loads captured by the physical test top load cells show smaller magnitudes. The values on the vertical axis are not shown for confidential reasons.

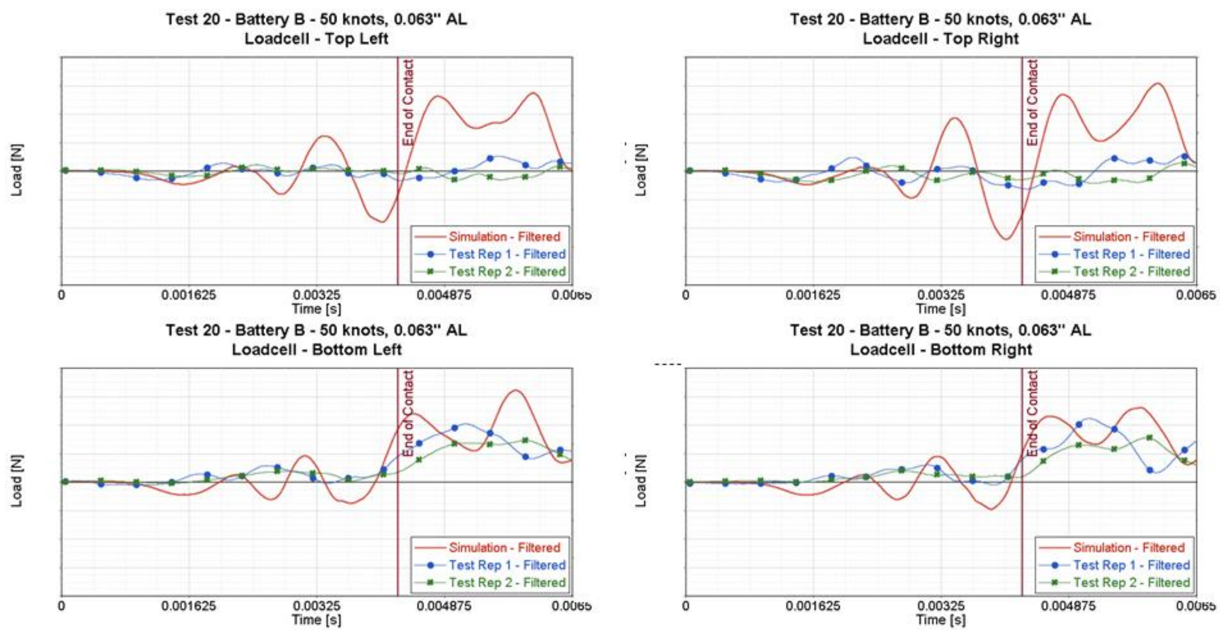


Figure 358. Load cell history data validation for battery B impact on 0.063” aluminum panel at 26.75 m/s (52.0 knots).

Figure 359 compares the strain data collected at both repetitions to the simulation strains. The simulation correlates with the test strains well, being close to iteration 1, chosen for the battery B FEM orientation. The values on the vertical axis are not shown for confidential reasons.

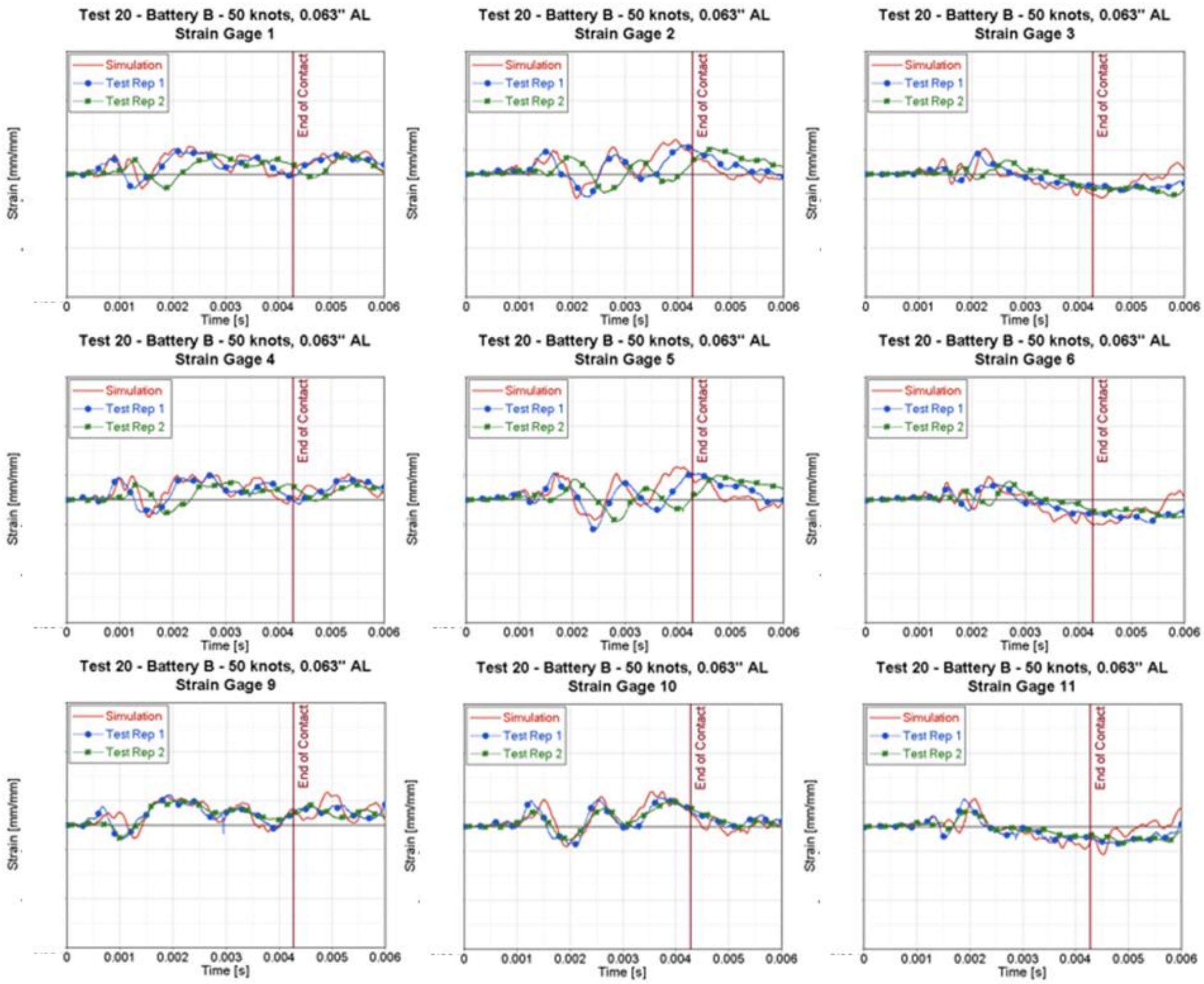


Figure 359. Strain comparison of strain gages 1-6 and 9-11 for battery B impact on 0.063” aluminum panel at 26.75 m/s (52.0 knots).

## A.21 TEST 21 – BATTERY AT 120 KNOTS – 1.6 MM AL PANEL

Test 21 consists of the impact of battery B with the 1.6 mm (0.063″) aluminum panel at a nominal velocity of 61.7 m/s (120 knots). Two iterations were carried out to evaluate data repeatability. For kinematics comparison, NIAR has identified iteration 2 as the repetition with the least deviation regarding the nominal test requirements. All batteries were fully charged previous to the test.

An initial velocity of 62.18 m/s (120.87 knots) was applied to the battery B FEM, corresponding to the velocity recorded for repetition 2 in the test documentation (APPENDIX B).

Figure 360 through Figure 363 show the comparison of the kinematics between the test and simulation at four different instances of the impact event.

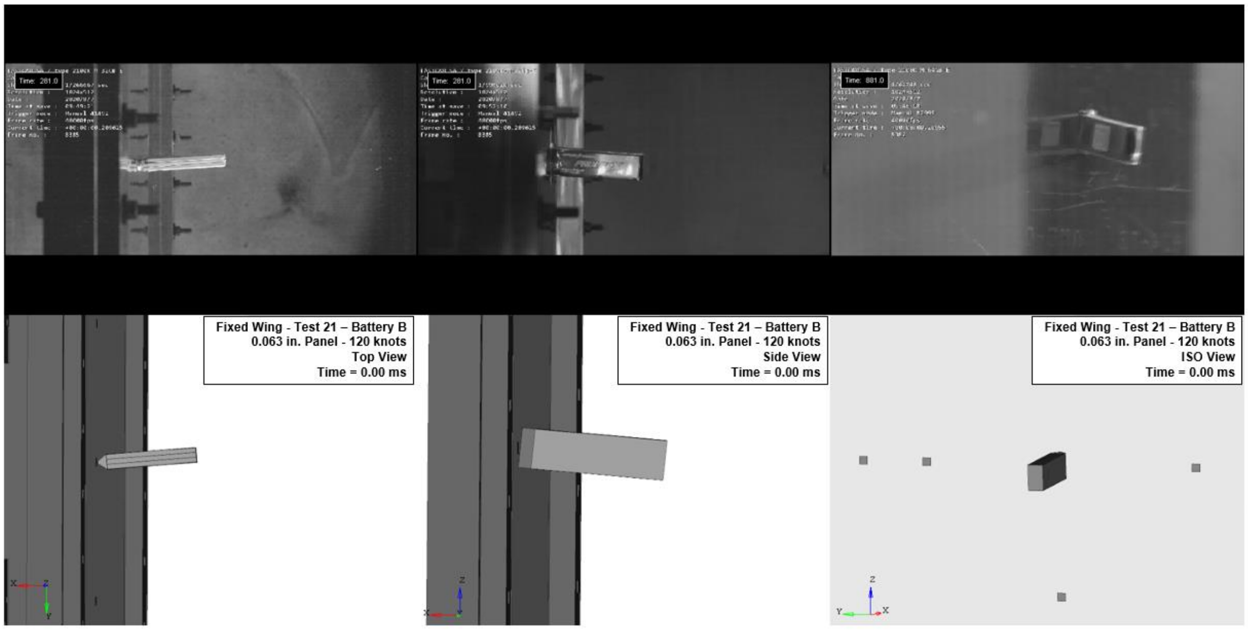


Figure 360. Comparison for battery B impact on 0.063” aluminum panel at 62.18 m/s (120.87 knots) at t = 0.00 ms (beginning of contact).

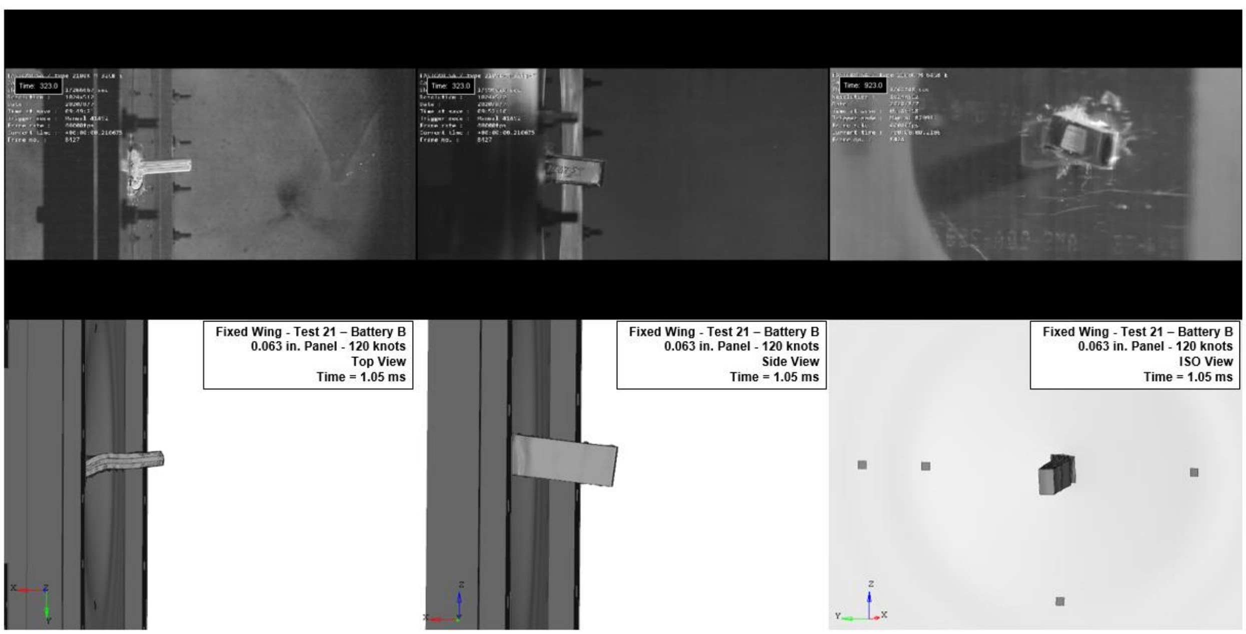


Figure 361. Comparison of battery B impact on 0.063” aluminum panel at 62.18 m/s (120.87 knots) at t = 1.05 ms.

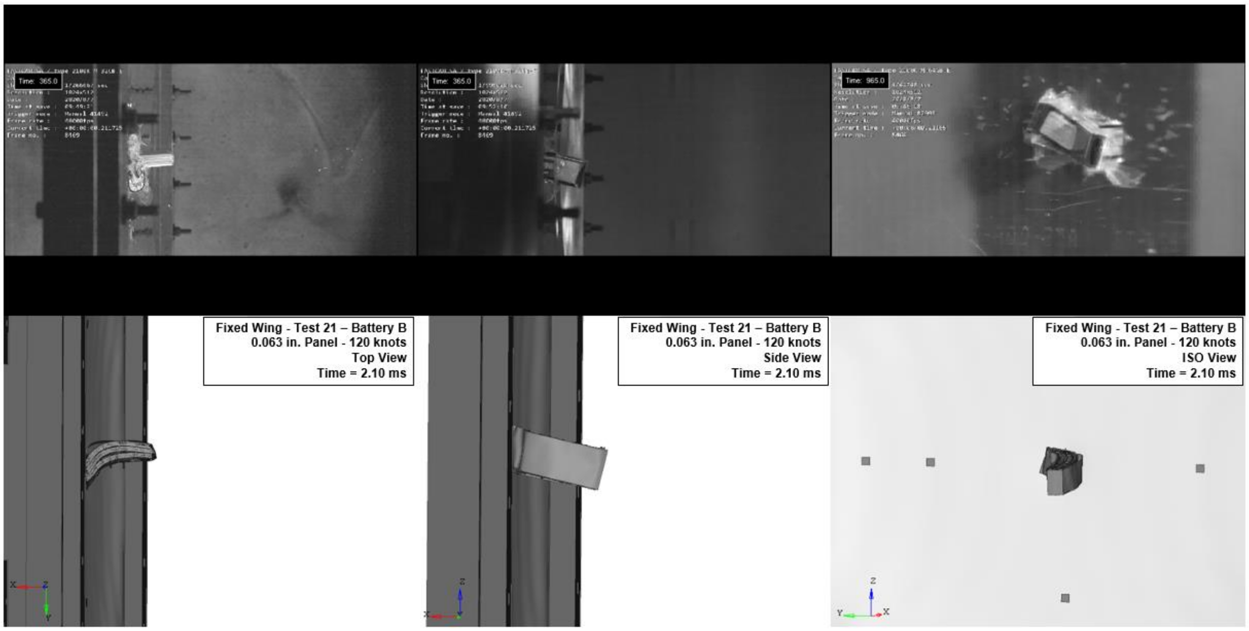


Figure 362 Comparison for battery B impact on 0.063" aluminum panel at 62.18 m/s (120.87 knots) at t = 2.10 ms.

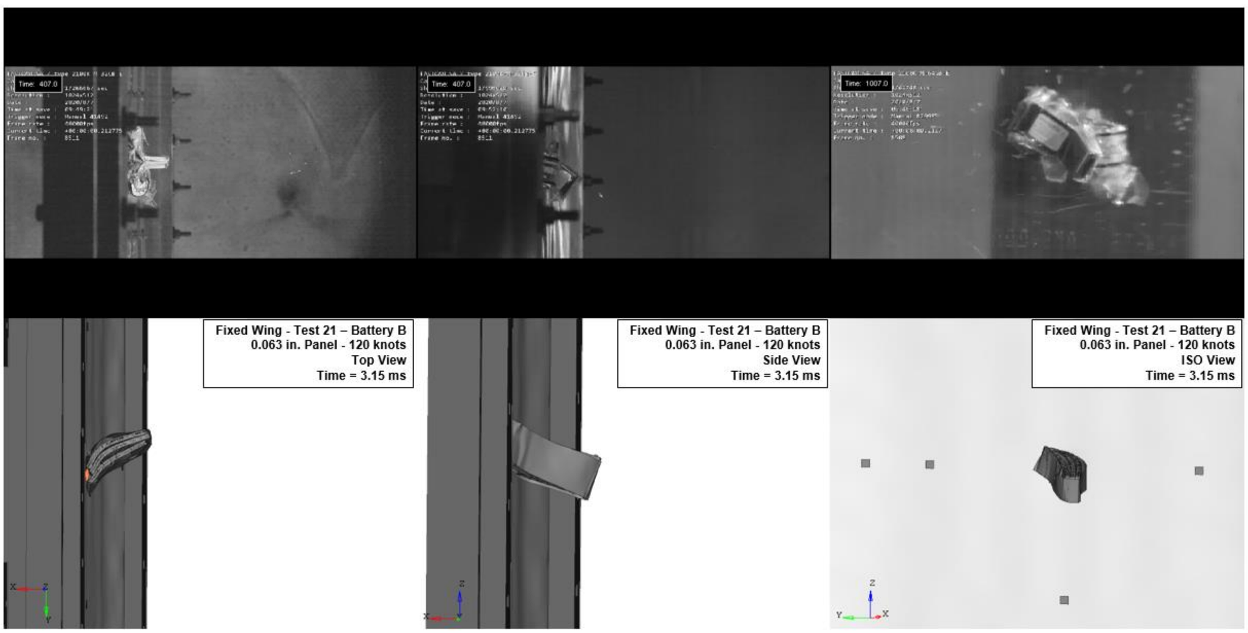


Figure 363 Comparison for battery B impact on 0.063" aluminum panel at 62.18 m/s (120.87 knots) at t = 3.15 ms (end of contact).

Figure 364 compares the simulation and test Y (horizontal) and Z (vertical) direction in-plane deformations and the out-of-plane displacements with a maximum displacement of the aluminum panel.

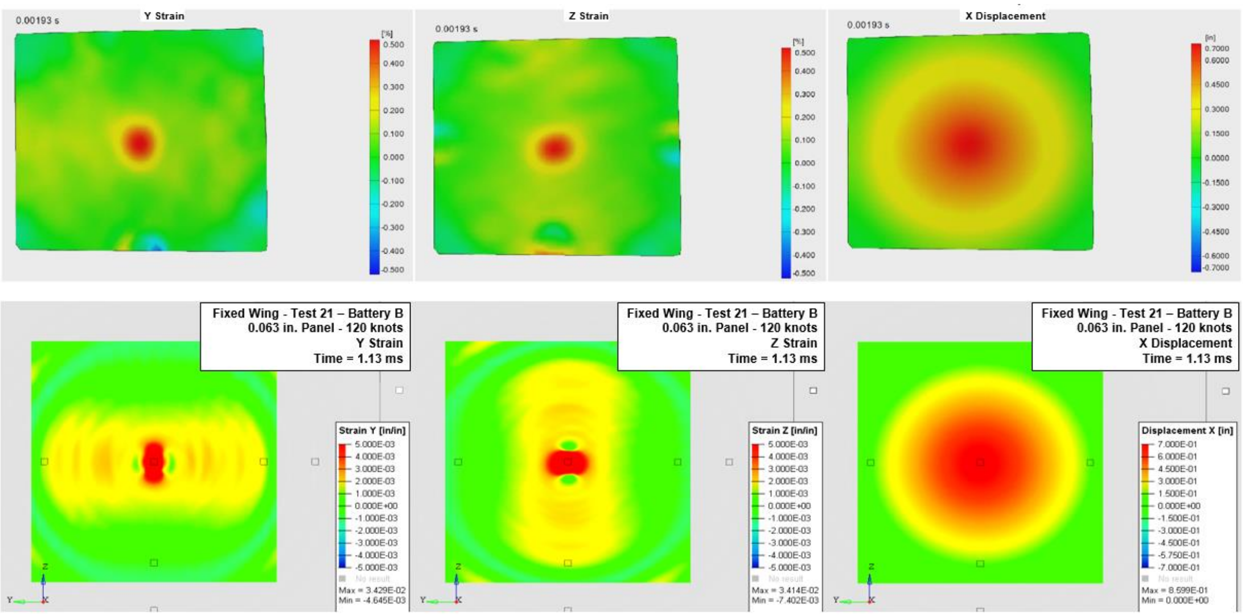

Figure 364. Comparison of test and simulation strains and displacements for battery B impact on 0.063” aluminum panel at 62.18 m/s (120.87 knots) at t = 1.50 ms (maximum displacement).

Figure 365 shows the out-of-plane displacement of the panel during the impact event obtained from the DIC data, and the simulation tracked displacements. The values on the vertical axis are not shown for confidential reasons.

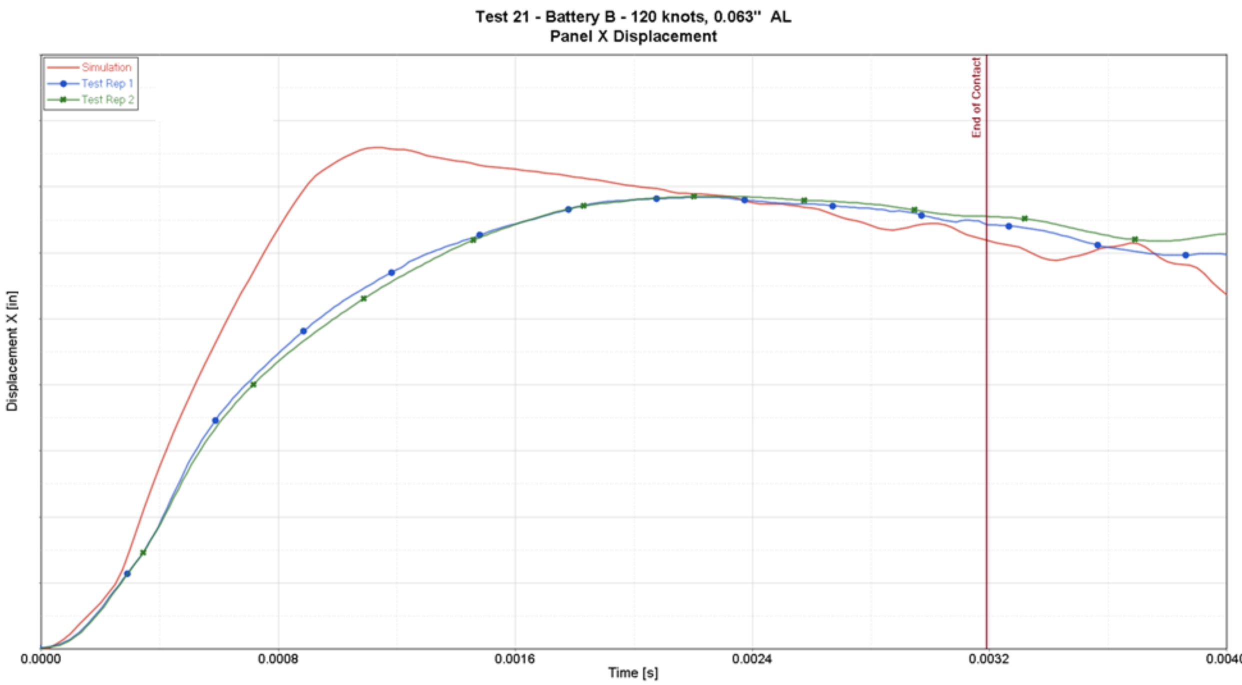


Figure 365. Comparison of the test and simulation out-of-plane displacements for battery B impact on 0.063” aluminum panel at 62.18 m/s (120.87 knots).

The physical panel was scanned after the test to compare the dimensions of the damaged area. Figure 366 compares the panel's damaged area dimensions for the test and simulation. Again, there is good agreement between the physical test and the predicted panel's damaged area.

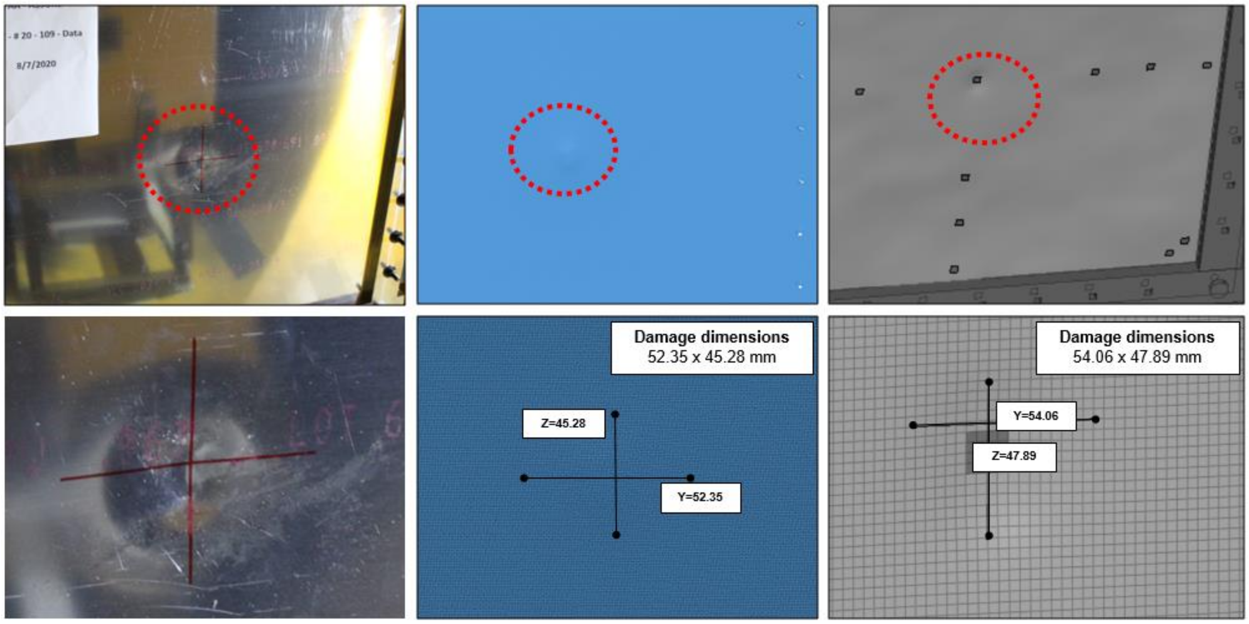


Figure 366. Comparison of the final damage of the panel for the test (left), scan (middle), and simulation (right) for battery B impact on 0.063" aluminum panel at 62.18 m/s (120.87 knots).

Figure 367 compares the physical and simulation projectile damage. The battery left an indentation on the physical test and simulation panel. Although the cells stayed attached, the test post-impact image shows damage to the plastic wrap and battery cells. Again, this is well captured by the FEM.

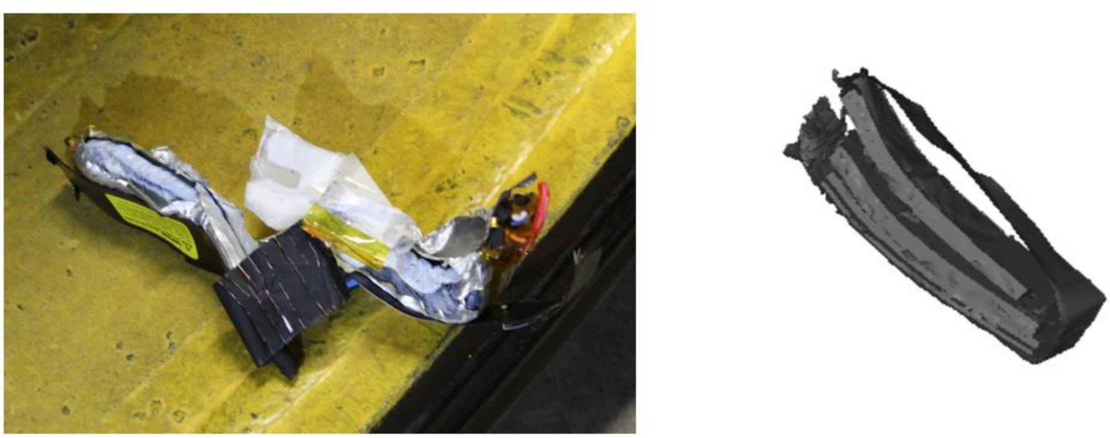

Figure 367. Comparison of the test (left) and simulation (right) projectile damage for battery B impact on 0.063" aluminum panel at 62.18 m/s (120.87 knots).

Figure 368 compares the load-time history of both test repetitions and the simulation load output. All the curves were filtered with a low-pass filter of 15,000 Hz. The load data shows good repeatability for both tests. The simulation captures the bottom load readings well and the top ones up to the end of the contact, marked with an asymptote. The values on the vertical axis are not shown for confidential reasons.

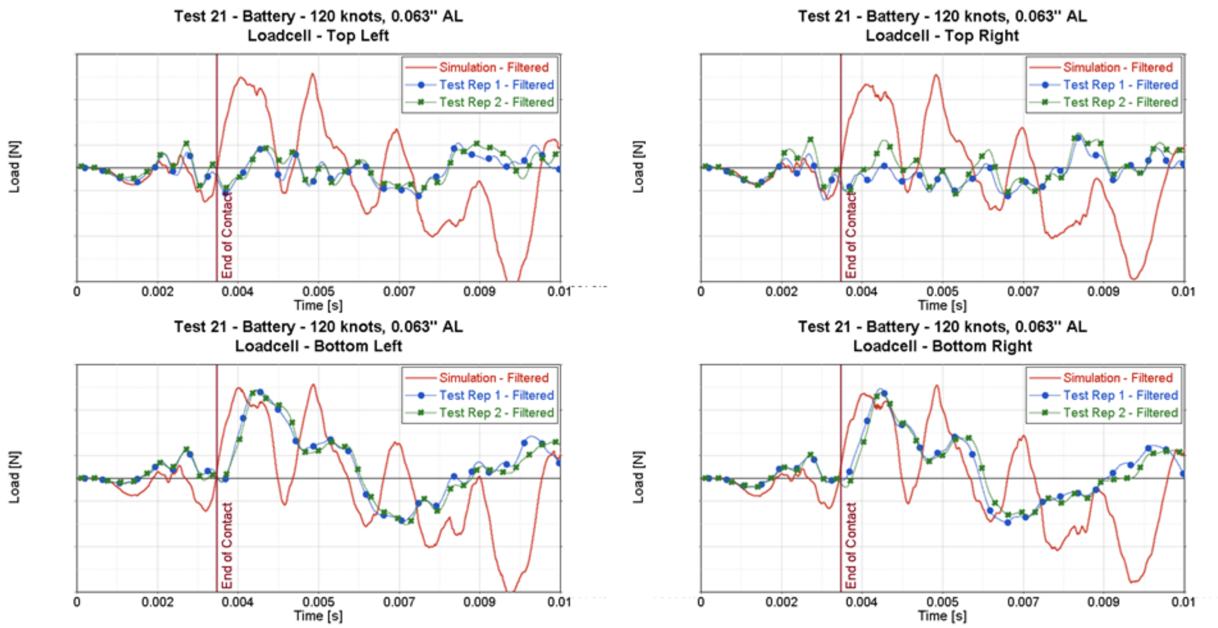


Figure 368. Load cell history data validation for battery B impact on 0.063” aluminum panel at 62.18 m/s (120.87 knots)

Figure 369 compares the strain data collected at both repetitions to the simulation strains. The FEM strains correlate to the test strain gages history data. The values on the vertical axis are not shown for confidential reasons.

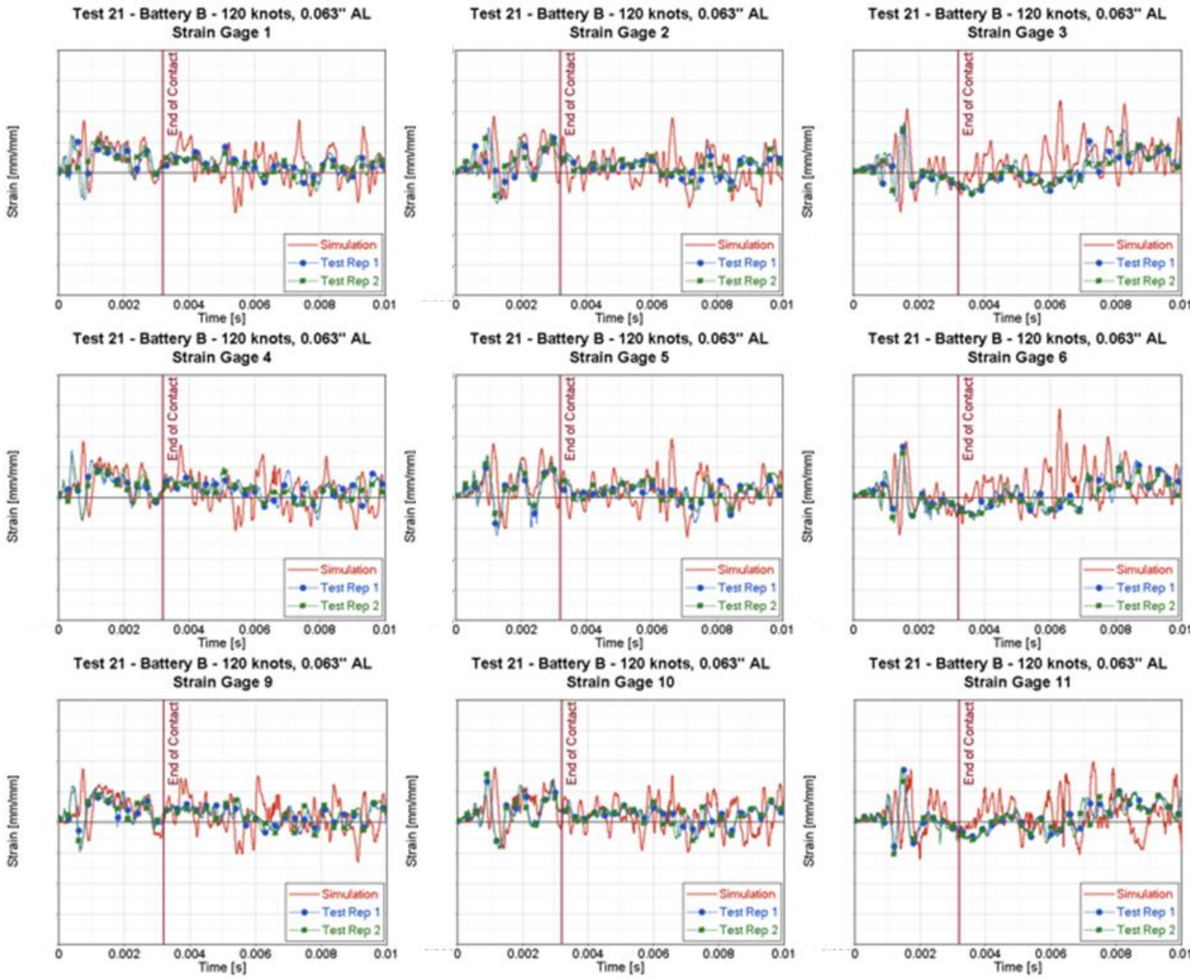


Figure 369. Strain comparison of strain gages 1-6 and 9-11 for battery B impact on 0.063” aluminum panel at 62.18 m/s (120.87 knots).

## A.22 TEST 22 – MOTOR AT 50 KNOTS – 1.6 MM AL PANEL

Test 22 consists of the impact of motor B with the 1.6 mm (0.063″) aluminum panel at a nominal velocity of 25.7 m/s (50 knots). Two iterations were carried out to evaluate data repeatability. For kinematics comparison, NIAR has identified iteration 1 as the repetition with the least deviation regarding the nominal test requirements.

An initial velocity of 25.21 m/s (49.0 knots) was applied to the motor B FEM, corresponding to the velocity recorded for repetition 2 in the test documentation (APPENDIX B).

Figure 370 through Figure 373 show the comparison of the kinematics between the test and simulation at four different instances of the impact event.

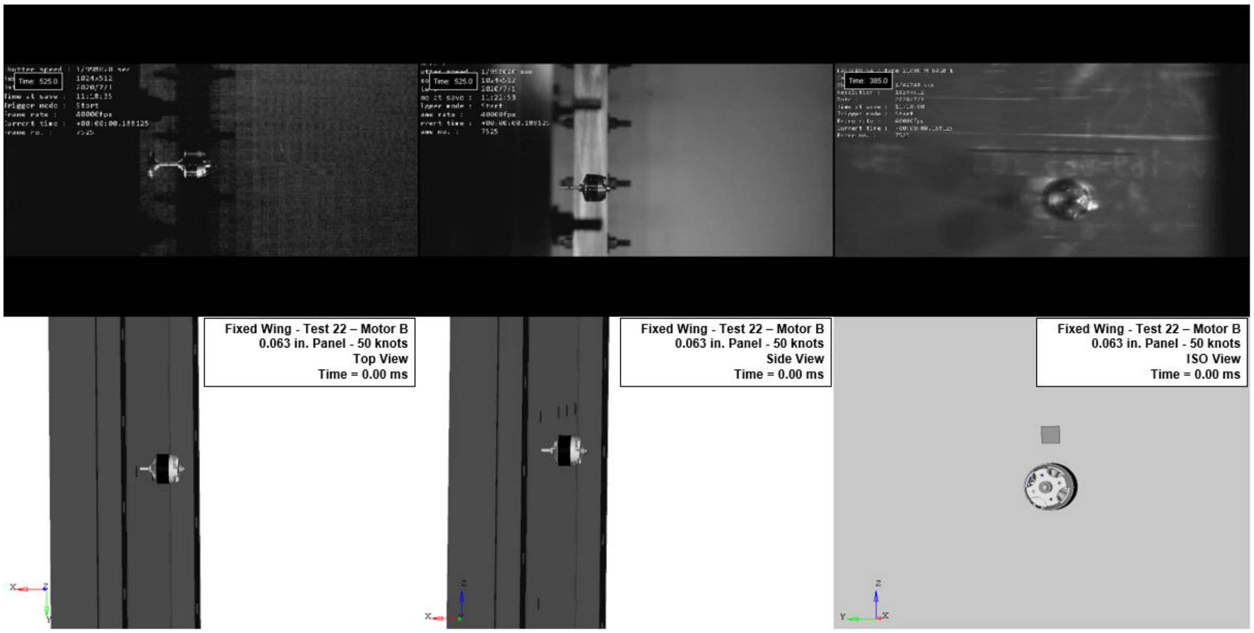


Figure 370. Comparison for motor B impact on 0.063” aluminum panel at 25.21 m/s (49.0 knots) at t = 0.00 ms (beginning of contact).

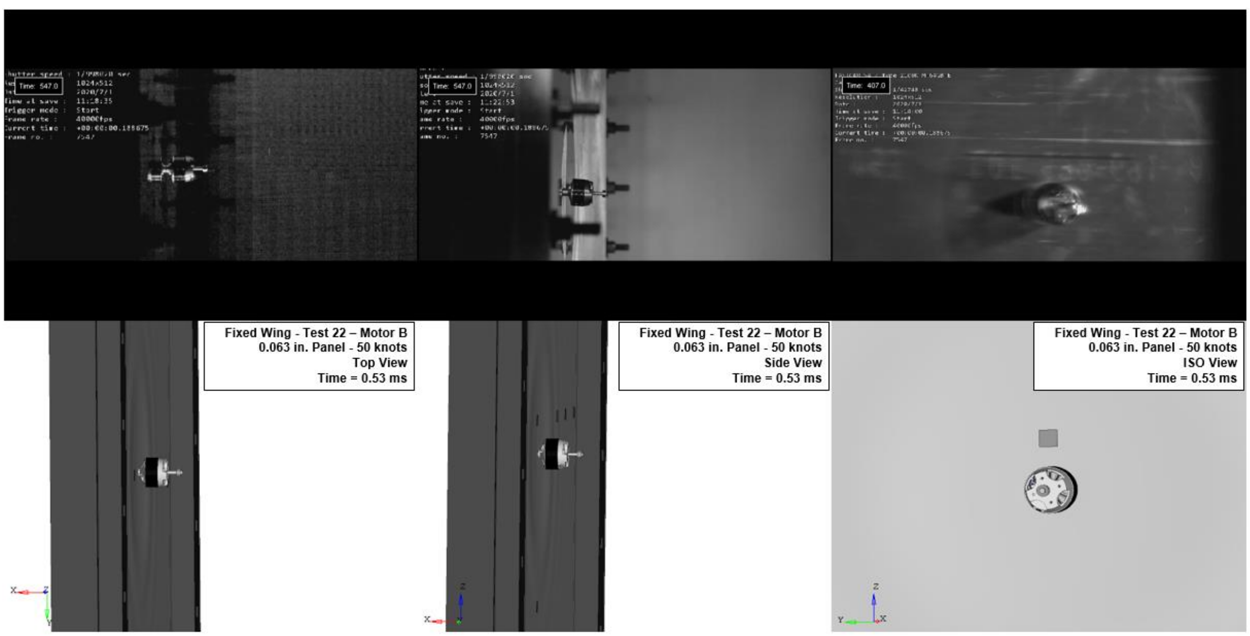


Figure 371. Comparison for motor B impact on 0.063” aluminum panel at 25.21 m/s (49.0 knots) at t = 0.53 ms (panel failure).

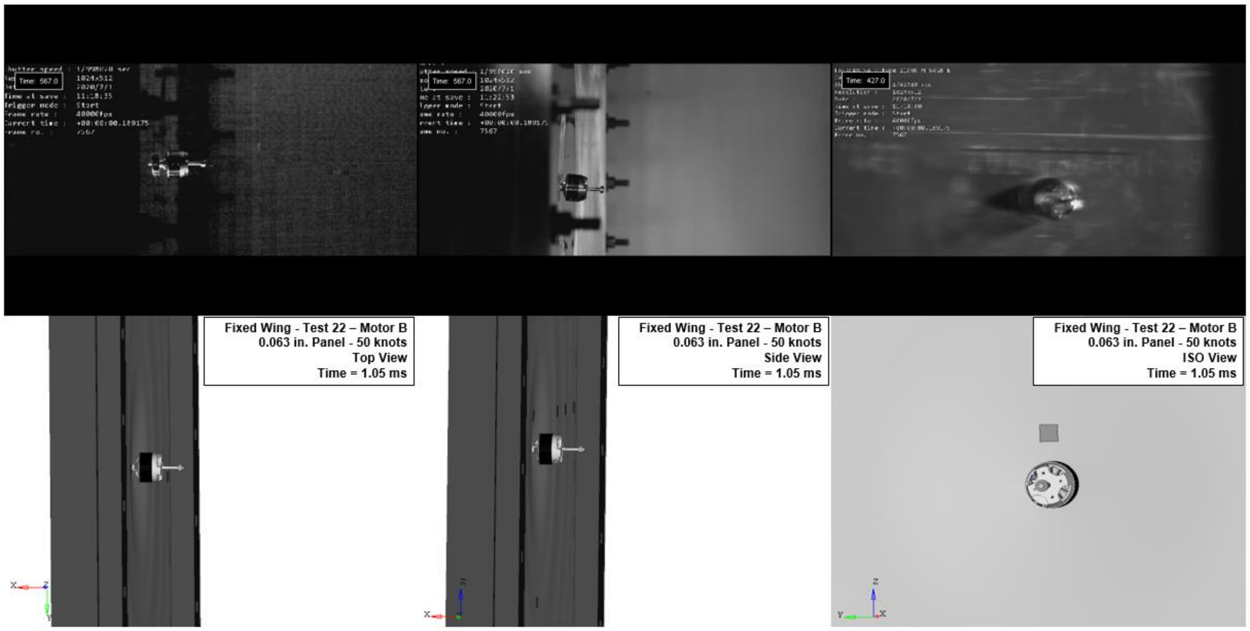


Figure 372 Comparison for motor B impact on 0.063” aluminum panel at 25.21 m/s (49.0 knots) at t = 1.05 ms.

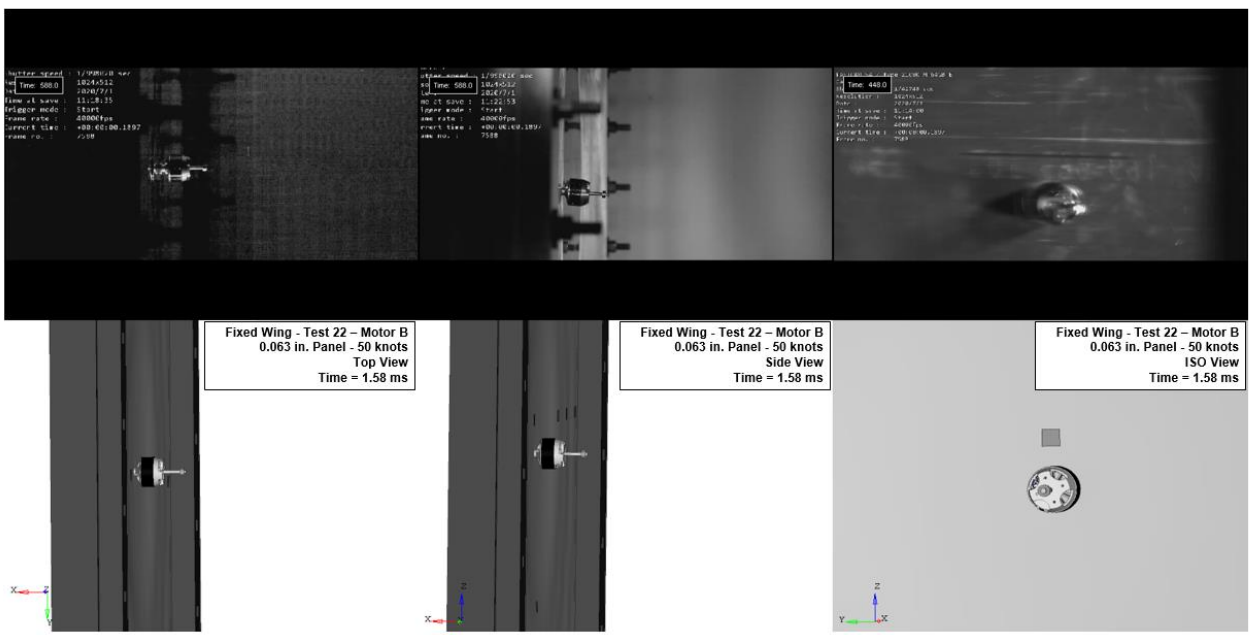


Figure 373 Comparison for motor B impact on 0.063” aluminum panel at 25.21 m/s (49.0 knots) at t = 1.58 ms (end of contact).

Figure 374 compares the simulation and test Y (horizontal) and Z (vertical) direction in-plane deformations and the out-of-plane displacements with a maximum displacement of the aluminum panel.

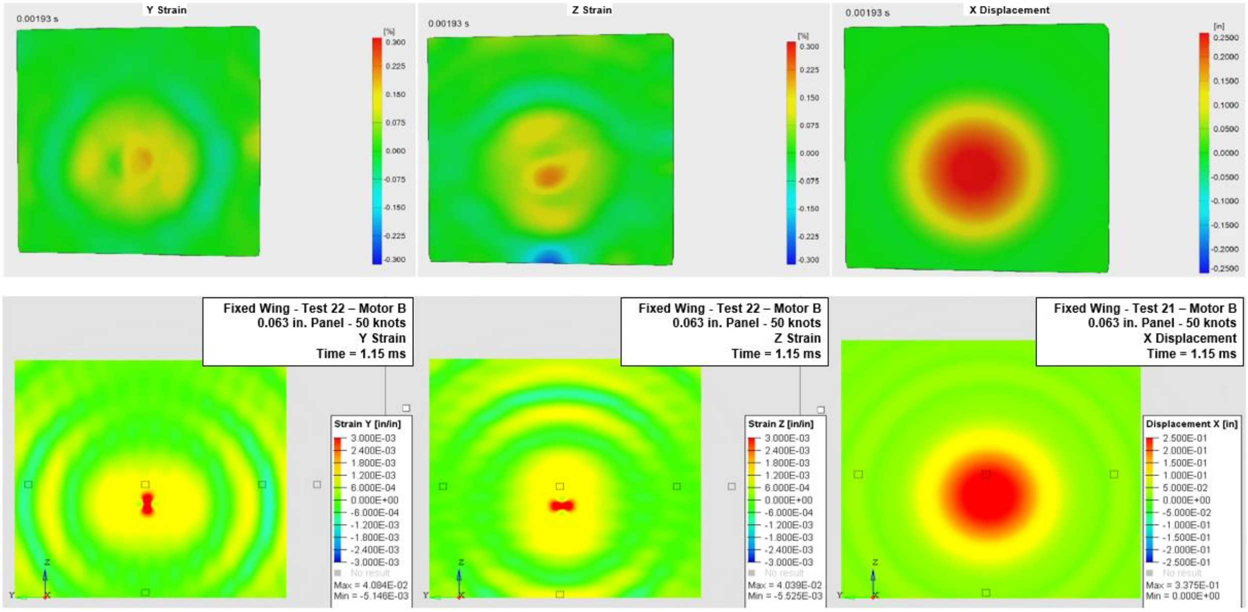


Figure 374. Comparison of test and simulation strains and displacements for motor B impact on 0.063” aluminum panel at 25.21 m/s (49.0 knots) at t = 1.50 ms (maximum displacement).

Figure 375 shows the out-of-plane displacement of the panel during the impact event obtained from the DIC data, and the simulation tracked displacements. The values on the vertical axis are not shown for confidential reasons.

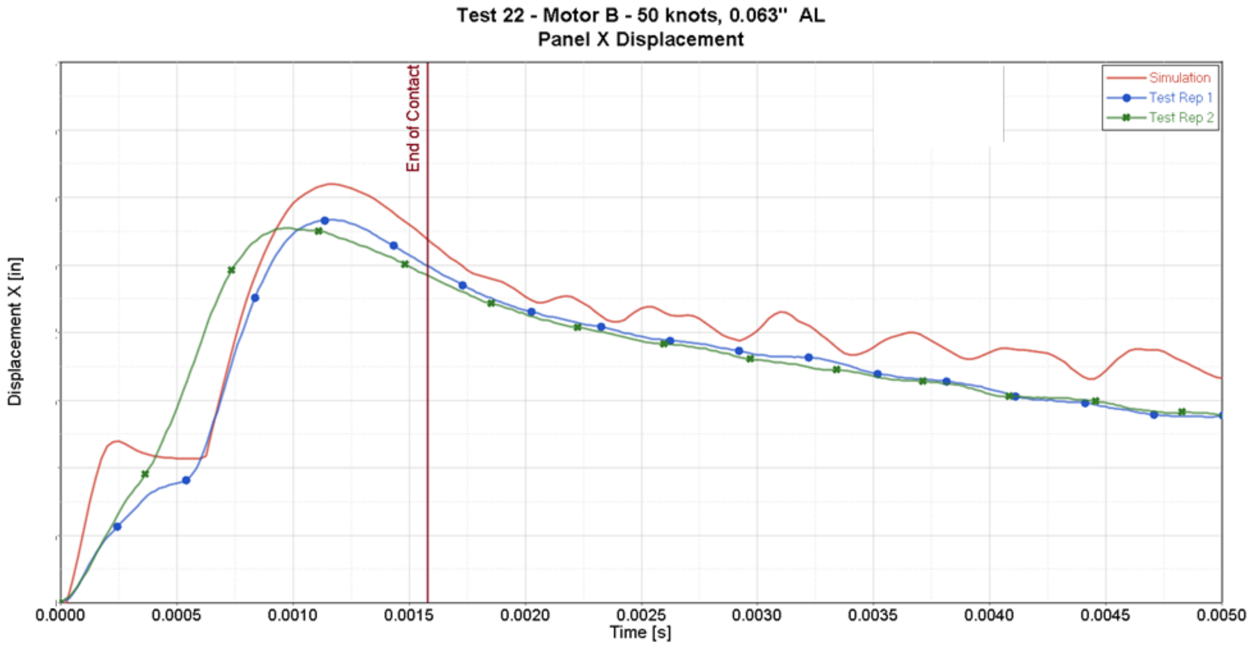


Figure 375. Comparison of the test and simulation out-of-plane displacements for motor B impact on 0.063” aluminum panel at 25.21 m/s (49.0 knots).

The physical panel was scanned after the test to compare the dimensions of the damaged area. Figure 376 compares the panel's damaged area dimensions for the test and simulation. Again, there is good agreement between the physical test and the predicted panel's damaged area.

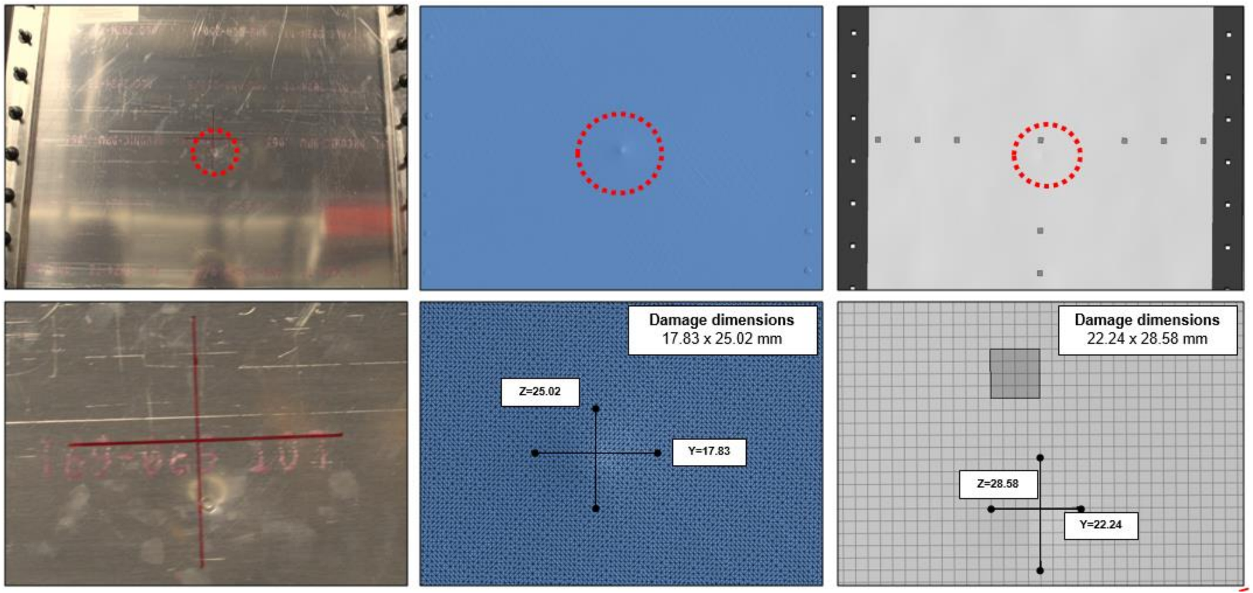


Figure 376. Comparison of the final damage of the panel for the test (left), scan (middle), and simulation (right) for motor B impact on 0.063" aluminum panel at 25.21 m/s (49.0 knots).

Figure 377 compares the physical and simulation projectile damage. For both physical tests and simulation, the motor sustained minimal damage.

Figure 377. Comparison of the test (left) and simulation (right) projectile damage for motor B impact on 0.063" aluminum panel at 25.21 m/s (49.0 knots)

Figure 378 compares the load-time history of both test repetitions and the simulation load output. Again, all the curves were filtered with a low-pass filter of 15,000 Hz. Again, the load data shows good repeatability for tests and simulation and confirms the good correlation of the FEM. The values on the vertical axis are not shown for confidential reasons.

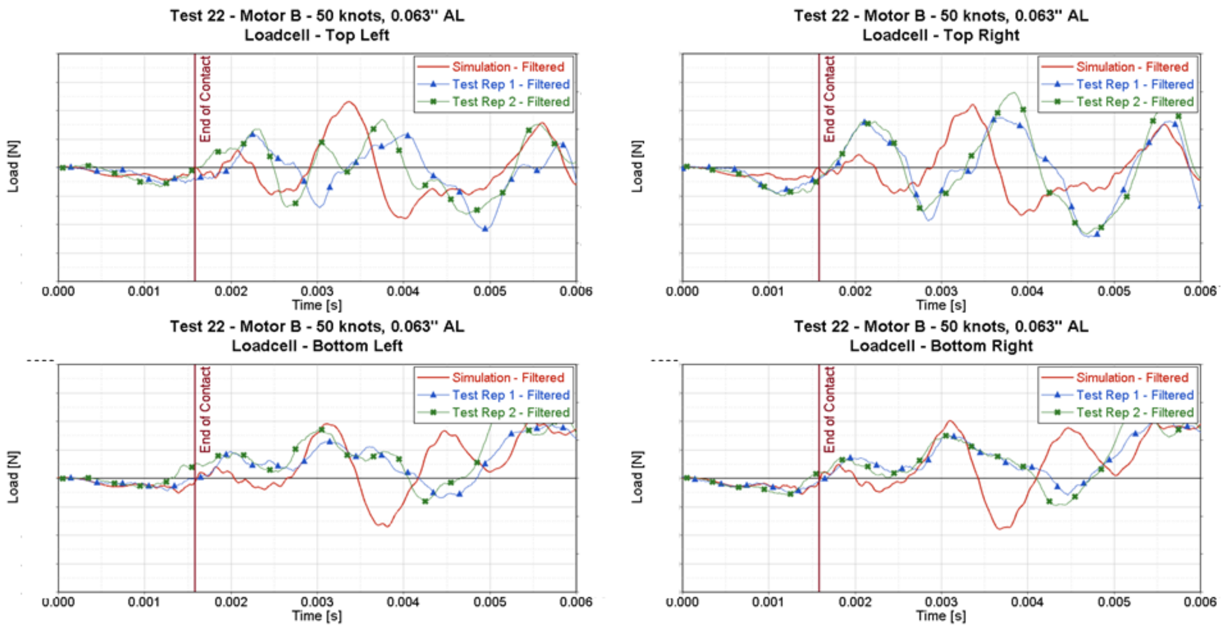


Figure 378. Load cell history data validation for motor B impact on 0.063" aluminum panel at 25.21 m/s (49.0 knots).

Figure 379 compares the strain data collected at both test iterations to the simulation strains. The FEM shows a good correlation to the test strain gages history data. For strain gage 4 in iteration 2, no data was available, and it has been shown as non-available (N/A). The values on the vertical axis are not shown for confidential reasons.

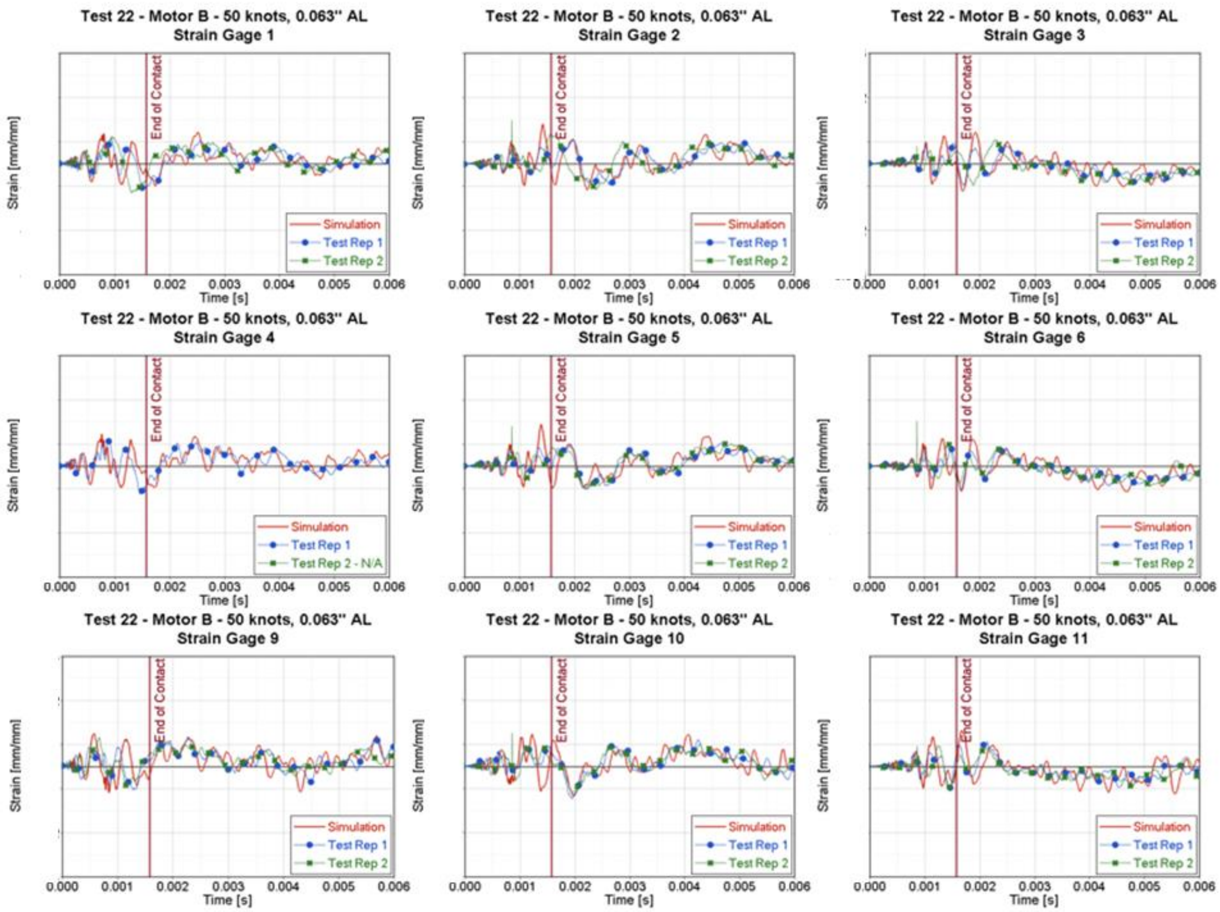


Figure 379. Strain comparison of strain gages 1-6 and 9-11 for motor B impact on 0.063" aluminum panel at 25.21 m/s (49.0 knots).

## A.23 TEST 22 – MOTOR AT 120 KNOTS – 1.6 MM AL PANEL

Test 23 consists of the impact of motor B with the 1.6 mm (0.063″) aluminum panel at a nominal velocity of 61.7 m/s (120 knots). Two iterations were carried out to evaluate data repeatability. For kinematics comparison, NIAR has identified iteration 1 as the repetition with the least deviation regarding the nominal test requirements.

An initial velocity of 63.28 m/s (123.0 knots) was applied to the motor B FEM, corresponding to the velocity recorded for repetition 1 in the test documentation (APPENDIX B).

Figure 380 through Figure 383 show the comparison of the kinematics between the test and simulation at four different instances of the impact event.

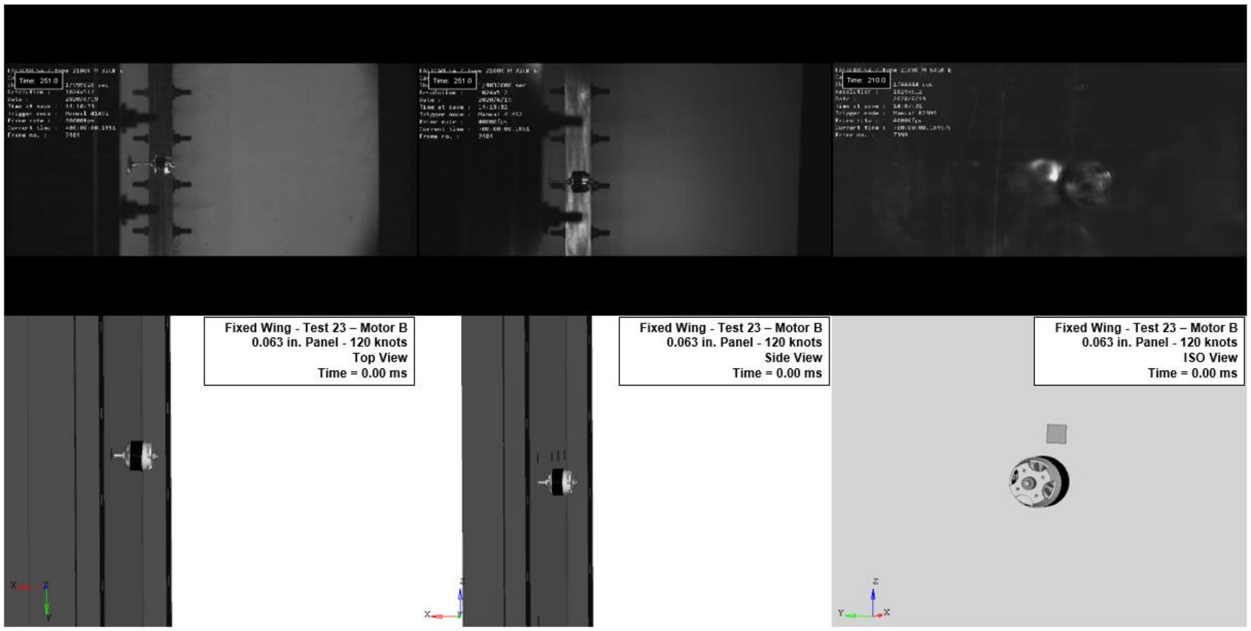


Figure 380. Comparison for motor B impact on 0.063” aluminum panel at 63.28 m/s (123.0 knots) at t = 0.00 ms (beginning of contact).

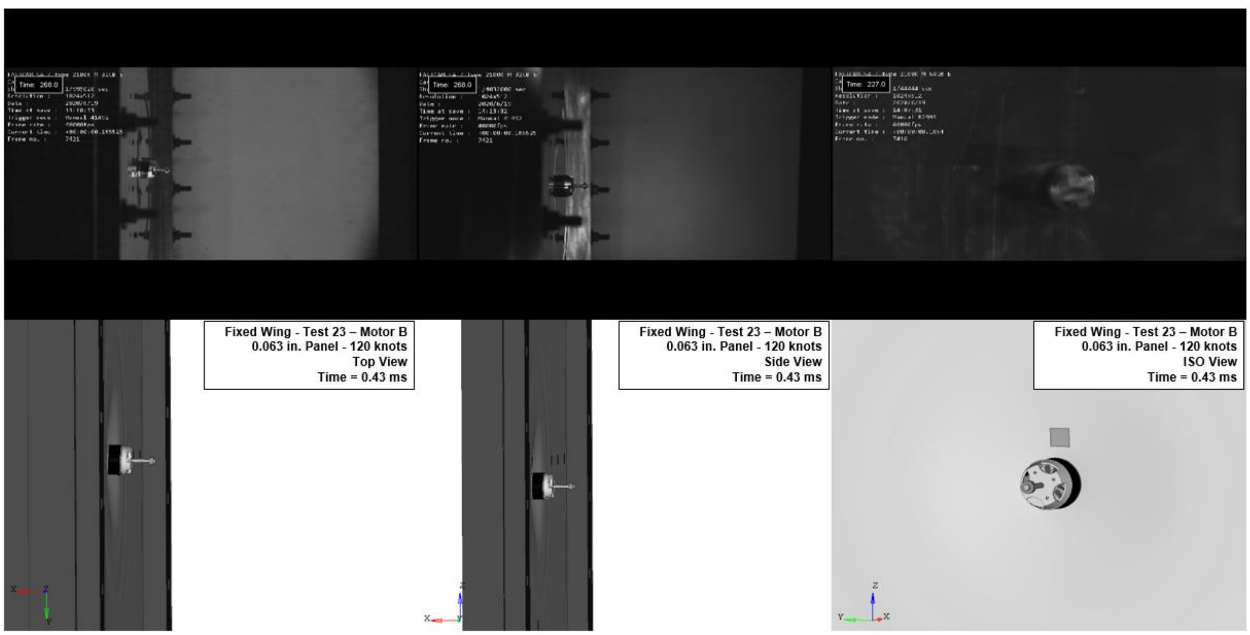


Figure 381. Comparison for motor B impact on 0.063” aluminum panel at 63.28 m/s (123.0 knots) at t = 0.43 ms (panel failure).

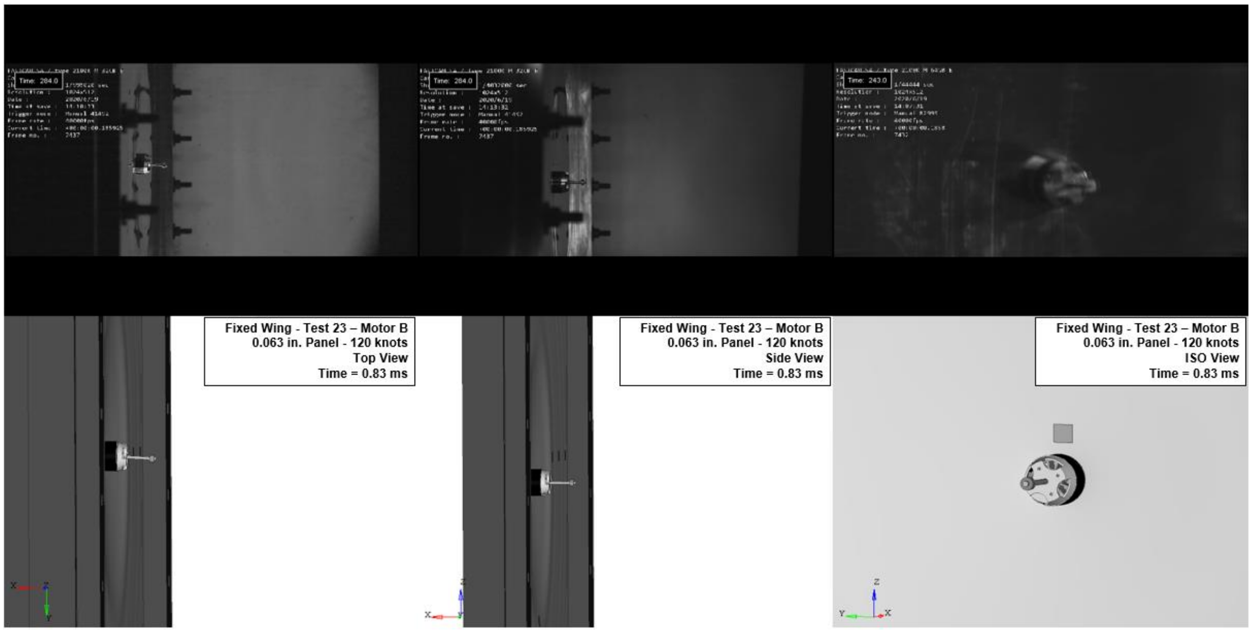


Figure 382 Comparison for motor B impact on 0.063” aluminum panel at 63.28 m/s (123.0 knots) at t = 0.83 ms.

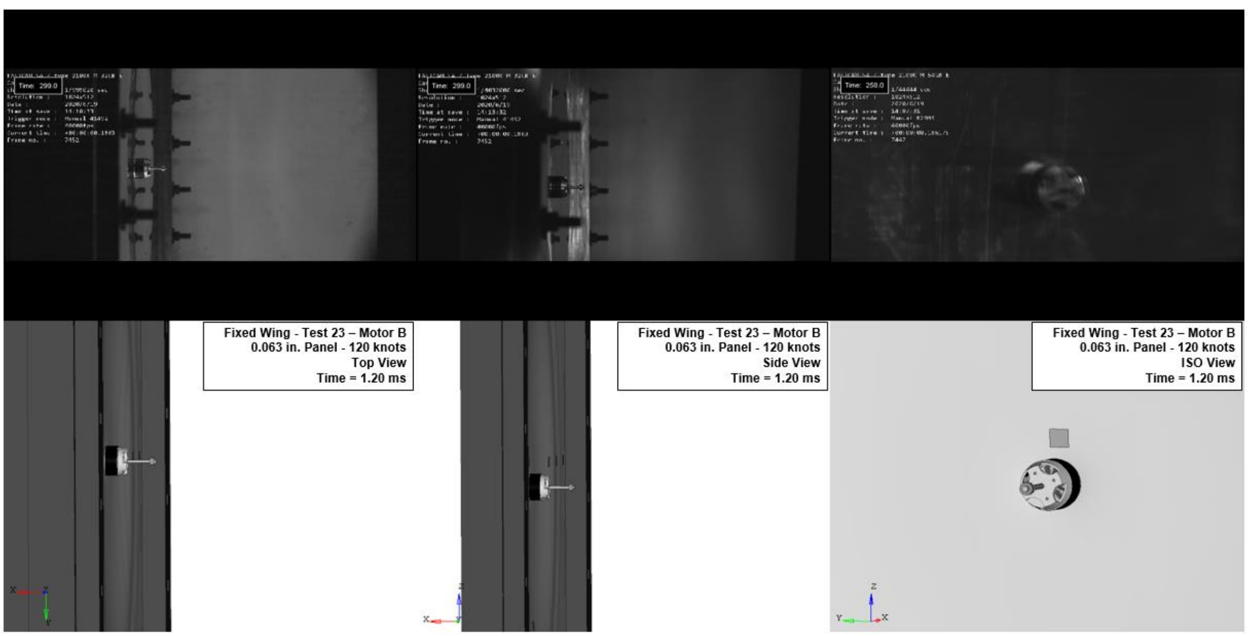


Figure 383 Comparison for motor B impact on 0.063” aluminum panel at 63.28 m/s (123.0 knots) at t = 1.20 ms (end of contact).

Figure 384 compares the simulation and test Y (horizontal) and Z (vertical) direction in-plane deformations and the out-of-plane displacements, for instance, with the aluminum panel's maximum displacement.

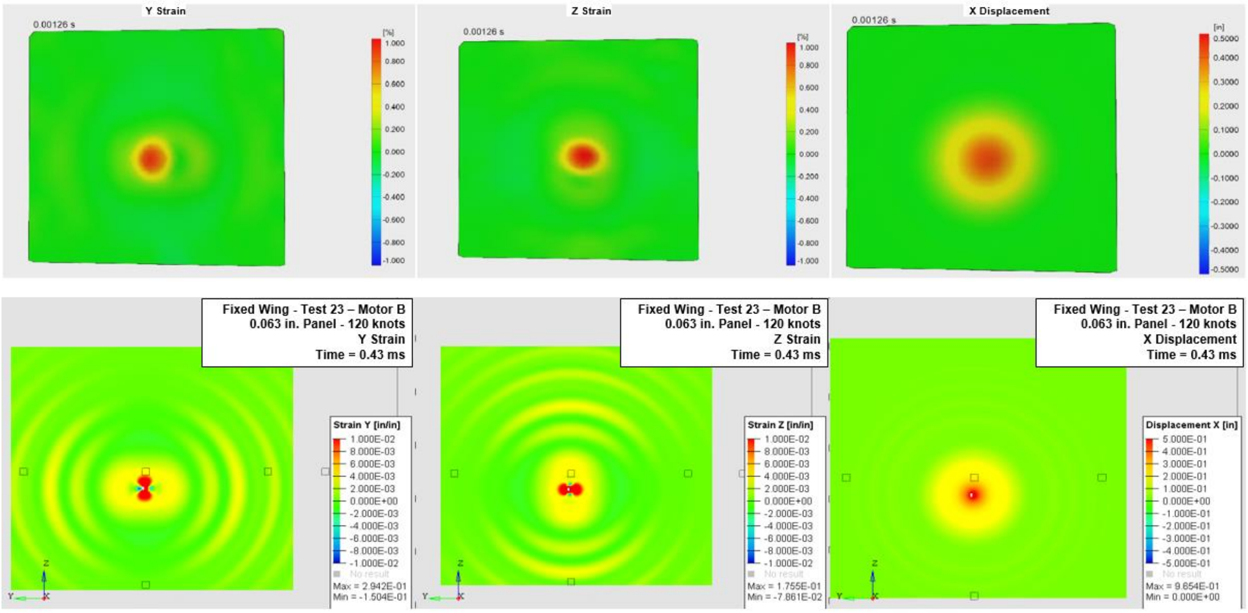


Figure 384. Comparison of test and simulation strains and displacements for motor B impact on 0.063" aluminum panel at 63.28 m/s (123.0 knots) at t = 1.50 ms (maximum displacement).

Figure 385 shows the out-of-plane displacement of the panel during the impact event obtained from the DIC data, and the simulation tracked displacements. The values on the vertical axis are not shown for confidential reasons.

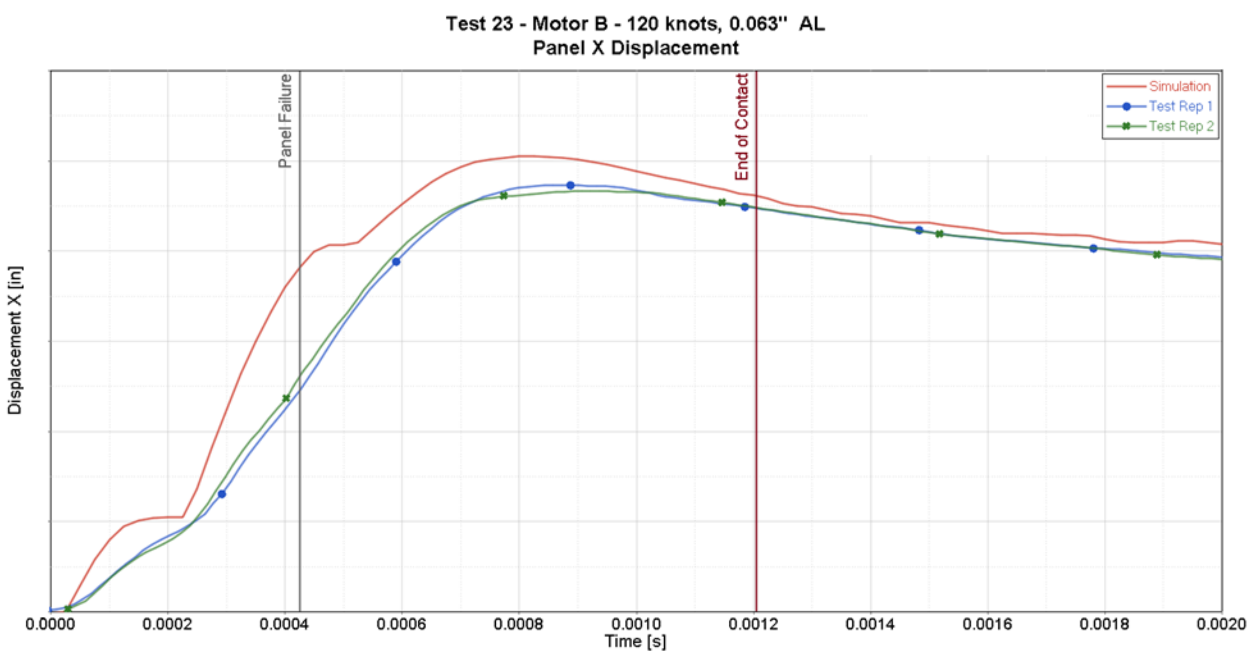


Figure 385. Comparison of the test and simulation out-of-plane displacements for motor B impact on 0.063" aluminum panel at 63.28 m/s (123.0 knots).

The physical panel was scanned after the test to compare the dimensions of the damaged area. Figure 386 compares the panel's damaged area dimensions for the test and simulation. Again, there is good agreement between the physical test and the predicted panel's damaged area.

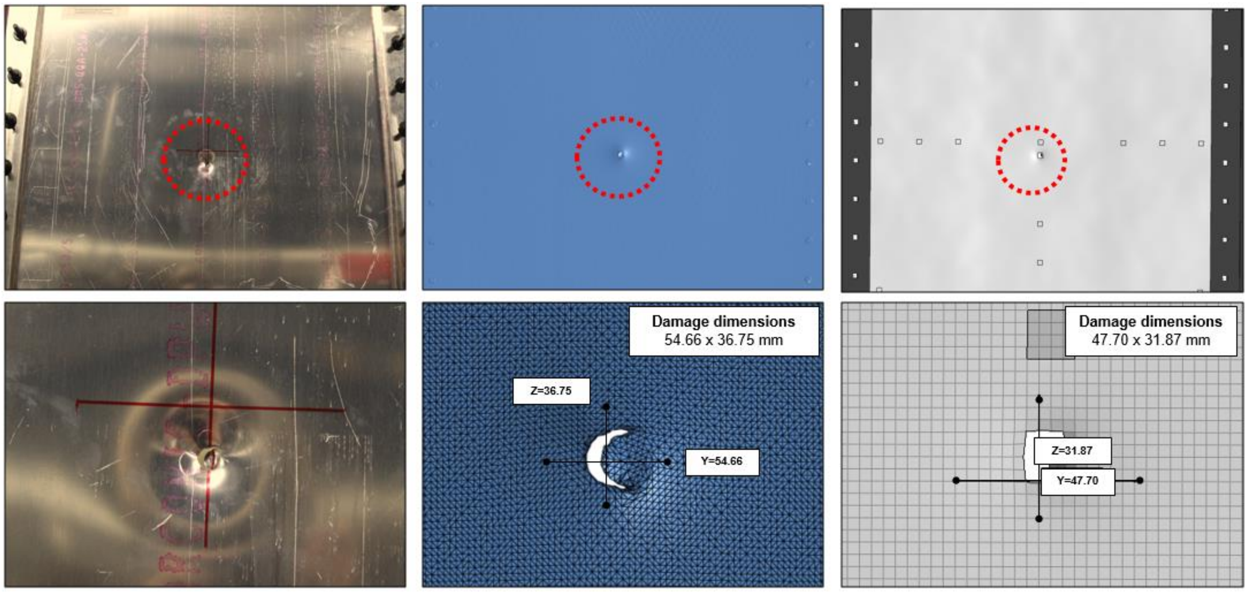


Figure 386. Comparison of the final damage of the panel for the test (left), scan (middle), and simulation (right) for motor B impact on 0.063" aluminum panel at 63.28 m/s (123.0 knots).

Figure 387 compares the physical and simulation projectile damage. For both physical test and simulation, the motor caused the panel's failure but did not go through it. However, the motor sustained minor damage, and the motor B FEM is well captured.

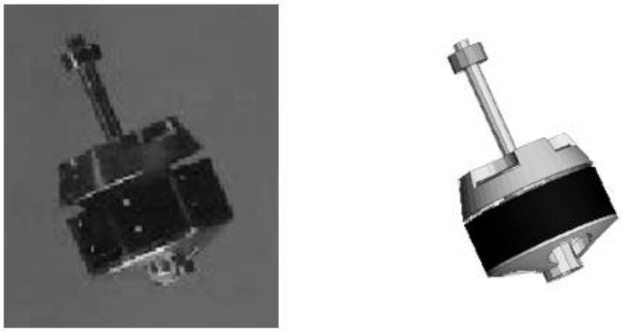

Figure 387. Comparison of the test (left) and simulation (right) projectile damage for motor B impact on 0.063" aluminum panel at 63.28 m/s (123.0 knots).

Figure 388 compares the load-time history of both test repetitions and the simulation load output. All the curves were filtered with a low-pass filter of 15,000 Hz. The load data shows good repeatability for test and simulation and confirms the good correlation up to the end of the contact, marked with an asymptote. However, the post-impact oscillations of the panel deviate from those of the physical test. The values on the vertical axis are not shown for confidential reasons.

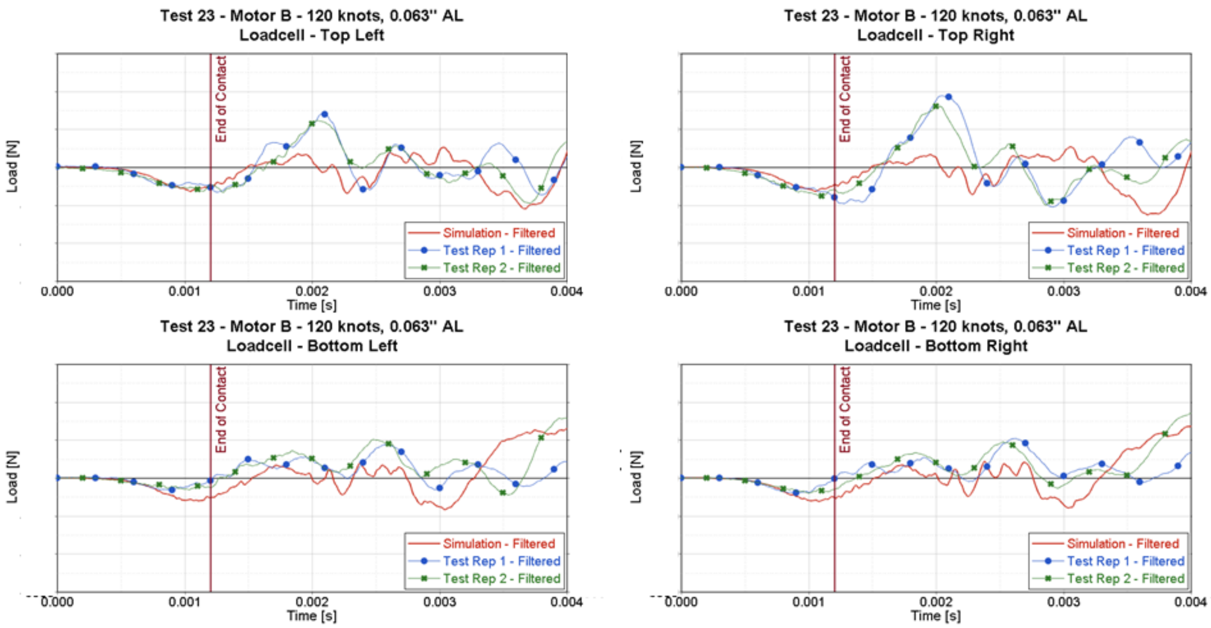


Figure 388. Load cell history data validation for motor B impact on 0.063” aluminum panel at 63.28 m/s (123.0 knots).

Figure 389 compares the strain data collected at both repetitions to the simulation strains. Again, there is a good correlation to the test strain gages history data. The values on the vertical axis are not shown for confidential reasons.

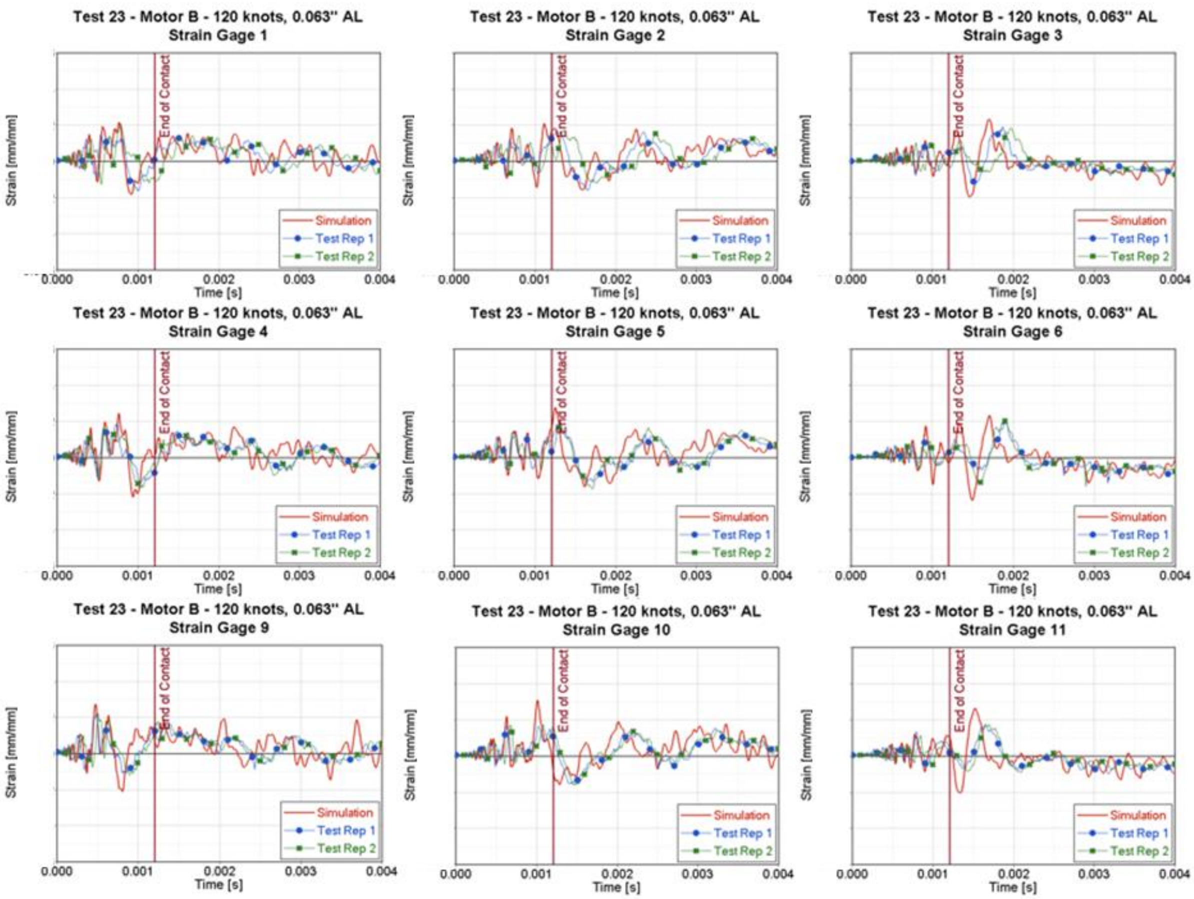


Figure 389. Strain comparison of strain gages 1-6 and 9-11 for motor B impact on 0.063" aluminum panel at 63.28 m/s (123.0 knots).

**DOT/FAA/AR-xx/xx**

Federal Aviation Administration
William J. Hughes Technical Center
Aviation Research Division
Atlantic City International Airport
New Jersey 08405

The FAA's Center of Excellence for UAS Research
ASSURE
Alliance for System Safety of UAS through Research Excellence

# Annex A to Task A16: Airborne Collision Severity Evaluation – Rotary Wing Structural Impact Test Report

4-1-2022

Final Report



U.S. Department of Transportation
**Federal Aviation Administration**

**NOTICE**

This report is available at the Federal Aviation Administration William J. Hughes Technical Center's Full-Text Technical Reports page: actlibrary.tc.faa.gov in Adobe Acrobat portable document format (PDF).

**Legal Disclaimer:** The information provided herein may include content supplied by third parties. Although the data and information contained herein has been produced or processed from sources believed to be reliable, the Federal Aviation Administration makes no warranty, expressed or implied, regarding the accuracy, adequacy, completeness, legality, reliability or usefulness of any information, conclusions or recommendations provided herein. Distribution of the information contained herein does not constitute an endorsement or warranty of the data or information provided herein by the Federal Aviation Administration or the U.S. Department of Transportation. Neither the Federal Aviation Administration nor the U.S. Department of Transportation shall be held liable for any improper or incorrect use of the information contained herein and assumes no responsibility for anyone's use of the information. The Federal Aviation Administration and U.S. Department of Transportation shall not be liable for any claim for any loss, harm, or other damages arising from access to or use of data or information, including without limitation any direct, indirect, incidental, exemplary, special or consequential damages, even if advised of the possibility of such damages. The Federal Aviation Administration shall not be liable to anyone for any decision made or action taken, or not taken, in reliance on the information contained herein.

## B.1 SCOPE

### B.1.1 Research Tasks

The University of Alabama in Huntsville's (UAH) role in the Task A16 project was divided into the following tasks occurring over a 46-month Period of Performance:

Task #2: Evaluate the severity of small Uncrewed Aircraft System (sUAS) collisions with Rotorcraft (WSU, UAH, MSU)

The Objective of Working Package 2 was to identify the damage severity of sUAS with Part 27 rotorcraft that typically operate at low altitudes. This task incorporated analyzing high-speed impacts of sUAS projectiles on target rotorcraft components to develop a rotorcraft crashworthiness evaluation standard. This task was sub-divided into 6 phases with UAH contributions in each phase except the fourth phase. UAH conducted a survey of registered Part 27 aircraft in the US that was used to determine the aircraft models in this category that were mostly likely to be impacted by a sUAS based on their higher numbers in the national airspace system. UAH conducted high-speed impacts of sUAS components testing on target specimens (aluminum panels and aluminum plates machined to represent an airfoil leading edge) and full sUAS impacts on rotorcraft windshields, blades, rotors and tail structures. It also supported NIAR-WSU in defining sUAS projectiles and target definitions and in developing of a calibrated, validated sUAS model. The report includes information related to both component-level impact testing and full sUAS impact testing.

### B.1.2 Research Questions.

The proposed research was intended to answer the following research questions and any related questions that may be developed through the research process:

Task A#2:

a) What are the hazard severity criteria for a sUAS collision (mass, kinetic energy, etc.)?
b) What is the severity of a sUAS collision with a rotorcraft in mid-air?
c) Can the severity of a sUAS mid-air collision with a rotorcraft be characterized into categories based on the sUAS? What would those categories look like?
d) Can a sUAS impact be classified similar to a bird strike?
e) What are the characteristics of a sUAS where it will not be a risk to an aircraft?

Task A: Assumptions and Limitations. The research will assume the following operating limitations:

a) The rotorcraft structure will be representative but not specific of any current rotorcraft system.
b) The blade models will be representative of the structural properties of a current rotorcraft, but not the aerodynamic features.
c) Material models used for any of the structural components will be based on already developed material models.
d) Rotorcraft components used in testing are subject to availability based on donations, aftermarket component availability, or salvage part availability.

### B.1.3 Objectives

The goal of UAH's research was to conduct testing to estimate the severity of sUAS collision with rotorcraft components based on credible impact conditions. This research also identified how an sUAS impacts rotorcraft structures and if the damage caused could be separated in categories similar to what was developed during Task A.3.

During FAA ASSURE TASK A3 – Airborne Collision Severity Research, quadcopter and fixed-wing models were validated at lower speeds from 100 to 250 knots with blunt force impacts against thin aluminum plates that were representative of the skin of an airplane, as well as aluminum plates that represent a rigid impact structure. The research focused on large commercial aircraft and business jets, but sUAS mostly operate at lower altitudes and are a risk to law enforcement and emergency medical rotorcraft, which are typically less than 7,000 lbs or Part 27 Normal Category Rotorcraft. The impact speeds during a main rotor blade impact, for an aircraft at cruise speed, on the advancing side of the rotor are much higher, with an initial estimated speed of 500 knots, and a slicing impact as opposed to a blunt force impact. As a result, a series of flat panel and "slicing" tests were conducted at this speed range to evaluate and calibrate the numerical model performance of these components.

This was accomplished in two steps. First, UAH conducted impacts of sUAS components like motors, camera payload and batteries from 50 to 500 knots against flat aluminum panels, which are representative of rotorcraft skin, and against 'sharp blades', that are representative of rotorcraft blades. Second, UAH conducted impact tests by launching full sUAS (DJI Phantom 3s) at velocities between 50 to 430 knots at rotorcraft blades, windshields, a tail rotor blade, a horizontal tail, and the upper portion of an aircraft cowling. This work was intended to identify how an sUAS will impact rotorcraft structure and if the damage caused could be separated in categories similar to what was developed during Task A.3.

Table 22. Test, Test Conditions, and Test Outputs.

| Test | Test Conditions | Key Output(s) |
|---|---|---|
| **sUAS Components High-Speed Impacts with AL plates** | sUAS Battery, Motor, and Camera impacts at speed from 50-500 kts on 2024-T3 aluminum sheet panels (41"x41" and of thickness 0.063" and 0.25", respectively) and 2024-T3 aluminum sharp blades (36"x10" and of 0.125" thickness). | Damage Assessment, High Speed Videos, Strain and Load measurements, Still Images, 3D Scan Cloud Data, and Digital Image Correlation System outputs |
| **sUAS High-Speed Impacts with helicopter components** | DJI Phantom 3 sUAS, with camera and legs removed, impacted against bi-layer glass windscreens (50-290 kts), a tail rotor blade (385 kts), main rotor blade sections (425 kts), and a horizontal tail (170 kts) | Damage Assessment, High Speed Videos, Strain and Load measurements, and Still Images |

### B.1.4 Relation of UAH's Efforts with Other Universities on the Task A16 Team

UAH's impact testing and the resulting video, still images, Digital Image Correlation (DIC) system data, load cell signals, and strain gage signals were used by NIAR's modelers to calibrate aircraft component models. The component-level model calibration supported modeling full aircraft impacts by enabling a progressive buildup of the full aircraft model from its constituent parts. Full aircraft impact test data was used to enable calibration of helicopter component models.

## B.2 UAH IMPACT TESTS

### B.2.1 Tests Location

All tests were performed at the US Army Space and Missile Defense Command (SMDC) Aerophysics Research Facility (ARF) which is located on Redstone Arsenal. This facility operates three two-stage light gas gun systems. ARF Researchers designed and built two custom gas guns for FAA Tasks A16 and A17. The component testing was accomplished using a single-stage gun, and the full aircraft testing was conducted using a gun with potential to function as either a single or dual-stage gas gun, based on shot requirements. Table 23 provides examples of several existing dual and single-stage guns at the SMDC ARF.

Table 23. Representative ARF Gas Guns.

| UAH ARF Launcher Systems | Pump Tube Length | Pump Tube Inside Diameter | Launch Tube Length | Available Launch Tube Inside Diameters | Primary Impact Chamber | Projectile Launch Mass Range | Projectile Velocity Range |
|---|---|---|---|---|---|---|---|
| | (m) | (mm) | (m) | (mm) | Diam x Length (m) | (gm) | (km/sec) |
| Large | 38.13 | 254 | 22.88 | 56, 57, 68, 70, 75, 78, 86, 100, 152 | 3 x 12.5 | 150 - 12,000 | 1 - 7.5 |
| Intermediate | 18.3 | 133 | 15.25 | 18, 29, 35 | 2.4 x 6.7 | 40 - 250 | 1 - 7.5 |
| Small | 13.42 | 108 | 7.47 | 19, 29 | 1.8 x 4.3 | 10 - 130 | 1 - 7.5 |
| Single Stage | NA | NA | 9.9 | 19, 32, 90 | 2.4 x 6.7 | 5 - 30 | 0.1 – 1.1 |

## B.2.2 Test Apparatus

### B.2.2.1 SUAS COMPONENTS TEST GAS GUN SYSTEM

An existing single stage compressed gas gun was modified for accelerating the motor, camera, and battery components of the sUAS to the desired equivalent impact velocity. This gun utilized a 38 ft long, 90mm inside diameter barrel adapted to an impact test section configured with orthogonal and DIC system camera ports, a scrubber system for hazardous gas removal, cable feed throughs for load cell, strain gage, and lighting power cables, as shown in Figure 390. The full system consisted of a bulk gas manifold, which provides nitrogen or helium storage and supplies gas to the pressure reservoir. Between the bulk gas manifold and the reservoir was a gas pressure booster pump for pressurization of the reservoir. The gas pressure in the reservoir was directly proportional to the capacity of the gun system to do work on and accelerate a projectile in the barrel. The reservoir was connected to the barrel via an adapter and ball valve, as shown in Figure 391. The ball valve was used to discharge gas from the reservoir to the barrel and fire the projectile. While the magnitude of the pressure in the reservoir represents the maximum capability of the gun to accelerate a projectile, the timing or rate of opening the valve provides control over the rate of acceleration of the projectile. Based on the requirement to fire the sUAS battery which is significantly larger and heavier than the sUAS motor and camera, an alternate gas pressure reservoir and larger ball valve were installed in the system at the end of the component test period to accelerate the larger, heavier, and more compliant batteries and mitigate battery deformation. The barrel was mounted and aligned on a heavy I-beam structure using adjustable stanchions. Stanchions mounted on the I-beam to support the barrel enabled barrel alignment and have roller interfaces with the barrel that allow for barrel movement up and down range to adjust the projectile and sabot fly-out distance. Fly-out distance, in conjunction with projectile velocity and sabot design, was critical to provide enough flight time for air loads to separate the sabot from the projectile in flight. Based on the wide range of projectile velocities that were used in the study, the ARF personnel used both reservoir pressure and breach position of the projectile to control muzzle velocity. Breach position of the projectile refers to its location within the barrel prior to firing. The barrel was connected to the reservoir and extends through a port into the impact tank (Figure 392). The barrel was aligned with the desired impact point for the projectile on the intended target using the adjustable stanchions. Figure 393 and Figure 394 show the Task A16 component targets were mounted to a support frame using a stainless-steel frame.

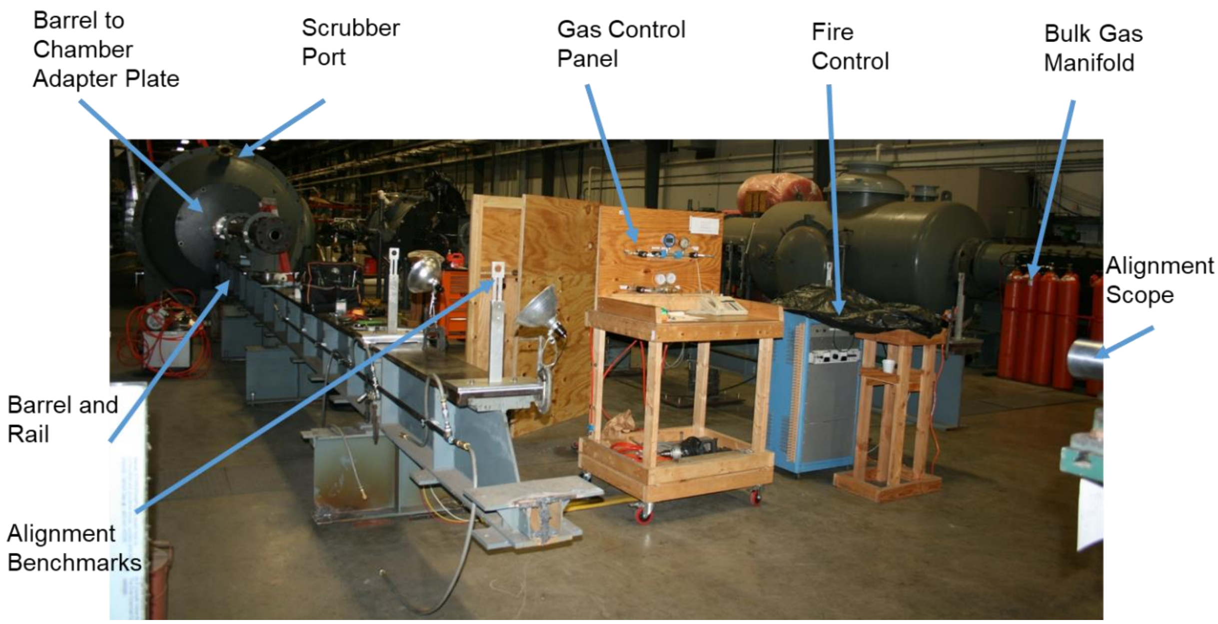


Figure 390. sUAS Component Impact Test Range Setup (Reservoir Not Shown).

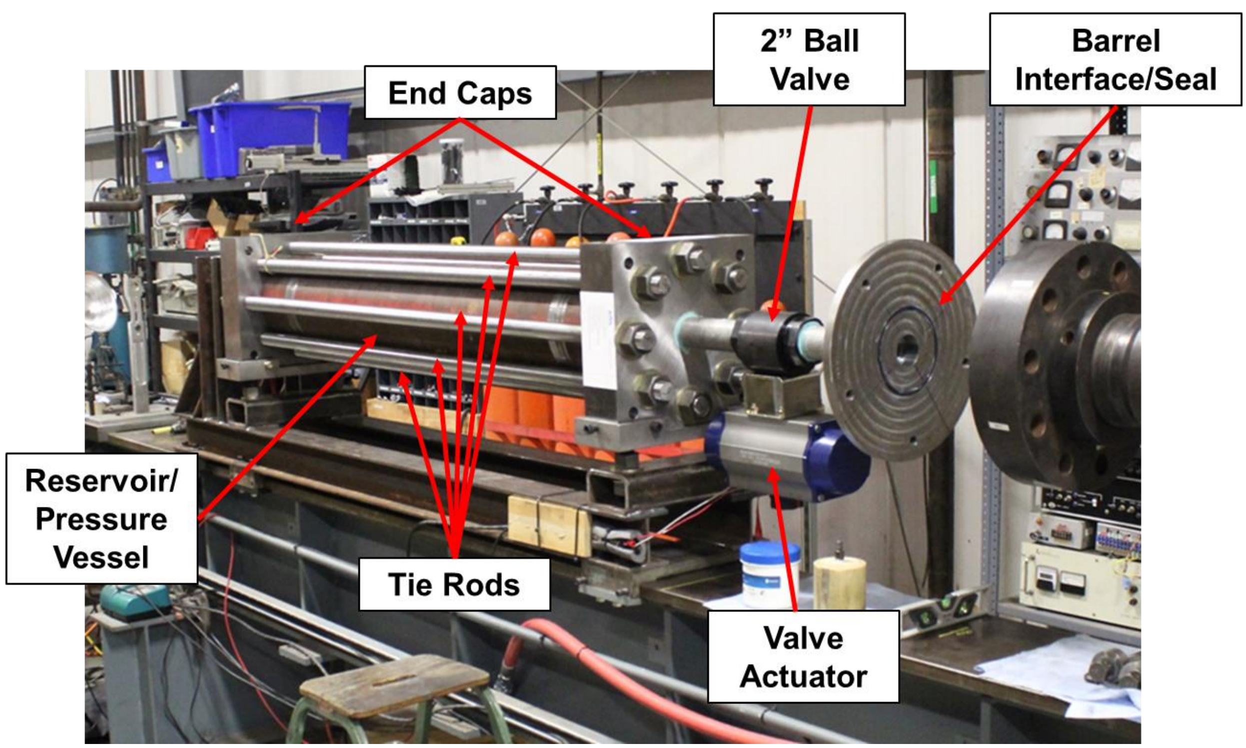


Figure 391. Pressure Reservoir, Valve and Barrel Adapter.

Figure 392. Barrel Extension with Supporting I-beam Structure and Alignment System.

Figure 393. Barrel extension and Target Fixture Frame (viewing down range).

Figure 394. Barrel Extension and Fixture Support Structure (viewing up range).

Given that the full DJI Phantom 3 is a uniquely shaped projectile, a new range and launching system was designed by SMDC ARF personnel to conduct these impact tests. This range has a proprietary design and images are not included in this document to protect the nature of the full sUAS range design. The full aircraft impact test range was designed to be a vacuum environment to prevent aerodynamic-induced tumbling of the full aircraft following release from the sabot. The projectile (aircraft and sabot) was launched using a track system in order to decouple the aircraft from the gun barrel. The design also allowed for firing a wider range of aircraft since different sabots can be designed for the track system, versus having to purchase large diameter gun barrels (in excess of 12" diameter) for testing with larger aircraft.

### B.2.2.2 PROJECTILES

sUAS components and full sUAS were the projectiles used for this research purpose. The specifications of these projectiles are summarized in Table 24.

Table 24. Projectiles Description used in Component and Full sUAS Impact Tests.

| Projectile | Type (Component/ Full sUAS) | Actual projectile | Weight | Dimensions |
|---|---|---|---|---|
| Motor A | Component | DJI Phantom 3 Motors | 1.80 oz | 1.28 x 1.11 x 1.11 in |
| Motor B | Component | Precision Hawk Motors | 3.20 oz | 5.09 x 1.66 x 0.91 in |
| Camera | Component | DJI Phantom 3 Cameras | 1.83 oz | 1.44 x 1.65 x 1.34 in |
| Battery A | Component | DJI Phantom 3 Batteries | 12.80 oz | 4.40 x 2.25 x 1.38 in |
| Battery B | Component | Precision Hawk Batteries | 11.83 oz | 5.09 x 1.66 x 0.91 in |
| DJI Phantom 3 | Full sUAS | DJI Phantom 3 with camera and legs removed | 32.0 oz | 11.5 x 3.5 x 11.5 in |

### B.2.2.3 TARGETS

For the sUAS component tests, three different targets were used. The first was a 2024-T3 aluminum panel of dimension 41”x41”x0.063” (LxWxD), the second was a 2024-T3 aluminum panel of dimension 41”x41”x0.25” (LxWxD), and the third was a 2024-T3 aluminum sharp blade of dimension 36”x10” (LxW) and maximum thickness of 0.125”. Figure 395 shows the Aluminum panel. The two different Aluminum panels had similar length and width but differed in thickness. Figure 396 shows the Aluminum sharp edge target.

Figure 395. Aluminum Panel (41”x41” LxW).


Figure 396. Aluminum Sharp Blade (36”x10” LxW).

### B.2.2.4 COMPONENT IMPACT TEST TARGET FIXTURES

For the 2024-T3 aluminum panel target, the test frame consisted of two square steel “picture frames” bolted together, sandwiching the test plate specimen in between. The frame had 1-in diameter through holes in all four corners for mounting the load cells between the test frame and steel cross members behind it. Figure 397 shows an image of the steel test frame holding the 2024-T3 aluminum panel target.

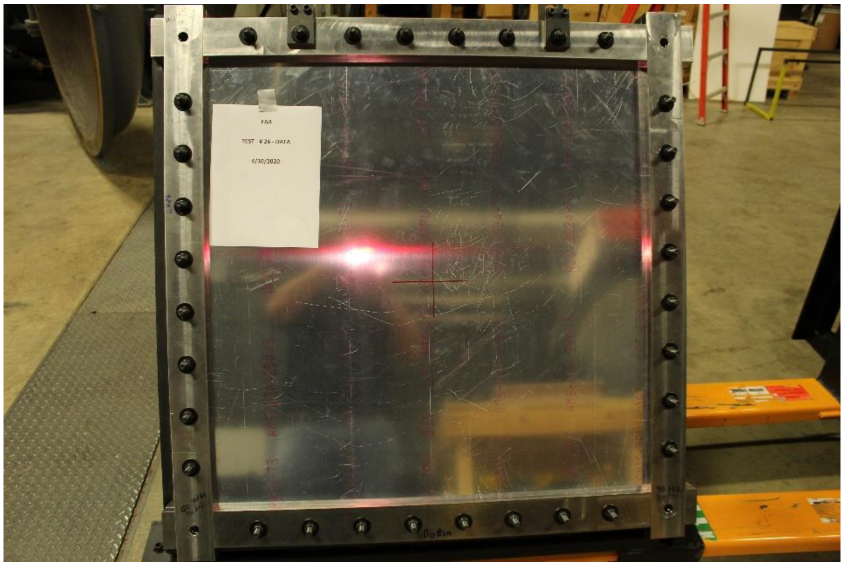

Figure 397. The Steel Test Frame holding the Aluminum Panel Target.

For the 2024-T3 aluminum blade target, the test frame consisted of one square steel frame with half lap joints at the corners. The corner holes on the frame were used to hang the frame on studs attached to the I-beam structure shown in Figure 394. Four load cells were placed between the frame and the I-beam structure to measure reaction loads during impacts for calibration of the component models during impact simulations that were conducted by NIAR. Figure 398 shows the aluminum blade targets which were bolted at the center of this square frame using four L-shape brackets. The sharp blade was sandwiched between two of the brackets on either side. The L-shape brackets had six holes on either side, one end was bolted to the frame and the other end was bolted to the sharp blade target and another bracket.

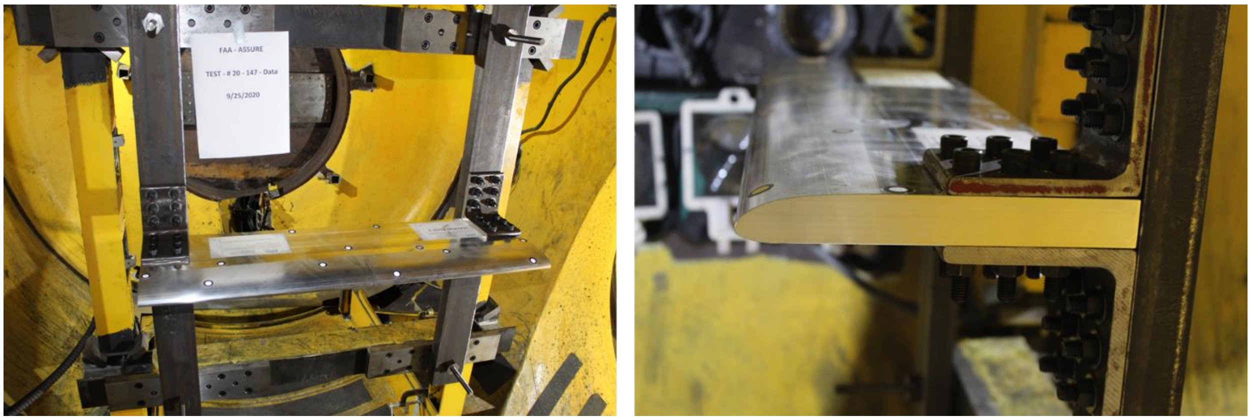

Figure 398. Aluminum Blade Target Fixture.

### B.2.2.5 PROJECTILE SABOT

A sabot was required to support the projectile in the middle of the barrel and provide a uniform loading surface during launch. A sabot trap, or stripper, was positioned at the end of the barrel to capture the sabot and allowed the projectile to continue on in free flight. The sabots for the motor and camera component projectiles were 3D-printed using ABS plastic. Figure 399 shows the sabot used for motor launches.

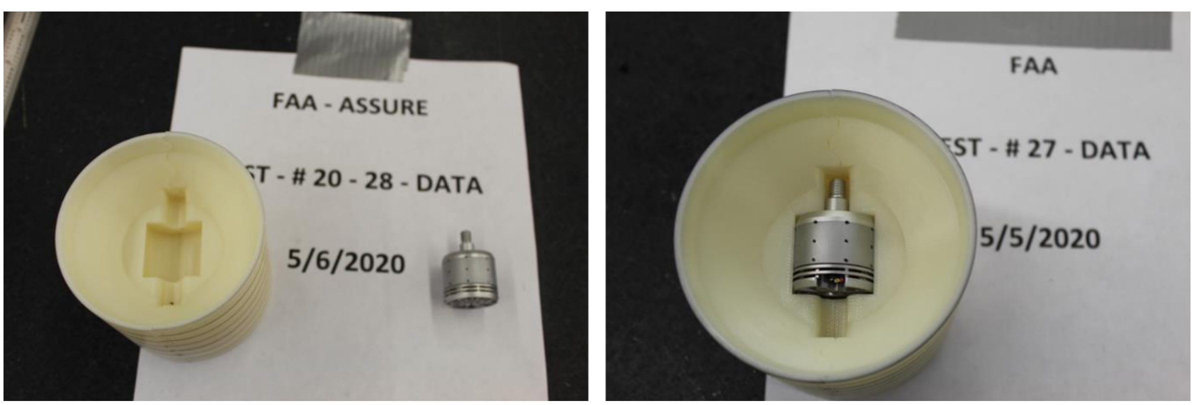


Figure 399. Motor A Sabot.

For the camera component, Figure 400 shows the sabot part made of 4 sabot leaves that separated in flight due to dynamic pressure and allowed the projectile to continue down range toward the target.

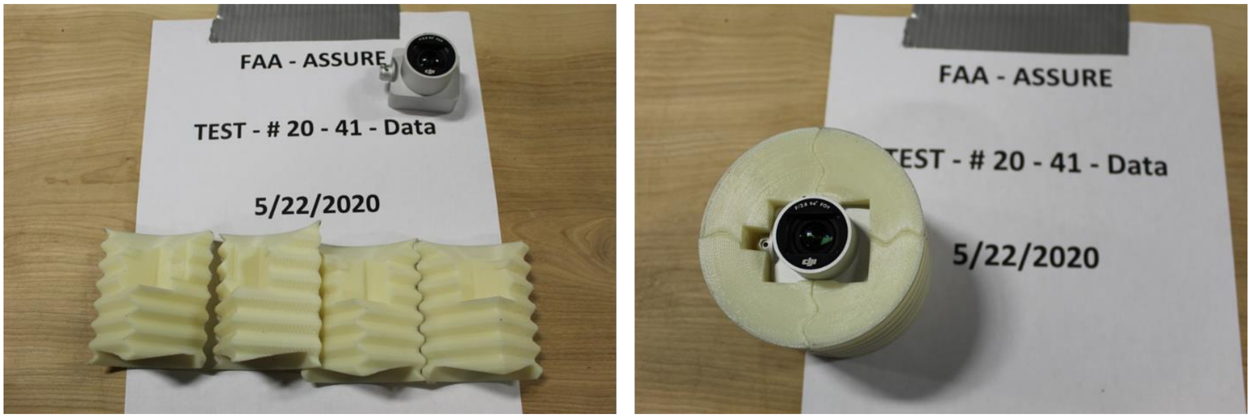


Figure 400. Camera Sabot.

For the battery component, Figure 401 shows the sabot part made of a fiberboard cylinder filled with hard foam and cut into two halves with the battery held between the two halves.


Figure 401. Battery Sabot.

### B.2.2.6 LOAD CELLS

The force transferred to the target frame due to the high-speed impact of the projectile on the target was recorded by four uniaxial load cells located at the corners of the target frame. A set of four ICP® quartz force ring, PCB Piezotronics 204C, with a 40,000 lbf compressive capacity and an upper frequency limit of 55,000 Hz was used for all the tests. They were preloaded to approximately 8,000 lbf before testing and allowed to discharge. This allowed for the measurement of tension as a negative voltage and compression as a positive voltage. A 4-channel, line powered, ICP® sensor signal conditioner, PCB Piezotronics 482C24, was used to process load cell measured signals to readout or recording devices. A Yokogawa DL750 ScopeCorder which can measure signals up to 10 million samples per second was used to record the load cells data. Figure 402 shows an image of the PCB Piezotronics ICP® 204C Quartz Force Ring and 482C24 Signal Conditioner, respectively. Figure 403 shows a schematic of the load cell connection to the ScopeCorder via the Signal Conditioner. Figure 404 shows the relative positions of the four load cells held between the steel frame and the target. The same corner-mounted load cell arrangement was used in the full sUAS impact testing.


Figure 402. PCB Piezotronics 204C ICP® Quartz Force Ring, (R) PCB Piezotronics 482C24 ICP® Signal Conditioner.

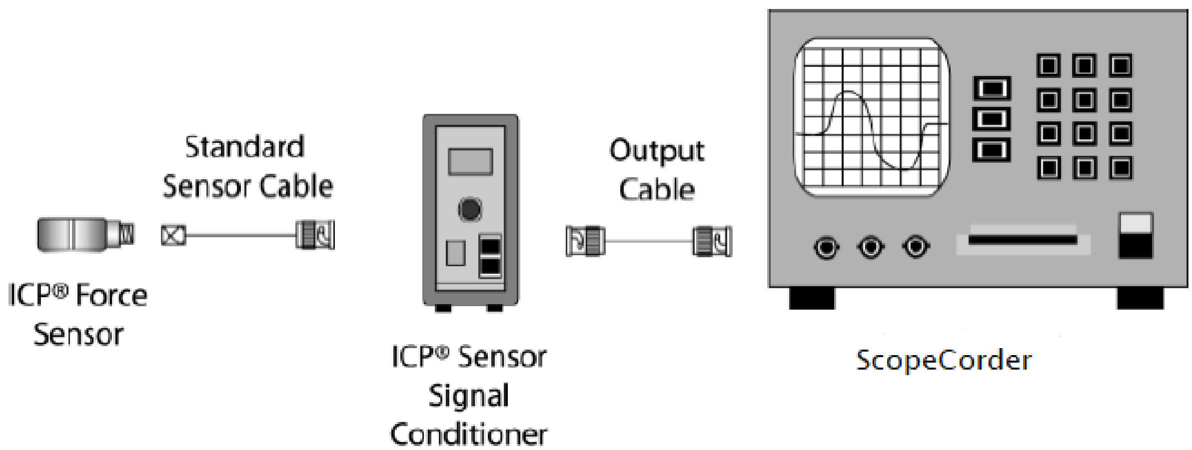


Figure 403. Load Cells Sensor System Schematic.

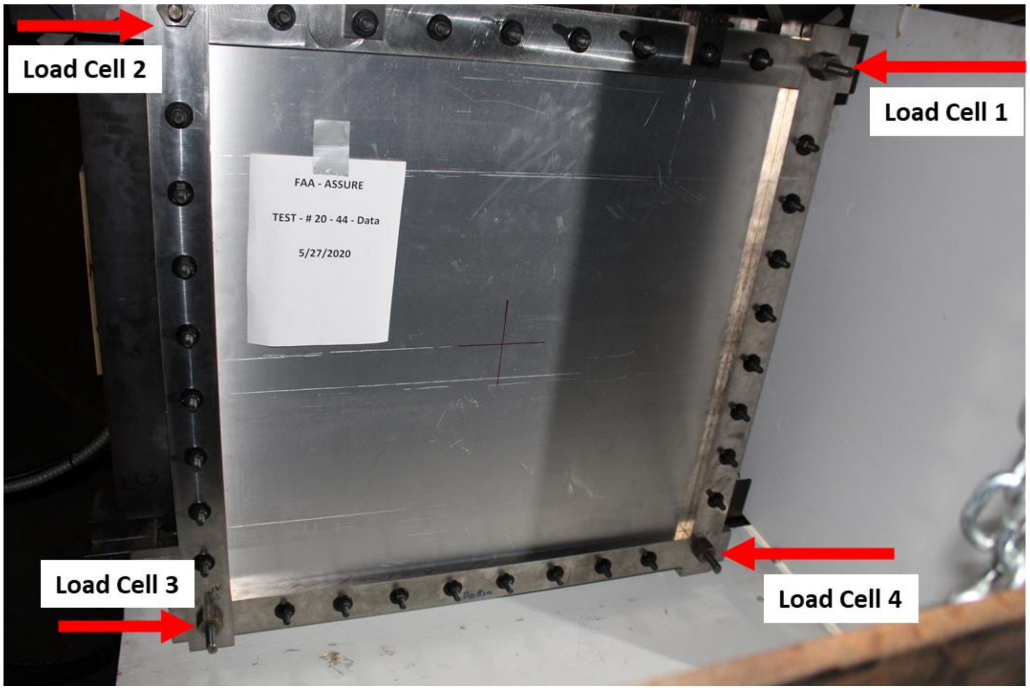


Figure 404. Load Cell Positions on an Aluminum Panel Target held between Steel Frame.

### B.2.2.7 STRAIN GAGES

The strain gage data acquisition was recorded at 1 MHz, or one data point every microsecond. UAH used MMF003247 linear strain gages from Micro-Measurements for measurement of local strain values on the aluminum panels and helicopter components during impact tests. These gages have a 350 (± 0.3%) ohm standard elongation strain with a gage factor of 2.155 (± 0.5%) and were 0.25" (±5%). A Hi-Techniques Synergy Universal Input Amplifier SY6216-4D-VC was used to receive data from the strain gages and store it at 1 MHz. Strain gage locations for the aluminum panels and helicopter components were documented in the NIAR Test Plan.

### B.2.2.8 HIGH-SPEED VIDEO CAMERAS

High-Speed Video Cameras were used to record the projectiles in flight and the resulting impact on the target. Photron FASTCAM SA-Z high speed cameras were used. These cameras can provide a one-megapixel (1024x1024) image resolution at 20,000 frames per second or frame rates beyond 2 million fps at reduced image resolution.

Four of these cameras were used for the component impact tests. Camera 1 and Camera 2 recorded data at 1024x512 resolution and at 40,000 frames per second while Camera 3 and Camera 4 recorded data at 512x512 resolution and at 40,000 frames per second. Figure 405 shows the orientation of these four high-speed Cameras. All the cameras were located outside the chamber and look in through ports. Camera 1 was positioned perpendicular to the shot line to measure velocity and projectile flight data. Plate surface was included in this top-down view. Camera 2 was also positioned perpendicular to the shot line, in order to measure velocity and projectile flight data. The aluminum panel surface was also included in this side view. Camera 3 was positioned on the side of the test chamber viewing target panel through angled mirror. It recorded the impact and dynamic response from a front view in line with and just below or above the projectile's flight path. This mirror was approximately 6 feet from the impact. Camera 4 was positioned on the opposite side of the Camera 3 location. Its view was directed at the muzzle to capture initial launch conditions of sabot and projectile assembly. An angled mirror could be optionally added to provide a view similar to Camera 3 but from opposite side. Full sUAS impact test camera setup diagrams were documented in the NIAR Full-Scale Test Plan.

The Photron FASTCAM Viewer 4 software was used to perform post-processing of the raw files. Additionally, projectile velocity was also measured using this software. The data from Camera 1 and 2 were used to measure velocity. Markers were placed on the projectile and the movement of the markers over 10 frames was observed in the software. A scale factor for each projectile was measured prior to any testing and applied to each high-speed video to determine impact velocity.

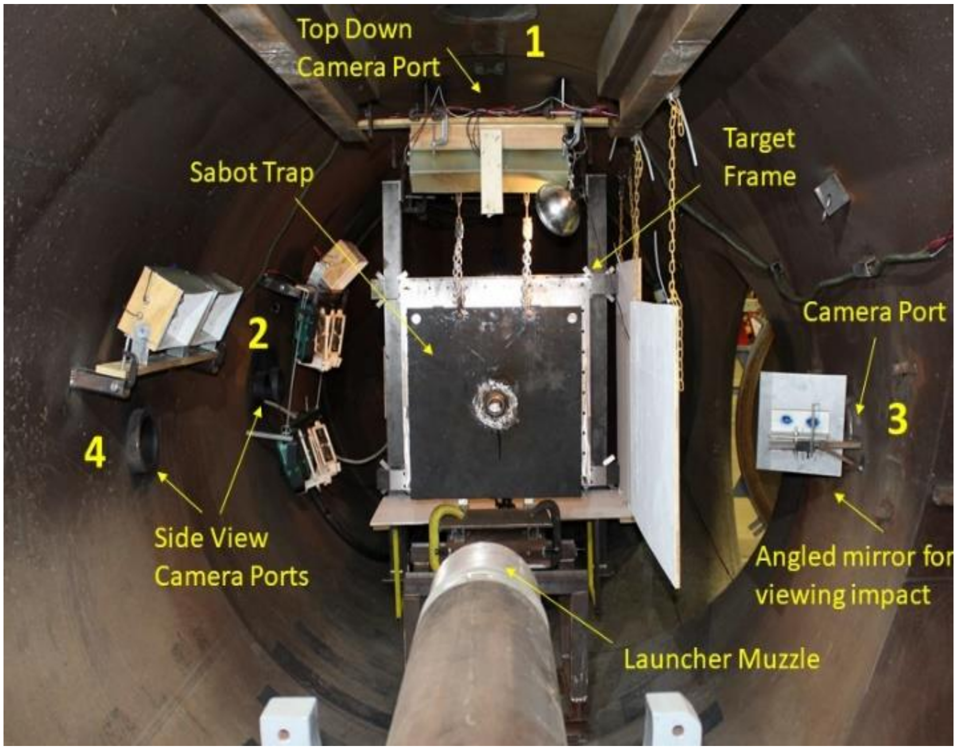


Figure 405. High-speed Cameras Location inside the Test Chamber.

### B.2.2.9 DIGITAL IMAGE CORRELATION SYSTEM

All component impact tests included the use of two high-speed cameras to capture data needed for a DIC system. This system used a pair of high-speed video cameras with a small angle between them to observe an object deforming at high rate – the back surface of the test article (aluminum flat panel) as it was struck by the projectile. Before testing, a semi-random dot pattern was applied on the back surface of the aluminum flat panel with spray paint. The semi-random dot pattern was drilled into a polycarbonate sheet which was placed on the panel and spray painted. Images of the deformation recorded by the camera pair were combined with a set of calibration images in DIC software to produce data of interest (deflections, strains, and their time-derivatives).

Two Photron FASTCAM SA-Z cameras were used to capture data needed for the DIC system on impact tests against aluminum panels. The DIC system was not used for the sharp edge aluminum plate or helicopter component full sUAS impact tests. These cameras captured data at 256x256 resolution and 100,000 frames per second. The camera field of view was 10.5"x10.5" and captured the back of the Aluminum panel targets. GOM Correlate software was used for performing the DIC analysis.

#### B.2.2.10 PRE AND POST PICTURES

Before and after a test was conducted, a high resolution, still images of the test setup and test articles were captured by a Canon DSLR.

#### B.2.2.11 PERMANENT DEFORMATION DAMAGE DOCUMENTATION

A 3D scan of the three target types used in the component impact tests was performed prior to test execution. Later, the 3D scan of each target, for every test, was performed after each impact test to record the permanent deformation of the target specimen. UAH used a Metra Scan 750 elite handheld optical CMM 3D scanner. This scanner has an accuracy of 0.0025 inches. The scans were performed on the rear end of the target specimen after it was fixed to the frames. The cloud data of the scans, before and after impact, were given to NIAR for further evaluation.

### B.2.3 Component Test Matrix Overview

A total of 46 component tests were conducted. Table 25 provides an overview of specifications of the projectiles, targets and the impact test conditions.

Table 25. Component Level Test Matrix.

| **Test#** | **Projectile** | **Velocity [knot]** | **Target** | **Purpose** | **Repetitions** | **Projectile Dimensions** | **Projectile Mass** |
|---|---|---|---|---|---|---|---|
| 1 | Battery* | 500 | Rotor Blade | Assess damage | 2 | 4.40x2.25x1.38in | 12.80 oz |
| 2 | Battery* | 500 | 0.063" Al. Panel | Penetration Yes/No | 2 | 4.40x2.25x1.38in | 12.80 oz |

| | | | | | | | |
|---|---|---|---|---|---|---|---|
| 3 | Battery* | 500 | 0.25” Al. Panel | Penetration Yes/No | 2 | 4.40x2.25x1.38in | 12.80 oz |
| 4 | Motor | 500 | 0.063” Al. Panel | Penetration Yes/No | 2 | 1.28x1.11x1.11in | 1.80 oz |
| 5 | Motor | 500 | 0.25” Al. Panel | Penetration Yes/No | 2 | 1.28x1.11x1.11in | 1.80 oz |
| 6 | Camera | 500 | 0.063” Al. Panel | Penetration Yes/No | 2 | 1.44x1.65x1.34 in | 1.83 oz |
| 7 | Camera | 500 | 0.25” Al. Panel | Penetration Yes/No | 2 | 1.44x1.65x1.34 in | 1.83 oz |
| 8 | Battery* | 50 | 0.063” Al. Panel | Penetration Yes/No | 2 | 4.40x2.25x1.38in | 12.80 oz |
| 9 | Battery* | 120 | 0.063” Al. Panel | Penetration Yes/No | 2 | 4.40x2.25x1.38in | 12.80 oz |
| 10 | Battery* | 120 | 0.25” Al. Panel | Penetration Yes/No | 2 | 4.40x2.25x1.38in | 12.80 oz |
| 11 | Motor | 120 | 0.063” Al. Panel | Penetration Yes/No | 2 | 1.28x1.11x1.11in | 1.80 oz |
| 12 | Motor | 50 | 0.063” Al. Panel | Penetration Yes/No | 2 | 1.28x1.11x1.11in | 1.80 oz |
| 13 | Camera | 120 | 0.063” Al. Panel | Penetration Yes/No | 2 | 1.44x1.65x1.34 in | 1.83 oz |
| 14 | Camera | 50 | 0.063” Al. Panel | Penetration Yes/No | 2 | 1.44x1.65x1.34 in | 1.83 oz |
| 15 | Battery* | 500 | Sharp Blade | Assess damage | 2 | 5.09x1.66x0.91in | 11.83 oz |
| 16 | Battery* | 500 | 0.063” Al. Panel | Penetration Yes/No | 2 | 5.09x1.66x0.91in | 11.83 oz |
| 17 | Battery* | 500 | 0.25” Al. Panel | Penetration Yes/No | 2 | 5.09x1.66x0.91in | 11.83 oz |
| 18 | Motor | 500 | 0.063” Al. Panel | Penetration Yes/No | 2 | 2.48x1.39x1.39 in | 3.20 oz |
| 19 | Motor | 500 | 0.25” Al. Panel | Penetration Yes/No | 2 | 2.48x1.39x1.39 in | 3.20 oz |
| 20 | Battery* | 50 | 0.063” Al. Panel | Penetration Yes/No | 2 | 5.09x1.66x0.91in | 11.83 oz |

| | | | | | | | |
|---|---|---|---|---|---|---|---|
| 21 | Battery* | 120 | 0.063” Al. Panel | Penetration Yes/No | 2 | 5.09x1.66x0.91in | 11.83 oz |
| 22 | Motor | 50 | 0.063” Al. Panel | Penetration Yes/No | 2 | 2.48x1.39x1.39 in | 3.20 oz |
| 23 | Motor | 120 | 0.063” Al. Panel | Penetration Yes/No | 2 | 2.48x1.39x1.39 in | 3.20 oz |

*Note 1. Batteries were fully charged

### B.2.4 Component Impact Test Method

The component impacts test matrix and requirements were provided by NIAR-WSU and UAH developed the test setup and conducted the tests. These tests involved high speed impact testing of a commercial quadcopter’s electric motors, cameras and batteries against full scale rotorcraft components statically supported within the test chamber.

The test preparation sequence inside the tank included target installation, sensor hookup, lighting checks, and camera setup. Aluminum panels were prepared for testing by drilling for fixturing, undergoing surface preparation, painting, and strain gage bonding and soldering. The aluminum sharp edge blade targets did not have any strain gages. Panels were match-drilled in order to mount within the fixture frame. The surface of the back side of the panel was cleaned and the strain gages were bonded to it. The aluminum panels were spray painted on the down range side with the strain gages already bonded to the surface. Wires were soldered to each of the strain gages on the down range side of each panel. Prior to test execution, each panel was bolted into the fixture and the strain gage wires were connected to the Synergy DAQ. The panel and frame assembly were hung on four corner-mounted studs with the load cells between the stainless-steel frame and the I-beam structure. The load cells were zeroed out and tightened to 8.000 lbf of preloading and then allowed to discharge to zero. This allowed the load cells to register both tensile and compressive loads. Finally, the aluminum panel is then placed inside the chamber. The high-speed cameras were calibrated and manually focused.

A calibration of the two high-speed cameras used for DIC system was also performed by taking capturing images of a calibration plate. A time-delay trigger was connected to the load cell DAQ, strain gages DAQ, high-speed cameras, DIC cameras, the gas gun valve. A transistor-transistor login signal was sent from the time-delay generator to all the equipment to capture data at the same time. All equipment and sensors were calibrated in the mornings on days when tests were performed.

Just before testing began, the gas gun was cleaned and prepared. Initially, simulated masses were shot at dummy targets to validate projectile alignment, projectile impact velocity, projectile impact angle, gun settings (reservoir pressure, valve actuation time) and gun alignment (error between actual impact and desired impact location & offset impact angle). Figure 406 shows images of the required impact angle for the battery, motor, and camera projectiles. The longitudinal axis of the battery was required to be normal to the surface of target at impact within a tolerance $< \pm 5^{\circ}$. The motor shaft was required to be normal to the surface of the target at impact within a tolerance < ± 5˚. The camera lens was required to be normal to the surface of the target at impact within a tolerance < ± 5˚. Additionally, the component must have impacted at the exact marked location on the target with a tolerance < ± 1 inch.

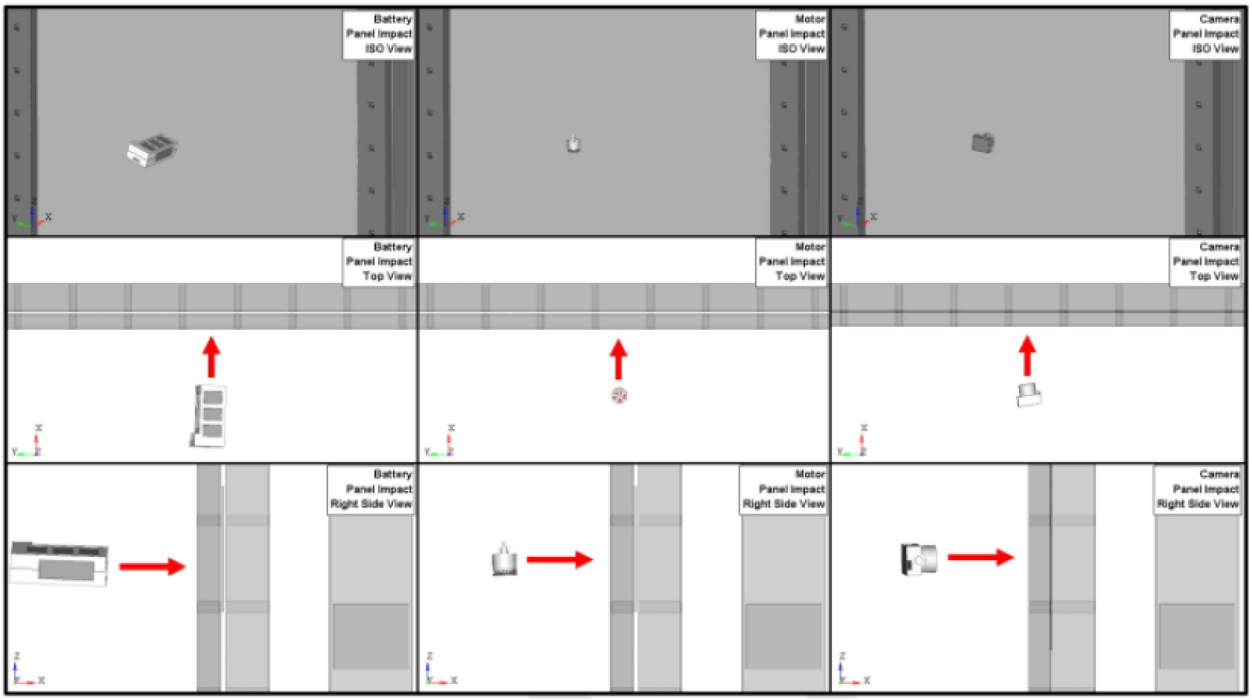


Figure 406. Projectile Orientations (Battery, Motor and Camera respectively).

Before the simulated masses or the actual components were fired, a test fire is performed to verify that the trigger causes all the equipment and sensors to record data at the same time. The trigger caused the valve on the gas gun to open, however, there was no gas or projectile. The lights in the chamber turned on momentarily and the high-speed cameras capture data. The quality of the high-speed cameras was verified. The strain gage wires were gently shaken and the aluminum panel was slightly pressed and released to verify that the wiring connections were good and the readings on the strain gages were not abnormal.

After verifying that the pre-test procedures were completed and all checks completed, the simulated masses were placed in the sabot and fired onto a dummy target made up of wood. After the gun alignment and settings were confirmed, the actual component was placed inside the sabot and fired on the target. The data captured by the equipment and sensors was verified. The panel and the frame were removed from the chamber and the panel was detached and a 3D scan was performed. The chamber was then cleaned and prepared for the next test.

B.2.5 Full Aircraft Test Matrix Overview

UAH conducted a total of 8 full sUAS impact tests. Table 25 provides an overview of specifications of the projectiles, targets and the impact test conditions.

Table 26. Full sUAS Impact Test Matrix.

| Test # | Projectile | Velocity [knot] | Target | UAS Mass [lb] | UAS Orientation |
|---|---|---|---|---|---|
| **0** | Mass Sim | | | | |
| **1** | Quadcopter UAS* | 340 | Tail Rotor Blade | 2.06 | FWD flying direction |
| **2** | Quadcopter UAS* | 500 | Main Rotor Blade | 2.06 | FWD flying direction |
| **3** | Quadcopter UAS* | 500 | Main Rotor Blade | 2.06 | FWD flying direction |
| **4** | Quadcopter UAS* | 175 | Horizontal Stabilizer | 2.06 | FWD flying direction |
| **5** | Quadcopter UAS* | 50 | Bi-Layer Windshield (Glass+PU) | 2.06 | FWD flying direction |
| **6** | Quadcopter UAS* | 175 | Bi-layer Windshield (Glass+PU) | 2.06 | FWD flying direction |
| **7**** | Quadcopter UAS* | TBD | Bi-layer Windshield (Glass+PU) | 2.06 | FWD flying direction |
| **8**** | Quadcopter UAS* | TBD | Bi-layer Windshield (Glass+PU) | 2.06 | FWD flying direction |

(*) Removed legs, gimbal, camera and propellers. **Batteries were fully charged prior to the tests.**

(**) An additional windshield test was conducted obtain UAS penetration through the windshield.

### B.2.6 Component Impact Test Method

UAH prepared for individual full sUAS impact tests using an iterative fixture design process with NIAR, strain gage instrumentation of helicopter components, configuration of camera arrays, and through developmental shots. RSESC provided Computer Aided Design (CAD) support to develop helicopter component fixture designs that were approved by the ARF range engineer and then sent to NIAR for meshing and use in impact simulations. If NIAR determined that there were design shortcomings with specific helicopter component fixtures, then the RSESC CAD designer completed design revisions, had the design reviewed by the ARF range engineer, and resubmitted the fixture design to NIAR for review. This process was repeated with each fixture design until NIAR approved of the design. Fixture designs included both the solid model of the design and a parts sheet that provided part numbers and part material specifications to support transition of the solid model to finite element analysis simulation use. ARF and RSESC technicians performed surface preparation and strain gage bonding to helicopter components based on the instrumentation diagrams in the NIAR full aircraft test plan prior to impact tests. ARF instrumentation personnel also configured the camera setups for each test based on the NIAR full sUAS impact test plan prior to impact tests. In order to determine gun conditions (reservoir pressures) ARF personnel conducted developmental shots prior to record tests. Gas gun, instrumentation, data acquisition and lighting triggering were executed in the same manner during full sUAS testing as during component-level impact tests.

## B.3 RESULTS

### B.3.1 sUAS Components Impact Testing

All 46 sUAS component tests were successfully performed. However, data for the Test 4 - Repetition 1 was not recorded due to a triggering issue that was rectified for other tests. For all the remaining tests, most of the data from all sensors and equipment was captured from either or both of the repetitions. During testing, the high-speed camera used by the DIC system had to be repaired and were unavailable for few weeks. During that time, one of the high-speed cameras looking at the impact was used for the DIC system and only three high speed cameras looked at the impact. For few tests, some of the strain gages recorded very high data points due to a bad connection and such data points were ignored. For some tests, the trigger had some errors and one or two high-speed cameras did not trigger data.

B.3.1.1 RESULTS OVERVIEW

| Test # | Projectile | Target | Rep. | Des Vel (kts) | Act Vel (kts) | Result |
|---|---|---|---|---|---|---|
| 1 | Battery A | Sharp Blade | 1 | 500 | 510.7 | Battery did not penetrate nor indent the blade. Battery shattered into multiple fragments but did pose a "Fire Risk" |
| | | | 2 | 500 | 516.6 | Battery did not penetrate nor indent the blade. Battery shattered into multiple fragments but did not pose a "Fire Risk" |
| 2 | Battery A | 0.063' Al. Panel | 1 | 500 | 503.6 | Battery penetrated the panel. Battery shattered into multiple fragments but did not pose a "Fire Risk" |
| | | | 2 | 500 | 500.6 | Battery penetrated the panel. Battery shattered into multiple fragments but did not pose a "Fire Risk" |
| 3 | Battery A | 0.25' Al. Panel | 1 | 500 | n/a | n/a |
| | | | 2 | 500 | 500.6 | Battery left an indentation on the panel. Battery shattered into multiple fragments but did not pose a "Fire Risk" |
| 4 | Motor A | 0.063' Al. Panel | 1 | 500 | 513 | Motor penetrated the panel. Motor broke into distinct pieces |
| | | | 2 | 500 | 507 | Motor penetrated the panel. Motor broke into distinct pieces |
| 5 | Motor A | 0.25' Al. Panel | 1 | 500 | 520 | Motor left an indentation on the panel. Motor was crushed |
| | | | 2 | 500 | n/a | Motor left an indentation on the panel. Motor was crushed |
| 6 | Camera | 0.063' Al. Panel | 1 | 500 | 508 | Camera penetrated the panel. Camera broke into distinct pieces |
| | | | 2 | 500 | 518 | Camera penetrated the panel. Camera was crushed. |
| 7 | Camera | 0.25' Al. Panel | 1 | 500 | 522 | Camera left an indentation on the panel. Camera was crushed |
| | | | 2 | 500 | 521 | Camera left an indentation on the panel. Camera was crushed |
| 8 | Battery A | 0.063' Al. Panel | 1 | 50 | 52 | Battery left a slight indentation on the panel. Battery broke into distinct pieces but no fire |
| | | | 2 | 50 | 51.5 | Battery left a slight indentation on the panel. Battery broke into distinct pieces but did not pose a "Fire Risk" |
| 9 | Battery A | 0.063' Al. Panel | 1 | 120 | 120.87 | Battery left an indentation on the panel. Battery posed a "Fire Risk" |
| | | | 2 | 120 | 118.5 | Battery left an indentation on the panel. Battery broke into distinct pieces and posed a "Fire Risk" |
| 10 | Battery A | 0.25' Al. Panel | 1 | 120 | 116 | Battery left an indentation on the panel. Battery broke into distinct pieces and posed a "Fire Risk" |
| | | | 2 | 120 | 122 | Battery left an indentation on the panel. Battery broke into distinct pieces and posed a "Fire Risk" |
| 11 | Motor A | 0.063' Al. Panel | 1 | 120 | 124 | Motor left an indentation on the panel and experienced minor crush. |
| | | | 2 | 120 | 120 | Motor left an indentation on the panel and experienced minor crush. |
| 12 | Motor A | 0.063' Al. Panel | 1 | 50 | 57 | Motor left an indentation on the panel and experienced minor crush. |
| | | | 2 | 50 | 57 | Motor left an indentation on the panel and experienced minor crush. |
| 13 | Camera | 0.063' Al. Panel | 1 | 120 | 121 | Camera left an indentation on the panel and had minor deformation. |
| | | | 2 | 120 | 123 | Camera left an indentation on the panel and had minor deformation. |

| | | | | | | |
|---|---|---|---|---|---|---|
| 14 | Camera | 0.063' Al. Panel | 1 | 50 | 53 | Camera left an indentation on the panel and had minor deformation. |
| | | | 2 | 50 | 48.6 | Camera left an indentation on the panel and had minor deformation. |
| 15 | Battery B | Sharp Blade | 1 | 500 | 510 | Battery did not penetrate nor indent the blade. Battery shattered into multiple fragments but did not pose a “Fire Risk” |
| | | | 2 | 500 | 499 | Battery did not penetrate nor indent the blade. Battery shattered into multiple fragments but did not pose a “Fire Risk” |
| 16 | Battery B | 0.063' Al. Panel | 1 | 500 | 510 | Battery penetrated the panel. Battery shattered into multiple fragments but did not pose a “Fire Risk” |
| | | | 2 | 500 | 500 | Battery penetrated the panel. Battery shattered into multiple fragments but did not pose a “Fire Risk” |
| 17 | Battery B | 0.25' Al. Panel | 1 | 500 | 500 | Battery left an indentation on the panel. Battery shattered into multiple fragments but did not pose a “Fire Risk” |
| | | | 2 | 500 | 501 | Battery left an indentation on the panel. Battery shattered into multiple fragments but did not pose a “Fire Risk” |
| 18 | Motor B | 0.063' Al. Panel | 1 | 500 | 527 | Motor penetrated the panel. Motor broke into distinct pieces |
| | | | 2 | 500 | 525 | Motor penetrated the panel. Motor remained mostly intact |
| 19 | Motor B | 0.25' Al. Panel | 1 | 500 | 527 | Motor left an indentation on the panel. Motor was crushed |
| | | | 2 | 500 | 522 | Motor left an indentation on the panel. Motor was crushed |
| 20 | Battery B | 0.063' Al. Panel | 1 | 50 | 52 | Battery did not leave an indentation on the panel. Battery broke into distinct pieces but did not pose a “Fire Risk” |
| | | | 2 | 50 | 52 | Battery did not leave an indentation on the panel. Battery broke into distinct pieces but did not pose a “Fire Risk” |
| 21 | Battery B | 0.063' Al. Panel | 1 | 120 | 120 | Battery left an indentation on the panel. Battery was crushed and posed a “Fire Risk” |
| | | | 2 | 120 | 121 | Battery left an indentation on the panel. Battery was crushed and posed a “Fire Risk” |
| 22 | Motor B | 0.063' Al. Panel | 1 | 50 | 49 | Motor left an indentation on the panel. Very Little deformation of motor |
| | | | 2 | 50 | 52 | Motor left an indentation on the panel. Very Little deformation of motor |
| 23 | Motor B | 0.063' Al. Panel | 1 | 120 | 123 | Motor partially pierced the panel but did not pass through. Motor broke into distinct pieces |
| | | | 2 | 120 | 123 | Motor partially pierced the panel but did not pass through. Motor broke into distinct pieces |

### B.3.1.2 AIRCRAFT COMPONENT IMPACT TEST RESULTS SUMMARY

A total of 46 test were performed for sUAS Components Impact testing. The test conditions and result summaries of each of these tests are described below.

#### B.3.1.2.1 TEST 1-1

| **General Test Information** | | | |
|---|---|---|---|
| Test Facility: | **SMDC-TC Aerophysics Research Facility** | Test Date | **9/25/2020** |
| ARF Test ID Number | **20-146** | NIAR Test ID Number | **1-1** |

| | |
|---|---|
| **Test Description** | 500 knot impact of Battery A on a Sharp Blade secured within a 17-4 stainless steel frame |

| **Test Conditions** | | | |
|---|---|---|---|
| Projectile | Battery A | Target Dimensions | 36” span, 9.987” chord length, 0.21 leading edge radius, 1.263” max. thickness |
| Projectile mass | 350.8 gm (0.773 lb.) | Nominal Impact Velocity (knots) | 500 |
| Target | 2024 aluminum plate with a representative airfoil leading edge | Actual Impact Velocity (knots) | 510.7 |

| **Test Setup** | | | |
|---|---|---|---|
| Target impact angle attained | Y | DIC system recorded properly | N/A |
| Gun alignment in tolerance | Y | All load cells recorded data | Y |
| All still camera images captured | Y | All strain gages recorded data | N/A |
| All high-speed cameras capture impact | Y | | |

| **Test Results Summary** |
|---|
| Battery A impacted the target in the nominal velocity range and correct orientation (longitudinal axis of the battery normal to the surface of the blade leading edge). During the test the battery did not penetrate through the sharp blade. The battery broke apart during impact.<br>Strain gages and DIC Cameras were not used in the Sharp Blade tests. |

| **Photos** | |
|---|---|
|  |  |
| Projectile and Sabot | Projectile Condition After Impact |
|  |  |
| Sharp Edge Blade with Battery Impact Marks | |

B.3.1.2.2 TEST 1-2

| **General Test Information** | | | |
|---|---|---|---|
| Test Facility: | **SMDC-TC Aerophysics Research Facility** | Test Date | **9/25/2020** |
| ARF Test ID Number | **20-147** | NIAR Test ID Number | **1-2** |

| **Test Description** | 500 knot impact of Battery A on a Sharp Blade secured within a 17-4 stainless steel frame |
|---|---|

| **Test Conditions** | | | |
|---|---|---|---|
| Projectile | Battery A | Target Dimensions | 36” span, 9.987” chord length, 0.21 leading edge radius, 1.263” max. thickness |
| Projectile mass | 350.8 gm (0.773 lb.) | Nominal Impact Velocity (knots) | 500 |
| Target | 2024 aluminum plate with representative airfoil leading edge | Actual Impact Velocity (knots) | 516.6 |

| **Test Setup** | | | |
|---|---|---|---|
| Target impact angle attained | Y | DIC system recorded properly | N/A |
| Gun alignment in tolerance | Y | All load cells recorded data | Y |
| All still camera images captured | Y | All strain gages recorded data | N/A |
| All high-speed cameras capture impact | Y | | |

| **Test Results Summary** |
|---|
| Battery A impacted the target in the nominal velocity range and correct orientation (longitudinal axis of the battery normal to the surface of the blade leading edge). During the test the battery did not penetrate through the sharp blade. The battery broke apart during impact.<br>Strain gages and DIC Cameras were not used in the Sharp Blade tests. |

<table>
<tr><th colspan="2">Photos</th></tr>
<tr><td>
</td><td></td></tr>
<tr><td>Projectile and Sabot</td><td>Projectile Condition After Impact</td></tr>
<tr><td>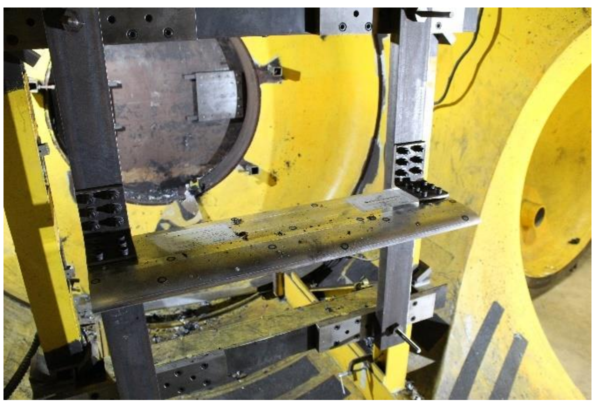</td><td></td></tr>
<tr><td colspan="2">Sharp Edge Blade with Battery Impact Marks</td></tr>
</table>

B.3.1.2.3 TEST 2-1

| **General Test Information** | | | |
|---|---|---|---|
| Test Facility: | **SMDC-TC Aerophysics Research Facility** | Test Date | **08/19/2020** |
| ARF Test ID Number | **20-115** | NIAR Test ID Number | **2-1** |

| | |
|---|---|
| **Test Description** | 500 knot impact of Battery A on a 0.063" thick 2024 aluminum panel secured within a 17-4 stainless steel frame |

| **Test Conditions** | | | |
|---|---|---|---|
| Projectile | Battery A | Target Dimensions | 41"x41"x0.063" |
| Projectile mass | 344.2 gm (0.758 lb.) | Nominal Impact Velocity (knots) | 500 |
| Target | 2024 aluminum panel | Actual Impact Velocity (knots) | 503.6 |

| **Test Setup** | | | |
|---|---|---|---|
| Target impact angle attained | Y | DIC system recorded properly | Y |
| Gun alignment in tolerance | Y | All load cells recorded data | Y |
| All still camera images captured | Y | All strain gages recorded data | Y |
| All high-speed cameras capture impact | Y | | |

| **Test Results Summary** |
|---|
| Battery A impacted the target in the nominal velocity range and correct orientation (battery longitudinal axis normal to the panel surface). During the test the battery penetrated through the aluminum panel and broke up into distinct pieces. |

| **Photos** | |
|---|---|
| 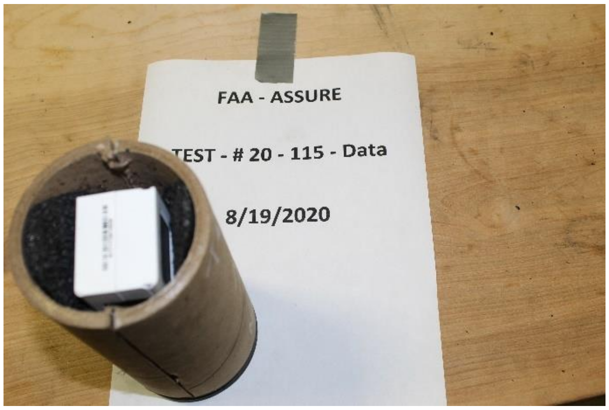 | N/A |
| Projectile and Sabot | Projectile Condition After Impact |
| 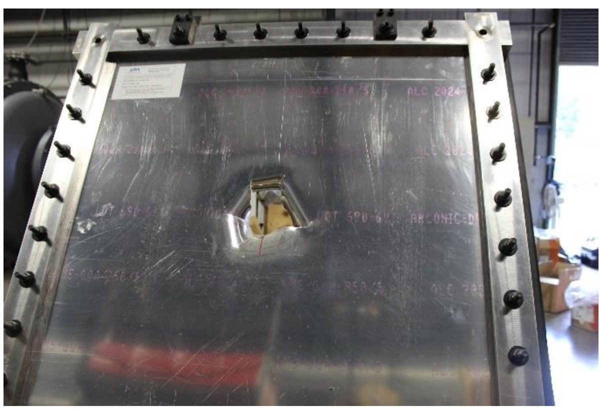 | 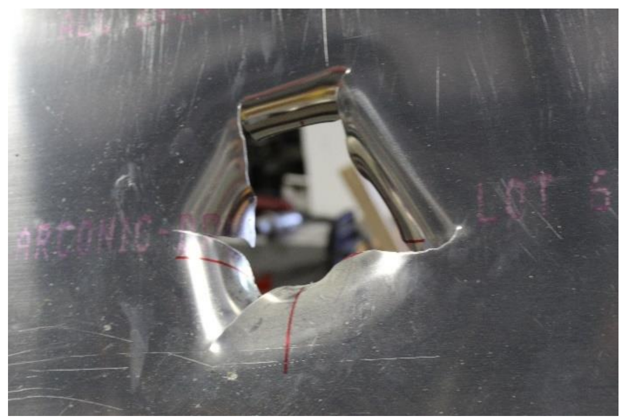 |
| Target Panel Showing Impact Perforation | |

B.3.1.2.4 TEST 2-2

| **General Test Information** | | | |
|---|---|---|---|
| Test Facility: | **SMDC-TC Aerophysics Research Facility** | Test Date | **8/26/2020** |
| ARF Test ID Number | **20-116** | NIAR Test ID Number | **2-2** |

| | |
|---|---|
| **Test Description** | 500 knot impact of Battery A on a 0.063” thick 2024 aluminum panel secured within a 17-4 stainless steel frame |

| **Test Conditions** | | | |
|---|---|---|---|
| Projectile | Battery A | Target Dimensions | 41”x41”x0.063” |
| Projectile mass | 343.4 gm (0.757 lb.) | Nominal Impact Velocity (knots) | 500 |
| Target | 2024 aluminum panel | Actual Impact Velocity (knots) | 500.6 |

| **Test Setup** | | | |
|---|---|---|---|
| Target impact angle attained | Y | DIC system recorded properly | Y |
| Gun alignment in tolerance | Y | All load cells recorded data | N |
| All still camera images captured | Y | All strain gages recorded data | Y |
| All high-speed cameras capture impact | Y | | |

| **Test Results Summary** |
|---|
| Battery A impacted the target in the nominal velocity range and correct orientation (battery longitudinal axis normal to the panel surface). During the test the battery penetrated through the aluminum panel and broke up into distinct pieces.<br>Load Cell 4, or the wire connection to it, sustained damaged during the test. Load Cell 4 showed sharp spike on impact. A new wire connection was installed after the test. This fixed the load cell 4 readings for future tests. |

<table>
<tr><th colspan="2">Photos</th></tr>
<tr><td></td><td>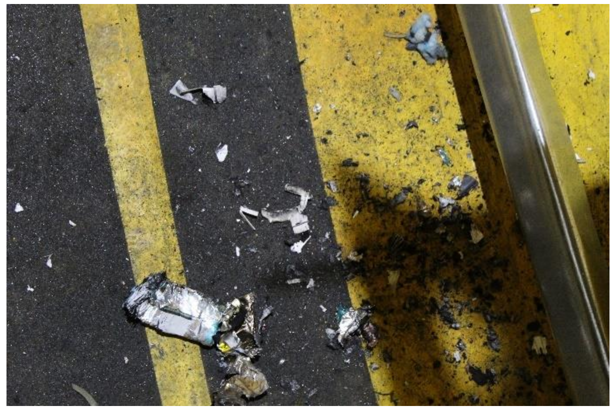</td></tr>
<tr><td>Projectile and Sabot</td><td>Projectile Condition After Impact</td></tr>
<tr><td>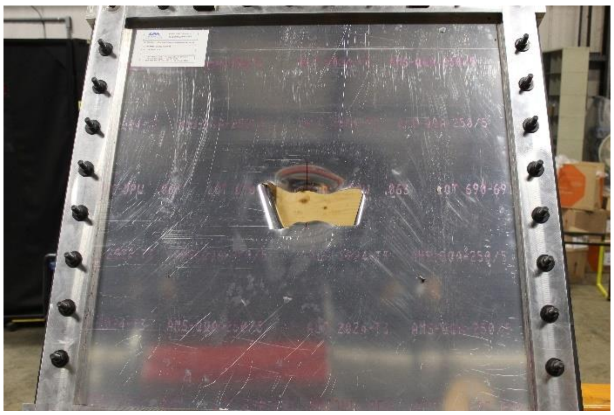</td><td>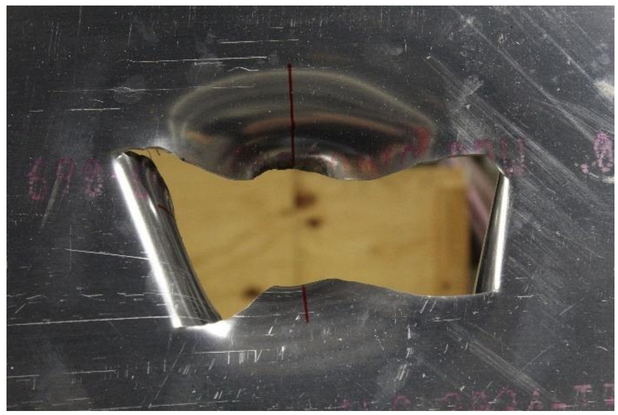</td></tr>
<tr><td colspan="2">Target Panel Showing Impact Perforation</td></tr>
</table>

B.3.1.2.5 TEST 3-1

| General Test Information | | | |
|---|---|---|---|
| Test Facility: | **SMDC-TC Aerophysics Research Facility** | Test Date | **9/2/2020** |
| ARF Test ID Number | **20-117** | NIAR Test ID Number | **3-1** |

| | |
|---|---|
| **Test Description** | 500 knot impact of Battery A on a 0.25” thick 2024 aluminum panel secured within a 17-4 stainless steel frame |

| Test Conditions | | | |
|---|---|---|---|
| Projectile | Battery A | Target Dimensions | 41”x41”x0.25” |
| Projectile mass | 342.9 gm (0.756 lb.) | Nominal Impact Velocity (knots) | 500 |
| Target | 2024 aluminum panel | Actual Impact Velocity (knots) | n/a |

| Test Setup | | | |
|---|---|---|---|
| Target impact angle attained | Y | DIC system recorded properly | N |
| Gun alignment in tolerance | Y | All load cells recorded data | N |
| All still camera images captured | N | All strain gages recorded data | N |
| All high-speed cameras capture impact | N | | |

| Test Results Summary |
|---|
| Battery A impacted the target in the nominal velocity range and correct orientation (battery longitudinal axis normal to the panel surface). During the test the battery did not penetrate through the aluminum panel and broke up into distinct pieces.<br>There was a delay between the cameras being triggered and the gun being triggered, thus, no data (high-speed, DIC, still images, strain and load cells) were captured. |

| Photos – None captured |
|---|

B.3.1.2.6 TEST 3-2

| General Test Information | | | |
|---|---|---|---|
| Test Facility: | **SMDC-TC Aerophysics Research Facility** | Test Date | **8/26/2020** |
| ARF Test ID Number | **20-118** | NIAR Test ID Number | **3-2** |

| | |
|---|---|
| **Test Description** | 500 knot impact of Battery A on a 0.25” thick 2024 aluminum panel secured within a 17-4 stainless steel frame |

| Test Conditions | | | |
|---|---|---|---|
| Projectile | Battery A | Target Dimensions | 41”x41”0.25” |
| Projectile mass | 343.4 gm (0.757 lb.) | Nominal Impact Velocity (knots) | 500 |
| Target | 2024 aluminum panel | Actual Impact Velocity (knots) | 500.6 |

| Test Setup | | | |
|---|---|---|---|
| Target impact angle attained | Y | DIC system recorded properly | Y |
| Gun alignment in tolerance | Y | All load cells recorded data | Y |
| All still camera images captured | Y | All strain gages recorded data | Y |
| All high-speed cameras capture impact | N | | |

| Test Results Summary |
|---|
| Battery A impacted the target in the nominal velocity range and correct orientation (battery longitudinal axis normal to the panel surface). During the test the battery did not penetrate through the aluminum panel and broke up into distinct pieces.<br>High Speed Camera 4 did not trigger. |

| **Photos** | |
|---|---|
|  |  |
| Projectile and Sabot | Projectile Condition After Impact |
| 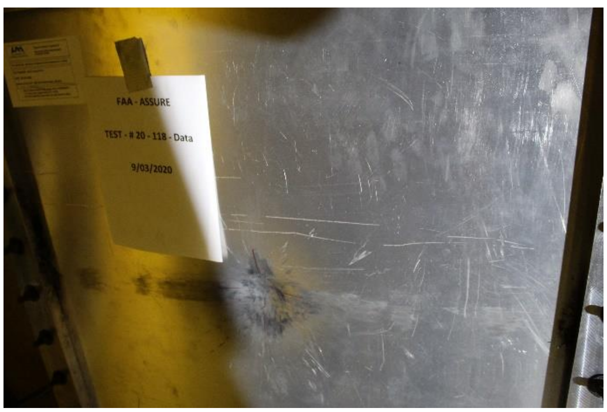 | 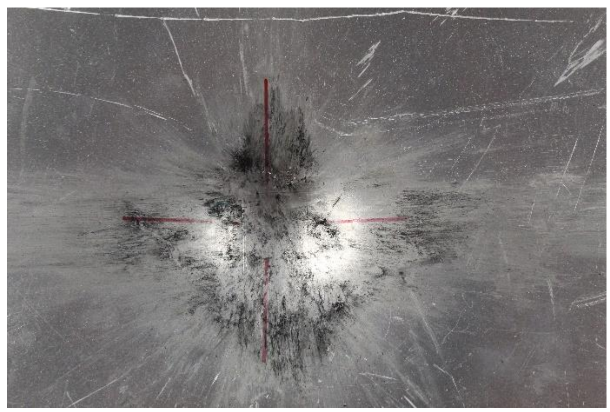 |
| Target Panel Showing Impact Indentation | |

B.3.1.2.7 TEST 4-1

| **General Test Information** | | | |
|---|---|---|---|
| Test Facility: | **SMDC-TC Aerophysics Research Facility** | Test Date | **4/24/2020** |
| ARF Test ID Number | **20-25** | NIAR Test ID Number | **4-1** |

| | |
|---|---|
| **Test Description** | 500 knot impact of Motor A on a 0.063” thick 2024 aluminum panel secured within a 17-4 stainless steel frame |

| **Test Conditions** | | | |
|---|---|---|---|
| Projectile | Motor A | Target Dimensions | 41”x41”0.063” |
| Projectile mass | 51.4 gm (0.133 lb.) | Nominal Impact Velocity (knots) | 500 |
| Target | 2024 aluminum panel | Actual Impact Velocity (knots) | 513 |

| **Test Setup** | | | |
|---|---|---|---|
| Target impact angle attained | Y | DIC system recorded properly | N |
| Gun alignment in tolerance | Y | All load cells recorded data | Y |
| All still camera images captured | Y | All strain gages recorded data | Y |
| All high-speed cameras capture impact | Y | | |

| **Test Results Summary** |
|---|
| Motor A impacted the target in the nominal velocity range and correct orientation (motor shaft normal to the panel surface). During the test the motor penetrated through the aluminum panel and broke up into several distinct pieces.<br>The DIC setup was incorrect and data was not recorded during this test. |

**Photos**


Projectile and Sabot

Projectile Condition After Impact

Target Panel Showing Impact Perforation

B.3.1.2.8 TEST 4-2

| General Test Information | | | |
|---|---|---|---|
| Test Facility: | **SMDC-TC Aerophysics Research Facility** | Test Date | **4/30/2020** |
| ARF Test ID Number | **20-26** | NIAR Test ID Number | **4-2** |

| | |
|---|---|
| **Test Description** | 500 knot impact of Motor A on a 0.063” thick 2024 aluminum panel secured within a 17-4 stainless steel frame |

| Test Conditions | | | |
|---|---|---|---|
| Projectile | Motor A | Target Dimensions | 41”x41”0.063” |
| Projectile mass | 51.1 gm (0.113 lb.) | Nominal Impact Velocity (knots) | 500 |
| Target | 2024 aluminum panel | Actual Impact Velocity (knots) | 507 |

| Test Setup | | | |
|---|---|---|---|
| Target impact angle attained | Y | DIC system recorded properly | Y |
| Gun alignment in tolerance | Y | All load cells recorded data | Y |
| All still camera images captured | Y | All strain gages recorded data | N |
| All high-speed cameras capture impact | Y | | |

| Test Results Summary |
|---|
| Motor A impacted the target in the nominal velocity range and correct orientation (motor shaft normal to the panel surface). During the test the motor penetrated through the aluminum panel and broke up into several distinct pieces.<br>Strain Gages 6 and 12 both had a single solder pad debond from the panel during the test. Strain gage 12 had very high reading, compared to other gages. Strain gage 6 appeared to measure correctly during the test. |

| **Photos** | |
|---|---|
|  | 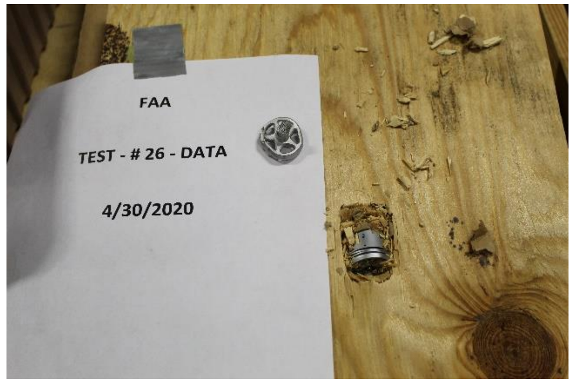 |
| Projectile and Sabot before Impact | Projectile Condition After Impact |
| 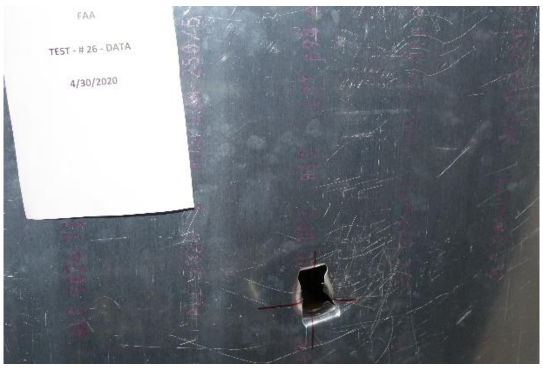 |  |
| Target Panel Showing Impact Perforation | |

B.3.1.2.9 TEST 5-1

| General Test Information | | | |
|---|---|---|---|
| Test Facility: | **SMDC-TC Aerophysics Research Facility** | Test Date | **5/5/2020** |
| ARF Test ID Number | **20-27** | NIAR Test ID Number | **5-1** |

| | |
|---|---|
| **Test Description** | 500 knot impact of Motor A on a 0.25" thick 2024 aluminum panel secured within a 17-4 stainless steel frame |

| Test Conditions | | | |
|---|---|---|---|
| Projectile | Motor A | Target Dimensions | 41"x41"0.25" |
| Projectile mass | 51.0 gm (0.112 lb.) | Nominal Impact Velocity (knots) | 500 |
| Target | 2024 aluminum panel | Actual Impact Velocity (knots) | 520 |

| Test Setup | | | |
|---|---|---|---|
| Target impact angle attained | Y | DIC system recorded properly | Y |
| Gun alignment in tolerance | Y | All load cells recorded data | Y |
| All still camera images captured | Y | All strain gages recorded data | Y |
| All high-speed cameras capture impact | Y | | |

| Test Results Summary |
|---|
| PH 3 electric motor impacted the target in the nominal velocity range and correct orientation (motor shaft normal to the panel surface). During the test the motor did not penetrate through the aluminum panel. The motor left an indentation on the panel. The motor was crushed as it impacted the panel. |

| Photos | |
|---|---|
| 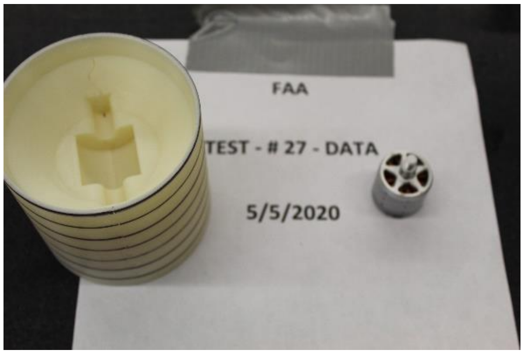 |  |
| Projectile and Sabot | Projectile Condition After Impact |
| 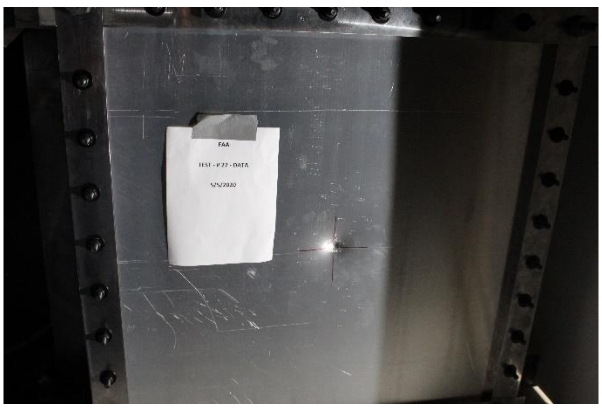 | 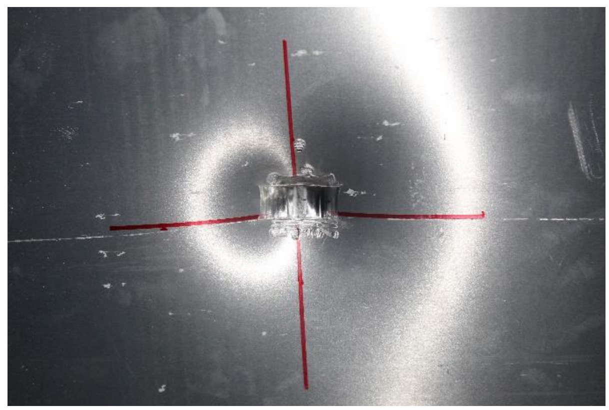 |
| Target Panel Showing Impact Perforation | |

B.3.1.2.10 TEST 5-2

| General Test Information | | | |
|---|---|---|---|
| Test Facility: | **SMDC-TC Aerophysics Research Facility** | Test Date | **5/6/2020** |
| ARF Test ID Number | **20-28** | NIAR Test ID Number | **5-2** |

| | |
|---|---|
| **Test Description** | 500 knot impact of Motor A on a 0.25" thick 2024 aluminum panel secured within a 17-4 stainless steel frame |

| Test Conditions | | | |
|---|---|---|---|
| Projectile | Motor A | Target Dimensions | 41"x41"x0.25" |
| Projectile mass | 50.6 gm (0.1116 lb.) | Nominal Impact Velocity (knots) | 500 |
| Target | 2024 aluminum panel | Actual Impact Velocity (knots) | N/A |

| Test Setup | | | |
|---|---|---|---|
| Target impact angle attained | Y | DIC system recorded properly | Y |
| Gun alignment in tolerance | Y | All load cells recorded data | Y |
| All still camera images captured | Y | All strain gages recorded data | Y |
| All high-speed cameras capture impact | N | | |

| Test Results Summary |
|---|
| Motor A impacted the target in the nominal velocity range and correct orientation (motor shaft normal to the panel surface). During the test the motor did not penetrate through the aluminum panel. The motor left an indentation on the panel. The motor was crushed as it impacted the panel.<br>A solenoid failure caused the gun to fire late. Therefore, the impact showed up later in the data for the load cells and the strain gages. High-Speed Data for Camera 1 and 2 was not captured due to this triggering error. Impact velocity which was calculated from the Camera 1 and 2 high speed video data could not be calculated for this test. |

| **Photos** | |
|---|---|
| 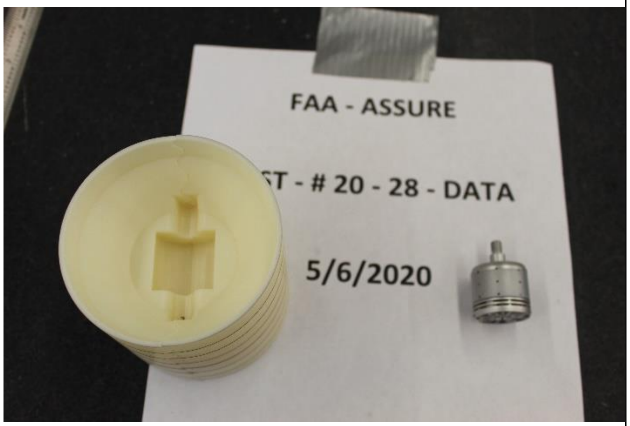 | 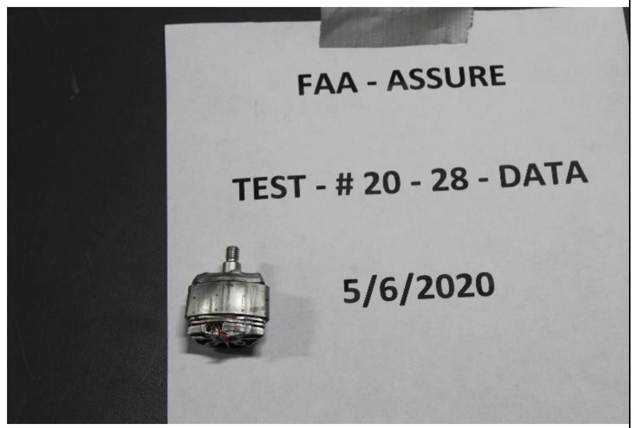 |
| Projectile and Sabot | Projectile Condition After Impact |
|  | 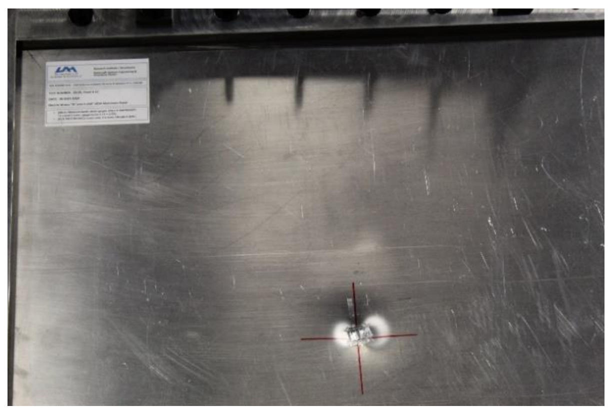 |
| Target Panel Showing Impact Indentation | |

B.3.1.2.11 TEST 6-1

| General Test Information | | | |
|---|---|---|---|
| Test Facility: | **SMDC-TC Aerophysics Research Facility** | Test Date | **05/22/2020** |
| ARF Test ID Number | **20-41** | NIAR Test ID Number | **6-1** |

| | |
|---|---|
| **Test Description** | 500 knot impact of Camera on a 0.063” thick 2024 aluminum panel secured within a 17-4 stainless steel frame |

| Test Conditions | | | |
|---|---|---|---|
| Projectile | Camera | Target Dimensions | 41”x41”x0.063” |
| Projectile mass | 51.9 gm (0.1144 lb.) | Nominal Impact Velocity (knots) | 500 |
| Target | 2024 aluminum panel | Actual Impact Velocity (knots) | 508 |

| Test Setup | | | |
|---|---|---|---|
| Target impact angle attained | Y | DIC system recorded properly | Y |
| Gun alignment in tolerance | Y | All load cells recorded data | Y |
| All still camera images captured | Y | All strain gages recorded data | Y |
| All high-speed cameras capture impact | Y | | |

| Test Results Summary |
|---|
| The camera impacted the target in the nominal velocity range and with the correct orientation (camera lens normal to the panel surface). During the test the camera penetrated through the aluminum panel. The camera broke up into distinct pieces. |

| **Photos** | |
|---|---|
| 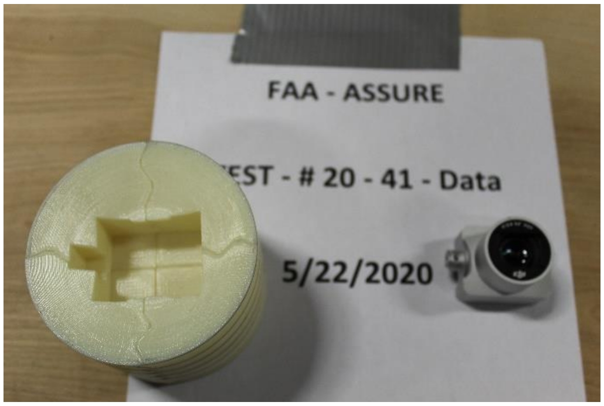 | 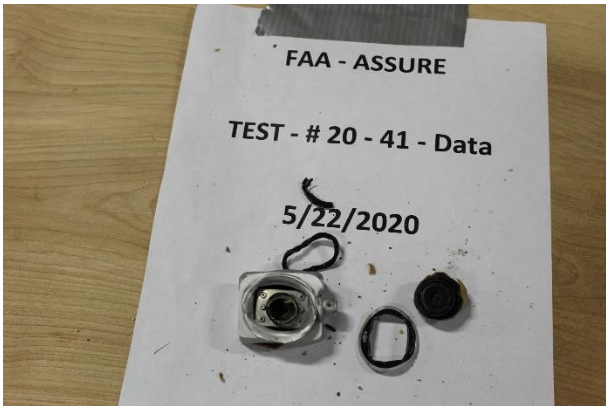 |
| Projectile and Sabot | Projectile Condition After Impact |
| 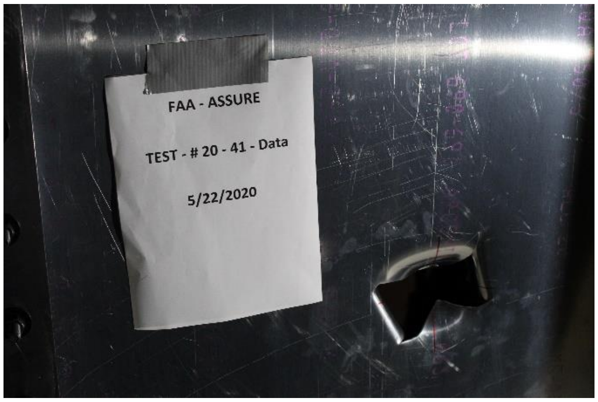 |  |
| Target Panel Showing Impact Perforation | |

B.3.1.2.12 TEST 6-2

| **General Test Information** | | | |
|---|---|---|---|
| Test Facility: | **SMDC-TC Aerophysics Research Facility** | Test Date | **05/26/2020** |
| ARF Test ID Number | **20-42** | NIAR Test ID Number | **6-2** |

| | |
|---|---|
| **Test Description** | 500 knot impact of Camera on a 0.063” thick 2024 aluminum panel secured within a 17-4 stainless steel frame |

| **Test Conditions** | | | |
|---|---|---|---|
| Projectile | Camera | Target Dimensions | 41”x41”0.063” |
| Projectile mass | 52.9 gm (.1166 lb.) | Nominal Impact Velocity (knots) | 500 |
| Target | 2024 aluminum panel | Actual Impact Velocity (knots) | 518 |

| **Test Setup** | | | |
|---|---|---|---|
| Target impact angle attained | Y | DIC system recorded properly | Y |
| Gun alignment in tolerance | Y | All load cells recorded data | Y |
| All still camera images captured | Y | All strain gages recorded data | Y |
| All high-speed cameras capture impact | Y | | |

| **Test Results Summary** |
|---|
| The camera impacted the target in the nominal velocity range and with correct orientation (camera lens normal to the panel surface). During the test the camera penetrated through the aluminum panel. The camera was crushed during the impact. |

| Photos | |
|---|---|
| 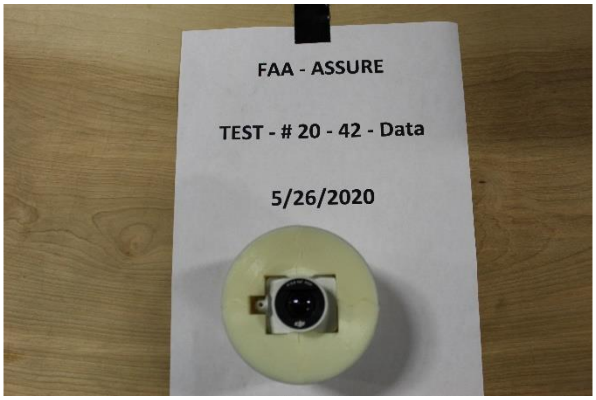 | 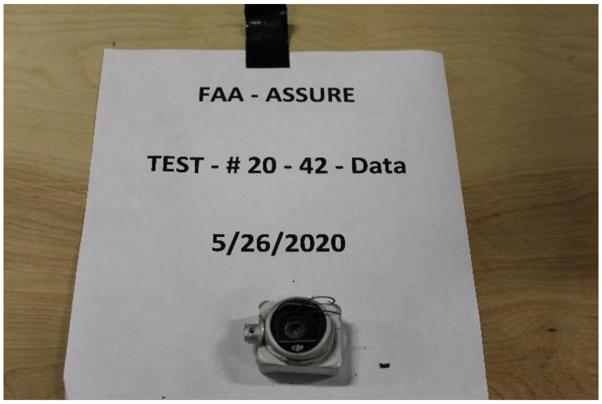 |
| Projectile and Sabot | Projectile Condition After Impact |
| 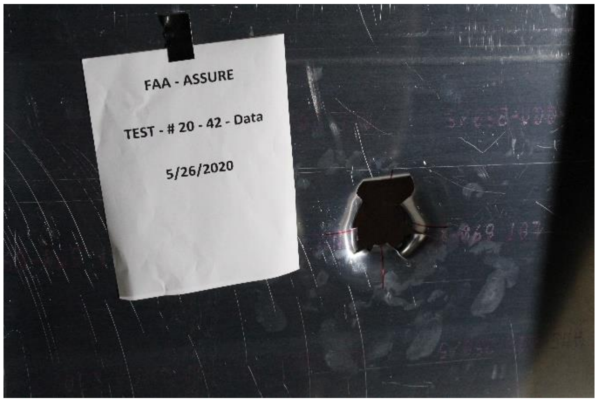 | 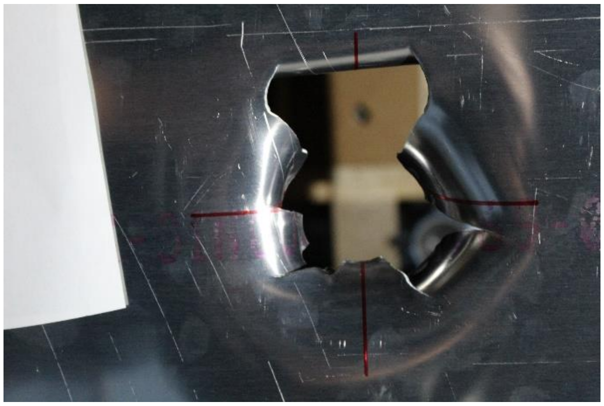 |
| Target Panel Showing Impact Perforation | |

B.3.1.2.13 TEST 7-1

| General Test Information | | | |
|---|---|---|---|
| Test Facility: | **SMDC-TC Aerophysics Research Facility** | Test Date | **05/26/2020** |
| ARFC Test ID Number | **20-43** | NIAR Test ID Number | **7-1** |

| | |
|---|---|
| **Test Description** | 500 knot impact of Camera on a 0.25” thick 2024 aluminum panel secured within a 17-4 stainless steel frame |

| Test Conditions | | | |
|---|---|---|---|
| Projectile | Camera | Target Dimensions | 41”x41”x0.25” |
| Projectile mass | 52.4 gm (0.1155 lb.) | Nominal Impact Velocity (knots) | 500 |
| Target | 2024 aluminum panel | Actual Impact Velocity (knots) | 522 |

| Test Setup | | | |
|---|---|---|---|
| Target impact angle attained | Y | DIC system recorded properly | Y |
| Gun alignment in tolerance | Y | All load cells recorded data | Y |
| All still camera images captured | Y | All strain gages recorded data | Y |
| All high-speed cameras capture impact | Y | | |

| Test Results Summary |
|---|
| Camera impacted the target in the nominal velocity range and correct orientation (camera lens normal to the panel surface). During the test the camera did not penetrate through the aluminum panel. The camera left an indentation on the panel. The camera was crushed as it impacted the panel. |

| Photos | |
|---|---|
| 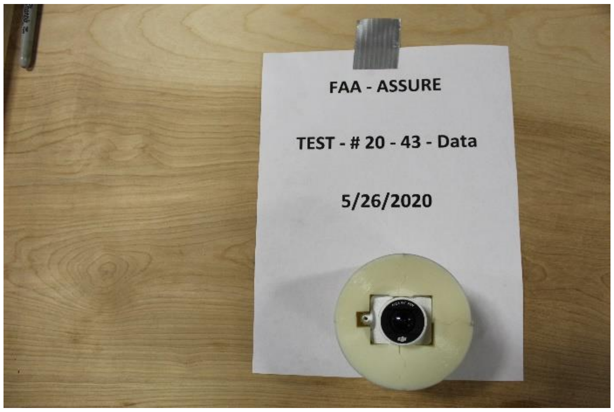 | 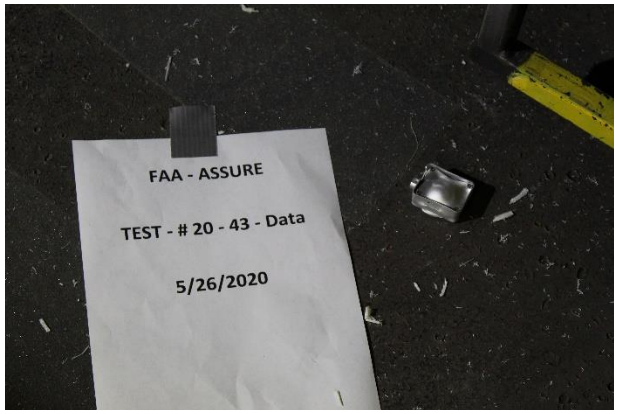 |
| Projectile and Sabot | Projectile Condition After Impact |
| 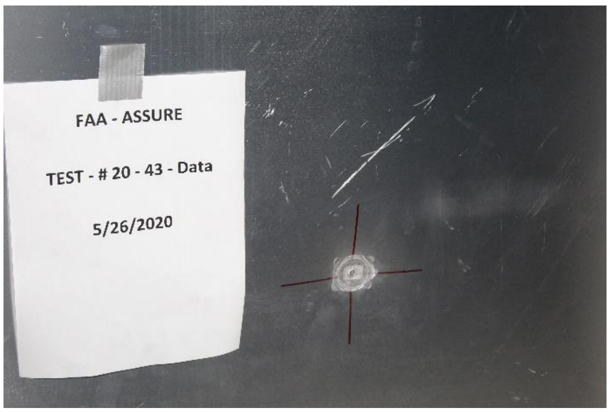 | 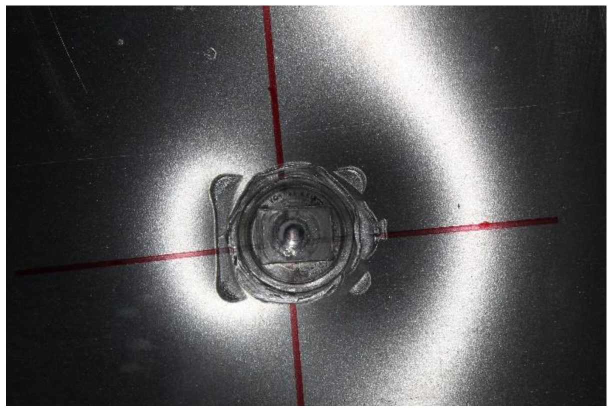 |
| Target Panel Showing Impact Indentation | |

B.3.1.2.14 TEST 7-2

| General Test Information | | | |
|---|---|---|---|
| Test Facility: | **SMDC-TC Aerophysics Research Facility** | Test Date | **05/27//2020** |
| ARF Test ID Number | **20-44** | NIAR Test ID Number | **7-2** |

| | |
|---|---|
| **Test Description** | 500 knot impact of Camera on a 0.25” thick 2024 aluminum panel secured within a 17-4 stainless steel frame |

| Test Conditions | | | |
|---|---|---|---|
| Projectile | Camera | Target Dimensions | 41”x41”x0.25” |
| Projectile mass | 53.1 gm (0.1171 lb.) | Nominal Impact Velocity (knots) | 500 |
| Target | 2024 aluminum panel | Actual Impact Velocity (knots) | 521 |

| Test Setup | | | |
|---|---|---|---|
| Target impact angle attained | Y | DIC system recorded properly | Y |
| Gun alignment in tolerance | Y | All load cells recorded data | Y |
| All still camera images captured | Y | All strain gages recorded data | N |
| All high-speed cameras capture impact | Y | | |

| Test Results Summary |
|---|
| Camera impacted the target in the nominal velocity range and with the correct orientation (camera lens normal to the panel surface). During the test the camera did not penetrate through the aluminum panel. The camera left an indentation on the panel. The camera was crushed as it impacted the panel.<br>Strain gage 4 read exceptionally high spike in strain and was noisier. The high reading and signal noise were likely due to a wiring issue that was fixed before the next test. |

**Photos**

| | |
|---|---|
|  |  |
| Projectile and Sabot | Projectile Condition After Impact |
| 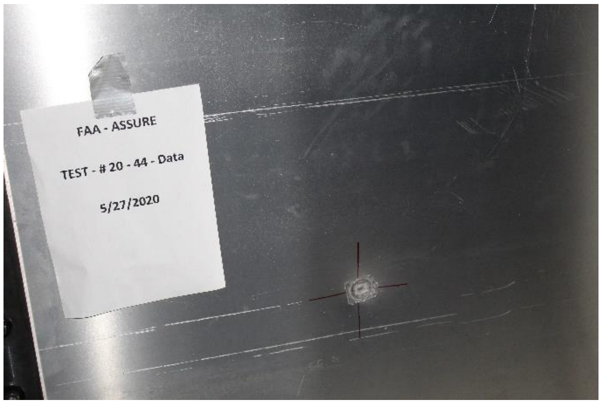 | 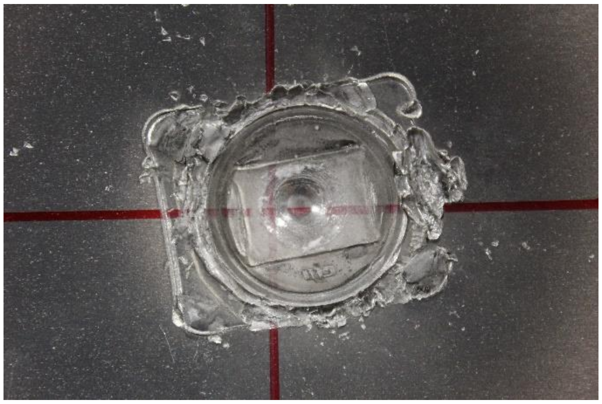 |

Target Panel Showing Impact Indentation

B.3.1.2.15 TEST 8-1

| General Test Information | | | |
|---|---|---|---|
| Test Facility: | **SMDC-TC Aerophysics Research Facility** | Test Date | **07/23/2020** |
| ARF Test ID Number | **20-92** | NIAR Test ID Number | **8-1** |

| | |
|---|---|
| **Test Description** | 50 knot impact of Battery A on a 0.063” thick 2024 aluminum panel secured within a 17-4 stainless steel frame |

| Test Conditions | | | |
|---|---|---|---|
| Projectile | Battery A | Target Dimensions | 41”x41”x0.063” |
| Projectile mass | 343.2 gm (0.7566 lb.) | Nominal Impact Velocity (knots) | 50 |
| Target | 2024 aluminum panel | Actual Impact Velocity (knots) | 52 |

| Test Setup | | | |
|---|---|---|---|
| Target impact angle attained | Y | DIC system recorded properly | Y |
| Gun alignment in tolerance | Y | All load cells recorded data | Y |
| All still camera images captured | Y | All strain gages recorded data | N |
| All high-speed cameras capture impact | Y | | |

| Test Results Summary |
|---|
| Battery A impacted the target in the nominal velocity range and with the correct orientation (battery longitudinal axis normal to the panel surface). During the test the battery did not penetrate the aluminum panel. The battery plastic frame broke into two pieces with the cell pack still attached to one half. The battery did not pose a “Fire Risk”. The battery left an indentation on the panel.<br>Strain gage 13 data was not recorded. |

**Photos**


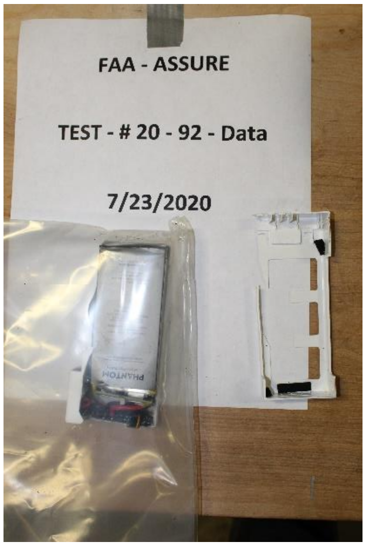


| Projectile and Sabot | Projectile Condition After Impact |
|---|---|

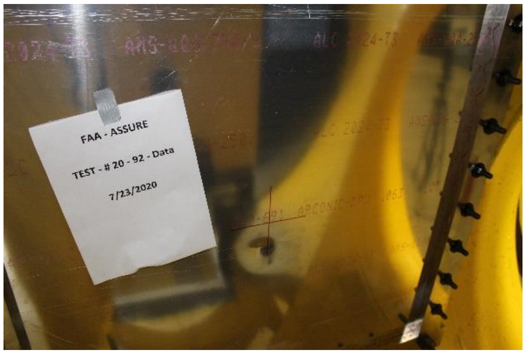


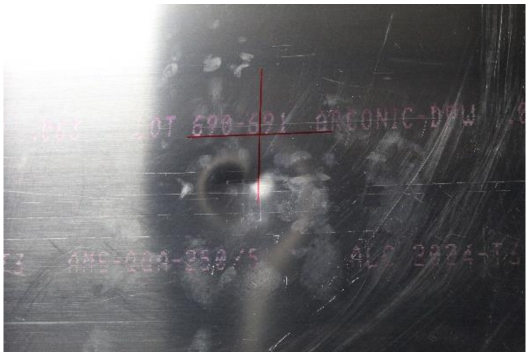

Target Panel Showing Impact Indentation

B.3.1.2.16 TEST 8-2

| General Test Information | | | |
|---|---|---|---|
| Test Facility: | **SMDC-TC Aerophysics Research Facility** | Test Date | **07/24/2020** |
| ARF Test ID Number | **20-93** | NIAR Test ID Number | **8-2** |

| | |
|---|---|
| **Test Description** | 50 knot impact of Battery A on a 0.063” thick 2024 aluminum panel secured within a 17-4 stainless steel frame |

| Test Conditions | | | |
|---|---|---|---|
| Projectile | Battery A | Target Dimensions | 41”x41”x0.063” |
| Projectile mass | 343.7 gm (0.7577 lb.) | Nominal Impact Velocity (knots) | 50 |
| Target | 2024 aluminum panel | Actual Impact Velocity (knots) | 51.5 |

| Test Setup | | | |
|---|---|---|---|
| Target impact angle attained | Y | DIC system recorded properly | Y |
| Gun alignment in tolerance | Y | All load cells recorded data | Y |
| All still camera images captured | Y | All strain gages recorded data | Y |
| All high-speed cameras capture impact | Y | | |

| Test Results Summary |
|---|
| Battery A impacted the target in the nominal velocity range and with the correct orientation (battery longitudinal axis normal to the panel surface). During the test the battery did not penetrate the aluminum panel. The battery plastic frame cracked but the part remained intact. The battery did not pose a “Fire Risk”. |

| **Photos** | |
|---|---|
|   |  |
| Projectile and Sabot | Projectile Condition After Impact |
| 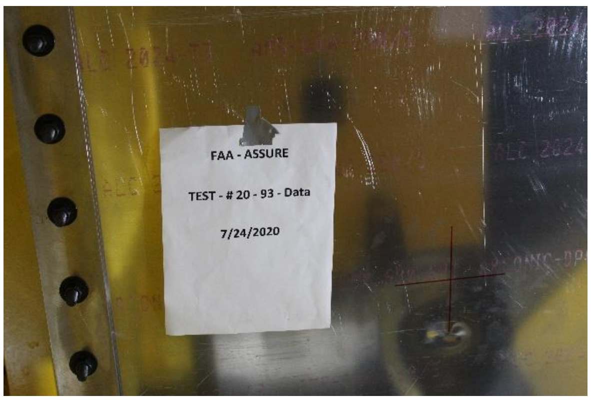  | 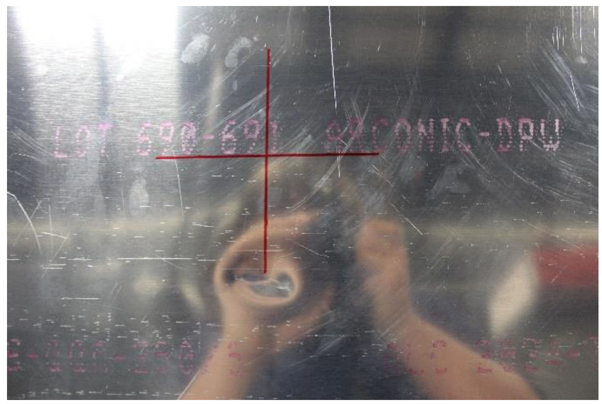 |
| Target Panel showing impact Indentation | |

B.3.1.2.17 TEST 9-1

| General Test Information | | | |
|---|---|---|---|
| Test Facility: | **SMDC-TC Aerophysics Research Facility** | Test Date | **8/5/2020** |
| ARF Test ID Number | **20-106** | NIAR Test ID Number | **9-1** |

| | |
|---|---|
| **Test Description** | 120 knot impact of Battery A on a 0.063” thick 2024 aluminum panel secured within a 17-4 stainless steel frame |

| Test Conditions | | | |
|---|---|---|---|
| Projectile | Battery A | Target Dimensions | 41”x41”x0.063” |
| Projectile mass | 342.6 gm (0.7553 lb.) | Nominal Impact Velocity (knots) | 120 |
| Target | 2024 aluminum panel | Actual Impact Velocity (knots) | 120.87 |

| Test Setup | | | |
|---|---|---|---|
| Target impact angle attained | Y | DIC system recorded properly | Y |
| Gun alignment in tolerance | Y | All load cells recorded data | Y |
| All still camera images captured | Y | All strain gages recorded data | Y |
| All high-speed cameras capture impact | Y | | |

| Test Results Summary |
|---|
| Battery A impacted the target in the nominal velocity range and with the correct orientation (battery longitudinal axis normal to the panel surface). During the test the battery did not penetrate through the aluminum panel. The battery broke into distinct pieces and posed a “Fire Risk”. The battery left an indentation on the panel. |

**Photos**

| | |
|---|---|
|   |  |
| Projectile and Sabot | Projectile Condition After Impact |
|   |  |

Target Panel Showing Impact Indentation

B.3.1.2.18 TEST 9-2

| **General Test Information** | | | |
|---|---|---|---|
| Test Facility: | **SMDC-TC Aerophysics Research Facility** | Test Date | **8/5/2020** |
| ARF Test ID Number | **20-107** | NIAR Test ID Number | **9-2** |

| | |
|---|---|
| **Test Description** | 120 knot impact of Battery A on a 0.063” thick 2024 aluminum panel secured within a 17-4 stainless steel frame |

| **Test Conditions** | | | |
|---|---|---|---|
| Projectile | Battery A | Target Dimensions | 41”x41”x0.063” |
| Projectile mass | 343.1 gm (.7564 lb.) | Nominal Impact Velocity (knots) | 120 |
| Target | 2024 aluminum panel | Actual Impact Velocity (knots) | 118.5 |

| **Test Setup** | | | |
|---|---|---|---|
| Target impact angle attained | Y | DIC system recorded properly | Y |
| Gun alignment in tolerance | Y | All load cells recorded data | Y |
| All still camera images captured | Y | All strain gages recorded data | Y |
| All high-speed cameras capture impact | Y | | |

| **Test Results Summary** |
|---|
| Battery A impacted the target in the nominal velocity range and with the correct orientation (battery longitudinal axis normal to the panel surface). During the test the battery did not penetrate through the aluminum panel. The battery broke into distinct pieces and posed a “Fire Risk”. The battery left an indentation on the panel. |

| Photos | |
|---|---|
| 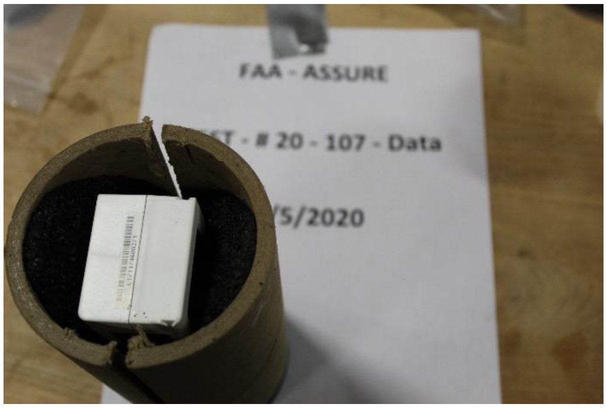  |  |
| Projectile and Sabot | Projectile Condition After Impact |
|   |  |
| Target Panel Showing Impact Indentation | |

B.3.1.2.19 TEST 10-1

| General Test Information | | | |
|---|---|---|---|
| Test Facility: | **SMDC-TC Aerophysics Research Facility** | Test Date | **8/4/2020** |
| ARF Test ID Number | **20-104** | NIAR Test ID Number | **10-1** |

| | |
|---|---|
| **Test Description** | 120 knot impact of Battery A on a 0.25” thick 2024 aluminum panel secured within a 17-4 stainless steel frame |

| Test Conditions | | | |
|---|---|---|---|
| Projectile | Battery A | Target Dimensions | 41”x41”x0.25” |
| Projectile mass | 343.8 gm (0.7579 lb.) | Nominal Impact Velocity (knots) | 120 |
| Target | 2024 aluminum panel | Actual Impact Velocity (knots) | 116 |

| Test Setup | | | |
|---|---|---|---|
| Target impact angle attained | Y | DIC system recorded properly | Y |
| Gun alignment in tolerance | Y | All load cells recorded data | Y |
| All still camera images captured | Y | All strain gages recorded data | Y |
| All high-speed cameras capture impact | Y | | |

| Test Results Summary |
|---|
| Battery A impacted the target in the nominal velocity range and correct orientation (battery longitudinal axis normal to the panel surface). During the test the battery did not penetrate through the aluminum panel. The battery left a very slight indention on the aluminum panel. The battery broke into two distinct pieces and posed a “Fire Risk”. |

| Photos | |
|---|---|
| 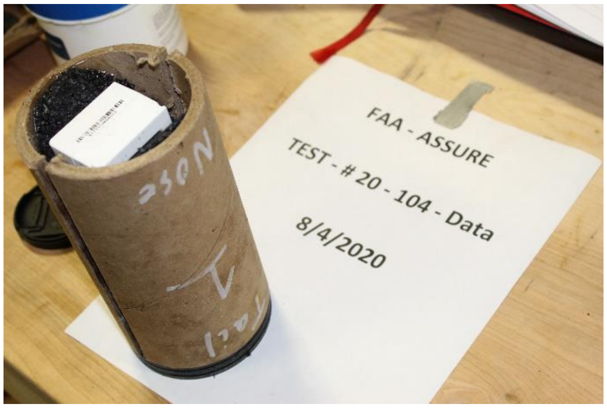 |  |
| Projectile and Sabot | Projectile Condition After Impact |
|  |  |
| Target Panel Showing Impact Indentation | |

B.3.1.2.20 TEST 10-2

| General Test Information | | | |
|---|---|---|---|
| Test Facility: | **SMDC-TC Aerophysics Research Facility** | Test Date | **8/4/2020** |
| ARF Test ID Number | **20-105** | NIAR Test ID Number | **10-2** |

| | |
|---|---|
| **Test Description** | 120 knot impact of Battery A on a 0.25” thick 2024 aluminum panel secured within a 17-4 stainless steel frame |

| Test Conditions | | | |
|---|---|---|---|
| Projectile | Battery A | Target Dimensions | 41”x41”x0.25” |
| Projectile mass | 334.5 gm (0.7595 lb.) | Nominal Impact Velocity (knots) | 120 |
| Target | 2024 aluminum panel | Actual Impact Velocity (knots) | 122 |

| Test Setup | | | |
|---|---|---|---|
| Target impact angle attained | Y | DIC system recorded properly | Y |
| Gun alignment in tolerance | Y | All load cells recorded data | Y |
| All still camera images captured | Y | All strain gages recorded data | Y |
| All high-speed cameras capture impact | Y | | |

| Test Results Summary |
|---|
| Battery A impacted the target in the nominal velocity range and correct orientation (battery longitudinal axis normal to the panel surface). During the test the battery did not penetrate through the aluminum panel. The battery left a slight indention on the aluminum panel. The battery broke into two distinct pieces and posed a “Fire Risk”. Red residue in the tank by the battery, post-impact, indicated that the battery and ambient moisture generated hydrofluoric acid. |

| **Photos** | |
|---|---|
| 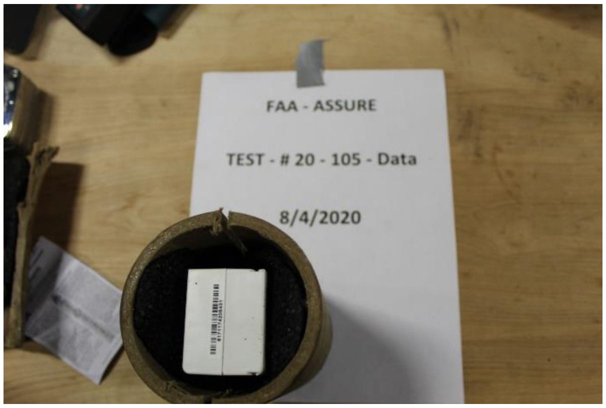 |  |
| Projectile and Sabot | Projectile Condition After Impact |
|  | 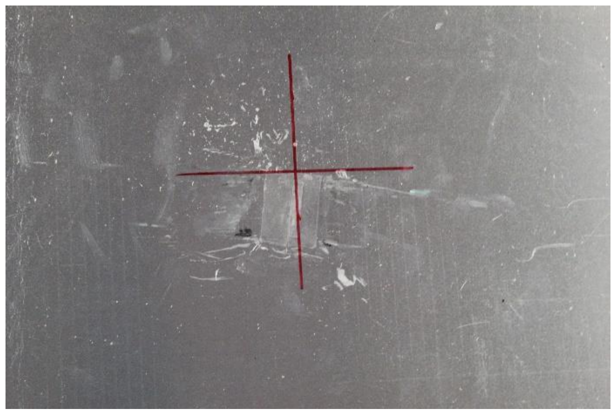 |
| Target Panel Showing Impact Marks | |

B.3.1.2.21 TEST 11-1

| General Test Information | | | |
|---|---|---|---|
| Test Facility: | **SMDC-TC Aerophysics Research Facility** | Test Date | **06/09/2020** |
| ARF Test ID Number | **20-55** | NIAR Test ID Number | **11-1** |

| | |
|---|---|
| **Test Description** | 120 knot impact of Motor A on a 0.063” thick 2024 aluminum panel secured within a 17-4 stainless steel frame |

| Test Conditions | | | |
|---|---|---|---|
| Projectile | Motor A | Target Dimensions | 41”x41”x0.063” |
| Projectile mass | 50.8 gm (0.1119 lb.) | Nominal Impact Velocity (knots) | 120 |
| Target | 2024 aluminum panel | Actual Impact Velocity (knots) | 124 |

| Test Setup | | | |
|---|---|---|---|
| Target impact angle attained | Y | DIC system recorded properly | Y |
| Gun alignment in tolerance | Y | All load cells recorded data | Y |
| All still camera images captured | Y | All strain gages recorded data | Y |
| All high-speed cameras capture impact | Y | | |

| Test Results Summary |
|---|
| Motor A impacted the target in the nominal velocity range and with the correct orientation (motor shaft normal to the panel surface). During the test the motor left an indention on the aluminum panel. The motor did not deform much nor did break. |

**Photos**


Projectile and Sabot

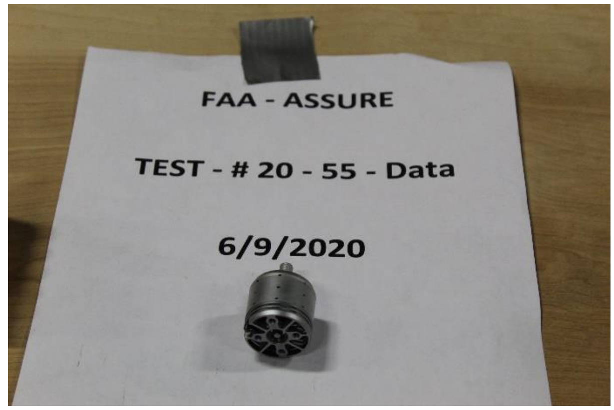


Projectile Condition After Impact

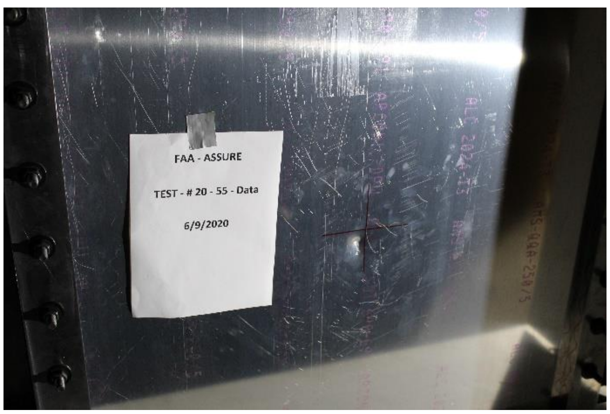


Target Panel Showing Impact Indentation

B.3.1.2.22 TEST 11-2

| General Test Information | | | |
|---|---|---|---|
| Test Facility: | **SMDC-TC Aerophysics Research Facility** | Test Date | **06/10/2020** |
| ARF Test ID Number | **20-56** | NIAR Test ID Number | **11-2** |

| | |
|---|---|
| **Test Description** | 120 knot impact of Motor A on a 0.063” thick 2024 aluminum panel secured within a 17-4 stainless steel frame |

| Test Conditions | | | |
|---|---|---|---|
| Projectile | Motor A | Target Dimensions | 41”x41”x0.063” |
| Projectile mass | 51.8 gm (0.1142 lb.) | Nominal Impact Velocity (knots) | 120 |
| Target | 2024 aluminum panel | Actual Impact Velocity (knots) | 120 |

| Test Setup | | | |
|---|---|---|---|
| Target impact angle attained | Y | DIC system recorded properly | Y |
| Gun alignment in tolerance | Y | All load cells recorded data | Y |
| All still camera images captured | Y | All strain gages recorded data | Y |
| All high-speed cameras capture impact | Y | | |

| Test Results Summary |
|---|
| Motor A impacted the target in the nominal velocity range and with the correct orientation (motor shaft normal to the panel surface). During the test the motor left a slight indention on the aluminum panel. The motor did not deform much nor did it break. |

| **Photos** | |
|---|---|
|  | 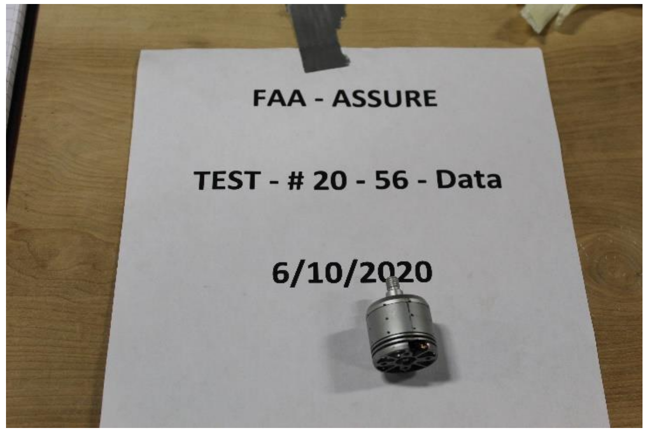 |
| Projectile and Sabot | Projectile Condition After Impact |
| 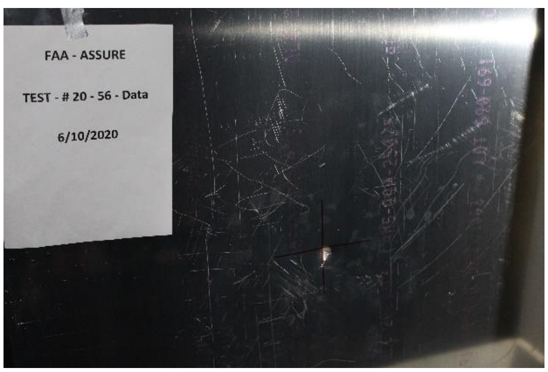 |  |
| Target Panel Showing Impact Indentation | |

B.3.1.2.23 TEST 12-1

| General Test Information | | | |
|---|---|---|---|
| Test Facility: | **SMDC-TC Aerophysics Research Facility** | Test Date | **07/02/2020** |
| ARF Test ID Number | **20-76** | NIAR Test ID Number | **12-1** |

| | |
|---|---|
| **Test Description** | 50 knot impact of Motor A on a 0.063” thick 2024 aluminum panel secured within a 17-4 stainless steel frame |

| Test Conditions | | | |
|---|---|---|---|
| Projectile | Motor A | Target Dimensions | 41”x41”x0.063” |
| Projectile mass | 51.3 gm (0.1131 lb.) | Nominal Impact Velocity (knots) | 50 |
| Target | 2024 aluminum panel | Actual Impact Velocity (knots) | 57 |

| Test Setup | | | |
|---|---|---|---|
| Target impact angle attained | Y | DIC system recorded properly | Y |
| Gun alignment in tolerance | Y | All load cells recorded data | Y |
| All still camera images captured | Y | All strain gages recorded data | Y |
| All high-speed cameras capture impact | N | | |

| Test Results Summary |
|---|
| Motor A impacted the target slightly higher than the nominal velocity range and, but it did impact in the correct orientation (motor shaft normal to the panel surface). During the test the motor left a slight indention on the aluminum panel. The motor did not deform much nor did break.<br>High-Speed Camera 3 was used as a temporary replacement for one of the DIC cameras thus there was no high-speed camera 3 video for this test. |

**Photos**

| | |
|---|---|
|  | 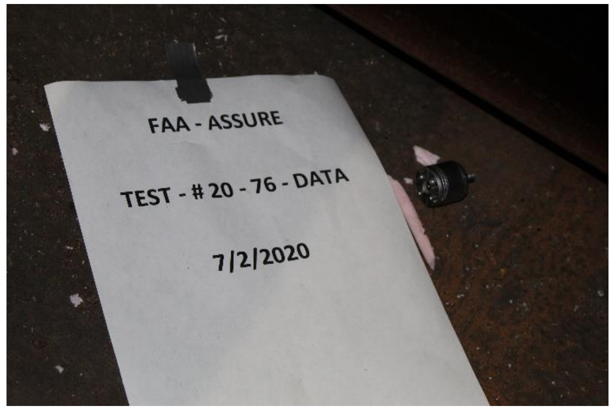 |
| Projectile and Sabot | Projectile Condition After Impact |
|  | 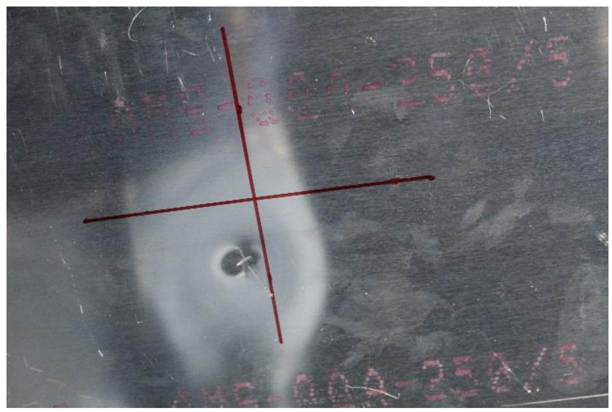 |
| Target Panel Showing Impact Indentation | |

B.3.1.2.24 TEST 12-2

| General Test Information | | | |
|---|---|---|---|
| Test Facility: | **SMDC-TC Aerophysics Research Facility** | Test Date | **07/02/2020** |
| ARF Test ID Number | **20-77** | NIAR Test ID Number | **12-2** |

| | |
|---|---|
| **Test Description** | 50 knot impact of Motor A on a 0.063” thick 2024 aluminum panel secured within a 17-4 stainless steel frame |

| Test Conditions | | | |
|---|---|---|---|
| Projectile | Motor A | Target Dimensions | 41”x41”x0.063” |
| Projectile mass | 50.8 gm (0.1119 lb.) | Nominal Impact Velocity (knots) | 50 |
| Target | 2024 aluminum panel | Actual Impact Velocity (knots) | 57 |

| Test Setup | | | |
|---|---|---|---|
| Target impact angle attained | Y | DIC system recorded properly | Y |
| Gun alignment in tolerance | Y | All load cells recorded data | Y |
| All still camera images captured | Y | All strain gages recorded data | Y |
| All high-speed cameras capture impact | N | | |

| Test Results Summary |
|---|
| Motor A impacted the target slightly higher than the nominal velocity range and correct orientation (motor shaft normal to the panel surface). During the test the motor left a slight indention on the aluminum panel. The motor did not deform much nor did break.<br>High-Speed Camera 3 was used as a temporary replacement for one of the DIC cameras thus there ~~is~~was no high-speed camera 3 video for this test. |

| Photos | |
|---|---|
|  |  |
| Projectile and Sabot | Projectile Condition After Impact |
|  | 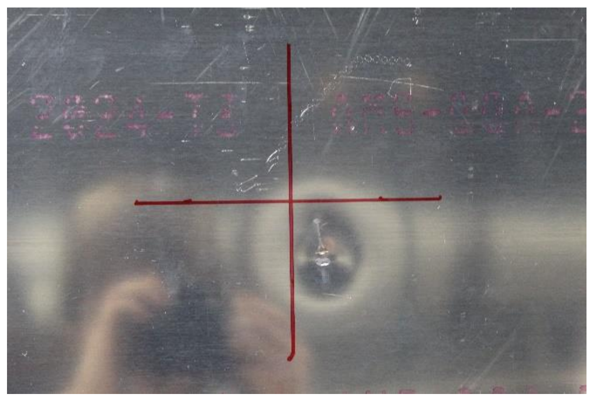 |
| Target Panel Showing Impact Indentation | |

B.3.1.2.25 TEST 13-1

| General Test Information | | | |
|---|---|---|---|
| Test Facility: | **SMDC-TC Aerophysics Research Facility** | Test Date | **06/16/2020** |
| ARF Test ID Number | **20-58** | NIAR Test ID Number | **13-1** |

| | |
|---|---|
| **Test Description** | 120 knot impact of Camera on a 0.063” thick 2024 aluminum panel secured within a 17-4 stainless steel frame |

| Test Conditions | | | |
|---|---|---|---|
| Projectile | Camera | Target Dimensions | 41”x41”x0.063” |
| Projectile mass | 51.3 gm (0.1131 lb.) | Nominal Impact Velocity (knots) | 120 |
| Target | 2024 aluminum panel | Actual Impact Velocity (knots) | 121 |

| Test Setup | | | |
|---|---|---|---|
| Target impact angle attained | Y | DIC system recorded properly | Y |
| Gun alignment in tolerance | Y | All load cells recorded data | Y |
| All still camera images captured | Y | All strain gages recorded data | Y |
| All high-speed cameras capture impact | N | | |

| Test Results Summary |
|---|
| Camera impacted the target in the nominal velocity range and correct orientation (camera lens normal to the panel surface). During the test the camera left a slight indention on the aluminum panel. The camera did not deform nor did break.<br>High-Speed Camera 3 was used as a temporary replacement for one of the DIC cameras thus there was no high-speed camera 3 video for this test. |

<table>
<tr><th colspan="2">Photos</th></tr>
<tr><td>
</td><td>N/A</td></tr>
<tr><td>Projectile and Sabot</td><td>Projectile Condition After Impact</td></tr>
<tr><td>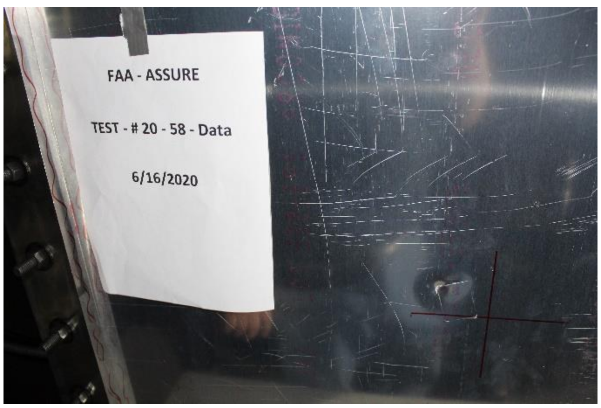
</td><td>
</td></tr>
<tr><td colspan="2">Target Panel Showing Impact Indentation</td></tr>
</table>

B.3.1.2.26 TEST 13-2

| **General Test Information** | | | |
|---|---|---|---|
| Test Facility: | **SMDC-TC Aerophysics Research Facility** | Test Date | **06/19/2020** |
| ARF Test ID Number | **20-60** | NIAR Test ID Number | **13-2** |

| | |
|---|---|
| **Test Description** | 120 knot impact of Camera on a 0.063” thick 2024 aluminum panel secured within a 17-4 stainless steel frame |

| **Test Conditions** | | | |
|---|---|---|---|
| Projectile | Camera | Target Dimensions | 41”x41”x0.063” |
| Projectile mass | 52.3 gm (0.1153 lb.) | Nominal Impact Velocity (knots) | 120 |
| Target | 2024 aluminum panel | Actual Impact Velocity (knots) | 123 |

| **Test Setup** | | | |
|---|---|---|---|
| Target impact angle attained | Y | DIC system recorded properly | Y |
| Gun alignment in tolerance | Y | All load cells recorded data | Y |
| All still camera images captured | Y | All strain gages recorded data | Y |
| All high-speed cameras capture impact | N | | |

| **Test Results Summary** |
|---|
| Camera impacted the target in the nominal velocity range and correct orientation (camera lens normal to the panel surface). During the test the camera left a slight indention on the aluminum panel. The camera did not deform nor did break.<br>High-Speed Camera 3 was used as a temporary replacement for one of the DIC cameras thus there was no high-speed camera 3 video for this test. |

**Photos**



| Projectile and Sabot | Projectile Condition After Impact |
|---|---|

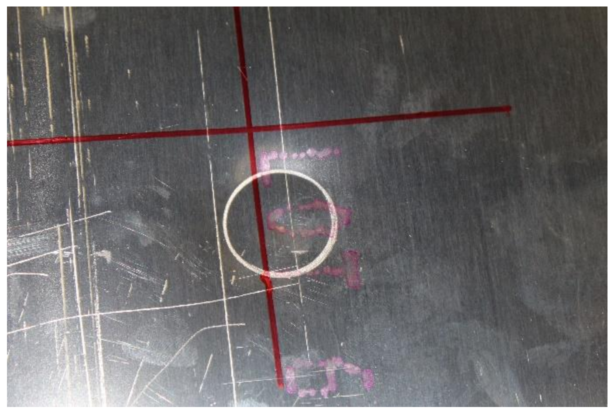

Target Panel Showing Impact Indentation

B.3.1.2.27 TEST 14-1

| General Test Information | | | |
|---|---|---|---|
| Test Facility: | **SMDC-TC Aerophysics Research Facility** | Test Date | **/2020** |
| ARF Test ID Number | **20-72** | NIAR Test ID Number | **14-1** |

| | |
|---|---|
| **Test Description** | 50 knot impact of Camera on a 0.063” thick 2024 aluminum panel secured within a 17-4 stainless steel frame |

| Test Conditions | | | |
|---|---|---|---|
| Projectile | Camera | Target Dimensions | 41”x41”x0.063” |
| Projectile mass | 52.3 gm (0.1153 lb.) | Nominal Impact Velocity (knots) | 50 |
| Target | 2024 aluminum panel | Actual Impact Velocity (knots) | 53 |

| Test Setup | | | |
|---|---|---|---|
| Target impact angle attained | Y | DIC system recorded properly | Y |
| Gun alignment in tolerance | Y | All load cells recorded data | Y |
| All still camera images captured | Y | All strain gages recorded data | Y |
| All high-speed cameras capture impact | N | | |

| Test Results Summary |
|---|
| Camera impacted the target in the nominal velocity range and correct orientation (camera lens normal to the panel surface). During the test the camera left a slight indention on the aluminum panel. The camera did not deform nor did break.<br>High-Speed Camera 3 was used as a temporary replacement for one of the DIC cameras thus there was no high-speed camera 3 video for this test. |

<table>
<tr><th colspan="2">Photos</th></tr>
<tr><td>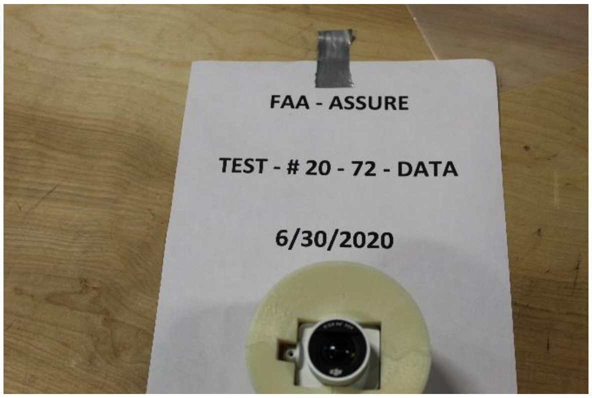
</td><td>
</td></tr>
<tr><td>Projectile and Sabot</td><td>Projectile Condition After Impact</td></tr>
<tr><td>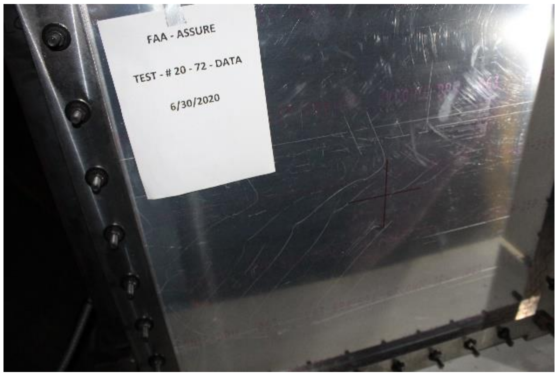
</td><td></td></tr>
<tr><td colspan="2">Target Panel Showing Impact Indentation</td></tr>
</table>

B.3.1.2.28 TEST 14-2

| General Test Information | | | |
|---|---|---|---|
| Test Facility: | **SMDC-TC Aerophysics Research Facility** | Test Date | **07/01/2020** |
| ARF Test ID Number | **20-73** | NIAR Test ID Number | **14-2** |

| | |
|---|---|
| **Test Description** | 50 knot impact of Camera on a 0.063” thick 2024 aluminum panel secured within a 17-4 stainless steel frame |

| Test Conditions | | | |
|---|---|---|---|
| Projectile | Camera | Target Dimensions | 41”x41”x0.063” |
| Projectile mass | 52.2 gm (0.1151 lb.) | Nominal Impact Velocity (knots) | 50 |
| Target | 2024 aluminum panel | Actual Impact Velocity (knots) | 48.6 |

| Test Setup | | | |
|---|---|---|---|
| Target impact angle attained | Y | DIC system recorded properly | Y |
| Gun alignment in tolerance | Y | All load cells recorded data | Y |
| All still camera images captured | Y | All strain gages recorded data | Y |
| All high-speed cameras capture impact | N | | |

| Test Results Summary |
|---|
| Camera impacted the target in the nominal velocity range and with the correct orientation (camera lens normal to the panel surface). During the test the camera left a slight indention on the aluminum panel. The camera did not deform nor did break.<br>High-Speed Camera 3 was used as a temporary replacement for one of the DIC cameras thus there was no high-speed camera 3 video for this test. |

<table>
<tr><th colspan="2">Photos</th></tr>
<tr><td>
</td><td>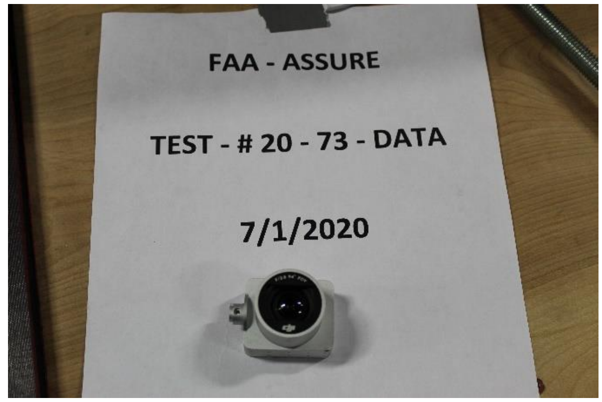
</td></tr>
<tr><td>Projectile and Sabot</td><td>Projectile Condition After Impact</td></tr>
<tr><td>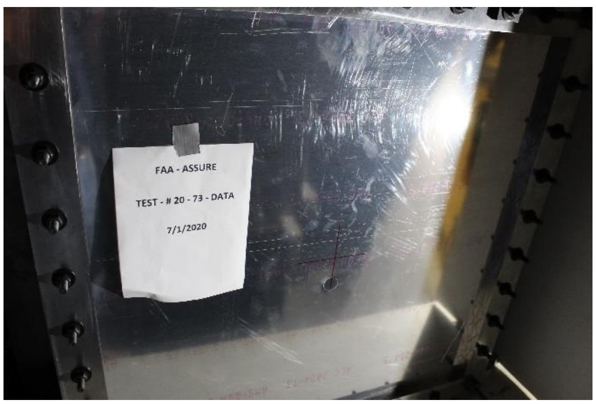
</td><td>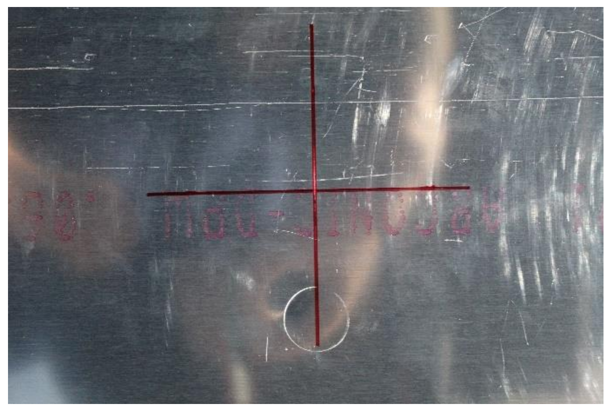</td></tr>
<tr><td colspan="2">Target Panel Showing Impact Indentation</td></tr>
</table>

B.3.1.2.29 TEST 15-1

| General Test Information | | | |
|---|---|---|---|
| Test Facility: | **SMDC-TC Aerophysics Research Facility** | Test Date | **9/25/2020** |
| ARF Test ID Number | **20-148** | NIAR Test ID Number | **15-1** |

| | |
|---|---|
| **Test Description** | 500 knot impact of Battery B on a Sharp Blade secured within a 17-4 stainless steel frame |

| Test Conditions | | | |
|---|---|---|---|
| Projectile | Battery B | Target Dimensions | 36” span, 9.987” chord length, 0.21 leading edge radius, 1.263” max. thickness |
| Projectile mass | gm (lb.) | Nominal Impact Velocity (knots) | 500 |
| Target | 2024 aluminum plate with a representative airfoil leading edge | Actual Impact Velocity (knots) | 509.5 |

| Test Setup | | | |
|---|---|---|---|
| Target impact angle attained | Y | DIC system recorded properly | N/A |
| Gun alignment in tolerance | Y | All load cells recorded data | Y |
| All still camera images captured | Y | All strain gages recorded data | N/A |
| All high-speed cameras capture impact | Y | | |

| Test Results Summary |
|---|
| Battery B impacted the target in the nominal velocity range and with the correct orientation (longitudinal axis of the battery normal to the surface of the blade leading edge). During the test the battery did not penetrate through the Sharp Blade. The battery shattered into multiple fragments.<br>Strain gages and DIC Cameras were not used in the Sharp Blade tests. |

| Photos | |
|---|---|
|  |  |
| Projectile and Sabot | Projectile Condition After Impact |
|  |  |
| Target Sharp Edged Blade Showing Impact Marks | |

B.3.1.2.30 TEST 15-2

| General Test Information | | | |
|---|---|---|---|
| Test Facility: | **SMDC-TC Aerophysics Research Facility** | Test Date | **9/24/2020** |
| ARF Test ID Number | **20-145** | NIAR Test ID Number | **15-2** |

| | |
|---|---|
| **Test Description** | 500 knot impact of Battery B on a Sharp Blade secured within a 17-4 stainless steel frame |

| Test Conditions | | | |
|---|---|---|---|
| Projectile | Battery B | Target Dimensions | 36” span, 9.987” chord length, 0.21 leading edge radius, 1.263” max. thickness |
| Projectile mass | 259.6 gm (0.572 lb.) | Nominal Impact Velocity (knots) | 500 |
| Target | 2024 aluminum plate with a representative airfoil leading edge | Actual Impact Velocity (knots) | 498.87 |

| Test Setup | | | |
|---|---|---|---|
| Target impact angle attained | Y | DIC system recorded properly | N/A |
| Gun alignment in tolerance | Y | All load cells recorded data | N |
| All still camera images captured | Y | All strain gages recorded data | N/A |
| All high-speed cameras capture impact | Y | | |

| Test Results Summary |
|---|
| Battery B impacted the target in the nominal velocity range and correct orientation (longitudinal axis of the battery normal to the surface of the blade leading edge). During the test the battery did not penetrate through the sharp blade. The battery shattered into multiple fragments.<br>Strain gages and DIC Cameras were not used in the Sharp Blade tests. |

| **Photos** | |
|---|---|
| 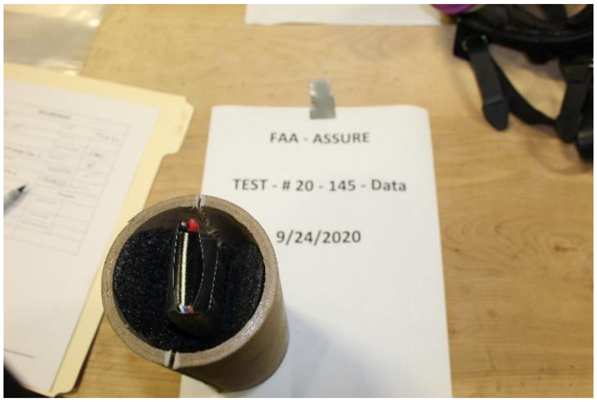  |  |
| Projectile and Sabot | Projectile Condition After Impact |
|  |  |
| Target Sharp Edged Blade Showing Impact Marks | |

B.3.1.2.31 TEST 16-1

| **General Test Information** | | | |
|---|---|---|---|
| Test Facility: | **SMDC-TC Aerophysics Research Facility** | Test Date | **9/10/2020** |
| ARF Test ID Number | **20-129** | NIAR Test ID Number | **16-1** |

| | |
|---|---|
| **Test Description** | 500 knot impact of Battery B on a 0.063” thick 2024 aluminum panel secured within a 17-4 stainless steel frame |

| **Test Conditions** | | | |
|---|---|---|---|
| Projectile | Battery B | Target Dimensions | 41”x41”x0.063” |
| Projectile mass | 264.8 gm (0.584 lb.) | Nominal Impact Velocity (knots) | 500 |
| Target | 2024 aluminum panel | Actual Impact Velocity (knots) | 509.5 |

| **Test Setup** | | | |
|---|---|---|---|
| Target impact angle attained | Y | DIC system recorded properly | Y |
| Gun alignment in tolerance | Y | All load cells recorded data | Y |
| All still camera images captured | Y | All strain gages recorded data | Y |
| All high-speed cameras capture impact | Y | | |

| **Test Results Summary** |
|---|
| Battery B impacted the target in the nominal velocity range and correct orientation (battery longitudinal axis normal to the panel surface). During the test the battery penetrated through the aluminum panel and broke up into distinct pieces. |

<table>
<tr><th colspan="2">Photos</th></tr>
<tr><td>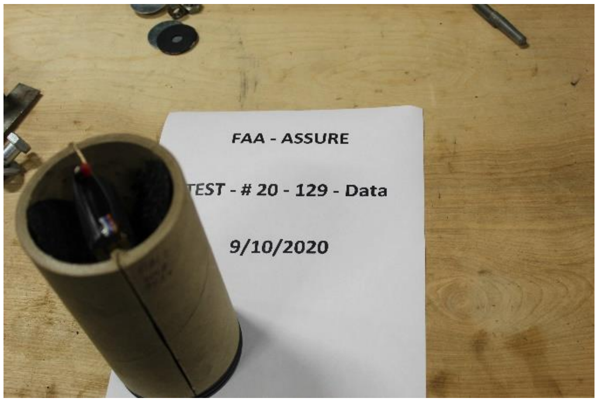
</td><td>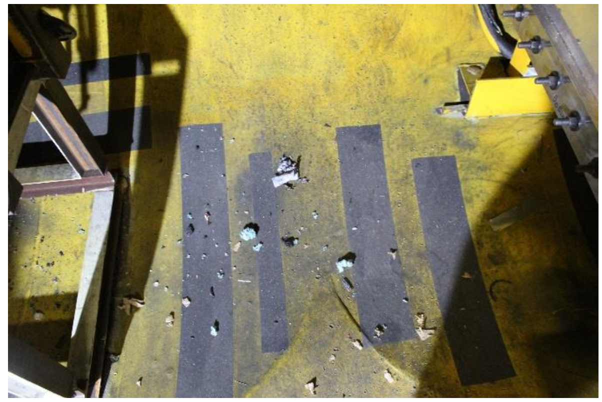</td></tr>
<tr><td>Projectile and Sabot</td><td>Projectile Condition After Impact</td></tr>
<tr><td>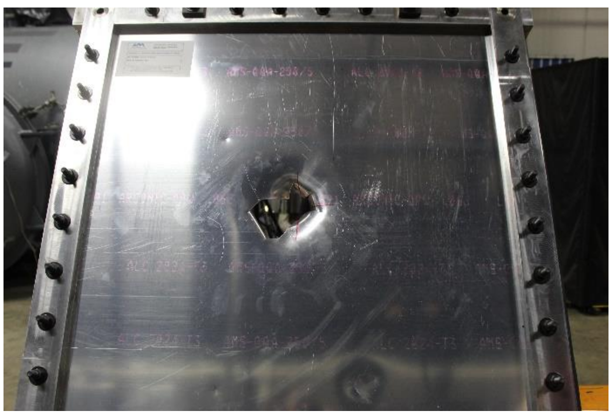</td><td>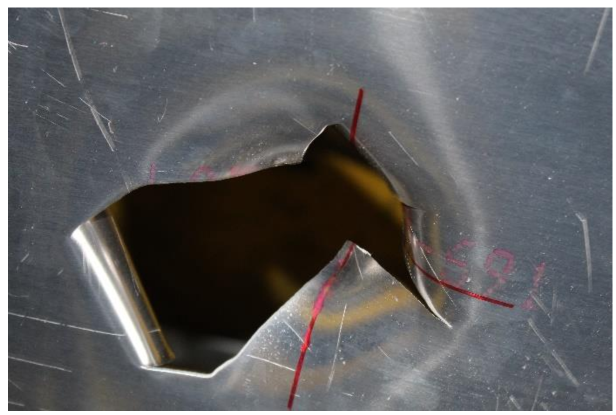</td></tr>
<tr><td colspan="2">Target Panel Showing Impact Perforation</td></tr>
</table>

B.3.1.2.32 TEST 16-2

| General Test Information | | | |
|---|---|---|---|
| Test Facility: | **SMDC-TC Aerophysics Research Facility** | Test Date | **9/11/2020** |
| ARF Test ID Number | **20-130** | NIAR Test ID Number | **16-2** |

| | |
|---|---|
| **Test Description** | 500 knot impact of Battery B on a 0.063” thick 2024 aluminum panel secured within a 17-4 stainless steel frame |

| Test Conditions | | | |
|---|---|---|---|
| Projectile | Battery B | Target Dimensions | 41”x41”x0.063” |
| Projectile mass | 259.6 gm (0.572 lb.) | Nominal Impact Velocity (knots) | 500 |
| Target | 2024 aluminum panel | Actual Impact Velocity (knots) | 499.46 |

| Test Setup | | | |
|---|---|---|---|
| Target impact angle attained | Y | DIC system recorded properly | Y |
| Gun alignment in tolerance | Y | All load cells recorded data | Y |
| All still camera images captured | Y | All strain gages recorded data | Y |
| All high-speed cameras capture impact | Y | | |

| Test Results Summary |
|---|
| Battery B impacted the target in the nominal velocity range and correct orientation (battery longitudinal axis normal to the panel surface). During the test the battery penetrated through the aluminum panel and broke up into multiple fragments. |

| Photos | |
|---|---|
|  | 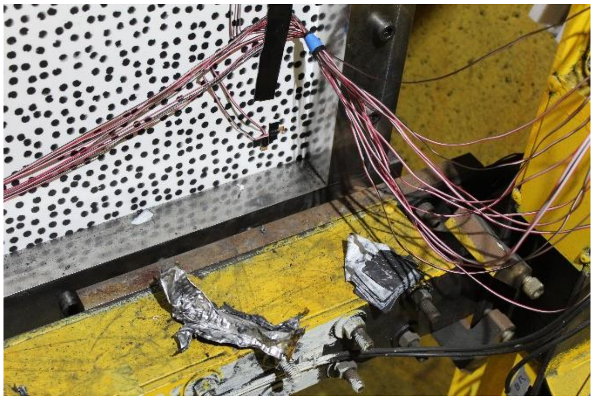 |
| Projectile and Sabot | Projectile Condition After Impact |
| 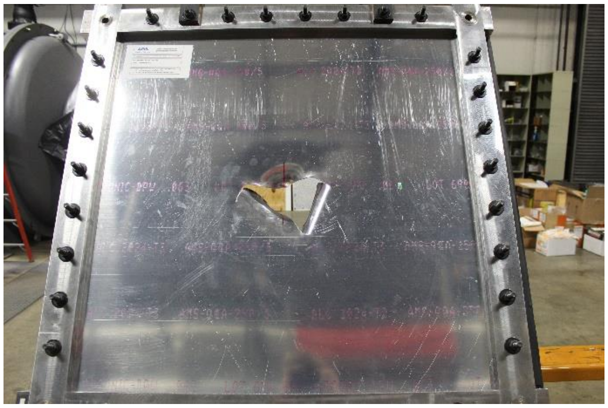 | 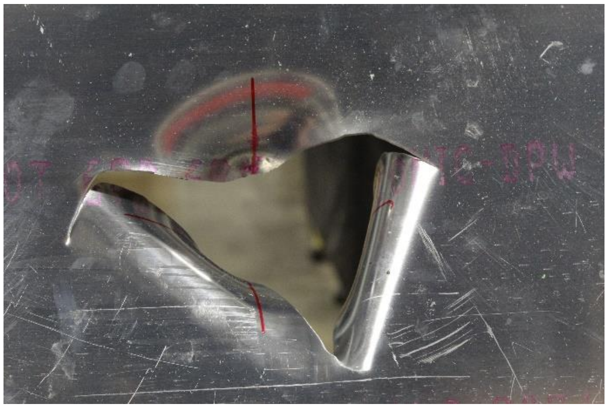 |
| Target Panel Showing Impact Perforation | |

B.3.1.2.33 TEST 17-1

| General Test Information | | | |
|---|---|---|---|
| Test Facility: | **SMDC-TC Aerophysics Research Facility** | Test Date | **9/8/2020** |
| ARF Test ID Number | **20-127** | NIAR Test ID Number | **17-1** |

| | |
|---|---|
| **Test Description** | 500 knot impact of Battery B on a 0.25" thick 2024 aluminum panel secured within a 17-4 stainless steel frame |

| Test Conditions | | | |
|---|---|---|---|
| Projectile | Battery B | Target Dimensions | 41"x41"x0.25" |
| Projectile mass | 263.9 gm (0.582 lb.) | Nominal Impact Velocity (knots) | 500 |
| Target | 2024 aluminum panel | Actual Impact Velocity (knots) | 499.46 |

| Test Setup | | | |
|---|---|---|---|
| Target impact angle attained | Y | DIC system recorded properly | Y |
| Gun alignment in tolerance | Y | All load cells recorded data | Y |
| All still camera images captured | Y | All strain gages recorded data | Y |
| All high-speed cameras capture impact | N | | |

| Test Results Summary |
|---|
| Battery B impacted the target in the nominal velocity range and with the correct orientation (battery longitudinal axis normal to the panel surface). During the test the battery did not penetrate through the aluminum panel but left an indentation on the panel. The battery broke up into many distinct pieces.<br>High Speed Camera 2 and 4 did not capture any data due to triggering issue. |

**Photos**

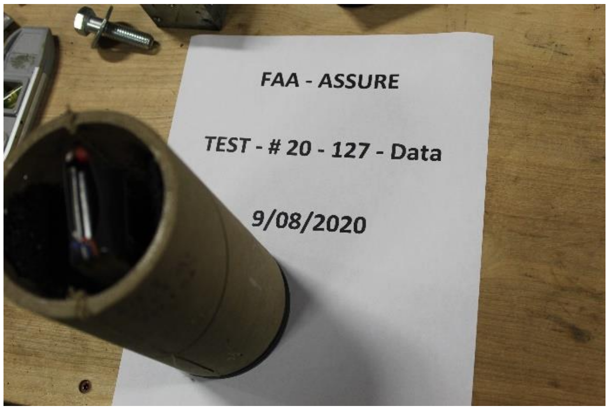


Projectile and Sabot

Projectile Condition After Impact

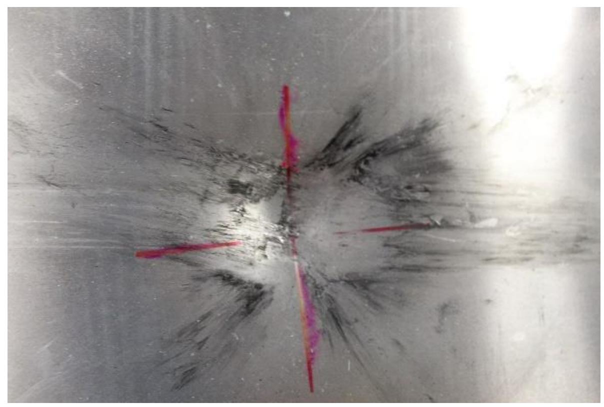

Target Panel Showing Impact Indentation

B.3.1.2.34 TEST 17-2

| General Test Information | | | |
|---|---|---|---|
| Test Facility: | **SMDC-TC Aerophysics Research Facility** | Test Date | **9/9/2020** |
| ARF Test ID Number | **20-128** | NIAR Test ID Number | **17-2** |

| | |
|---|---|
| **Test Description** | 500 knot impact of Battery B on a 0.25” thick 2024 aluminum panel secured within a 17-4 stainless steel frame |

| Test Conditions | | | |
|---|---|---|---|
| Projectile | Battery B | Target Dimensions | 41”x41”x0.25” |
| Projectile mass | 264 gm (0.582 lb.) | Nominal Impact Velocity (knots) | 500 |
| Target | 2024 aluminum panel | Actual Impact Velocity (knots) | 501.2 |

| Test Setup | | | |
|---|---|---|---|
| Target impact angle attained | Y | DIC system recorded properly | Y |
| Gun alignment in tolerance | Y | All load cells recorded data | Y |
| All still camera images captured | Y | All strain gages recorded data | Y |
| All high-speed cameras capture impact | Y | | |

| Test Results Summary |
|---|
| Battery B impacted the target in the nominal velocity range and with the correct orientation (battery longitudinal axis normal to the panel surface). During the test the battery did not penetrate through the aluminum panel and left an indentation on the panel. The battery broke up into many distinct small pieces. |

**Photos**


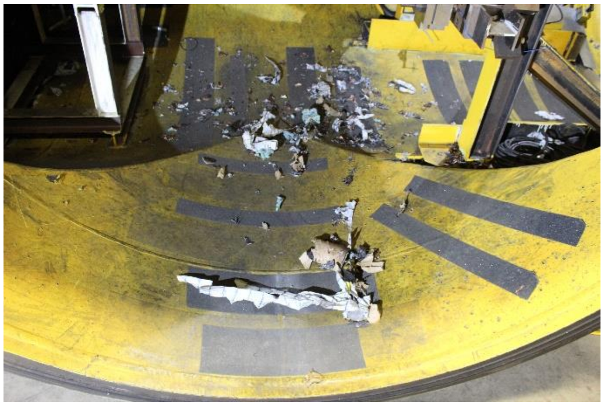

Projectile and Sabot

Projectile Condition After Impact

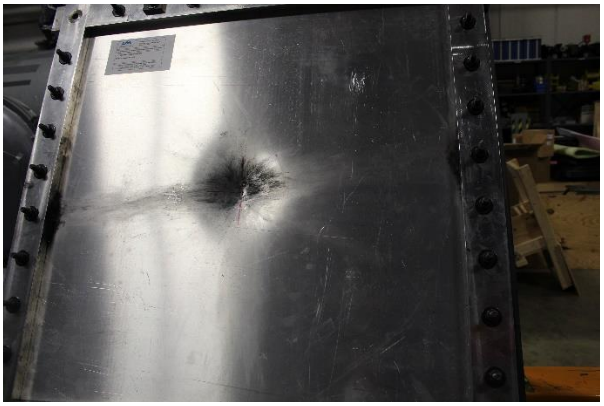

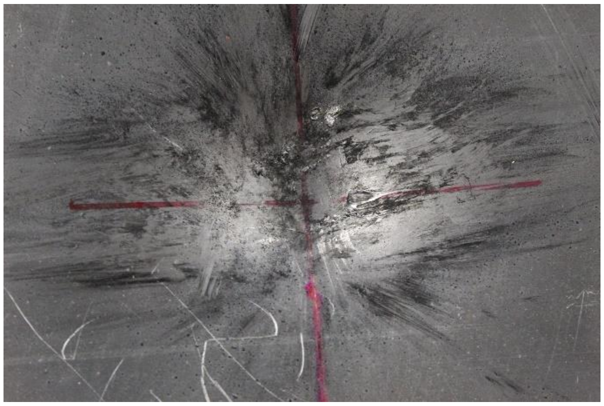

Target Panel Showing Impact Indentation

B.3.1.2.35 TEST 18-1

| **General Test Information** | | | |
|---|---|---|---|
| Test Facility: | **SMDC-TC Aerophysics Research Facility** | Test Date | **5/15/2020** |
| ARF Test ID Number | **20-35** | NIAR Test ID Number | **18-1** |

| | |
|---|---|
| **Test Description** | 500 knot impact of Motor B on a 0.063” thick 2024 aluminum panel secured within a 17-4 stainless steel frame |

| **Test Conditions** | | | |
|---|---|---|---|
| Projectile | Motor B | Target Dimensions | 41”x41”x0.063” |
| Projectile mass | 75.9 gm (0.1673 lb.) | Nominal Impact Velocity (knots) | 500 |
| Target | 2024 aluminum panel | Actual Impact Velocity (knots) | 527 |

| **Test Setup** | | | |
|---|---|---|---|
| Target impact angle attained | Y | DIC system recorded properly | Y |
| Gun alignment in tolerance | Y | All load cells recorded data | Y |
| All still camera images captured | Y | All strain gages recorded data | Y |
| All high-speed cameras capture impact | N | | |

| **Test Results Summary** |
|---|
| Motor B impacted the target in the nominal velocity range and with the correct orientation (motor shaft normal to the panel surface). During the test the motor penetrated through the aluminum panel. The motor broke up into several distinct pieces.<br>High Speed Camera 3 failed to record data. |

**Photos**



| Projectile and Sabot | Projectile Condition After Impact |
|---|---|


Target Panel Showing Impact Perforation

B.3.1.2.36 TEST 18-2

| General Test Information | | | |
|---|---|---|---|
| Test Facility: | **SMDC-TC Aerophysics Research Facility** | Test Date | **5/18/2020** |
| ARF Test ID Number | **20-36** | NIAR Test ID Number | **18-2** |

| | |
|---|---|
| **Test Description** | 500 knot impact of Motor B on a 0.063” thick 2024 aluminum panel secured within a 17-4 stainless steel frame |

| Test Conditions | | | |
|---|---|---|---|
| Projectile | Motor B | Target Dimensions | 41”x41”x0.063” |
| Projectile mass | 76.0 gm (0.1676 lb.) | Nominal Impact Velocity (knots) | 500 |
| Target | 2024 aluminum panel | Actual Impact Velocity (knots) | 525 |

| Test Setup | | | |
|---|---|---|---|
| Target impact angle attained | Y | DIC system recorded properly | Y |
| Gun alignment in tolerance | Y | All load cells recorded data | Y |
| All still camera images captured | Y | All strain gages recorded data | Y |
| All high-speed cameras capture impact | Y | | |

| Test Results Summary |
|---|
| Motor B impacted the target in the nominal velocity range and correct orientation (motor shaft normal to the panel surface). During the test the motor penetrated through the aluminum panel. The motor remained mostly intact, and only lost a collet which was used to set the shaft position within the motor. |

**Photos**


Projectile and Sabot


Projectile Condition After Impact

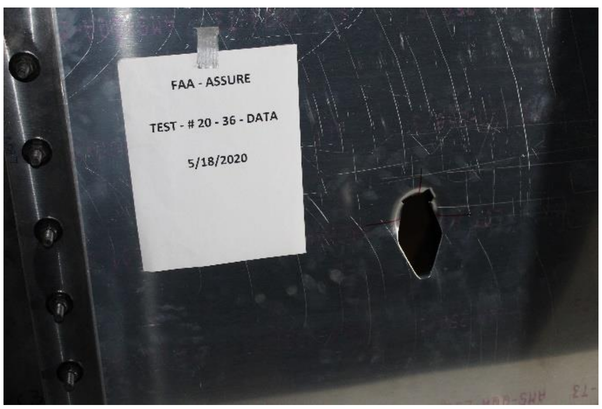


Target Panel Showing Impact Perforation

B.3.1.2.37 TEST 19-1

| General Test Information | | | |
|---|---|---|---|
| Test Facility: | **SMDC-TC Aerophysics Research Facility** | Test Date | **5/18/2020** |
| ARF Test ID Number | **20-37** | NIAR Test ID Number | **19-1** |

| | |
|---|---|
| **Test Description** | 500 knot impact of Motor B on a 0.25” thick 2024 aluminum panel secured within a 17-4 stainless steel frame |

| Test Conditions | | | |
|---|---|---|---|
| Projectile | Motor B | Target Dimensions | 41”x41”x0.25” |
| Projectile mass | 76.1 gm (0.1678 lb.) | Nominal Impact Velocity (knots) | 500 |
| Target | 2024 aluminum panel | Actual Impact Velocity (knots) | 527 |

| Test Setup | | | |
|---|---|---|---|
| Target impact angle attained | Y | DIC system recorded properly | Y |
| Gun alignment in tolerance | Y | All load cells recorded data | N |
| All still camera images captured | Y | All strain gages recorded data | Y |
| All high-speed cameras capture impact | N | | |

| Test Results Summary |
|---|
| Motor B impacted the target in the nominal velocity range and correct orientation (motor shaft normal to the panel surface). During the test the motor did not penetrate through the aluminum panel. It left an indentation on the panel. The motor was crushed as it impacted the panel.<br>High Speed Camera 3 failed to record data. Noise in load cells caused the trigger to go off between arming and fire command. No load cell data was recorded during impact as a result. |

| Photos | |
|---|---|
| <br> | 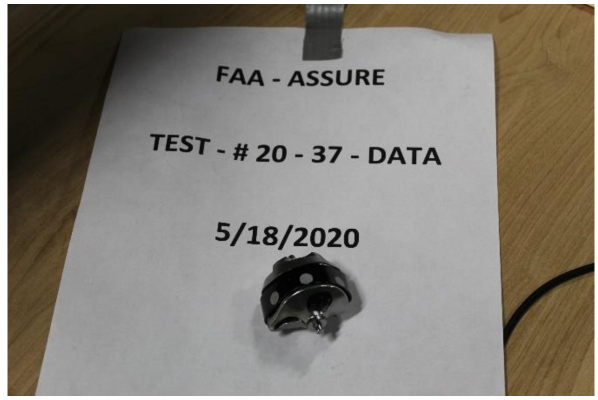<br> |
| Projectile and Sabot | Projectile Condition After Impact |
| 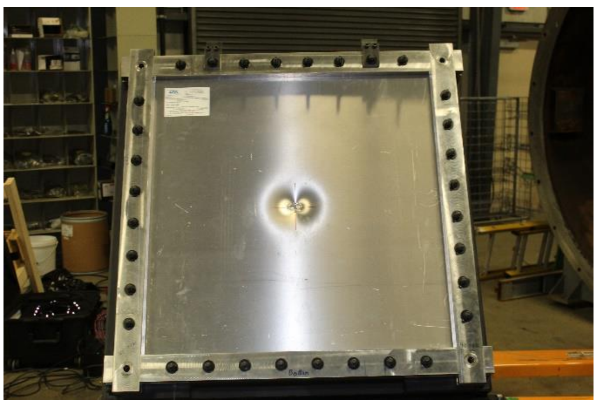 | 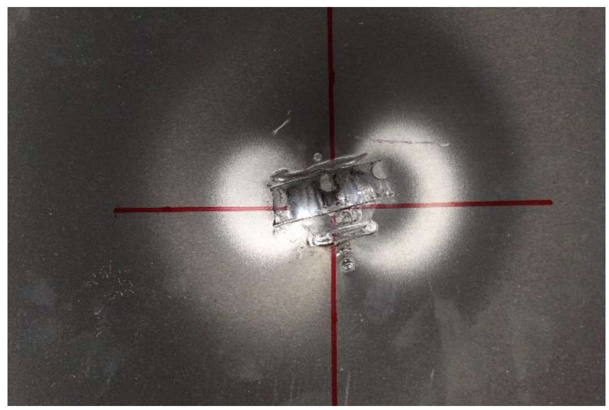 |
| Target Panel Showing Impact Indentation | |

B.3.1.2.38 TEST 19-2

| General Test Information | | | |
|---|---|---|---|
| Test Facility: | **SMDC-TC Aerophysics Research Facility** | Test Date | **5/19/2020** |
| ARF Test ID Number | **20-38** | NIAR Test ID Number | **19-2** |

| | |
|---|---|
| **Test Description** | 500 knot impact of Motor B on a 0.25” thick 2024 aluminum panel secured within a 17-4 stainless steel frame |

| Test Conditions | | | |
|---|---|---|---|
| Projectile | Motor B | Target Dimensions | 41”x41”x0.25” |
| Projectile mass | 76.5 gm (0.1687 lb.) | Nominal Impact Velocity (knots) | 500 |
| Target | 2024 aluminum panel | Actual Impact Velocity (knots) | 522.5 |

| Test Setup | | | |
|---|---|---|---|
| Target impact angle attained | Y | DIC system recorded properly | Y |
| Gun alignment in tolerance | Y | All load cells recorded data | Y |
| All still camera images captured | Y | All strain gages recorded data | Y |
| All high-speed cameras capture impact | Y | | |

| Test Results Summary |
|---|
| Motor B impacted the target in the nominal velocity range and correct orientation (motor shaft normal to the panel surface). During the test the motor did not penetrate through the aluminum panel. It left an indentation on the panel. The motor was crushed as it impacted the panel. |

| **Photos** | |
|---|---|
|  | 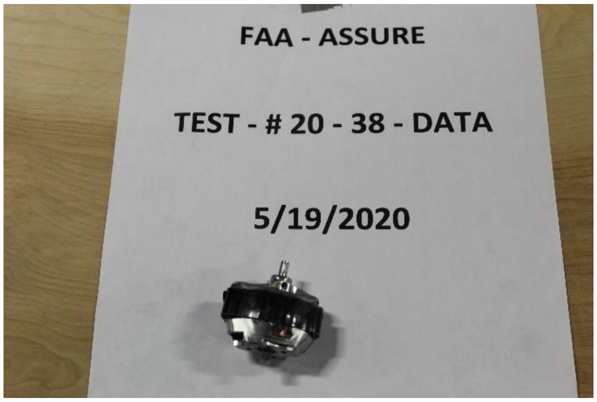 |
| Projectile and Sabot | Projectile Condition After Impact |
| 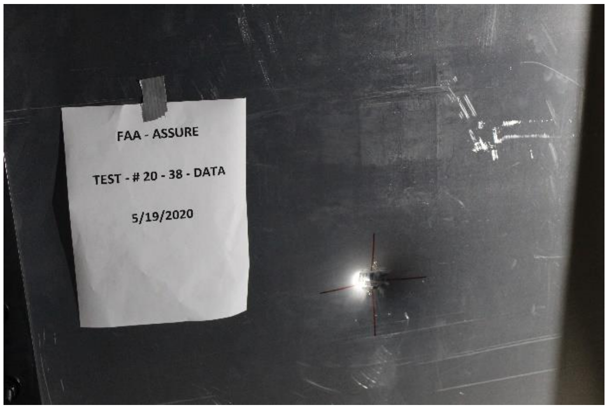 | 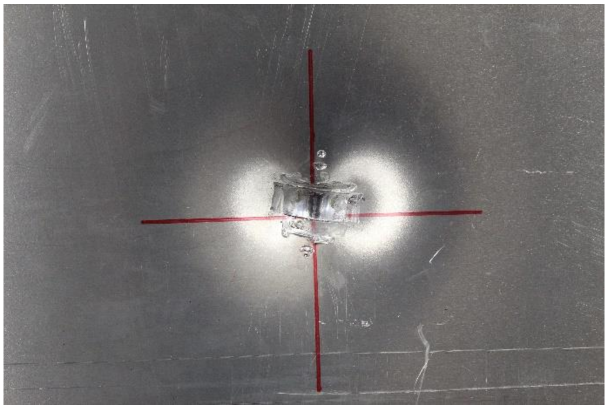 |
| Target Panel Showing Impact Indentation | |

B.3.1.2.39 TEST 20-1

| General Test Information | | | |
|---|---|---|---|
| Test Facility: | **SMDC-TC Aerophysics Research Facility** | Test Date | **07/24/2020** |
| ARF Test ID Number | **20-94** | NIAR Test ID Number | **20-1** |

| | |
|---|---|
| **Test Description** | 50 knot impact of Battery B on a 0.063” thick 2024 aluminum panel secured within a 17-4 stainless steel frame |

| Test Conditions | | | |
|---|---|---|---|
| Projectile | Battery B | Target Dimensions | 41”x41”x0.063” |
| Projectile mass | 264.4 gm (0.5829 lb.) | Nominal Impact Velocity (knots) | 50 |
| Target | 2024 aluminum panel | Actual Impact Velocity (knots) | 52 |

| Test Setup | | | |
|---|---|---|---|
| Target impact angle attained | Y | DIC system recorded properly | Y |
| Gun alignment in tolerance | Y | All load cells recorded data | Y |
| All still camera images captured | Y | All strain gages recorded data | Y |
| All high-speed cameras capture impact | N | | |

| Test Results Summary |
|---|
| Battery impacted the target in the nominal velocity range and correct orientation (battery longitudinal axis normal to the panel surface). During the test the battery did not dent or penetrate the aluminum panel. The battery was slightly crushed after it impacted the panel. The battery did not pose a “Fire Risk”.<br>High Speed Camera 4 did not record data. |

**Photos**


Projectile and Sabot

Projectile Condition After Impact

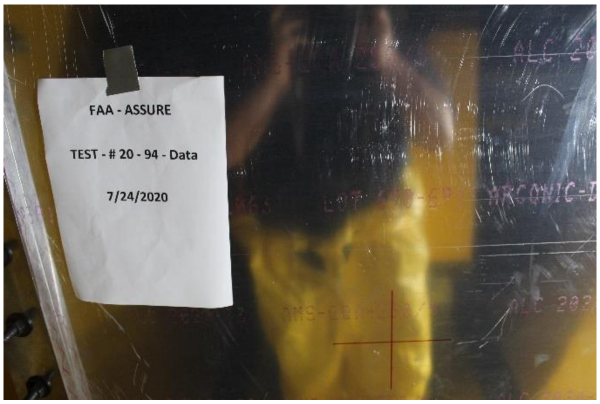


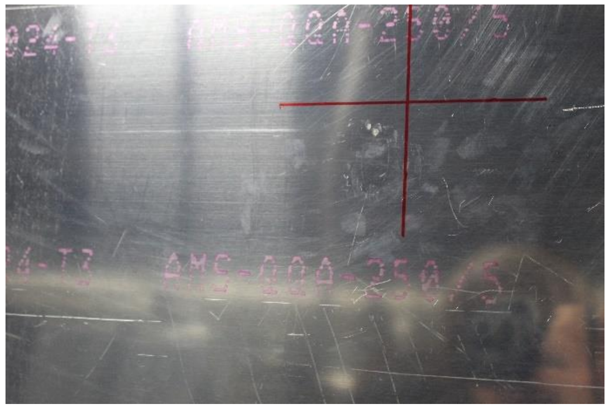

Target Panel after Impact with Minimal Damage

B.3.1.2.40 TEST 20-2

| **General Test Information** | | | |
|---|---|---|---|
| Test Facility: | **SMDC-TC Aerophysics Research Facility** | Test Date | **07/24/2020** |
| ARF Test ID Number | **20-95** | NIAR Test ID Number | **20-2** |

| | |
|---|---|
| **Test Description** | 50 knot impact of Battery B on a 0.063” thick 2024 aluminum panel secured within a 17-4 stainless steel frame |

| **Test Conditions** | | | |
|---|---|---|---|
| Projectile | Battery B | Target Dimensions | 41”x41”x0.063” |
| Projectile mass | 264.4 gm (0.5829 lb.) | Nominal Impact Velocity (knots) | 50 |
| Target | 2024 aluminum panel | Actual Impact Velocity (knots) | 52 |

| **Test Setup** | | | |
|---|---|---|---|
| Target impact angle attained | Y | DIC system recorded properly | Y |
| Gun alignment in tolerance | Y | All load cells recorded data | Y |
| All still camera images captured | Y | All strain gages recorded data | Y |
| All high-speed cameras capture impact | Y | | |

| **Test Results Summary** |
|---|
| Battery B impacted the target in the nominal velocity range and correct orientation (battery longitudinal axis normal to the panel surface). During the test the battery left a minor indentation on the aluminum panel. The battery was crushed near the end where it impacted the panel. The battery did not pose a “Fire Risk”. |

<table>
<tr><th colspan="2">Photos</th></tr>
<tr><td>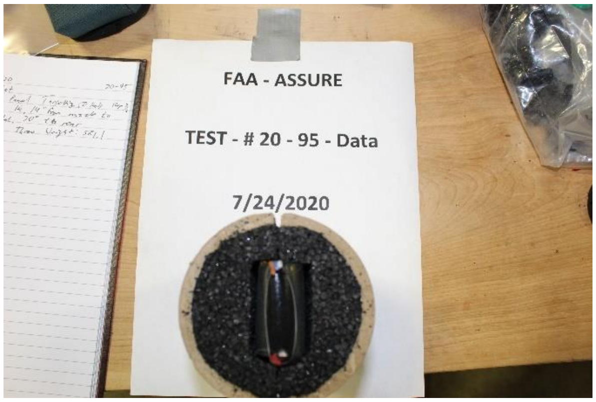
</td><td></td></tr>
<tr><td>Projectile and Sabot</td><td>Projectile Condition After Impact</td></tr>
<tr><td>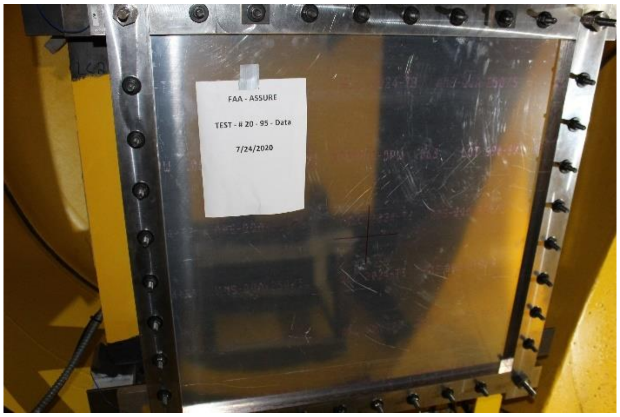
</td><td></td></tr>
<tr><td colspan="2">Target Panel Showing Impact Indentation</td></tr>
</table>

B.3.1.2.41 TEST 21-1

| **General Test Information** | | | |
|---|---|---|---|
| Test Facility: | **SMDC-TC Aerophysics Research Facility** | Test Date | **8/5/2020** |
| ARF Test ID Number | **20-108** | NIAR Test ID Number | **21-1** |

| | |
|---|---|
| **Test Description** | 120 knot impact of Battery B on a 0.063” thick 2024 aluminum panel secured within a 17-4 stainless steel frame |

| **Test Conditions** | | | |
|---|---|---|---|
| Projectile | Battery B | Target Dimensions | 41”x41”x0.063” |
| Projectile mass | 264 gm (0.582 lb.) | Nominal Impact Velocity (knots) | 120 |
| Target | 2024 aluminum panel | Actual Impact Velocity (knots) | 119.68 |

| **Test Setup** | | | |
|---|---|---|---|
| Target impact angle attained | Y | DIC system recorded properly | Y |
| Gun alignment in tolerance | Y | All load cells recorded data | Y |
| All still camera images captured | Y | All strain gages recorded data | Y |
| All high-speed cameras capture impact | Y | | |

| **Test Results Summary** |
|---|
| Battery B impacted the target in the nominal velocity range and correct orientation (battery longitudinal axis normal to the panel surface). During the test the battery indented the panel. The battery was crushed when it impacted the panel. The battery posed a “Fire Risk” after the impact. |

| Photos | |
|---|---|
| <br> |  |
| Projectile and Sabot | Projectile Condition After Impact |
| 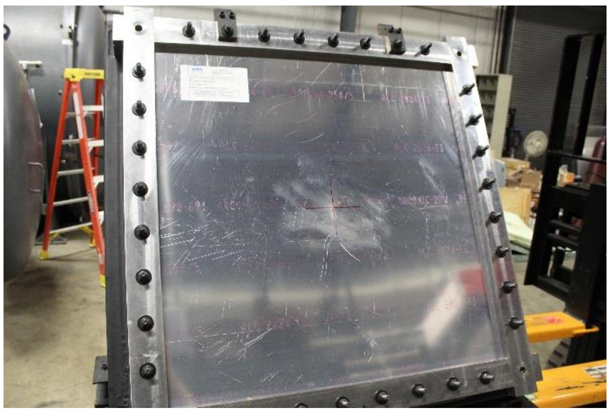 | 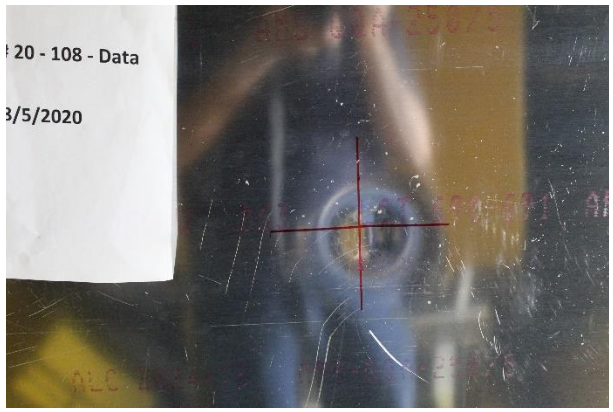<br> |
| Target Panel Showing Impact Indentation | |

B.3.1.2.42 TEST 21-2

| **General Test Information** | | | |
|---|---|---|---|
| Test Facility: | **SMDC-TC Aerophysics Research Facility** | Test Date | **8/7/2020** |
| ARF Test ID Number | **20-109** | NIAR Test ID Number | **21-2** |

| **Test Description** | 120 knot impact of Battery B on a 0.063” thick 2024 aluminum panel secured within a 17-4 stainless steel frame |
|---|---|

| **Test Conditions** | | | |
|---|---|---|---|
| Projectile | Battery B | Target Dimensions | 41”x41”x0.063” |
| Projectile mass | 265.1 gm (0.5844 lb.) | Nominal Impact Velocity (knots) | 120 |
| Target | 2024 aluminum panel | Actual Impact Velocity (knots) | 120.87 |

| **Test Setup** | | | |
|---|---|---|---|
| Target impact angle attained | Y | DIC system recorded properly | Y |
| Gun alignment in tolerance | Y | All load cells recorded data | Y |
| All still camera images captured | Y | All strain gages recorded data | Y |
| All high-speed cameras capture impact | Y | | |

| **Test Results Summary** |
|---|
| Battery B impacted the target in the nominal velocity range and correct orientation (battery longitudinal axis normal to the panel surface). During the test the battery indented the panel. The battery was crushed when it impacted the panel. The battery posed a “Fire Risk” after the impact. |

| **Photos** | |
|---|---|
|  | 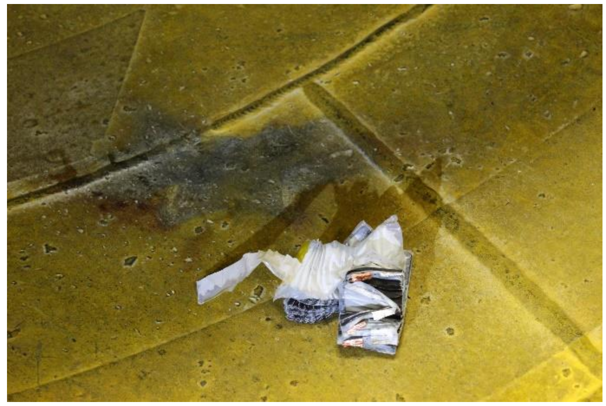 |
| Projectile and Sabot | Projectile Condition After Impact |
| 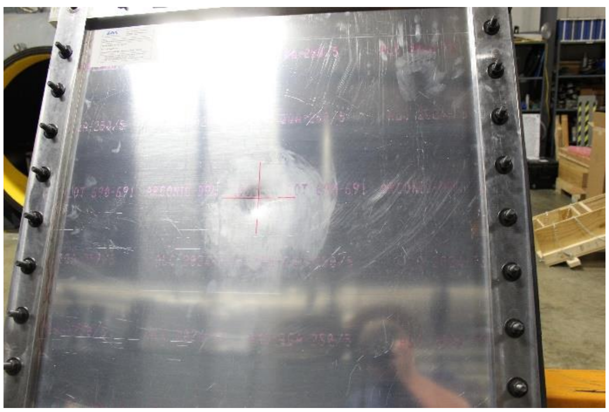 | 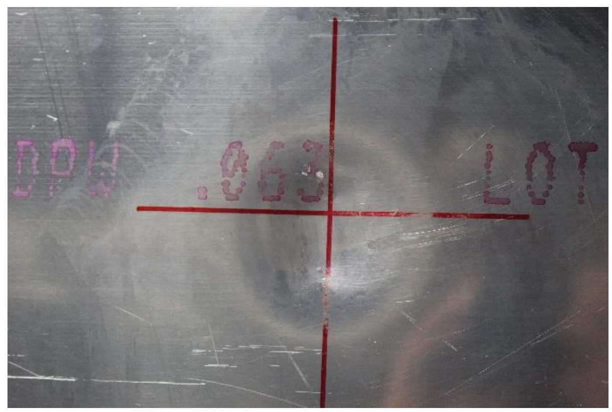 |
| Target Panel Showing Impact Indentation | |

B.3.1.2.43 TEST 22-1

| General Test Information | | | |
|---|---|---|---|
| Test Facility: | **SMDC-TC Aerophysics Research Facility** | Test Date | **07/01/2020** |
| ARF Test ID Number | **20-74** | NIAR Test ID Number | **22-1** |

| | |
|---|---|
| **Test Description** | 50 knot impact of Motor B on a 0.063” thick 2024 aluminum panel secured within a 17-4 stainless steel frame |

| Test Conditions | | | |
|---|---|---|---|
| Projectile | Motor B | Target Dimensions | 41”x41”x0.063” |
| Projectile mass | 76.2 gm (0.1679 lb.) | Nominal Impact Velocity (knots) | 50 |
| Target | 2024 aluminum panel | Actual Impact Velocity (knots) | 49 |

| Test Setup | | | |
|---|---|---|---|
| Target impact angle attained | Y | DIC system recorded properly | Y |
| Gun alignment in tolerance | Y | All load cells recorded data | Y |
| All still camera images captured | Y | All strain gages recorded data | Y |
| All high-speed cameras capture impact | N | | |

| Test Results Summary |
|---|
| Motor B impacted the target in the nominal velocity range and correct orientation (motor shaft normal to the panel surface). During the test the motor did not penetrate through the aluminum panel but left an indentation. The motor did not break or get crushed after the impact.<br>High-Speed Camera 3 was used as a temporary replacement for one of the DIC cameras thus there was no high-speed camera 3 video for this test. |

| **Photos** | |
|---|---|
| 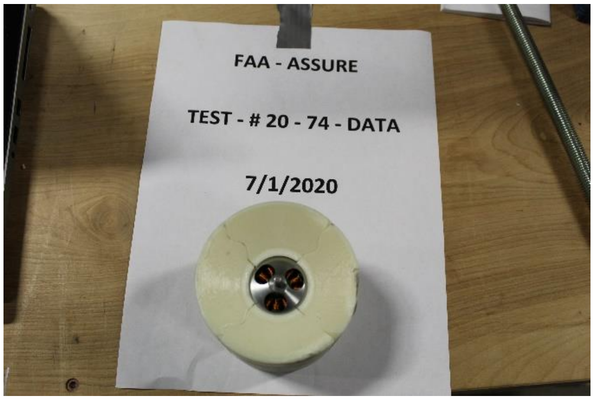 | 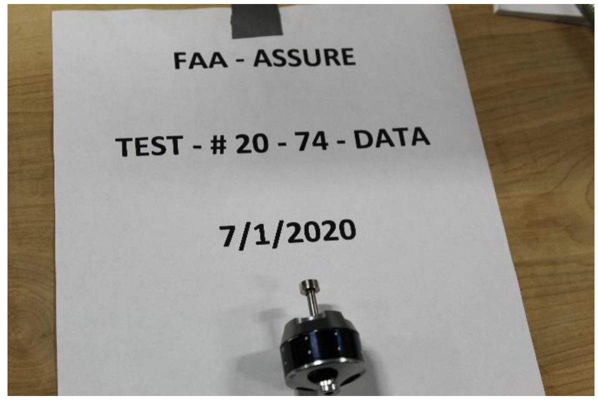 |
| Projectile and Sabot | Projectile Condition After Impact |
| 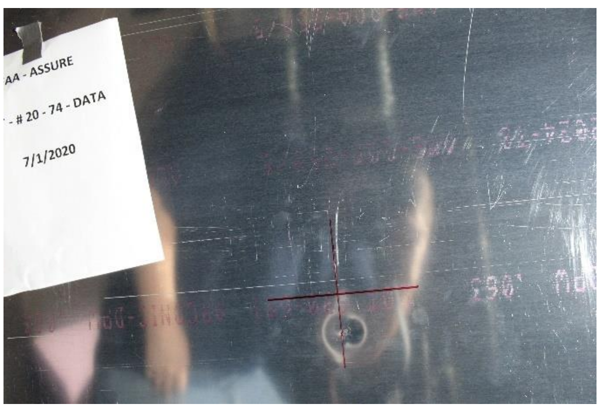 | 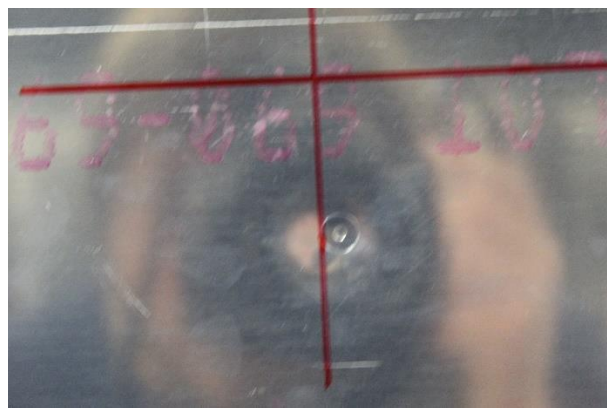 |
| Target Panel Showing Impact Penetration | |

B.3.1.2.44 TEST 22-2

| General Test Information | | | |
|---|---|---|---|
| Test Facility: | **SMDC-TC Aerophysics Research Facility** | Test Date | **07/01/2020** |
| ARF Test ID Number | **20-75** | NIAR Test ID Number | **22-2** |

| | |
|---|---|
| **Test Description** | 50 knot impact of Motor B on a 0.063” thick 2024 aluminum panel secured within a 17-4 stainless steel frame |

| Test Conditions | | | |
|---|---|---|---|
| Projectile | Motor B | Target Dimensions | 41”x41”x0.063” |
| Projectile mass | 76.6 gm (0.1689 lb.) | Nominal Impact Velocity (knots) | 50 |
| Target | 2024 aluminum panel | Actual Impact Velocity (knots) | 52 |

| Test Setup | | | |
|---|---|---|---|
| Target impact angle attained | Y | DIC system recorded properly | Y |
| Gun alignment in tolerance | Y | All load cells recorded data | Y |
| All still camera images captured | Y | All strain gages recorded data | N |
| All high-speed cameras capture impact | N | | |

| Test Results Summary |
|---|
| Motor B impacted the target in the nominal velocity range and correct orientation (motor shaft normal to the panel surface). During the test the motor did not penetrate through the aluminum panel but left an indentation. The motor did not break nor get crushed after the impact.<br>High-Speed Camera 3 was used as a temporary replacement for one of the DIC cameras thus there was no high-speed camera 3 video for this test. SG4 read exceptionally high data. This could have been due to a bad connection. |

| Photos | |
|---|---|
| 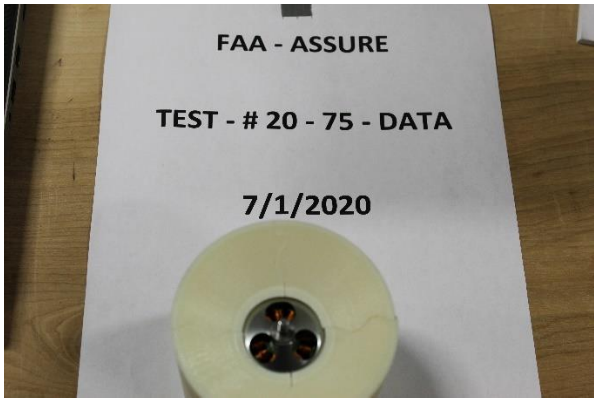 | 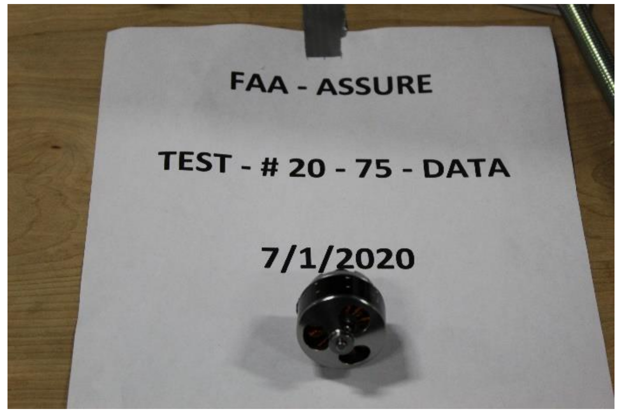 |
| Projectile and Sabot | Projectile Condition After Impact |
|  | 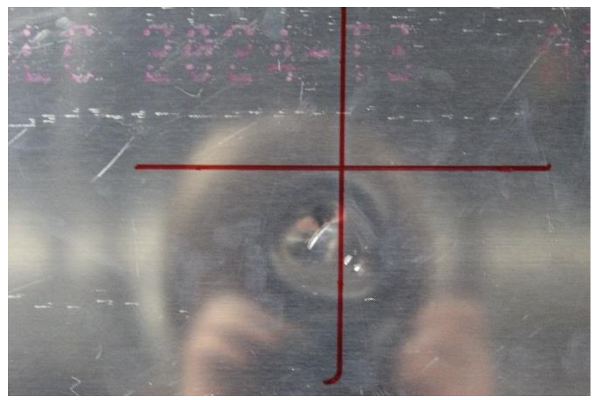 |
| Target Panel Showing Impact Indentation | |

B.3.1.2.45 TEST 23-1

| **General Test Information** | | | |
|---|---|---|---|
| Test Facility: | **SMDC-TC Aerophysics Research Facility** | Test Date | **06/19/2020** |
| ARF Test ID Number | **20-61** | NIAR Test ID Number | **23-1** |

| **Test Description** | 120 knot impact of Motor B on a 0.063” thick 2024 aluminum panel secured within a 17-4 stainless steel frame |
|---|---|

| **Test Conditions** | | | |
|---|---|---|---|
| Projectile | Motor B | Target Dimensions | 41”x41”x0.063” |
| Projectile mass | 76.7 gm (0.1691 lb.) | Nominal Impact Velocity (knots) | 120 |
| Target | 2024 aluminum panel | Actual Impact Velocity (knots) | 123 |

| **Test Setup** | | | |
|---|---|---|---|
| Target impact angle attained | Y | DIC system recorded properly | Y |
| Gun alignment in tolerance | Y | All load cells recorded data | Y |
| All still camera images captured | Y | All strain gages recorded data | Y |
| All high-speed cameras capture impact | N | | |

| **Test Results Summary** |
|---|
| Motor B impacted the target in the nominal velocity range and correct orientation (motor shaft normal to the panel surface). During the test the motor pierced the aluminum panel, but did not go fully through the panel. The motor broke into two pieces.<br>High-Speed Camera 3 was used as a temporary replacement for one of the DIC cameras thus there was no high-speed camera 3 video for this test. |

| **Photos** | |
|---|---|
| 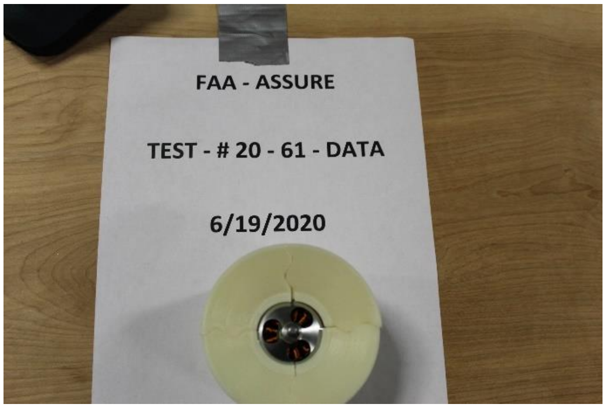 |  |
| Projectile and Sabot | Projectile Condition After Impact |
| 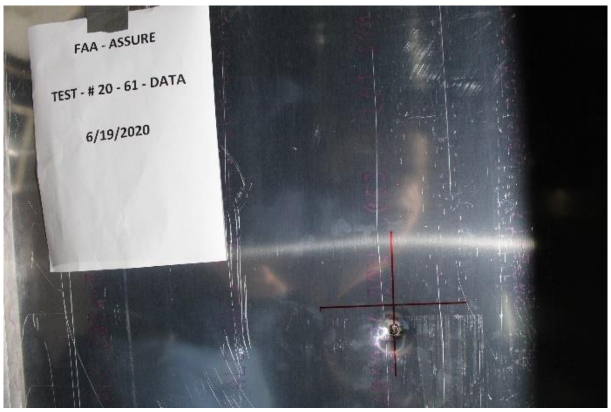 |  |
| Target Panel Showing Impact Perforation | |

B.3.1.2.46 TEST 23-2

| General Test Information | | | |
|---|---|---|---|
| Test Facility: | **SMDC-TC Aerophysics Research Facility** | Test Date | **06/22/2020** |
| ARF Test ID Number | **20-62** | NIAR Test ID Number | **23-2** |

| | |
|---|---|
| **Test Description** | 120 knot impact of Motor B on a 0.063” thick 2024 aluminum panel secured within a 17-4 stainless steel frame |

| Test Conditions | | | |
|---|---|---|---|
| Projectile | Motor B | Target Dimensions | 41”x41”x0.063” |
| Projectile mass | 76.8 gm (0.1693 lb.) | Nominal Impact Velocity (knots) | 120 |
| Target | 2024 aluminum panel | Actual Impact Velocity (knots) | 123 |

| Test Setup | | | |
|---|---|---|---|
| Target impact angle attained | Y | DIC system recorded properly | Y |
| Gun alignment in tolerance | Y | All load cells recorded data | Y |
| All still camera images captured | Y | All strain gages recorded data | Y |
| All high-speed cameras capture impact | N | | |

| Test Results Summary |
|---|
| Motor B impacted the target in the nominal velocity range and correct orientation (motor shaft normal to the panel surface). During the test the motor pierced the aluminum panel without going through the panel. The motor broke into two pieces.<br>High-Speed Camera 3 was used as a temporary replacement for one of the DIC cameras thus there was no camera 3 video for this test. |

| **Photos** | |
|---|---|
| 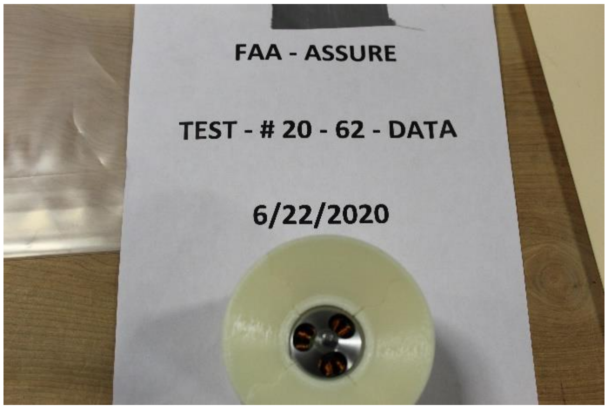 |  |
| Projectile and Sabot | Projectile Condition After Impact |
|  |  |
| Target Panel Showing Impact Perforation | |

## B.4 FULL SUAS IMPACT TEST RESULTS

### B.4.1 Full sUAS Impact Testing

UAH conducted full sUAS impact testing against helicopter components as shown in Table 27. UAH uploaded the full sUAS impact test data sets that include strain gage and load cell signal data, high speed videos, and still images to the NIAR ftp site for use in model calibration following each individual test.

#### B.4.1.1 FULL AIRCRAFT IMPACT TEST RESULTS OVERVIEW

Table 27. Full sUAS Impact Testing Summary (as Executed).

| Test # | Projectile | Target | Desired Velocity (kts) | Actual Velocity (kts) | Result |
|---|---|---|---|---|---|
| 1 | DJI Phantom 3 | Tail Rotor Blade | 340 | | Catastrophic failure with debonding between composite fibers throughout the test article. Blade experienced high bending (>45 deg) during impact. |
| 2-1 | DJI Phantom 3 | Main Rotor Blade | 500 | 425 | No-Test because of glancing impact. Two motors impacted and fractured composite blade spar. Deformation of the lead ballast rod in the blade nose. |
| 2-2 | DJI Phantom 3 | Main Rotor Blade | 500 | 425 | No-Test because of glancing impact. Two motors impacted and fractured composite blade spar. Deformation of the lead ballast rod in the blade nose. |
| 2-3 | DJI Phantom 3 | Main Rotor Blade | 500 | 425 | Single motor impact that fractured the composite blade spare and deformed the lead ballast rod in the blade nose. |
| 2-4 | DJI Phantom 3 | Main Rotor Blade | 500 | 425 | Battery impact with the leading edge fractured the composite blade spar and split open the glued joint of the upper and lower blade shell at the trailing edge of the blade. Deformation of the lead ballast rod in the blade nose. |
| 5 | DJI Phantom 3 | Horizontal Stabilizer | 175 | 425 | Leading edge deformation with motors left embedded in the stabilizer. Damage was localized to the metal skin of the lead edge with no damage propagation more than two inches from the impact point. |
| 6 | DJI Phantom 3 | Bi-Layer Windscreen | 50 | 44 | Superficial scratches left on windscreen. |
| 7 | DJI Phantom 3 | Bi-Layer Windscreen | 175 | 165 | >90% of the windscreen was fractured and cracked. Film on the inside of the windscreen remained intact. |

| | | | | | |
|---|---|---|---|---|---|
| 8 | DJI Phantom 3 | Bi-Layer Windscreen | 290 | 290 | Aircraft impact broke a hole in the windscreen and battery contents were ejected through the windscreen and would have entered an aircraft cockpit. Film on the inside of the windscreen broke and a large number of glass shards broke off and the inside of an aircraft cockpit would be sprayed with glass shards. |

### B.4.1.2 FULL AIRCRAFT IMPACT TEST RESULTS

#### B.4.1.2.1 TEST #1 TAIL ROTOR BLADE

| **General Test Information** | | | |
|---|---|---|---|
| Test Facility: | **SMDC-TC Aerophysics Research Facility** | Test Date | **5-14-21** |
| ARF Test ID Number | **2-144** | NIAR Test ID Number | **1** |

| | |
|---|---|
| **Test Description** | DJI Phantom 3 Impact against a tail rotor blade |

| **Test Conditions** | | | |
|---|---|---|---|
| Projectile | DJI Phantom 3 with camera and legs removed | Target Dimensions | |
| Projectile mass | 912g | Nominal Impact Velocity (knots) | 385 |
| Target | 3.5 lbs | Actual Impact Velocity (knots) | 385 |

| **Test Setup** | | | |
|---|---|---|---|
| Target impact angle attained | Yes | DIC system recorded properly | N/A |
| Gun alignment in tolerance | Yes | All load cells recorded data | Yes |
| All still camera images captured | Yes | All strain gages recorded data | Yes |
| All high-speed cameras capture impact | Yes | | |

| **Test Results Summary** |
|---|
| The tail rotor blade was structurally compromised by the sUAS impact. |

<table>
<tr><th colspan="2">Photos</th></tr>
<tr><td>


</td><td>

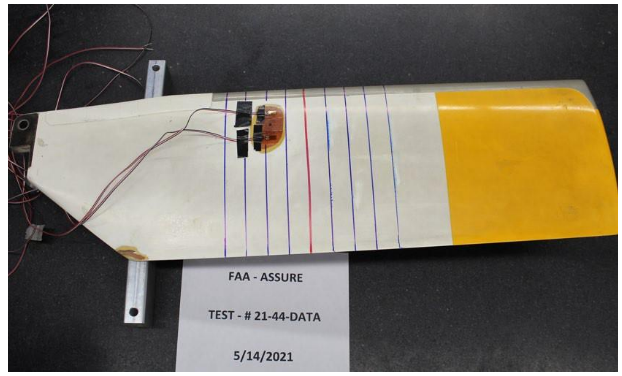


</td></tr>
<tr><td>

</td><td>

*Post impact target images not included in report. Post-test article provided to NIAR for analysis.*

</td></tr>
</table>

B.4.1.2.2 TEST 2-1 MAIN ROTOR BLADE

| General Test Information | | | |
|---|---|---|---|
| Test Facility: | **SMDC-TC Aerophysics Research Facility** | Test Date | **8-10-21** |
| ARF Test ID Number | **21-92** | NIAR Test ID Number | **2-1** |

| | |
|---|---|
| **Test Description** | DJI Phantom 3 Impact against a main rotor blade section centered on the 75% blade spanwise position of the full main rotor blade |

| Test Conditions | | | |
|---|---|---|---|
| Projectile | DJI Phantom 3 with camera and legs removed | Target Dimensions | 20” x 40” x 1.5” |
| Projectile mass | 912g | Nominal Impact Velocity (knots) | 500 |
| Target | 16.2 lbs | Actual Impact Velocity (knots) | 430 |

| Test Setup | | | |
|---|---|---|---|
| Target impact angle attained | No | DIC system recorded properly | N/A |
| Gun alignment in tolerance | Yes | All load cells recorded data | Yes |
| All still camera images captured | Yes | All strain gages recorded data | Yes |
| All high-speed cameras capture impact | Yes | | |

**Test Results Summary**

Unable to conduct a 500 kts impact based on launcher limitations. This was briefed to NIAR and the FAA in advance of the test.

The sUAS dropped below the intended target line and only one motor impacted the blade leading edge. The motor that impacted the blade broke off of the sUAS and left a dent in the leading edge of the blade. The motor impact crushed the leading edge of the composite spare and deformed the metal rod in the leading edge of the spar. The impact created chordwise fractures in the composite spar. The motor was crushed to approximately half of its pre-impact width/diameter during the impact.

| Photos | |
|---|---|
|  | 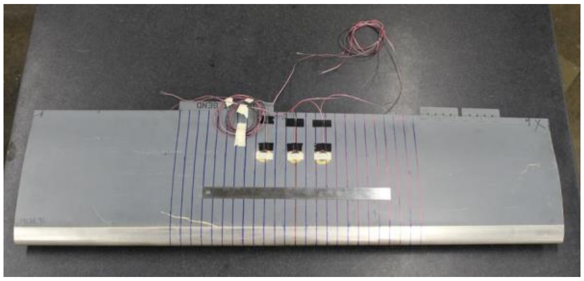 |
| 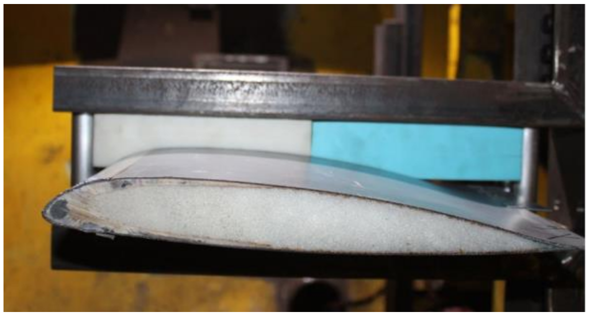 | 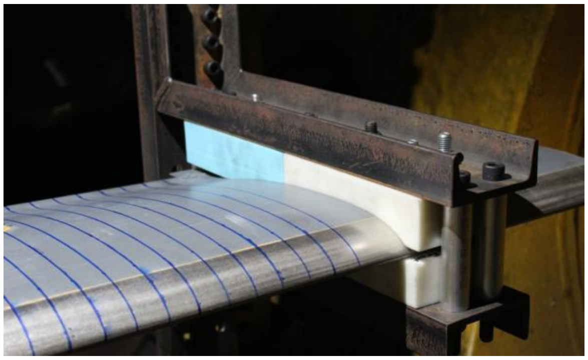 |
| 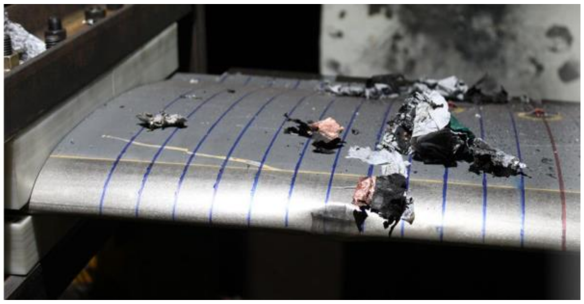 | 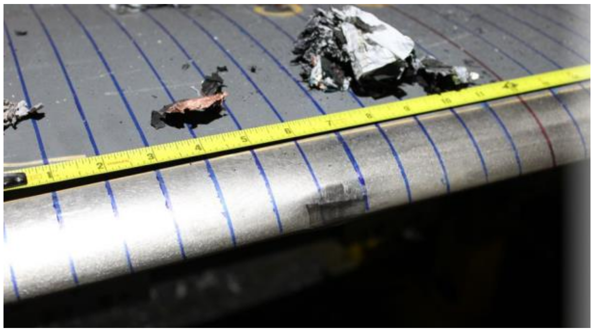 |

B.4.1.2.3 TEST 2-2 MAIN ROTOR BLADE

| General Test Information | | | |
|---|---|---|---|
| Test Facility: | **SMDC-TC Aerophysics Research Facility** | Test Date | **9-21-21** |
| ARF Test ID Number | **21-113** | NIAR Test ID Number | **2-2** |

| | |
|---|---|
| **Test Description** | DJI Phantom 3 Impact against a main rotor blade section centered on the 75% blade spanwise position of the full main rotor blade |

| Test Conditions | | | |
|---|---|---|---|
| Projectile | DJI Phantom 3 with camera and legs removed | Target Dimensions | 20” x 40” x 1.5” |
| Projectile mass | 919g | Nominal Impact Velocity (knots) | 500 |
| Target | 16.2 lbs | Actual Impact Velocity (knots) | 425 |

| Test Setup | | | |
|---|---|---|---|
| Target impact angle attained | No, shot trajectory was low | DIC system recorded properly | N/A |
| Gun alignment in tolerance | Yes | All load cells recorded data | Yes |
| All still camera images captured | Yes | All strain gages recorded data | Yes |
| All high-speed cameras capture impact | Yes | | |

| Test Results Summary |
|---|
| This test article was reused after Test 2-1 (ARF test number 21-92).<br><br>The sUAS trajectory was low such that only one motor impact the main rotor blade leading edge. This impact created a second indentation on the blade because there was already a motor impact on the blade leading edge from Test 2-1. After the test was completed, NIAR sectioned the blade at the impact point and observed that the leading edge of the composite spar was crushed, the leading-edge metal rod was deformed and the impact resulted in numerous chordwise fractures within the composite spar structure. There was debonding between the composite spar and the inner foam core of the main rotor blade. The sUAS was destroyed following its impact with the range backstop. Because this blade was sectioned after two impact tests were conducted using it as the target, it is not possible to correlate all damage to specific tests. |

| **Photos** | |
|---|---|
|  | *Pre-impact images of the blade were not available* |
| <br>**Test 21-92 and 21-113 Blade –** LE Dents |  |
| *There were no other post-impact test images of the impact point from test 21-113 on the blade.* | |

B.4.1.2.3 TEST 2-3 MAIN ROTOR BLADE

| **General Test Information** | | | |
|---|---|---|---|
| Test Facility: | **SMDC-TC Aerophysics Research Facility** | Test Date | **10-13-21** |
| ARF Test Number | **21-125** | NIAR Test Number | **2-3** |

| | |
|---|---|
| **Test Description** | DJI Phantom 3 Impact against a main rotor blade section centered on the 75% blade spanwise position of the full main rotor blade |

| **Test Conditions** | | | |
|---|---|---|---|
| Projectile | DJI Phantom 3 with camera and legs removed | Target Dimensions | 20” x 40” x 1.5” |
| Projectile mass | 919.2g | Nominal Impact Velocity (knots) | 500 |
| Target | 16.2 lbs | Actual Impact Velocity (knots) | 430 |

| **Test Setup** | | | |
|---|---|---|---|
| Target impact angle attained | Yes, but aircraft pitch angle was high | DIC system recorded properly | N/A |
| Gun alignment in tolerance | Yes | All load cells recorded data | |
| All still camera images captured | Yes | All strain gages recorded data | Missing one strain gage |
| All high-speed cameras capture impact | Yes | | |

| **Test Results Summary** |
|---|
| Blade was oriented vertically to avoid dropping below target.<br><br>Aircraft yaw angle was large based on a poor sabot separation. The sUAS impacted with part of the battery and center body and one motor. There were minor dents in the blade leading edge from the motor impact. The sUAS was completely destroyed and the battery did not pose a “Fire Risk” after the impact. |

| Photos | |
|---|---|
|  |  |
| 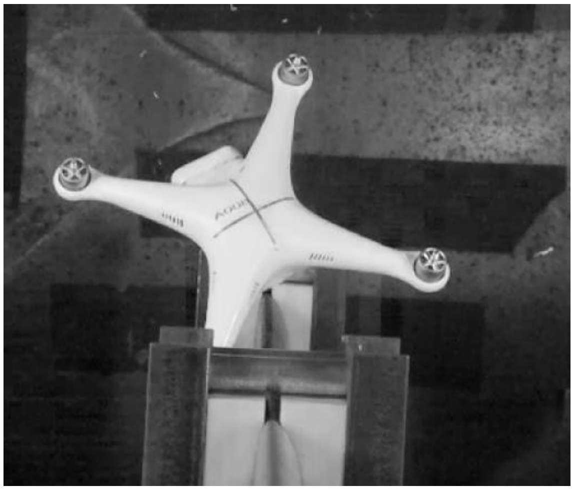 |  |
| 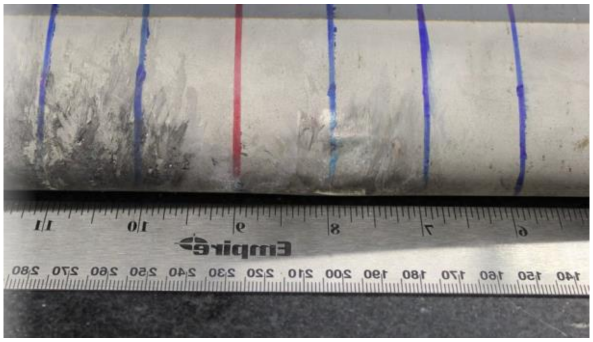 | |

B.4.1.2.4 TEST 2-4 MAIN ROTOR BLADE

| **General Test Information** | | | |
|---|---|---|---|
| Test Facility: | **SMDC-TC Aerophysics Research Facility** | Test Date | **10-14-22** |
| ARF Test ID Number | **21-126** | NIAR Test ID Number | **2-3** |

| | |
|---|---|
| **Test Description** | DJI Phantom 3 Impact against a main rotor blade section centered on the 75% blade spanwise position of the full main rotor blade |

| **Test Conditions** | | | |
|---|---|---|---|
| Projectile | DJI Phantom 3 with camera and legs removed | Target Dimensions | 20” x 40” x 1.5” |
| Projectile mass | 919.4g | Nominal Impact Velocity (knots) | 500 |
| Target | 16.2 lbs | Actual Impact Velocity (knots) | 440kts |

| **Test Setup** | | | |
|---|---|---|---|
| Target impact angle attained | Yes | DIC system recorded properly | N/A |
| Gun alignment in tolerance | Yes | All load cells recorded data | Yes |
| All still camera images captured | Yes | All strain gages recorded data | Yes |
| All high-speed cameras capture impact | Yes | | |

| **Test Results Summary** |
|---|
| Blade was oriented vertically, which was annotated in the latest revision of the NIAR Task A16 Test Plan for Full sUAS impact tests.<br><br>The DJI Phantom 3 impacted with roll, pitch and yaw angles within limits and the center body/battery was the only portion of the aircraft that impacted the rotor blade leading edge. The blade flexed during the impact, but only sustained minor leading-edge dents. NIAR’s post-impact blade dissection showed that the metallic leading-edge strip debonded from the blade lower surface skin during the impact. The upper and lower surfaces of the blade debonded from the internal foam core. The sUAS impact also caused the trailing edge skin to split open and leave a gap between the upper and lower surface skin on the section directly aft of the leading edge impact area. The sUAS was destroyed and there was no “Fire Risk” based on how the impact destroyed the battery cells. |

**Photos**

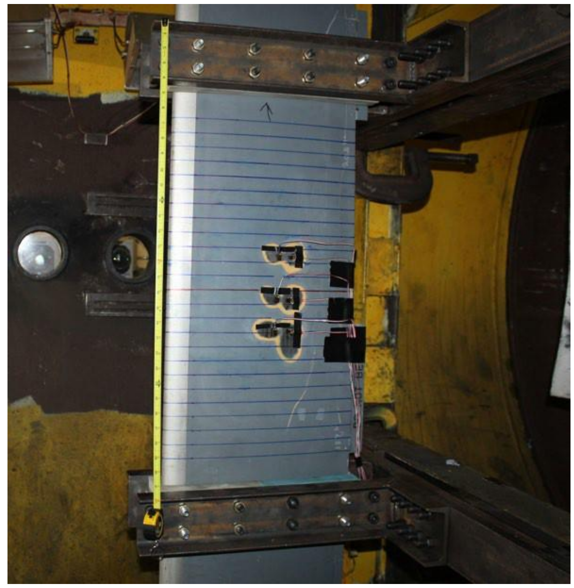

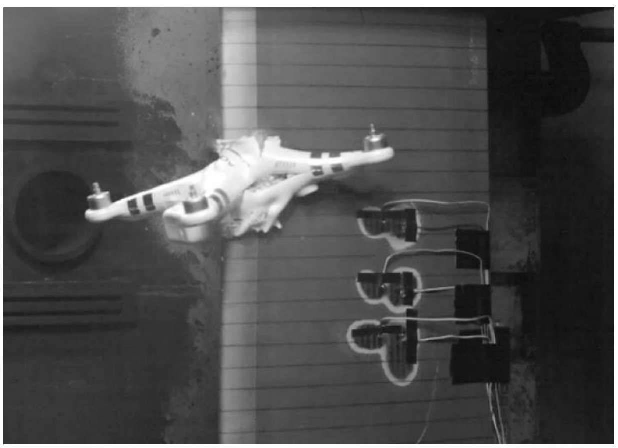

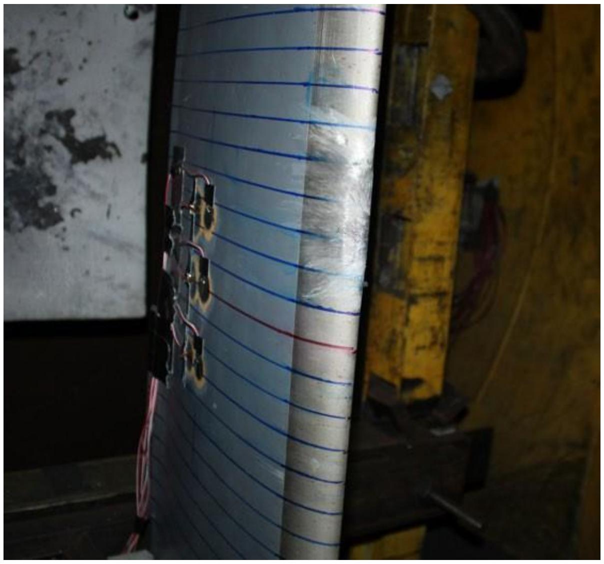

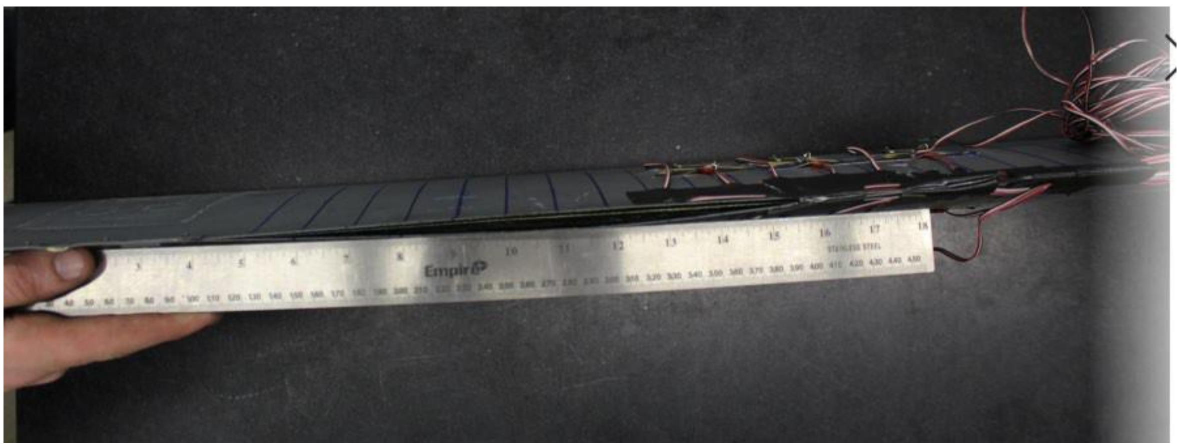

B.4.1.2.5 TEST 2-4 HORIZONTAL TAIL

| General Test Information | | | |
|---|---|---|---|
| Test Facility: | **SMDC-TC Aerophysics Research Facility** | Test Date | **8-3-2021** |
| ARF Test ID Number | **21-90** | NIAR Test ID Number | **2-4** |

| | |
|---|---|
| **Test Description** | DJI Phantom 3 Impact against Horizontal Tail |

| Test Conditions | | | |
|---|---|---|---|
| Projectile | DJI Phantom 3 without legs and camera | Target Dimensions | 20” x 40.4” x 2” |
| Projectile mass | 908.6 g | Nominal Impact Velocity (knots) | 175 |
| Target | 44.95 lbs | Actual Impact Velocity (knots) | 180 |

| Test Setup | | | |
|---|---|---|---|
| Target impact angle attained | Yes | DIC system recorded properly | N/A |
| Gun alignment in tolerance | Yes | All load cells recorded data | Yes |
| All still camera images captured | Yes | All strain gages recorded data | Yes |
| All high-speed cameras capture impact | Yes | | |

**Test Results Summary**

The center body of the aircraft flew under the horizontal tail and a single motor impacted the horizontal tail. The impacting motor and plastic motor mount broke off of the Phantom 3 and embedded in the leading edge of the horizontal tail. This impact resulted in breaks and dents in the leading-edge skin, but this plastic deformation was limited to a 4.25” span across the leading edge of the horizontal tail.

The test setup was modified from the test plan in the following manner. The 3/8” bolts that attached the horizontal tail side plates where torqued to the engineering reference’s recommended 40 ft-lbf after the bolts stripped at the 80 ft-lbf of torque specified in the test plan.

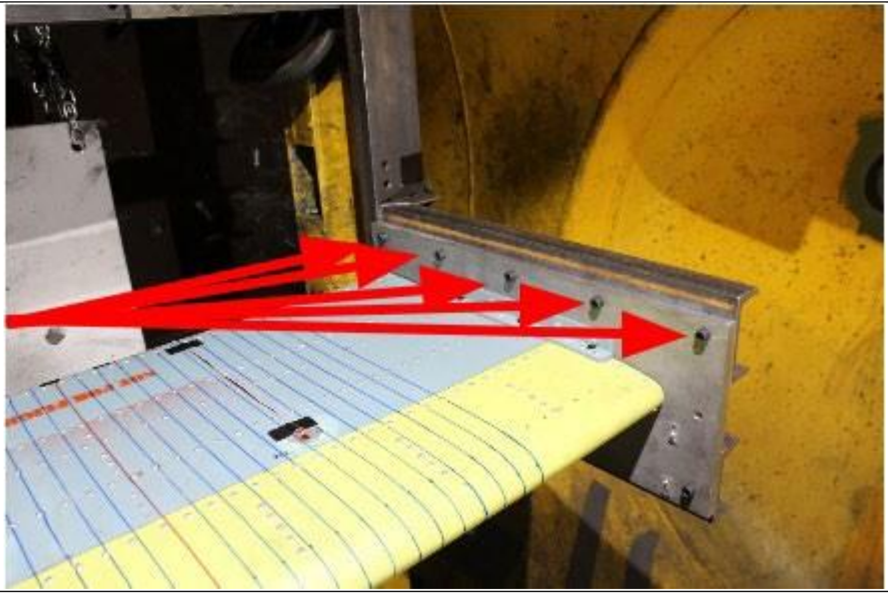

**Photos**

| | |
|---|---|
|  | 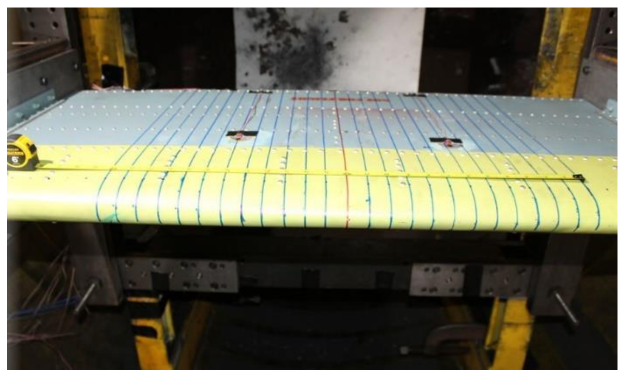 |
| 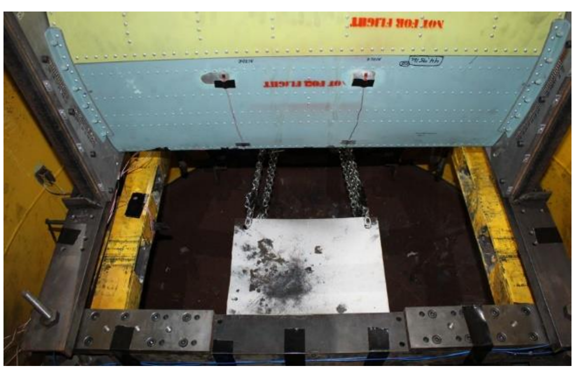 |  |

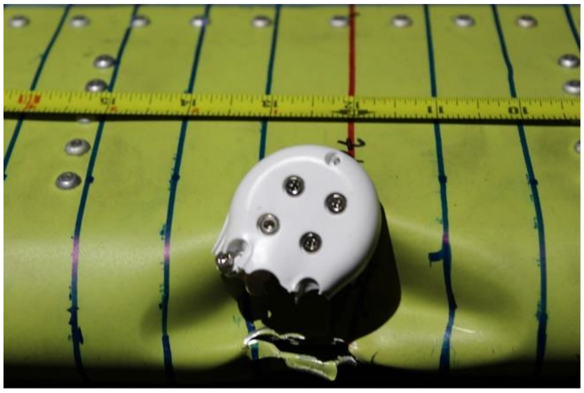

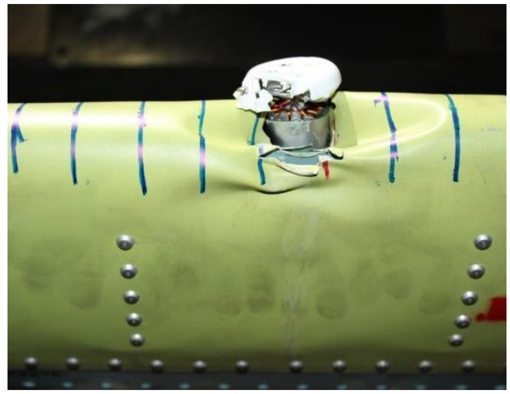

B.4.1.2.6 TEST 5 BI-LAYER WINDSCREEN

| **General Test Information** | | | |
|---|---|---|---|
| Test Facility: | **SMDC-TC Aerophysics Research Facility** | Test Date | **11-5-21** |
| ARF Test ID Number | **21-134** | NIAR Test ID Number | **5** |

| | |
|---|---|
| **Test Description** | DJI Phantom 3 impact test against a bi-layer windscreen |

| **Test Conditions** | | | |
|---|---|---|---|
| Projectile | DJI Phantom 3 with camera and legs removed | Target Dimensions | In UAH solid model files |
| Projectile mass | 933.9g | Nominal Impact Velocity (knots) | 50 |
| Target | 99.75 lbs | Actual Impact Velocity (knots) | 44 |

| **Test Setup** | | | |
|---|---|---|---|
| Target impact angle attained | No, angle was low | DIC system recorded properly | N/A |
| Gun alignment in tolerance | Yes | All load cells recorded data | Yes |
| All still camera images captured | Yes | All strain gages recorded data | Yes |
| All high-speed cameras capture impact | Yes | | |

| **Test Results Summary** |
|---|
| The DJI Phantom 3 impacted in a nose-low attitude and the impacting arms deformed during impact. The windscreen surface was scratched, but there was no structural damage to the windscreen the sUAS deflected upwards and landed behind the windscreen. Following the test, the windscreen was inspected for internal fractures in vicinity of the impact point. There were no visible fractures in the windscreen after the impact. There was minor damage to the drone and battery, which is shown in post-impact pictures. There was no post-impact battery “Fire Risk”. |

**Photos**



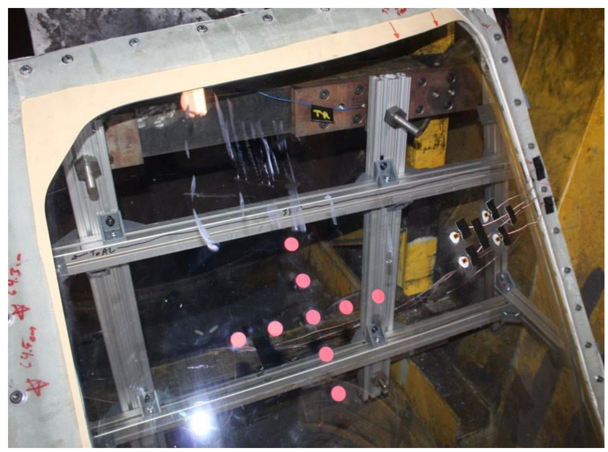

B.4.1.2.7 TEST 6 BI-LAYER WINDSCREEN

| **General Test Information** | | | |
|---|---|---|---|
| Test Facility: | **SMDC-TC Aerophysics Research Facility** | Test Date | **10-19-21** |
| ARF Test ID Number | **21-127** | NIAR Test ID Number | **6** |

| **Test Description** | DJI Phantom 3 impact test against a bi-layer windscreen |
|---|---|

| **Test Conditions** | | | |
|---|---|---|---|
| Projectile | DJI Phantom 3 with camera and legs removed | Target Dimensions | In UAH solid model files |
| Projectile mass | 917.7g | Nominal Impact Velocity (knots) | 175 |
| Target | 99.4 lbs | Actual Impact Velocity (knots) | 160 |

| **Test Setup** | | | |
|---|---|---|---|
| Target impact angle attained | Yes | DIC system recorded properly | N/A |
| Gun alignment in tolerance | Yes | All load cells recorded data | Yes |
| All still camera images captured | Yes | All strain gages recorded data | Yes |
| All high-speed cameras capture impact | Yes | | |

| **Test Results Summary** |
|---|
| DJI Phantom 3 impacted 2 inches below target point. The aircraft upper and lower shells broke apart and the battery was ejected. The battery remained intact and did not pose a “Fire Risk”. The aircraft body and battery deflected upwards and would have impacted the lower side of the main rotor in vicinity of the aircraft hub. The aircraft impact shattered >90% of the windscreen glass; however, the film on the inside of the glass remained intact and shards did not break off of the backside of the windscreen. |

| **Photos** | |
|---|---|
| 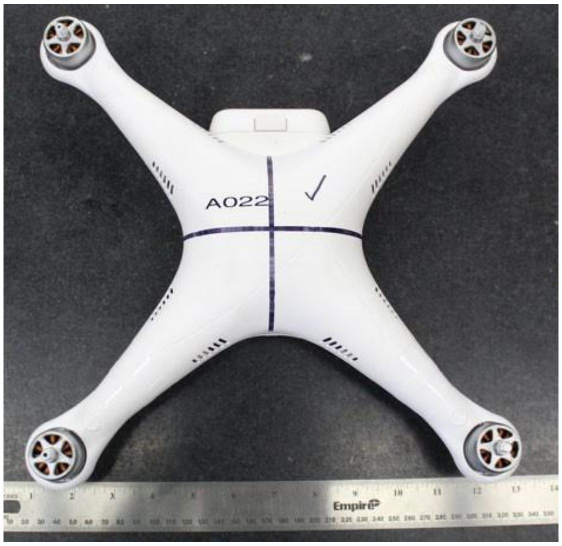 | 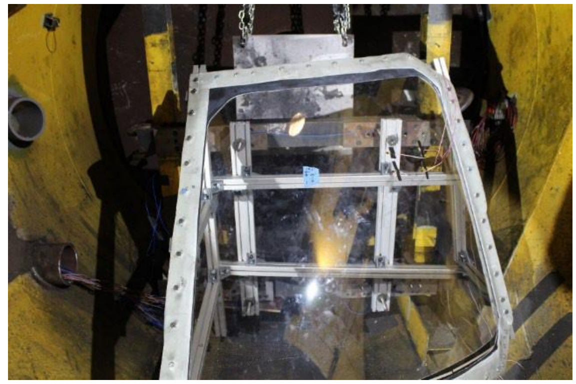 |
|  |  |

| | |
|---|---|
|  |  |

B.4.1.2.8 TEST 7 BI-LAYER WINDSCREEN

| **General Test Information** | | | |
|---|---|---|---|
| Test Facility: | **SMDC-TC Aerophysics Research Facility** | Test Date | **12-8-2021** |
| ARF Test ID Number | **21-143** | NIAR Test ID Number | **7** |

| **Test Description** | DJI Phantom 3 impact test against a bi-layer Windscreen |
|---|---|

| **Test Conditions** | | | |
|---|---|---|---|
| Projectile | DJI Phantom 3 with camera and legs removed | Target Dimensions | See UAH solid model files given to NIAR |
| Projectile mass | 918.2g | Nominal Impact Velocity (knots) | 290 |
| Target | 99.75 | Actual Impact Velocity (knots) | 290 |

| **Test Setup** | | | |
|---|---|---|---|
| Target impact angle attained | Yes | DIC system recorded properly | N/A |
| Gun alignment in tolerance | Yes | All load cells recorded data | Yes |
| All still camera images captured | Yes | All strain gages recorded data | Yes |
| All high-speed cameras capture impact | Yes | | |

| **Test Results Summary** |
|---|
| DJI Phantom 3 impacted 2 inches below target point. The aircraft upper and lower shells spread apart and the battery was breached the windscreen. As the battery breached the windscreen, the cells broke apart and became a cloud of lithium ion polymer dust on the back side of the windscreen. The front side of the windscreen was shattered and a large cloud of shards and glass dust came off of the front side of the windscreen during and after the impact. The film on the back side of the windscreen broke and glass shards came out of the back side of the windscreen. |

**Photos**